



Rôle physiologique et pathologique de la kinésine Kif21b au cours de la migration neuronale

José Rivera Alvarez

► To cite this version:

José Rivera Alvarez. Rôle physiologique et pathologique de la kinésine Kif21b au cours de la migration neuronale. Human health and pathology. Université de Strasbourg, 2022. English. NNT : 2022STRAJ105 . tel-04056679

HAL Id: tel-04056679

<https://theses.hal.science/tel-04056679>

Submitted on 3 Apr 2023

HAL is a multi-disciplinary open access archive for the deposit and dissemination of scientific research documents, whether they are published or not. The documents may come from teaching and research institutions in France or abroad, or from public or private research centers.

L'archive ouverte pluridisciplinaire **HAL**, est destinée au dépôt et à la diffusion de documents scientifiques de niveau recherche, publiés ou non, émanant des établissements d'enseignement et de recherche français ou étrangers, des laboratoires publics ou privés.

ÉCOLE DOCTORALE DES SCIENCES DE LA VIE ET DE LA SANTE

Institut de Génétique et de Biologie Moléculaire et Cellulaire

THÈSE présentée par :

José RIVERA ALVAREZ

Soutenue le : **6 décembre 2022**

pour obtenir le grade de : **Docteur de l'université de Strasbourg**

Discipline/ Spécialité : Aspects moléculaires et cellulaires de la biologie

Physiological and pathological role of the kinesin Kif21b during neuronal migration

THÈSE dirigée par :

Dr Juliette GODIN

CR, INSERM, IGBMC, Illkirch

RAPPORTEURS :

Dr. Fiona FRANCIS

DR, UMR-S 2170 Inserm Sorbonne Université, Paris

Dr. Alexandre BAFET

CR, CNRS UMR144, Institut Curie, Paris

EXAMINATEUR INTERNE :

Dr. Sylvie FRIANT

DR, GMGM- UMR7156 – Université de Strasbourg

INVITEE:

Dr. Anne-Cécile REYMANN

CR, IGBMC, Illkirch

*To those who are gone,
but I keep alive through my thoughts and actions*

ACKNOWLEDGEMENTS

I would like to thank the members of my thesis committee: Dr. Fiona Francis, Dr. Alexandre Baffet, Dr. Sylvie Friant and Dr. Anne-Cécile Reymann for evaluating this work and providing me with their valuable input.

I express my gratitude to my thesis supervisor, Juliette Godin, whose guidance and encouragement have always been a source of inspiration. Thanks for giving me the opportunity to participate in a fascinating project where I learnt things from different areas, it's been a pleasure making discoveries about the developing brain during these years. Thank you for the patience and confidence during the realization of this work.

Thanks to all the people in my team: to Laure for laying the foundations of the work with Kif21b during cortex development, it was great learning from you, I've been always amazed and inspired by all the work you did; to Peggy, for all the help provided during these years, for the *in utero* electroporations, genotypings, and your charming presence; to Efil for always being willing to give advice, for being an endless source of good ideas, for helping me to not drown, and so many other things; thanks to Noemie for helping me with the experiments during this last part of my PhD, it's been great working with you; to Charlotte for being a great labmate and a very generous human being; to Pierre, for the interesting discussion about our projects, and for teaching me how to properly hold a bottle of wine; gracias Aline for the feedback during the presentations. Thanks also to Jordi, Hakima, Romain and all the members of the lab that were part of this experience.

I would like to express my gratitude to all the people that collaborated with their expertise in different areas that complemented this project. We are the best example that progress in science, the same as in any other area, is possible just by the collective effort where everyone gives their passion and talent. A big thank you to Claire, for your work with recombinant Kif21b; to Roxane, for your help with *In vitro* actin experiments; and Ludovic, for your assistance during the super resolution acquisition and processing.

Thanks to the people of the platforms: cell culture facility, imaging platform (especially Elvire Guiot, Erwan Grandgirard and Yves Lutz), proteomic platform (especially Bastian Morlet) and molecular biology platform (Therry Lerouge and Paola Rosolillo).

To my friends here in Strasbourg: Dana, Juliana, Moni, Roberto, Isra, Yuri, Olga, Lillia, Ale, Hector, José Tomas, I am really thankful to all of you for making these difficult times a bit easier. One of the best things about my time here was meeting you guys.

Gracias, mamá por tu cariño y por tu apoyo incondicional en todas las cosas que emprendo, también gracias por ser el mejor ejemplo de amor, tenacidad y resiliencia que podría existir.

And last but not least, I would like to thank me.

TABLE OF CONTENTS

LIST OF FIGURES	7
ABBREVIATIONS	8
CHAPTER I.- CEREBRAL CORTEX DEVELOPMENT AND RADIAL MIGRATION.....	9
1 Early stages of cortex formation.....	10
2 Progenitor cells.....	11
2.1 Neuroepithelial cells.....	11
2.2 Radial glia.....	12
2.3 Apical radial glia dynamics.....	13
2.4 Intermediate progenitors.....	16
3 Neuronal migration in the cortex	18
3.1 Tangential migration	18
3.2 Migration of projection neurons.....	20
<u>3.2.1 Projection neurons migrate in a stepwise fashion</u>	<u>21</u>
<u>3.2.2 Multipolar phase and transition to bipolar phase</u>	<u>22</u>
<u>3.2.2a Extracellular signals in MP-BP transition.....</u>	<u>23</u>
<u>3.2.2b Cell adhesions in MP-BP transition</u>	<u>24</u>
<u>3.2.2c Regulation of gene expression</u>	<u>25</u>
<u>3.2.3 Locomotion.....</u>	<u>27</u>
<i>3.2.3a Extracellular factors and receptors</i>	<i>27</i>
<i>3.2.3b Cell adhesions and membrane trafficking.....</i>	<i>31</i>
<i>3.2.3c Cell signaling- Cdk5 and Jnk</i>	<i>33</i>
<i>3.2.3d Nucleokinesis regulation.....</i>	<i>34</i>
<i>3.2.3e Cytoskeleton regulation.....</i>	<i>35</i>
1. CHAPTER II. CYTOSKELETON DYNAMICS AND PARTICIPATION IN RADIAL MIGRATION	36
1. Actin cytoskeleton dynamics.....	36
1.1 Regulators of actin organization	37

1.1.1 Arp2/3 and participation in filament branching	37
1.1.2 Actin bundling proteins.....	38
1.1.3 Filament disassembly.....	40
1.1.4 Rho family of small GTPases	41
1.1.5 Other actin related proteins involved in radial migration	43
1.2 Actomyosin contraction and contractile structures	46
1.2.1 Myosins.....	46
1.2.2 Actomyosin contraction	47
2. Microtubules dynamics	50
2.1 Microtubules organizing centers	51
2.2 The tubulin code.....	52
2.3 Microtubules associated proteins	54
2.3.1 Plus-tip binding MAPs.....	54
2.3.2 Lattice binding MAPs	55
2.3.3 Microtubule stabilizing MAPs	57
3. Microtubule motor proteins.....	60
3.1 Dyneins and associated proteins	60
3.2 Kinesins.....	62
3.2.1 Kinesins regulatory mechanisms	63
3.2.1a Kinesins inhibition	63
3.2.1b cargo recruitment/release	65
3.2.1c Regulatory functions on microtubules dynamics.....	66
3.2.2 Cortical malformations associated to kinesins dysfunctions.....	66
3.2.3 Participation of kinesins in radial migration	68
4. Kif21b.....	72
4.1 Neurotransmitter receptors regulation.....	72
4.2 Regulation on microtubules dynamics	73
4.3 Structural regulation	75
4.4 Kif21b in human health.....	76

AIMS OF THE PROJECT	77
RESULTS	79
ARTICLE 1: Mutations in the KIF21B gene cause neurodevelopmental disorders through imbalanced canonical motor activity.....	80
ARTICLE 2: Further delineation of KIF21B-related neurodevelopmental disorders ...	81
ARTICLE 3: The kinesin Kif21b regulates radial migration of cortical projection neurons through non canonical function on actin cytoskeleton.....	82
DISCUSSION	83
1. KIF21B relevance for human neurodevelopmental disease.....	83
1.1 Test of a possible dominant negative function.....	85
1.2 Kif21b mutations induced a gain of function of the protein	85
1.3 Relieve in auto-inhibition is related to pathological outcomes in other kinesins.....	87
1.4 Study in other neuronal types	88
1.5 Contribution of this work to the knowledge of kinesins in cortical development	88
2. Kif21b in physiological condition – a detailed glance at migration	88
2.1 Kif21b participates in locomotion, but not in multipolar-bipolar transition	89
2.2 Kif21b motility does not participate in radial migration	90
2.3 Implication of the motor domain during migration.....	91
2.4 Kif21b is an actin binding protein.....	94
2.5 Kif21b regulates actin dynamics in migrating neurons.....	95
2.6 Other roles of Kif21b regulating actin cytoskeleton dynamics.....	97
2.7 Hypothesized microtubules actin crosslink	99
2.8 Summary.....	100
3. General conclusion.....	100
BIBLIOGRAPHY	101

LIST OF FIGURES

1. Cerebral cortex structure	9
2. Early central nervous system and cortex development	10
3. Neuroepithelium and Radial glial cells	12
4. Different cell types composing the developing cortex	13
5. Neuronal migration in the cerebral cortex	17
6. Interneurons migration cycle	18
7. Development of cortical structures	19
8. Phases of radial migration	20
9. Multipolar-bipolar transition	24
10. Morphological changes during locomotion	26
11. Locomotion regulatory mechanisms	31
12. F-actin structure	34
13. Lamellipodial structure	35
14. Filopodial structures	37
15. Rho family of small GTPases	40
16. Graphical summary of actin related proteins regulating radial migration	43
17. Contraction of actomyosin cytoskeleton in sarcomere structure present in skeletal muscle	45
18. Different contractile structures formed by actomyosin cytoskeleton	45
19. Microtubules dynamic instability	47
20. Microtubule associated proteins	54
21. Dynein structure	58
22. Kinesin superfamily proteins	59
23. Kinesins regulating neuronal migration	24
24.- Structure of Kif21b with its main domains and subdomains	69

ABBREVIATIONS

AAA: ATPases associated with diverse cellular activities	MCD: Malformations of cortical development
AP Apical Progenitors	MGE: Medial ganglionic eminences
ATP: Adenosine triphosphate	MCD: Malformations of cortical development
BLBP: Brain lipid binding protein	MHC: Myosin heavy chain
BP: Basal progenitor	MLC: Myosin light chain
CC: Coiled coil	MP: Multipolar
CLASP: Cytoplasmic linker associated protein	MT: Microtubules
CLIP: Cytoplasmic Linker protein	MZ: Marginal Zone
CP: Cortical Plate	MTOC: Microtubule organizing center
Cux: Cut like homeobox	NBEA: Neurobeachin
Dcx: Doublecortin	NMDA: N-methyl-D-Aspartate
Dclk: Doublecortin-like kinase	PACT: Pericentrin-AKAP-450 centrosomal targeting
E: Embryonic day	Pax6: Paired box 6 protein
EB: End binding protein	PCM: Pericentriolar matrix
GABA: gamma-aminobutyric acid	rCC: regulatory coiled coil
GAP: GTPase activating protein	RG: Radial glia
GEF: Guanine Exchange factor	Shh: Sonic hedgehog
GFP: Green fluorescent protein	shRNA: short hairpin RNA
GDP: Guanosine diphosphate	siRNA: small interfering RNA
GTP: Guanosine triphosphate	SP: Subplate
INM: Interkinetic nuclear migration	SVZ: Sub-Ventricular Zone
IUE: <i>In utero</i> electroporation	Tbr2: T-box brain protein 2
IP: Intermediate Progenitors	WT: Wild type
IZ: Intermediate Zone	
kD: Kilodaltons	
KBP: Kinesin Binding protein	
KLC: Kinesin Light chain	
KI: Knock-In	
KIF: Kinesin family	
KHC: Kinesin heavy chain	
KO: Knock-out	
LGE: Lateral ganglionic eminence	
Lis1: Lissencephaly 1	
LP: Leading process	
MAP: Microtubules associated protein	
MAPK: Mitogen activated protein kinase	

INTRODUCTION

CHAPTER I.- CEREBRAL CORTEX DEVELOPMENT AND RADIAL MIGRATION

The cerebral cortex is the outermost and largest portion of the brain, and it is required for the integration of motor, sensory and cognitive information in order to provide functions like language, reasoning and voluntary movement, to mention some. The processing of this information requires a rich interconnection between cortical areas and subcortical structures (Shipp, 2007). The two main neuronal types that compose the cortex are pyramidal excitatory neurons, being around 80% of the total, and inhibitory interneurons, making the remaining 20%. Pyramidal neurons produce glutamate as neurotransmitter and project to other regions of the cortex and subcortical areas, while interneurons make short inhibitory local connections using γ -amino butyric acid (GABA) as neurotransmitter. Importantly, both types of neurons are generated in different sites in the embryonic brain (for review see C. G. Silva et al., 2019).

According to their degree of folding cortices can be classified in two classes, lissencephalic, where the structure is smooth and lacks folding, such as the case for rodents; and gyrencephalic, where the cortex is folded and develops bulges and grooves, for example in human and ferrets (**Fig. 1**) (for review, see Rakic, 2009). Defects of cortical folding produce disabling pathological outcomes in humans that are related to intellectual disability and epilepsy (For review, see Fernández et al., 2016).

Despite the differences in folding, one evolutionary conserved feature in mammalian cortex is the arrangement of neurons in 6 layers parallel to the cortical surface, each with a different morphological and biochemical composition. Deep layers (V and VI), connecting mainly to sub-cortical targets, express markers such as *Ctip2* and *Tbr2*; while superficial layers (II, III and IV), connecting intra-cortically, express *Cux2* and *Lhx2* (for review, see Molyneaux et al., 2007).

This neuronal arrangement is determined since embryonic stages, where many processes involving progenitor proliferation and differentiation, neuronal migration and maturation are necessary to happen at the right time and place. Interestingly, this organization in 6 neuronal layers is generated in a similar fashion in mammals, with an inside-out integration of neurons, where early born neurons integrate in deep layers, and newly generated neurons integrate to more superficial layers (Angevine & Sidman, 1961; Rakic, 1974). Thanks to the conserved mechanisms generating the cortex during development, knowledge about corticogenesis has been often enriched from studies coming from mouse models, from where basic principles can be extracted and then applied in different mammalian models, including human (Luhmann & Fukuda, 2020).

In the following section, basic aspects of early corticogenesis and neurogenesis (progenitors biology) will be briefly explained and then, neuronal migration (the focus of this thesis) will be explored in more detail.

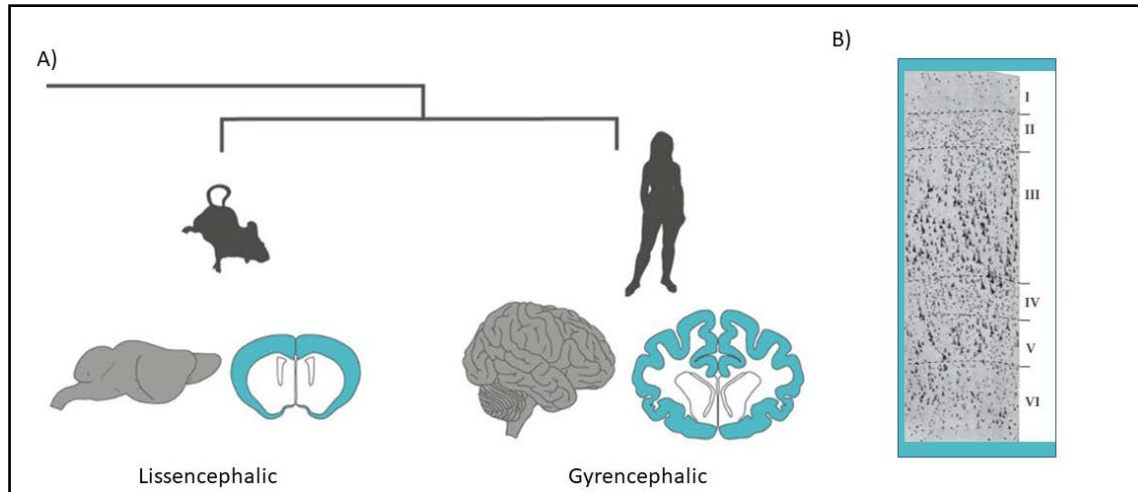


Figure 1. Cerebral cortex structure. Mammalian cortex (highlighted in green) can be divided in two types depending on the degree of folding: lissencephalic (rodent in the example) and gyrencephalic (human in the example) (Modified from Espinós et al., 2022). B) Cerebral cortices possess a six layered structure conserved among mammals, each layer with unique morphological and molecular characteristics (From Parent, 1996).

1. Early stages of cortex formation

The development of central nervous system (CNS) starts with neurulation, the process of neural tube formation and closure (Wilde et al., 2014). It begins with the formation of the neural plate, a thickened portion of the dorsal ectoderm induced by the chemical signals derived from the notochord in the mesoderm. Later on, the neural plate folds in the midline until the borders fuse and close together to form the neural tube (**Fig. 2A**) (Rubenstein et al., 1998; Wilde et al., 2014). The rostral end of the neural tube gives rise to three main vesicles: the forebrain, midbrain and hindbrain. The forebrain further divides into diencephalon and telencephalon, the structure giving rise among other parts, to the cerebral cortex (**Fig. 2B**) (Davidson, 1989).

Different kinds of neurons are generated from diverse proliferative regions in the telencephalon, the dorsal telencephalon gives rise to pyramidal neurons, while the ventral telencephalon, composed by the ganglionic eminences (GEs), produces many different types of interneurons (Nadarajah & Parnavelas, 2002). For this reason, the telencephalon requires a dorso-ventral regionalization, which is achieved by the induction of different molecules. Wnt signalling components are important for telencephalon dorsalization, the same as the expression of the transcription factor Gli3, which absence disrupts the expression of the marker of dorsal telencephalon Emx1, as well as generation of structures such as choroid plexus and cortical hem (Theil et al., 1999; Tole et al., 2000). Sonic hedgehog (Shh) in the other hand, is a morphogen that participates in telencephalon ventralization by repressing

Gli3, as it was shown by Rallu, et al, (2002) where *Gli3* KO produces ventralization defects, something that is partially restored by *Gli3* / *Shh* double KO (Rallu et al., 2002). Moreover, ventralization is also supported by positive feedback produced between FoxG1 and FGF (Hébert & Fishell, 2008).

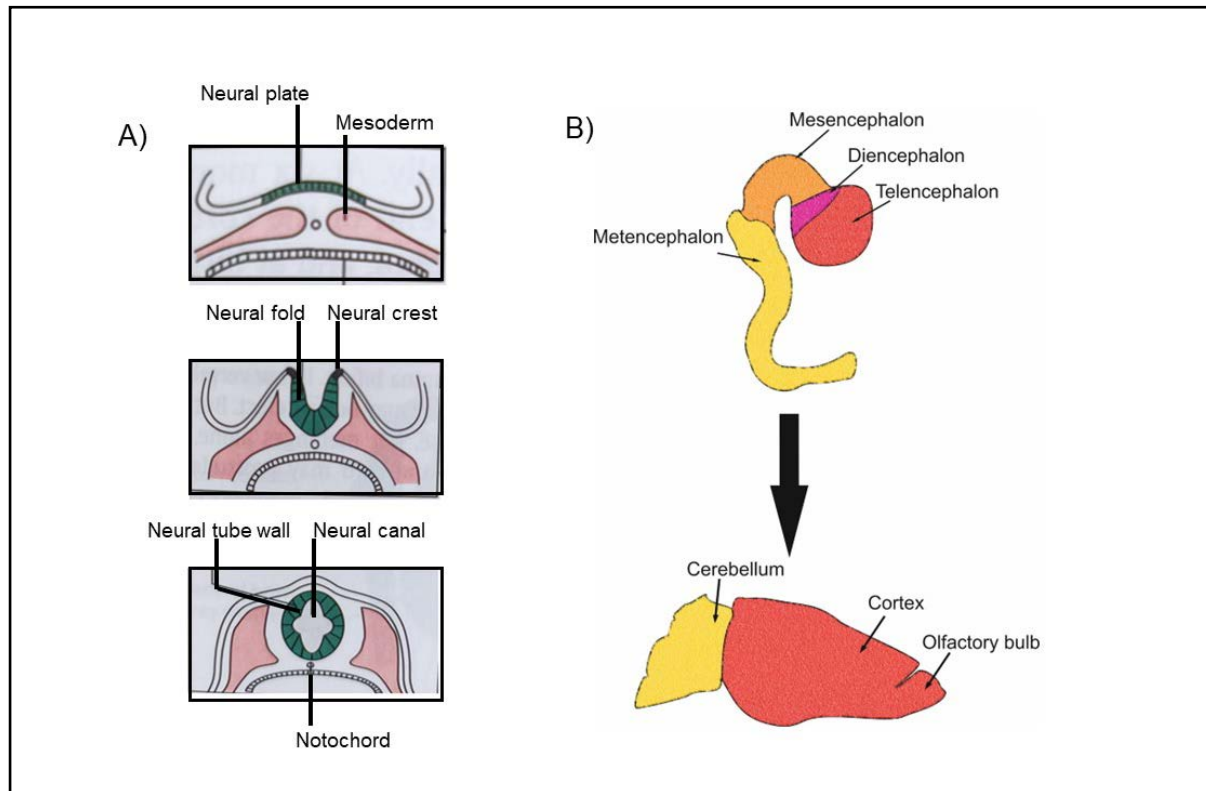


Figure 2. Early central nervous system and cortex development. A) During early stages of central nervous system (CNS) development, the neural plate generates from the ectoderm to further fold and give rise to the neural crest and later on, produces the neural tube by closing by the edges (modified from Greenstein & Greenstein, 2000). B) Early vesicles forming at the front of the neural tube, from where the telencephalon gives rise to the adult cortex.

2. Progenitor cells

2.1 Neuroepithelial cells

After the neural tube is closed at embryonic day 9 (E9) in mouse, the first cortical progenitors organize in a Neuroepithelium (NE), a pseudostratified epithelium which cells divide symmetrically to amplify the progenitor pool, and whose basal surface is directed towards the ventricle and the apical surface faces the outer surface. Molecularly, the NE is characterized by the presence of tight junctions and the expression of the intermediate filament nestin (Götz & Huttner, 2005). The nuclei, accommodated in different places gives rise to the pseudostratified structure, undergo interkinetic nuclear migration

(INM), a process where, depending on the phase of the cell cycle, the nucleus locates in different apico- basal regions, with cells in G1 undergoing apico-basal nuclear migration (directed to the outer surface) and cells in G2 undergoing basal-apical nuclear migration (directed to the ventricle), with mitosis occurring at the apical site (**Fig. 3A**) (Fujita, 1962, 1963; reviewed in Miyata et al., 2015).

Since amplification of the NE progenitor pool is essential to produce the right number of cortical cells, the mechanisms controlling self-renewal / differentiation are one of the most interesting topics concerning neuroepithelia. Recently, it was shown in human pluripotent stem cells differentiated into dorsal forebrain NE cells, that activation of FGF and inhibition of BMP and Activin A signalling are required for long term renovation of NE cells. Low activity of GSK-3, AKT and CATENIN- β 1 were also important to support clonal expansion of dorsal forebrain NE cells (Varga et al., 2022). Studies comparing human, gorillas and chimpanzees brain organoids, showed that one of the reasons humans produce a larger number of neurons is because human NE present with shorter cell cycle length, and a delayed transition to radial glia, giving more time to amplify the progenitors pool (Kwiecinski, et al. 2021). Hence, these first steps controlling NE numbers are important to produce the right number of progenitors and neurons in later steps.

2.2 Radial Glia

At E11 in mice, NEs undergo molecular and morphological changes that give rise to the Radial Glia (RG), the main neural progenitor in the brain that produces the different neuronal and glial lineages. RG can be recognized from NE for their different markers, morphology and strategies of division (Malatesta et al., 2003). Two main types of RG cells are found in the mammalian cortex: The apical radial glia (aRG), and the basal radial glia (bRG) (**Fig. 3**) (For review see Fenlon, 2022).

aRG locate their soma in the region constituting the VZ and extend a long basal process that attaches to the pial surface (facing the outer surface), and a short apical process contacting the ventricle (internal surface) including the presence of a cilium (Rakic, 1972). bRG on the other hand, often lack the apical process contacting the ventricle, and their soma is located in the basal part of the SVZ (Fietz et al., 2012; Hansen et al., 2010) (**Fig. 3B**). bRG possess high self-renewing capacity, increasing the potential to generate neurons. They are more abundant in mammals with gyrencephalic cortex, where the formation of folded cortices requires a high neuronal production (Farkas & Huttner, 2008).

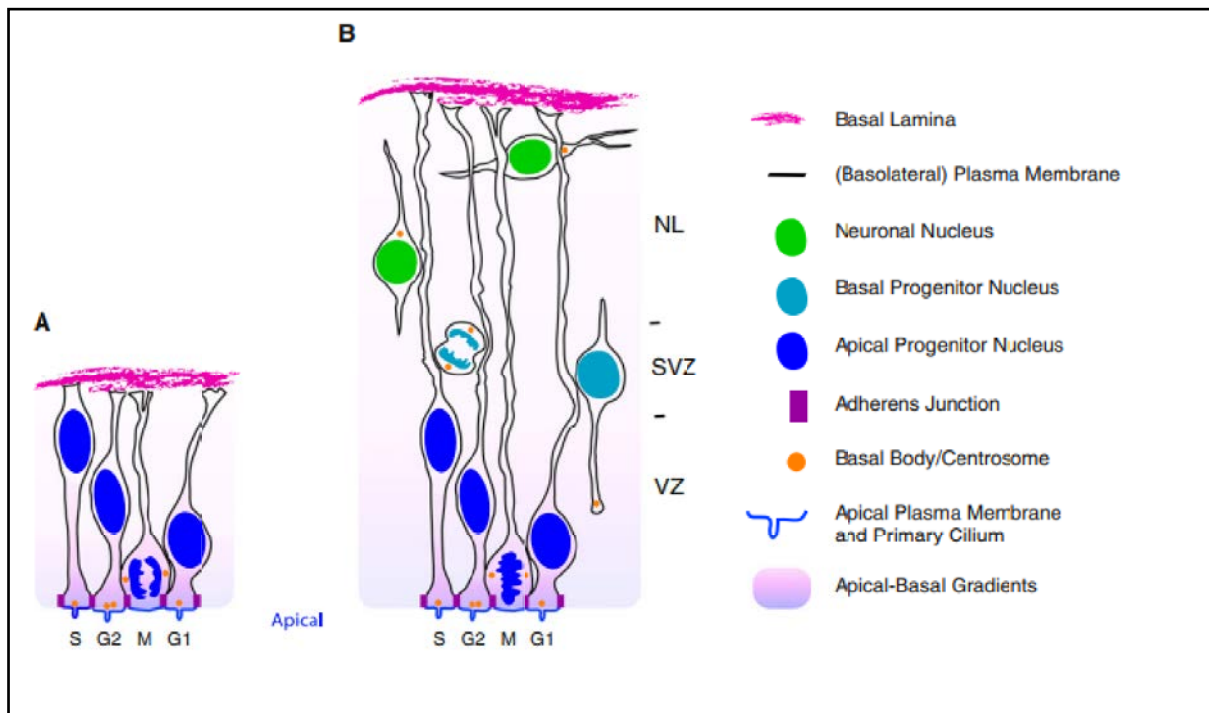


Figure 3. Neuroepithelium and Radial glial cells. A) Representation of Neuroepithelial cells, forming a pseudostratified epithelium, characterized by interkinetic nuclear migration (INM), where the nucleus is located in different apico-basal localizations depending on the phase of the cell cycle, they possess a primary cilium at the apical (ventricular) surface. B) Apical progenitors possess a long basal process spanning the whole thickness of the cortex, and undergo INM in the VZ, where they localize their nuclei. Basal progenitors in the other hand, often lack the contact with the ventricular surface (Taverna & Huttner, 2010).

2.3 Apical radial glia dynamics

aRG is defined by its markers, mainly BLBP (Feng et al., 1994), Glast (Shibata et al., 1997) and the transcription factor Pax6 (Götz et al., 1998). aRG undergo INM, locating their nucleus in different apico-basal regions of the VZ depending on the phase of the cell cycle they are passing through (Takahashi et al., 1993;). The aRG pool is increased by symmetrical divisions, where each progenitor gives rise to two cells of the same type. Otherwise, the aRG divide asymmetrically and produce neurons either directly, giving birth to one neuron and one aRG; or indirectly, producing one aRG and one intermediate progenitor (IP), which increases the final neuronal output. Newly born neurons use the aRG basal process as a scaffold to migrate until they integrate in the cortical plate (**Fig. 4**) (Kawaguchi, 2021).

Regarding neurogenic potential, studies using quantitative clonal analysis in mouse (Mosaic Analysis with Double Markers) have demonstrated that once entered in neurogenic phase (starting at E11 in

mouse), aRG can produce between 8 and 9 neurons distributed along all the layers of the cortex. Accordingly, *Otx1* KO (present in some progenitor cells) induces defective production of neurons in all neuronal layers (Gao et al., 2014).

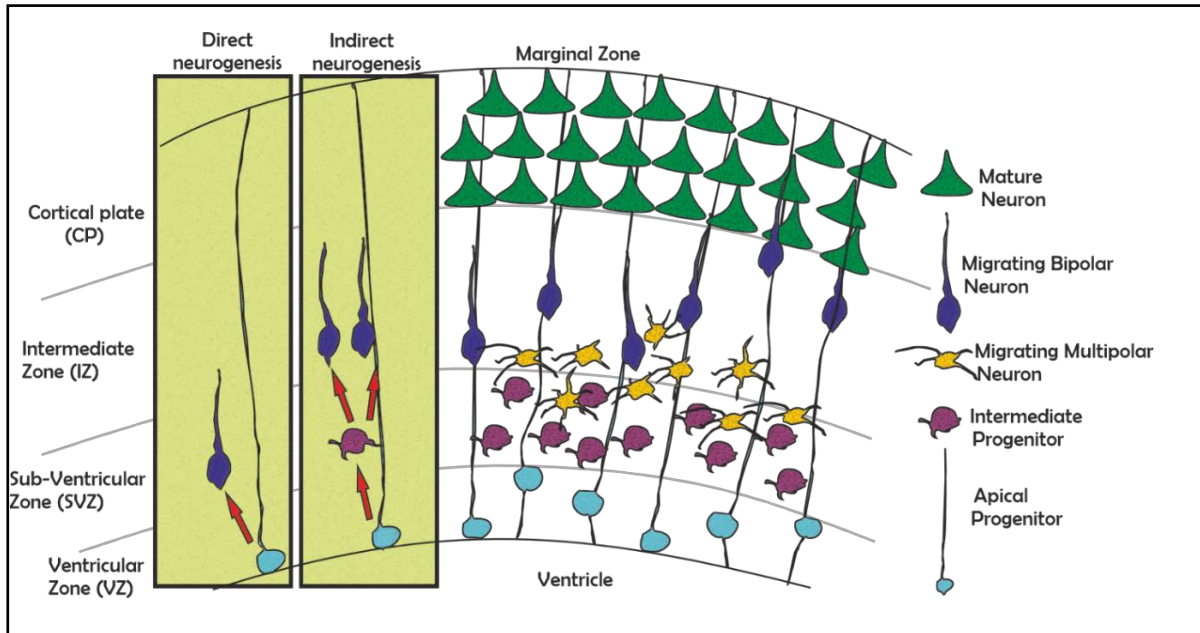


Figure 4. Different cell types composing the developing cortex. Apical radial glia (light blue) span the entire thickness of the cortex, with the apical end-feet contacting the ventricle and the basal process reaching the pial surface or marginal zone. Direct and indirect neurogenesis are indicated in the yellow squares, where APs can give rise to neurons (deep blue) directly or through the mediation of Intermediate progenitors (purple).

Once generated, neurons pyramidal neurons require a scaffold to migrate, that is the reason of the importance of the structural integrity of the aRG, required for neuronal migration. Cell adhesions are important factors regulating maintenance of morphological integrity of aRG and besides influencing cell interactions (for review see Sokpor et al., 2022), they are implicated in cytoskeleton integrity and cell signalling pathways. aRG cells are known to form contacts between them mainly by adherent junctions present at their apical side, where an actin “belt-like” structure is linked by proteins like cadherins, ZO-1 and β -catenin (Chenn et al., 1998; Hatakeyama et al., 2014). These structures are responsible to provide the aRG with shape and polarity, since the KO of their adherent junctions’ components are known to induce mis-localization and malformations of these progenitors, associated with cortical malformations (Uzquiano et al., 2018).

Components of the aRG require to be well-distributed in a polarized manner in the basal process, soma and apical region. The basal process presents some interesting features, such as varicosities, which consist in protuberances that contain clusters of receptors that increase in number during

mitotic phase, and in addition, they contain MT organizing centres independent from the centrosome, and dependent on the protein CAMPSAP (Coquand et al., 2021). Moreover, the basal end feet, contacting the pial surface, contributes to the binding of extracellular components from the basal lamina and to the reception of mitogenic signals from the meninges and other surrounding cells (Taverna et al., 2014).

At the apical side of aRG, the centrosome anchors the primary cillium and works as an antenna that receives extracellular regulatory signals like TGF- β , IGF, Sonic Hedgehog and Wnts coming from the CSF and that regulate progenitor dynamics (Martín et al., 2006; Falk et al., 2008; Lehtinen et al., 2011). When aRG enter into mitosis, the centrosome disassembles and distributes its centrioles to the poles of the mitotic spindle (Farkas & Huttner, 2008; Taverna et al., 2014).

Besides the mentioned factors in CSF, aRG are exposed to signals coming from different sources, such as the migrating neurons and meninges, all of them influencing cell behaviour and cell cycle dynamics (Taverna et al., 2014). Dysregulation of Wnt signaling, for example, produces an increase in the number of aRG at the expense of IPs and neurons (da Silva et al., 2021). Meninges at the basal side of the aRG, are the source of retinoic acid, which regulate progenitor dynamics by decreasing aRG amplification and inducing differentiation (Siegenthaler et al., 2009).

At the end of the neurogenic period, aRG transition from neurogenesis to gliogenesis, generating all the glial cells of the CNS such as astrocytes, oligodendrocytes and ependymal cells. This transition requires secretion of cardiotrophin-1 from the new-born neurons as a feedback mechanism, activating the JAK-STAT signalling pathway (Barnabé-Heider et al., 2005).

The high degree of neuronal diversity is influenced since the progenitor stage, and some studies have addressed this topic. Early transplantation studies show that cells generated for the deep layers (early born) are able to generate superficial neurons when transplanted at late neurogenic periods (generating superficial neurons), but the opposite is not true for neurons committed to superficial layer phenotypes. This indicates that deep layer neurons possess a higher degree of plasticity than superficial layers (Frantz & McConnell, 1996). Further studies revealed that genes like Cux1 and Cux2 (Nieto et al., 2004) expressed in neurons are already present in progenitors in the VZ. However, these cells are able to produce neurons and also glia from different layers (not necessarily Cux1 and 2) in the cortex, as indicated by Eckler et al (2015).

Transcriptomic analysis of aRG indicates that early born progenitors (E12, E13) are regulated mainly by intrinsic factors (nuclear proteins and cell cycle regulators), while late aRG (E14, E15) are predominantly regulated extrinsically (ion channels, lipid metabolism) (Telley et al., 2019). Another important feature is that aRG present age specific transcriptional programs that are transmitted to their daughter neurons, meaning that the high neuronal diversity that characterizes the cortex is

generated since the progenitor stage (Telley et al., 2019). Nevertheless, influence in cell fate due to plasticity of the progeny cannot be neglected.

Another investigation by single cell transcriptomics looked at the different types of progenitor cells in the ganglionic eminences, the site of interneurons generation. Authors saw that these progenitors possessed a transcriptional signature defined by their time and place of generation, supporting the idea that neurons are already defined to their fate since the progenitor stage (Mi et al., 2018). But adding complexity to this phenomenon, another study on interneuron progenitors discovered by RNA-sequencing approaches with genetic fate mapping, that interneurons undergo a common maturation program before branching into distinct precursor states that give emergence to the high interneuron diversity (Mayer et al., 2018).

Overall, dynamics and structure of RG are essential aspects that require to be finely tuned in order to produce the right amount and type of neurons and guide them to their final place of localization in the cortex.

2.4 Intermediate progenitors

Indirect neurogenesis requires the production of IPs, which amplify the final number of produced neurons. After they arise from aRG asymmetric divisions, they delaminate from the VZ and locate in the SVZ by the mediation of factors like the centrosomal protein AKNA, that regulates organization of centrosomal microtubules (Camargo Ortega et al., 2019). IPs possess lower proliferative capacity than APs and normally they undergo a self-consuming symmetric division giving rise to two neurons (Haubensak et al., 2004; Miyata et al., 2004; Noctor et al., 2004). IPs are defined by the presence of the T-box transcription factor Tbr2, which downregulates the expression of the aRG transcription factor Pax6 (Englund et al., 2005).

The role of IPs is not limited to the amplification of the neuronal numbers, they regulate cortex morphogenesis by the induction of instructive roles in other cells. This is the case for the contacts they establish with aRG, where the interaction of the Delta1 ligand in IPs with the Notch receptors 1-3 in the aRG, produces a feedback mechanism generated to keep stem cell identity in aRG; blocking of Notch activation induces aRG precocious differentiation into IPs (Nelson et al., 2013).

Another example is the secretion of chemical attractant signals, like Cxcl12, which is inductive to the ingression of thalamocortical tracts into the cortex (Abe et al., 2015). This is in accordance with the fact that IPs express genes associated with axon guidance, neurite growth and excitability, like Unc5d, Plexin and Netrins (Bedogni & Hevner, 2021). Blood vessels are another component of the IPs niche, whose function is hypothesised to be important for providing with integrins and collagen to enhance signalling pathways like TGF β in the IPs (Javaherian & Kriegstein, 2009). The balance between the

production of aRG, IPs and neurons relies on a species-dependent dynamic of intrinsic and extrinsic factors. The factors regulating progenitor activities include transcription factors, epigenetic landscape, signalling pathways, environmental cues and interaction between cells, to mention some examples (Paridaen & Huttner, 2014).

3. Neuronal migration in the cortex

As noted previously, cortical neurons are born in two germinative regions, the dorsal and ventral telencephalon. The first generates pyramidal excitatory (glutamate expressing) neurons, comprising nearly 80% of the cortical neurons, that migrate in a radial fashion; while the second produce inhibitory (GABA expressing) interneurons, that are part of the remaining 20% and migrate in a tangential fashion (**Fig. 5**). Despite having in common a highly polarized structure characterized by the presence a soma and a leading process, mechanisms driving migration in different neuronal types are diverse, showing different cellular structures, dynamics and ways of regulation (C. G. Silva et al., 2019).

Thus, mechanisms described that regulate pyramidal neurons migration might differ from interneurons, or other neurons, like cerebellar granular neurons, another common neuronal type studied regarding migration. Differences are due to the particular origin of each neuronal type and the microenvironment (cells and extracellular components) that they have to go through (A. H. Hansen & Hippenmeyer, 2020; Solecki et al., 2004; Sultan et al., 2013). In the next section it will be explained the mechanisms driving interneuron migration and more deeply, pyramidal neuron migration, since that is the focus of this work.

3.1 Tangential migration

Interneurons migrating from the ventral telencephalon arise from the ganglionic eminences (GE), more specifically from medial (MGE), and caudal (CGE) ganglionic eminences. In these regions, interneuron progenitors express markers like *Dlx1/2* (Anderson et al., 1997; Petryniak et al., 2007) and *Mash1* (Casarosa et al., 1999). Progenitors born specifically from the MGE are positive for *Nkx2.1* (Fogarty et al., 2007), while CGE progenitors express *CoupTF1/2* (Tripodi et al., 2004).

After becoming immature neurons, they migrate in a tangential way of migration, that requires the cells to move long distances through the parenchyma until they reach the dorsal pallium (Anderson et al., 2001). Interneurons migrate mainly through two main streams, one in the marginal zone and the other in the SVZ, from where they disperse in the cortical plate by attaching to the radial glia to locate in their respective layer (**Fig. 5**) (Marin & Rubenstein, 2001).

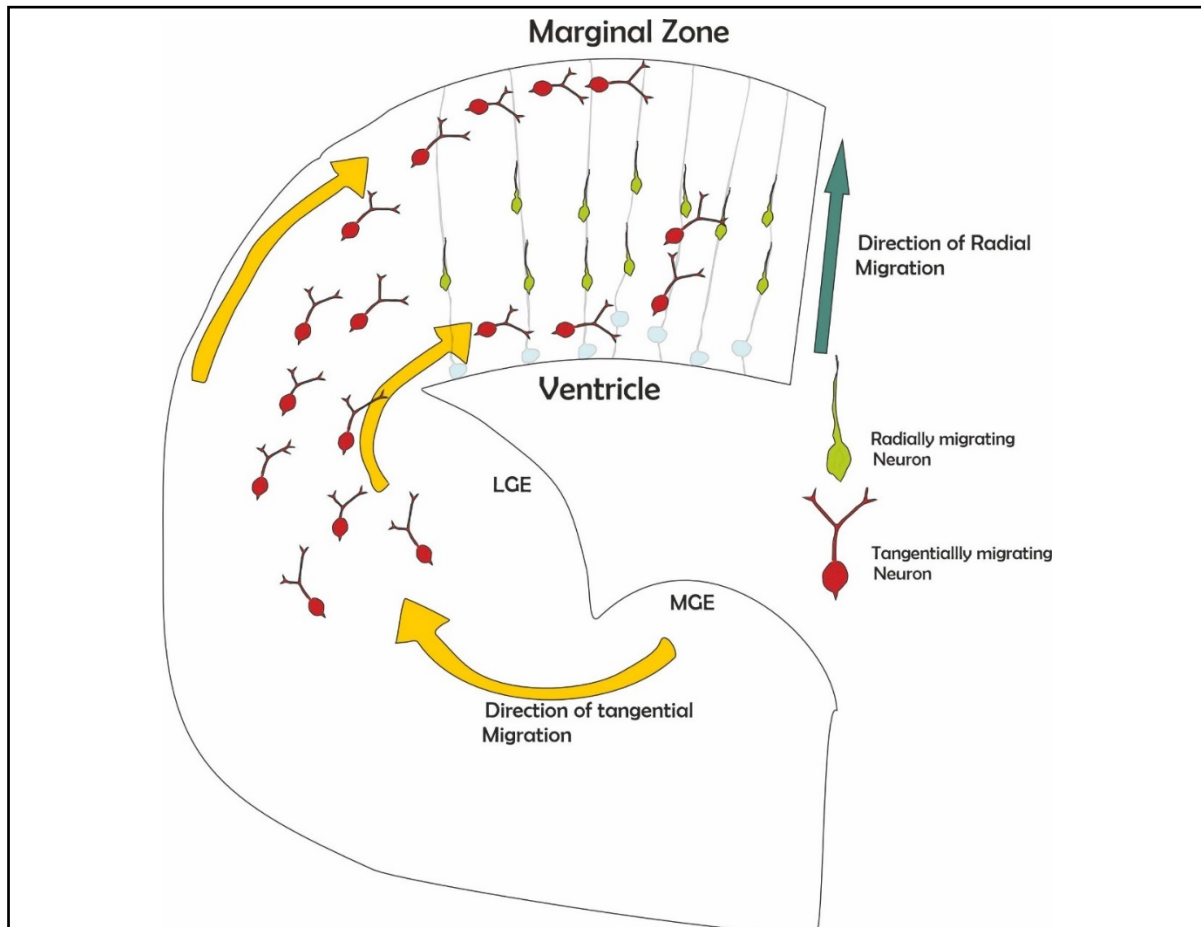


Figure 5. Neuronal migration in the cerebral cortex. There are two ways of neuronal migration in the cortex: radial (direction indicated by the green arrow), where pyramidal neurons (green), born in the SVZ of the dorsal telencephalon, move in a vertical direction to the marginal zone; and tangential migration (direction indicated by the yellow arrow), where interneurons (red), born in the ganglionic eminences (MGE and LGE in the drawing), migrate long distances until they reach the dorsal telencephalon and continue migration until they disperse in the cortex.

At the cellular level, migrating interneurons present a bifurcating and dynamic leading process with a growth cone-like structure at the end of each branch. At the beginning of each interneuron migration cycle, the cell extends two exploratory branches, followed by the extension of one of them in the direction of the chemo-attractant and the retraction of the other branch (Martini et al., 2009). At the same time, a dilation in the leading process (or swelling) is generated at the front of the soma and a fast forward movement of the soma (saltatory movement) is produced to make the neuron move (Bellion et al., 2005) (**Fig. 6**). Among the chemical clues followed by interneurons, it is possible to find the chemokine Cxcl12, secreted by IPs in the SVZ of the dorsal pallium (Sessa et al., 2010). Cortical interneurons show a high degree of morphological, biochemical and electrophysiological diversity and

depending on the site of the GEs where they are generated, they will integrate as a particular type. Among the main types of interneurons integrated in the cortex, it is possible to find neurons positive for Calbindin (CB), Parvalbumin (PV), Somatostatin (SST) and 5HTR3a; moreover, each class can be subdivided in different groups (de Felipe, 1993).

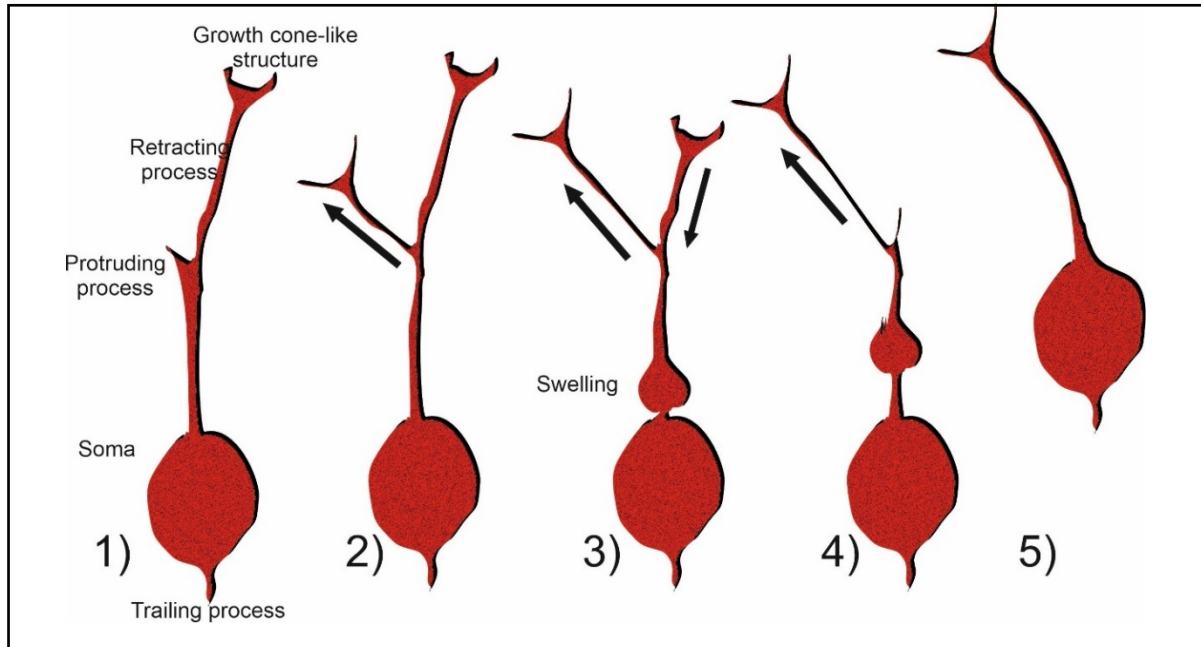


Figure 6. Interneurons migration cycle. Migrating interneurons present a bifurcating leading process, in which one branch extends in direction of the chemoattractant while the other branch collapses (1-4), followed by the saltatory movement of the nucleus in direction of the protruding process directed to the chemoattractant signal (5).

3.2 Migration of projection neurons

Neurons born from the proliferative regions in the dorsal telencephalon go through radial migration, a process in which neurons move vertically from the SVZ to the cortical plate using the basal process of the Radial progenitors to reach their target. As it happens with tangential migration, this event requires cyclic morphological changes from the migrating neurons, but in this case, it involves different phases, namely multipolar phase, locomotion and somal translocation (Peregrina & del Toro, 2020). At early stages of corticogenesis, the first wave of neurons generated is able to locate above the SVZ by somal translocation, a movement where neurons extend a branched leading process to the pial surface, followed by the pulling of the cell body in the direction of the leading process. This process generates the first layer of neurons, known as the preplate (**Fig. 7A**) (Kriegstein & Noctor, 2004; Molyneaux et al., 2007).

As subsequent waves of neurons are generated and the cortex enlarges, neurons require to migrate longer distances and switch from somal translocation to radial migration, characterized by the use of the RG basal process as a scaffold to migrate and to populate the upper layers of the preplate in an inside-out sequence, bypassing the previously generated neurons and forming the cortical plate (Nadarajah et al., 2001;).

With the appearance of the cortical plate, the preplate splits into subplate and marginal zone (**Fig. 7B and C**). The marginal zone is populated by Cajal-Retzius cells, a type of neuron which fulfil a role in radial migration by the secretion of the chemoattractant glycoprotein reelin. After the neurons occupy their respective layer in the cortex, they complete their differentiation programs by producing mature dendrites and finishing axon extension (**Fig. 7E**) (Allendoerfer & Shatz, 1994; Price et al., 1997).

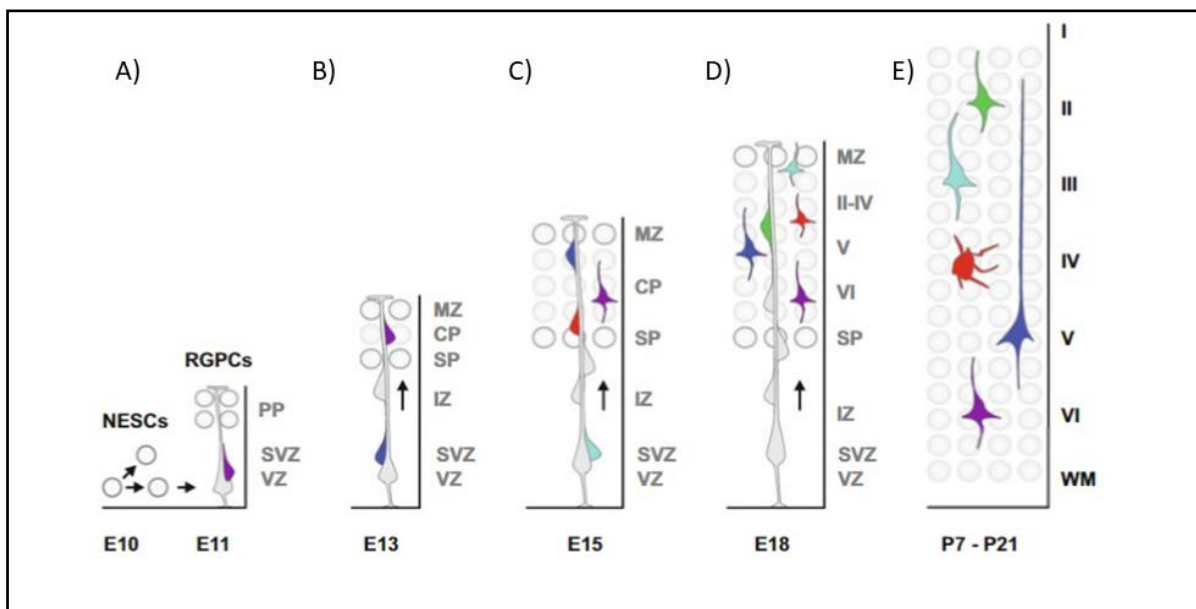


Figure 7. Development of cortical structures. A) First generated neurons give rise to the preplate, which is split B) in Marginal Zone (MZ) and Subplate (SP) after the incorporation of new neurons, forming the Cortical plate (CP). C) The CP incorporates new neurons increasing in thickness and different layers are established (D) until the mature cortex is formed with all its six layers (E). Below each stage is indicated the Embryonic (E10-18) or Postnatal (P7-21) corresponding day (Modified from Hippenmeyer, 2014).

3.2.1 Projection neurons migrate in a stepwise fashion

Migration of projection neurons from their place of birth in their germinative zone in the SVZ to their place of incorporation in the cortical plate requires a series of steps that have been well defined by

time-lapse studies in cortical slices (**Fig. 8**). After their birth, neurons transit to a multipolar (MP) phase characterized by the continuous protrusion and retraction of processes during a time that has been estimated to take approximately 24 hours (Noctor et al., 2004). Later, they transit to a bipolar (BP) phase, in what is known as the MP-BP transition, and once they acquire BP morphology, they go through locomotion, a phase characterized by the attachment of the BP neuron to the basal process of the RG, and finally when they reach the marginal zone, they conclude migration by detaching from the basal process, using a movement known as final somal translocation (Nadarajah et al., 2001). In the next sections I will describe the processes and mechanisms behind these phases of migration.

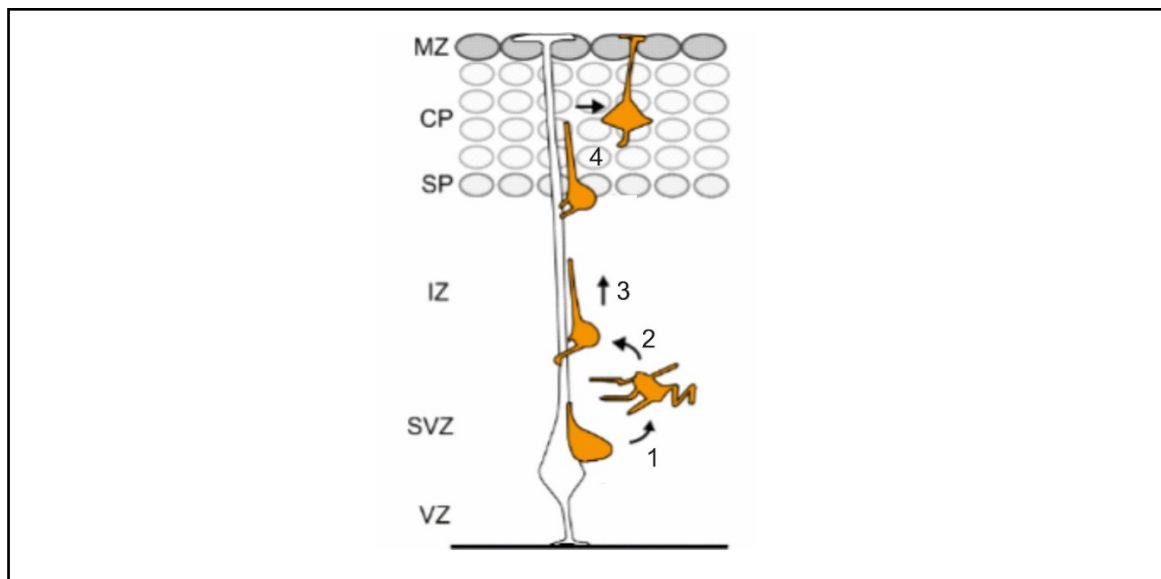


Figure 8. Phases of radial migration. - Radially migrating neuron (yellow) goes through different phases, starting with transition to a multipolar stage (1), in which it remains approximately 24 hours, then it transitions to a bipolar morphology (2) to start locomotion, using the AP as a track to migrate. Finally, when the neuron installs in the cortical plate, it undergoes somal translocation (4), where the neuron attaches to the pial surface to locate its soma in the upper neuronal layer. VZ: ventricular zone, SVZ: Sub-ventricular zone, IZ: Intermediate zone, SP : subplate, CP : Cortical plate, MZ : Marginal zone. (Modified from Hansen & Hippenmeyer, 2020)

3.2.2 Multipolar phase and transition to bipolar phase

Soon after neurons are born from progenitors, they acquire a BP morphology, defined by the fast protrusion and retraction of multiple short processes in different directions. During this phase, neurons move in a random fashion, changing direction frequently while they remain at the boundary SVZ/IZ during approximately 24 hours (Noctor et al., 2004).

The MP-BP transition involves organelles and cytoskeleton re-arrangements to assemble the structure of the forming BP neuron. Among the main cellular re-arrangements, the neuron requires the movement of the centrosome and Golgi to the front of the nucleus in the proximal part of the leading process, pointing towards the marginal zone, and the distribution of the microtubules (MT) cytoskeleton around the nucleus in the core of the leading process (Hatanaka et al., 2004; de Anda et al., 2010). Some of the extracellular factors, interactions and cell signalling events shaping MP morphology or MP-BP transition are studied (**Fig. 9**), nevertheless, the precise inductive factors of the MP phase and its causes remain a mystery.

3.2.2.a Extracellular signals in MP-BP transition

Some of the extracellular factors known to regulate the MP phase are neurotransmitters and neurotrophic factors. Neurotransmission by glutamate or serotonin, for example, regulates the MP-BP transition. Subplate neurons, establish direct contacts with multipolar neurons to release glutamate and by this means facilitate transition to a BP phase in a NMDA receptor dependent way. This is shown by the fact that there is accumulation of MP neurons in the SVZ when the electrical activity of subplate neurons is blocked (Ohtaka-Maruyama et al., 2018). Serotonin regulates MP-BP transition through the mediation of the 5-HT₆R receptor, as it was noticed by the delay in transition upon depletion of the 5-HT₆R receptor, this phenotype is partially rescued by the co-expression of Cdk5/p35. However, the site of provenance of the neurotransmitter is not clear (Jacobshagen et al., 2014).

The role of neurotrophic factors has been studied for tyrosine kinase receptors TrkB and TrkC, responsive to brain derived neurotrophic factor (BDNF). Both of them are expressed in the SVZ/IZ and their double inactivation produces defects in the MP-BP transition, with an increased accumulation in the MP phase at the IZ (Nakamuta et al., 2011). Downstream of BDNF, the GTPase α -chimerin is one of the targets that has been involved in both, the MP morphology and the MP-BP transition. On one hand, α -chimerin KD neurons at the MP stage show decreased number of protrusions, and on the other hand, they fail to establish a leading process to transit to the BP morphology, staying in a rounded shape. The signalling pathway involves the downstream activation of the microtubule binding protein CRMP (Ip et al., 2012).

About extracellular matrix components, chondroitin sulphate binds to different proteins (for example, growth factors) and regulates among different processes, neuronal migration. It was seen by *in utero* electroporation of shRNAs that downregulation of the enzymes producing chondroitin sulphate UST and 4,6-ST sulfotransferases, produce defects in migration by arresting neurons in MP phase at the IZ (Ishii & Maeda, 2008). In agreement with this, downregulation of Chondroitin sulphate and

Neuroglycan C (another extracellular matrix protein) by knock-down of the transcriptional factor PHF6 induces arrest in MP in the IZ (C. Zhang et al., 2013).

Reelin is a ligand secreted by Cajal-Retzius cells, and it is known to bind the VLDLR and ApoER2 receptors and activating the adapter protein Dab1. It influences MP-BP transition by activating the Ras-related GTPase Rap1, which in turn re-orient the MP neurons by regulating the surface trafficking of N-cadherin. Inhibition of any of the components of this pathway arrest migrating neurons in the IZ in a MP stage (Jossin & Cooper, 2011). Interestingly, the ligand DCC also binds to VLDLR and ApoER2 and also inducing Dab1 phosphorylation. As it is expected with this shared signalling, silencing of DCC by *in utero* electroporation of a shRNA produces arrest of migrating neurons in the IZ impairing MP to BP transition (Zhang et al., 2018).

These are some clear examples that the MP cells require diverse external stimuli in order to produce the right morphology of protrusion-retraction of its processes and subsequently start the BP phase. As it will be explained in future sections, some of these factors are still required for locomotion in the BP phase.

3.2.2b Cell adhesions in MP-BP transition

One of the most well-known pathways regulating MP phase involves the gap junction protein connexin 43 (Cx43), expressed in MP neurons. Cx43 KD induces arrest at the MP phase in the SVZ. Notably, this phenotype is rescued by over-expression of p27, indicating a downstream role of this protein (Liu et al., 2012). In line with this, p27 silencing in migrating neurons produces rounded MP neurons with fewer processes compared to the controls, a phenotype induced by the over activation of the actin severing protein cofilin (Kawauchi et al., 2006). In this same study, p27 was shown to be activated by a phosphorylation at Ser10 by Cdk5 (Kawauchi et al., 2006), which is an important node for cell signalling at different stages of neuronal migration (Ohtaka-Maruyama & Okado, 2015). The importance of Cdk-5 to transition for a MP to a BP state was demonstrated by Ohshima, et al, where they saw that the expression of a dominant negative form of Cdk5 and the Cdk5 KO induces delay of MP neurons in the SVZ/IZ (Ohshima et al., 2007).

At the same time, two cell adhesion molecules, N-cadherin and NEGR1, play a role in MP-BP transition by regulating the localization and stabilization of Fibroblast growth factor receptor (FGFr): N-cadherin by avoiding its ubiquitination and NEGR1 by avoiding its lysosomal degradation (Kon et al., 2019; Szczurkowska et al., 2018). FGF in turn, is necessary to induce the transition of MP phase to BP state, using a pathway that led to Erk1/2 phosphorylation (Kon et al., 2019). N-cadherin importance in MP-BP transition is showed by Barnat, et al, that demonstrated that Huntingtin (Htt) regulates neuronal migration through Rab11 dependent recycling of N-cadherin, where neurons with deleted Htt are

arrested at the SVZ/IZ with a MP morphology (Barnat et al., 2017). Additionally, Xu, et al (2015) observed that N-cadherin mediates contacts with the basal process of the AP during MP-BP transition for polarization of the neuron and extension of the nascent axon (Xu et al., 2015). They showed this by inducing the expression of a dominant negative form of N-cadherin in embryonic cortices and showing arrest of MP cells in IZ, later on, with an *In Vitro* system, they demonstrated that the contact between a radial glial cell and a neuron induces axon extension, which is impaired after silencing of N-cadherin in the progenitor (Xu et al., 2015).

A revealing study that showed a mechanism of cell adhesions regulation during MP phase to transition to BP stage is the one made by Epifanova, et al (2021), where they show that during MP stage, neurons need to decrease their levels of integrins to become BP. This decrease is regulated by the expression of the transcription factor Zeb2, which cKO in neurons produces MP neurons that move slowly and with shorter sideways distances during this phase. In this same study, they showed that the Zeb2 regulation in adhesion is dependent on the repression of Nrp1.

Regarding the role of membrane trafficking, TBC1D24 was studied, a protein that regulates exchange between plasma membrane and endocytic compartments through the mediation of the GTP-binding protein ARF6 (D'Souza-Schorey & Chavrier, 2006). The KD of *TBC1D24* induces defects in migration due to delayed MP-BP transition, additionally, it induces maturation defects at postnatal stages (Falace et al., 2014).

With this information in mind, we can observe that even in this stage of random movement of the neuron, cell adhesions are still an important factor to regulate MP neuronal morphology and transition to the BP phase, although the exact mechanisms underlying these events are not clear.

3.2.2c Regulation of gene expression

Different factors are known to regulate gene expression in MP phase, one of them is the histone methyltransferase Prdm8, which was shown necessary to maintain neurons in a MP stage. Overexpression of Prdm8 induces an arrest of neurons in a MP stage in the IZ, while the KD produces the opposing effect, inducing more cells reaching the cortical plate in a premature way (M. Inoue et al., 2014). Another factor necessary to maintain neurons in MP phase is Foxp2, for which downregulation by the miRNAs miR-9 and miR-132 is required for neurons to transit to BP phase. This was seen by over-expression of a version of *Foxp2* resistant to the mentioned miRNAs, which induced an increase of MP neurons in the IZ (Clovis et al., 2012).

Dynamic expression of the transcription factor FoxG1 is regulated at the MP phase. At entry of MP stage, neurons decrease their levels of FoxG1 to induce an increase in Unc5D, nevertheless, to exit this phase, they need to increase again FoxG1, as shown by Miyoshi & Fishell, 2012. They observed

that KD of FoxG1 induces a mis-localization of the neurons in their final position, with a failure of a MP-BP transition and a subsequent change in expression of genes associated to cytoskeleton and polarity, like Dcx, Dlk, Tubb2b, Cdk5 and Rac1. On the other hand, over expression of a form of FoxG1 with gain of function produces defects in Unc5D expression (Miyoshi & Fishell, 2012). Interestingly, Unc5D is also regulated by the previously mentioned Prdm8, where overexpression of the transcription factor induces decreased levels of the receptor (M. Inoue et al., 2014).

This FoxG1 way of regulation adds another layer of complexity to the MP neurons, and the study of these fluctuating levels of transcription factors and their associated genes will give a better understanding of the nature of the MP phase.

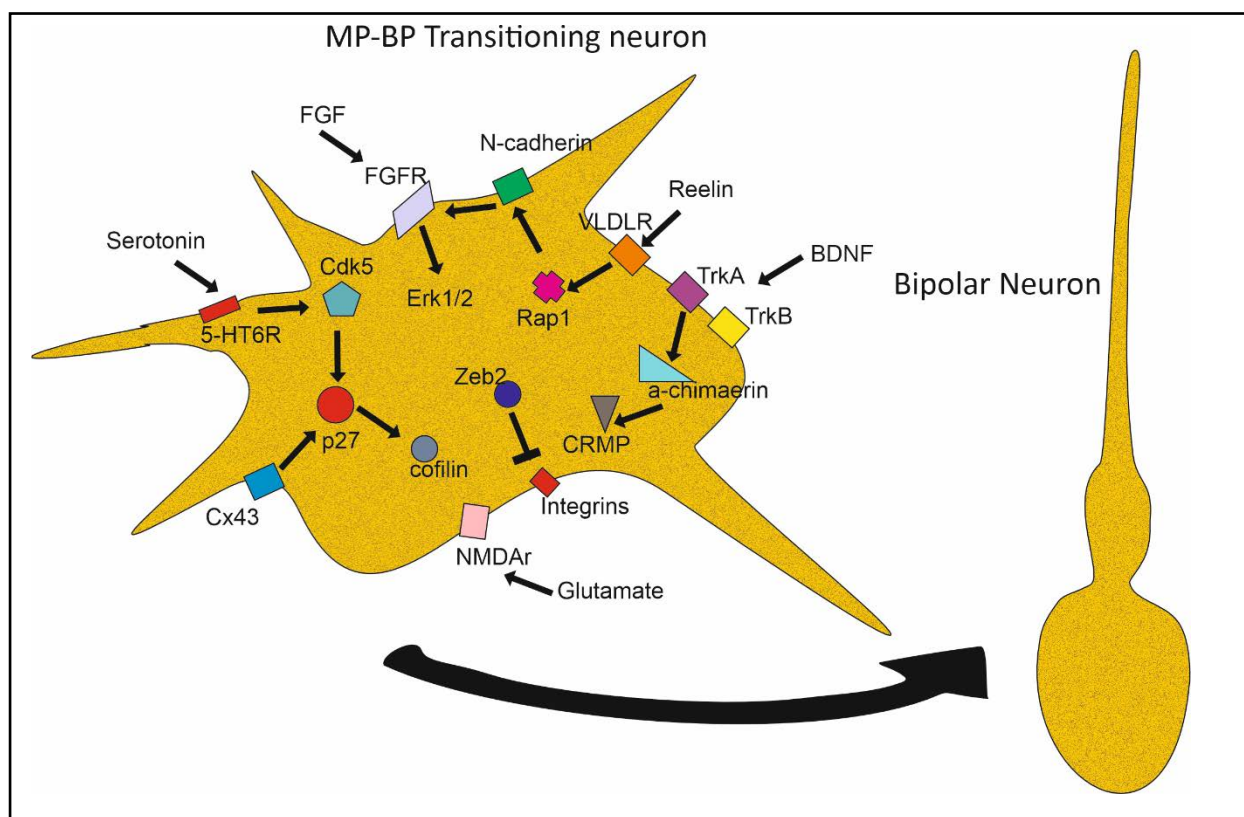


Figure 9. Multipolar-bipolar transition. Main molecular mechanisms taking place to transition from multipolar morphology to a bipolar locomoting stage, involving cell adhesions, extracellular signals (chemoattractants, neurotransmitters and growth factors), receptors to those molecules, and signalling pathways, that often lead to the activation of proteins that participate in cytoskeleton re-arrangement.

3.2.3 Locomotion

After the MP-BP transition, neurons start the locomotion phase, a mode of migration in which neurons attach to the basal process of the RG, using it as a track to reach the cortical plate. During this migratory event, the neuron goes through a challenging journey that requires the movement between different cells and extracellular matrix components, involving a series of cyclic movements defined by morphological changes in its different neuronal compartments (Nakazawa & Kengaku, 2020).

First, the neuron extends a leading process in the direction of the marginal zone, next, it produces a cytoplasmic dilation, known as swelling, at the proximal part of the leading process. Third, the soma, containing the nucleus, undergoes a saltatory movement, or nucleokinesis, where it elongates and enters the previously formed swelling. Then, the nucleus initiates a pause that takes several minutes, and again the leading process extends, initiating another cycle of movement, meanwhile, a trailing process in the rear of the neuron is left behind, forming the future axon (**Fig. 10**) (Noctor, et al. 2004; Schaar & McConnell, 2005; Tsai et al., 2007).

The locomoting neuron has an internal architecture characterized by the presence of the centrosome and golgi apparatus in the swelling, and with the MT emanating from the centrosome and extending the plus ends in direction to the leading process and to the trailing process, creating a cage-like structure wrapping the nucleus (Tsai et al., 2007).

After reaching the place in the cortical plate where they will integrate, neurons undergo somal translocation, a movement that requires the attachment of the leading process to the marginal zone and the detachment of the neuron from the basal process of the radial glia to locate in their final position (Nadarajah et al., 2001).

Compartmentalization of the BP neurons in different structures is regulated by factors regulating polarization, being one of them a set of kinases that include the Liver Kinase B1 (LKB1) and its downstream targets SAD1 and SAD2. The effect of LKB1 downregulation is the arrest of neurons in the IZ, with neurons in a BP state with multiple branches emanating from the leading process and defective formation of the axon (Barnes et al., 2007). This phenotype is common upon depletion of proteins that participate in polarity.

3.2.3a Extracellular factors and receptors

Locomotion is a process tightly regulated by different factors that modulate morphology, velocity, position and coordination between cyclic movements (**Fig. 11**). Unsurprisingly, the different components of the extracellular matrix participate actively in locomotion. In the case of β 1-Integrin, important in cell-extracellular matrix adhesion, when knocked down in all the cells in the CNS, it produces migratory defects, affecting neuronal layering, but this is not reproduced upon neuronal

specific KO, indicating that neurons require $\beta 1$ -Integrin to migrate in a non-autonomous manner, mostly dependent on the radial glial contacts (Belvindrah et al., 2007).

Highlighting the role of extracellular matrix as a promoter of migration, laminin $\gamma 1$ deficiency (glycoprotein abundant in basal membrane) was seen to affect neuronal migration in a cKO of this protein using Cre CaMKII as driver expression. Authors observed that cells that were depleted of laminin $\gamma 1$, were unable to reach the cortical plate at the same numbers as the control cortices. Downstream, the cKO brains had decreased levels of phosphorylated Akt and GSK3- β (Chen et al., 2009).

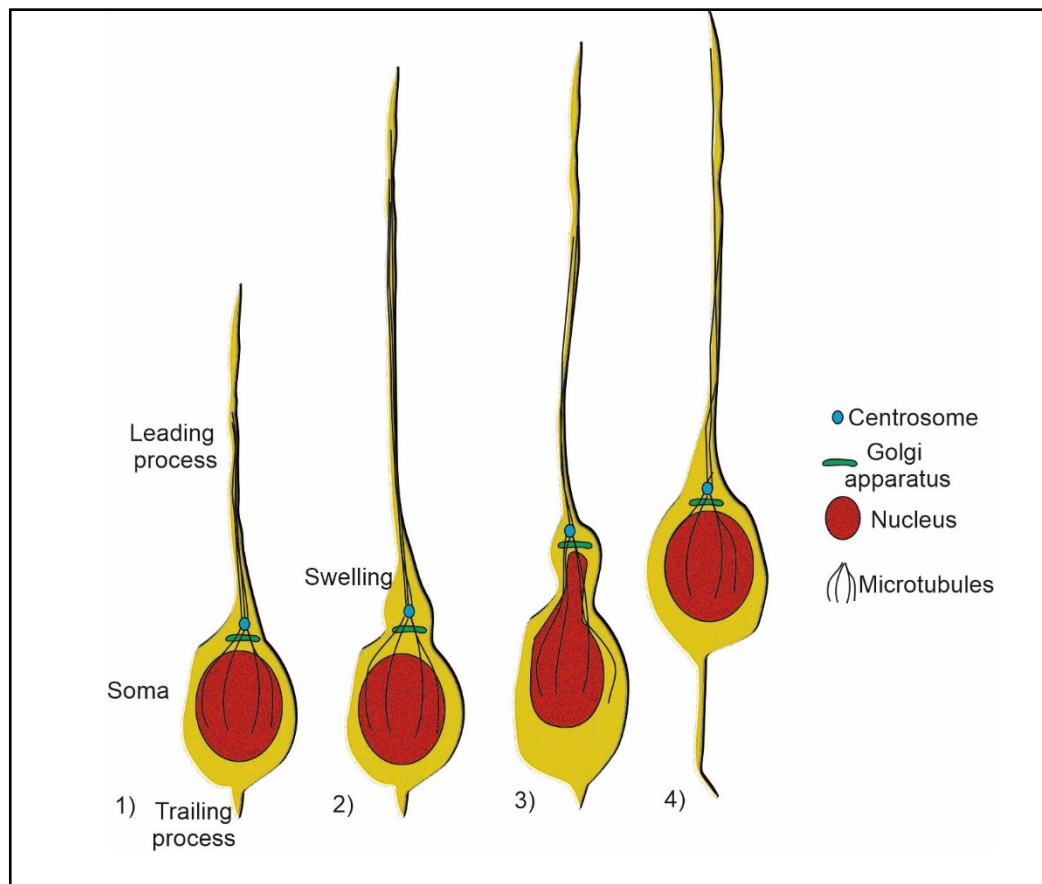


Figure 10. Morphological changes during locomotion. Neuronal locomotion is characterized by the sequence of cyclic steps in which the cell first extends the leading process in direction to the marginal zone (1-2), then, it engorges a swelling in the front of the nucleus, where the centrosome and Golgi apparatus are localized (2-3). Then, the contents of the soma, including the nucleus enter the swelling and the neuron moves forward, in a movement known as nucleokinesis (3-4).

Related to Laminins, although not expressed in neurons, cKO in nervous tissue of dystroglycan, a receptor that mediates interactions with laminins, and is important in the integrity of the pial

membrane and aRG, induces among many other defects, neurons that migrate excessively and reach the marginal zone in a premature way (Myshrall et al., 2012), indicating that adhesions with the matrix in some cases act as locomotion inhibitors.

Neuroglycan C and chondroitin sulphate proteoglycan 5 are glycosaminoglycans of the extracellular matrix for which expression is downregulated upon KD of the transcription factor PHF6, with consequences in neuronal migration that include migratory delay with bipolar cells with over branching or absent branching (C. Zhang et al., 2013), in a phenotype that together with the MP-BP transition defect (section 3.2.2a), points to the importance of Chondroitin sulphate in neuronal polarization. The L1-cell adhesion molecule (L1cam) binds to many extracellular ligands such as proteoglycan, neurocan, integrins, contactin and itself by homophilic interactions. Neurons knocked down for L1cam present with delayed migration and aberrant expression of layer specific transcription factors including Ctip2 and Satb2 (Itoh & Fushiki, 2015), probably by defective signalling pathways that participate in cell specification of those neuronal types.

Netrin-G1 and Netrin-G2, which are ligands bound to the cell membrane by a GPI anchor, have been demonstrated to play a role during radial migration, and silencing of either of these proteins at E14.5 induces the permanent arrest of migrating neurons at the IZ, as it was observed in cortices of electroporated mice with shRNAs at P1 and P7. Nevertheless, the further mechanisms related to Netrin-G1 and G2 are not solved (Heimer et al., 2020).

Neogenin is a membranal protein highly expressed in the IZ that prevents early entry of neurons in the cortical plate, as it was seen by the premature entry of migrating neurons in this region 2 days after KD of the gene by *in utero* electroporation, while in the control condition most neurons were presented in the IZ. Neogenin is regulated by Lrig2, that prevents ectodomain shedding by the metalloprotease ADAM17 (van Erp et al., 2015).

Reelin is another important extracellular factor, secreted by Cajal-Retzius cells in the marginal zone, it binds to the VLDLR and ApoER2 lipoprotein receptors, producing the phosphorylation of the adapter Dab1 and being involved in the stabilization of the actin cytoskeleton and cell adhesions. Among the main phenotypes of the KO mouse for *reelin* is the inverted position of the neurons in the cortex. Reelin regulates locomotion at different steps, it participates in cofilin inactivation to stabilize the actin cytoskeleton, mediates N-cadherin cell adhesions and finally for somal translocation it participates in the adhesion to fibronectin in the marginal zone (Dulabon et al., 2000; Hirota & Nakajima, 2017).

Locomoting neurons are influenced by neurotransmitters, such as serotonin, which regulates neuronal velocity during this phase. Riccio et al observed that excessive serotonin accumulation induces decrease in locomotion speed as seen in time-lapse experiments. A similar result was produced by the

KO of the serotonin transporter SERT (Riccio et al., 2011). Similarly, KD of the serotonin receptor 5-HT₆R induces decrease in locomotion velocity, a defect that is rescued by the expression of Cdk5 (Jacobshagen et al., 2014), which targets many intracellular targets.

Heterotrimeric G proteins Gi2 and G α i1, known for their role in the inhibition of adenylate cyclase, play different roles during locomotion. For Gi2, it was shown arrest of BP neurons in the IZ, presenting features such as branched leading process, decreased velocity and defective migratory pathways (Hamada et al., 2017). In the case of G α i1, known for its role as inhibitor of adenylate cyclase, it was shown to be important for neuronal migration. KD of G α i1 induces a decrease in migrating neurons reaching the cortical plate, with increased size of the leading process and additional increase in the distance from the nucleus to the centrosome, as measured in fixed slices (Hamada, et al. 2020).

Regarding glutamatergic neurotransmission, silencing of the subunits GluN1 and GluN2B of the NMDA receptor were reported to produce arrest of migrating neurons, and in the case of GluN2B silencing, neurons develop an increased dendritic complexity in their ectopic place of location (Jiang et al., 2015). Since glutamate levels at early postnatal stages (P3) in mouse cortex decrease as development proceeds due to astrocytes uptake (Hanson et al., 2019), it is possible to think that at embryonic stages glutamate concentration is high in absence of astrocytes regulating its concentration (Medvedeva & Pierani, 2020).

Glutamatergic neurotransmission is known by the stimulation of calcium currents inside neurons, and calcium influx in migrating neurons has been studied by the design of DREADD, an artificial receptor-ligand system that increases Ca²⁺ transient frequencies. It was observed that upon expression of DREADD by the migrating neurons, with a subsequent increase in Ca²⁺ currents, this induces migration delay in the IZ due to an increased number of pauses during locomotion and increased number of branches, but not to changes in velocity (Hurni et al., 2017). In a similar manner, either the KD of the K⁺ channel KCNK or expression of its dominant negative mutations induce arrest of migrating neurons in the SVZ, with an increase of calcium currents similar to the DREADD expressing neurons (Bando et al., 2014).

Related to GABAergic neurotransmission, Furukawa et al showed that GABA plays a role in decreasing speed of migrating neurons, and administration of the inhibitor SR95531 induces migrating neurons to reach faster the cortical plate than the controls. In the same study, they found abundant presence of the GABA_AR agonist taurine in cortical plate, which potentially regulates GABA related processes at these site (Furukawa et al., 2014).

Overall, in its journey to the cortical plate, the neuron finds a high range of extracellular ligands that finely regulate locomotion, including factors of the extracellular matrix, growth factors and neurotransmitters, that trigger a complex array of intracellular pathways regulating the different parameters of locomotion.

3.2.3b Cell adhesions and membrane trafficking

Polarization and locomotion are highly influenced by endocytosis and membrane trafficking related pathways, in which Rab proteins are highly implicated. Overexpression of a dominant negative of Rab5 or its KD by shRNA, induce arrest of migrating BP neurons at the IZ, with a large fraction of those neurons presenting with an over-branched leading process. In this same study, dynamin inhibition in migrating neurons induced arrest in the IZ, with the same effect produced by Rab11 KD (Kawauchi et al., 2010).

Furthermore, these defects associated to membrane trafficking are linked to a dysfunction in cell adhesions, and it was shown that migratory defects produced by Rab5 KD, are partially rescued by N-cadherin over-expression (Kawauchi et al., 2010). Another study showing a similar relationship between membrane trafficking and cell adhesions, indicates the role of the Rab23 protein regulating N-cadherin. In this case it was shown that Rab23 silencing induces detachment of the locomoting neurons from the basal processes of RG and produces defects in velocity and directionality in an Erk 1/2 dependent fashion. All those defects are rescued by the co-expression of N-cadherin (Hor & Goh, 2018). Shikanai showed the same effect of detachment from the basal process of the RG by KD of N-cadherin (Shikanai et al., 2011). Another way by which N-cadherin regulation shows involvement in locomotion is by the regulatory activity of the miRNAs miR369 and miR496, that when overexpressed, produce a migratory delay in lower cortical plate and IZ, but this effect is counteracted by the expression of N-cadherin (Rago et al., 2014).

N-cadherin trafficking is also mediated by Htt, for which KO in neurons produces aberrant N-cadherin distribution and mis localization of migrating neurons as a consequence. These defects were rescued by the expression of Rab11, indicating the importance of vesicular trafficking of N-cadherin during radial migration. In the same way that this mechanism regulates MP-BP transition (section 3.2.2b), Htt depleted neurons present with an increased number of pauses while migrating, slowing down migration velocity (Barnat et al., 2017).

The pair of protocadherins that function as receptor-ligand DCHS1-FAT4 were shown to produce defects in migration in human organoids of patients with periventricular heterotopia (abnormal accumulation of neurons around the ventricles). More specifically, neurons with those defects present with slower migratory velocities and defective directionality, and some of the genes for which

regulation is altered in these neurons are Ephrins, Dcc and ItgB1, which are upregulated, while Map1, Snc and Gria2 are downregulated (Klaus et al., 2019).

Another kind of cell adhesion participating in locomotion is the gap junction protein Cx43, which is important in the stabilization of the leading process and nucleokinesis. It has been seen that upon silencing of Cx43, multiple branches are produced in the leading process and a defective nucleokinesis presents with shorter distance in every migratory cycle. The mechanisms involved implicate the adhesive properties of Cx43, but not its property as a ion channel, as seen by rescue experiments. Interestingly, dynamics of Cx43, as seen by the expression of a Cx43 bound to EYFP, involve movement of the protein to the swelling previous to nucleokinesis. Since adhesion molecules regulate cytoskeleton, the authors found that depletion of Cx43 produces a reduction in levels of F-actin in the migrating neuron (Elias et al., 2007).

In contrast, receptors Flrt1/3, transmembrane glycoproteins defined by the presence of 10 leucine rich repeats and a fibronectin type-II domain, work by downregulating neuronal migration speed in physiological conditions, as it was shown by del Toro, et al, where they saw that the double KO of Flrt 1/3 induces increase in the speed of neuronal migration, forming an abnormal accumulation of cells in the cortical plate (del Toro et al., 2017).

Silencing of the endoplasmic reticulum protein C6orf70 was shown to induce delay in migration in embryonic cortices of rats, in line with the phenotype seen in patients with mutation or haploinsufficiency of the gene who develop periventricular heterotopia (abnormal accumulation of neurons around the ventricular zone) (Conti et al., 2013).

In addition to the aforementioned mechanisms in which N-cadherin is implicated, it also regulates somal translocation. The decrease of N-cadherin has shown important for this step, and in this case, Rab7 was shown necessary to reduce N-cadherin levels for a correct positioning of the neurons at this final step of locomotion (Kawauchi et al., 2010). Another contribution of cadherins comes from cadherin-6, which is down-regulated for the final positioning of the migrating neurons. This protein acts through its RGD domain of binding to integrins to bind extracellular matrix components and to position the neuron in the right orientation, this contribution is mediated by Zeb2, which allows repression of cadherin 6 (Epifanova et al., 2021). The ending of neuronal locomotion is also mediated by the protein SPARC-1, which is expressed in the zone of the aRG corresponding to the cortical plate. In this way, SPARC-1 produces detachment of the migrating neurons in order to localize the cells in their final positions in this layer (Gongidi et al., 2004). In a similar manner, apical detachment of aRG for loss of the endothelin converting enzyme 2 (ECE2) produce defects in migration, but in these cases, neurons accumulate in the deep layers of the mouse cortex and also produce abnormal migration in human cortical organoids (Buchsbaum et al., 2020).

With all these mentioned components, it is clear that an efficient locomotion requires a proper attachment of the neuron to its surroundings. Additionally, the correct recycling of these attachments, like it is often observed for N-cadherin, is essential for the neuron to complete a successful migration.

3.2.3c Cell signalling - Cdk5 and Jnk

Similar to what happens in the MP phase, Cdk5 is an important regulatory node that controls neuronal morphology and movement, in this case through the phosphorylation of targets like Dcx, Lis1 and p27. It was seen that inhibition of Cdk5 activity reduced locomotion speed with a corresponding lack of swelling formation at the leading process and defective nuclear morphology (Nishimura et al., 2014). Furthermore, these phenotypes were reproduced by silencing p27 or Dcx, indicating that they might be involved in the Cdk5 signalling pathway (Nishimura et al., 2014). Upstream of Cdk5, one of its regulatory proteins is PKC δ , whose levels of expression regulate the stability of the subunit p35. It was seen that silencing of PKC δ induces arrest of neurons in the IZ, and that this defect is rescued by the co-expression of p35 (Zhao et al., 2009).

Cdk5 down-regulation produces a decrease in velocity of migrating neurons, a characteristic that was proposed to be a product of over-branching (Gupta et al., 2003; Ohshima et al., 2007), however, branching was shown to be not important for this locomotor phenotype (Martínez-Martínez et al., 2019).

The c-Jun N-terminal kinase (Jnk), member of the Mitogen activated protein kinases superfamily, participates in nucleokinesis, it has been shown that its inhibition by pharmacological agents like rottlerin and SP600125 and shRNA for Jnk2 produce defects in nuclear elongation during locomotion (Nishimura et al., 2010; Zhang et al., 2016). Kawauchi (2003) demonstrated that DN of Jnk induced decrease in the size of the leading process due to microtubules abnormalities, similar to the phenotype presented by neurons incubated with SP600125 (Kawauchi et al., 2003).

Further discoveries proved that Jnk2 was involved in radial migration through a TGB- β non-canonical (Smad independent) signalling pathway, dependent on the mediation by the protein TAK (TGB- β Activated kinase), that interacts with POSH (a factor of the Rac1 signalling pathway) and Wdr62 (Zhang et al., 2016).

Some of the already mentioned extracellular ligands and receptors (section 3.2.3a) are responsible to trigger these intracellular pathways, which seem to be common nodes to regulate the way neurons locomote.

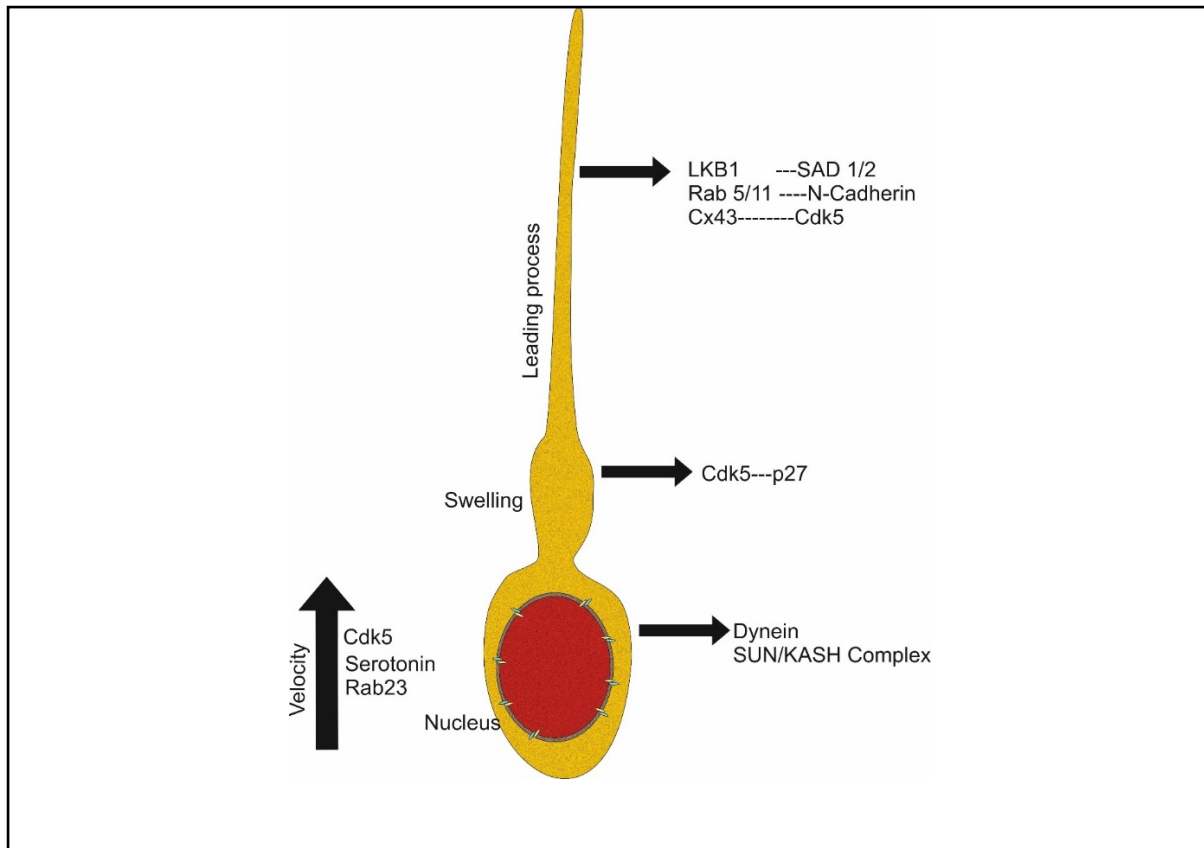


Figure 11. Locomotion regulatory mechanisms. Extracellular factors, receptors and signalling pathways that participate in locomotion regulating velocity and morphological characteristics in leading process, swelling and nucleus.

3.2.3d Nucleokinesis regulation

The movement of the nucleus in the locomotion phase requires both high resistance to mechanical stress, and at the same time, flexibility to travel through narrow spaces imposed by the extracellular environment. Additionally, the nucleus is equipped with the motor proteins that transport this large cargo during the saltatory movement (Tsai et al., 2007). Neuronal nuclei possess a double membrane that in the internal face is delimited by the nuclear lamina, composed of intermediate filaments that provide stiffness to the nucleus. This was studied by Coffinier et al., 2011, who showed that specific deficiencies of lamin B1 and B2 produce defects in neuronal migration associated to nuclear malformations (Coffinier et al., 2011).

Nuclear lamina link the nucleus with the cytoskeleton, more specifically by the intervention of the LINC (Linker of nucleus and cytoskeleton) complex, composed by the SUN (Sad1 and Unc-84) complex in the internal side of the nuclear membrane and the KASH (Klarsicht, ANC-1, and Syne Homology) complex spanning the nuclear envelope lumen and the outer region of the nucleus. This last one, connects the MT to the motor proteins dynein/Lis complex and kinesins (Nakazawa & Kengaku, 2020;

Zhang et al., 2009). This nucleus-motor protein coupling allows the saltatory movement of the nucleus, as it was seen in the case of dynein, for which depletion promotes migratory defects related to the uncoupling of the nucleus with the centrosome in pyramidal migrating neurons (Shu et al., 2004), a discovery that was also found to be true in granular cerebellar neurons (Tanaka et al., 2004).

Cadherin-2 and 4 are involved in neuronal migration through regulation of nucleokinesis, where cKO for each one produces defective migration, and the effect is potentiated by the cKO of both cadherins. The defects include an abnormally long and thin leading process and closer distance between nucleus and centrosome. The mechanism proposed is through mediation of α -catenin, that produces rescue of neuronal positioning when expressed together with the dominant negative form of cadherins. Moreover, LIS1 also rescues the migration phenotype with decreased size of the leading process (Martinez-Garay, et al. 2016).

Despite some knowledge acquired about how actin cytoskeleton controls nucleokinesis in cortical interneurons and cerebellar granular neurons (Bellion, et al. 2005; Martini & Valdeolmillos, 2010; Solecki et al., 2009), there is scarce research addressing how the actin cytoskeleton regulates nuclear movement and in general neuronal migration in pyramidal neurons. This issue will be addressed in section 1.5 of Chapter II.

3.2.3e Cytoskeleton regulation

As previously mentioned, the cytoskeleton takes a fundamental role during the dynamic events involved during radial migration. Most cellular processes converge to remodel the microtubules and actin cytoskeletons in order to provide polarity, dynamicity, mechanical force and resistance to produce migration. In the next section it will be explained the structure and functions of the cytoskeletal components and how they participate in radial migration.

CHAPTER II.- CYTOSKELETON DYNAMICS AND PARTICIPATION IN RADIAL MIGRATION

The cytoskeleton comprises different types of filaments that confer mechanical support, polarity, and migratory faculties to the cell. The main cytoskeleton polymers are comprised by the Microtubules (MT) cytoskeleton, Actin filaments (F-Actin) and Intermediate filaments. The former two are the most studied cytoskeleton types, but more functions are being revealed for the intermediate filaments, an important component of the nuclear envelope involved in mechanical resistance of the nucleus during neuronal migration (See chapter I 3.2). Even though the different cytoskeletons are classically conceived as working in separate ways, it is getting clear that there is an interdependency between them to coordinate many biological phenomena, including neuronal migration (Akhshi et al., 2014; Cammarata et al., 2016).

Septins, another type of cytoskeletal protein considered as the fourth cytoskeletal element (Mostowy & Cossart, 2012), participate in radial migration, as it was demonstrated by silencing of Septin-14 or Septin-4, that induced delay in migration at the IZ and low layers of the cortical plate, with decreased size of the leading process of the migrating neurons. The C-terminal domain of Septin-14, interacting with Septin-4, was shown to be important for the migratory function (Shinoda et al., 2010).

Being a process where the cell undergoes multiple cyclic changes, neuronal migration requires a cytoskeleton that is on one hand capable of constant re-organization, and on the other hand, that provides mechanical resistance to the stress imposed by the microenvironment (Nakazawa & Kengaku, 2020).

1. Actin cytoskeleton dynamics

Actin filaments accomplish a plethora of functions in all eukaryotic cells. The way they assemble to form different structures and change in response to the needs of the cell make the actin cytoskeleton one of the most dynamic and adaptable structures in the cell. This dynamic behaviour requires the association with many regulatory proteins to assemble and disassemble filaments, bundles, branches and crosslinking structures.

Actin monomers (globular or G-actin) are 42 kDa proteins composed of 375 amino acids, arranged in 4 domains. In mammals there are six isoforms expressed by different genes, three of them code for α -Actin (muscular), one for β -Actin (non-muscular) and two for γ -Actin (smooth muscle and non-muscle cells) (Dugina et al., 2019; Pollard, 2016). G-Actin associates to ATP nucleotides and assemble into a polarized helical filament that possess a barbed, or fast-growing end; and a pointed, or slow-growing end (**Fig. 12**). The main limiting factor for filaments formation is nucleation, a step that

requires the association of dimers and trimers to start the elongation of the filament (Blanchoin, et al. 2014).

Inside the cell, most actin monomers are complexed with profilin, preventing spontaneous association to F-actin, unless nucleation factors bind to the complexed actin-profilin, enabling a fast binding of G-actin to the barbed end of the existing filaments. This rapid polymerization can be activated when the cell requires a burst of actin polymerization, such as the case of endocytosis, cell motility or cytokinesis (Chesarone & Goode, 2009).

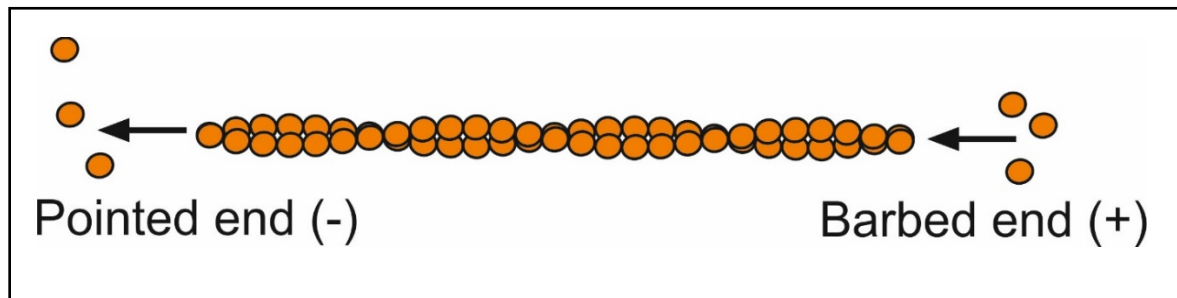


Figure 12. F-actin structure. The actin filament is a polarized structure providing different dynamics, with a pointed end (shrinking) and a Barbed end (growing)

1.1.- Regulation of actin organization

1.1.1.- Arp2/3 and participation in filament branching

The protein Arp2/3 catalyses the polymerization of a new filament in the side of a pre-existing filament to produce a branched structure. In order to act as a polymerizing agent, Arp2/3 requires the activity of the nuclear promoting factor (NPF) WASp/SCAR/WAVE to associate its subunits and mimic the structure of actin dimers to stimulate the addition of more G-Actin subunits. This mechanism of F-actin polymerization is involved in the formation of lamellipodia, focal adhesions and endocytic patches (Chesarone & Goode, 2009; Pollard, 2016).

This kind of branched structure is important for migration because extensive networks of actin branches are generated to push forward the membrane in lamellipodial structures. This growth requires to be controlled by capping proteins that bind to the barbed ends of the filaments in order to produce multiple branched structures that accumulate, forming a dense mesh (**Fig. 13**) (Blanchoin et al., 2014). During radial migration, the depletion of Arp2/3 in migrating neurons (Dcx+ population) induces arrest in IZ, which indicates that neurons need Arp2/3 to undergo locomotion (Wang et al., 2016). Contributing to this information, studies *in vitro* in human derived neurospheres showed that defects in migration produced by the biallelic loss of CTNA2, the gene encoding for α -catenin, are produced by overactivation of Arp2/3, producing shorter distances migrated and shorter leading processes (Schaffer et al., 2018).

WAVE2 mechanisms during radial migration have been addressed more in detail, and it has been seen that its KD in radially migrating neurons produce defects in MP-BP transition due to defects in protrusions extension during MP morphology. Depletion of WAVE2 or its associated partner Abi2 produce decrease in growth cone like structures in MP protrusions, in line with the role of these proteins as regulators of growth cone (Xie et al., 2013).

Hence, actin branching seems to be important for the process, although the precise implication is not clear, as the migration of the neuron is not based in the protrusion of a lamellipodium.

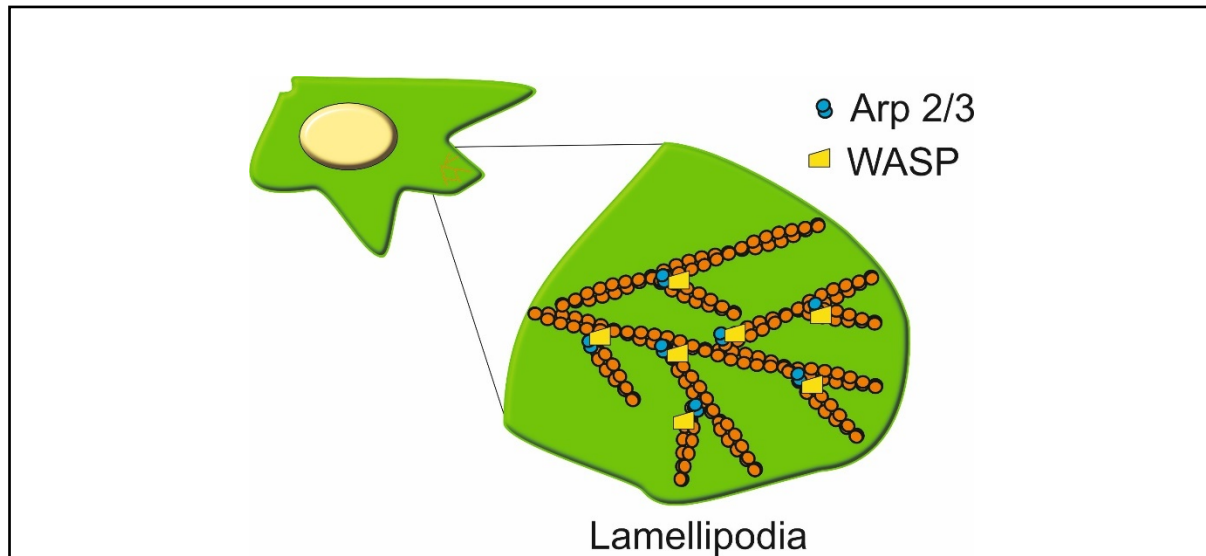


Figure 13. Lamellipodial structure. Actin branching requires Arp2/3 and WASP proteins in order to coordinate protrusion of lamellipodial structures.

1.1.2 Actin bundling proteins

Formins are a type of actin nucleating proteins that also work as elongating factors, but in contrast to Arp 2/3, formins elongate linear filaments. Their mechanism of function requires the binding of the dimeric donut shaped FH2 domain to the barbed end of the filament, in which it adds processively new actin subunits. This recruitment happens at their FH1 domain, characteristic by its poly-proline sequence that binds profilin-actin complexes to transfer them to the FH2 domain (Chesarone & Goode, 2009).

Another elongating factor is Ena/VASP, a tetramerizing protein that protects the barbed end of the filament from capping proteins and binds to profilin-actin to extend the filament (Winkelman et al., 2014). The mechanism of elongation is through the binding of actin-profilin to the proline-rich region in the central region of Ena/VASP, while the binding of the protein to the actin filament is through the N-terminal domain EVH2 to cap the barbed end (Winkelman et al., 2014).

Both formins and Ena/VASP proteins contribute to the formation of filopodia, finger-like motile protrusions at the edge of the cells, by binding to the barbed end of the filaments and assisting in the elongation of the linear structure. To maintain stabilization between parallel filaments, the action of actin proteins like fascin, α -actinin, fimbrin and epsin is required to increase collective stiffness by elaborating filament bundles (**Fig. 14**) (Svitkina, 2018; Coles & Bradke, 2015). In particular, α -actinin dysregulation by KO of IP6K (enzyme producing phosphatidyl inositol), induces aberrant radial migration, first by inducing a migratory delay, and later on by inducing cells that do not stop migrating where they are supposed to. The observed defects are also associated to decreased activity of the focal adhesion kinase (FAK) (Fu et al., 2017).

Ena/VASP proteins participate in the correct positioning of neurons in the layer they integrate, and neurons that originally should integrate in deep layers, upon Ena/VASP depletion, integrate in upper layers. Despite this abnormal positioning, neurons presented normal morphology when integrated in the cortical plate (Lin Goh et al., 2002). Further discoveries revealed that the protein Mena, belonging to the Ena/VASP family is expressed in MP neurons, and *in utero* electroporation of a vector that sequestered Ena/VASP members produced a decrease in processes projecting from the MP neurons (Yoshinaga et al., 2012), in line with the role of these proteins in formation of protrusions.

Actin assemblies can also be found in the form of crosslinked structures, associated by proteins like filamin, dystrophin or spectrin. The extent of crosslinking provides the actin assemblies with different microstructures and mechanical properties, forming scaffolds for processes like adhesion and migration (for review see Blanchoin et al., 2014). Filamin A is one of the most studied actin-crosslinkers in cortical development, since it is known that mutations in the *Filamin A* gen are associated to periventricular heterotopia (Fox et al., 1998; Parrini et al., 2006), a cortical malformation associated to defects in migration, where neurons accumulate ectopically along the ventricles. In animal models, it was shown that KD of *Filamin A* by IUE of RNAi alters neuronal migration in rat embryonic cortex, forming heterotopic accumulations of neurons similar to what happens in patients with heterotopia (Carabalona, et al. 2012).

The KD of *Filamin A* produces defects in migration by increased expression and defective localization of Big2, a factor that anchors Protein kinase A in the membrane and directs vesicle trafficking and membrane stability (J. Zhang et al., 2013), factors that as it was seen in previous sections, are essential for locomotion. Decrease of FILIP (Filamin-A interacting protein), a negative regulator of Filamin-A is required to start migration. Accordingly, expression of FILIP induces neuronal migratory delays in cortical explants (Nagano et al., 2002).

Decrease in Filamin A is seen upon expression of a WT and a mutant version of DLGAP4 in RPE1 cells, with increase in filopodial structures and decrease in lamellipodia (Romero et al., 2022). DLGAP4 is a

protein that previously was seen as a participant in the organization of glutamate synapses (Takeuchi et al., 1997). Interestingly, both overexpression and KD of *Dlgap4* in migrating neurons induces mispositioning in the cortical plate, with neurons spread in lower layers of the cortical plate in comparison to the control. Defects in progenitors' morphology and dynamics due to actin cytoskeleton disruption contribute to these neuronal migration defects (Romero et al., 2022). Moreover, Filamin A increase also induces aberrant migration. This was seen upon KO of MEKK4, which induced increase in the levels of Filamin A in the forebrain with resulting ectopic clusters of neurons. Accordingly, and this effect was produced directly by overexpressing Filamin A (Sarkisian, et al. 2006), showing how balance in physiological activities is essential for correct development.

The participation of all these factors highlights the importance that actin dynamics and different actin structures have in the regulation of the migratory process.

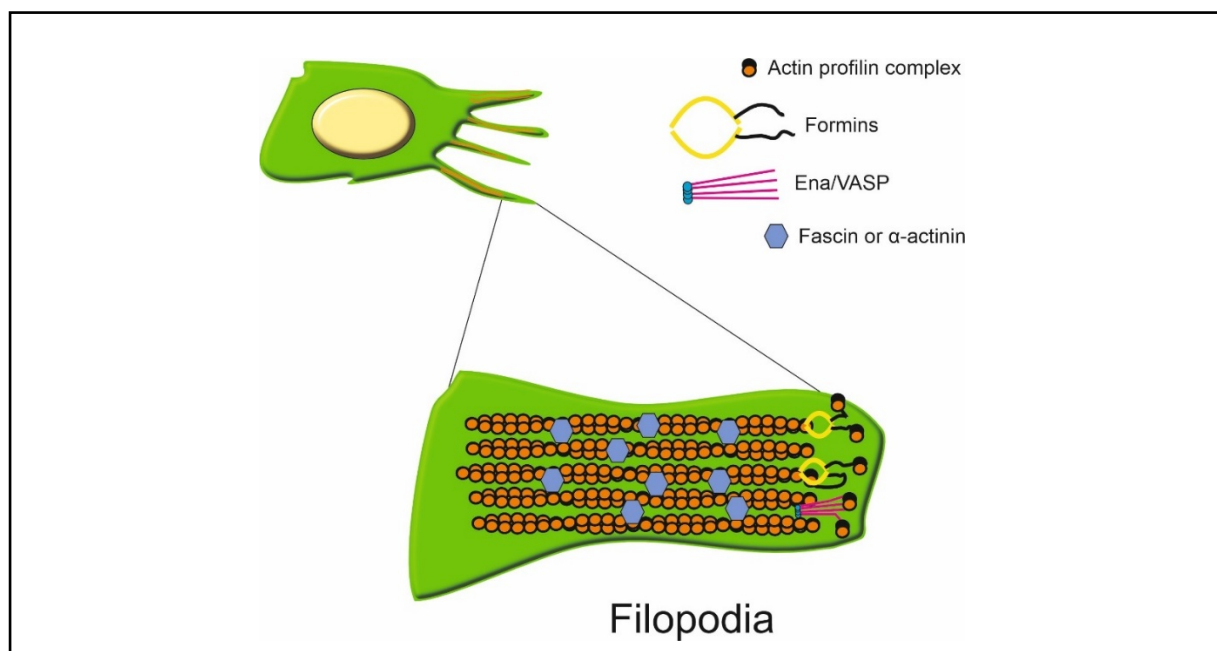


Figure 14. Filopodial structures. Conformation of the actin cytoskeleton in the formation and stabilization of the filopodia, requiring actin bundling proteins, like fascin; and actin polymerizing factors like formins and Ena/VASP.

1.1.3 Filament disassembly

Actin filaments disassembly is important to reconfigure structures in response to different physiological stimuli and to replenish the pool of polymerizable actin. Importantly, actin disassembly is known to participate in the elaboration of motile structures like lamellipodia, filopodia and growth

cones (Narita, 2020). Two main proteins are known to participate in actin disassembly: Actin depolymerizing factor (ADF)/cofilin and gelsolin (Pollard, 2016).

ADF/cofilin associates with higher affinity to ADP-Actin than ATP bound actin, producing a mechanical twitch in the filament that weakens the lateral contacts between actin monomers, destabilizing the structure and producing its disassembly (Winterhoff & Faix, 2015). ADF/Cofilin is highly regulated by factors like pH, association to other proteins, and phosphorylation at Ser3, which inhibits binding to the filaments (Narita, 2020). Because binding to the filament by itself is inefficient to induce the severing activity, ADF/Cofilin requires association to proteins like Aip1, coronin or Srv2/Cap to accelerate actin disassembly (Winterhoff & Faix, 2015).

Cofilin is relevant for radial migration in a way mediated by Reelin, knowing that Reelin induces phosphorylation of LIM Kinase 1, which subsequently phosphorylates cofilin in serine 3 to inactivate its interaction with actin (Frotscher et al., 2017). Chai et al. discovered that the transfection by *in utero* electroporation of either a non-phosphorylatable or a pseudo-phosphorylated cofilin in the serine 3 induce defects in neuronal migration (Chai et al., 2016). Among the main features of the defective neurons are the delay in migration as well as the presence of super-numerary and shorter leading processes. When observed by time-lapse, neurons transfected with both versions of cofilin, the same as the reeler mice, presented with inverted layering of the migrating neurons (Bellenchini, et al 2007). Gelsolin is activated by the presence of calcium, producing a release from auto-inhibition and inducing multitude of activities, including severing of the actin filament, capping of the barbed end, and sequestering of the actin monomers (Nag et al., 2013; Pollard, 2016).

These findings show how actin disassembly is important for regulation of the neuronal morphology during migration, associated to a defective migration.

1.1.4 Rho family of small GTPases

One important aspect of actin biology is how the cell controls the elaboration of actin assemblies in different cellular structures at the right time. One of its most important ways of regulation is through the activity of Rho GTPases, being Cdc42, Rac1 and RhoA the most well-known members of this family of proteins.

The way they work is by propagating a signalling cascade in their activated GTP-bound state, which can be hydrolysed to an inactivated GDP-bound state by their own phosphatase activity or by a GAP (GTP Activating Protein). Later on, they can be again activated by interaction with a GEF (Guanidine Exchange Factor) to exchange GDP for GTP (**Fig. 15 A**). GDI (Guanine-nucleotide dissociation inhibitors) bind to the Rho GTPase and inhibit the dissociation of the guanine nucleotide, preventing their activation (Hodge & Ridley, 2016).

Although not exclusively, it has been shown that Rac1 promotes the formation of lamellipodia via the WAVE complex, activating Arp 2/3; or by the activation of the p21-Activated kinase (PAK). It has been described that both constitutively active and dominant negative Rac1 induce arrest of migrating neurons in IZ (Konno et al., 2005). Upstream of Rac1, the GEF factor STEF is involved in this neuronal migration phenotype, since dominant negative introduction of this protein induces a similar phenotype to the one described for Rac1 (Kawauchi et al., 2003). About the effector Pak1, it was shown that overexpression of its constitutive active form produces arrest of locomoting neurons in the IZ, with curved, branched and disoriented leading processes, while the same effects are produced with its KD by the expression of a shRNA. Detaching from the basal process of the APs was suggested by the authors (Causeret et al., 2009).

More detailed studies revealed that the Rac1 scaffold POSH (Plenty of SH3) is involved in radial migration. It was observed that its KD by *in utero* electroporation produced arrest of migration in the IZ, inducing defects in the formation of swellings and inducing shorter nucleus-centrosome distances during migration. Moreover, POSH KD induced mis-localization in Rac1 (Yang et al., 2012).

Cdc42 is more commonly known to be involved in filopodia growth by formins recruitment and maintenance of cell polarity by establishment of the Par complex (Par3, Par6, aPKC) (**Fig. 15 B**) (Kühn et al., 2015). Similar to Rac1, both constitutively active and dominant negative Cdc42 induce arrest in neuronal migration, although at a lower degree (Konno et al., 2005).

The Rho sub-family is associated to the formation of contractile structures like stress fibres and focal adhesions, being RhoA the most studied member of this family, and its main downstream effectors being ROCK, PIP5K and mDia (**Fig. 15 B**) (Murali & Rajalingam, 2014; Spiering & Hodgson, 2011). Regarding its role in radial migration, Cappello, et al. described that it regulates velocity of migration, and when depleted specifically in neurons in a cKO, neurons show increased locomotion speed. However, more drastic defects were seen in a more general cKO deleting Rho also in progenitors (Emx+), where an important arrest of migrating neurons was observed (Cappello et al., 2012). RhoA activity is positively regulated by the PlexinB2 receptor by recruiting RhoGEFs and by the inhibition of Rnd3. KD of PlexinB2 induced delayed migration with supernumerary branches (Azzarelli et al., 2014). In addition, Xhu, et al (2015) observed that expression of a dominant negative form of RhoA produced arrest of MP cells in the IZ. The authors showed that Rho pathway was induced by N-cadherin contacts between radial glia and transitioning MP-BP neurons. However, another study showed that the defective migration (MP cells stuck in IZ) produced by the KD of the adhesion molecule Cntn1, was rescued by a dominant negative version of RhoA, implicating that RhoA is a negative regulator of migration.

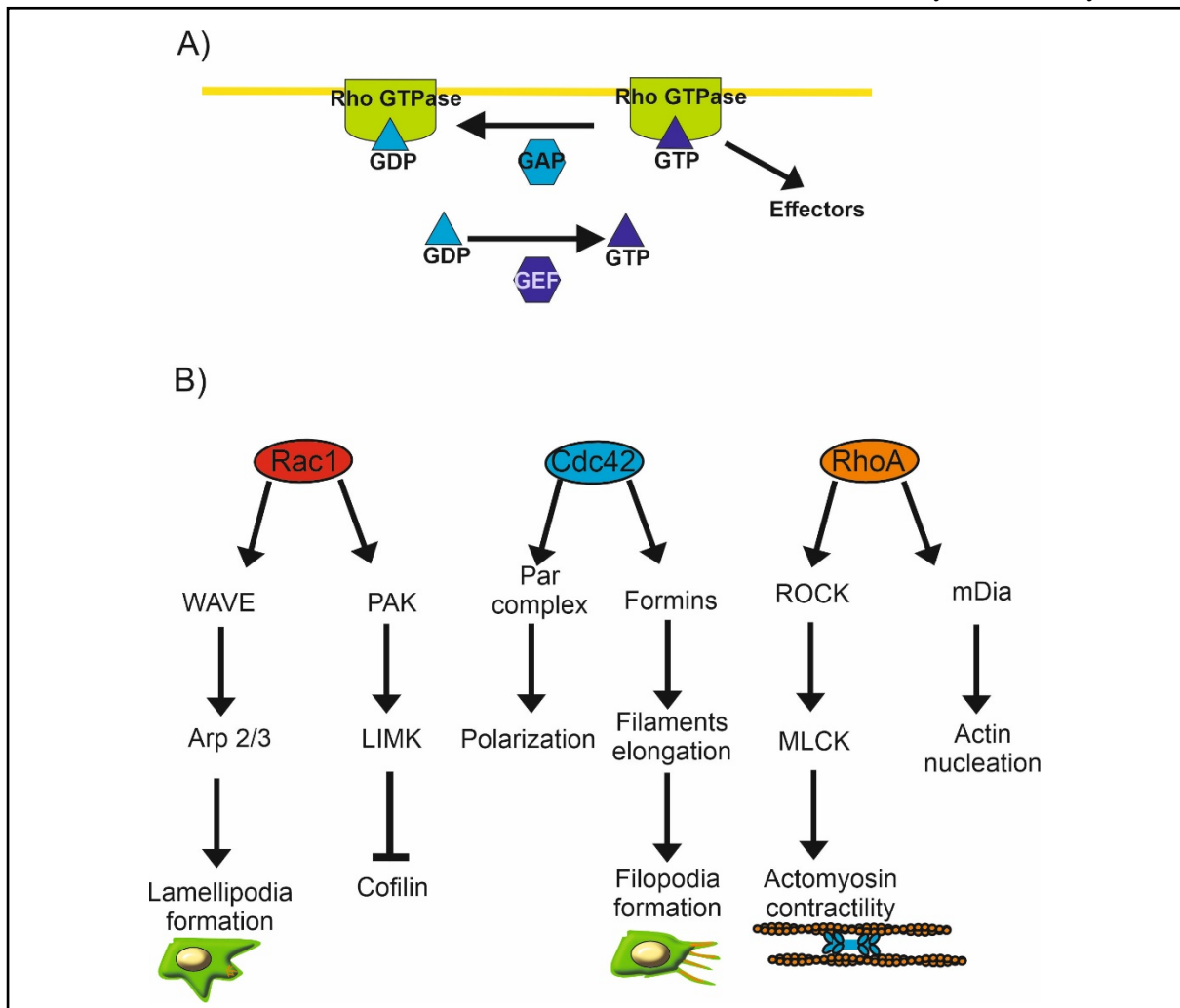


Figure 15. Rho family of small GTPases. A) Mechanism of activation /deactivation of small GTPases by exchange of their GTP /GDP nucleotide, where GAP induces the hydrolysis of the GTP bound to the Rho GTPase and GEFs participate in GTP exchange for GDP in the inactive state. **B)** Some of the main effectors of the most studied small GTPases related to actin structure arrangements.

1.1.5 Other actin related proteins involved in radial migration

As it has been mentioned in the previous sections the study of radial migration of pyramidal neurons associated to actin cytoskeleton is mostly related to the studies of silencing or overexpression of proteins that bind actin or regulate actin dynamics, in **Table 1** and **Figure 16** is shown a summary of the actin related proteins treated in this section.

Neuronal tyrosine-phosphorylated adaptor for the PI3-Kinase (Nyap2) is a protein that participates in actin cytoskeleton remodelling by its interaction with proteins like WAVE or PI3K (Cantrell 2001; Jaworski et al. 2005; Kumar et al. 2005). Its importance for radial migration was shown by both KD and overexpression in embryonic cortices by *in utero* electroporation (Wang et al., 2019). Overexpression of Nyap2 induced increased velocity of neuronal migration, with a phenotype of over branching of the

leading process, with the super-numerary branches being thicker and shorter. Faster migration was seen as a result of this phenotype. Accordingly, the opposite effect was seen with KD of *Nyap2*, where MP neurons were arrested at the IZ. Additionally, BP neurons in the KD presented with longer and thinner leading processes (Wang et al., 2019).

It was seen that the KD of Drebrin -like protein (Dbr1) induces neuronal migration arrest, a phenotype explained by defects in the multipolar phase of migration, in which the KD neurons have less processes than the WT neurons. In this same work, the authors showed that the abnormal neuronal positioning is rescued by co-electroporation of N-cadherin (Inoue et al., 2019), highlighting again the important role of this adhesion molecule during radial migration.

Actin-MT crosslinking protein MACF1 was seen to be important for radial migration when Ka et al., 2014 knocked-down the expression by *in utero* electroporation in cortical neurons, observing an increased number of branches in the leading process and similarly as in POSH KD, there was a decrease in the distance soma- centrosome during migration.

Table 1.-Actin related proteins and their mechanisms associated to radial migration (Studied by *in utero* electroporation)

Actin related protein	Effect on migration and at the cellular level
Actin nucleation and branching	
Nyap1 (S. Wang et al., 2019)	Over-expression. - Accelerated velocity / Shorter and branched leading process. Knock-Down. - Slower velocity / Longer and thinner leading process
WAVE-Abl complex (M. J. Xie et al., 2013)	Knock-Down. - Arrest in SVZ/IZ / Fail in MP-BP transition with defective protrusions in MP neurons
Arp 2/3 (P. S. Wang et al., 2016)	Knock-Down. - Neurons arrested in SVZ/IZ
Ena/VASP (Yoshinaga et al., 2012)	Knock-Down. - Neurons arrested in SVZ/IZ / MP neurons projecting less processes
RhoA family of proteins and related	
POSH (T. Yang et al., 2012)	Knock-Down. - Slower velocity / Defective (lack of) swelling formation and shorter soma-centrosome distance.
Rac1 (Konno et al., 2005)	Constitutively active and Dominant negative. - Arrest in SVZ/IZ

Cdc42 (Konno et al., 2005)	Overexpression of a dominant negative. - Migration delay
RhoA (Capello et al., 2012)	Conditional Knock - Out in migrating neurons. - Faster migration / Increased migration speed, normal morphology
PlexinB2 (Azarelli et al., 2014)	Knock-Down. - Arrested migration with supernumerary branches
Filament disassembly	
Cofilin (Chai et al., 2016)	Phosphomutated and phosphomimetic. - Slower velocity / Shorter and supernumerary leading processes
Filament crosslinking	
Filamin A (Zhang et al., 2013)	Knock-Down and Conditional Knock-Out (tamoxifen induced). - Arrest of neurons in IZ / Decrease of focal adhesions in MEF cells. Overexpression. - Arrest in neuronal migration in lower cortical plate.
Microtubule-Actin crosslinking	
Dbnl (Butkevich et al., 2015)	Knock-Down. - Slower velocity / Decreased branching of multipolar stage
MACF1 (Ka et al., 2014)	Knock-Down. - Arrested migration in SVZ/IZ / Shorter and supernumerary leading processes, shorter soma-centrosome distances.
Contraction	
fMyo10 (Ju et al., 2014)	Knock-Down. - Arrested migration in SVZ/IZ / Misdirection of LP
hMyo10 (Ju et al., 2014)	Knock-Down. - Arrested migration in SVZ/IZ / Impaired MP-BP transition

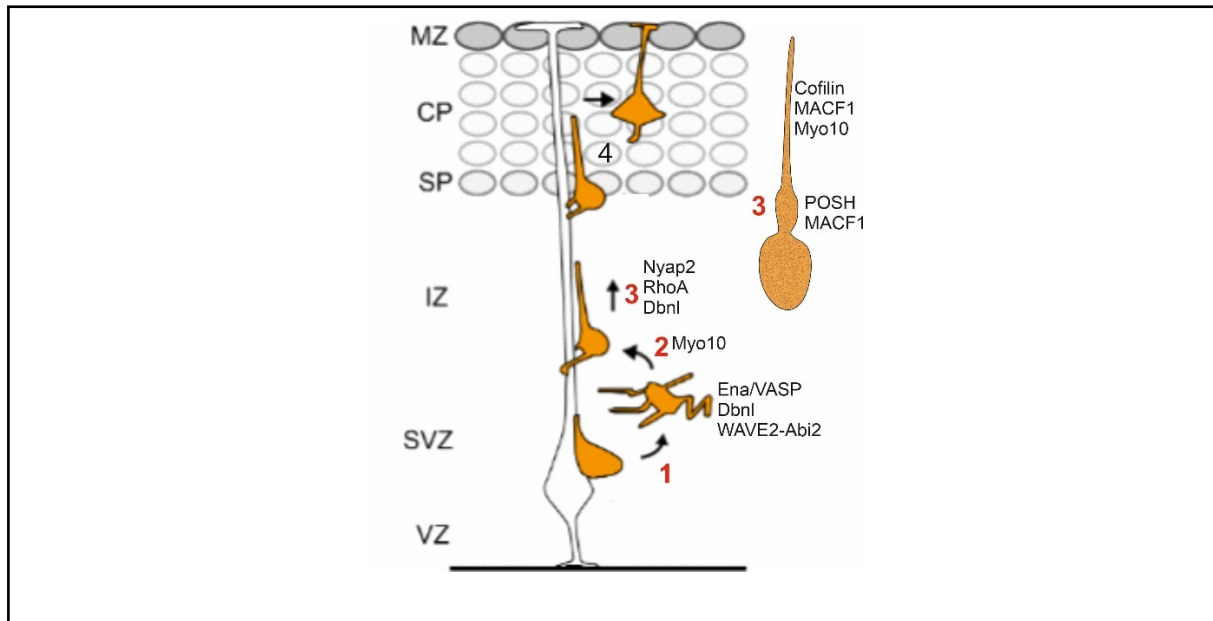


Figure 16.- Graphical summary of actin related proteins regulating radial migration

(Modified from Hansen & Hippenmeyer, 2020)

1.2 Actomyosin contraction and contractile structures

1.2.1 Myosins

Myosins are a superfamily of motor proteins that comprises 35 classes. Myosin heavy chain (MHC) bind to the actin filaments and generate force through the hydrolysis of ATP. All MHC are composed of an N-terminal motor domain, that binds to actin and hydrolyses ATP using Mg^{2+} as a cofactor; an intermediate IQ domain (or neck domain) that binds to myosin light chains (MLC) or calmodulin; and a C-terminal tail domain, necessary for dimerization (Masters et al., 2017).

Binding to MLC is necessary to regulate stability and function of the MHC, and it has been reported that depending on the myosin type, up to 17 MLCs can bind to a single MHC. Filament forming myosins are better known as “conventional myosins” because they were the first myosins discovered in muscle, and then were found to be highly distributed in eucaryotic cells (Heissler & Sellers, 2014). Conventional myosins possess 2 IQ domains, each of them binding to one MLCs, being these the regulatory light chain (RLC) and essential light chain (ELC). Myosins can be regulated by phosphorylation, and in the case of Myosin-2, phosphorylation at Serine 19 in the RLC activates the motor protein by relieving the auto-inhibited interaction of the motor domain with the tail (Heissler & Sellers, 2014).

“Unconventional myosins” on the other hand, bind in their neck domain to calmodulin instead of a MLC, indicating a role of calcium binding for the function of these type of myosins. They are classically viewed as organelle transporters, but also fulfil a wide variety of roles, such as actin organization,

transcription and chromatin organization (Fili et al., 2017; Woolner & Bement, 2009). Importantly for radial migration, two isoforms of unconventional myosin 10, full length (fMyo10) and headless (hMyo10, missing the motor domain), were shown to be essential for this process, although in a differential way. KD of either fMyo10 or hMyo10 induces arrest in the IZ, nevertheless, the defect produced by fMyo10 is related to a defect in leading process directionality of BP neurons, while hMyo10 depleted neurons are arrested in MP phase (Ju et al., 2014). Further investigation about the mechanism that Myo10 uses to drive radial migration, showed that arrest in SVZ/IZ are rescued by overexpression of N-cadherin, and that Myo10 keeps the adhesion molecule in a surface localization (Lai et al., 2015).

Although it is known the important role that actomyosin contraction plays in neuronal migration, little is known about the mechanisms regulating the process, as it will be explained in the next chapter.

1.2.2 Actomyosin contraction

One of the most important features of the actin cytoskeleton is the capacity to contract, generating mechanical forces that among other functions, produce actin ring constriction, vesicle fission, muscle contraction, or changes in cell morphology. The way it works is mostly known for the studies made in muscle contraction, where it assembles in structures known as sarcomeres. Here, actin filaments are embedded by their barbed ends in a region called the Z-disk, composed of different stabilizing proteins, including α -actinin. Antiparallel filaments of actin are associated by myosins, which produce forces that pull the actin filaments close to each other in an ATP dependent manner (**Fig. 17**) (Sutherland & Lesko, 2020).

In this process of muscular contraction, there are proteins that keep the stability of the contracted filaments. Among them, some of the most important are tropomodulins, capping the pointed end; CapZ, capping the barbed end at the Z disk; and nebulin as a giant protein that provides stability binding along the filament and to both the Z disk containing the barbed end, and the pointed end capping proteins (**Fig. 17**) (Yuen & Ottenheijm, 2020).

In other systems, contraction of the anti-parallel actin filaments has been shown to act in different manners, depending on the number and type of myosins, the length and conformation of actin filaments, as well as the associated actin bundling proteins (Sutherland & Lesko, 2020). Since the composition of these filaments differs from that of the sarcomere, these alternative modes of contraction can induce actin fragmentation due to a buckling activity in the filaments, making necessary a cycle of actin polymerization and assembly before the machinery is newly disassembled with each cycle of contraction (**Fig. 18**) (Murrell et al., 2015).

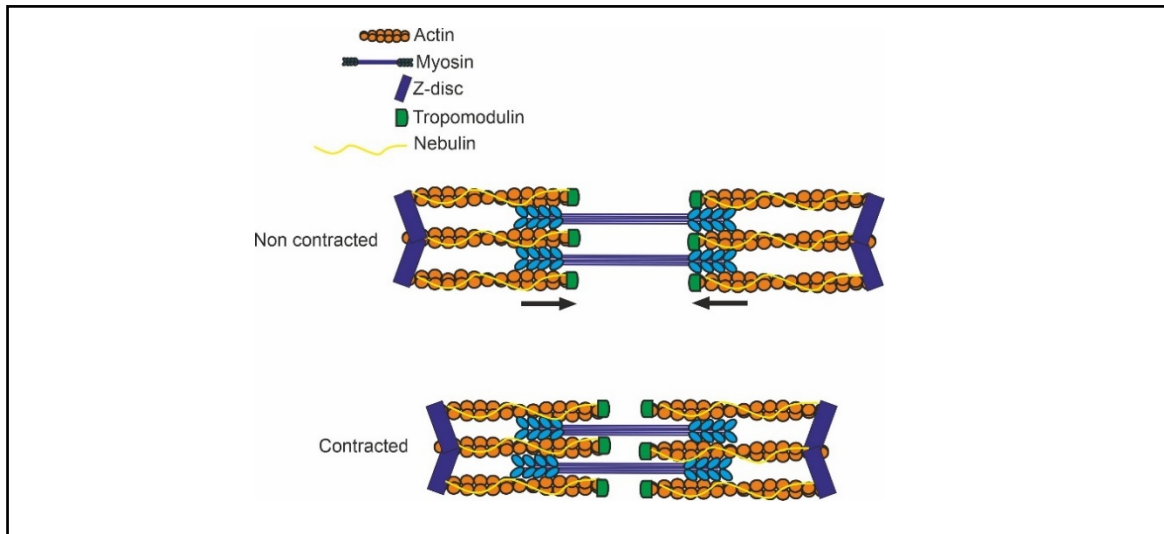


Figure 17. Contraction of actomyosin cytoskeleton in sarcomere structure present in skeletal muscle. In this mode of actomyosin contraction, different elements contribute to stabilize the actin filaments by binding to their both ends (tropomodulin at the pointed end, and Z-disk proteins at the barbed end). In the same way, large proteins, like nebulin, stabilize the filament by binding along its length.

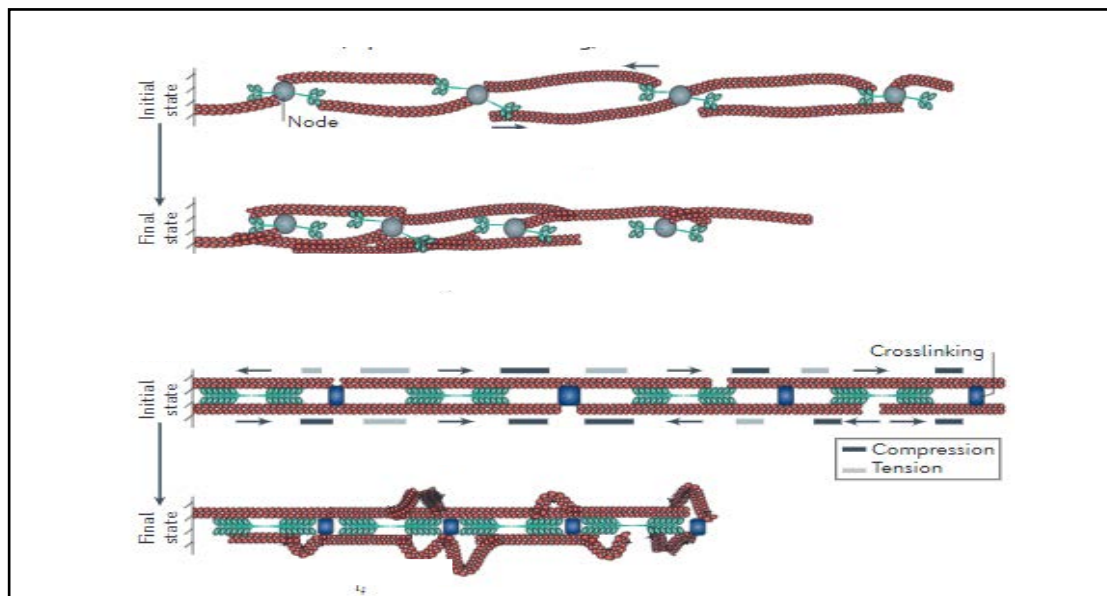


Figure 18. Different contractile structures formed by actomyosin cytoskeleton. Actin filaments can be under a buckling activity, promoting disassembly of the filament and requiring re-assembly to re-start the cycle of contraction (From Murrell et al., 2015)

Contractile structures described for different cell types include stress fibres, traverse arcs, blebs and the cell cortex. Stress fibres and transverse arcs are both based on actin bundled structures, in the first case, stress fibres are located ventrally in different types of migrating cells and are anchored to focal adhesions, while transverse arcs lack those adhesions. The cell cortex consists in a shell composed of an actomyosin mesh covering the inner face of the cellular membrane, bound to it by the ERM (ezrin, radixin, moesin) protein complex. The degree of branched actin and amount of myosin molecules composing the cellular cortex provides with different levels of tension to the cell (Kelkar et al., 2020).

Blebs are regions that extrude from the cell in a bubble-like fashion, produced by the flow of hydrostatic pressure due to the lack of a cellular cortex in these parts. These blebs are then filled-up by the actomyosin cytoskeleton and through interaction with cell adhesions, produce a forward movement (Adams et al., 2021).

Among the different ways in which actin dynamics can provide locomotion to the cell, contraction plays a pivotal role in neuronal migration, as it was seen for interneurons and cerebellar neurons. It was described in cortical interneurons expressing the F-actin reporter Life-Act, that actin concentrates at the rear of the cell before nucleokinesis, a dynamic in which actin return to basal levels after nucleokinesis. These cyclic changes have been correlated with the dynamics of myosin activity and nucleokinesis (Martini & Valdeolmillos, 2010). Among the mechanisms driving this contraction during interneurons nucleokinesis, p27 presents an inhibitory activity on contractility by decreasing RhoA activity. As a result, p27 KO neurons showed increased phosphorylation in MLC-II, leading to defective nucleokinesis (Godin et al., 2012).

Actomyosin contraction was investigated also in migrating cerebellar granular neurons. Solecki, et al. mentions that cerebellar neurons require actomyosin contraction at the proximal edge of the leading process before nucleokinesis in a dynamic similar to that of the rear end of interneurons (Solecki et al., 2009). During radial migration, myosin plays an important role for nucleokinesis, and inhibition incubation in the myosin inhibitor blebbistatin produces arrested nuclear movement, with the expression of the RNAi for myosin IIB producing the same effect (Tsai et al., 2007).

Addressing actin dynamics in pyramidal neurons during radial migration, in the study by Mererynk, et al (2022) by combining CRISPR genetic edition by *in utero* electroporation, they endogenously tagged the β -actin gene with the Myc epitope. They visualized the label of the tag in both aRG and migrating neurons. In these last, actin labelling was mainly at the processes of the MP neurons and the leading process of locomoting neurons (Meyerink et al., 2022). Nevertheless, studies about actomyosin contraction during radial migration in pyramidal neurons are missing and research about it needs to be performed in order to understand these mechanisms.

2. Microtubules dynamics

The MT cytoskeleton is composed by hetero dimers of α and β -tubulin, associated in the form of 13 polarized protofilaments that couple laterally to form a hollow tube of 25 nm in diameter. MTs experience a process known as dynamic instability, in which the plus end of the filament possesses a high tendency to grow (rescue) and shrink (catastrophe), and the minus end at the opposite tip of the filament presents a slower dynamic of growth than the plus end (**Fig. 19**). The plus end tip binds with more affinity to $\alpha\beta$ -tubulin dimers bound to GTP, while the subunits forming the lattice are normally associated to GDP (Akhmanova & Steinmetz, 2015).

MTs bring different functions to the cell: formation of the tracks for long distance intracellular transport, they work as a placement for organelle positioning, formation of the mitotic spindle, assembly of cilia and flagella, and the transduction of mechanical energy (Rafiq et al., 2019). Among the most studied factors known to influence MT dynamics and functions, are the different α and β -tubulin isotypes that can form them, the association to Microtubule Associated Proteins (MAPs), and post-translational modifications (PTMs) (Goodson & Jonasson, 2018; Kapitein & Hoogenraad, 2015). In the next sections these factors will be explained, and **Table 2** summarizes some of the most important MT proteins and MAPs associated to defects of neuronal migration.

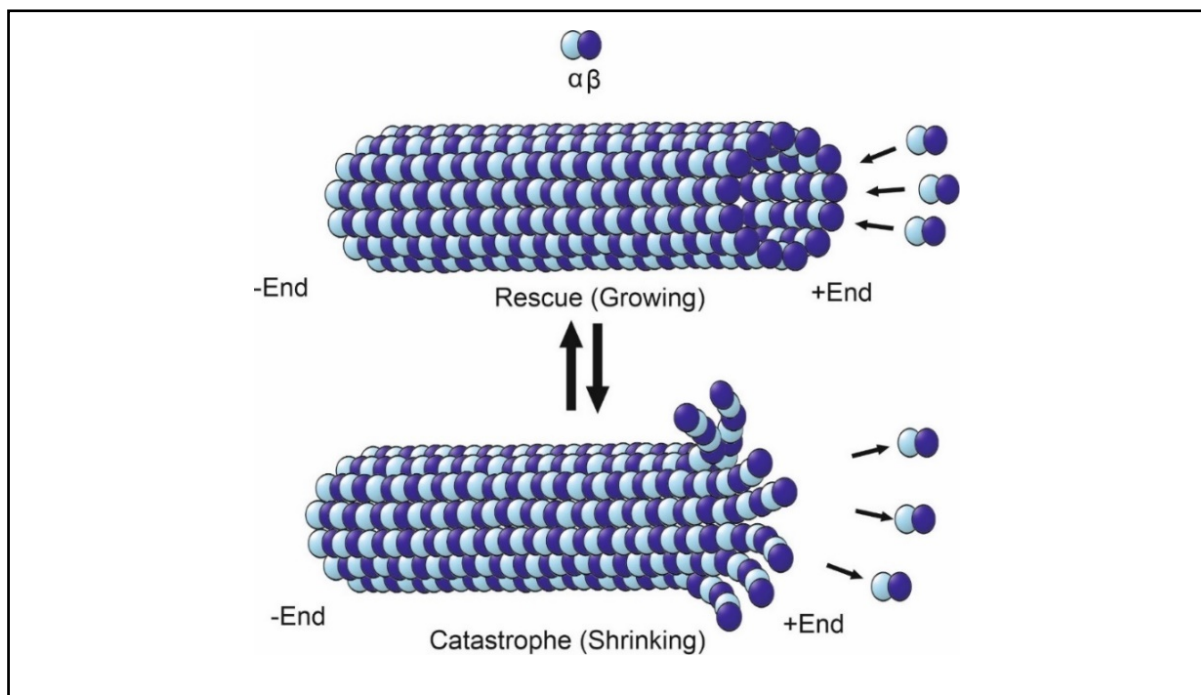


Figure 19. Microtubule dynamic instability. The MT is a polarized filament, composed of α/β tubulin heterodimers, with both a minus and a plus end. It is characterized by a phenomenon known as dynamic instability, where the plus end is able to switch from a stable (rescue) to a depolymerizing state (catastrophe).

2.1 Microtubule organizing centres

The main MT organizing centre (MTOC) is located at the centrosome, a cellular structure composed of two centrioles surrounded by pericentriolar material (PCM). One of the most important centrosomal organizers is pericentrin, a protein that contains a PACT domain at its C-terminal part, required to form associations with other proteins like CEP215, CEP192, CEP85L and NEDD1, which are important to recruit the γ -Tubulin Ring Complex (γ -TuRC) (Zheng et al., 1995). This complex is the most important and well-known centre for MT formation *de novo*, and as the name indicates, it relies on γ -Tubulin to initiate MT polymerization (Kollman et al., 2011).

Apart from centrosomes, there are additional places for MT nucleation and anchoring, such as the Golgi apparatus, which takes advantage of its MT organizing centre function to regulate local vesicle transportation. In this case, the protein AKAP450 interacts with the Golgi membranal protein GM130, that is thought to recruit γ -tubulin in order to start MT (Zhu & Kaverina, 2013). The calmodulin-regulated spectrin-associated protein (CAMSAP) binds to the minus ends of free, uncapped MTs and slows down their growth, in addition to being an important non-centrosomal centre for MT organization in differentiated cells, such as neurons (Hendershott & Vale, 2014).

Since the centrosome is the main MTOC in migrating neurons, proteins involved in its organization are important for a correct migration. Example of these are the proteins CEP85 and γ -tubulin, whose KD induces arrest of neurons at the IZ associated with abnormal nucleus-centrosome distancing during locomotion, and for γ -tubulin KD the pausing time during locomotion cycles was increased (Ivanova et al., 2019; Kodani et al., 2020). Interestingly, CEP85 was shown important in organization of centrosomal proteins in a CDK5 dependent fashion (Kodani et al., 2020).

The centrosome shows dynamic changes during the whole radial migration process. During MP phase, it is located in a random fashion while the neuron protrudes and retracts multiple processes. In locomoting phase, with the BP shape formed, it localizes at the front of the nucleus, changing localization in a cyclic manner, being localized in the proximal part of the leading process and moving forward together with the swelling just before nucleokinesis takes place (Umeshima et al., 2007).

The protein complex composed by Ndel/Lis1 is known to participate in MT stabilization and centrosome dynamics during different stages of cortical development, and some studies have addressed its importance for radial migration (Shu et al., 2004; Youn et al., 2009). It was seen that their individual KD by *in utero* electroporation produces arrest of the migrating cells in the SVZ/IZ with an increased nucleus-centrosome distance (Shu, et al. 2004), moreover, and Tsai et al (2005) observed defects of MP-BP transition with the expression of a shRNA for Lis1 (Tsai et al., 2005).

To study the role of Lis1 in neuronal migration at the cellular level, Tsai et al (2007) tested two different RNAi to inhibit Lis1 at different levels and saw that potent inhibition of Lis1 produced decreased

nucleus – centrosome distance, while the opposite happened with a less potent RNAi, inducing increased space between the nucleus and centrosome. This centrosome's driving role is also mediated by dynein, as seen by impairments in centrosome dynamics upon dynein RNAi expression. In this same study the authors observed that nuclear movement was dependent on myosin (discussed in section 1.2.2) and dynein (Tsai et al., 2007).

In another study, it was seen that the reduction of the protein levels of either Ndel or Lis1 (genetic mutations reducing 50% and 65% of the protein levels) was enough to decrease locomotion speed and for the case of Ndel, the decrease in its levels induced supernumerary branches and defective directionality. In line with this, full KO of both proteins individually was able to completely abolish migration (Youn et al., 2009).

Then, the importance of the processes happening in the MTOC involving MT dynamics and activity of motor proteins is essential for pyramidal neurons to complete the different steps of migration.

2.2 The tubulin code

The tubulin code is a concept that explains that the combinatorial differences between tubulins isotypes and their different PTMs contribute to the functional differences in MTs across cell types and MTs filaments in the same cell type. Concerning MT isotypes, it is known that in mammals there are 9 genes encoding for α -tubulin and 9 genes encoding for β -tubulin, some of which are exclusively expressed in specific cell types, such as β -tubulin isotype III (TUBB3), expressed in the central nervous system (Janke & Magiera, 2020 Kapitein & Hoogenraad, 2015; Wloga & Gaertig, 2011). Expression of tubulin isoforms is dynamic during development and changes according to the needs of the cell. As an example, it was studied in mouse brains during development that expression of the mRNAs for Tuba1a, Tuba1b, Tuba1c, Tubb2a, Tubb2b, Tubb3 and Tubb5 was enriched in whole brain at embryonic stages in mouse (E14.5) (Hausrat et al., 2021).

The mutation of different tubulin isotypes, such as TUBA1A, TUBB2B and TUBG1, can be found in patients with defects in cortical gyrification (Stouffer et al., 2016), and the study for some of these tubulin isoforms shows interesting results about the cellular phenotypes in migrating neurons. Saillour, et al. showed that β III-tubulin KD induces arrest of migration in IZ at least due to an alteration in the MP phase. In this study, *in utero* electroporation of a shRNA to deplete β III-tubulin induces decrease in the protrusions from MP neurons and hence, they become more rounded while transiting through this stage (Saillour, et al. 2014). Tuba1a mutation S140G, affecting the binding to GTP is also seen to affect migration, corresponding to the lissencephaly (smooth cortex) in patients with the mutation in its homolog α III-tubulin (Keays et al., 2007). In the same way, mutations in TUBB2B are

found in patients with polymicrogyria (excessive gyri) and when silenced in mice by *in utero* electroporation of shRNA, they are seen to induce migration arrest (Jaglin et al., 2009).

Acetylation is one of the most common PTMs, happening mainly at the Lys40 residue at the luminal part of the filament. Additionally, secondary chains of poly glycine and polyglutamate can be added to different glutamate residues at the C-terminal region of α and β -tubulins, in a reaction catalysed by the Tubulin Tyrosine Ligase Like (TTLL) enzymes (Wloga & Gaertig, 2011). It was shown acetylation is important for radial migration in the study of Creppe et al, where neurons silenced for the Elongator complex, implicated in α -tubulin acetylation, showed delayed migration and aberrant maturation, an effect emulated by the expression of a non acetylatable form of α -tubulin (Creppe et al., 2009). Similarly, upon depletion of the protein SrpX2, projection neurons fail to migrate, and administration of the deacetylase inhibitor tubacin rescues the phenotype (Salmi et al., 2013).

Besides acetylation, Lys40 can be trimethylated, an effect produced by the enzyme SET Domain containing 2 (STED2). Knock-down of this protein induces arrest of neurons in the IZ, with an increased proportion of MP cells and BP neurons with an abnormally overbranched leading process. These functions are rescued by tri methylation-mimicking tubulin and by the truncated STED2 that keeps enzymatic activity (X. Xie et al., 2021).

Removal of residues acts as another important PTM that regulates MTs composition. Among the most important are the removal of tyrosine from the C-terminal part of α -tubulin by VASH proteins; and the subsequent removal of glutamate residues from detyrosinated α -tubulin, generating $\Delta 2$ and $\Delta 3$ tubulins. These last are generated by the Cytosolic Carboxypeptidases (CCPs) (Janke & Magiera, 2020). Contrasting with this role, Carboxypeptidase E overexpression is known to induce increased polyglutamylation, while decreased glutamylation is seen upon knock-down of the gene. It was shown that knock-down of Carboxypeptidase E produces defects in radial migration (Liang et al., 2019), and that overexpression of Carboxypeptidase E with truncated zinc-binding motif, necessary for glutamylation, induces defects in migration with excessive accumulation of MP neurons at the IZ, suggesting that this motif implicated in polyglutamylation, is not involved in the phenotype (Liang et al., 2022).

The function and catalysing enzymes for other PTMs, such as ubiquitylation, sumoylation and palmitoylation, are less known and require further research (Janke & Magiera, 2020). The different combinatorial tubulin isoforms and post-translational modifications can affect the different protein binding to the MT and motility parameters of motor proteins, such as binding, velocity and processivity (Sirajuddin et al., 2014).

2.3 Microtubule associated proteins

In addition to the tubulin code, MTs require interactions with a diverse array of MT Associated Proteins (MAPs) to display various functions and determine their localization in the cell. Binding of MAPs modulates MT activities in order to stabilize, bundle, cross-link or sever the filaments. They can associate either to the lattice or to the tips (plus and minus) of the MT (**Fig. 20**). Motor proteins are other kinds of proteins that associate to MT, but they will be discussed later.

2.3.1 Plus-tip binding MAPs

The family of the end binding proteins (EBs) comprise a group of proteins that bind to the plus-end of the MT filament and is represented in mammals by three members: EB1, EB2 and EB3. They bind MTs through their N-terminal domain, referred as the calponin homology domain, that additionally shows affinity for actin, contributing to a crosslink activity of both cytoskeletons. EBs dimerize with other proteins, like APC or STIM1 by their C terminal region containing an EB-homology domain. They are known to provide the MTs with processive growth and reduce the number of catastrophes. Additionally, they function as hubs to integrate signalling pathways that regulate MT organization (Sayas & Avila, 2014; Mustyatsa et al., 2017).

Adenomatous Polyposis Coli 2 (APC2) protein lost by knock-out produces defects in cortical lamination, as seen by abnormal localization of layers expressing Cux1, Ctip2 and FoxP2. These defects were induced by migration disruption and were also accompanied by a rise in apoptosis. In cultured neurons it was seen that APC2 is a factor that interacts with both actin and MT (Shintani et al., 2012). In contrast to APC2, APC does not participate in radially migrating neurons (Eom et al., 2014).

CLASP (CLIP-associating protein) proteins recognize the MT plus-ends and bind them to promote rescue and suppress catastrophes of the MTs, activity enhanced by the association to EB proteins (Akhmanova et al., 2001). These proteins also have a role in MT-actin crosslinking, being involved in the attachment of MT to the actin cortex, actin filaments transportation or focal adhesions assembly/disassembly (Alkemade et al., 2022; Juanes et al., 2019). CLASPs are known to provide stability and directionality during neurite growth (Beffert et al., 2012) and it has effectors of the Reelin signalling pathway, important regulators of radial migration (discussed in previous sections). Besides incorrect positioning, neurons knocked down for *CLASP2* show increased nucleus centrosome distance and disrupted neuronal polarity of radially migrating neurons. CLASP was seen to interact with Dab1 by a phosphorylation of GSK-3 β (Dillon et al., 2017).

XMAP215 is a protein that binds to the MT plus-end via the tumour overexpressed gene (TOG) domains, it acts both as a polymerase of the MT filament or as a catastrophe inducer (Brouhard et al., 2008; Farmer et al., 2021). Actually, binding of the TOG domains is altered upon V409I and V409A

missense mutations of TUBA1A, reducing recruitment of XMAP215, inducing increased MT polymerization rates and tubulin acetylation levels. The expression of these TUBA1A mutations (V409I and V409A) induces defects in migration with more neurons positioned at the SVZ/IZ (Hoff et al., 2022).

FGF13 is a member of the FGF family that in contrast to most of its members, it is not secreted. It is a protein that binds MT, providing stabilization and inducing polymerization, it is located normally at the growth cones. Silencing the expression of *FGF13* in migrating neurons leads to defects in MP-BP transition, with depleted neurons found mostly in the IZ presenting a MP morphology, and the neurons that become BP present a highly branched leading process. These defects were rescued by *Dcx*, a protein that participates in MT stabilization (Wu et al., 2012).

Being the plus end of the MT a site where multiple processes are regulated and different interactions happen, it is not surprising to know that dysregulation of the proteins at these sites affect radial migration dynamics and morphology.

2.3.2 Lattice binding MAPs

MAPs associated to the lattice are well-known by their role in assembly, stabilization and in some cases bundling MTs. Their presence can influence, either positively or negatively, the binding of other MAPs and motor proteins, influencing the distribution of organelles like mitochondria and endoplasmic reticulum, and diverse cellular components (Kapitein & Hoogenraad, 2015).

Tau regulation is highly dependent on phosphorylation, as it can be noticed by its 85 putative sites for this PTM (Wegmann et al., 2021). There are 6 isoforms in the brain with a molecular weight ranging from 55 to 62 kDa. They contain the following domains: N-terminal domain, a proline rich region, a repeat domain and C-terminal domain; the repeat domain being the one interacting with the MTs (Goedert, 2018). Acute reduction of Tau levels by *in utero* electroporation of a shRNA induces arrest in migration in the SVZ/IZ with morphological defects in migrating neurons, showing thin and crooked leading processes, additionally it affects mitochondria motility and distribution, affecting also postnatal development of dendritic structures (Sapir et al., 2012).

Defects in migration induced by *p600* KD produce neurons with thin and crooked leading processes. *p600* being a protein that links MT to endoplasmic reticulum, it was seen that neurons depleted of *p600* presented also decreased levels and abnormal distribution of endoplasmic reticulum. Interestingly, these neurons also presented lower levels of acetylated tubulin (Su et al., 2008).

Similar to Tau, MAP2 presents with repeats of MT binding domains that differ in number depending on the isoform expressed (MAP2A, MAP2B, MAP2C). Some MAPs, like MAP2, MAP4 and tau have been demonstrated to bind actin by their MT binding domains in a non-overlapping manner. Since their MT

binding domains are repeated, they can use some repeats to bind MT and other repeats to bind actin, as is the case for tau (Bodakuntla et al., 2019; Elie et al., 2015). Specifically for the case of Tau, it was shown by studies *In vitro* that its presence is involved in the coordinated growth of MT and actin filaments in a hybrid manner, with the two cytoskeletons growing in the same direction and position (Elie et al., 2015).

MAP2 is known to be specific for MT in soma and dendrites of mature neurons (Dehmelt & Halpain, 2004). KO of both MAP2 and MAP1B show synergistic effects that affect neuronal migration, as shown by Teng et al (2001), where the double knock-out for Map2 and Map1b presented delay in migrating neurons and defective lamination. The MT of the double KO neurons showed decreased spacing between filaments (Teng et al., 2001).

MAP6 has been demonstrated as a factor that stabilizes axons by binding MT. In the case of migrating neurons, KD of *MAP6* produces migratory delay with abnormal development of axons and leading process, being absent in some cases. *In vitro*, it was shown that palmitoylation is required to move MAP6 from vesicular compartments to MT, inducing like this neuronal polarization (Tortosa et al., 2017).

Doublecortin (Dcx) is a 49 kDa MAP found in developing neurons, it binds to MT via Dcx domains, DC1 and DC2, present at the N and C terminal respectively and linked by an unstructured linker. Dcx binds directly to 4 adjacent tubulin dimers in the region between adjacent protofilaments, providing stability and strength to the lattice (Bodakuntla et al., 2019; Moslehi et al., 2017).

The microtubule stabilizer DCX, whose gene is located in the X chromosome, is mutated in a heterozygous manner in female patients with subcortical band heterotopia (abnormal accumulation of neurons below the cortex), while hemizygous mutations in males produce lissencephaly (des Portes et al., 1998; Pilz et al., 1998). Despite this high importance in human health, studies in animal models require a deeper analysis: KO in mouse presents with normal cortical lamination and the defects are present mainly in hippocampus (Corbo et al., 2002), while defects in migration are seen by acute depletion of Dcx in rat by *in utero* electroporation of RNAi (Bai et al., 2003). Nevertheless, defects in cortical lamination appear with double KO of Dcx and Dcx like-kinase (Dclk), indicating a compensatory effect of Dclk in mouse (Deuel et al., 2006).

MT bundling is necessary for some important cell processes, like the assembly of the mitotic spindle during anaphase. For this process, PRC1 is well known to participate in MT bundling in antiparallel fibres in order to establish the correct architecture of the mitotic spindle to segregate chromosomes in a proper way (Hannabuss et al., 2019), nevertheless, its role in neuronal migration is not studied.

The importance of all these elements indicates that regulation of MT stability, bundling, and interaction with other proteins provided by all these lattice binding proteins, the same than in other biological processes, is important for regulation of the migratory process.

2.3.3 MT destabilizing MAPs

MTs severing is performed by the proteins katanin, spastin and fidgetin, that form part of the AAA (ATPases Associated with diverse cellular Activities) superfamily of P loop ATPases (Goodson & Jonasson, 2018). Katanin, the most studied of the MT severing proteins, is a heterodimeric protein constituted by the catalytic subunit p80 (80kDa) and the regulatory subunit p60 (60kDa), this second showing its highest degree of activity upon hexamerization. Their severing activity generates MT fragments that can be transported to neuronal branches to contribute to axon and dendritic development. (Ghosh et al., 2012). Since p60 full knock-out is embryonically lethal, it was studied in haploinsufficiency, and heterozygous mice presented with migratory delay and cells in BP stage often showing an absent leading process (Lombino et al., 2019).

Destabilization of MT can be performed by stathmin (a 17kDa protein), either by binding to α and β -tubulin dimers, avoiding their integration into filaments; or by interacting with the plus-end tips and blocking the addition of tubulin dimers and increasing the rate of catastrophes (Chauvin & Sobel, 2015). Stathmin-2 is phosphorylated by Jnk1 at the serine 62 and 73, and absence of these phosphorylations produce a phenotype similar to that of Jnk1 knock-down, with defects in MP-BP transition, showing increased exit from MP phase. These defects are rescued by the expression of a phospho-mimetic version of Stathmin 2, which was shown to increase MT stability (Westerlund et al., 2011).

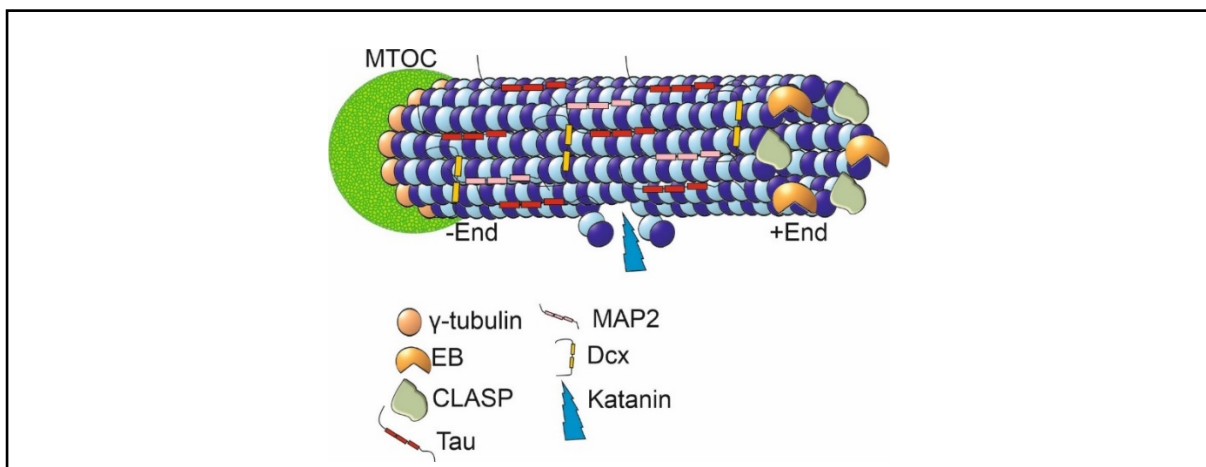


Figure 20. Microtubule associated proteins. Different classes of MT associated proteins binding either to the plus ends and the lattice, which are normally associated to provide stabilization to the filament, and katanin as an example of MT severing protein, that removes dimers from the lattice.

Table 2.- Microtubule binding proteins participating in neuronal migration (excluding kinesins, explained in further sections)

Protein	Cellular function	Effect on migration and at the cellular level
Tubulin variants		
βIII-tubulin (Saillour et al., 2014)	MT subunit	Knock-Down. - Arrest in SVZ/IZ / Impairment in MP morphology, they become rounded
TUBB2B (Jagglin, et al. 2009)	MT subunit	Knock-Down. - Arrest in SVZ/IZ
TUBA1A (Keays et al., 2007; Hoff et al., 2022)	MT subunit	S140G missense mutation. - Lamination defects V409I and V409A mutations. - Neuronal arrest at SVZ/IZ with MP morphology
Centrosomal regulatory proteins		
Cep85 (Kodani et al., 2020)	Maintenance of centrosome integrity	Knock-Down. - Arrest in IZ/SVZ
γ-tubulin (Ivanova et al., 2019)	MT nucleator in the centrosome	Knock-Down. - Arrest in SVZ/IZ / Mislocalized centrosome Y92C Knock-In. - Arrest in SVZ/IZ / Increased pauses and pausing time
Proteins of the dynein complex		
DYNC1H (Willemsen et al., 2012)	MT motor protein in retrograde fashion	Knock-Down. - Arrested nucleokinesis and defect in centrosome movement
BICD2 (Ravenscroft et al., 2016; Tsai et al., 2020)	Adaptor protein	Conditional knock-Out.- Elongated and branched leading process. Knock-Down with K775X rescue.- Migration arrest with defect in nucleokinesis but not swelling
Ndel (Shu et al., 2004b; Youn et al., 2009)	Regulatory of dynein movement	Knock-Down. - Neuronal arrest in SVZ/IZ Hypomorphic Knock-Out. - Lamination defects / Decreased velocity, multiple LP branching Knock-Out. - Absence of migration
LIS1 (Shu et al., 2004; Tsai et al., 2007; Youn et al., 2009)	Mediates interactions of dynein with other proteins of the complex	Knock-Down. - Neuronal arrest in SVZ/IZ / Impaired nucleokinesis and centrosome movement Hypomorphic Knock-Out. - Decreased velocity Knock-Out .- Lamination defects / Absence of migration
Lattice binding proteins		
Tau (Sapir et al., 2012)	MT stability	Knock-Down. - Migration delay / Thin and crooked leading process, defective mitochondria distribution
Dcx (Bai et al., 2003; Corbo et al., 2002)	MT stability	Knock-Out. - No effects Knock-Down. - Neuronal arrest in IZ / Stalled MP cells

MAP6 (Tortosa et al., 2017)	MT stability	Knock-Down. - Migratory delay / Neurons fail to form leading processes and axons
Carboxypeptidase E (Liang et al., 2022)	MT glutamylation	Knock-Down. - Arrest of migrating neurons in MP phase
p600 (Su et al., 2008)	Interaction MT- Endoplasmic Reticulum	Knock-Down. - Decreased and incorrect distribution of ER, defective leading process
Plus tip binding proteins		
CLASP2 (Dillon et al., 2017)	Promotes rescue and rescues catastrophes.	Knock-Down. - Delay in migration and lamination defects / Disrupted polarity, decreased nucleus -centrosome distance
APC2 (Shintani et al., 2012)	Promotes MT growth	Knock-Out. - Lamination defects and increased apoptosis
FGF13 (Wu et al., 2012)	Provides stability and induces MT polymerization	Knock-Down. - Arrested neurons at SVZ/IZ / Neurons arrested in MP phase, highly branched BP neurons.
Microtubules severing proteins		
p60 (katanin subunit) (Lombino et al., 2019)	Generation of MT fragments	Haploinsufficiency. - arrested migration / Migrating neurons with absent leading process
Stathmin-2 (Westerlund et al., 2011)	Inhibition of MT growth by binding to the +tip or sequestering subunits	Phosphomimetic Stathmin-2 and KD. - induces increased migration velocity / Accelerated MP-BP transition

3 Microtubule motor proteins

One of the most important features for every developmental process is the efficient transport of cellular components to the place they will be needed by the cell. This is achieved by the action of motor proteins, such as kinesins, dyneins and myosins. The first two use the MT network as their tracks to transport different cargoes, with the difference that most kinesins move in an anterograde fashion (to the + end) and dyneins move in a retrograde fashion (to the – end). On the other hand, myosins (previously described) use the actin filaments as the trails for their motor activity (Konjikusic et al., 2021).

3.1 Dyneins and associated proteins regulating neuronal migration

In contrast to the high number of kinesins that regulate anterograde transport (discussed later), retrograde transport in the cytoplasm is solely by dynein 1 (cytoplasmic dynein). The other members of the dynein family participate in cilia transport, where dynein-2 carries intra-flagellar transport, bringing signalling components from the tip of the cilia to the base. Another type of dynein is implicated in the structural arrangement of the axoneme, where it helps to keep the MT doublets arranged in a circular manner (Vuolo et al., 2020)

Dynein-1 is a complex of 1.4 MDa, composed of a dimer of six polypeptides, with dynein heavy chain-1 (DHC) as the largest, with a molecular weight of 530 kDa. The C-terminal domain of DHC contains the region that hydrolyses ATP and produces the motor activity. This ATPase domain is organized in a ring of 6 asymmetrical modules (AAA1-6), from which the first 4 bind and hydrolyse ATP (**Fig. 21**) (Bhabha et al., 2016). From domains AAA4 and 5, two coiled coil domains extend to form the stalk of the dynein, and at the base of the stalk, it is found the MT binding domain (MTBD). The movement of dynein is promoted by AAA5 and 6, that transmit the conformational changes happening in AA1 by the ATP hydrolysis (Canty et al., 2021; Carter et al., 2016).

The dynein tail is composed by the N-terminal part of the DHC and two copies of five accessory chains and is responsible for cargo binding and dynein dimerization. Essential for dynein function is the interaction with dynactin, a 1.1 MDa protein complex composed of 23 subunits. The interaction of Dynactin with dynein-1 is assembled by the activity of cargo adaptors Bicaudal-D and Hook family of proteins (Canty et al., 2021).

During radial migration, dynein accumulates at the swelling reaching a peak before nucleokinesis. Moreover, expression of RNAi of dynein heavy chain arrest nucleokinesis and produces defects in

centrosomal movement (Tsai et al., 2007). Many different proteins have been described to participate in the dynein complex to regulate neuronal migration. One of the mechanisms by which dynein regulates locomotion is by interaction with the LINC complex in the external side of the nucleus by interaction with the Syne-2 protein, regulating the centrosome-nucleus distance during migration (X. Zhang et al., 2009).

The giant protein Nesprin-2 (800 KDa), recruits molecular motors, including dynein and kinesin-1 to couple nucleus-centrosome distance and regulate leading process size. This effect was seen to be dependent on an interaction with BicD2, which acts as an adapter protein (Gonçalves et al., 2020). This Bic2D participation was also seen involved in the locomotor phase in a Nex-Cre driven cKO mouse line, where the leading process is longer than control and, in this case, branched (Ravenscroft et al., 2016). Another protein of this complex that participates in neuronal migration is N-acetylglucosamine kinase (NAGK), that interacts with the dynein complex dynein-Lis1-NudC, these last two also necessary for migration regulation, as seen in migratory defects induced by NudC RNAi (Cappello et al., 2011). The protein Lis1 promotes binding of dynein-1 with dynactin, as discussed previously (section 2.1 of this chapter) both dynein and Lis1 are required for centrosome movement (Tsai, et al. 2007). Importantly, the importance of the dynein protein complex is highlighted by the fact that mutations of their components are related to diseases associated with defective neuronal migration like lissencephaly, pachygyria and different kind of heterotopias (Alkuraya et al., 2011; Toyo-oka et al., 2003; Willemsen et al., 2012b).

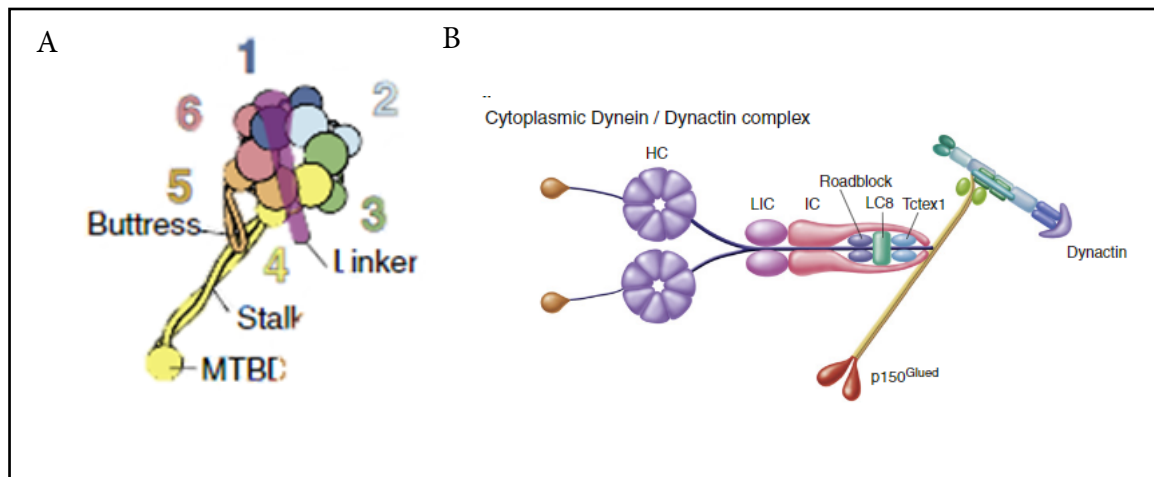


Figure 21. Dynein structure. A) Structure of the cytoplasmic dynein, showing the ATPase domain organized in a ring of 6 modules, the stalk and MT binding domain B) Dynactin is a dynein associated complex required for motor processivity, it is composed by multiple subunits (from Carter et al., 2016 and Hirokawa et al., 2010).

3.2 Kinesins

Kinesins are a diverse group of proteins composed by 45 members in mouse, which are divided into 16 subfamilies (For review, see Kalantari & Filges, 2020). They are characterized by three main domains: motor domain, containing the MT binding domain and an ATPase activity necessary for motility; a coiled coil domain associated with kinesin oligomerization and a tail domain that associates to cargoes directly or through the mediation of adaptor proteins (**Fig. 22**). Additionally, kinesins can influence MT dynamics in different ways (Kalantari & Filges, 2020).

Kinesins can be classified according to the location of the motor domain in the kinesin. The N-type are the most common kinesins, in which the motor domain is in the N terminal region of the protein and their motility is in direction to the plus end of the MTs. The C-type are kinesins in which the motor domain is in the C terminus (*Kifc1*, *Kifc2* and *Kifc3*), and differently from N-kinesins, they move to the minus end of the MTs. The third type of kinesin is the M-type (*Kif2a*, *Kif2b*, *Kif2c*), which are kinesins where the motor domain is in the central part of the protein, and their most important feature is their MT severing activity (Lawrence et al., 2004; Hirokawa et al., 2010). In the next sections I will first describe their regulatory mechanisms, and then their role in neuronal migration.

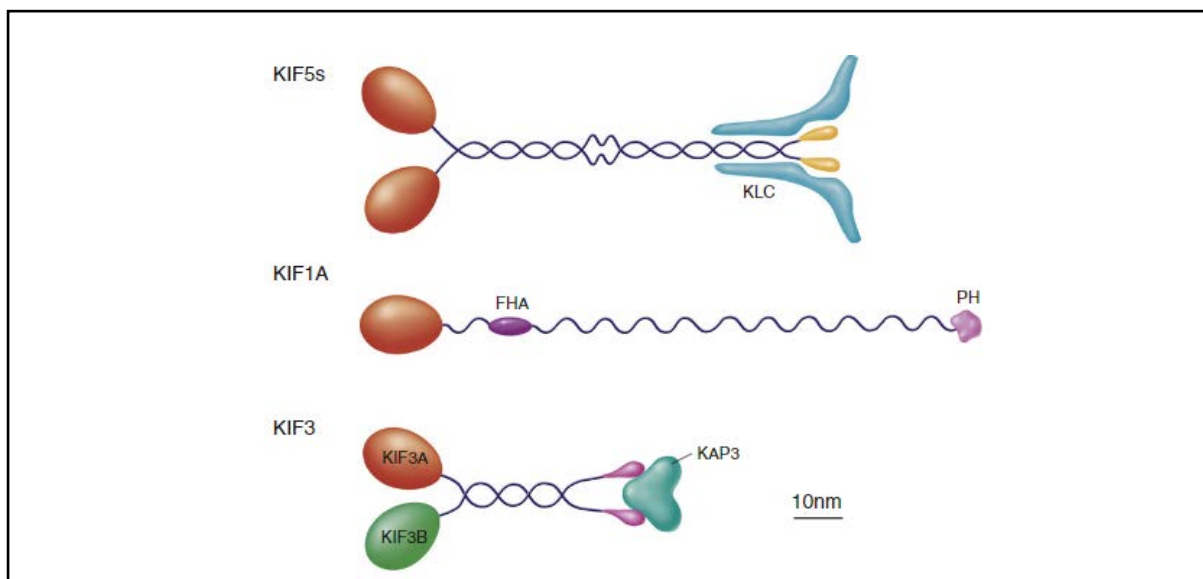


Figure 22. Kinesin superfamily proteins. Kinesins are constituted by three main domains: motor domain, coiled coil domain and a tail domain. They associate in oligomers of different numbers and depending on the kinesin, contain different features. It is shown as an example the heterotetrameric Kinesin 1 (KIF5C), the monomeric KIF1A and the homodimeric KIF3B (from Hirokawa, et al. 2010)

Kinesins activities need to be modulated in order to localize the protein at specific cell compartments, bind to specific cargoes, switch to activated/deactivated states, and exert influence on MT dynamics (Verhey & Hammond, 2009). Most kinesins work as functional processive motors by the formation of

oligomers, being dimeric forms the most common found. In the case of kinesin 1, however, it forms heterotetramers formed by two kinesin heavy chains (KHC) and two kinesin light chains (KLC) (Kuznetsov et al., 1988). For kinesin 3 motors, besides the homodimers forming members, there are some kinesins of this family that form heterotrimers (KIF3A, KIF3B, KAP) (Yamazaki et al., 1996). Moreover, kinesin 5 members form homotetramers to crosslink MT in anti-parallel orientations during mitotic spindle formation (Kashina et al., 1996; Alsabban et al., 2020; van den Wildenberg et al., 2008). Kinesins selectivity for specific MT tracks in the cell (for example those in axons or dendrites) can be explained in part by the PTMs decorating the MT and the MAPs associated to them. In the case of MAPs, it is known that they differentially give access to motors. In an *in vitro* study, it was seen that Tau, MAP2 and Dcx inhibit landing and motility of Kinesin 1 at the MT lattice, while the opposite can be seen for MAP7. Meanwhile, for kinesin 3, MAP7, MAP2 and tau are inhibitory, while Dcx, DCLK1 and MAP9 increase the kinesin processivity (Monroy et al., 2020)

3.2.1.- Kinesins regulatory mechanisms

3.2.1a- Kinesins inhibition

Kinesins can adopt auto-inhibited folded conformations that block their own activity when their function is not required in the cell, avoiding interaction with MT and unnecessary ATP hydrolysis. Autoinhibition is seen very often among kinesins, it was shown at least in members of the kinesin families 1, 2, 3, 4 and 7. It requires hinge domains in the coiled coil part of the protein in order to establish a folded conformation where the motor domain contacts the CC or the tail domains (Alsabban et al., 2020; Verhey & Hammond, 2009).

There are different ways to relieve autoinhibition, binding of a cargo is one of them, as described for KIF16B, of the family 3 of kinesins. Mutation of its PX domain in the tail, inhibits cargo binding and keeps KIF16B motor in a monomeric inactive state, while the normal WT KIF16B becomes a highly processive motor when dimerized upon cargo binding. This dimerization is dependent of the neck-coil (NC) segment, serving as a site of contact with the rest of the CC domain in autoinhibited state (Soppina et al., 2014). Also, from the family 3 of kinesins, KIF13B is activated upon partner binding, that in this case was identified as the human Disk Large protein (hDlg). After binding of hDlg with the stalk domain, KIF13B increases its ATPase activity by 10-fold (Yamada et al., 2007).

For kinesin 1, one of the ways in which it relieves its autoinhibition requires the association of the FEZ1 protein to the KHC tail domain and JIP1 to the KLC subunit to free the motor domain and induce the MT based motility (Blasius et al., 2007). Interestingly, in *Drosophila* neurons, it was studied that Kinesin-1 was differentially distributed depending on the conformation of the protein, being the autoinhibited form present in the dendrites, and the active conformation present in axons. Depletion

of the autoinhibited form disrupted dendrites development and cargo distribution, in this case Golgi outpost accumulated in the axon (Kelliher et al., 2018). Related to radial migration, JIP1, partner of the KLC subunit to relieve autoinhibition, is necessary for polarization during neuronal migration, as demonstrated by Deng, et al. (2014), that upon *JIP1* depletion by *in utero* electroporation in mouse, this produced severe defects in migration as a result of arrested migrating neurons in MP phase and further postnatal defects in Golgi distribution and axon extension (Deng et al., 2014).

KIF11 and CENPE (from the family 7 of kinesins), both possess autoinhibited conformations where the motor domain interacts with the terminal part of the tail domain. They require phosphorylation in the tail domain by MPS1 or CDK1 to induce the protein unfolding from the autoinhibited state with the subsequent increased association to the MT (Espeut et al., 2008). KIF3A, subunit of the heterotrimeric KIF3 complex, also hinders its activity by interaction of the motor with the tail domain, and phosphorylation in the tail domain by CaMKII produces conformational changes that lead to opening of the kinesin (K. Chen et al., 2018).

For KIF21A, from the family 4, it was demonstrated that mutations in its regulatory CC (rCC) domain are responsible for congenital fibrosis of the extraocular muscles type 1 (CFEOM1) (van der Vaart et al., 2013). The mutation R954W, found in patients with CFEOM1, was found to induce an increase in the processivity of Kif21a when observed in COS-7 cells. In addition to this, motor domain (MD) co-precipitated with the tail domain of the WT, but not with the mutated R954W tail (van der Vaart et al., 2013).

Besides autoinhibition, kinesins activity is stopped by the interaction with different partners. One example of this happens for many kinesins (families 2, 3, 8 and 12) that interact with the kinesin binding protein (KBP), expressed abundantly in brain. Disruption of KBP expression induces defects in neuronal development and is associated to syndromes that present neurological problems (Alves et al., 2010; Drerup et al., 2016; Lyons et al., 2008). KBP associates to the MT binding elements of the motor domain, preventing binding of the kinesin in the lattice (Atherton et al., 2020). Binding of KBPs regulates organelles transport and distribution, as it was seen by mitochondria or vesicles, where KD of KBP in cultured neurons induces increased vesicular anterograde transport associated to the release of the different inhibited kinesins (Wozniak et al., 2005; Kevenaar et al., 2016). In light of the importance of KBP in kinesin regulation, it is not surprising to notice that depletion of KBP in neurons by *in utero* electroporation in cortex induced migratory arrest in SVZ/IZ with defects in dendritic arborization and impaired axon extension, producing loss of neurons postnatally for increased apoptosis (Chang et al., 2019).

3.2.1b.- Cargo recruitment / release

Cargo recruitment to the kinesins involve different mechanisms, the most notorious are the use of cargo adapters and the recognition of specific phospholipids in vesicles. Regarding cargo adapters, for kinesin 1, its binding to Trk receptor needs involvement of Rab27b, S1p1 and CRMP-2. The assembly of this complex requires the activity of different signalling pathways (Arimura et al., 2009). Another case of cargo recruitment by protein complexes is the binding of melanosomes to KIF1B in zebrafish, in which protein kinase A (PKA) phosphorylates LC3B in order to recruit SKIP and bind the melanosome to the kinesin (Subramaniam et al., 2021).

The transport of different RNA species requires the interaction with specific adapters. One example of an adaptor that recruits mRNAs is the atypical tropomyosin Tm1-I, that assists the binding of *oscar* mRNA to kinesin-1 to transport it to the posterior pole of the *Drosophila* oocyte (Dimitrova-Paternoga et al., 2021). Another form of RNA association is through the binding of the RNA binding protein (RBP) SFQP, that associates neurotrophin-regulated transcripts to the kinesin 1 through the mediation of the adapter KLC1 in order to transport the RNAs along the axon (Fukuda et al., 2021). Of note, in cortex, SFQP levels are highly expressed during embryonic stages, and these levels decrease after postnatal stages. Moreover, when downregulating SFQP by *In Utero Electroporation* of a shRNA, radial migration is impaired and neurons that normally are in superficial layers, are located in deep layers of the cortex without showing defects in specification or survival (Saud et al., 2017).

For recognition to phosphoinositides, pleckstrin homology (PH) domains in KIF1A/KIF1B interact with membranes containing phosphatidylinositol-4,5-bisphosphate (PIP₂), while PX domain of KIF16B binds to phosphatidylinositol-3-bisphosphate (PI(3)P), which is important for interaction with early endosomes (Akhmanova & Hammer, 2010; Antón et al., 2021).

Cargo release can be regulated by different PTMs, like phosphorylation, an example of this is the interaction with kinases of the Jnk pathway, which are known to induce dissociation of KIP1 protein from the Kinesin 1 in *Drosophila* (Horiuchi et al., 2008). For KIF17 it was seen that the factor involved in kinesin-cargo dissociation is the calcium dependent protein CaMKII, that phosphorylates the tail region of the kinesin and regulates the release from NMDA containing vesicles. This mechanism of release is effective for synapse proteins required to be delivered upon the action potential (Guillaud et al., 2008).

Another way by which kinesins release their cargo in neurons is mediated by the recognition of GTP enriched plus ends at the MT, found mainly in proximity to dendritic spines. In this mechanism, KIF1A moves processively in the lattice until it finds the GTP enriched region at the tip, where it detaches,

with the subsequent delivery of cargoes that are required at the synapse, such as synaptophysin and the glutamate transporter vGlut1 (Guedes-Dias et al., 2019).

3.2.1c.- Regulatory functions in microtubule dynamics

Besides the canonical motor function, kinesins can exert a regulatory role in MT dynamics by influencing elongation, pausing or shrinking of the filament. Among the kinesins with this activity, there are some that only serve as MT remodelers and others that possess both remodelling and motor functions.

Kinesin 13 family (KIF2A, KIF2B, KIF2C), which members are unable to generate directed movement along the MT lattice, includes the most studied kinesins regarding MT destabilization (Mennella et al., 2005). Other kinesins, like KIF19A (family 8), which keeps motile activity, is also responsible for increasing MT catastrophes (D. Wang et al., 2016). These kinds of kinesins recognize and attach both ends of the MT filament, and when that happens, they use ATP hydrolysis in order to remove tubulin dimers, inducing the catastrophe events in the filament (Ohi et al., 2021; D. Wang et al., 2016).

For growth and stabilization of the MT, the processive kinesin CENPE (kinesin 7) is an important player that participates in kinetochore activity, since it is a kinesin that binds to the GTP enriched plus end of the MT and increasing growth rate by 2-fold (Drummond, 2011). KIF17 is another kinesin that stabilizes MT by acting at plus ends with proteins like EB1 and APC, interacting with those via the motor domain (Jaulin & Kreitzer, 2010).

Inhibiting shrinking/growth dynamics and providing with a pausing effect on the filament is the role that some kinesins, like KIF4, KIF21B and KIF18A, produce on the MT. In the case for KIF4A, this was shown important for stabilization of MT in the mitotic spindle and avoiding excessive growth that could produce defects on chromosome distribution, another function of these kind of kinesins is the control in the size of certain cellular structures, avoiding overgrowth (Sturgill & Ohi, 2013).

These examples show that kinesins localization, activity and cargo transportation are controlled at different levels to provide specific functions to these motor proteins. In addition, the non-canonical functions that many kinesins fulfil on MT dynamics are necessary to the correct functioning of the cell.

3.2.2.- Cortical malformations associated to kinesins dysfunctions

Kinesins, as an essential part of the MT cytoskeleton, are necessary for the correct development of the cerebral cortex. Their malfunctioning is responsible for many disabling diseases affecting cortex formation, such as microcephaly, lissencephaly, heterotopia or pachygyria. The multiple

malformations of cortical development (MCD) in which kinesins participate (**Table 3**) is a signature of the large variety of cellular processes in which they are involved.

Patients carrying mutations in the MT disassembling kinesin KIF2A present different phenotypes, including pachygyria, lissencephaly and microcephaly (Cavallin et al., 2017; Poirier et al., 2013), indicating an important role for the disassembly of MT in the regulation of human cortical development. Interestingly, some residues are more commonly mutated, such as p.His321 or p.Ser317, both found in the motor domain (Poirier et al., 2013).

The homotetrameric kinesin 5 (Eg-5, also called Kif11) participates in mitotic spindle regulation, an important process for progenitors' dynamics (Ferenz et al., 2010). In that regard, all the kinesin 5 mutations (truncations and missense mutations) are responsible for microcephaly at different degrees in 11 observed patients (Ostergaard et al., 2012). Interestingly, besides progenitors' regulation, kinesin 5 also participates in neuronal migration (next section). Another kinesin associated to mitotic spindle regulation and which malfunction is associated to microcephaly is CENPE (*KIF10*), in which a compound heterozygous mutation (D933N and K1355E) was the responsible for this phenotype in two siblings (Mirzaa et al., 2014).

Another interesting phenomenon is the variety of phenotypes that can be produced by mutations located in different parts of the same kinesin. This happens in KIF2A, where mutations in His321Asp produces a series of defects (heterotopia, pachygyria, microcephaly) different from the ones found in patients with the mutation in pSer317Asp (Lissencephaly, pachygyria), both located in the motor domain. These kinds of phenomena can be explained by different factors, including the relevance of different domains to different biological processes, the activity of other genes or environmental factors (Klingler et al., 2021; Kalantari & Filges, 2020).

A patient carrying an X-linked associated mutation in KIF4A presented with intellectual disability, the mutation was found to produce a truncated version of the kinesin. It was shown to be presented in an X linked recessive inherited manner, since 5 males in different generations were also affected (Willemsen et al., 2014). KIF4A as mentioned earlier, is expected to fulfil a role in MT pausing and stability.

Some kinesins affect corticogenesis in the stage of neuronal maturation, such as KIF7 and KIF1A (Barakeh et al., 2015; Cheon et al., 2017), both of them affecting among other things the development of the corpus callosum, the bundle of axons connecting both hemispheres and that is important in intra-cortical communication.

Taken together, these clinical studies show that kinesins work at the core of diverse biological processes required for corticogenesis, and hence, they are essential for the development of a cortex with a healthy function.

Table 3.- Kinesins affected in patients with cortical malformations				
Kinesin	Family	Malformations of cortical development	Mutation	References
KIF5C	1	Pachygyria Microcephaly	p.Glu237Val or p.Glu237Lys p.Glu237Val	Michels et al., 2017 Poirier et al., 2013
KIF14	3	Microcephaly	p.Gly459Arg or p.Ser841Phe	Makrythanasis et al., 2018
KIF1A	3	Thinning of corpus callosum and microcephaly	p.Thr258Met	Cheon et al., 2017
KIF4A	4	Intellectual disability, mild lissencephaly	Deletion in a splice site leading to skipping exon 15 of the protein	Willemsen et al., 2014
KIF7	4	Agenesis of corpus callosum Agenesis of corpus callosum and hydrocephaly	Homozygous truncating mutations	Barakeh et al., 2015 Putoux et al., 2011
KIF11	5	Microcephaly	7 truncating variants, 3 missense mutations in the motor domain, and 1 missense mutation in the C terminal tail	Ostergaard et al., 2012
KIF23	5	Microcephaly	p.LeuHis	Karaca et al., 2015
KIF10 (CENPE)	7	Microcephaly	Compound heterozygous mutation (p.Asp933Asn and p.Lys1355Glu)	Mirzaa et al., 2014
KIF6	9	Megalencephaly	p.Leu398Glnfs	Konjikusic et al., 2018
KIF26A	11	Subcortical band heterotopia	p.Gln455Arg	Jamuar et al., 2014
KIF26B	11	Microcephaly, ventriculomegaly, Schyencephaly	Biallelic loss of function mutations	Quian, et al. 2022
KIF2A	13	Heterotopia, pachygyria and microcephaly Pachygyria and microcephaly Lissencephaly, Pachygyria	p.His321Asp p. Ser317Asp pHis321Pro or p.Ser317Asn	Poirier et al., 2013 Poirier et al., 2013 Cavallin et al., 2017

3.2.3.- Participation of kinesins in radial migration

To understand how defective kinesins lead to the catastrophic diseases presented in the previous section, it is necessary to know the physiological cellular role in which they participate either in

progenitors, migrating neurons or neuronal maturation. Regarding this topic, the understanding of kinesins biology in cortical development is very limited, with just some kinesins studied (**Table 4 and figure 23**), but certainly, further work remains to be done.

Progenitor cells require a tight regulation of cell cycle and chromosome organization, a function in which at least 12 kinesins are involved (Kalantari & Filges, 2020). Some of the functions they carry are related with chromosomal organization, mitotic spindle formation and cytokinesis (Kalantari & Filges, 2020; Wordeman, 2010). For this reason, microcephaly is one of the most common MCD related to kinesins mutations, as can be noticed in table 3. This has been studied for example for Kif2a and Kif20b, for which mutation and KO respectively, increase the amount of cell death in progenitors and neurons, phenotypes that explain microcephaly in patients that carry mutations in those genes (Gilet et al., 2020; Janisch et al., 2013). For KIF1A, the KD by *in utero* electroporation of the shRNA induces decrease in the number of neurogenic divisions compared to the symmetric divisions producing Pax6+ cells (Carabalona, et al. 2016), which can lead to microcephaly as a result.

Besides defects in cell survival for Kif20b knock-out, there is aberrant neuronal migration after depletion of the protein by KD using *in utero* electroporation, characterized by inability of the cells to transition from MP to BP, additionally, distribution of Golgi is also disrupted in these neurons (Sapir et al., 2013). These results agree with studies where Kif20b mutations induce polarization defects in cultured cortical neurons (McNeely et al., 2017). Shootin 1, a protein that participates in induction of polarization by influencing PI3K distribution (Toriyama et al., 2006), was seen to be an important partner of Kif20b to regulate these phenotypes during migration (Sapir et al., 2013).

In addition to the phenotype in progenitors, KIF1A deficiency is responsible for an accumulation of neurons in MP phase at the SVZ/IZ, without affecting locomotor phase velocity or morphology. Nevertheless, arrested cells in MP phase presented with precocious expression of the mature neuronal marker Tbr1, a phenotype that was seen to be non-autonomous, dependent on the secretion of BDNF (Carabalona et al., 2016).

Being a protein for which mutations produce different phenotypes, it makes sense that Kif2a affects also neuronal migration, as it was shown also by Gilet, et al (2021), where they found defects in the transition from MP to BP neurons in the KI of the mutation p.His321His driven by Nex-Cre (Gilet et al., 2020). Adding complexity to Kif2a biology, three different isoforms, products of alternative splicing, are differentially expressed during cortical development. Out of the three isoforms, there are two that support radial migration, the one that does not participate misses 20 residues at the N terminal portion of the protein. Meanwhile, the two isoforms important for radial migration interact with mitochondrial proteins in more abundance than the non-participating, as seen in an interactome study (Akkaya et al., 2021).

Kinesin 5, previously seen to be mutated in patients with microcephaly, participates in the locomotion phase of migration. Upon depletion of Kinesin 5 by *in utero* electroporation of a shRNA, neurons migrate faster and protrude shorter leading process than the controls. Accordingly, when Kinesin 5 was over-expressed, neurons showed delayed migration with a larger leading process (Falnikar et al., 2011).

For neuronal maturation, the schizophrenia related Kif3b is involved in corpus callosum formation (Alsabban et al., 2020b), a feature altered in patients with the disease (Downhill et al., 2000). The mechanism responsible for this phenotype was found to be a decrease in dendritic spines and abnormal growth cone morphology (Alsabban et al., 2020).

Importantly, KIF13B's participation in neuronal migration was seen by KD in radially migrating neurons, finding that less cells are able to reach the cortical plate and that those cells present polarity defects with decreased axon extension. An interaction with myosin X, also participating in neuronal migration (Myosin section 1.2.1 in this chapter) was suggested as a mechanism involved in these defects (Yu et al., 2020).

Despite the high amount of evidence indicating the participation of kinesins in cortical development and their importance for human health, the mechanisms that these kinesins play in physiological roles are far from being elucidated, as can be noticed by the difference between the identified genes (**Table 3**) and the cellular roles attributed to them (**Table 4**).

Table 4.- Cellular mechanisms associated to kinesins and kinesins regulatory proteins that participate in corticogenesis		
Kinesin	Family	Model studied and phenotypes
Kif3b (Alsabban et al., 2020)	2	KD.- Decreased corpus callosum thickness due to growth cone and dendritic spines defects
KIF13B (Yu et al., 2020)	3	KD.- Decrease in cells reaching the cortical plate and defective polarity.
KIF1A (Carabalona et al., 2016)	3	KD and mutation p.R18W expression induce failure in MP-BP transition. It also presented decrease in neurogenic divisions in progenitors
KIF11 (Kinesin 5) (Falnikar, 2011)	5	KD.- increases velocity in neuronal migration
Kif20b (Janisch et al., 2013; Sapir et al., 2013)	6	KO.- Increased apoptosis in progenitors KD.- Neuronal migration arrest in IZ due to defects in MP-BP transition and neuronal polarization
Kinesin 6 (Falnikar et al., 2013)	9	KD.- arrest of MP neurons in the IZ -

Kif26a Quian, et al. 2022	11	KD.- Migration arrest with defective MP-BP transition
Kif2a (Gilet et al., 2020)	13	cKI of the mutation p.His321Asp with Nex-Cre.- decreases MP-BP transition and shows increased cell death in IPs and neurons
Kif2a isoforms (Akkaya et al., 2021)	13	KD and rescue with Kif2a.1, Kif2a.2 and Kif2a.3 isoforms: Isoforms Kif2a.1 and Kif2a.2 participate in migration.
KIF1C (Muralidharan et al., 2022)	14	KD.- Decrease in average speed and directionality of neurons.
Kinesin regulatory proteins	Regulatory role	Model studied and phenotypes
KBP (Chang et al., 2019)	Binds to motor domain to inhibit kinesins activity	KD.- Migration arrest with postnatal defects in dendritic arborization and axon extension.
JIP1 (Deng et al., 2014)	Binds to KLC subunit of Kinesin 1 to relieve autoinhibition	KD.- Migration arrest in MP phase with postnatal defects in polarization, Golgi distribution and axonal extension.
SFPQ (Saud et al., 2017)	Adapter between kinesin-1 and neurotrophin regulated transcripts	KD.- Neuronal mis-localisation.

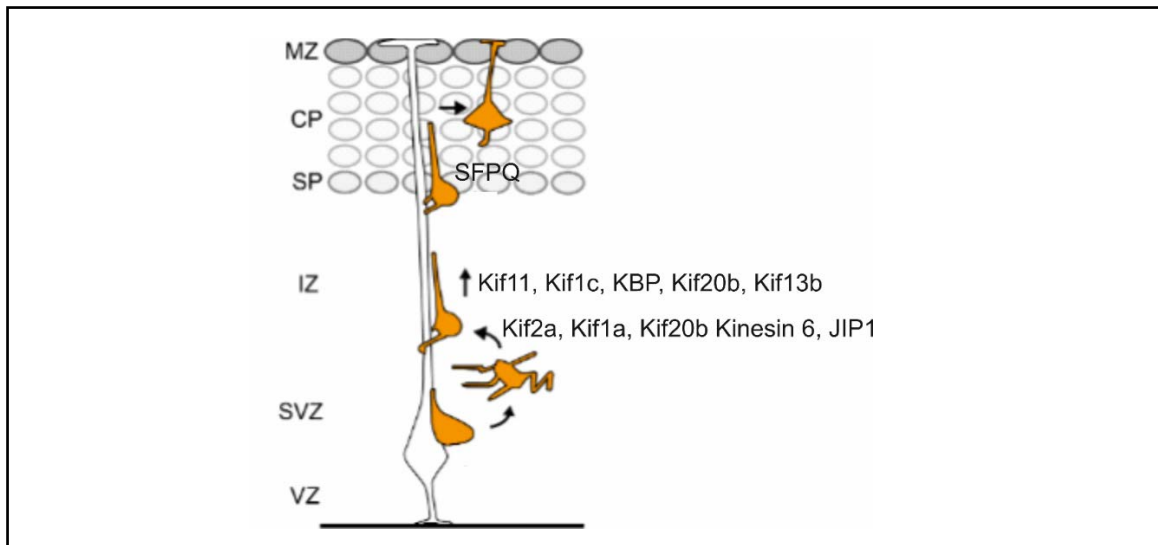


Figure 23.- Kinesins regulating neuronal migration. Kinesins and kinesin related proteins studied regarding their role in the different phases of neuronal radial migration (Modified from Hansen & Hippenmeyer, 2020)

4. Kif21b

Kif21b is a plus end directed kinesin belonging to the family 4 of kinesins and it is expressed in brain, spleen and testes; its gene localizes on the chromosome 1 and expresses a protein of 1637 aa. Its closest relative is Kif21a, sharing 61% of identity and expressed in most tissues. Both of them form homodimers, nevertheless, they were not found to form heterodimers between them (Marszalek et al., 1999; van Riel et al., 2017). In brain, Kif21b is expressed in neurons, and first studies in hippocampal neurons initially described it as a kinesin for which expression was restricted to dendrites (Marszalek et al., 1999), but further work revealed that it is actually present in all neuronal compartments, including dendrites, axon and soma (Ghiretti et al., 2016).

Kif21b is composed of three main domains those being the motor domain, containing the ATPase activity and MT binding site; the coiled coil domain, that is divided in different subdomains, being CC1, CC2 and rCC; and the tail domain, composed of seven consensus WD-40 repeats (**Fig. 24**). Besides the MD, there are two other additional sites of MT interaction, being those in the CC2 domain (residues 696-1163) and in the WD40 domain (1236-1624) (van Riel et al., 2017). These additional MT binding sites are not well understood, but it is known that the one in the WD40 domain is used by Kif21b to switch from MT filaments with anti-parallel orientation in dendrites (Masucci et al., 2021).

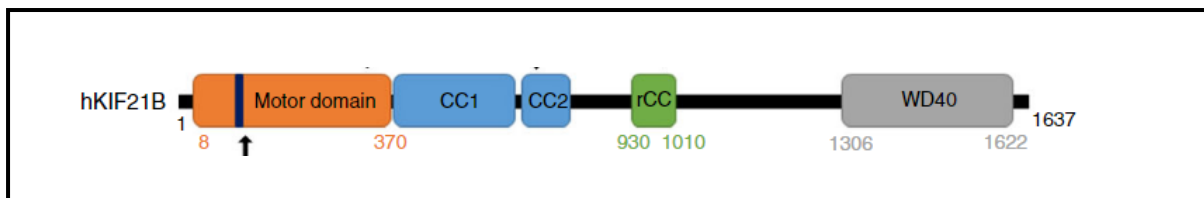


Figure 24. Structure of Kif21b with its main domains and subdomains. In orange it is depicted the motor domain, with the ATP binding domain; in blue, the subdomains CC1 and CC2; in green, the rCC, responsible for regulation of auto-inhibition; and in grey, the WD40 domain (Asselin, et al. 2020).

Besides the classical cargo transport role, it has been shown *in vitro* and *In vivo* that Kif21b regulates MT length and stability (Muhia et al., 2016; Ghiretti et al., 2016; van Riel et al., 2017). Furthermore, it participates in cell signalling in dendritic spines to regulate their morphology during long term depression in hippocampal neurons (Morikawa et al., 2018)

4.1 Neurotransmitter receptors regulation

Most of the studies related to Kif21b in CNS have been centred in adult hippocampus, specifically on the regulation of dendritic length, as well as dendritic spines morphology and functionality. Part of

these regulatory mechanisms on dendrites come from the fact that Kif21b drives the trafficking of different neurotransmitter receptors and controls MT dynamics.

Regarding the neurotransmitter regulation, it was seen that Kif21b interacts with different subunits of the GABA_AR receptor in cultured neurons, and after the KD of Kif21b, there was a decrease of the GABA_AR γ 2 receptor expression at the cell surface, specifically at the extra synaptic sites (Labonté et al., 2014). Something similar happens regarding the subunit GluN2B of the NMDA receptor (glutamate receptor), where Kif21b KO neurons presented less surface receptor than their WT counterpart, and the effect was dependent on the membrane protein trafficking neurobeachin (NBEA), which interacts with Kif21b (Gromova et al. 2018).

To elucidate how Kif21b exerts its function in the neurons, some interacting partners have been identified, among them, some endosomal trafficking related proteins, such as Neurobeachin (NBEA), Rab4 and Rab7, indicative of the role of Kif21b in vesicular traffic (Morikawa et al., 2018; Gromova et al., 2018). About the specific cargoes of Kif21b, it was seen that the Tyrosine receptor kinase B (TrkB) is transported by Kif21b together with its ligand BDNF, transporting it mainly in a retrograde manner in dendrites (Ghiretti, et al. 2016). Mitochondria is another target related to Kif21b, since its transport duration is reduced in Kif21b KO neurons, nevertheless, a more direct relationship is missing (Muhia, et al. 2016). Therefore, there is few information concerning the cargoes transported by Kif21b.

Cell signalling is another point of control where Kif21b exerts regulation. Kif21b was shown as a mediator of dendritic spines shrinking in response to Long Term Depression (LTD) by internalization of the GluR2 subunit of AMPA receptors. The mechanism described for this spine remodelling is through the fusion of Kif21b containing vesicles with ELMO/Dock1 containing vesicles, bringing the fused vesicles outside of the spine. This exit inactivates Rac1 GTPase in the spine, remodelling actin-cytoskeleton through Pak1 (Morikawa et al., 2018).

The described molecules and cell processes regulated by Kif21b in adult brain have as a consequence the regulatory activity on behavioural aspects in mouse, such as memory acquisition in a fear conditioning test (Muhia et al., 2016), which is impacted negatively in KO mouse where the dendrites and dendritic spines length is decreased; and social interaction, where the Kif21b KO mouse possesses dysfunctional dendritic spines with a concomitant decrease in social recognition (Gromova et al., 2018) or defective fear extinction due to problems in LTD (Morikawa et al., 2018).

4.2.- Regulation on microtubules dynamics

As described for other kinesins in previous sections, Kif21b possesses a dual role of motor protein and MT dynamics regulating kinesin. However, despite the fact that most studies describe Kif21b as a MT

pausing protein, there is controversy about the activity of Kif21b as an inducer of catastrophes (**Table 5**).

Ghiretti, et al observed in experiments of MT *in vitro* that incubation of the filaments with the full length (FL) Kif21b increased the number of catastrophes, but at the same time, increased the growth of the filament. This effect was replicated by addition of only the C terminal tail of the kinesin (residues 657-1624), being the binding domain to the MT mainly at the plus tip ending. In line with this, they also observed that MT dynamics, as measured by EB3-GFP comet lifetime, were increased upon Kif21b silencing in hippocampal neurons, indicating a modulating (stopping) role for Kif21b with respect to the MT (Ghiretti et al., 2016).

Accordingly, Muhia, et al saw by EB3-mCherry tracking experiment in HeLa cells, that the overexpression of Kif21b, the truncated 1-620 and an immotile version (mutated in the residue T96N) produced a decrease in the size of MT length, and that the FL but not the truncated construct (1-620) induced an increase in the number of MT catastrophes (Muhia et al., 2016).

To investigate more deeply the role of Kif21b in MT dynamics, Van Riel et al observed in EB3-GFP assays in COS-7 cells, that the FL protein transfection led to a decrease in MT growth, and it accumulated in the plus-end tips of the MT filaments, in contrast to the MD-CC1 part of the protein alone, that does not decrease growth or accumulate on the tips. *In vitro* experiments to look for MT growth revealed two things: one is that when Kif21b reached the tip of the MT, the filament stabilizes and stops growing, and the second phenomenon that happens is the increase in MT catastrophes upon arrival at the plus-end tip. Another observation they made is that velocity of the kinesin increases from 0.63 $\mu\text{m/s}$ to 1.23 $\mu\text{m/s}$ in HeLa cells when truncating the tail domain (using just the MD-CC1 domains) (van Riel et al., 2017).

In a similar way, it was shown that Kif21b is required in T cells to shorten the size of the MT, required to reposition the centrosome during immunological synapse formation. It was seen that upon Kif21b KO in T cells, the MT were overgrown, and the centrosome failed to localize in the region of the immunological synapse, a phenotype rescued by induction of catastrophes by incubation with viniblastine (Hooikaas et al., 2020).

Supporting Kif21b MT pausing activity, Massucci, et al observed that addition of recombinant FL or MD stabilizes the filament by decreasing MT growth rate. Interestingly, they also observed that upon increasing Kif21b FL concentration, both the growth rate and catastrophe frequency decreased with increasing concentration (from 5 nm to 50 nm). Additionally, they saw that in dendrites, where the MT have mixed polarity, the Kif21b tail domain is necessary to switch from different filaments (Masucci et al., 2021).

Some discrepancies have been found regarding Kif21b localization and function on the MT. Van Riel, et al and Hooikas, et al showed that binding to the plus-end induces a pausing effect, while Ghiretti, et al (2016) although the authors also found this binding to the plus-end, they associated it with increased catastrophes. Massucci, et al (2021), on the other hand, observed that binding of Kif21b to the lattice stabilized the MT, but not by binding to the plus-end.

To understand the reason of the discrepancies coming from these studies, it is necessary to analyse the conditions in which the experiments are done, including cell system used, buffer conditions, protein concentration, among others, in order to interpret the results, as it is the case for Massucci, et al, where increased Kif21b has a differential effect on MT, increasing MT catastrophes.

Table 5.- MT dynamics influenced by Kif21b				
Reference	Activity on Microtubules			
	Stabilization	Increase in growth rate	Catastrophe inducer	Binding to plus end
Muhia, et al. 2016	-	- (KD)/+(KO)	+	NS
Ghiretti, et al. 2016	-	+	+	+ for catastrophe induction
Van Riel, et al. 2017	+	-	+	+ for stabilization
Hooikas, et al. 2020	-	-	+	+ for catastrophe induction
Massucci, et al. 2021	+	-	+	-

+ : positive influence, - : negative influence NS : Not seen

4.3 Kif21b structural regulation

In previous sections it was explained how autoinhibition is essential for kinesins physiology, maintaining a balance between activated/inactivated motors. This is also the case for kinesins of the family 4, including Kif21b and its closest relative Kif21a, as it was described in section 3.2.1a of this chapter.

Importantly, the region responsible for autoinhibition in Kif21a is conserved in Kif21b, as structural studies show where the rCC (residues 931-1010 in Kif21b) domain forms an antiparallel coiled coil in order to allow interaction with the MD-CC1 with the rest of the CC domain. It was reported that *in vitro*, the MD-CC part of Kif21b (containing rCC) by itself fails to interact with the MT, nevertheless, after the deletion of the rCC, the MD-CC was able to bind to MT (van Riel et al., 2017).

The ubiquitin E3 ligase TRIM3 regulates the velocity of Kif21b in a function independent of protein degradation. It was seen that upon *Trim3* KO, the speed of Kif21b (coupled to fluorescent protein mCherry) was reduced from 1.4 $\mu\text{m/s}$ to approximately 0.5 $\mu\text{m/s}$, with a subsequent increase in the number of stationary particles. In a yeast two hybrid experiment, it was seen that Trim 3 binds Kif21b in the CC domain (residues 401-1100) (Labonté et al., 2014).

Another interesting fact of Kif21b is that in dendrites, where MT polarity is mixed, it possesses a bias to retrograde transport, using MT where the plus end is pointing towards the soma. However, the direction of transport can switch, as it was shown in *in vitro* experiments and in neurons. This MT switch was seen to be dependent on the tail domain, since the MD by itself cannot perform this switching activity (Massucci; et al. 2021).

4.4.- KIF21B in human health

The role of Kif21b has been mainly associated as a locus of risk for development of multiple sclerosis and Alzheimer Disease (AD) (Goris et al., 2010). Related to AD, it was seen that KIF21B is 5 times more expressed in patients with AD than in patients without dementia, mainly in people below 62 years of age (Kreft et al., 2014). In addition, KIF21B was recently identified as a gene of risk associated to Parkinson disease (PD) with a missense mutation in the tail domain (p.A1079T) and one in the motor domain (p.R211C) in patients with late onset of the disease (symptoms starting around 60 years old) (Gialluisi et al., 2021).

There is very limited information relating Kif21b to neurodevelopment, being the only study of Kannan et al., 2017 showing that the Kif21b KO mouse shows microcephaly at adult stages, with the presence of a thinner corpus callosum than its WT counterpart. Nevertheless, studies addressing Kif21b function during cortical development are missing and the relationship between Kif21b and neuronal migration (since Kif21b is a neuronal protein) needs to be addressed.

AIMS OF THE PROJECT

Factors controlling radial migration of pyramidal neurons, including extracellular molecules, receptors, cell adhesions and signaling pathways, converge to instruct changes in MT and actin cytoskeletons happening during radial migration. Kinesins are MT motor proteins for which dysfunctions are implicated in many malformations of cortical development with disabling outcomes in the patients that suffer from them. Therefore, it is necessary to uncover the physiological and pathological mechanisms in which these kinesins participate to drive brain cortex formation.

For this reason, we decided to study Kif21b, a kinesin expressed in neurons, with important roles in neuronal plasticity in the adult brain and microtubules dynamics, but for which roles during embryonic development were not studied before this project. Hence, the aims of this project were the following:

1) Elucidate the importance of KIF21B for human cortex development.

To achieve this objective, I studied the role of pathological variants present in patients with cortical malformations and intellectual disabilities. Using the mouse as a working model, I over-expressed by *In utero* electroporation the KIF21B versions present in patients with the aim to study defects in radial migration and associated mechanisms that induce abnormal development of the cortex. Importantly, I was able to elucidate from different lines of evidence that regulation by relieve in autoinhibition of Kif21b is impaired in pathological condition. Among the main factors observed supporting this are the following: 1) WT protein is unable to rescue the phenotype, indicating a gain of function of the protein, 2) Kif21b lacking the rCC domain (involved in autoinhibition) induces migratory delay, 3) Immotile versions of the mutant proteins are unable to produce the defective migration. These results can be found in Asselin, et al. 2020 and Narayanan, et al. 2022

2) Study the mechanisms involved in radial migration during physiological conditions

Knowing that Kif21b regulates neuronal migration during cortical development, I studied the mechanisms involved in radial migration during physiological conditions by depleting the expression of *Kif21b* in neurons. To dissect the different functions of the protein during the process, this project had the aim to address in detail the Kif21b regulatory domains participating during neuronal migration. Another objective of this project was to define the stages of migration in which Kif21b is involved by studies using *time-lapse* microscopy. The information provided by this approach allowed me to discover regulatory mechanisms and go deeper into them. Another aim of this project, the elucidation of the cellular mechanisms in which Kif21b participates during migration, was clarified by the observation that motility of the kinesin is dispensable for migration. While studying the interactions of Kif21b with other proteins by mass spectrometry, I discovered actin as the main interacting protein, an association unseen previously for kinesins. Then I aimed to go deeper into the

nature of this actin-Kif21b interaction and the importance of its role for neuronal migration. Furthermore, I described that the depletion of Kif21b produces defects in actomyosin contraction during radial migration.

RESULTS

ARTICLE 1:

Mutations in the KIF21B gene cause neurodevelopmental disorders through imbalanced canonical motor activity

Laure Asselin, José Rivera Alvarez, Solveig Heide, Camille S. Bonnet, Peggy Tilly, Hélène Vitet, Chantal Weber, Carlos A. Bacino, Kristin Baranaño, Anna Chassevent, Amy Dameron, Laurence Faivre, Neil A. Hanchard, Sonal Mahida, Kirsty McWalter, Cyril Mignot, Caroline Nava, Agnès Rastetter, Haley Streff, Christel Thauvin-Robinet, Marjan M. Weiss, Gladys Zapata, Petra J. G. Zwijnenburg, Frédéric Saudou, Christel Depienne, Christelle Golzio, Delphine Héron & Juliette D. Godin

My contribution to this work consisted in the elucidation of the mechanisms leading to defective pyramidal neuronal migration upon expression of three KIF21B missense variants found in patients with intellectual disability and neurodevelopmental disorders. I found through different approaches that mutations of KIF21B lead to defects in autoinhibition, inducing excessive activity of the protein. In line with this hypothesis, expression in neurons of the mutant versions of KIF21B truncated in the ATP binding domain, and hence, devoid of motility, are no longer able to induce migratory defects.

ARTICLE



<https://doi.org/10.1038/s41467-020-16294-6>

OPEN

Mutations in the *KIF21B* kinesin gene cause neurodevelopmental disorders through imbalanced canonical motor activity

Laure Asselin^{1,2,3,4}, José Rivera Alvarez^{1,2,3,4,20}, Solveig Heide^{5,6,7,20}, Camille S. Bonnet^{1,2,3,4,20}, Peggy Tilly^{1,2,3,4}, Hélène Vitet⁸, Chantal Weber^{1,2,3,4}, Carlos A. Bacino^{9,10}, Kristin Baranaño¹¹, Anna Chassevent¹¹, Amy Dameron¹², Laurence Faivre^{13,14}, Neil A. Hanchard⁹, Sonal Mahida¹⁵, Kirsty McWalter¹², Cyril Mignot^{5,6,7,16}, Caroline Nava^{5,16}, Agnès Rastetter¹⁶, Haley Streff^{9,10}, Christel Thauvin-Robinet^{13,17}, Marjan M. Weiss¹⁸, Gladys Zapata¹⁰, Petra J. G. Zwijsen¹⁸, Frédéric Saudou⁸, Christel Depienne^{1,2,3,4,16,19}, Christelle Golzio^{1,2,3,4}, Delphine Héron^{5,6,7} & Juliette D. Godin^{1,2,3,4}✉

KIF21B is a kinesin protein that promotes intracellular transport and controls microtubule dynamics. We report three missense variants and one duplication in *KIF21B* in individuals with neurodevelopmental disorders associated with brain malformations, including corpus callosum agenesis (ACC) and microcephaly. We demonstrate, in vivo, that the expression of *KIF21B* missense variants specifically recapitulates patients' neurodevelopmental abnormalities, including microcephaly and reduced intra- and inter-hemispheric connectivity. We establish that missense *KIF21B* variants impede neuronal migration through attenuation of kinesin autoinhibition leading to aberrant *KIF21B* motility activity. We also show that the ACC-related *KIF21B* variant independently perturbs axonal growth and ipsilateral axon branching through two distinct mechanisms, both leading to deregulation of canonical kinesin motor activity. The duplication introduces a premature termination codon leading to nonsense-mediated mRNA decay. Although we demonstrate that *Kif21b* haploinsufficiency leads to an impaired neuronal positioning, the duplication variant might not be pathogenic. Altogether, our data indicate that impaired *KIF21B* autoregulation and function play a critical role in the pathogenicity of human neurodevelopmental disorder.

A list of author affiliations appears at the end of the paper.

The development of the mammalian cerebral cortex depends on microtubule (MT)-related processes that coordinate birth, migration and differentiation of excitatory and inhibitory neurons. MT cytoskeleton acts in concert with microtubule associated proteins (MAP) and motor proteins to promote the structural changes that underlie key developmental events such as neurogenesis, migration, neuritogenesis, axon pathfinding and synapse formation. Kinesin superfamily proteins (KIFs) are important molecular motors that control MT organization and dynamics in both axons and dendrites and mediate intracellular transport of various cargo, including vesicles, organelles, cellular proteins and mRNAs, along MTs^{1,2}. The importance of both the force-generating and MT-regulating functions of KIFs for brain development has become evident with loss of function studies demonstrating defects in mitosis^{3–9}, cytokinesis^{10,11}, polarity³, migration^{12–14}, axonal growth and branching^{14–18}, survival¹⁹ and synaptogenesis^{20–24}. Further reflecting the key role of KIFs in neuronal development, variants in human KIF-encoding genes (*KIF4A*²⁴, *KIF7*^{25–28}, *KIF11*²⁹, *KIF2A*^{30–32}, *KIF5C*^{24,28,30,33}, *KIF1A*^{28,34}, *KIF6*³⁵, *KIF14*^{11,36,37}, *KIF26A*²⁸) have been associated with various neurodevelopmental disorders, including malformation of cortical development (MCD), acrocallosal syndrome, ciliopathies, epilepsy and intellectual disability. Most KIF variants have been predicted to be highly pathogenic in silico but their direct implication in disease and the underlying pathophysiological mechanisms have only been elicited for only a few of them^{11,26,35,38}.

The MT-plus-end directed kinesin-4 motor KIF21B is mainly expressed in spleen, testes and central nervous tissues and is particularly enriched in neurons^{39,40}. Within neurons, KIF21B is present in both axons and dendrites and especially abundant in growth cones^{40,41}. KIF21B has dual functions in neurons. First, it promotes intracellular transport through its N-terminal processive motor activity^{21,42–44}. However, except for BDNF-TrkB signaling endosomes⁴⁴, 2-subunit-containing GABAA receptor⁴⁵ and neurobeachin recycling endosomes⁴³, our knowledge of KIF21B-transported cargoes is very limited. Second, KIF21B influences MT dynamics through distinct MT binding domains^{21,42,44}. KIF21B positively regulates MTs dynamicity in dendrites by favoring MT growth and catastrophes^{21,44}. In addition, in vitro studies demonstrate that KIF21B can also act as a MT pausing factor by accumulating at the MT-plus ends⁴². Notably, KIF21B functions can be modulated by neuronal activity, which favors KIF21B trafficking activity at the expense of MT dynamics regulatory function⁴⁴ as well as through an auto-inhibitory interaction between the N-terminal motor domain and an internal regulatory coiled-coil region (rCC)^{42,46}.

KIF21B homozygous knockout (KO) mice display severe morphological abnormalities including microcephaly and partial loss of commissural fibers⁴⁷, cognitive deficits^{21,43,48} and altered synaptic transmission^{21,23}. Together with the reduced dendritic complexity and spines density observed in KIF21B^{−/−} neurons in culture²¹, these results highlight a critical role for KIF21B in brain development and function. Though, there are no clear KIF21B-related neurodevelopmental disorders, a duplication of the locus bearing KIF21B has been found in individuals with neurodevelopmental delay and intellectual disability (ID)⁴⁹.

Here we provide the evidence of a causal relationship between variants in KIF21B and neurodevelopmental disorders. We report the identification of three missense variants and one truncating variant in patients with neurodevelopmental delay and brain malformations including corpus callosum (CC) agenesis (ACC) and microcephaly. By combining in vivo modeling tools, we show that KIF21B pathogenic variants impede neuronal migration and connectivity through at least two distinct mechanisms both leading to dysregulation of canonical kinesin motor activity.

Taken together our data suggest that KIF21B is a novel gene for ID associated with heterogeneous brain morphological anomalies.

Results

Identification of human KIF21B variants. Using trio whole-exome sequencing, we identified a de novo variant (NM_001252100.1, c.2032A>C, p.Ile678Leu) in the KIF21B gene in a first patient (P1) presenting with developmental delay, learning and motor disabilities, associated with isolated complete agenesis of the corpus callosum (ACC) (Fig. 1a, e, Table 1, Supplementary Note 1). Through the GeneMatcher platform⁵⁰, variants in KIF21B were found in three additional patients. Patient 2 (P2) (NM_001252100.1, c.937C>A, p.Gln313Lys) presented with severe ID associated with microcephaly (Fig. 1b, f); patient 3 (P3) (NM_001252100.1, c.3001G>A, p.Ala1001Thr) presented with global developmental delay and mild to moderate ID (Fig. 1c) but normal brain structure at the MRI. This variant was inherited from the father, who presented with developmental delay and learning difficulties; and patient 4 (P4) (NM_001252100.1, c.2959_2962dup, p.Asn988Serfs*4) presented with mild developmental delays and hypotonia, but no brain structural anomalies on brain MRI (Fig. 1d, g). The three identified KIF21B missense variants occur within highly conserved residues positioned in the motor domain (NM_001252100.1, c.937C>A, p.Gln313Lys-P2), the regulatory coiled-coil (rCC) region (NM_001252100.1, c.3001G>A, p.Ala1001Thr-P3), and the coiled-coil domain (NM_001252100.1, c.2032A>C, p.Ile678Leu-P1) (Fig. 1h, Supplementary Fig. 1a–c). The fourth variant is a duplication (NM_001252100.1, c.2959_2962dup, p.Asn988Serfs*4-P4) that leads to the introduction of a premature termination codon in exon 20. RT-qPCR analysis and sequencing of KIF21B transcripts isolated from P4's blood revealed haploinsufficiency, likely due to the degradation of the mutant mRNA by nonsense-mediated decay (Supplementary Fig. 1d, e). All variants were predicted pathogenic by commonly used in silico software (Polyphen-2, Mutation Taster, SIFT and CADD; Supplementary Fig. 1f) and co-segregated with the phenotype in each pedigree (Fig. 1a–d). Of note, we found two other de novo variants of unknown significance in patients: one hemizygous variant in ARHGAP4 (chromosome X) in P1 that also segregated in his healthy brother and one de novo in UBR3 (NM_172070.3, c.5023G>C; p.Glu1675Gln) in P4, that showed a weak pathogenic score based on in silico predictions. None of the four KIF21B variants is reported in public databases, including dbSNP, 1000 Genomes and gnomAD. Overall, we identified variants in KIF21B gene in four patients presenting with mild to severe neurodevelopmental delay associated with heterogeneous brain malformations (Table 1, Supplementary Note 1).

Kif21b expression is restricted to neurons. We first examined the expression pattern of Kif21b in the mouse developing cortex. Although levels of Kif21b mRNA transcripts are rather stable during development (Fig. 2a), protein expression tends to increase from embryonic day (E) 12.5 to postnatal day (P) 2 (Fig. 2b). mKif21b transcripts were mostly observed in the cortical plate (CP) and almost entirely excluded from the ventricular (VZ) and sub-ventricular (SVZ) zones, where progenitors and newborn neurons reside (Supplementary Fig. 2a). As corticogenesis proceeds, mKif21b mRNAs accumulated in the intermediate zone, which is enriched in growing axons (Supplementary Fig. 2a). Immunolabeling of E12.5 to E18.5 embryo brain sections showed a restricted expression of mKif21b proteins to postmitotic compartments of the neuronal epithelium with a particularly intense signal in the axon-rich zone

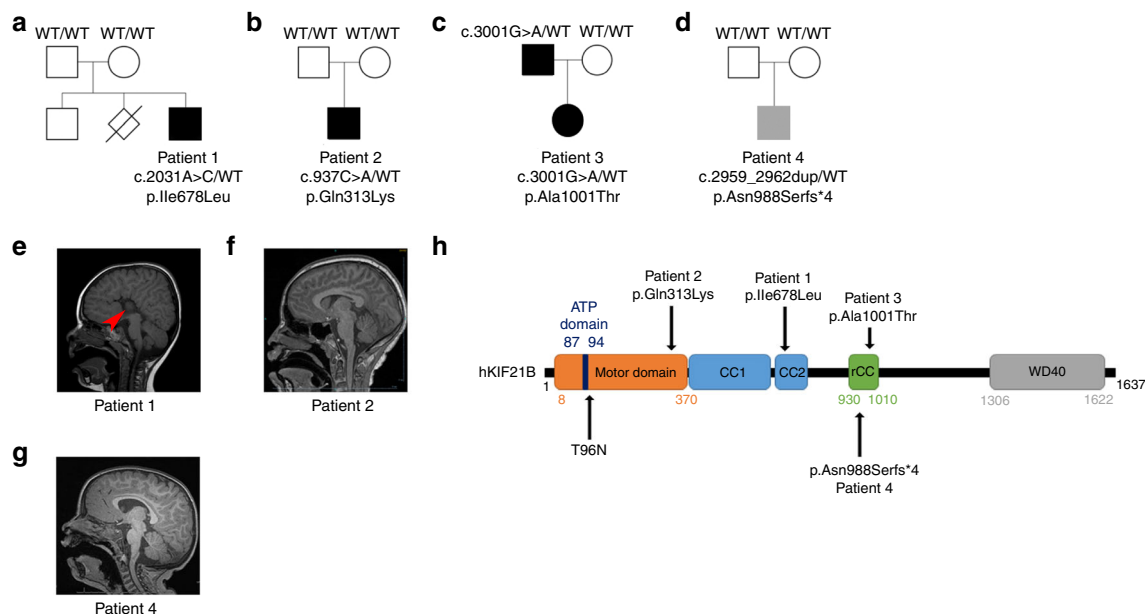


Fig. 1 Patients with *KIF21B* variants. **a–d** Pedigrees of patients with identified *KIF21B* variants. **e–g** Sagittal brain section of patient's MRI showing a complete agenesis of the corpus callosum in patient 1 (**e**, red arrow) and microcephaly in patient 2 (**f**). **h** Schematic representation of the human *KIF21B* (hKIF21B) protein indicating the different domains (motor domain, ATP binding site, coiled-coil domain (CC) 1 and 2, regulatory coiled-coil domain (rCC) and WD40 domain) and the position of the mutated amino acids for patient 1 (p.Ile678Leu), 2 (p.Gln313Lys), 3 (p.Alala1001Thr) and 4 (p.Asn988SerfsX4). T96N substitution that abolishes *KIF21B* mobility is also depicted.

(Fig. 2c and Supplementary Fig. 2b, c). mKif21b staining specificity was validated by the absence of labeling in *Kif21b* knockout brain sections at birth (Supplementary Fig. 2e, f). Further immunostainings with antibodies against mKif21b and β III-Tubulin or Tbr2 that label neurons and intermediate progenitors respectively, confirmed that Kif21b is exclusively expressed in post mitotic neurons at all stages of development (Fig. 2c, d and Supplementary Fig. 2b, c). To undoubtedly exclude any expression of Kif21b in progenitors, we analyzed mKif21b protein in progenitor (YFP[−]; CD24[−]) and neuron populations (YFP⁺; CD24⁺) isolated from Rosa26-lox-STOP-YFP; NEX^{CRE/+} E16.5 cortices by fluorescent-activated cell sorting. No Kif21b protein was detected in cortical progenitors by immunoblotting (Supplementary Fig. 2d). Although Kif21b was previously thought to be mainly localized to dendrites⁴⁰, our data suggest an axonal localization in the developing cortex (Supplementary Fig. 2b). To ascertain the axonal distribution of mKif21b, we used a 2-chambers microfluidic device to analyze separately the axons from cell bodies and dendrites⁵¹ (Fig. 2e, f). Channels separating both chambers are 450- μ m-long so only axons from neurons located in the proximal compartment can reach the distal chamber⁵¹. Immunolabelings of mouse primary cortical neurons with Kif21b and Tau antibodies in these devices confirmed the expression of Kif21b in Tau-positive axons and its accumulation at the axonal tips (Fig. 2e, f). Kif21b is thus moderately but stably expressed in both dendrites and axons of postmitotic neurons from early to late corticogenesis.

***KIF21B* variants impair migration of projection neurons.** To evaluate the pathogenic nature of *KIF21B* variants, we assessed the consequences of overexpressing hKIF21B variants on neuronal migration using in utero electroporation (IUE) in mice. Given that KIF21B is a post mitotic kinesin, we used plasmids allowing expression of human KIF21B under the control of the NeuroD promoter (NeuroD-hKIF21B). Transfection in N2A neuroblastoma cell line showed even expression of wild-type (WT) and all three missense hKIF21B variants by western blot, suggesting that

p.Gln313Lys, p.Ile678Leu and p.Alala1001Thr missense variants are unlikely to affect the production, stability or turnover of the hKIF21B proteins (Supplementary Fig. 3a). Consistently, cycloheximide chase experiments in N2A cells revealed a similar half-life of WT and mutant hKIF21B proteins (Supplementary Fig. 3b).

To investigate the effects of the variants on neuronal positioning, we individually induced neuron-specific expression of the hKIF21B mutants using IUE of NeuroD-hKIF21B constructs together with a NeuroD-IRES-GFP reporter plasmid in mouse embryonic cortices at E14.5. Four days after IUE, whereas most of the GFP⁺ postmitotic neurons expressing full-length WT-hKIF21B reached the CP as in the control (Fig. 3a), neurons expressing missense variants accumulated in the intermediate zone, with a decrease of 27.7%, 60.3% and 23% of the cells reaching the upper CP in the p.Gln313Lys, p.Ile678Leu and p.Alala1001Thr conditions, respectively (Bonferroni adjusted $P = 0.0001$) (Fig. 3b). Noteworthy, hKIF21B missense variants likely disturbed neuronal migration in a cell-autonomous manner as their expression did not affect cell survival and glia scaffold integrity (Supplementary Fig. 3c). To assess the functional consequences of the p.Asn988Serfs*4 protein truncated variant (Supplementary Fig. 1d), we silenced mKif21b specifically in post mitotic neurons using IUE of CRE-dependent inducible shRNA vector⁵² together with a NeuroD-CRE-IRES-GFP construct at E14.5. Efficacy of the two shRNAs was confirmed by RT-qPCR (−61.4% for sh-Kif21b #1, −45.1% for sh-Kif21b #2) (Supplementary Fig. 3d). Four days after IUE, *Kif21b*-silenced neurons displayed migration defects compared to control shRNA-electroporated cells with a reduction of 23.5% and 32.2% of cells distributed in the upper CP for sh-Kif21b #1 and sh-Kif21b #2, respectively (Supplementary Fig. 3e, f). To note, the migratory phenotype induced by sh-Kif21b #2 was fully recovered by co-electroporation of wild-type NeuroD-mKif21b construct (Supplementary Fig. 3e, f). Most of the cells overexpressing the p.Gln313Lys and p.Alala1001Thr mutants or silenced for *Kif21b* showed a correct positioning with nearly all cells found in

Table 1 Clinical summary of patients with *hKIF21B* variants.

	Patient 1	Patient 2	Patient 3	Patient 4
Age at last evaluation	10 y	12 y 1 m	9 y	3 y 8 m
Sex	Male	Male	Female	Male
Genetics				
Gene	KIF21B	KIF21B	KIF21B	KIF21B
NM_001252100.1	c.2032A>C	c.937C>A	c.3001G>A	c.2959_2962dupGCCA
HGVs protein	p.Ile678Leu	p.Gln313Lys	p.Ala1001Thr	p.Asn988Serfs*4
nomenclature				
Inheritance	De novo	De novo	Inherited from the affected father	De novo
Pregnancy and delivery				
Pregnancy	Normal	Oligohydramnios and IUGR	Normal	Small for gestational age
Height (perc)/weight (perc)/head circumference (perc) at birth	51 cm (97th p), 3.750 kg (97th p), 33 cm (15th p)	49 cm (49th p), 2.584 kg (7th p), 32 cm (5th p)	3.480 kg (50th p)	46.4 cm (7th p), 2.633 kg (5.87th p), *34 cm (25th p) *Measurements done at age 6 days
Neonatal findings	None	Nuchal cord at birth and was blue, mild respiratory distress, but discharged with mother	None	Feeding issues, NG tube
Developmental stages				
Age of sitting (months)	10	Does not	14	9
Age of walking (months)	18	Does not	24	15–16
Language delay	Yes	Yes	Yes	No
Age of first words (m: months, y: years)	36 m		36 m	12 m
Age of first sentences (m: months, y: years)	NA		N/A	24 m
Current language ability	Short sentences, dysarthria	Non-verbal	Sentences	Short sentences
Intellectual disability (ID)	Borderline	Severe	Mild to moderate	Mild
Estimated level of ID (mild, moderate, severe)				
Age at evaluation (y)	10 y		9 y	
Total IQ	66–79 (WISC V)		54–59 (WISC V)	
Clinical examination				
Age at examination (years)	5 y	12 y 1 m	3 y 9 m	3 y 8 m
Height (SD)/weight (SD)/head circumference (SD)	118 cm (+1.5), 21.3 kg (+2), 52 cm (+0.5)	139 cm (−1.3), 20 kg (−3.4), 48.5 cm (−3.9)	99 cm (−1.1), 17.8 kg (+1.8), 49.6 cm (−0.2)	90.7 cm (−1.67), 16.3 kg (+0.09), 50.7 cm (+0.72)
Neurologic examination	Slow	Poor visual fixation, constant tongue thrusting, poor gag, poor head control, bilateral ankle tightness, right wrist contracture	Mildly hypertonic legs	Hypotonia
Dysmorphic features	Plagiocephaly	Large eyes, fleshy ears, hypertelorism	Epicanthic folds, mild ptosis, tented upperlip	Upslanting palpebral fissures, prominent eyebrows, broad nose with bulbous tip, anteverted nares, Micrognathia. Right-sided Duane syndrome
Brain imaging (MRI)				
Age at examination (m: months, y: years)	3 y	6 m and 12 y	2 y	1 y 9 m
Brain anomalies (MRI)	Complete agenesis of the corpus callosum	Normal	No structural abnormalities, myelination not completed yet. Normal differentiation white and gray matter. No focal lesions. Normal spectroscopy	A few scattered punctate foci of T2 prolongation in subcortical white matter and periventricular white matter of bilateral cerebral hemispheres with no associated restricted diffusion or hemorrhage
Other				History of falling spells with normal EEG. Severe constipation, Central sleep apnea, History of feeding issues requiring G tube

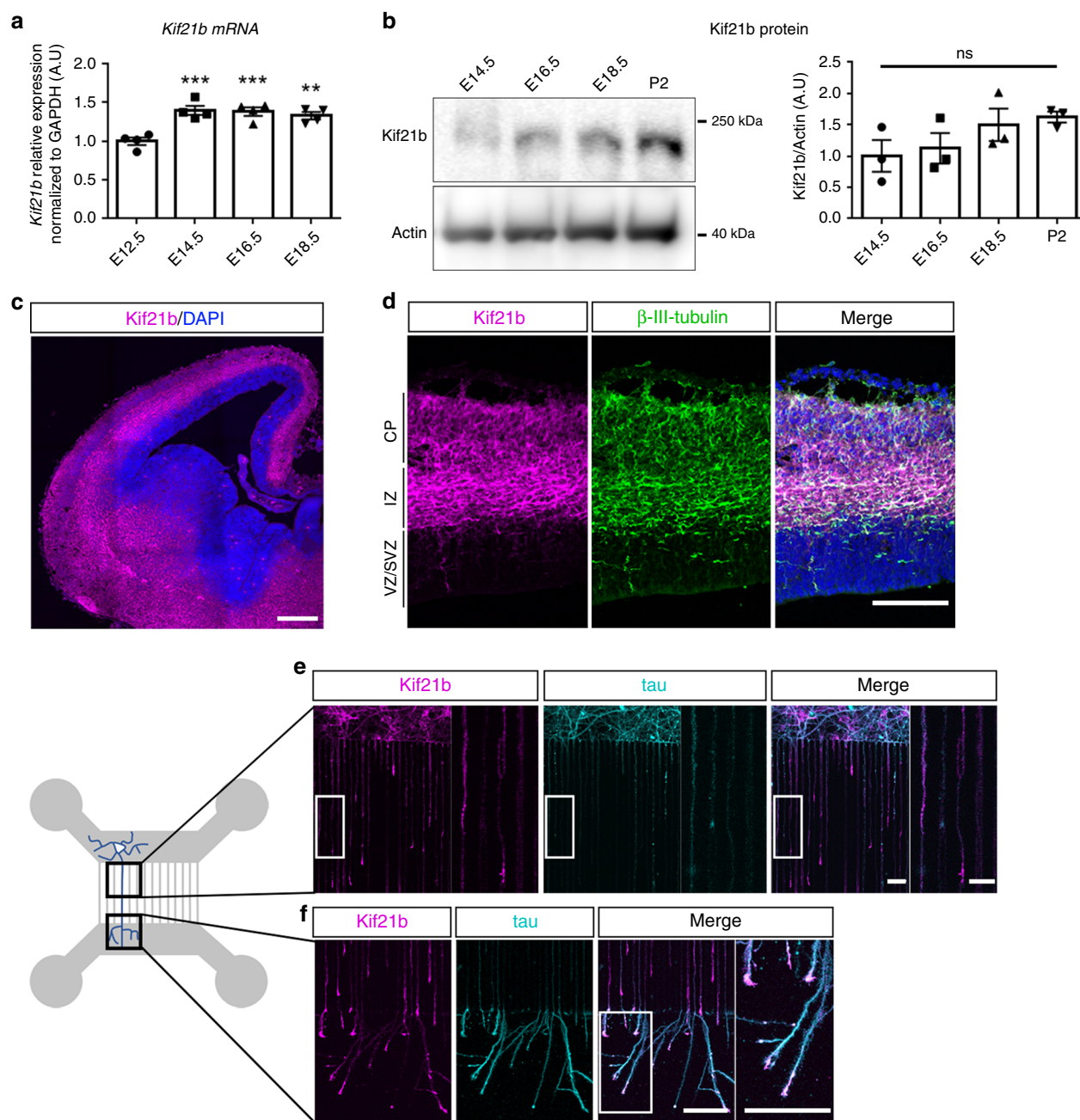


Fig. 2 *Kif21b* expression in mouse developing cortex. **a** RT-qPCR analyses showing expression of *Kif21b* transcripts in mouse cortices at different embryonic stages (from E12.5 to E18.5) ($n = 4$ brains per stage). **b** Western blot analyses of mouse cortical extracts showing similar expression of Kif21b protein from E14.5 to P2 ($n = 3$ brains per stage). **a, b** Data are represented as means \pm S.E.M. Significance was calculated by one-way ANOVA (Bonferroni's multiple comparisons test), ns non-significant; $^{**}P < 0.005$; $^{***}P < 0.001$. **c, d** E14.5 mouse forebrain coronal sections immunolabelled for Kif21b (magenta) and β -III-tubulin (neuronal marker, green) and counterstained with DAPI (blue) showing that Kif21b expression is restricted to post mitotic neurons. **e, f** Left panel: schematic representation of a 2-compartments microfluidic chamber. Cortical neurons (in cyan) plated in the upper chamber (gray) grow their axons through 450- μ m-long microchannels. The length of the microchannels allows axons but not dendrites to reach the lower chamber. Right panel: immunolabeling of Kif21b (magenta) and tau (axonal marker, cyan) on mouse primary cortical neurons at DIV5 in microdevices showing expression of Kif21b in axons (**e**) with an enrichment in growth cones (**f**). CP cortical plate, IZ intermediate zone, SVZ subventricular zone, VZ ventricular zone. Scale bars, (**c**) 250 μ m and (**d-f**) 100 μ m, magnifications (**e, f**) 20 μ m. Source data are provided in the Source Data file.

the upper layer of the cortex after birth, indicating a delay in migration rather than a permanent arrest (Fig. 3c, d, Supplementary Fig. 3g, h). By contrast, the p.Ile678Leu variant induced a permanent migration defect as a large number of p. Ile678Leu-expressing neurons remained in the white matter and deep-layers at P2 (Fig. 3c, d). Remarkably, p.Ile678Leu-expressing

projection neurons permanently arrested in the white matter were expressing the upper-layer marker Cux1, which supports a faulty migration rather than specification defects (Fig. 3e). Altogether, these results demonstrate that missense hKIF21B variants and *Kif21b* haploinsufficiency impede, to various extents, the radial migration of projection neurons.

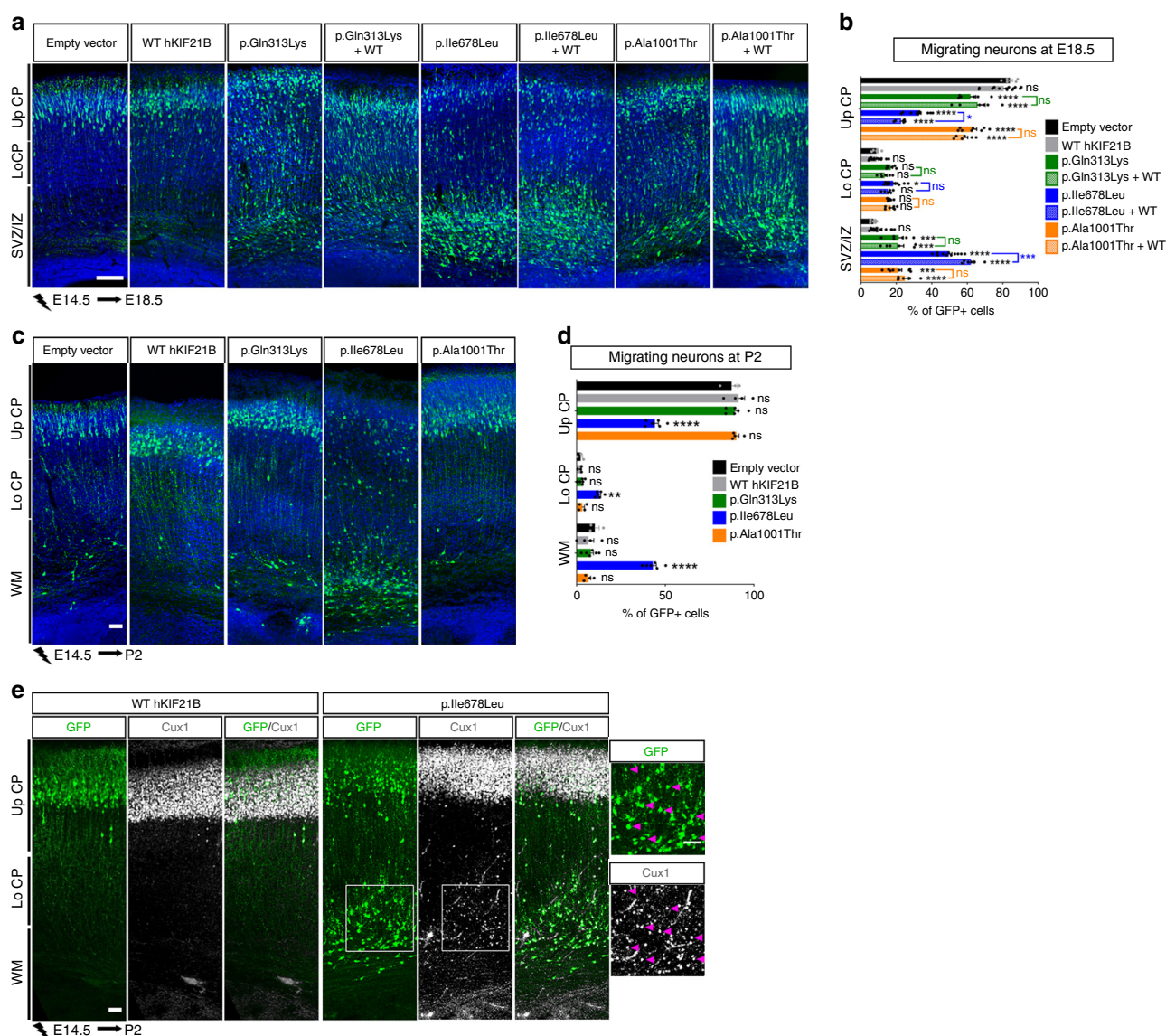
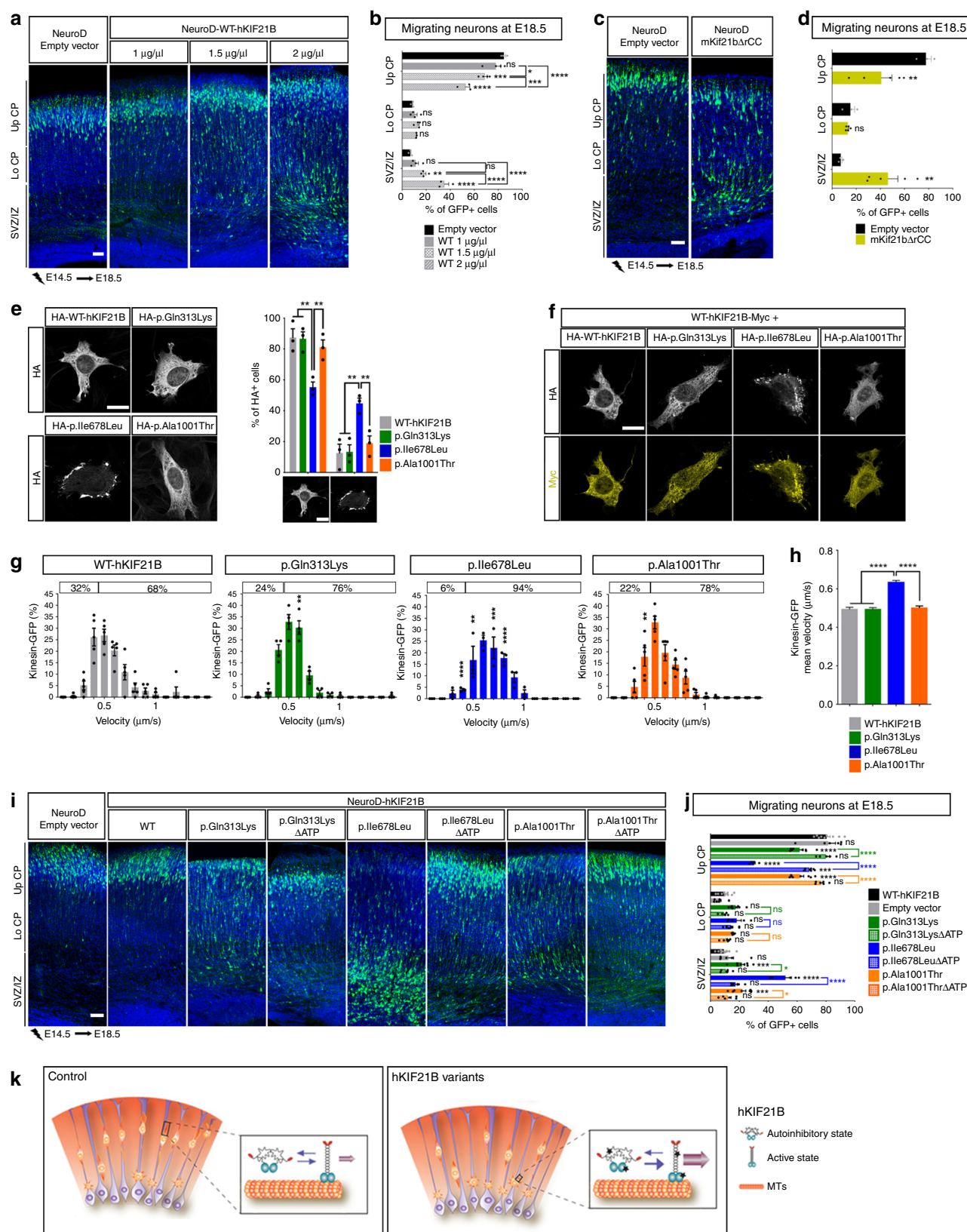


Fig. 3 Expression of hKIF21B missense variants induces abnormal neuronal migration. **a, c** Coronal sections of E18.5 (**a**) or P2 (**c**) mouse cortices electroporated at E14.5 with NeuroD-IRES-GFP empty vector (1 μ g/ μ L) or WT, p.Gln313Lys, p.Ile678Leu or p.Ala1001Thr NeuroD-hKIF21B or co-expressing WT-hKIF21B together with mutated hKIF21B constructs (ratio 1:1). GFP-positive electroporated cells are depicted in green. Nuclei are stained with DAPI. **b, d** Analysis (means \pm S.E.M.) of the percentage of electroporated GFP-cells in different regions (Up CP: upper cortical plate, Lo CP: lower cortical plate, IZ: intermediate zone, SVZ: subventricular zone) showing effect of expressing hKIF21B variants. Data were analyzed by two-way ANOVA (Bonferroni's multiple comparisons test). Number of embryos analyzed: **b** Empty vector, $n = 6$; WT, $n = 13$; p.Gln313Lys, $n = 6$; p.Ile678Leu, $n = 11$; p.Ala1001Thr, $n = 8$. Rescue experiments: $n = 6$ for each condition. **d** Empty vector, $n = 3$; WT, $n = 4$; p.Gln313Lys, $n = 6$; p.Ile678Leu, $n = 6$; p.Ala1001Thr, $n = 4$. ns non-significant; * $P < 0.05$; ** $P < 0.005$; *** $P < 0.001$; **** $P < 0.0001$. **e** Cux1-immunolabeling (gray) of P2 coronal sections of mouse brains electroporated at E14.5 with the WT or p.Ile678Leu NeuroD-hKIF21B constructs showing no specification defects of arrested neurons (green). Scale bars (**a, c, e**) 50 μ m. Source data are provided in the Source Data file.

KIF21B variants lead to aberrant KIF21B motility activity. To understand the molecular mechanisms by which variants in hKIF21B gene lead to defective radial migration, we tested for restoration of the hKIF21B variant-induced phenotype by increasing amount of wild-type protein. IUE of wild-type hKIF21B together with hKIF21B mutants at a 1:1 ratio failed to rescue the migration phenotype (Fig. 3a, b). Strikingly, neurons overexpressing large amount of WT-hKIF21B (2 units of NeuroD-hKIF21B) failed to reach the upper CP 4 days after IUE (Fig. 4a, b). Collectively, these results raise the possibility that hKIF21B variants impair migration by enhancing KIF21B activity in a dominant manner. One possible mechanism by which hKIF21B mutants might exert this effect is by relieving

autoinhibition imposed by the rCC to the motor domain as shown for CFEOM-causing variants in KIF21A^{46,53,54}, a kinesin-4 family member that shares 61% identity with KIF21B⁴⁰. Consistent with the hypothesis that KIF21B hyperactivation cause migration phenotypes, expression of a truncated mouse mKif21b protein that lacks the rCC domain (1 unit of NeuroD-mKif21b Δ rCC) led to faulty migration (Fig. 4c, d).

To test whether identified variants alter KIF21B autoinhibition, we next sought to explore the functions of KIF21B that were enhanced by KIF21B autoinhibition release in mutant conditions. Given the processive activity of KIF21B, we assessed the effect of the variants on KIF21B motility activity. Using immunofluorescence, we first compared the localization of the wild-type (WT)



and the three missense mutant proteins in ST cells transfected with pcDNA-HA-hKIF21B cDNA constructs (Fig. 4e, Supplementary Fig. 4a). Although WT, p.Gln313Lys and p.Ala1001Thr proteins showed similar diffuse cytoplasmic localization, the p.Ile678Leu KIF21B protein tended to form aggregates localized

mainly at the periphery of the cells, suggesting an enhanced motility toward the plus end of the microtubules (Fig. 4e). To note, WT and all mutant proteins showed similar distribution in soma and neurites when overexpressed in primary cortical neurons (Supplementary Fig. 4c). Interestingly, in 100% of the

Fig. 4 hKIF21B variants induce abnormal migration through enhanced KIF21B motor activity. **a, c, i** Coronal sections of E18.5 cortices, 4 days after IUE with the indicated NeuroD-IRES-GFP constructs. GFP-positive electroporated cells are depicted in green. Nuclei are stained with DAPI. **b, d, j** Percentage (means \pm S.E.M.) of electroporated cells in upper (Up CP) and lower (Lo CP) cortical plate, intermediate (IZ) and subventricular zone (SVZ), showing the effect of increasing (**b**) amount or (**d**) activity of hKIF21B and (**j**) contribution of the processive activity to the phenotype. Data were analyzed by two-way ANOVA (Bonferroni's multiple comparisons test). Number of embryos analyzed: **b** Empty vector and WT 2 $\mu\text{g}/\mu\text{L}$, $n = 3$; WT 1 and 1.5 $\mu\text{g}/\mu\text{L}$, $n = 4$; **d** $n = 3$ for each condition; **j** Empty vector, $n = 9$; WT, $n = 6$; p.Gln313Lys, $n = 8$; p.Ile678Leu, $n = 5$; p.Alal001Thr, $n = 8$; p.Gln313Lys Δ ATP, $n = 5$; p.Ile678Leu Δ ATP, $n = 8$; p.Alal001Thr Δ ATP, $n = 6$. **e** Immunolabeling of ST cells transfected with indicated HA-tagged hKIF21B constructs showing impaired localization of p.Ile678Leu variant. Histogram (means \pm S.E.M.) represents the percentage of cells with a diffuse versus an impaired localization of the HA-tagged proteins. Data were analyzed by two-way ANOVA (Bonferroni's multiple comparisons test). Number of cells analyzed: WT, $n = 467$; p.Gln313Lys, $n = 429$; p.Ile678Leu, $n = 540$; p.Alal001Thr, $n = 387$; from three independent experiments. **f** Immunolabeling of ST cells transfected with the indicated Myc- and HA-tagged hKIF21B constructs showing that the p.Ile678Leu variant alters the localization of the WT protein. **g, h** Live imaging of Cos7 cells transfected with the indicated GFP-tagged hKIF21B constructs. Histograms (means \pm S.E.M.) represent (**g**) velocities distribution and (**h**) mean velocities. 20–32 cells from 3–5 independent experiments were analyzed by (**g**) two-way ANOVA or (**h**) one-way ANOVA (Bonferroni's multiple comparisons test). Total number of particles analyzed: WT, $n = 203$; p.Gln313Lys, $n = 182$; p.Ile678Leu, $n = 195$; p.Alal001Thr, $n = 237$. ns non-significant; * $P < 0.05$; ** $P < 0.005$; *** $P < 0.001$; **** $P < 0.0001$. Scale bars: (**a, c, i**) 50 μm ; (**e, f**) 20 μm . **k** Model: WT KIF21B switches between an autoinhibition and an active (purple arrows) state. hKIF21B variants (marked by a star) conformation favors the active state. KIF21B hyper-motility (pink arrow) leads to migration defects. Source data are provided in the Source Data file.

ST cells where the p.Ile678Leu variant is mislocalized, the cellular localization of the WT protein is altered, suggesting that the p.Ile678Leu protein might act as a dominant negative protein (Fig. 4f). In accordance, the p.Ile678Leu variant is competing with the WT protein to form KIF21B homodimer. Indeed, anti-Myc immunoprecipitation on extracts from HEK293T cells expressing myc-tagged WT, HA-tagged WT and WT or p.Ile678Leu GFP-tagged hKIF21B proteins revealed that the binding of the Myc and HA-tagged WT proteins was affected by the expression of the p.Ile678Leu missense variant (Supplementary Fig. 4d). We further analyzed the processivity of mutant hKIF21B in Cos7 cells transfected with GFP-tagged hKIF21B constructs (Supplementary Fig. 4b). Live-cell imaging revealed a shift of GFP-hKIF21B velocity toward high speed for all variant proteins compared to the WT protein (Fig. 4g). Notably the p.Ile678Leu variant showed a more drastic effect with an increased average velocity of 28% compared to the WT protein (Fig. 4h). We next assessed the effect of hKIF21B variants on the trafficking of BDNF vesicles and mitochondria, two potential cargoes of KIF21B^{21,44}. Fast videomicroscopy experiments performed in Cos7 cells transfected with WT and mutant pcDNA-HA-hKIF21B cDNA (Supplementary Fig. 4b) and BDNF-mCherry or Mito-RFP constructs did not reveal any change in the dynamics of neither BDNF-mCherry-containing vesicles (Supplementary Fig. 4e–g) or mitochondria (Supplementary Fig. 4h, i), suggesting that hKIF21B variants might lead to excessive motility of other unidentified cargoes. Collectively, these data indicate that the variants enhanced KIF21B processive activity through lessening of the kinesin autoinhibition.

We finally tested the effect of expressing immotile hKIF21B mutant proteins on neuronal migration. We performed IUE of truncated WT and mutant hKIF21B that lacks the ATP binding domain (Fig. 1h) in wild-type E14.5 mouse cortices. Although a significant number of neurons expressing the p.Gln313Lys, p.Ile678Leu and p.Alal001Thr hKIF21B variants were trapped in the IZ at E18.5, most of the cells expressing the immotile variants (NeuroD-p.Gln313Lys- Δ ATPhKIF21B, NeuroD-p.Ile678Leu- Δ ATPhKIF21B, NeuroD-p.Alal001Thr- Δ ATPhKIF21B) showed a correct distribution (Fig. 4i, j, Supplementary Fig. 3a), demonstrating that preventing the motility of the mutant proteins decreases the severity of the migration phenotype. These results confirmed that the mutant protein impairs radial migration at least by enhancing KIF21B motility activity through the release of the kinesin autoinhibition (Fig. 4k). Collectively, our data indicate that modulation of kinesin autoregulation is critical in KIF21B-associated cortical migration phenotypes.

KIF21B p.Gln313Lys variant reduced head size in zebrafish.

Considering the presence of microcephaly in the subject with p.Gln313Lys variant, we asked whether this mutant could induce head size defects in an appropriate animal model. We therefore turned toward the developing zebrafish embryo, a model that has been extensively used for microcephaly modeling, the measure of head size being a relevant proxy for brain size⁵⁵. drKIF21B protein is broadly distributed in zebrafish larval brain at 5 days post-fertilization (dpf), a stage characterized by strong upregulation of *drKIF21B* transcripts (Supplementary Fig. 5a, b). Larvae injected with p.Gln313Lys human mRNA showed a significant and physiologically relevant reduction of head size compared to control at 5 dpf (–6%, Welch two sample *t*-test $P = 1.185 \times 10^{-9}$), therefore exhibiting a phenotype analogous to the microcephaly observed in the human clinical condition (Fig. 5). By contrast, introduction of WT mRNAs or the two other missense variants (p.Alal001Thr and p.Ile678Leu), that do not lead to head circumference defects in patients, barely affected zebrafish head size (Fig. 5, Supplementary Fig. 5c, d). These data suggest that this particular p.Gln313Lys variant in the motor domain of KIF21B likely drives the microcephaly phenotype observed in the individual carrier.

p.Gln313Lys KIF21B variant does not impair proliferation.

We next sought to understand the mechanisms by which the p.Gln313Lys variant impairs brain size. Expression of hKIF21B missense variants in mouse cortical neurons did not induce cell death (Supplementary Fig. 3c), excluding the possibility that the microcephaly phenotype arises from a poor survival of neurons. Although KIF21B expression is restricted to neurons, we further tested whether expression of the p.Gln313Lys variant could non-cell autonomously affect the progenitors' biology. We performed IUE of NeuroD-p.Gln313Lys hKIF21B at E14.5 in wild-type cortices and analyzed the progenitors located in the electroporated area at E16.5. The total number and the proliferative fraction (Ki67⁺) of both apical (Pax6⁺) and intermediate progenitors (Tbr2⁺) were indistinguishable from control condition (Supplementary Fig. 5e–j), suggesting that the brain size phenotype induced by the p.Gln313Lys hKIF21B variant was unlikely to have arisen from impaired neurogenesis. Altogether these results suggested that neither impaired birth nor poor survival of neurons or their progenitors contributed to the microcephaly phenotype observed in the subject with the p.Gln313Lys variant.

p.Ile678Leu hKIF21B variant expression impedes axonogenesis.

The corpus callosum (CC), the major commissure connecting

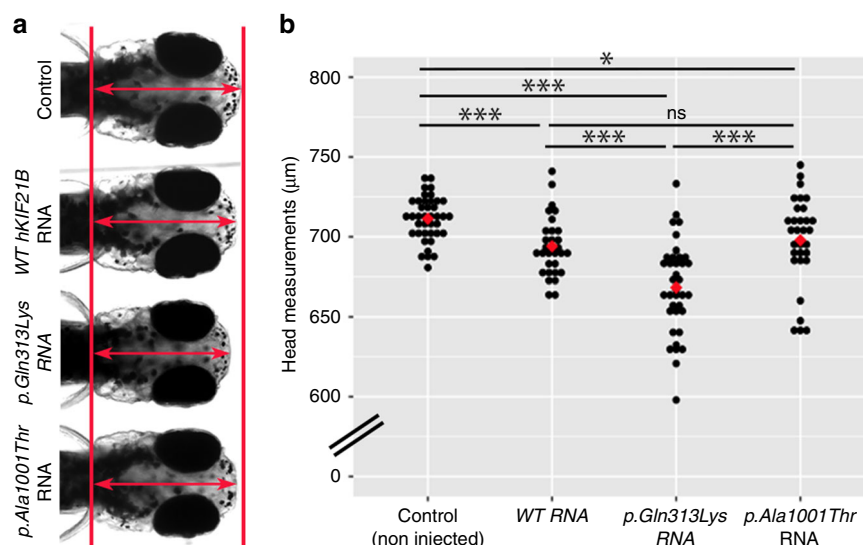


Fig. 5 Expression of p.Gln313Lys hKIF21B decreases head size in zebrafish larvae. a Dorsal view of representative control zebrafish larvae (non-injected) or injected with 100 pg of wild-type (WT) or mutated *hKIF21B* mRNAs (p.Gln313Lys and p.Ala1001Thr) at 5 days post-fertilization (5 dpf). Double arrow indicates the distance between the forebrain and hindbrain, a measure used as a proxy for head size. **b** Dot plot of the head measurements (red double arrow) of control and injected larvae at 5 dpf. Red diamond corresponds to the mean of the batch measured. Number of embryos analyzed for this specific batch: control, $n = 40$; WT, $n = 31$; p.Gln313Lys, $n = 38$; p.Ala1001Thr, $n = 31$. Experiments were repeated six times for non-injected control embryos ($n = 231$), four times for WT-injected embryos ($n = 127$), three times for p.Gln313Lys-injected embryos ($n = 108$) and four times for p.Ala1001Thr-injected embryos ($n = 158$). ns, non-significant, $*P < 0.05$, $**P < 0.005$, $***P < 0.001$. Significance was calculated by unpaired two-tailed Student's *t*-test or a Welch's two sample *t*-test between control and RNA-injected larvae. ns non-significant, $*P < 0.05$, $**P < 0.005$, $***P < 0.001$. Source data are provided in the Source Data file.

the two cerebral hemispheres, is formed of hundreds of millions of axons projecting contralaterally from the callosal projection neurons. Callosal axons cross the midline around birth to reach, in the first postnatal week, the contralateral cortex where they branch extensively at layer II/III and V. Given the ACC in the patient carrying the p.Ile678Leu variant, we investigated how the missense variants in *hKIF21B* lead to aberrant inter-hemispheric connectivity by introducing WT or mutant cDNA (NeuroD-hKIF21B) together with a mScarlet-expressing vector (pCAG2-mScarlet) in wild-type callosal projection neuron via IUE of E15.5 mouse cortical progenitors. The p.Gln313Lys substitution variant was used as a negative control as we did not expect any commissural defects according to the patient clinical features (Table 1). At P4, soon after the axons cross the midline and at P8, when axons start invading the contralateral CP, neither the expression of WT-hKIF21B nor of any of the variants perturbed midline crossing, as indicated by an equivalent scarlet intensity on each side of the CC (Fig. 6a–c, Supplementary Fig. 6a–c). In addition, at P22, when callosal axons achieve their adult-like arborization pattern, axons correctly invaded the homotopic contralateral cortex and successfully branched in layer II–III and V in all conditions (Supplementary Fig. 6g, h). Nonetheless, expression of the p.Ile678Leu, but not WT nor p.Gln313Lys mutant reduced by half the density of scarlet-positive axons in the white matter compared to the control both at P4 and P8 (–49.7% at P8, $P = 0.0043$) (Fig. 6a, b, d, e, Supplementary Fig. 6a, b, d). These defects were unlikely due to delayed innervation, as the poor inter-hemispheric connections persisted at P22 (Supplementary Fig. 6e, f). Rerouting through alternate commissures was also excluded as no aberrant axonal projections were observed after electroporation of callosal neurons and as no other commissures were shown enlarged in the patient (P1). Altogether, these results indicate that the faulty CC innervation is due to an impaired axonal growth rather than to defective contralateral targeting. Accordingly, we

measured the length of the longest neurites in primary cortical neurons transfected with pcDNA-HA-hKIF21B cDNA constructs. Although primary cortical neurons expressing WT-hKIF21B or p.Ala1001Thr and p.Gln313Lys hKIF21B variants showed normal axonal growth, expression of p.Ile678Leu mutant severely impaired axonogenesis at DIV2 and DIV5 (Fig. 6f, g, Supplementary Fig. 7a, b). To dig deeper into the pathogenic mechanism of the p.Ile678Leu hKIF21B variant, we performed a complementation experiment by co-electroporating p.Ile678Leu hKIF21B with increasing amounts of WT-hKIF21B at E15.5 and analyzed the percentage of projecting neurons at P8. Equivalent amounts of WT-hKIF21B failed to rescue the CC innervation phenotype (Fig. 6b, e). Further in vitro analysis of neurite length in primary cortical neurons expressing WT-hKIF21B together with p.Ile678Leu hKIF21B mutant at a 1:1 ratio confirmed the lack of rescue of axonal growth (Fig. 6f, g). We next reasoned that the p.Ile678Leu variant might exert its effect through attenuation of KIF21B autoinhibition. Accordingly, primary neurons transfected with two units of NeuroD-hKIF21B displayed shorter longest neurites in vitro (Fig. 6f, g), suggesting that enhanced KIF21B activity induces axonogenesis defects. To corroborate these findings in vivo, we assessed the ability of neurons electroporated with ΔATP p.Ile678Leu variant (NeuroD-p.Ile678Leu-ΔATPhKIF21B) to project axons contralaterally at P8 (Fig. 6b, c, e). There was no significant difference between the control and the immotile p.Ile678Leu-ΔATPhKIF21B, suggesting that the p.Ile678Leu variant impedes CC innervation through aberrant motor activity. Consistent with a hyperactivation of KIF21B, neurons expressing NeuroD-mKif21bΔrCC failed to project axons at P8 (Fig. 6b, e). Altogether these results indicate that the loss of inter-hemispheric connectivity induced by the p.Ile678Leu hKIF21B variant, and the subsequent release of KIF21B autoinhibition, arises from impaired axonal growth rather than defective innervation and arborization in the contralateral cortex.

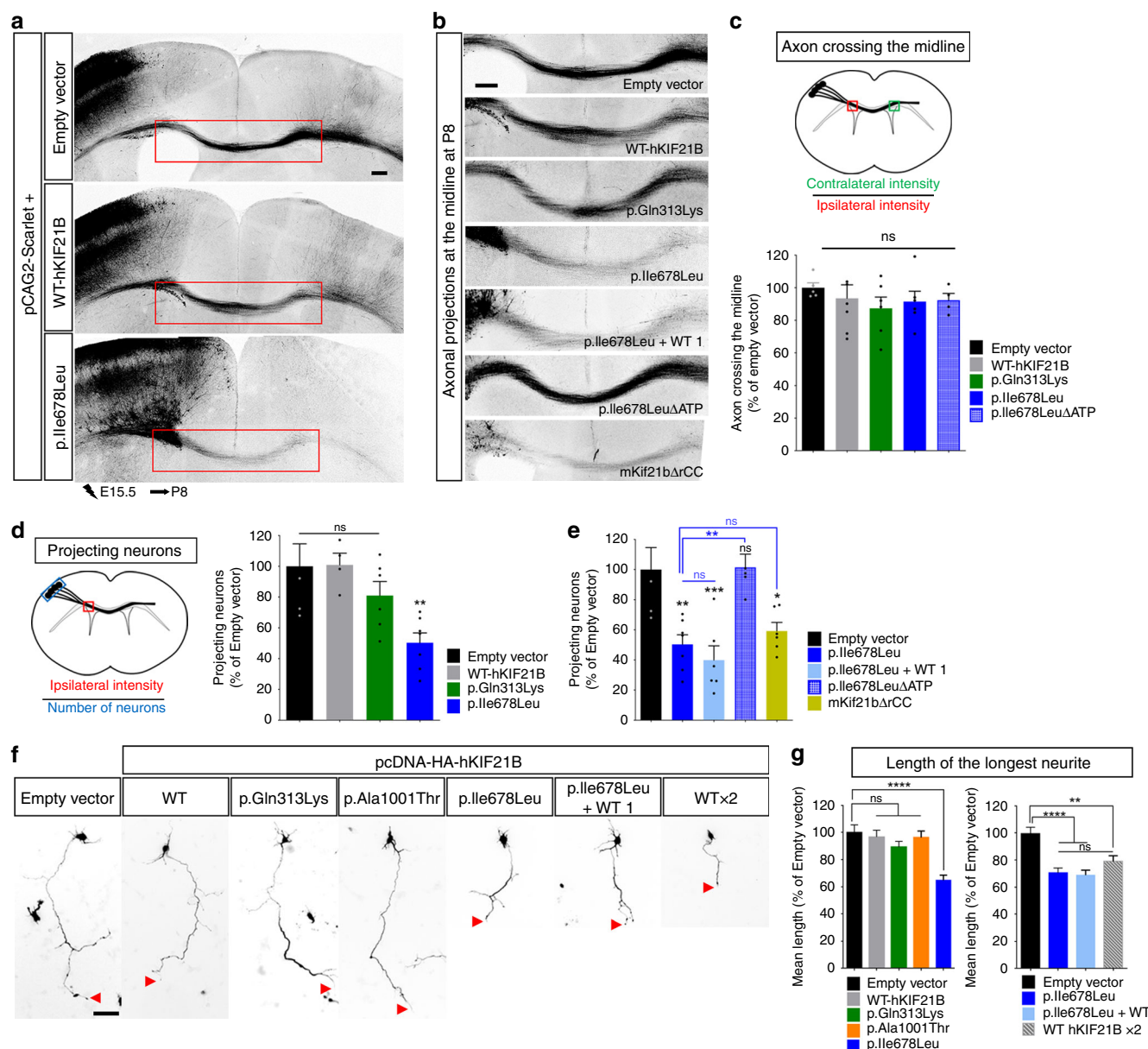
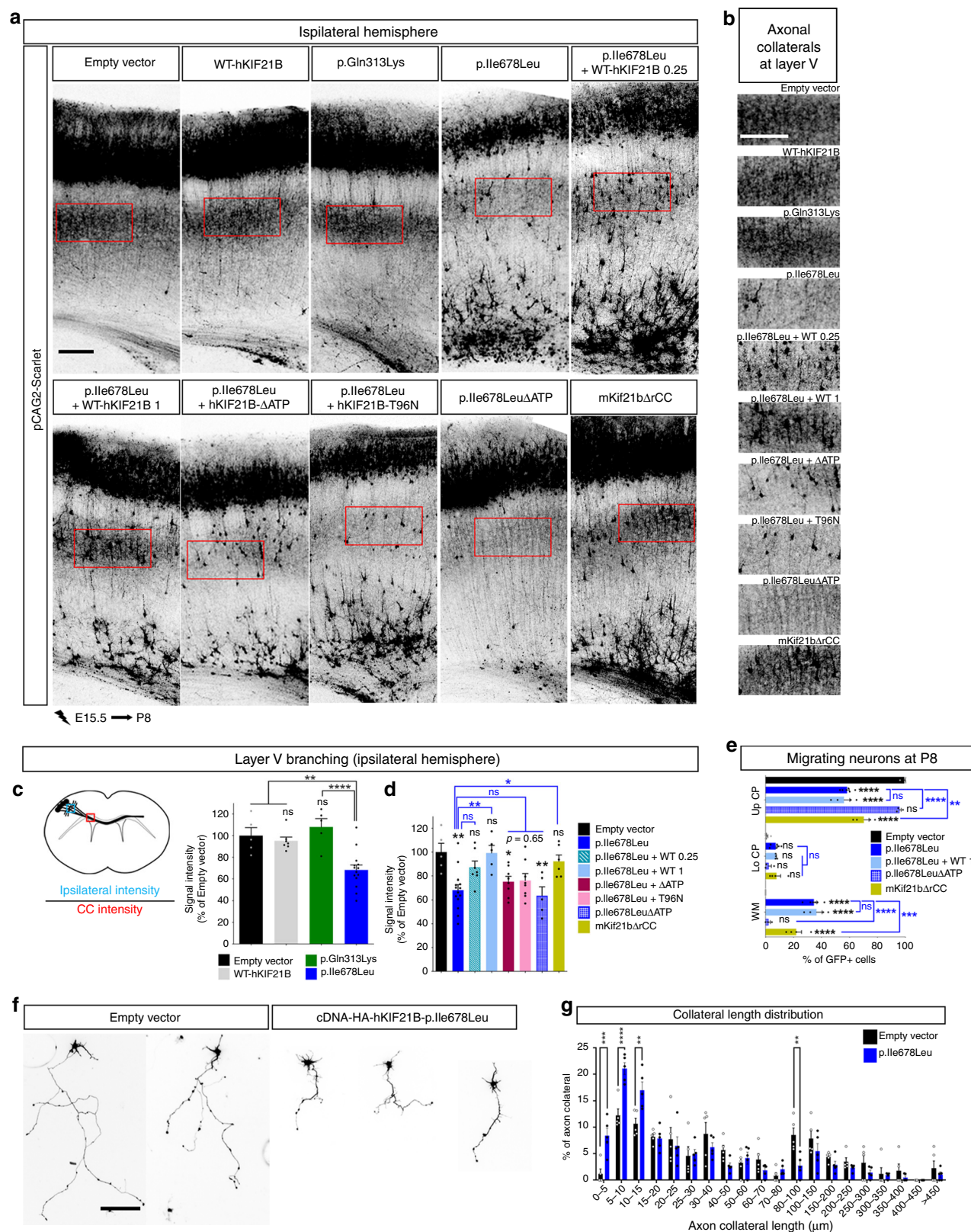


Fig. 6 p.Ile678Leu hKIF21B variant impedes inter-hemispheric connectivity. **a** Coronal sections of P8 brains after IUE with pCAG2-Scarlet and indicated NeuroD-IRES-GFP constructs. **b** Close-up views of the red boxed area in **a** showing impaired axonal inter-hemispheric connectivity upon expression of the p.Ile678Leu variant or the hyperactive mKif21bΔrCC but not upon expression of WT, p.Gln313Lys or immotile p.Ile678LeuΔATP. Rescue experiments were done by co-expressing p.Ile678Leu-hKIF21B (1 μg/μL) together with WT-hKIF21B constructs at 1 μg/μL (p.Ile678Leu + WT 1). Scale bars, 250 μm. **c**, **d** Upper (**c**) or left (**d**) panels, schematic describing methods used to quantify the percentage (**c**) of axon crossing the midline and (**d**) of projecting neurons. Lower (**c**) or right (**d**) panels, histograms presenting the percentage (**c**) of axon crossing the midline and (**d**, **e**) of projecting neurons. Data (means ± S.E.M.) were analyzed by one-way ANOVA (Bonferroni's multiple comparisons test). Number of pups analyzed: **c** Empty vector, *n* = 5; WT, *n* = 7; p.Gln313Lys, *n* = 6; p.Ile678Leu, *n* = 6; p.Ile678LeuΔATP, *n* = 4; **d**, **e** empty vector, *n* = 5; WT, *n* = 4; p.Gln313Lys, *n* = 6; p.Ile678Leu, *n* = 7; p.Ile678LeuΔATP, *n* = 5; p.Ile678Leu + WT, *n* = 6; mKif21bΔrCC, *n* = 6. **f** Representative DIV2 cortical neurons transfected at DIV0 with pCAG2-Scarlet together with empty pcDNA-HA or WT (at 1 (WT) or 2 μg/μL (WT ×2)) or mutant pcDNA-HA-hKIF21B constructs. Rescue experiments were done by co-expressing mutated p.Ile678Leu hKIF21B variant together with NeuroD-WT-hKIF21B (ratio 1:1; p.Ile678Leu + WT 1). Red arrowheads point to the axon tip. **g** Quantification of the longest neurite length (axon) at DIV2. Bars represent the means of the longest neurite length ± S.E.M. Significance was calculated by one-way ANOVA (Bonferroni's multiple comparisons test). Number of neurons analyzed: (left graph) Empty vector, *n* = 94; WT, *n* = 96; p.Gln313Lys, *n* = 104; p.Ile678Leu, *n* = 144; p.Ala1001Thr, *n* = 133, from four (Empty vector, WT, p.Ile678Leu) or three (p.Gln313Lys, p.Ala1001Thr) independent experiments; (right graph) empty vector, *n* = 132; WT 2 μg/μL, *n* = 125; p.Ile678Leu + WT, *n* = 146; p.Ile678Leu, *n* = 134; from four independent experiments. ns non-significant; **P* < 0.05; ***P* < 0.005; ****P* < 0.001; *****P* < 0.0001. Scale bars, (**a**) 200 μm, (**b**) 250 μm (**f**) 50 μm. Source data are provided in the Source Data file.

hKIF21B p.Ile678Leu variant impairs ipsilateral connectivity. Callosal neurons not only branch contralaterally, but also send multiple ipsilateral axon collaterals within layer II-III and even more strongly to layer V. We further examined whether this

hKIF21B missense variant also impacts the establishment of intracortical connections. We performed IUE of WT and mutant hKIF21B in wild-type embryos at E15.5 and analyzed ipsilateral cortical collaterals at P8. Although callosal neurons expressing



WT or p.Gln313Lys hKIF21B displayed prominent ipsilateral branching, overexpression of the p.Ile678Leu variant greatly reduced the intracortical branching (-32% , Bonferroni adjusted $P = 0.0016$) (Fig. 7a-c). Co-electroporation of p.Ile678Leu hKIF21B variant with either half or equivalent dose of WT-hKIF21B gradually restored the intrahemispheric connectivity

phenotype, suggesting that p.Ile678Leu hKIF21B possibly impairs formation of ipsilateral collaterals through a dominant negative mechanism (Fig. 7a, b, d). Notably, migration defects were not rescued in these experiments (Fig. 7e) demonstrating that the branching phenotype is not an indirect consequence of neuron mispositioning. Conversely, p.Ile678Leu- Δ ATPhKIF21B

Fig. 7 p.Ile678Leu hKIF21B variant impairs ipsilateral axon collaterals formation. **a** Representative images of ipsilateral P8 cortices after IUE, with pCAG2-Scarlet and indicated NeuroD-IRES-GFP constructs. Rescue experiments were done by co-expressing mutated p.Ile678Leu hKIF21B together with increasing amount of WT-hKIF21B (at 0.25 $\mu\text{g}/\mu\text{L}$ (WT 0.25) or 1 $\mu\text{g}/\mu\text{L}$ (WT 1)) or equivalent amount of hKIF21B- ΔATP or hKIF21B-T96N, that both lost their processivity. **b** Close-up views of red boxed area in **(a)** showing axon ipsilateral branching within layer V for all the indicated conditions. **c–e** Histograms (means \pm S.E.M.) showing **(c, d)** the quantification of the ipsilateral branching in layer V (intensity of scarlet signal in layer V (blue box) normalized on the intensity of the scarlet signal in the corpus callosum (red box) — as shown on the schematic in the upper panel) and **(e)** the distribution of electroporated neurons in three different regions (Up CP (upper cortical plate), Lo CP (lower cortical plate), and WM (White matter)). Data from were analyzed by **(c, d)** one-way ANOVA or **(e)** two-ways ANOVA (Bonferroni's multiple comparisons test). Number of pups analyzed: **c, d** Empty vector, $n = 5$; WT, $n = 7$; p.Gln313Lys, $n = 5$; p.Ile678Leu, $n = 14$; p.Ile678Leu + WT 0.25 $\mu\text{g}/\mu\text{L}$, $n = 7$; p.Ile678Leu + WT 1 $\mu\text{g}/\mu\text{L}$, $n = 5$; p.Ile678Leu + ΔATP , $n = 8$; p.Ile678Leu + T96N, $n = 8$; p.Ile678Leu ΔATP , $n = 5$; mKif21b ΔrCC , $n = 6$; **e** Empty vector, $n = 5$; p.Ile678Leu, $n = 6$; p.Ile678Leu + WT 1 $\mu\text{g}/\mu\text{L}$, $n = 4$; p.Ile678Leu ΔATP , $n = 3$; mKif21b ΔrCC , $n = 4$. **f** Representative DIV5 cortical neurons transfected at DIV2 with pCAG2-Scarlet together with the indicated pcDNA-HA-hKIF21B constructs. **g** Distribution (means \pm S.E.M.) of axonal collateral branches length at DIV5. Significance was calculated by two-way ANOVA (Bonferroni's multiple comparisons test). Number of collaterals analyzed: Empty vector, $n = 265$; p.Ile678Leu, $n = 385$; from 51 (Empty vector) and 66 (p.Ile678Leu) neurons from five independent experiments. ns non-significant, * $P < 0.05$; ** $P < 0.005$; *** $P < 0.001$; **** $P < 0.0001$. Scale bars, **(a, b)** 250 μm , **(f)** 150 μm . Source data are provided in the Source Data file.

overexpressing neurons that migrated normally (Fig. 7e), failed to send axonal collaterals ipsilaterally in layer V (Fig. 7a, b, d). Also, those neurons (p.Ile678Leu- ΔATP hKIF21B) showed normal axonal growth (Fig. 6b, c, e), ruling out the possibility that defective intracortical branching arises from impaired axonogenesis (Fig. 7a, b, d). Accordingly, branching defects likely arose from impaired collateral growth as revealed by in vitro analysis of axon branching in primary neurons at DIV5. Expression of p.Ile678Leu hKIF21B variant but not WT nor p.Gln313Lys or p.Ala1001Thr mutants led to a shift of branch length toward short branch classes that resulted in a large decrease of the mean length of axon collaterals (Fig. 7f, g, Supplementary Fig. 7a, c, d). Consistent with a dominant negative effect, intrahemispheric connectivity is not affected upon KIF21B hyperactivation with neurons expressing NeuroD-mKif21b ΔrCC displaying normal ipsilateral collaterals (Fig. 7a, b, d). We finally investigated which function of WT-hKIF21B was negatively modulated by the mutant protein. We induced expression of p.Ile678Leu variant together with hKIF21B that either cannot bind (NeuroD- ΔATP hKIF21B; Fig. 1h) or hydrolyze ATP (T96N-hKIF21B; Fig. 1h)²¹ at a 1:1 ratio using IUE at E15.5. Both constructs failed to rescue the branching phenotype induced by p.Ile678Leu hKIF21B at P8, suggesting that p.Ile678Leu hKIF21B exerts its dominant negative effect on the processive activity of KIF21B (Fig. 7a, b, d, Supplementary Fig. 3a). Collectively, our results showed that the p.Ile678Leu variant alters the intrahemispheric connectivity beyond its effect on migration and axonal growth through a dominant negative effect on motility.

Discussion

Our findings highlight the critical role of KIF21B in the regulation of processes involved in cortical development and implicate variants in *KIF21B* in ID and brain malformation. We identified three missense variants and one duplication of four nucleotides. The duplication leads to a frameshift introducing a premature termination codon in exon 20. The resulting mutant mRNA is likely degraded by nonsense-mediated mRNA decay. Although we demonstrated in mice that *Kif21b* haploinsufficiency leads to an impaired neuronal positioning (Supplementary Fig. 3d–f), the p.Asn988Serfs*4 protein truncated variant is possibly not pathogenic. Indeed, hKIF21B gene might partially tolerate loss-of-function variants: in the gnomAD (Genome Aggregation Database, v2.1.1 “non-neuro”) populations that is supposed to be depleted in severe pediatric conditions, 28 loss-of-function variants have been reported. Nonetheless, the ratio of the observed/expected loss-of-function variants in the gnomAD populations is

low (0.32, confidence interval 0.23–0.43), still questioning the penetrance of loss-of-function variants in *KIF21B*.

Our study provides the molecular mechanisms by which the identified variants lead to an abnormal brain phenotype. We showed that all missense variants, to various extents, impaired neuronal migration by enhancing KIF21B motor activity. Several lines of evidence suggest that hKIF21B missense variants exert a gain-of-function effect by enhancing KIF21B motility activity through lessening of the kinesin autoinhibition (Fig. 4). First, WT-hKIF21B is unable to rescue the variant-induced migratory defects at equivalent dose (Fig. 3a, b). Second, the phenotype induced by overexpression of the variants is phenocopied by the expression of a constitutively active form of KIF21B (that is truncated for the rCC domain) (Fig. 4c, d). Third, loss of ATP binding is sufficient to abrogate the phenotype induced by the missense variants (ΔATP -hKIF21B; Figs. 4i, j and 7e). Fourth, mutant hKIF21B proteins showed enhanced microtubule-based motility compared to the WT protein (Fig. 4g, h). How do hKIF21B variants lead to autoinhibition release? KIF21B autoinhibition is mediated by a regulatory segment (rCC) within the second coiled-coil domain (CC2, Fig. 1h) that fastens the CC2 domain to the motor head^{42,46}. We hypothesize that the position of the missense variants within the motor (p.Gln313Lys), coiled-coil (p.Ile678Leu) and rCC (p.Ala1001Thr) domains (Fig. 1h) alters the protein conformation so that it varies the impact on the intramolecular interaction between the motor and the internal coiled-coil domains. This model raises the possibility that the level of disruption of these interactions correlates with the degree of autoinhibition release imposed by the different missense variants and therefore dictates the severity of the phenotype. In accordance, the increase in KIF21B processivity correlated with the extent of migration defects, the velocity of the p.Ile678Leu variant being the most drastically enhanced (Fig. 4g, h). We therefore propose a model in which a minimal level of autoinhibition is required to ensure proper function of KIF21B in the developing cortex. Below this threshold, the more KIF21B gets overactivated, the more severe and broad the phenotypes will present. In this model, the p.Gln313Lys and p.Ala1001Thr variants would partially relieve autoinhibition, whereas the p.Ile678Leu variant would completely loose autoinhibition. Consistently, p.Gln313Lys and p.Ala1001Thr KIF21B induce a delay of migration, whereas the p.Ile678Leu variant leads to a permanent arrest of migration and an additional connectivity phenotype (Figs. 3 and 6).

Beyond autoinhibition, maintaining a proper level of KIF21B activity seems to be crucial for its function during development. Indeed, *KIF21B* haploinsufficiency also leads to migratory defects. Whether those defects are caused by a loss of trafficking or MT

regulator functions is not clear and should be further assessed. Overall, the model could be expanded to a threshold of activity, below (haploinsufficiency) or above (identified missense variants) which KIF21B would not be properly functional leading to neurodevelopmental defects.

Convergent evidence suggests that the p.Ile678Leu variant alters axon branching through a dominant negative effect on KIF21B processivity (Fig. 7). First, co-expression of increasing amount of WT-hKIF21B together with the mutant protein gradually restored the intrahemispheric connectivity phenotype. Second, an immotile form of KIF21B failed to rescue the variant-induced branching defect. Third, expression of a constitutive active form (Δ rCC) of KIF21B does not affect the formation of axon branches. Fourth, p.Ile678Leu- Δ ATPhKIF21B overexpressing neurons display abnormal ipsilateral collaterals. Fifth, consistent with a dominant negative effect, the WT KIF21B protein fails to form homodimer and is mislocalized when co-expressed with the p.Ile678Leu variant. Intriguingly, the p.Ile678Leu variant also perturbs axonal growth (Fig. 6) and migration (Figs. 3 and 4) through attenuation of autoinhibition, suggesting, as discussed above, a possible gain-of-function effect. To reconcile these seemingly conflicting findings, we propose that it could imply that KIF21B regulates the trafficking of different cargoes in axon and branches. p.Ile678Leu-induced overactivation of KIF21B might therefore lead to excessive motility of specific cargoes within axons. Conversely, the same variant could impede the transport of branch-specific cargoes by interfering with the function of the wild-type protein. At this time, none of the few KIF21B cargoes identified is specific to axon or branches^{44,45}, so further work is needed to identify cargoes in the different cellular compartments and validate this hypothesis.

Expression of the KIF21B p.Gln313Lys variant recapitulates the microcephaly phenotype observed in the reported subject. Given that introduction of the p.Alal001Thr variant that is expected to attenuate KIF21B autoinhibition at the same extent as the p.Gln313Lys substitution variant, but does not reduce brain size in zebrafish (Fig. 5), the hyperactivation of KIF21B is unlikely to be driving the phenotype of microcephaly. In a search for possible microcephaly-underlying mechanism, we exclude any non-cell autonomous effect on progenitors' proliferation, or any impact on cell survival. Abnormal postnatal neuronal maturation may also contribute to the global microcephaly phenotype. Accordingly microcephaly may worsen with time: the patient carrying the KIF21B p.Gly313Lys variant was born with a head circumference (HC) of 32 cm (5th percentile), but microcephaly progressed and at the age of 12 was 48.5 cm (<1st percentile, -3.9 SD). These maturation defects may result from regulation of neuronal soma size^{56,57} or from connectivity defects. Although the axonal branching is not impaired in callosal neurons overexpressing the microcephaly-related variant, we cannot rule out the possibility that reduced dendritic arborization of projection neurons influences the microcephaly phenotype.

In conclusion, the mechanism proposed here for the role of KIF21B in attenuating (p.Gln313Lys and p.Alal001Thr) or abrogating autoinhibition (p.Ile678Leu) of one or several kinesin functions, might be expanded to other kinesins (KIF1A²⁸, KIF5C³⁰, KIF7²⁶, KIF4A²⁴) known to be regulated by autoinhibition and for which the pathophysiological mechanisms underlying the migration and inter-hemispheric connectivity phenotypes have not yet been elucidated. In addition, autoinhibition of kinesins has been implicated in several physiological processes including the regulation of innervation, synaptogenesis and compartment-specific localization of cargo^{53,54,58,59}. Our results indicate that fine-tuning of KIF21B activities is critical for proper neuronal migration and axonal growth, adding novel physiological roles of kinesin autoinhibition.

Methods

Whole-exome sequencing (WES). A parent-offspring trio approach was used for whole-exome sequencing (WES) in each family. Exomes were sequenced using DNA isolated from blood according to standard procedures. Informed consent was obtained from all participants in accordance with site-specific institutional review board. Patient 1: The SeqCap EZ MedExome Enrichment Kit (Roche) was used for library preparation with 12 samples multiplexing, according to manufacturer's protocol. This library was then sequenced on a NextSeq 500 (Illumina) with a 2 × 150 bp high output flowcell. The bioinformatic analyses was conducted by Polyweb using BWA 0.7.12, picard-tools-1.121, GenomeAnalysisTK-2014.3-17-g0583013, SNPEff-4.2. Patient 2: The SeqCap EZ VCRome 2.0 (Roche) was used for library preparation. Exome libraries were sequenced on an Illumina HiSeq 2500 instrument and the following sites are used to search for previously described gene pathogenic variants and polymorphisms: the Human Gene Mutation Database (HGMD), the single Nucleotide Polymorphism database (dbSNP), 1000 genomes, HapMap data. Patient 3: Exome capture was done using the Nimblegen SeqCap EZ Exome v3 (Nimblegen). Exome libraries were sequenced on an Illumina HiSeq instrument (Illumina, San Diego, USA) with 150 bp paired-end reads at a median coverage of 100×. Sequence reads were aligned to the hg19 reference genome using BWA. Variants were subsequently called by the GATK unified genotyper, and annotated using a custom diagnostic annotation pipeline. Patient 4: Exome was captured using the Clinical Research Exome kit (Agilent Technologies, Santa Clara, CA). Massively parallel (NextGen) sequencing was done on an Illumina system with 100 bp or greater paired-end reads. Reads were aligned to human genome build GRCh37/UCSC hg19, and analyzed for sequence variants using GeneDx's XomeAnalyzer (a custom-developed variant annotation, filtering and viewing interface for WES data)⁶⁰. The general assertion criteria for variant classification are publicly available on the GeneDx ClinVar submission page (<http://www.ncbi.nlm.nih.gov/clinvar/submitters/26957/>).

Inclusion and genetic studies were approved by local ethics committee in France (CCP Ile de France, CPP No. 71-10/ ID RCB: 2010-A00802-37) and USA (Institutional Review Board at Baylor College of Medicine, protocol H-29697 and at the John Hopkins School of Medicine).

Cloning and plasmid constructs. Wild-type (WT) human *KIF21B* cDNA (NCBI Reference Sequence: NM_001252100.1) was obtained from Vector Builder by gene synthesis and subcloned by restriction-ligation into the NeuroD-iresGFP⁶¹, the pcDNA3.1+/N-HA and in the pEGFP-N1 vectors. Myc-tagged hKIF21B constructs were obtained by replacing the GFP sequence of the pEGFP-N1 containing the hKIF21B gene by a Myc-tag sequence. Human *KIF21B* variants c.937C>A (p.Gln313Lys), c.2032A>C (p.Ile678Leu), c.3001G>A (p.Alal001Thr) and the c.288C>T (T96N) substitution that abolishes KIF21B mobility²¹ were created from WT CDS by Sequence and Ligation Independent Cloning (SLIC). hKIF21B ATP binding site (amino acids 87–94; UniProtKB O75037) was deleted by SLIC from NeuroD-WT-hKIF21B-iresGFP, NeuroD-hKIF21B-p.Gln313Lys-iresGFP, NeuroD-hKIF21B-p.Ile678Leu-iresGFP and NeuroD-hKIF21B-p.Alal001Thr-iresGFP to generate p.Ile678Leu- Δ ATPhKIF21B WT- Δ ATPhKIF21B, p.Gln313Lys- Δ ATPhKIF21B, p.Ile678Leu- Δ ATPhKIF21B and p.Alal001Thr- Δ ATPhKIF21B constructs, respectively.

Wild-type mouse *Kif21b* CDS was isolated from E18.5 cDNA mouse cortices by PCR and a new isoform has been amplified. This isoform is 4920 bp-long and has an insertion (c.4905_4906 ins C; NM_001039472.2) that leads to a frameshift and to the introduction of a premature stop codon in exon 35. This isoform has been subcloned by restriction-ligation into the NeuroD-iresGFP plasmid. This new isoform has also been fused to eGFP in the N-terminal part (pEGFP-C1-WT-mKif21b) via subcloning in pEGFP-C1 plasmid (NovoPro V12024). The amino acids 930–1010 corresponding to autoinhibitory domain (rCC)⁴² were deleted by site-directed mutagenesis to generate NeuroD-mKif21b- Δ rCC construct. Mouse *Kif21b* 3'UTR sequence (NCBI Reference Sequence: NM_001039472.2) were amplified by PCR and cloned by restriction-ligation into the pEGFP-C1 plasmid and fused to eGFP in the N-terminal part. pCR-BluntII-TOPO-mKif21b 3'UTR used to synthesize RNA probes was generated by cloning part of the mKif21b 3'UTR (255 bp, Genepaint template T36548) in pCR-BluntII-TOPO vector.

shRNAs against coding sequence 3390–3410 (NM_001252100.1) (sh-*Kif21b* #1) or the 3'-UTR (sh-*Kif21b* #2) of mouse *Kif21b* were generated by annealing of sense and antisense oligos, the resulting duplex were subcloned in pCALSL-mir30⁵² backbone vector digested with *Xho*I and *Eco*RI. The following oligos were used: sh-*Kif21b* #1:

sense: 5'TCGAGaaggtatattgtctgtgacagtgagcgcCCACGATGACTTCAAGTTCAAtagtgagccacagatgtaTTGAACCTGAAGTCATCGTGGtgctactgctcctg 3'; antisense: 5'AATTTCcaggcagtaggcaCCAGATGACTTCAAGTTCAAtacatctgtgcttactaTTGAACCTGAAGTCATCGTGGtgctactgctcagcaatataccttC 3'; sh-*Kif21b* #2: sense: 5'TCGAGaaggtatattgtctgtgacagtgagcGCCTTTAAACACAGAGTATAtagtgagccacagatgtaTATACTCTGGTGTGTTAAAGGCTgctactgctcctg 3'; antisense: 5'AATTTCcaggcagtaggcaGCCTTTAAACACAGAGTATAtacatctgtgcttactaTATACTCTGGTGTGTTAAAGGCTgctactgctcagcaatataccttC 3'; Scrambled shRNA: Sense: 5'TCGAGaaggtatattgtctgtgacagtgagcGCCTGATGCGCGATGCGTAAATTTtagtgaagccacagatgtaAATTAATTCAGCGTATGCGGATgctcctgctg 3'; Antisense: 5'AATTTCcaggcagtaggcaGCGCGATAGCGCT

AATAATTTTtacatctgtgcttactaAAATTATTAGCGCTATCGCGCgctcactgcaacagcaataactctC 3'

pCAG2-mScarlet and pSCV2-CAG-mVENUS⁶¹ expressing vectors were provided by J. Courchet (INMG, Lyon, France). Plasmid DNAs used in this study were prepared using the EndoFree plasmid purification kit (Macherey Nagel).

Mice. All animal studies were conducted in accordance with French regulations (EU Directive 86/609 – French Act Rural Code R 214-87 to 126) and all procedures were approved by the local ethics committee and the Research Ministry (APAFIS#15691-201806271458609). Mice were bred at the IGBMC animal facility under controlled light/dark cycles, stable temperature (19 °C) and humidity (50%) condition and were provided with food and water ad libitum.

Timed-pregnant wild-type (WT) NMRI (Janvier-labs) and CD1 (Charles River Laboratories) females were used for in utero electroporation (IUE) of sh-*Kif21b* and NeuroD-hKIF21B constructs, respectively, at embryonic day 14.5 (E14.5). Hybrid F1 females were obtained by mating inbred 129/SvJ females (Janvier-labs) with C57BL/6J males (Charles River Laboratories). F1 females were crossed with C57BL/6J males (Charles River Laboratories) to obtain timed-pregnant females for IUE at E15.5.

Kif21b KO mice were generated using the International Mouse Phenotyping Consortium targeting mutation strategy⁶² and obtained from UC Davis/ KOMP repository (Kif21b^{tm1a(KOMP)wt}). Genotyping was done as follows: Genomic DNA was extracted from tail biopsies using PCR reagent (Viagen) supplemented with Proteinase K (1 mg/mL), heated at 55 °C for 5 h. Proteinase K was inactivated for 45 min at 85 °C, and cell debris was removed by centrifugation. Samples were processed for PCR using the following primers: KIF21B forward: 5'-GGGGTACTT TCCATTGACCCAG-3', KIF21B reverse: 5'-GAAGGGACCAACCTGGGC-3' for KIF21B targeted exon amplification and Mq forward 5'-GCTATGACTGGG CACAACAGACAATC-3' and Mq reverse 5'-CAAGGTGAGATGACAGAG ATCCTG-3' for Neomycin gene amplification. The presence of the wild-type and knockout alleles was indicated by 346 and 261 bp products, respectively, which were detected on a 2% agarose gel.

In utero electroporation (IUE). Timed-pregnant mice were anesthetized with isoflurane (2 L per min of oxygen, 4% isoflurane in the induction phase and 2% isoflurane during surgery operation; Tem Segal). The uterine horns were exposed, and a lateral ventricle of each embryo was injected using pulled glass capillaries (Harvard apparatus, 1.0 OD*0.58 ID*100 mmL) with Fast Green (1 µg/µL; Sigma) combined with different amounts of DNA constructs using a micro injector (Eppendorf Femto Jet). We injected 1 µg/µL of WT or mutant NeuroD-hKIF21B-IRES-GFP constructs together with 0.5 µg/µL of empty NeuroD-IRES-GFP vector at E14.5. 1.5 µg/µL of NeuroD-IRES-GFP vector were used as control. We injected 1 µg/µL of NeuroD:Cre-GFP vector together with 3 µg/µL of either Cre inducible pCALSL-miR30-shRNA-*Kif21b* #1 or #2 or pCALSL-miR30-sh-scramble sequence and 1 µg/µL of NeuroD-IRES-GFP or NeuroD-mKif21b-IRES-GFP (rescue experiment). For axonal pathfinding experiments, we injected 1 µg/µL of NeuroD-IRES-GFP (empty or containing WT or mutated human KIF21B cDNA) together with 0.8 µg/µL of pCAG2-mScarlet at E15.5. For rescue experiments, we co-injected 1 µg/µL of NeuroD-IRES-GFP (WT or mutated human KIF21B cDNA) together with 0.25, 0.5 or 1 µg/µL of the indicated NeuroD-IRES-GFP constructs. Plasmids were further electroporated into the neuronal progenitors adjacent to the ventricle by discharging five electric pulses (40 V) for 50 ms at 950 ms intervals using electrodes (diameter 3 mm; Sonidel CUY650P3) and ECM-830 BTX square wave electroporator (VWR international). After electroporation, embryos were placed back in the abdominal cavity and the abdomen was sutured using surgical needle and thread. For E16.5 and E18.5 analysis, pregnant mice were killed by cervical dislocation 2 and 4 days after surgery. For postnatal analysis, electroporated pups were killed 2, 4, or 8 days after birth (P2, P4, P8) by head sectioning or 22 days after birth (P22) by terminal perfusion.

Mouse brain fixation, cutting and immunolabeling. E12.5 to P8 animals were killed by head sectioning and brains were fixed in 4% paraformaldehyde (PFA, Electron Microscopy Sciences) in Phosphate buffered saline (PBS, HyClone) 2 h at room temperature (RT) or overnight (O/N) at 4 °C. P22 animals were killed by terminal perfusion of PBS then 4% PFA followed by overnight post-fixation at 4 °C in 4% PFA. For Kif21b expression pattern (Fig. 2 and Supplementary Fig. 2), immunolabeling was performed on cryosections as follows: after fixation, brains were rinsed and equilibrated in 20% sucrose in PBS overnight at 4 °C, embedded in Tissue-Tek O.C.T. (Sakura), frozen on dry ice and coronal sections were cut at the cryostat (12 to 18 µm thickness, Leica CM3050S) and processed for In situ hybridization or immunolabeling. Sections were maintained at -80 °C. For IUE analyses (Figs. 3–7, Supplementary Figs. 3–7), immunolabeling was performed on vibratome sections as follows: after fixation, brains were rinsed and embedded in a solution of 4% low-melting agarose (Bio-Rad) and cut into coronal sections (60-µm-thick for E18.5 and P2 mice, 100-µm-thick for P4 to P22 mice) using a vibrating-blade microtome (Leica VT1000S, Leica Microsystems) and processed for immunolabeling. Sections were maintained in PBS-azide 0.05% for short-term storage and in an Antifreeze solution (30% Ethyleneglycol, 20% Glycerol, 30% D₂O, 20% PO₄ Buffer) for long-term storage.

For cryosections only, an antigen retrieval was performed by boiling sections in sodium citrate buffer (0.01 M, pH 6) during 15 min. Cryo- and vibratome sections were permeabilized and blocked with 5% Normal Donkey Serum (NDS, Dominic Dutcher), 0.1% Triton X-100 in PBS. Slides were incubated with primary antibodies diluted in blocking solution overnight at 4 °C and secondary antibodies diluted in PBS-0.1% Triton one hour at room temperature, whereas cell nuclei were identified using DAPI (1 mg/mL Sigma). Slices were mounted in Aquapolymount mounting medium (Polysciences Inc). All primary and secondary antibodies used for immunolabeling are described in Supplementary Table 1.

RNA in situ hybridization. Mouse *Kif21b* sense and antisense probes were synthesized from pCR-BluntII-TOPO-mKif21b 3'UTR by either *Bam*HI digestion followed by synthesis with T7 RNA polymerase (Roche) (sense probe) or *Eco*RV digestion followed by synthesis with SP6 RNA polymerase (Roche) (antisense probe). Kif21b digoxigenin-labeled probes using the DIG RNA labeling Kit SP6/T7 (Roche) according to the manufacturer's protocol. In situ hybridization was performed on E12.5 to E18.5 WT NMRI coronal embryonic brain cryosections as follow: sections were first rinsed in Phosphate buffered saline (PBS, HyClone) and dehydrated for 5 min in successive ethanol baths (70%, 95% and 100%) diluted in sterile milliQ water. The same amount of each antisense or sense Kif21b digoxigenin-labeled probes were diluted at 0.1 µg/µL in pre-warm Hybridization Buffer (4 M NaCl 0.2 M, 5 mM EDTA pH 8, 10 mM Tris-HCl pH 7.5, 10 mM NaH₂PO₄·2H₂O, 10 mM Na₂HPO₄, 2 mg/mL Ficoll, 2 mg/mL polyvinylpyrrolidone, 2 mg/mL bovine serum albumin, 10% Dextran Sulfate, 1 mg/mL Yeast tRNA (ThermoFisher Scientific), 50% deionized formamide) and denatured for 10 min at 70 °C. Sections were then incubated with the probe mix in a water-bath O/N at 70 °C in a sealed humidified chamber. Slides were then washed twice with the pre-warmed 1× Saline Sodium Citrate solution (SSC, 0.15 M NaCl, 15 mM Na Citrate) at 70 °C for 30 min and in the 0.2× SSC solution for one hour at 70 °C and for 5 min at RT. Slides were then washed twice in the MABT solution (0.1 M Maleic Acid, 0.15 M NaCl, 0.1% Tween-20, pH 6) for 30 min at RT under slow agitation and blocked in MABT solution supplemented with 2% blocking reagent (Roche) and 20% heat-inactivated Normal Donkey Serum (NDS, Dominic Dutcher) for 1 hour at RT. Slides were then incubated with the anti-DIG antibody (Abcam ab76907, 1:2500 diluted in blocking solution) O/N in humidified chamber at 4 °C. Slides were then washed four times in MABT for 15 min at RT then twice in Alkaline Phosphatase Buffer (NTMT, 100 mM NaCl, 100 mM Tris pH 9.5, 50 mM MgCl₂·H₂O, 0.1% Tween-20) for 10 min at RT and stained in NTMT supplemented with NBT (Sigma-Aldrich, 0.3 mg/mL) and BCIP (Sigma-Aldrich, 0.175 mg/mL) for 4 hours at RT in a box protected from the light. Reaction was stopped by transferring slides into PBS for 15 min, then slides were post-fixed in PFA4% diluted in PBS for 10 min at 4 °C. Slides were then washed 3 times in PBS for 10 min, air-dried and mount in Pertex mounting medium (Leica Microsystems). Images were taken using a microscope (Leica M420) connected to a Photometrics camera with the CoolSNAP software (v. 1.2).

Primary neuronal culture, magnetofection and immunolabeling. Cortices from E15.5 CD1 mouse embryos were dissected in cold PBS supplemented with BSA (3 mg/mL), MgSO₄ (1 mM, Sigma), and D-glucose (30 mM, Sigma). Cortices were dissociated in Neurobasal media containing papain (20 U/mL, Worthington) and DNase I (100 µg/mL, Sigma) for 20 min at 37 °C, washed 5 min with Neurobasal media containing Ovomucoid (15 mg/mL, Worthington), and manually triturated in OptiMeM supplemented with D-glucose (20 mM). Cells were then plated at 2 × 10⁵ cells per 24-well plate coated with poly-D-lysine (1 mg/mL, Sigma) overnight at 4 °C and cultured for 2–5 days in Neurobasal medium supplemented with B27 (1×), L-glutamine (2 mM) and penicillin (5 units/mL)–streptomycin (50 mg/mL). To transfected cultured neurons, we performed magnetofection at DIV0 (for analysis at DIV2) or DIV2 (for analysis at DIV5) using NeuroMag (OZ Bioscience) according to the manufacturer's protocol. Cells were fixed at DIV2 or DIV5 for 15 min at room temperature in 4% PFA, 4% sucrose in PBS, and incubated for 1 h in 0.1% Triton X-100, 5% NDS in PBS. Primary antibodies were incubated overnight at 4 °C and secondary antibodies were incubated for 1 h at room temperature (see Supplementary Table 1 for antibodies). DNA was stained using DAPI (1/1000). Slides were air-dried and mounted in Aquapolymount mounting medium (Polysciences Inc).

Fluorescent-activated cell sorting (FACS). Cortices from 3 to 4 E16.5 mouse Rosa26-loxSTOP-YFP; NEXCRE/+ embryos were dissected and dissociated as described above. After dissociation, cells were resuspended in 500 µL of staining solution (10% Fetal Bovine Serum (FBS) + 0.02% Sodium Azide in PBS) and stained for 20 min on ice in dark with CD24-APC Antibody (0.06 µg/100 µL final; clone M1/69, ThermoFisher Scientific (#17-0242-82)). Cells were then washed twice with HBSS (Gibco) and passed through a 40 µm filter (Falcon FACS). YFP-/CD24- population was sorted to enrich for progenitors and YFP+/CD24+ population was used to enrich for neurons using the BD Aria II flow cytometer with 488 and 633 lasers to excite YFP and APC respectively. Littermate YFP- embryos (Rosa26-loxSTOP-YFP; NEXCRE-) were processed the same way, stained with the Rat IgG2b-APC isotype control antibody (clone eB149/10H5, ThermoFisher Scientific (#17-4031-82)) and used as controls to set the YFP and CD24 gates.

Microfluidic fabrication and neurons plating. Design of polydimethylsiloxane microfluidic device is based on the one described by Taylor et al.⁵¹ with modifications of the size of the microchannels (3-μm width, 3-μm height and 450-μm length to reduce the number of axons per microchannels)⁶³. Briefly, microfluidics chambers were positioned and sealed on Iwaki boxes using plasma cleaner and then coated with poly-D-lysine (0.1 mg/mL) in the upper chamber, and with poly-D-lysine (0.1 mg/mL) and laminin (10 μg/mL) in the lower chamber. After overnight incubation at 4 °C microfluidic devices were washed two times with Neurobasal medium and once with growing medium (Neurobasal medium supplemented with 2% B27, 2 mM Glutamax, and 1% penicillin/streptomycin). Microchambers were then placed in the incubator until neurons were plated. Primary cortical neurons were prepared as follows: E15.5 C57Bl/6J mouse embryos were collected and cortices were dissected, followed by papain and cysteine digestion and trypsin inhibitor incubation. After mechanical dissociation, cortical neurons were resuspended in growing medium (5 × 10⁶ cells in 120 μL) and plated in the upper chamber with a final density of ~7000 cells/mm². Neurons were kept in the incubator for 1 h. Then, the two compartments were gently filled with growing medium.

Immunostaining in microchambers was performed from DIV5 culture⁶⁴: after 30 min fixation in 4% PFA/Sucrose dissolved in PBS, all the compartments were blocked with a solution containing BSA 1%, normal goat serum 2%, Triton X-100 0.1%. For these two solutions, a bigger volume in the upper chamber was applied to create a pressure gradient. After 1 h incubation with blocking solution, neurites in both compartments were incubated overnight at 4 °C with primary antibody recognizing KIF21B and Tau. Secondary antibodies were added the following day for 4 h and microchambers were maintained in PBS for a few days in the dark at 4 °C (see Supplementary Table 1 for antibodies).

RNA extraction, cDNA synthesis and RT-qPCR. To assess Kif21b mRNA expression in mouse and zebrafish, total RNA was extracted from the cortices of WT NMRI mouse embryos or from whole zebrafish (*Danio rerio*) embryos (AB strain) at different time points of development, with TRIzol reagent (ThermoFisher Scientific). We used mKif21b ex2-3 and drKIF21B ex2-3 primers to target *mKif21b* or *zKif21b* cDNA and mGAPDH or drElfA (Elongation factor 1-α) as housekeeping genes normalizer (Table 2). shRNA-*Kif21b* knock-down efficacy was assessed by RT-qPCR. Total RNA was prepared from HEK293T cells overexpressing sh-scrambled or shRNA-*Kif21b* #2 together with pEGFP-C1-3'UTR mKIF21B or from HEK 293K cells overexpressing sh-scrambled or shRNA-*Kif21b* #1 together with pEGFP-C1-WT-mKif21b. We used GFP primers to target the 3' UTR sequence of *mKif21b* cDNA fused to GFP and mKIF21B ex2-3 primers to target *mKif21b* cDNA. We used mGAPDH or Hprt1 primers as housekeeping genes normalizer (Table 2). cDNA samples were synthesized with SuperScript IV Reverse Transcriptase (Invitrogen) and submitted to DNase I treatment (TurboDNase, ThermoFisher). RT-qPCR was performed in a LightCycler PCR instrument (Roche) using SYBR Green Master Mix (Roche). RT-qPCR was also performed to assess the degradation of the mutant mRNA by nonsense-mediated decay (NMD). A blood sample was obtained from patient 4 in PAXgene Blood RNA Tube (Qiagen, Germantown, CA, USA) and total RNA extracted using Qiagen PAXgene Blood miRNA kit (Qiagen, Germantown, CA, USA). As controls, total RNA was prepared with TRIzol reagent (ThermoFisher Scientific) from blood sample obtained three male individuals aged between 3 and 8 years who do not carry any *KIF21B* variants in PAXgene Blood RNA Tube. We used hKIF21B ex2-3 and hKIF21B ex33-34 coupled primers to target *hKIF21B* cDNA and hTBP as housekeeping gene normalizer.

Cell culture, transfections and immunolabeling. All cells used in this study are provided by the cell culture platform of the IGBMC (Strasbourg), are guaranteed mycoplasma free (PCR test Venorgem) and have not been authenticated. Mouse neuroblastoma N2A (ATCC) cells and Cos7 (ATCC) cells were cultured in DMEM (1 g/L glucose, GIBCO) supplemented with 5% Fetal Calf Serum (FCS) and Gentamycin 40 μg/mL in a humidified atmosphere containing 5% CO₂ at 37 °C. Human embryonic kidney (HEK) 293T cells were cultured in DMEM (1 g/L glucose) (GIBCO) supplemented with 10% FCS, penicillin 100 UI/mL, streptomycin

100 μg/mL in a humidified atmosphere containing 5% CO₂ at 37 °C. Mouse ST cells are neuronal progenitor cell lines from E14 striatal primordia of WT embryos immortalized using tsA58 SV40 large T antigen⁶⁵. ST cells were cultured DMEM (1 g/L glucose) supplemented with 10% FCS heat-inactivated, non-essential amino acids, penicillin 100 UI/mL, streptomycin 100 μg/mL and G418 400 μg/mL in a humidified atmosphere containing 5% CO₂ at 33 °C. Cells were transfected using Lipofectamine 2000 (Invitrogen) according to the manufacturer's protocol. Expression of transfected genes was analyzed 48 h after transfection by immunoblotting. For localization experiments, ST cells were fixed 48 h after transfection for 5 min in -20 °C MeOH/AcOH solution (1:1), and incubated for 1 h in 0.5% Triton X-100, 5% NDS in PBS. Primary antibodies were incubated overnight at 4 °C and secondary antibodies were incubated for 1 h at room temperature (see Supplementary Table 1 for antibodies). DNA was stained using DAPI (1/1000). Slides were air-dried and mounted in Aquapolymount mounting medium (Polysciences Inc).

Immunoprecipitation. Immunoprecipitation (IP) experiments were done using the Pierce Anti-Myc Magnetic Beads kit (ThermoScientific) according to the manufacturer's protocol. HEK293T cells were transfected with the indicated HA-tagged, GFP-tagged and Myc-tagged constructs (ratio 1:1:2) using X-treme GENE 9 DNA transfection reagent (Roche). Cells were lysed 24 h after transfection in ice-cold IP buffer from the kit, supplemented with EDTA-free protease inhibitors (cOmplete™, Roche) and 0.01 M phosphatase inhibitor PMSF, for 30 min on ice. Cells debris were removed by high speed centrifugation at 4 °C for 15 min. After protein concentration measurement, samples were diluted to 1 μg/μL. Half of the protein were kept (Input) and diluted in 2× Laemmli Elution Buffer (Bio-Rad) containing 2% β-mercaptoethanol. 400 μg of proteins were then incubated with 15 μL of pre-washed magnetic Myc-coupled beads for 2 h at 4 °C under gentle shaking. Beads were collected using a magnetic stand and supernatants were discarded. Beads were then washed twice with IP buffer and proteins were eluted at 95 °C by adding 2× Laemmli Elution Buffer containing 2% β-mercaptoethanol. The same volume of sample for all condition were loaded and analyzed by western blot as described below.

Protein extraction and western blot. Proteins from mouse cortices (E14.5 to P2) or from transfected cells (N2A, HEK293T, Cos7 and ST cells) were extracted as follows: cells were lysed in RIPA buffer (50 mM Tris pH 8.0, 150 mM NaCl, 5 mM EDTA pH 8.0, 1% Triton X-100, 0.5% sodium deoxycholate, 0.1% SDS) supplemented with EDTA-free protease inhibitors (cOmplete™, Roche) for 30 min, then cells debris were removed by high speed centrifugation at 4 °C for 25 min. Protein concentration was measured by spectrophotometry using Bio-Rad Bradford protein assay reagent. Samples were denatured at 95 °C for 10 min in Laemmli buffer (Bio-Rad) supplemented with 2% β-mercaptoethanol and then resolved by SDS-PAGE and transferred onto nitrocellulose membranes. Membranes were blocked in 5% milk in PBS buffer with 0.1% Tween (PBS-T) and incubated overnight at 4 °C with the appropriate primary antibody in blocking solution. Membranes were washed three times in PBS-T, incubated at room temperature for 1 h with HRP-coupled secondary antibodies (Invitrogen) at 1:10,000 dilution in PBS-T, followed by three times PBS-T washes. Visualization was performed by quantitative chemiluminescence using SuperSignal West Pico PLUS Chemiluminescent Substrate (Sigma). Signal intensity was quantified using ImageQuant LAS 600 (GE Healthcare). Primary and secondary coupled HRP antibodies used for western blot are described in Supplementary Table 1. Relative protein expression was quantified using ImageJ software (Java 1.8.0_112).

Cycloheximide (CHX) treatment. To assess the protein half-life of WT- and mutated hKIF21B proteins, treatments using the translational inhibitor cycloheximide (CHX) were performed. N2A cells were cultured on 6-well plates and transfected with the adequate NeuroD- hKIF21B constructs using Lipofectamine 2000 (Invitrogen) according to the manufacturer's protocol. The day after, cells were treated with CHX (Sigma) diluted in media at 10 μg/mL for either 2, 4, 6, 8 or

Table 2 List of primers used for RT-qPCR.			
Gene	Specie	Forward sequence	Reverse sequence
mKIF21B ex2-3	Mouse	AAGGCTGCTTTGAGGGCTAT	AAAGCCGGTGCCCATAGTA
hKIF21B ex3-4	Human	GTCAGTCTCGCCTCATCCA	CTCTGCACGTTCACTCTGGGT
hKIF21B ex33-34	Human	TCATGGGCTCCCGAGATAAC	CTTGTCGCGATTGGGGATTT
drKIF21B ex2-3	Zebrafish	TCATCGAGGGCTGCTTTGAG	GACACGCTCACGTCAAACC
GFP		TACGGCAAGCTGACCCTGAAGT	GAAGTCGTGCTGCTTCATGTGG
mGAPDH	Mouse	TGATGACATCAAGAAGGTGGTGAAG	TCCTTGGAGGCCATGTAGGCCAT
drElfA	Zebrafish	CTTCTCAGGTCTGACTGTGC	CCGCTAGCAATTACCTCC
hTBP	Human	CGGCTGTTTAAGTCTCGCTTC	CACACGCCAAGAACAACAGTGA
Hprt1	Human	AGGCGAACCTCTCGGCTTTC	TCATCATCACTAATCACGACGCC

10 h. Cells were lysed as described above. For analysis, 10 µg of protein of each sample were loaded on a SDS-gel followed by western blotting analysis as described above. Experiments consisted of at least three independent replicates. Relative protein expression was quantified using ImageJ software (Java 1.8.0_112).

Zebrafish manipulation. Zebrafish (*D. rerio*) embryos (AB strain) maintenance and experiments were performed as described here https://zfinfo.org/zf_info/zfbook/cont.html#cont1. Human WT and mutant full-length cDNA were cloned into pCS2 vector and transcribed using the SP6 Message Machine kit (Ambion). We injected 1 nL of diluted RNAs (WT or mutants) at 100 ng/µL into wild-type zebrafish eggs at 1- to 2-cell stage. Length of the head was measured at 5 dpf as shown by the double arrow headed red lines (Fig. 5a). All the experiments were repeated at least three times and an unpaired two-tailed Student's *t*-test or a Welch's two samples *t*-test (when the variances are unequal) was performed to determine significance. All images were taken using a macroscope (Leica M420) dedicated to brightfield acquisitions equipped with a Coolsnap CF camera controlled by Coolsnap software. To perform zebrafish whole-mount immunolabeling, larvae were fixed at 5 dpf in Dent's fixative (80% methanol, 20% dimethylsulfoxide [DMSO]) overnight at 4 °C. The larvae were rehydrated slowly by decreasing concentrations of methanol. Larvae were then washed in PBS buffer with 0.1% Tween (PBS-T). After bleaching for 30 min in (10% H₂O₂ in PBS-T with KOH (0.5 g/mL)), the larvae were rinsed in PBS-T, twice for 10 min each. Then larvae were permeabilized with proteinase K, then post-fixed with 4% PFA and washed in PBS-T. PFA-fixed larvae were washed in IF buffer (0.1% Tween-20, 1% BSA in PBS) for 10 min, then incubated in the blocking buffer (10% FBS, 1% BSA in PBS) for 1 h at room temperature. Larvae were incubated with primary antibody diluted in blocking solution, overnight at 4 °C (see Supplementary Table 1 for antibodies). After two washes in IF Buffer for 10 min each, larvae were incubated in secondary antibody diluted in blocking solution 2 h at room temperature. Larvae were washed in IF buffer for 10 min, twice. All images were taken using an epifluorescence macroscope at ×5 magnification equipped with a Coolsnap CF camera controlled by Coolsnap software v1.2.

Image acquisition and analysis. Cell counting and in vivo branching analyses were done in at least three different brain slices of at least three different embryos or pups for each condition. After histological examination, only brains with comparative electroporated regions and efficiencies were conserved for quantification.

For neuronal migration analyses, proliferation analyses and brain immunofluorescence experiments, a *z* stack of 1.55 µm was acquired in 1024 × 1024 mode using a confocal microscope (Leica TCS SP5 equipped with an hybrid camera and a HC PL APO ×20/0.70 objective) controlled by Leica Las X software v3.7 and analyzed using ImageJ software (Java 1.8.0_112). Cortical wall areas (upper cortical plate (Up CP), lower cortical plate (Lo CP), intermediate zone (IZ), subventricular zone (SVZ)/ventricular zone (VZ)) were identified according to cell density (nuclei staining with DAPI). The total number of GFP-positive cells in the embryonic brain sections was quantified by counting positive cells within a box of fixed size and the percentage of positive cells in each cortical area was calculated. For proliferation analyses, the total number of markers-positive cells in embryonic brain sections was quantified by counting positive cells in the intermediate zone (IZ) and in the subventricular zone (SVZ) below the electroporated region using square of 100-µm width or 50-µm width, respectively, with anatomically matched positions in experimental groups.

For in vivo branching analyses, a *z* stack of 3 µm was acquired in 1024 × 1024 mode using confocal microscope (Leica TCS SP5 equipped with an hybrid camera and a PL FL ×10/0.30 objective) and analyzed using ImageJ software (Java 1.8.0_112). For axonal midline crossing analyses, the fluorescence within a box of fixed size placed at the contralateral side of the midline of the brain section was measured and divided by the fluorescence at the ipsilateral side of the midline area (Fig. 6c). This value was normalized to empty vector (control) value. For projecting neurons analyses, the fluorescence intensity within a box of fixed size placed at the ipsilateral side of the midline of the brain section was measured using ImageJ (Java 1.8.0_112) and this value was divided by the number of Scarlet-positive neurons within a box of fixed size placed at the upper cortical plate (Fig. 6d). For quantification of layer V (ipsilateral) collateral branching, a box of fixed size was drawn encompassing layer V and the fluorescence area within this box was measured. This value was then divided by the fluorescence at the ipsilateral side of the midline area (Fig. 7c). We quantified contralateral branching⁶⁶ as follows: fluorescence within a box of fixed size placed contralaterally is measured on a vertical axis (from ventricular boundaries to pial surface) and converted from pixel size to percentile (0%: ventricular zone, 100%: pial surface) using the ProfilePlot plugin from FIJI software. Signal intensity of 100% is set as the maximum signal intensity in migration percentile 0 to 20 (considered as the white matter).

For in vitro branching analyses, primary neuronal cultures were done independently at least two (DIV5) or three (DIV2) times. DIV2 and DIV5 axonal length measures were performed in 125–146 and 30–66 independent cells respectively. For DIV5 axon collateral length distribution analyses, measures were performed in 187–385 collaterals from 30 to 66 independent cells. Images were acquired using upright fluorescence (DM 4000B; Leica) equipped with a HC PLAN APO20/×0.70 objective and a CoolSnap FX monochrome camera (Photometrics)

controlled by Leica Las X software v3.7. To measure the axonal length (longest neurite) at DIV2 and DIV5, the longest Scarlet-positive-labeled neurite was traced and the length was measured using Simple Neurite Tracer plugin (https://imagej.net/Simple_Neurite_Tracer) from FIJI software. Branch number and length was measured at DIV5 using Simple Neurite Tracer plugin.

For variant subcellular localization analysis (Fig. 4e, f), a *z* stack of 0.13 µm was acquired in 1024 × 1024 mode using a confocal microscope (Leica TCS SP5 equipped with an hybrid camera, using a HCX PL APO ×63/1.40–0.60 oil objective) controlled by Leica Las X software v3.7. For each condition, 67 to 229 independent cells from three independent transfections were segregated according to the subcellular localization of HA-tagged constructs (diffuse localization versus impaired localization).

Live-cell imaging procedure and analysis. Cos7 cells were grown on 35-mm glass bottom microwell dishes No. 0 (MatTek, U.S.A.). Cells were transfected with the different pcEGFP-N1-hKIF21B constructs or co-transfected with BDNF-mCherry (gift from Gary Banker, Oregon Health and Science University, Portland, USA) or Mito-RFP (gift from Hélène Puccio, IGBMC, Illkirch, France) and the different pcDNA3.1+/N-HA-hKIF21B constructs or empty vector with a DNA ratio of 1:2 as described above. Live-cell imaging was done 24 h after transfection. Live videomicroscopy was performed on an inverted microscope Leica CSU W1 DM18 (Leica) with an Adaptive Focus Control (AFC) controlled by Metamorph software v 7.6, using an HCX PL APO Lambda blue ×63/1.40 oil objective or an HC PL APO 100 × 1.47 oil objective. The microscope and the chamber were kept at 37 °C and 5% CO₂. Images were collected using an Orca Flash 4.0 camera with an exposure time of 80–150 ms. Images were acquired every 250 ms for 30 s to 1 min. Single GFP-positive kinesin were tracked using Manual Tracking plugin (<https://imagej.nih.gov/ij/plugins/track/track.html>) from Fiji software. For each condition, 182–203 kinesin particles in 25–32 independent cells were analyzed from at least three independent transfections. BDNF vesicles velocities and RFP-positive mitochondria were obtained from kymograph analysis, using FIJI plugin Kymo Tool-Box v.1.01 (https://github.com/fabricecordelieres/IJ-Plugin_KymoToolBox/releases). For each condition, 250–322 BDNF particles in 10–19 independent cells were analyzed from at least three independent transfections. For each condition, 173–256 Mito-RFP particles in 19–31 independent cells were analyzed from four independent transfections.

Statistics and reproducibility. Immunofluorescence, in situ hybridization, FACS-sorting and western blot experiments (Figs. 2c–e and 3e; Supplementary Figs. 2a–d, 3c, 4c, 5b) were repeated three times independently and gave similar results. Experiments on Kif21b WT and knockout mouse brain (Supplementary Fig. 2e, f) were performed on *n* = 3 and *n* = 5 different brains per genotype, respectively, and gave similar results. Western blot expression profile of NeuroD-IRES-GFP constructs (Supplementary Fig. 3a), HA-tagged, Myc-tagged (Supplementary Fig. 4a) and GFP-tagged constructs (Supplementary Fig. 4b) were performed once. For in utero electroporation experiments, only brains with comparative electroporated regions and efficiencies were conserved for quantification and statistical analyzes. Analysis of IUE experiments were performed blinded. For one embryo or pup brain, cell counting and in vivo branching analyses were performed in three different slices. The exact numbers (*n*) of samples, animals, cells, particles, axons or branches used to derive statistics are mentioned in figure legends along with the respective data and are also reported in Supplementary Data 1. The number of times each experiment was repeated independently (i.e. the number of independent transfection or magnetofection) and statistical tests are mentioned in figure legends along with the respective data whenever possible, and are also reported in Supplementary Data 1. Statistical details (adjustments made for multiple comparisons, confidence intervals and exact *P*-values) for Figs. 2a; 3b, d; 4b, d, e—right panel, g, h, j; 5b; 6d, e, g; 7c–e, g; Supplementary Figs. 3d, f; 4d—right panel, f, g; 6d; 7b–d, are reported in Supplementary Data 1. All statistics were calculated using Prism (GraphPad, version 6) and are represented as mean ± S.E.M. Graphs were generated using Prism and images were assembled with Adobe Photoshop 13.0.1 (Adobe Systems).

Reporting summary. Further information on research design is available in the Nature Research Reporting Summary linked to this article.

Data availability

The source data underlying Figs. 2a, b; 3b, d; 4b, d, e, g, h, j; 5b; 6c, d, e, g; 7c, d, e, g; and Supplementary Figs. 1d; 2d, f; 3a, b, d, f, h; 4a, b, d, f, g, h, i; 5a, d, g, j; 6c, d, h; 7b, c, d are provided as a Source Data file. All other relevant data included in the article are available from the authors upon request. The following databases and in silico software were used in the study: Human Gene Mutation Databases (<http://www.hgmd.cf.ac.uk/ac/introduction.php?lang=english>), the single Nucleotide Polymorphism database (<http://ftp.ncbi.nih.gov/snp/>), genome aggregation database (gnomAD, <https://gnomad.broadinstitute.org/>), 1000 genomes (<https://www.internationalgenome.org/>), Polyphen-2 (<http://genetics.bwh.harvard.edu/pph2/>), Mutation Taster (<http://www.mutationtaster.org/>), Sorting Intolerant from Tolerant (SIFT, <https://sift.bii.a-star.edu.sg/>) and Combined Annotation Dependent Depletion (CADD, <https://cadd.gs.washington.edu/>).

The three *hKIF21B* missense variants have been deposited in LOVD (Leiden Open Variation Database) v3.0 (<https://databases.lovd.nl/shared/genes/KIF21B>) under the accession numbers 0000663938 (p.Ile678Leu), 0000663939 (p.Gln313Lys) and 0000663940 (p.Ala1001Thr).

Received: 17 June 2019; Accepted: 26 April 2020;

Published online: 15 May 2020

References

- Hirokawa, N. Kinesin and dynein superfamily proteins and the mechanism of organelle transport. *Science* **279**, 519–526 (1998).
- Hirokawa, N. & Tanaka, Y. Kinesin superfamily proteins (KIFs): various functions and their relevance for important phenomena in life and diseases. *Exp. Cell Res.* **334**, 16–25 (2015).
- Caraballona, A., Hu, D. J. & Vallee, R. B. KIF1A inhibition immortalizes brain stem cells but blocks BDNF-mediated neuronal migration. *Nat. Neurosci.* **19**, 253–262 (2016).
- Chen, J. L., Chang, C. H. & Tsai, J. W. Gli2 rescues delays in brain development induced by Kif3a dysfunction. *Cereb. Cortex* **29**, 751–764 (2018).
- Foerster, P. et al. mTORC1 signaling and primary cilia are required for brain ventricle morphogenesis. *Development* **144**, 201–210 (2017).
- Sun, D. et al. Regulation of neural stem cell proliferation and differentiation by Kinesin family member 2a. *PLoS ONE* **12**, e0179047 (2017).
- Tsai, J. W., Lian, W. N., Kemal, S., Kriegstein, A. R. & Vallee, R. B. Kinesin 3 and cytoplasmic dynein mediate interkinetic nuclear migration in neural stem cells. *Nat. Neurosci.* **13**, 1463–1471 (2010).
- Wilson, S. L., Wilson, J. P., Wang, C., Wang, B. & McConnell, S. K. Primary cilia and Gli3 activity regulate cerebral cortical size. *Dev. Neurobiol.* **72**, 1196–1212 (2012).
- Geng, A. et al. KIF20A/MKLP2 regulates the division modes of neural progenitor cells during cortical development. *Nat. Commun.* **9**, 2707 (2018).
- Janisch, K. M. et al. The vertebrate-specific Kinesin-6, Kif20b, is required for normal cytokinesis of polarized cortical stem cells and cerebral cortex size. *Development* **140**, 4672–4682 (2013).
- Reilly, M. L. et al. Loss of function mutations in KIF14 cause severe microcephaly and kidney development defects in humans and zebrafish. *Hum. Mol. Genet.* **28**, 778–795 (2018).
- Falnikar, A., Tole, S. & Baas, P. W. Kinesin-5, a mitotic microtubule-associated motor protein, modulates neuronal migration. *Mol. Biol. Cell* **22**, 1561–1574 (2011).
- Falnikar, A., Tole, S., Liu, M., Liu, J. S. & Baas, P. W. Polarity in migrating neurons is related to a mechanism analogous to cytokinesis. *Curr. Biol.* **23**, 1215–1220 (2013).
- Homma, N. et al. Kinesin superfamily protein 2A (KIF2A) functions in suppression of collateral branch extension. *Cell* **114**, 229–239 (2003).
- Liu, M. et al. Kinesin-12, a mitotic microtubule-associated motor protein, impacts axonal growth, navigation, and branching. *J. Neurosci.* **30**, 14896–14906 (2010).
- Myers, K. A. & Baas, P. W. Kinesin-5 regulates the growth of the axon by acting as a brake on its microtubule array. *J. Cell Biol.* **178**, 1081–1091 (2007).
- Peretti, D., Peris, L., Rosso, S., Quiroga, S. & Caceres, A. Evidence for the involvement of KIF4 in the anterograde transport of L1-containing vesicles. *J. Cell Biol.* **149**, 141–152 (2000).
- Xu, M. et al. Kinesin-12 influences axonal growth during zebrafish neural development. *Cytoskeleton* **71**, 555–563 (2014).
- Midorikawa, R., Takei, Y. & Hirokawa, N. KIF4 motor regulates activity-dependent neuronal survival by suppressing PARP-1 enzymatic activity. *Cell* **125**, 371–383 (2006).
- Kondo, M., Takei, Y. & Hirokawa, N. Motor protein KIF1A is essential for hippocampal synaptogenesis and learning enhancement in an enriched environment. *Neuron* **73**, 743–757 (2012).
- Muhia, M. et al. The kinesin KIF21B regulates microtubule dynamics and is essential for neuronal morphology, synapse function, and learning and memory. *Cell Rep.* **15**, 968–977 (2016).
- Nakajima, K. et al. Molecular motor KIF5A is essential for GABA(A) receptor transport, and KIF5A deletion causes epilepsy. *Neuron* **76**, 945–961 (2012).
- Swarnkar, S., Avshalomov, Y., Raveendra, B. L., Grinman, E. & Puthanveetil, S. V. Kinesin family of proteins Kif11 and Kif21B act as inhibitory constraints of excitatory synaptic transmission through distinct mechanisms. *Sci. Rep.* **8**, 17419 (2018).
- Willemsen, M. H. et al. Involvement of the kinesin family members KIF4A and KIF5C in intellectual disability and synaptic function. *J. Med. Genet.* **51**, 487–494 (2014).
- Najmabadi, H. et al. Deep sequencing reveals 50 novel genes for recessive cognitive disorders. *Nature* **478**, 57–63 (2011).
- Putoux, A. et al. KIF7 mutations cause fetal hydrolethrus and acrocallosal syndromes. *Nat. Genet.* **43**, 601–606 (2011).
- Dafinger, C. et al. Mutations in KIF7 link Joubert syndrome with Sonic Hedgehog signaling and microtubule dynamics. *J. Clin. Invest.* **121**, 2662–2667 (2011).
- Jamuar, S. S. et al. Somatic mutations in cerebral cortical malformations. *N. Engl. J. Med.* **371**, 733–743 (2014).
- Ostergaard, P. et al. Mutations in KIF11 cause autosomal-dominant microcephaly variably associated with congenital lymphedema and chorioretinopathy. *Am. J. Hum. Genet.* **90**, 356–362 (2012).
- Poirier, K. et al. Mutations in TUBG1, DYNC1H1, KIF5C and KIF2A cause malformations of cortical development and microcephaly. *Nat. Genet.* **45**, 639–647 (2013).
- Tian, G. et al. A patient with lissencephaly, developmental delay, and infantile spasms, due to de novo heterozygous mutation of KIF2A. *Mol. Genet. Genomic Med.* **4**, 599–603 (2016).
- Cavallin, M. et al. Recurrent KIF2A mutations are responsible for classic lissencephaly. *Neurogenetics* **18**, 73–79 (2017).
- Michels, S. et al. Mutations of KIF5C cause a neurodevelopmental disorder of cortical development. *Am. J. Med. Genet. A* **173**, 3127–3131 (2017).
- Ohba, C. et al. De novo KIF1A mutations cause intellectual deficit, cerebellar atrophy, lower limb spasticity and visual disturbance. *J. Hum. Genet.* **60**, 739–742 (2015).
- Konjikusik, M. J. et al. Mutations in Kinesin family member 6 reveal specific role in ependymal cell ciliogenesis and human neurological development. *PLoS Genet.* **14**, e1007817 (2018).
- Filges, I. et al. Exome sequencing identifies mutations in KIF14 as a novel cause of an autosomal recessive lethal fetal ciliopathy phenotype. *Clin. Genet.* **86**, 220–228 (2014).
- Makrythanasis, P. et al. Biallelic variants in KIF14 cause intellectual disability with microcephaly. *Eur. J. Hum. Genet.* **26**, 330–339 (2018).
- Broix, L. et al. Ciliogenesis and cell cycle alterations contribute to KIF2A-related malformations of cortical development. *Hum. Mol. Genet.* **27**, 224–238 (2018).
- Labonte, D., Thies, E. & Kneussel, M. The kinesin KIF21B participates in the cell surface delivery of gamma2 subunit-containing GABAA receptors. *Eur. J. Cell Biol.* **93**, 338–346 (2014).
- Marszałek, J. R., Weiner, J. A., Farlow, S. J., Chun, J. & Goldstein, L. S. Novel dendritic kinesin sorting identified by different process targeting of two related kinesins: KIF21A and KIF21B. *J. Cell Biol.* **145**, 469–479 (1999).
- Huang, C. F. & Banker, G. The translocation selectivity of the kinesins that mediate neuronal organelle transport. *Traffic* **13**, 549–564 (2012).
- van Riel, W. E. et al. Kinesin-4 KIF21B is a potent microtubule pausing factor. *Elife* **6**, e24746 (2017).
- Gromova, K. V. et al. Neurobeachin and the kinesin KIF21B are critical for endocytic recycling of NMDA receptors and regulate social behavior. *Cell Rep.* **23**, 2705–2717 (2018).
- Ghiretti, A. E. et al. Activity-dependent regulation of distinct transport and cytoskeletal remodeling functions of the dendritic kinesin KIF21B. *Neuron* **92**, 857–872 (2016).
- Labonte, D. et al. TRIM3 regulates the motility of the kinesin motor protein KIF21B. *PLoS ONE* **8**, e75603 (2013).
- Bianchi, S. et al. Structural basis for misregulation of kinesin KIF21A autoinhibition by CFEOM1 disease mutations. *Sci. Rep.* **6**, 30668 (2016).
- Kannan, M. et al. WD40-repeat 47, a microtubule-associated protein, is essential for brain development and autophagy. *Proc. Natl Acad. Sci. USA* **114**, E9308–E9317 (2017).
- Morikawa, M., Tanaka, Y., Cho, H. S., Yoshihara, M. & Hirokawa, N. The molecular motor KIF21B mediates synaptic plasticity and fear extinction by terminating Rac1 activation. *Cell Rep.* **23**, 3864–3877 (2018).
- Olson, H. E. et al. Micro-duplications of 1q32.1 associated with neurodevelopmental delay. *Eur. J. Med. Genet.* **55**, 145–150 (2012).
- Sobreira, N., Schiettecatte, F., Valle, D. & Hamosh, A. GeneMatcher: a matching tool for connecting investigators with an interest in the same gene. *Hum. Mutat.* **36**, 928–930 (2015).
- Taylor, A. M. et al. A microfluidic culture platform for CNS axonal injury, regeneration and transport. *Nat. Methods* **2**, 599–605 (2005).
- Matsuda, T. & Cepko, C. L. Controlled expression of transgenes introduced by in vivo electroporation. *Proc. Natl Acad. Sci. USA* **104**, 1027–1032 (2007).
- Cheng, L. et al. Human CFEOM1 mutations attenuate KIF21A autoinhibition and cause oculomotor axon stalling. *Neuron* **82**, 334–349 (2014).
- van der Vaart, B. et al. CFEOM1-associated kinesin KIF21A is a cortical microtubule growth inhibitor. *Dev. Cell* **27**, 145–160 (2013).
- Golzio, C. et al. KCTD13 is a major driver of mirrored neuroanatomical phenotypes of the 16p11.2 copy number variant. *Nature* **485**, 363–367 (2012).

56. Igarashi, A. et al. Nuclear PTEN deficiency causes microcephaly with decreased neuronal soma size and increased seizure susceptibility. *J. Biol. Chem.* **293**, 9292–9300 (2018).
57. Thomanetz, V. et al. Ablation of the mTORC2 component rictor in brain or Purkinje cells affects size and neuron morphology. *J. Cell Biol.* **201**, 293–308 (2013).
58. Kelliher, M. T. et al. Autoinhibition of kinesin-1 is essential to the dendrite-specific localization of Golgi outposts. *J. Cell Biol.* **217**, 2531–2547 (2018).
59. Niwa, S. et al. Autoinhibition of a neuronal kinesin UNC-104/KIF1A regulates the size and density of synapses. *Cell Rep.* **16**, 2129–2141 (2016).
60. Retterer, K. et al. Clinical application of whole-exome sequencing across clinical indications. *Genet Med* **18**, 696–704 (2016).
61. Hand, R. & Polleux, F. Neurogenin2 regulates the initial axon guidance of cortical pyramidal neurons projecting medially to the corpus callosum. *Neural Dev.* **6**, 30 (2011).
62. Skarnes, W. C. et al. A conditional knockout resource for the genome-wide study of mouse gene function. *Nature* **474**, 337–342 (2011).
63. Zala, D. et al. Vesicular glycolysis provides on-board energy for fast axonal transport. *Cell* **152**, 479–491 (2013).
64. Virlogeux, A. et al. Reconstituting corticostriatal network on-a-chip reveals the contribution of the presynaptic compartment to Huntington's disease. *Cell Rep.* **22**, 110–122 (2018).
65. Trettel, F. et al. Dominant phenotypes produced by the HD mutation in STHdh(Q111) striatal cells. *Hum. Mol. Genet* **9**, 2799–2809 (2000).
66. Courchet, J. et al. Terminal axon branching is regulated by the LKB1-NUAK1 kinase pathway via presynaptic mitochondrial capture. *Cell* **153**, 1510–1525 (2013).

Acknowledgements

This work was funded by grants from INSERM (ATIP-Avenir program, J.D.G.), the Fyssen foundation (J.D.G.), the French state funds through the Agence Nationale de la Recherche under the project JCJC CREDO ANR-14-CE13-0008-01 (J.D.G.), CILAXCAL (C.D.) and AXION ANR-18-CE16-0009-01 (F.S.), and the program Investissements d'Avenir labeled (ANR-10-IDEX-0002-02, ANR-10-LABX-0030-INRT, to J.D.G. and C.G.), the Fondation pour la recherche sur le cerveau (F.S.), INSERM/CNRS and University of Strasbourg. N.A.H. and G.Z. are supported by USDA Grant Number 3092-51000-057-04S. L.A. and J.R.A. are funded through the IGBMC PhD program (ANR-10-IDEX-0002-02, ANR-10-LABX-0030-INRT). L.A. is currently supported by Fondation pour la recherche médicale (FDT201805005184). P.T. and C.W. are, respectively, research assistant and research engineer at the University of Strasbourg. J.D.G. and C.G. are INSERM investigators. F.S. is a professor at Univ. Grenoble Alpes. H.V. is supported by a PhD fellowship from Association Huntington France. We thank the Imaging Center of IGBMC (ici.igbmc.fr), in particular, Elvire Guiot and Erwan Grandgirard for their assistance in the imaging experiments. We are grateful to the staff of the mouse facilities of the Institut Clinique de la souris (ICS) and Institut de Génétique et de Biologie Moléculaire et Cellulaire (IGBMC), the staff of the zebrafish facility of the IGBMC and, the molecular biology service (in particular Thierry Lerouge and Paola Rossolillo) for their involvement in the project. We thank Sandra Bour and IGBMC communication service. We also thank Dr Courchet, Dr Banker, Dr Puccio and member of Chelly lab for sharing reagents and for discussion. We are really grateful to Pr Jamel Chelly and Dr Laurent Nguyen for their continuous support, discussion and time reading this manuscript. We warmly thank Dr Sandrine Humbert and Dr Binnaz Yalcin for helpful comments and advices. We are also grateful to members of J.D.G. and Chelly

laboratories for discussion and technical assistance. In particular, we thank Dr Efil Bayam for cell sorting and advices in writing the manuscript. We thank Dr Gabrielle Rudolf for reading the manuscript and for her suggestions. We finally thank Paula Hernandez for her help collecting patient samples.

Author contributions

L.A. and J.R.A. conceived and designed the experiments, performed the experiments, performed statistical analysis and analyzed the data related to cellular, and functional studies in mice. P.T. provided technical assistance and performed in utero electroporation. C.G. and C.S.B. conceived, designed and performed experiments in zebrafish. C.W. provided technical assistance for zebrafish studies. S.H., K.B., C.A.B., A.C., A.D., S.M., L.F., N.A.H., K.M., C.M., H.S., C.T.R., M.M.W., P.J.G.Z., G.Z. and D.H. contributed clinical and imaging data and follow-up of patients and families. S.H., A.R., C.N. and C.D. contributed to the generation of whole-exome sequencing, bioinformatics tools and analysis of sequencing data. H.V. and F.S. conceived and performed the expression analysis in microdevices. J.D.G. conceived, coordinated and supervised the study, designed experiments, analyzed data and wrote the manuscript.

Competing interests

A.D. and K.M. are employees of GeneDx, Inc. The other authors declare no competing interest.

Additional information

Supplementary information is available for this paper at <https://doi.org/10.1038/s41467-020-16294-6>.

Correspondence and requests for materials should be addressed to J.D.G.

Peer review information *Nature Communications* thanks the anonymous reviewer(s) for their contribution to the peer review of this work. Peer reviewer reports are available.

Reprints and permission information is available at <http://www.nature.com/reprints>

Publisher's note Springer Nature remains neutral with regard to jurisdictional claims in published maps and institutional affiliations.



Open Access This article is licensed under a Creative Commons Attribution 4.0 International License, which permits use, sharing, adaptation, distribution and reproduction in any medium or format, as long as you give appropriate credit to the original author(s) and the source, provide a link to the Creative Commons license, and indicate if changes were made. The images or other third party material in this article are included in the article's Creative Commons license, unless indicated otherwise in a credit line to the material. If material is not included in the article's Creative Commons license and your intended use is not permitted by statutory regulation or exceeds the permitted use, you will need to obtain permission directly from the copyright holder. To view a copy of this license, visit <http://creativecommons.org/licenses/by/4.0/>.

© The Author(s) 2020

¹Institut de Génétique et de Biologie Moléculaire et Cellulaire, Illkirch, France. ²Centre National de la Recherche Scientifique, UMR7104, Illkirch, France. ³Institut National de la Santé et de la Recherche Médicale, INSERM, U1258 Illkirch, France. ⁴Université de Strasbourg, Strasbourg, France. ⁵Département de Génétique, AP-HP, Hôpital de la Pitié-Salpêtrière, Paris, France. ⁶Groupe de Recherche Clinique (GRC) "Déficiência Intellectuelle et Autisme", UPMC, Paris, France. ⁷Centre de Référence Déficiences Intellectuelles de Causes Rares, Hôpital de la Pitié-Salpêtrière, Paris, France. ⁸Univ. Grenoble Alpes, INSERM, U1216, CHU Grenoble Alpes, Grenoble Institut Neurosciences, Grenoble, France. ⁹Department of Molecular and Human Genetics, Baylor College of Medicine, Houston, TX, USA. ¹⁰Texas Children's Hospital, Houston, TX, USA. ¹¹Department of Neurogenetics, Kennedy Krieger Institute, Baltimore, MD 21205, USA. ¹²GeneDx, Gaithersburg, MD 20877, USA. ¹³Centre de Référence Anomalies du Développement et Syndromes Malformatifs, Fédération Hospitalo-Universitaire Médecine Translationnelle et Anomalies du Développement (TRANSLAD), Centre Hospitalier Universitaire Dijon et Université de Bourgogne, Dijon, France. ¹⁴Equipe GAD, INSERM LNC UMR 1231, Faculté de Médecine, Université de Bourgogne Franche-Comté, Dijon, France. ¹⁵Department of Neurology, Boston Children's Hospital, Boston, MA 02115, USA. ¹⁶INSERM, U 1127, CNRS UMR 7225, Faculté de Médecine de Sorbonne Université, UMR S 1127, Institut du Cerveau et de la Moelle épinière, ICM, Paris, France. ¹⁷Centre de Référence Déficiences Intellectuelles de Causes Rares, Centre Hospitalier Universitaire Dijon, Dijon, France. ¹⁸Department of Clinical Genetics, Amsterdam UMC, Vrije Universiteit Amsterdam, Amsterdam, The Netherlands. ¹⁹Institute of Human Genetics, University Hospital Essen, University of Duisburg-Essen, Essen, Germany. ²⁰These authors contributed equally: José Rivera Alvarez, Solveig Heide, Camille S. Bonnet ✉email: godin@igbmc.fr

Supplementary Information

Mutations in the *KIF21B* kinesin gene cause neurodevelopmental disorders through imbalanced canonical motor activity

Asselin et al

Content:

- **Supplementary Note 1:** Clinical features of patients with *KIF21B* variants
- **Supplementary Figure 1:** Patients with *KIF21B* mutations, related to Figure 1.
- **Supplementary Figure 2:** Kif21b expression in mouse developing cortex, related to Figure 2.
- **Supplementary Figure 3:** Expression of *hKIF21B* missense variants induce abnormal neuronal migration, related to Figure 3.
- **Supplementary Figure 4:** KIF21B missense variants induce abnormal neuronal migration through enhanced KIF21B motor activity, related to Figure 4.
- **Supplementary Figure 5:** Overexpression of the p.Gln313Lys *hKIF21B* variant does not impair proliferation in the developing mouse brain, related to Figure 5.
- **Supplementary Figure 6:** p.Ile678Leu *hKIF21B* variant impedes interhemispheric connectivity through aberrant motor activity, related to Figure 6.
- **Supplementary Figure 7:** Overexpression of p.Ile678Leu *hKIF21B* variant impairs ipsilateral intracortical axon collaterals formation through a dominant negative effect on motility, related to figure 7.
- **Supplementary Table 1:** List of primary and secondary antibodies used in this work.

Supplementary Note 1: Clinical features of patients with *KIF21B* variants

Patient 1 (NM_001252100.1, c.2032A>C, p.Ile678Leu)

Patient 1 is the second child of healthy, Caucasian, non-consanguineous parents. He was born at full term with normal growth parameters and had an uncomplicated neonatal course. Concerns about development were raised at 18 months when he started walking. He had an uneven gait, stereotypies and no speech. Brain MRI at age two years revealed isolated complete agenesis of the corpus callosum (Fig. 1e). He presented with down-slanting palpebral fissures and downturned corners of the mouth. His first words were at 36 months. He currently has appropriate expressive language despite persistent dysarthria. He was evaluated at six years and nine months (WISC IV) and total IQ was 78 which is consistent with borderline intellectual disability (ID). He has learning disabilities and is therefore cared for in a medico educational institution. He takes methylfenidate due to hyperactivity. Most recent neurological examination was unremarkable. The patient has muscle stiffness, but benefits from physical therapy to ease pain.

Patient 2 (NM_001252100.1, c.937C>A, p.Gln313Lys)

Patient 2 is the child of healthy, non-consanguineous, African American parents. The pregnancy was complicated by intra uterine growth restriction and oligohydramnios. He was born at 38 weeks gestation with height at 49cm (49th percentile), weight at 2.584kg (7th percentile) and head circumference at 32cm (5th percentile). He had a nuchal cord at birth transient cyanosis associated with mild respiratory distress, but was discharged home without complications. He presented with severe developmental delay. He was unable to sit and was non-verbal. Clinical examination at 12 years old showed growth difficulties with weight at 20kg (<1st percentile), height at 139 cm (8th percentile) and microcephaly with head circumference at 48.5cm (<1st percentile, -3.9 SD). He had poor visual fixation with constant tongue thrusting and poor head control. He presented with bilateral ankle tightness, and right wrist contracture.

Patient 3 (NM_001252100.1, c.3001G>A, p.Ala1001Thr)

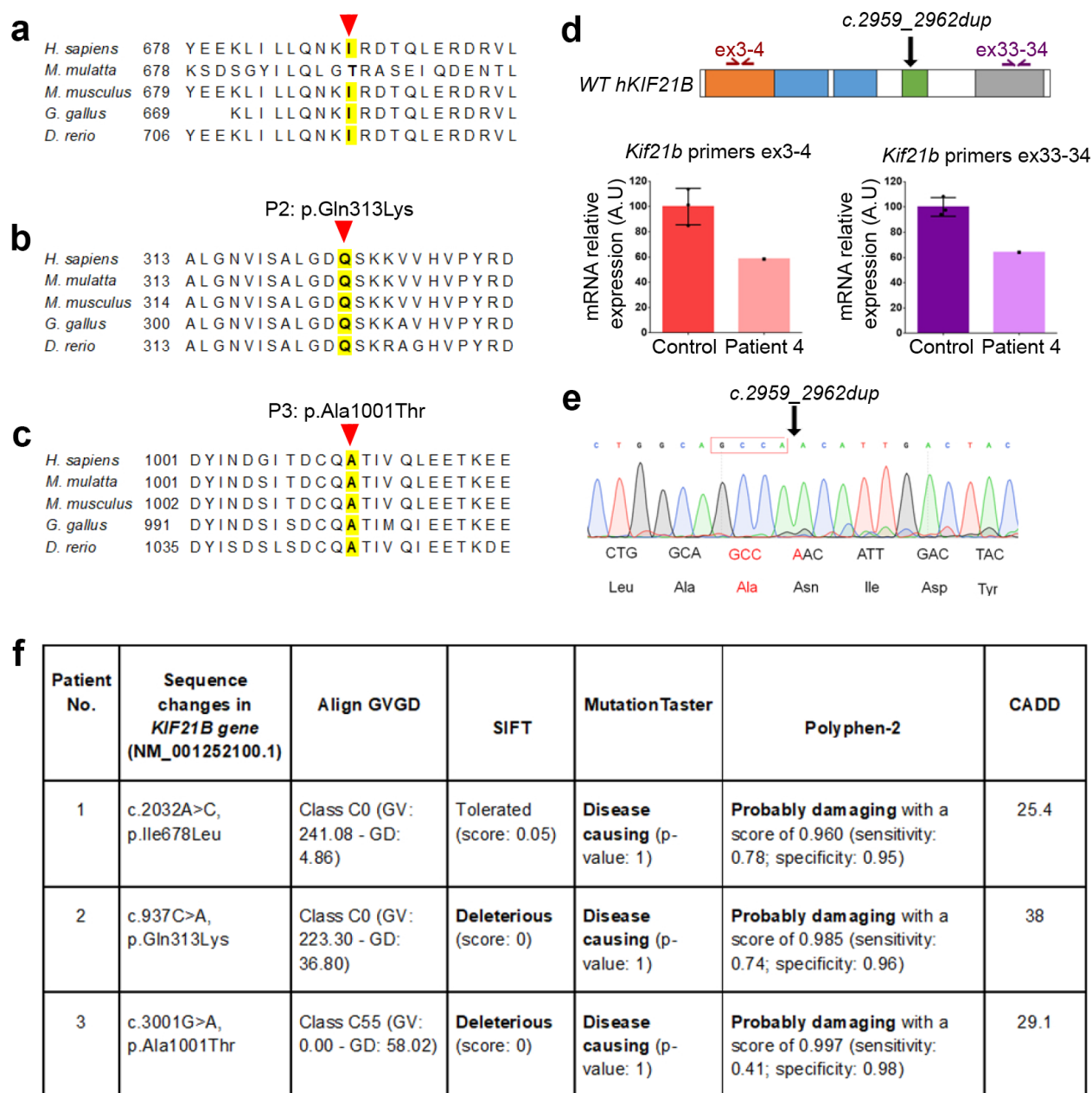
Patient 3 is a girl of non-consanguineous Dutch parents. Both parents have a reported personal history of mild intellectual disability. The father is a carrier of the variant and present with developmental delay and

learning difficulties. The pregnancy was routine and she was born at full term with normal growth parameters. Her psychomotor development was delayed, she sat at ten months and walked at 24 months. She said her first words at 36 months of age. At age five years, she was able to speak in sentences. She was evaluated at nine years and verbal and performance IQ were 54 and 59 respectively, which is consistent with mild to moderate ID. Upon clinical examination, she had mild dysmorphic features including epicanthal folds, mild ptosis, and tented upperlip. Her legs were mildly hypertonic. The brain MRI did not show any structural abnormalities.

Patient 4 (NM_001252100.1, c.2959_2962dup, p.Asn988Serfs*4)

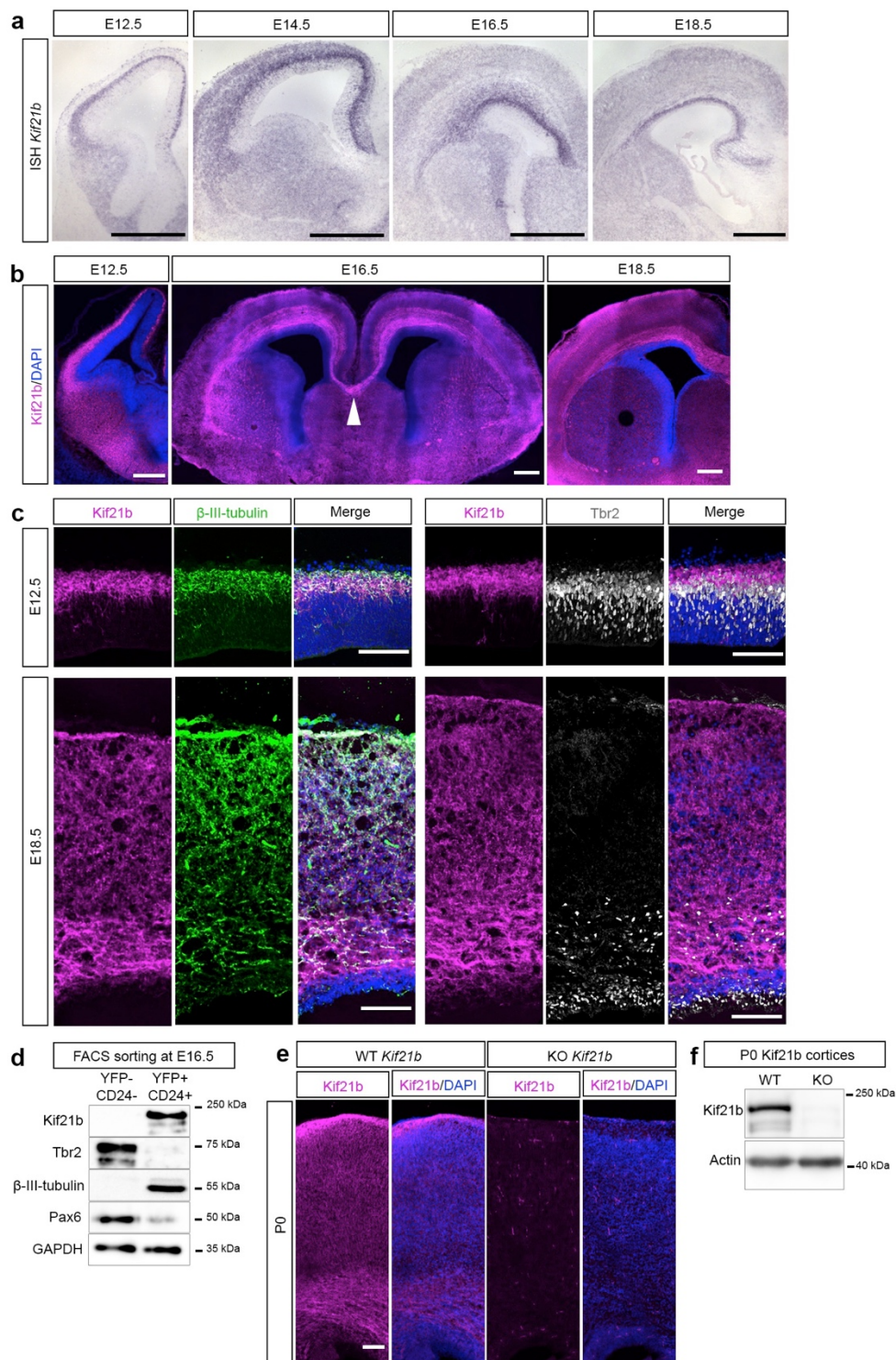
Patient 4 was born to non-consanguineous parents. Mother had a seizure disorder and she took Topiramate during the pregnancy. Antenatal ultrasound was positive for the fetus measuring small for gestational age. He was born at 38 weeks gestation by cesarean section secondary to repeat maternal seizures. Neonatal mensurations confirmed hypotrophy with birth height at 43 cm (<1st percentile) and birth weight at 2633 g (8th percentile). He had feeding difficulties in the neonatal period requiring an NG tube. Problems persisted and he received a G-tube at 18 months. Currently, he takes mainly by mouth and uses the G-tube for medications. He has a history of moderate to severe constipation. At 37 months of age, he had a developmental quotient of 97 consistent with a history of mild global developmental delays. He was diagnosed with right Duane syndrome and has central sleep apnea requiring C pap after adenoidectomy. He had a chromosome microarray (CMA) that was non-diagnostic; it showed he was a carrier for Poretti-Boltshauser syndrome [OMIM: 615960] due to a single heterozygous LAMA1 deletion and a gain on 22q11.23 with no clinical consequence associated. He has also had normal mitochondrial sequencing.

Supplementary Figure 1: Patients with *KIF21B* variants, related to Figure 1.



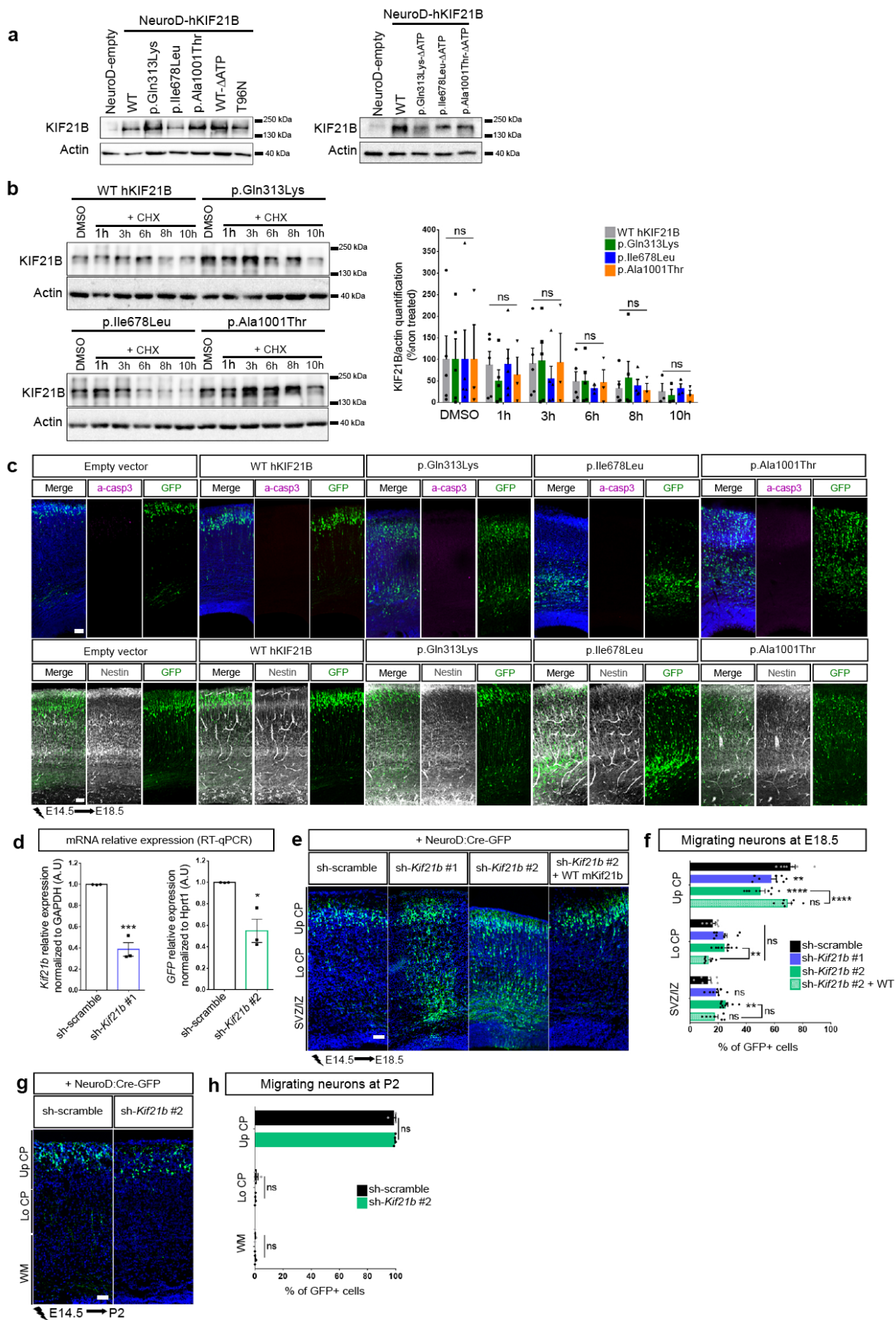
(a-c) Alignment of the *KIF21B* protein across several species (human, macaque, mouse, fish, chicken, zebrafish) shows the conservation of the mutated amino acid residue (red arrow head) in patients. (d) RT-qPCR analyses showing a decrease of *KIF21B* mRNA expression in Patient 4 (carrying a duplication c.2959_2962dup, p.Asn988SerfsX4). Three male individuals were used as control and each dot represent one independent measure. Data are represented as means \pm S.E.M. Position of the primers used for qPCR are shown in the upper panel. (e) Chromatogram showing the results of Sanger sequencing of RNA isolated from Patient 4's blood. (f) *In silico* prediction of sequence changes identified in patients, based on human *KIF21B* transcript variant 1 (RefSeq: NM_001252100.1). Source data are provided in the Source Data file.

Supplementary Figure 2: Kif21b expression in mouse developing cortex, related to Figure 2.



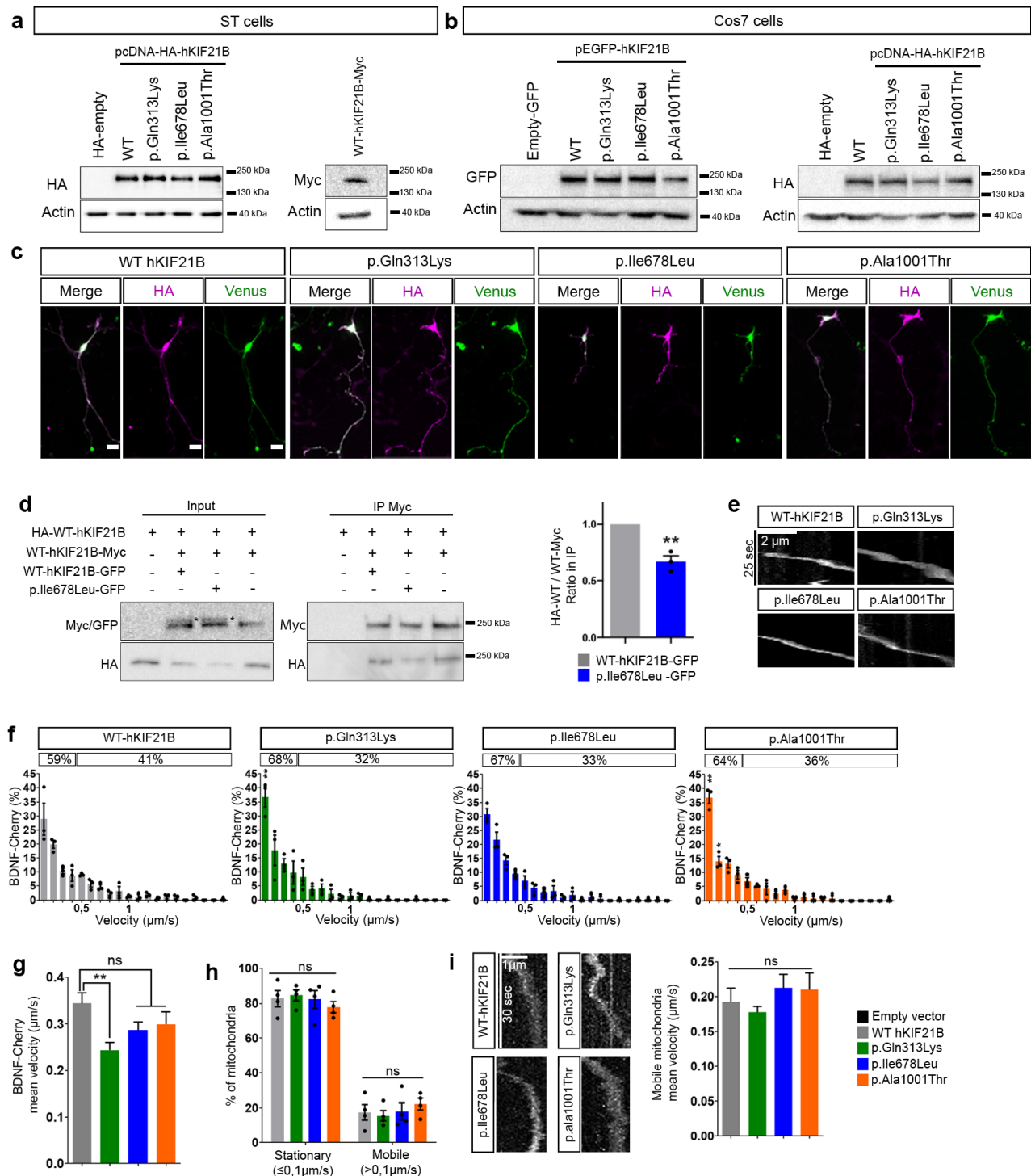
(a) *In situ* hybridization of mouse brain sections (from E12.5 to E18.5) showing mKif21b transcripts distribution. (b-c) E12.5, E16.5 and E18.5 mouse brains section immunolabelled for Kif21b (magenta), β -III-tubulin (neuronal marker, green) and Tbr2 (intermediate progenitor marker, light grey) showing restricted expression of Kif21b in post-mitotic neurons and enrichment in the axon-rich zone (b, white arrowhead). (d) Western blot of extracts from progenitors (YFP-; CD24-, expressing Pax6 and Tbr2 transcription factors) and neurons (YFP+; CD24+, expressing β -III-tubulin) isolated by FACS from Rosa26-loxSTOP-YFP; NEX^{CRE/+} E16.5 mouse cortices showing that Kif21b expression is restricted to neuronal population (n=3 independent experiments). GAPDH was used as a loading control. (e) Immunolabelling of Kif21b on P0 wild-type (WT) or Kif21b knock-out (KO) mouse brain confirm the specificity of the Kif21b staining. (f) Western blot of extracts from WT or Kif21b KO cortices showing the absence of Kif21b expression in KO brain (n=3 brains per genotype). Scale bars, (a) 500 μ m, (b) 250 μ m and (c, e) 100 μ m. (b, c, e) Nuclei are stained with DAPI. Source data are provided in the Source Data file.

Supplementary Figure 3: Expression of *hKIF21B* missense variants induce abnormal neuronal migration, related to Figure 3.



(a) Western blot of extract from N2A cells transfected with the indicated NeuroD-IRES-GFP constructs showing similar expression of both WT and mutant hKIF21B protein. Actin was used as a loading control. (b) Cycloheximide (CHX, 10µg/ml) treatment for the indicated duration show similar half-life of WT and mutant hKIF21B proteins. Data (means \pm S.E.M) were analyzed by two-way ANOVA, Bonferroni's multiple comparisons test, ns, non-significant. Experiments were repeated five times for WT, p.Gln313Lys and p.Ile678Leu conditions and three times for pAla1001Thr condition. (c, upper panel) Activated caspase3 (a-casp3, magenta)- or (lower panel) nestin (grey)-immunolabelling of E18.5 mouse brain coronal sections electroporated at E14.5 with the indicated NeuroD-hKIF21B IRES-GFP constructs, showing no apoptosis defects and no glia scaffold impairment. GFP positive electroporated cells are depicted in green. Nuclei are stained with DAPI. (d) RT-qPCR of HEK293T cells transfected with the indicated constructs showing *Kif21b* knock-down efficiency. Data (means \pm S.E.M) from 3 independent experiments were analyzed by unpaired two-tailed Student t-test, *P < 0.05; ***P < 0.001. (e, g) Coronal sections of (e) E18.5 or (g) P2 mouse brains electroporated at E14.5 with NeuroD:Cre-GFP together with either Cre inducible shRNA-*Kif21b* #1 or #2 or sh-scramble sequence. Rescue experiments were done by co-expressing NeuroD:Cre-GFP, inducible shRNA-*Kif21b* #2 together with WT-hKIF21B at 1 µg/µl. GFP positive electroporated cells are depicted in green. Nuclei are stained with DAPI. (f, h) Histograms (means \pm S.E.M) showing the distribution of GFP-positive neurons in different regions (Up CP, Upper cortical plate; Lo CP, Lower cortical plate; IZ, intermediate zone; SVZ, subventricular zone) for all conditions as indicated. Significance was calculated by two-way ANOVA (Bonferroni's multiple comparisons test). Number of embryos analyzed: (f) sh-scramble, n=7; sh-*Kif21b* #1, n=8; sh-*Kif21b* #2, n=9; sh-*Kif21b* #2 + WT, n=7; (h) sh-scramble, n=4; sh-*Kif21b* #2, n=4.; ns, non-significant; **P < 0.005; ****P < 0.0001. Scale bars (c, e, g), 50 µm. Source data are provided in the Source Data file.

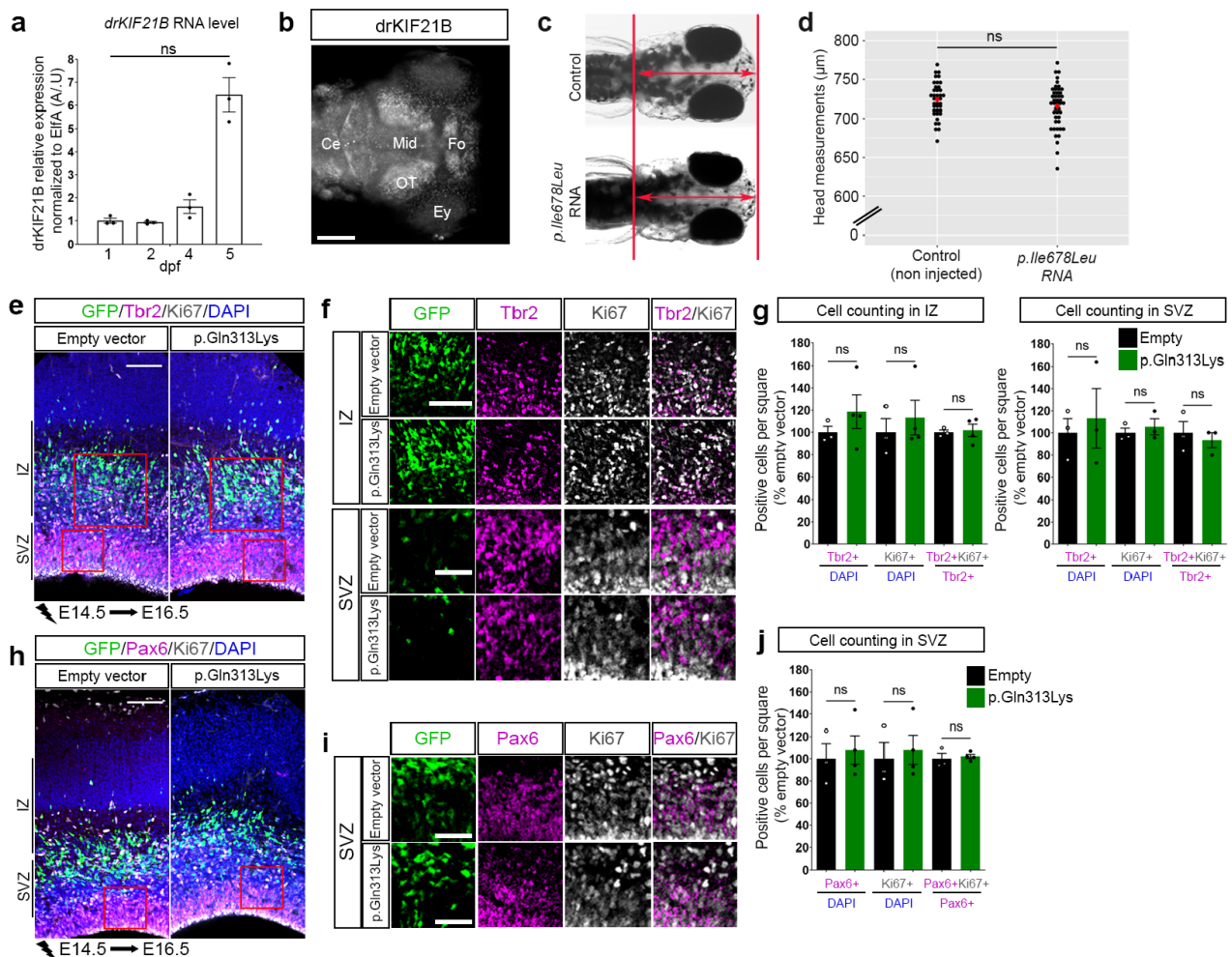
Supplementary Figure 4: hKIF21B missense variants induce abnormal neuronal migration through enhanced KIF21B motor activity, related to Figure 4.



(a, b) Western blot of extract from (a) ST cells transfected with the indicated HA-tagged or Myc-tagged constructs or (b) Cos7 cells transfected with the indicated GFP-tagged constructs or HA-tagged constructs, showing similar expression of both WT and mutant hKIF21B protein. Actin was used as a loading control. (c) HA-immunolabelling of primary cortical neurons transfected with WT or mutant HA-tagged hKIF21B cDNA constructs together with pCAGGs-mVenus showing distribution of KIF21B (HA, magenta) in soma, dendrites and axons at DIV2. Scale bars, 20 μ m. (d) WT hKIF21B immunoprecipitation (Myc beads, IP Myc) experiments in HEK293T cells transfected with the indicated HA-tagged, Myc-Tagged and GFP-tagged constructs showing that the p.Ile678Leu variant is competing with the wild type protein to form KIF21B homodimer. Whole cell lysates are shown as input. The asterisk shows the band corresponding to the GFP-tagged protein. Histograms (means \pm S.E.M) represent the quantitative assessment of the band intensities of the coimmunoprecipitated

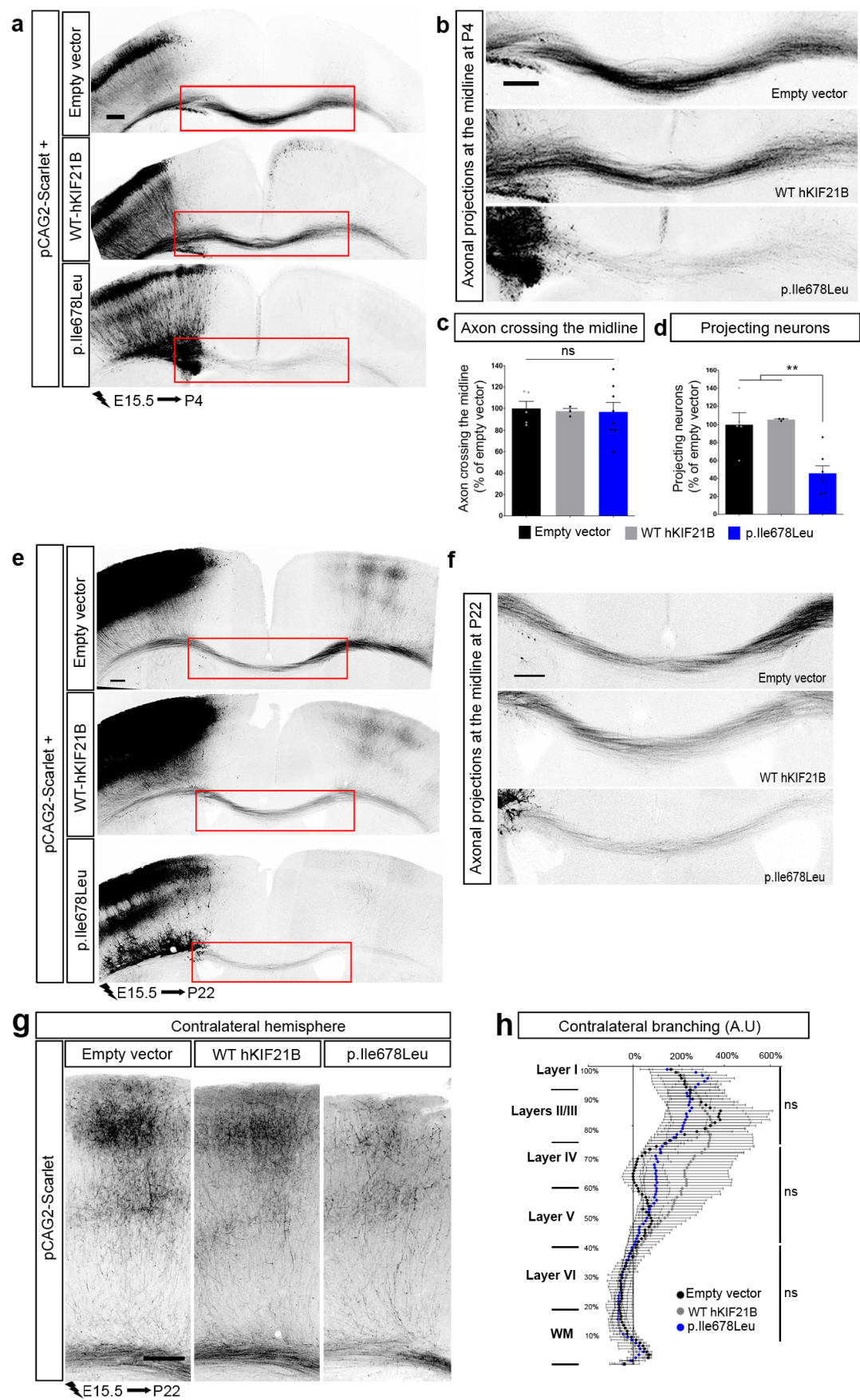
versus immunoprecipitated WT proteins from 3 independent experiments (unpaired two-tailed Student t-test, $**P < 0.005$). **(e-i)** Cos7 cells were co-transfected with BDNF-Cherry or Mito-RFP plasmids together with WT or mutant HA-tagged hKIF21B constructs and analyzed by videomicroscopy. Kymographs illustrate the motility of BDNF vesicles **(e)** or mitochondria **(i)** in time (y, sec) and space (x, μm). Histograms (means \pm S.E.M) represent the distribution of BDNF particles velocities **(f)**, the percentage of stationary mitochondria (velocity $\leq 0,1\mu\text{m/s}$) *versus* mobile mitochondria (velocity $>0,1\mu\text{m/s}$) **(h)** and the mean velocities of **(g)** BDNF particles and **(i)** mobile mitochondria. Data were analyzed **(f, h)** by two-way ANOVA or **(g, i)** by one-way ANOVA (Bonferroni's multiple comparisons test). **(f, g)** Total number of BDNF particles analysed in 10 to 19 cells: WT, n=322; p.Gln313Lys, n=255; p.Ile678Leu, n=307; pAla1001Thr, n=250. Experiments were repeated three times for all conditions. **(h, i)** Total number of mitochondria analysed in 19 to 31 cells: WT, n=177; p.Gln313Lys, n=256; p.Ile678Leu, n=189; pAla1001Thr, n=173. Experiments were repeated four times for all conditions. ns, non-significant; $*P < 0.05$; $**P < 0.005$. Source data are provided in the Source Data file.

Supplementary Figure 5: Overexpression of the p.Gln313Lys *hKIF21B* variant does not impair proliferation in the developing mouse brain, related to Figure 5.



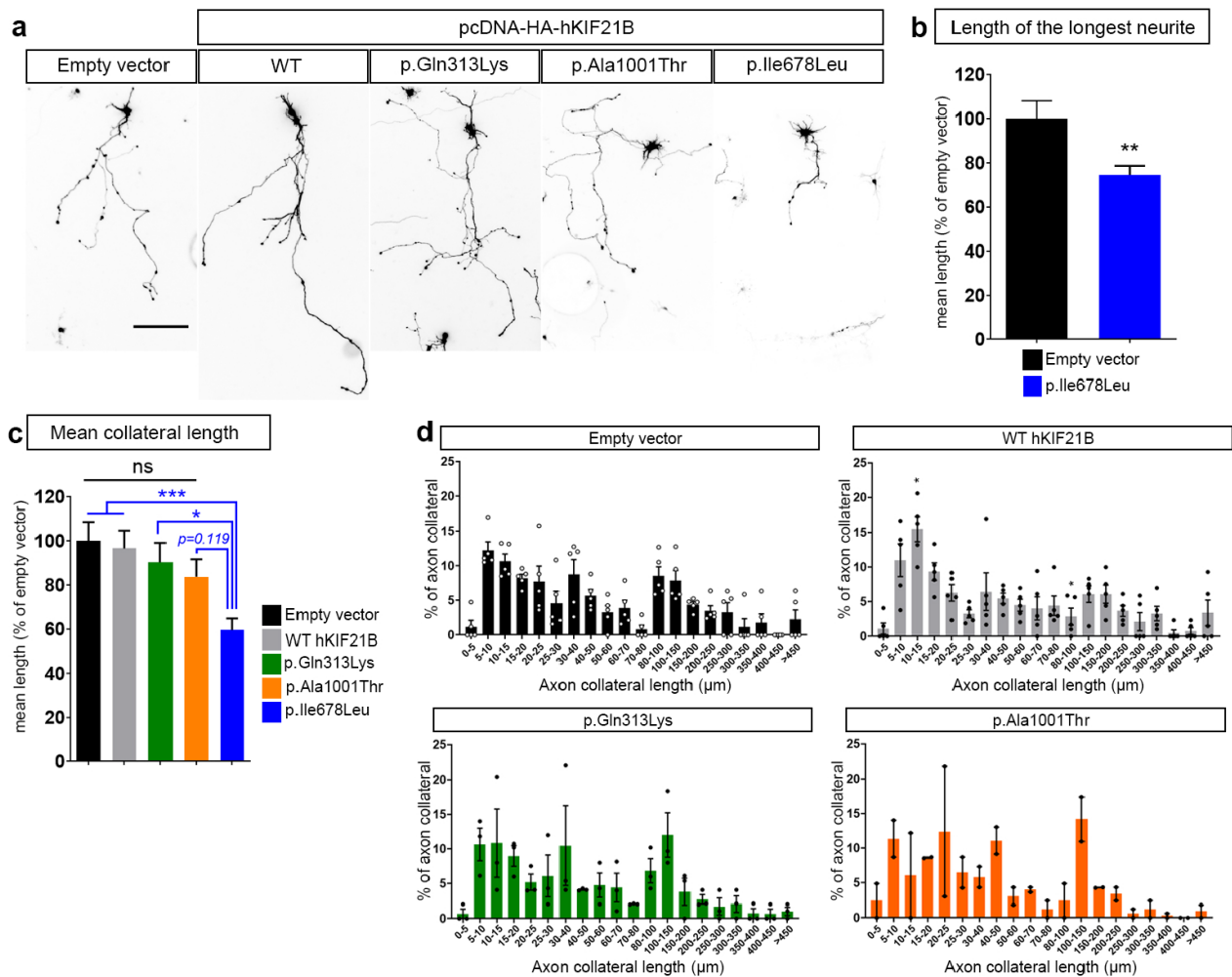
(a) qRT-PCR analyses show expression of *drKif21b* transcripts in developing zebrafish larvae at 1, 2, 4 and 5 days post-fertilization (dpf). Data (means \pm S.E.M) from 3 technical replicates per stage were analyzed by one-way ANOVA (Bonferroni's multiple comparisons test). ns, non-significant. (b) Kif21b-immunolabelling (grey) of whole zebrafish larvae show Kif21b enrichment in different region of the brain (OT, optic tectum; Ey, eye; Fo, forebrain; Mid, midbrain; Ce, cerebellum). (c) Dorsal view of representative control zebrafish larvae (non-injected) or injected with 100 pg of *p.lle678Leu hKIF21B* RNAs at 5 dpf. Double arrow indicates the distance between the forebrain and hindbrain, a measure used as a proxy for head size. (d) Dot plot of the head measurements (red double arrow) of control and RNA-injected larvae at 5dpf. Red diamond corresponds to the mean of the batch measured. Significance was calculated by unpaired two-tailed Student t-test comparisons between control and RNA-injected larvae. Number of embryos analyzed for this specific batch: control, n=45; *p.lle678Leu*, n=39. Experiments were repeated three times for each condition. Total Number of embryos analyzed: control, n=107; *p.lle678Leu*-injected embryos, n=105. ns, non-significant. (e, f, h, i) *Tbr2* (magenta) (e, f) of *Pax6* (magenta) (h, i) and Ki67 (grey) double immunolabeling of coronal sections of E16.5 mouse cortices electroporated at E14.5 with NeuroD-IRES-GFP empty vector or NeuroD-hKIF21B-p.Gln313Lys. GFP positive electroporated cells are depicted in green. Nuclei are stained with DAPI. (g, j) Analysis (means \pm S.E.M) of the percentage of *Tbr2*-positive cells, *Pax6*-positive cells, Ki67-positive cells or cells double positive for *Tbr2* (g) or *Pax6* (i) and Ki67 in the intermediate zone (IZ) or sub-ventricular zone (SVZ) in a fixed-size square represented in (e) and (h). Data were analyzed by unpaired two-tailed Student t-test. Number of embryos analyzed for (g) IZ countings, WT, n=4; p.Gln313Lys, n=3; and for (g, j) SVZ countings, WT, n=3; p.Gln313Lys, n=3. ns, non-significant. Scale bars, (b) 10 μm ; (e, h) 100 μm (f, upper panel) 100 μm , (f, lower panel and i) 50 μm . Source data are provided in the Source Data file.

Supplementary Figure 6: p.Ile678Leu hKIF21B variant impedes interhemispheric connectivity through aberrant motor activity, related to Figure 6.



(a, e) Coronal sections of **(a)** P4 or **(e)** P22 mouse brains after IUE with pCAG2-Scarlet and a NeuroD-IRES-GFP empty vector or WT or p.Ile678Leu NeuroD-hKIF21B-IRES-GFP constructs at E15.5. **(b, f)** Close-up views of the red boxed area in **(a)** or **(e)** showing impaired axonal interhemispheric connectivity upon expression of the p.Ile678Leu variant both at P4 and P22. **(c-d)** Histograms (means \pm S.E.M) presenting the quantification of **(c)** the percentage of axon crossing the midline and **(d)** the percentage of projecting neurons for all conditions tested as indicated at P4. Data were analyzed by one-way ANOVA (Bonferroni's multiple comparisons test). Number of pups analyzed: **(c)** empty vector, n=5; WT, n=3; p.Ile678Leu, n=8; **(d)** empty vector, n=5; WT, n=3; p.Ile678Leu, n=7. ns, non-significant, **P < 0.005. **(g)** Contralateral side of P22 mouse brain coronal sections electroporated with pCAG2-Scarlet and a NeuroD-IRES-GFP empty vector or WT or p.Ile678Leu NeuroD-IRES-GFP constructs at E15.5 showing no terminal branching defects for all conditions tested. **(h)** Quantification of normalized pScarlet fluorescence along the radial axis of the cortical wall in the contralateral cortex. Data (means \pm S.E.M) were analyzed by two-way ANOVA (Bonferroni's multiple comparisons test). Number of animals analyzed: empty vector, n=6; p.Ile678Leu, n=4; ns, non-significant. Scale bars **(a, b, e, f and g)**, 250 μ m. Source data are provided in the Source Data file.

Supplementary Figure 7: Overexpression of p.Ile678Leu hKIF21B variant impairs ipsilateral intracortical axon collaterals formation through a dominant negative effect on motility, related to figure 7.



(a) Representative DIV5 cortical neurons magnetofected at DIV2 with pCAG2-Scarlet together with control empty pcDNA-HA or WT, p.Gln313Lys, p.Ala1001Thr or p.Ile678Leu pcDNA-HA-hKIF21B constructs. Scale bar, 150 μ m. (b,c) Quantification of (b) the longest neurite length (axon) or (c) the mean of collaterals length at DIV5 after overexpression of the indicated constructs. (d) Distribution of axon collateral branches length at DIV5 after overexpression of the indicated constructs. (b-d) Data (means \pm S.E.M) of (b) the longest neurite length, (c) the mean of collateral length or (d) the distribution of axon collaterals length were analyzed by (b) unpaired two-tailed Student t-test, (c) one-way ANOVA or (d) two-ways ANOVA (Bonferroni's multiple comparisons test). (b) Number of cells analyzed: empty vector, n=66; p.Ile678Leu, n=51; from five independent experiments. (c, d) Number of collaterals analyzed: empty vector, n=265; WT, n=322; p.Gln313Lys, n=192; p.Ile678Leu, n=385; p.Ala1001Thr, n=187; in 51, 62, 66, 37 or 30 cells respectively, from five (empty vector, WT, p.Ile678Leu), three (p.Gln313Lys) or two (p.Ala1001Thr) independent experiments. ns, non-significant; *P < 0.05; **P < 0.005; ***P < 0.001. Source data are provided in the Source Data file.

Supplementary Table 1: List of primary and secondary antibodies used in this work.

Antibody	Host	Dilution	Used for	Compagny	reference
β -III-tubulin	Mouse	1/200	IHC, WB	Eurogentec	MMS-435P-0100
Caspase-3	Rabbit	1/100	IHC	R and D system	AF835
Cux1	Rabbit	1/200	IHC	Proteintech	HPA003317
GFP	Goat	1/500	IHC, WB	Abcam	ab6673
GFP	Chicken	1/500	IHC	Abcam	GFP-1020
HA	Rat	1/1000	IF, WB	Sigma-Aldrich	11867423001
Myc-Tag	Rabbit	1/1500	IF, WB	Cell Signalling	71D10
KIF21B	Rabbit	1/200	IHC, IF, WB	Sigma-Aldrich	HPA027274
KIF21B	Rabbit	1/500	IF (zebrafish staining)	Abcam	ab135410
Pax6	Rabbit	1/500	IHC	Biologends	901301
Tau	Mouse	1/1000	IF	Millipore	MAB3420
Tbr2	Rat	1/250	IHC, WB	EBiosciences	14-4875-80
Actin coupled HRP	Mouse	1/100 000	WB	Sigma-Aldrich	A3854
Goat-mouse-HRP	Mouse	1/10 000	WB	ThermoFisher Sc.	G-21040
Goat-rabbit-HRP	Rabbit	1/10 000	WB	ThermoFisher Sc.	G-21234
Goat-rat-HRP	Rat	1/10 000	WB	ThermoFisher Sc.	62-9520
Donkey-goat-488	Goat	1/1000	IF	ThermoFisher Sc.	A-11055
Donkey-mouse-488	Mouse	1/1000	IF	ThermoFisher Sc.	A-21202
Donkey-mouse-555	Mouse	1/1000	IF	ThermoFisher Sc.	A-31570
Donkey-rabbit-488	Rabbit	1/1000	IF	ThermoFisher Sc.	R-37118
Donkey-rabbit-555	Rabbit	1/1000	IF	ThermoFisher Sc.	A-31572
Donkey-rat-488	Rat	1/1000	IF	ThermoFisher Sc.	A-21208
Ki67 coupled-570	Rat	1/500	IF	eBioscience	41 5698 80

IHC, immunohistochemistry, IF, immunofluorescence; WB, western blot.

ARTICLE 2:

Further delineation of KIF21B-related neurodevelopmental disorders


**Dhanya Lakshmi Narayanan, José Rivera Alvarez, Peggy Tilly, Michelle C. do Rosario,
Vivekananda Bhat, Juliette D. Godin and Anju Shukla**

In this study, I demonstrated that the KIF21B variant p.Ser505Arg, found in a patient with intellectual disability and speech delay, induces migratory delay of pyramidal neurons. This was done by analysing the neuronal positioning in E18.5 cortices electroporated at E14.5 with the KIF21B p.Ser505Arg variant, finding defective distribution of the neurons upon expression of the mutant KIF21B. This finding expanded the evidence showing KIF21B as a gene of susceptibility for intellectual disability.

ARTICLE



Further delineation of *KIF21B*-related neurodevelopmental disorders

Dhanya Lakshmi Narayanan^{1,2,7}, José Rivera Alvarez^{3,4,5,6,7}, Peggy Tilly^{3,4,5,6}, Michelle C. do Rosario¹, Vivekananda Bhat¹, Juliette D. Godin^{3,4,5,6} and Anju Shukla¹ 

© The Author(s), under exclusive licence to The Japan Society of Human Genetics 2022

Kinesin Family Member 21B (*KIF21B*) encoded by *KIF21B* (MIM*608322), belongs to the Kinesin superfamily proteins, which play a key role in microtubule organisation in neuronal dendrites and axons. Recently, heterozygous variants in *KIF21B* were implicated as the cause of intellectual disability and brain malformations in four unrelated individuals. We report a 9-year-old male with delayed speech, hyperactivity, poor social interaction, and autistic features. A parent-offspring trio exome sequencing identified a novel de novo rare heterozygous variant, NM_001252102.2: c.1513A>C, p.(Ser505Arg) in exon 11 of *KIF21B*. In vivo functional analysis using in utero electroporation in mouse embryonic cortex revealed that the expression of Ser505Arg *KIF21B* protein in the cerebral cortex impaired the radial migration of projection neurons, thus confirming the pathogenicity of the variant. Our report further validates pathogenic variants in *KIF21B* as a cause of neurodevelopmental disorder.

Journal of Human Genetics; <https://doi.org/10.1038/s10038-022-01087-0>

INTRODUCTION

Kinesin Superfamily proteins (KIFs) play a major role in microtubule organisation and transport of various intracellular cargo in neuronal axons and dendrites [1]. Kinesin Family Member 21B (*KIF21B*), encoded by *KIF21B* (MIM*608322), is a protein belonging to the KIFs and is expressed mainly in neurons, spleen, and testes [2]. In the neuronal axons and dendrites, *KIF21B* regulates microtubule dynamics and promotes intracellular transport [3]. Homozygous *Kif21b* knock-out mice display microcephaly, altered synaptic transmission, cognitive defects and reduced dendritic complexity, implying a critical role of *KIF21B* in neuronal development and function [4–6]. Recently, four unrelated individuals with developmental delay, intellectual disability, nonspecific facial dysmorphism and corpus callosal agenesis were described harbouring heterozygous variants in *KIF21B* [7]. We describe a novel de novo variant in *KIF21B* in an individual with intellectual disability and hyperactivity, providing further evidence to the gene-disease association.

MATERIALS AND METHODS

Case report

A 9-year-old male was evaluated for delayed speech, hyperactivity, and poor social interaction. He is the firstborn child of non-consanguineous parents (Fig. 1A). His mother had an uneventful antenatal period. He was born at term with a birth weight of 2.8 kg (−0.4 SD). He cried immediately after birth and had an uncomplicated neonatal course. He had a delay in attaining age-appropriate milestones. He could stand without support only by 1 year and 4 months of age. He started babbling by 9 months of age and could say only bisyllables by 4 years of age. He had poor eye contact

and did not respond to his name, had hyperactivity and reduced attention span. He did not play with other children. At 3 years, evaluation by Vineland Social Maturity Scale showed a score of 81, indicating a dull normal level of social and adaptive functioning. The Modified Checklist for Autism in Toddlers Score at 3 years was 3, indicating a moderate risk for autism spectrum disorder. He never had seizures or any history of neuroregression. At 9 years of age, he was able to jump, say a few words and write single words. He needed assistance in grooming and showering. He attended sessions with a special educator. He was on atomoxetine and risperidone and parents felt that his hyperactivity had reduced. On examination, his weight was 24.8 kg (+0.8 SD), height was 133 cm (+0.5 SD) and head circumference was 53 cm (0 SD). He had a long face, broad eyebrows, multiple lentigines on face and back and bilateral fifth digit clinodactyly. Neurological examination was normal. Brain evoked response audiometry was normal. Magnetic resonance imaging of the brain did not show any structural malformation (Fig. 1B, C). Fragile X screening and chromosomal microarray returned normal results.

Whole exome sequencing

Informed consent was taken from the family. This study was approved by the Institutional Ethics committee. Genomic DNA was extracted from the blood of the proband and parents using QIAamp DNA Blood Mini Kit (QIAGEN, Valencia, CA; cat # 51106). A parent-offspring trio exome sequencing (Illumina, Inc., San Diego, California, USA) was performed using Agilent SureSelect Clinical Research Exome v3 (CREv3) capture kits, as described earlier [8]. Annotation was performed by in-house pipeline against the GRCh38 version of the human genome. The variants were analysed and prioritised using our in-house filtering strategy. Only rare variants with a minor allele frequency of <1% were considered for downstream analysis. Intronic and intergenic variants were excluded and exonic and splice site variants were prioritised based on the observed

¹Department of Medical Genetics, Kasturba Medical College, Manipal, Manipal Academy of Higher Education, Manipal, India. ²DBT/Wellcome Trust India Alliance Early Career Fellow, Manipal, India. ³Institut de Génétique et de Biologie Moléculaire et Cellulaire, Illkirch, France. ⁴Centre National de la Recherche Scientifique, UMR7104 Illkirch, France. ⁵Institut National de la Santé et de la Recherche Médicale, INSERM, U1258 Illkirch, France. ⁶Université de Strasbourg, Strasbourg, France. ⁷These authors contributed equally: Dhanya Lakshmi Narayanan, José Rivera Alvarez. ✉email: godin@igbmc.fr; anju.shukla@manipal.edu

Received: 24 June 2022 Revised: 21 September 2022 Accepted: 22 September 2022

Published online: 06 October 2022

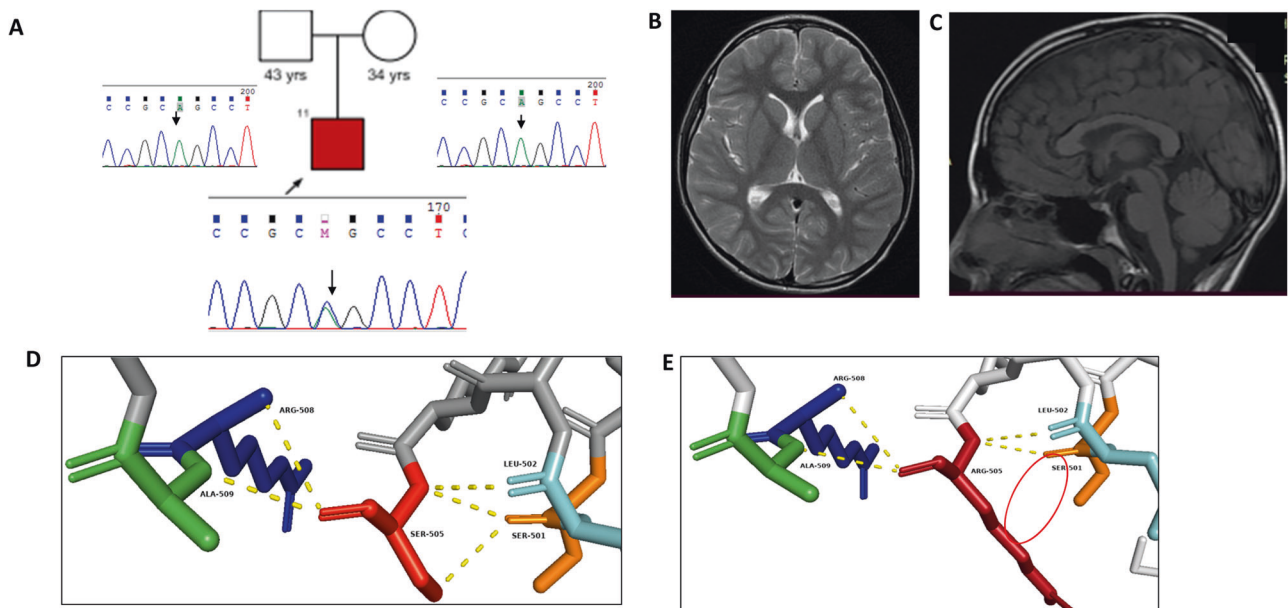


Fig. 1 **A** Pedigree of the family and Sanger sequencing chromatograms showing de novo variant in the proband. **B, C** Normal MRI brain in the proband. **D, E** Modelling of wild-type (**D**) and mutant (**E**) KIF21B protein showing abrogation of one of the two polar contacts with Ser501

phenotype and multiple in silico pathogenicity tools. All the different inheritance patterns were considered in variant prioritisation. The variant was validated and segregated in the family members by Sanger sequencing.

In silico protein modelling and analysis

In silico modelling was carried out using the structure of KIF21B available in Uniprot (AF-075037-F1). The resultant protein model was loaded on PyMol (The PyMOL Molecular Graphics System, Version 1.2r3pre, Schrödinger, LLC) and in silico mutagenesis was performed to deduce the structure of the mutant proteins. This was followed by analyses of the alteration in polar contacts of the wild-type (WT) residue (Ser505) with their neighbouring amino acids as compared to the mutant residue (Arg505). The structural effect of the variants was predicted using HOPE (<http://www.cmbi.ru.nl/hope/>).

In vivo functional analysis

Human *KIF21B* variant c.1513A>C (p.Ser505Arg) was generated from NeuroD-hKIF21B-WT by sequence and ligation independent cloning. Mouse neuroblastoma N2A (ATCC) cells were cultured and transfected with WT and mutant plasmid constructs. Forty-eight hours post transfection, the cells were collected and lysed, and western blotting was done. In utero electroporation (IUE) of pregnant mice was carried out. Dissected brains from embryos at E18.5 and newborns at day postnatal (P2) were processed and DAPI was used as a cell nuclei marker. Detailed methodology is provided in the Methods section in the Supplementary material.

RESULTS

Whole exome sequencing and variant interpretation

A parent-offspring trio exome sequencing showed a de novo heterozygous variant, NM_001252102.2: c.1513A>C, p.(Ser505Arg) in exon 11 of *KIF21B*. Sanger sequencing confirmed this variant (Fig. 1A). The variant was absent in population databases like gnomAD and our in-house database of 1861 individuals. Multiple in silico analysis tools like MutationTaster, ClinPred and CADD predicted the variant to be deleterious. PhastCons score was 0.995 indicating that the amino acid was conserved across species (Fig. 2A).

In silico protein modelling and analysis

In silico protein modelling predicted that the mutant residue, Arg505, is likely to result in abrogation of one of the two polar

contacts with Ser501 (Fig. 1D, E). HOPE predicted the WT residue (Ser505) to have a positive charge, causing repulsion of ligands or other residues with the same charge in the protein. The replacement of the smaller WT residue with the bigger, less hydrophobic mutant amino acid at this position could lead to collisions and result in the probable loss of hydrophobic interactions in the core or surface of the protein.

In vivo functional analysis

Next, we examined the pathogenicity of the p.Ser505Arg mutation in vivo in mouse embryonic cortex [7]. Transfection of mouse N2A neuroblastoma cells with WT and mutant constructs revealed comparable protein levels (Fig. 2B), indicating that the p.Ser505-Arg variant was unlikely to impair the expression of the KIF21B protein. We induced expression of the NeuroD-hKIF21B-S505R mutant specifically in migrating neurons using IUE. Electroporated cells were identified by co-electroporation of the NeuroD-IRES-GFP reporter plasmid. Distribution of GFP⁺ electroporated neurons was analysed 4 days after IUE at E18.5 (Fig. 2C). While most of the control neurons (NeuroD-Empty) and the neurons expressing full length WT hKIF21B reached the upper cortical plate (UpCP) 4 days after IUE, the neurons expressing the p.Ser505Arg variant failed to migrate properly with a significant decrease of cells reaching the UpCP (−29, 84% compared to the control) and a corresponding increase of cells accumulating in the subventricular zone/intermediate zone was observed (Fig. 2D). Most of the cells overexpressing the p.Ser505Arg variant showed a correct positioning with nearly all cells found in the upper layer of the cortex after birth, indicating a delay in migration rather than a permanent arrest (Fig. 2E). As shown for the previously identified *KIF21B* variants [7], this result demonstrates that the p.Ser505Arg KIF21B variant impairs the radial migration of projection neurons, thus suggesting the pathogenicity of this variant.

DISCUSSION

KIF21B, located on 1q32.1, has 37 exons and encodes KIF21B protein with 1623 amino acids. The human KIF21B protein (hKIF21B) has an ATP-binding site, motor domain, coiled-coil domains 1 and 2 (CC1 and CC2), regulatory coiled-coil domain (rCC) and WD40 domain [7]. KIF21B is expressed in abundance in

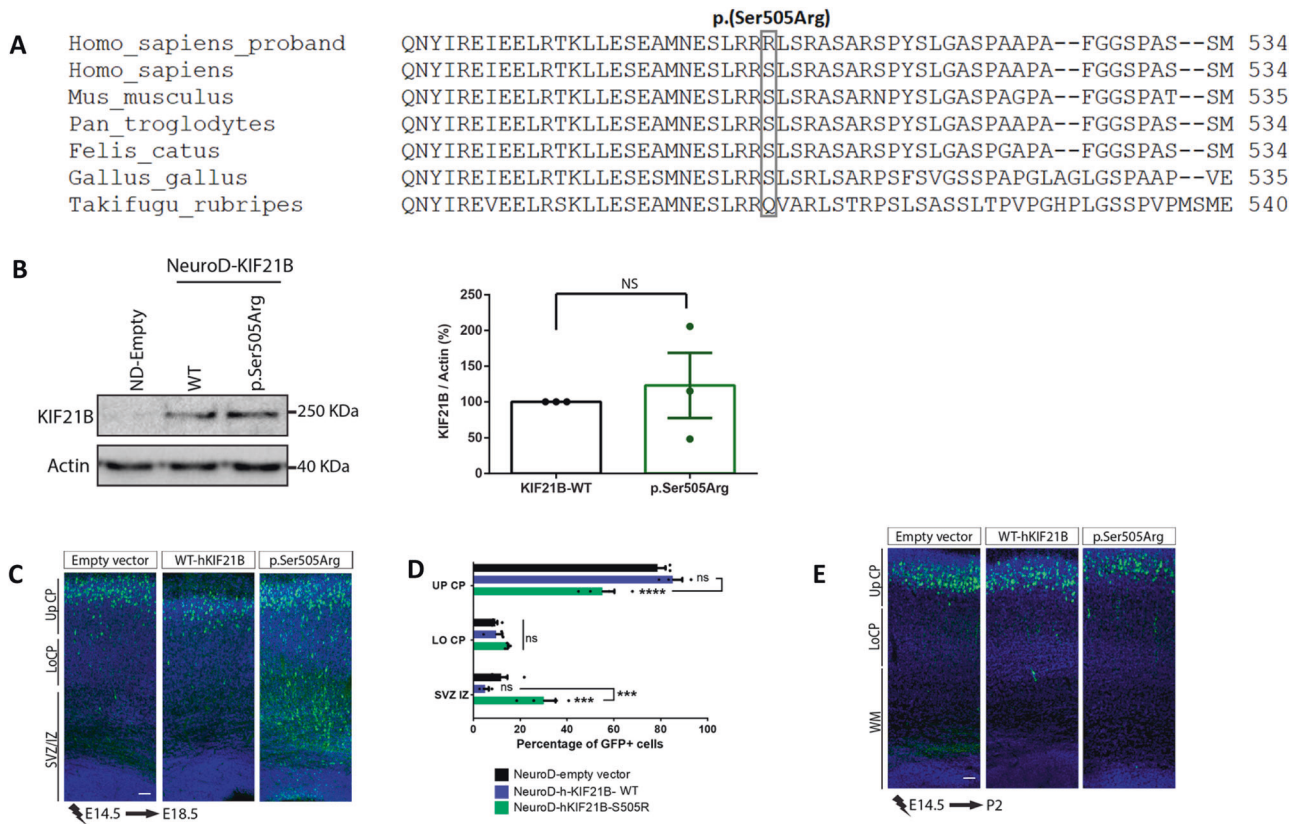


Fig. 2 **A** The amino acid Ser at 505 position is conserved across species. **B** Western blot of extract from N2A cells transfected with the indicated NeuroD-IRES-GFP constructs showing similar expression of both WT and mutant hKIF21B protein. Actin was used as a loading control. Graph represents quantification of three independent experiments (mean \pm SEM). Significance was calculated using *t*-test. **C, E** Coronal sections of E18.5 (**C**) and P2 (postnatal stage 2) (**E**) mouse cortices electroporated at E14.5 with NeuroD:Cre-GFP empty vector or NeuroD-hKIF21B WT or p.Ser505Arg. GFP-positive electroporated cells are depicted in green. Nuclei are stained with DAPI. **D** Histograms (mean \pm SEM) showing the distribution of GFP-positive neurons at E18.5 in different regions (Up CP, Upper cortical plate; Lo CP, Lower cortical plate; IZ, intermediate zone; SVZ, subventricular zone; WM: White matter) for all conditions as indicated. Significance was calculated by two-way ANOVA (Bonferroni's multiple comparisons test). Number of embryos analysed: **C, D** Empty vector, $n = 4$; WT, $n = 3$; p.Ser505Arg, $n = 4$. NS not significant, *** $P < 0.001$; **E** Empty vector, $n = 4$; WT, $n = 5$; p.Ser505Arg, $n = 7$. Scale bars (**C, E**) 50 μ m

both axons and dendrites of post-mitotic neurons. It has two different functions in neurons. First, it aids in intracellular transport of cargos. Second, it controls the microtubule organisation and favours microtubular growth [2].

We describe a 9-year-old male with KIF21B-related neurodevelopmental disorder who presented with intellectual disability, speech delay, autism, and attention deficit hyperactivity. All the affected individuals have global developmental delay, mild to severe intellectual disability and speech involvement in the form of delayed speech, dysarthria, or absent speech. Although some facial dysmorphic features were present in all of them, neither a consistent nor a recognisable pattern was observed in the affected individuals. None of them has seizures. Except for agenesis of corpus callosum, which was identified in one previously reported individual, none of them has any structural brain abnormalities. Microcephaly was observed only in one individual [7]. Table 1 shows a comparison of the clinical characteristics of the individual in this study with the previously reported individuals [7].

The five variants reported to date including the one in the present individual include four missense variants and one truncating variant. Only one of the previously reported individuals had inherited the variant from her affected father. All the others, including the individual in our study, had de novo variants. The previously reported missense variants were in the highly conserved domains of hKIF21B. The variant, NM_001252100.1, c.937C>A, p.Gln313Lys was in the motor domain, the variant, NM_001252100.1, c.3001G>A, p.Ala1001Thr was in the rCC

domain and the variant NM_001252100.1, c.2032A>C, p.Ile678Leu, was in the coiled-coiled domain 2.

The previous *in vivo* studies performed for the reported missense variants and the KIF21B haploinsufficiency, have explored the possible underlying mechanisms of the neurodevelopmental phenotype seen in these individuals. Studies in all three affected individuals with missense variants revealed impaired radial migration of projection neurons in mouse cortices attributed to attenuation of kinesin autoinhibition [7]. Incremental amounts of WT protein together with hKIF21B mutants failed to rescue the migration phenotype. Hence, the molecular mechanism proposed for the missense variants was a gain of function effect, which resulted in loss of autoinhibition and a subsequent increase in KIF21B motor activity. The motor activity of KIF21B directly correlated with the severity of the neuronal migration defect. The authors hypothesised that for adequate functioning of KIF21B in the developing mice cortex, a minimum level of autoinhibition is required. This autoinhibition is maintained by the rCC domain which helps to connect the CC2 domain to the motor head. The presence of the missense variants likely leads to a change in the conformation of KIF21B protein and thus loss of these interactions within the protein, resulting in enhanced KIF21B motility activity. The expression of a truncated mouse mKif21b protein that lacks the rCC domain also resulted in a phenotype similar to that induced by overexpression of the variants.

Of the missense variants reported previously, the p.Gln313Lys and p.Ala1001Thr variants were shown to impede but not arrest

Table 1. Comparison of characteristics of individuals with *KIF21B*-related neurodevelopmental disorder

Features	Individual 1	Individual 2	Individual 3	Individual 4	Current study
Age	10 years	12 years 1 month	9 years	3 years 8 months	9 years
Gender	Male	Male	Female	Male	Male
Antenatal and immediate postnatal period	Uneventful	Oligohydramnios, IUGR, cord around neck at birth	Uneventful	Mother had seizure disorder, feeding issues, SGA	Uneventful
Global developmental delay	+	+	+	+	+
Intellectual disability	Borderline	Severe	Mild to moderate	Mild	Mild
Stereotypic behaviour	+	+	–	–	+
Hyperactivity	+	–	–	–	+
Speech	Dysarthria	Absent	Speaks in sentences at 5 years	Short sentences	Says a few words at 9 years
Dysmorphic features	Plagiocephaly, down-slanting palpebral fissures, downturned corners of the mouth	Large eyes, fleshy ears, hypertelorism	Epicanthic folds, mild ptosis, tented upper lip	Up slanting palpebral fissures, prominent eyebrows, broad nose with bulbous tip, anteverted nares, micrognathia, right-sided Duane syndrome	Long face, broad eyebrows, multiple lentiginos on face and back and bilateral fifth digit clinodactyly
Head circumference	52 cm (+0.5 SD)	48.5 cm (–3.9 SD)	49.6 cm (–0.2 SD)	50.7 cm (+0.72 SD)	53 cm (0 SD)
MRI brain	Isolated complete agenesis of the corpus callosum	Normal	Normal	A few scattered punctate foci of T2 prolongation in subcortical white matter and periventricular white matter	Normal
Variant	c.2032A>C p.Ile678Leu	c.937C>A p.Gln313Lys	c.3001G>A p.Ala1001Thr	c.2959_2962dupGCCA, p.Asn988Serfs*4	c.1513A>C p.Ser505Arg
Zygosity	De novo	De novo	Inherited from affected father	De novo	De novo
Any other feature	–	–	–	Central sleep apnoea	–

+ present, – absent, SD standard deviation, SGA small for gestational age, IUGR intrauterine growth retardation

the migration in the mice cortices. This could possibly explain the absence of any neuroimaging findings suggestive of neuronal migration defects in individuals harbouring these variants. The novel variant reported in the present individual, i.e., NM_001252102.2: c.1513A>C, p.(Ser505Arg), is located in the CC1 domain. The delayed radial migration phenotype in the mouse cortices was recapitulated in the variant observed in the present individual as well, without any alteration in the amount or stability of the protein. As predicted in the earlier studies, this could be attributed to the changes in the conformation of the KIF21B protein and subsequent loss of interaction within its domains. The S505R variant is thus more likely to result in migration impediment as seen previously in Q313K and A1001T variants rather than permanent migration defect. This correlates with the absence of migration defects and a normally developed corpus callosum in the present individual.

In contrast, the p.Ile678Leu variant was shown to cause a permanent migration defect as well as perturb the axonal growth and ipsilateral branching. This correlated with the agenesis of corpus callosum observed in the individual harbouring this variant. Concurrent to the microcephaly noted in the individual with *KIF21B* p.Gln313Lys variant, reduced head size was noted in zebrafish. However, there was no impairment of neuronal proliferation or survival and hence the mechanism for microcephaly phenotype remains largely unknown [7]. Even though haploinsufficiency of *Kif21b* in mice was shown to result in impaired neuronal migration, the authors concluded that the truncating variant (NM_001252100.1, c.2959_2962dup, p.Asn988-Serfs*4) described in individual 4 by them was probably not pathogenic [7]. Hence, of the four individuals reported to date with de novo variants in *KIF21B*, variant pathogenicity could be concluded only in three individuals harbouring the missense variants.

Our report further validates *KIF21B*-related neurodevelopmental disorder. As predicted by the function of *KIF21B* and the impact of the variants, the phenotypes associated with the gene are likely to be broad. Hence, report of further individuals/studies is likely to inform us about the spectrum of this disorder.

REFERENCES

- Hirokawa N. Kinesin and dynein superfamily proteins and the mechanism of organelle transport. *Science*. 1998;279:519–26.
- Marszalek JR, Weiner JA, Farlow SJ, Chun J, Goldstein LS. Novel dendritic kinesin sorting identified by different process targeting of two related kinesins: KIF21A and KIF21B. *J Cell Biol*. 1999;145:469–79.
- Ghiretti AE, Thies E, Tokito MK, Lin T, Ostap EM, Kneussel M, et al. Activity-dependent regulation of distinct transport and cytoskeletal remodeling functions of the dendritic kinesin KIF21B. *Neuron*. 2016;92:857–72.
- Muhia M, Thies E, Labonté D, Ghiretti AE, Gromova KV, Xompero F, et al. The kinesin KIF21B regulates microtubule dynamics and is essential for neuronal morphology, synapse function, and learning and memory. *Cell Rep*. 2016;15:968–77.
- Kannan M, Bayam E, Wagner C, Rinaldi B, Kretz PF, Tilly P, et al. WD40-repeat 47, a microtubule-associated protein, is essential for brain development and autophagy. *Proc Natl Acad Sci USA*. 2017;114:E9308–17.
- Morikawa M, Tanaka Y, Cho HS, Yoshihara M, Hirokawa N. The molecular motor KIF21B mediates synaptic plasticity and fear extinction by terminating Rac1 activation. *Cell Rep*. 2018;23:3864–77.

- Asselin L, Rivera Alvarez J, Heide S, Bonnet CS, Tilly P, Vitet H, et al. Mutations in the KIF21B kinesin gene cause neurodevelopmental disorders through imbalanced canonical motor activity. *Nat Commun*. 2020;11:2441.
- Girisha KM, von Elsner L, Neethukrishna K, Muranjan M, Shukla A, Bhavani GS, et al. The homozygous variant c.797G>A/p.(Cys266Tyr) in PISD is associated with a Spondyloepimetaphyseal dysplasia with large epiphyses and disturbed mitochondrial function. *Hum Mutat*. 2019;40:299–309.

ACKNOWLEDGEMENTS

We thank the family for their co-operation. This work was funded by grants from INSERM (ATIP-Avenir programme, JDG), the French state funds through the Agence Nationale de la Recherche under the project JCJC CREDO ANR-14-CE13-0008-01 (JDG) and the programme Investissements d'Avenir labelled (ANR-10-IDEX-0002-02, ANR-10-LABX-0030-INRT, to JDG), INSERM/CNRS and University of Strasbourg. This work of the Interdisciplinary Thematic Institute IMCBio, as part of the ITI 2021-2028 programme of the University of Strasbourg, CNRS and Inserm, was supported by IdEx Unistra (ANR-10-IDEX-0002), and by SFRI-STRAT'US project (ANR 20-SFRI-0012) and EUR IMCBio (ANR-17-EURE-0023) under the framework of the French Investments for the Future Program. JRA was funded through the IGBMC PhD programme (ANR-10-IDEX-0002-02, ANR-10-LABX-0030-INRT). JRA is currently supported by the Fondation pour la recherche médicale. PT is a research assistant at the University of Strasbourg. JDG is INSERM investigator. We are grateful to the mouse facility of the Institut Clinique de la Souris (ICS) for taking care of the mice, to the Molecular Biology service of the IGBMC (in particular Thierry Lerouge) for their collaboration in making the plasmids used in this study and to Noémie Schwaller for her technical help. We acknowledge the National Institutes of Health, United States for funding the study titled, 'Genetic Diagnosis of Neurodevelopmental Disorders in India' (1R01HD093570-01A1). DLN is a DBT/Wellcome Trust India Alliance Early Career Clinical and Public Health Research Fellow.

AUTHOR CONTRIBUTIONS

DLN collected clinical data, and drafted the manuscript. JRA performed the experiments on mice and analyzed the data. PT performed experiments on mice. MCDR did in-silico modeling. VB was involved in collecting clinical information. JDG and AS supervised the work and design of research.

COMPETING INTERESTS

The authors declare no competing interests.

ADDITIONAL INFORMATION

Supplementary information The online version contains supplementary material available at <https://doi.org/10.1038/s10038-022-01087-0>.

Correspondence and requests for materials should be addressed to Juliette D. Godin or Anju Shukla.

Reprints and permission information is available at <http://www.nature.com/reprints>

Publisher's note Springer Nature remains neutral with regard to jurisdictional claims in published maps and institutional affiliations.

Springer Nature or its licensor holds exclusive rights to this article under a publishing agreement with the author(s) or other rightsholder(s); author self-archiving of the accepted manuscript version of this article is solely governed by the terms of such publishing agreement and applicable law.

Supplementary materials

In vivo functional analysis in mouse embryonic cortex

Cloning: Human *KIF21B* variant c.1513A>C (p. Ser505Arg) was generated from NeuroD-hKIF21B-WT by sequence and ligation independent cloning (SLIC). Plasmids were prepared by using NucleoBond Xtra Maxi Plus kit for transfection-grade plasmid DNA (Machery-Nagel).

Mice: Mice were bred at the Institute Clinique de la Souris (ICS) animal facility under controlled light/dark cycle, temperature and humidity conditions and were provided with food and water *ad libitum*. For the *In-Utero Electroporation (IUE)* experiments, time-pregnant CD1 female mice (Charles River Laboratories) were used. Mice studies were made in accordance with French guidelines (EU Directive 86/609 – French Act Rural Code R 214-87 to 126) and procedures were approved by the local ethics committee and the Research Ministry (APAFIS# 15691 – 20180627 148609).

In Utero Electroporation (IUE): Time-pregnant mice were anaesthetised with isoflurane (Tem Segal). After exposition of the uterine horns, plasmid solutions containing 0.5 µg/µL of NeuroD-IRES-GFP, 1 µg/µL of Fast Green (Sigma) and 1 µg/µL of empty NeuroD vector, NeuroD-hKIF21B-WT or NeuroD-hKIF21B-S505R were injected into the lateral ventricles of the embryos using pulled glass capillaries (Harvard apparatus, 1.0 OD*0.58 ID*100 mmL).

Electroporation was performed by the application of five electric pulses (40V) for 50 ms at 950 ms intervals with electrodes (diameter 3 mm; Sonidel CUY650P3) and ECM-830 BTX square wave electroporator (VWR international). Following electroporation, embryos were re-introduced into the abdominal cavity of the mother. Pregnant mice were killed four days after IUE (at E18.5) by cervical dislocation. E18.5 and P2 animals were sacrificed by head sectioning and brains were dissected in ice cold PBS.

Brain processing and immunolabeling: Dissected brains from E18.5 embryos or newborn at P2 were fixed in 4% paraformaldehyde (PFA, from Electron Microscopy Sciences) in Phosphate Buffered Saline

(PBS) overnight at 4°C. After rinsing, brains were embedded in 4% low melting point agarose (Bio-Rad) in PBS and 60 µm coronal sections were sliced using a vibratome (Leica VT10000S, Leica Microsystems). Free-floating sections were blocked and permeabilized by incubating them in Normal Donkey Serum (NDS, Dominic Dutsher), 0.1% Triton X-100 in PBS. Sections were incubated in primary antibody goat anti-GFP (1:600, Abcam ab6673) diluted in blocking solution overnight at 4°C and after rinsing, the sections were incubated in secondary antibody donkey anti-goat 488 (1:1 000, ThermoFisher Sc, A-11055) diluted in blocking solution for 1 h at room temperature (RT). DAPI (1 mg/ml) was used as a cell nuclei marker. Brain slices were mounted with Aquapolymount mounting medium (Polysciences Inc.).

Image analysis: Confocal images were acquired using a microscope Leica TCS SP5 equipped with a hybrid camera and a HC PL APO x20/0.70 objective and the Leica Las X software v3.7. To analyse images the ImageJ software was used. Cortical layers were identified by differences in cell density as distinguished by DAPI staining. For neuron quantification in the different layers, a box divided in bins was located in the images and the GFP+ cells in each bin were counted and designed to their corresponding layer. GraphPad Prim version 6 software was used for statistical analysis.

Cell culture, transfection and western blotting: Mouse neuroblastoma N2A (ATCC) cells were cultured in DMEM (1 g/L glucose, GIBCO) supplemented with 5% Foetal Calf Serum and gentamycin 40 µg/mL in a humidified 5% CO₂ atmosphere at 37°C. N2A cells were transfected using Lipofectamine 2000 (Invitrogen) and 1 µg of plasmid. 48 h after transfection cells were collected and lysed with RIPA buffer (50 mM Tris pH 8.0, 150 mM NaCl, 5 mM EDTA pH 8, 0.1% Triton X-100, 0.5% sodium deoxycholate, 0.1% SDS) supplemented with EDTA-free protease inhibitors (cOmplete, Roche), cell debris were removed by high speed centrifugation at 4°C and proteins were quantified with Bradford protein reagent (Bio-Rad). Laemmli buffer supplemented with 2% β-mercaptoethanol was added to the samples and then boiled for 10 min. Samples were subjected to SDS-PAGE and then transferred to PVDF membranes overnight. Membranes were blocked with 5% milk in PBS, 0.1% Tween (PBS-T) for

1h at RT and then incubated with primary antibody Rabbit anti-Kif21b (1/2000, Sigma-Aldrich, 11867423001) 4 h at RT followed by secondary antibody Goat anti-Rabbit-HRP (1/10000, Thermofisher, G-21234) for 1 h at RT. Actin was blotted using Mouse anti-Actin coupled to HRP (1/50000, Sigma Aldrich, A3854). Finally, the membranes were exposed to Supper Signal West Pico PLUS Chemiluminescent Substrate (Sigma) and the signal was detected by the imager ImageQuant LAS 600 (GE Healthcare).

ARTICLE 3:

The kinesin Kif21b regulates radial migration of cortical projection neurons through non canonical function on actin cytoskeleton

José Rivera Alvarez, Laure Asselin, Peggy Tilly, Roxane Benoit, Claire Batisse, Ludovic Richert, Julien Batisse, Bastien Morlet, Florian Levet, Noémie Schwaller, Yves Mély, Marc Ruff, Anne-Cécile Reymann, Juliette D. Godin

In this work I showed that *Kif21b* depletion in cortical pyramidal neurons induces defects in locomotion that lead to a migratory delay. Interestingly, neuronal migration is independent of the Kif21b motor function, but dependent on the motor domain. I showed how the rescue of the *Kif21b* depletion by co-expressing Kif21b truncated in the motor domain (Δ MD) produces just a partial rescue of the migratory defects, indicating the involvement of the motor domain in some parameters of migration and the rest of the protein in other parameters. By looking for protein partners, I found unexpectedly that Kif21b is an actin binding protein, an interaction that I was able to corroborate through different means, and showing a direct interaction, demonstrating like that for the first time that a kinesin interacts with the actin cytoskeleton. Moreover, I demonstrated that *Kif21b* depletion induces actin dynamics defects during migration of pyramidal neurons.

The kinesin Kif21b regulates radial migration of cortical projection neurons through a non-canonical function on actin cytoskeleton.

José Rivera Alvarez^{1,2,3,4,8}, Laure Asselin^{1,2,3,4,8}, Peggy Tilly^{1,2,3,4}, Roxane Benoit^{1,2,3,4}, Claire Batisse^{1,2,3,4}, Ludovic Richert^{4,5}, Julien Batisse^{1,2,3,4}, Bastien Morlet^{1,2,3,4}, Florian Levet^{6,7}, Noémie Schwaller^{1,2,3,4}, Yves Mély^{4,5}, Marc Ruff^{1,2,3,4}, Anne-Cécile Reymann^{1,2,3,4}, Juliette D. Godin^{1,2,3,4,9,*}

1. Institut de Génétique et de Biologie Moléculaire et Cellulaire, IGBMC, Illkirch, F-67404, France.

2. Centre National de la Recherche Scientifique, CNRS, UMR7104, Illkirch, F-67404, France.

3. Institut National de la Santé et de la Recherche Médicale, INSERM, U1258, Illkirch, F-67404, France.

4. Université de Strasbourg, Strasbourg, F-67000, France.

5. Laboratoire de Bioimagerie et Pathologies, Centre National de la Recherche Scientifique, UMR 7021, Illkirch, F-67404, France.

6. University of Bordeaux, CNRS, UMR 5297, Interdisciplinary Institute for Neuroscience, IINS, Bordeaux, F-33000, France.

7. University of Bordeaux, CNRS, INSERM, Bordeaux Imaging Center, BIC, UAR 3420, US 4, Pessac, F-33600, France.

8. These authors contributed equally to this work.

9. Lead contact

* Corresponding author: godin@igbmc.fr

Abstract

Completion of neuronal migration is critical for brain development. Kif21b is a plus-end directed kinesin motor protein that promotes intracellular transport and controls microtubule dynamics in neurons. Here we report a physiological function of Kif21b during radial migration of projection neurons in the mouse developing cortex. *In vivo* analysis in mouse and live imaging on cultured slices demonstrate that Kif21b regulates the radial glia-guided locomotion of new-born neurons independently of its motility on microtubules. Unexpectedly we show that Kif21b directly binds and regulates the actin cytoskeleton both *in vitro* and *in vivo* in migratory neurons. We establish that Kif21b-mediated regulation of actin cytoskeleton dynamics influences branching and nucleokinesis during neuronal locomotion. Altogether, our results reveal atypical roles of Kif21b on the actin cytoskeleton during migration of cortical projection neurons.

Keywords

Kinesin, Kif21b, Actin, Radial migration, Nucleokinesis, glia-guided locomotion, Cytoskeleton, Microtubule, Neuronal polarization

Introduction

The cerebral cortex is a central structure of the mammalian brain that commands all higher-order functions. It contains a large number of specialized types of excitatory projection neurons, inhibitory interneurons and glia that are distributed within layers and are regionally organized into specialized areas responsible of motor, sensory, and cognitive functions (Greig et al., 2013; Jabaudon, 2017; Rash and Grove, 2006). Proper functioning of the neocortex depends on the active migration of the two major classes of cortical neurons, the pyramidal projection neurons that primarily engage in radial migration (Molyneaux et al., 2007) and the GABAergic interneurons that undergo tangential migration (Wonders and Anderson, 2006). Consequently, in human, abnormal cortical layering leads to cortical malformation and is often associated with epilepsy and intellectual disability (Barkovich et al., 2012; Fernandez et al., 2016; Francis and Cappello, 2020; Guerrini and Dobyns, 2014).

To reach their final position in the cortical plate, projection neurons first undergo somal translocation and then, as the cortical wall thickens, they switch to a multimodal radial migration that is accompanied by a series of highly coordinated morphological changes (Nadarajah et al., 2001; Noctor et al., 2004). Newborn projection neurons first adopt a multipolar morphology and migrate randomly in the intermediate zone (LoTurco and Bai, 2006; Tabata and Nakajima, 2003). Then, they undergo a multipolar-to-bipolar transition to initiate locomotion along the radial glia scaffold. During this locomotion phase, the displacement of projection neurons is paced by successive cycles of nucleokinesis (Martinez-Garay et al., 2016; Tanaka et al., 2004a; Tanaka et al., 2004b) as well as occasional pauses (Hurni et al., 2017). Once the glia-guided locomotion is completed, the projection neurons connect to the pia and undergo a final somal translocation to settle at appropriate position in the cortical plate (Nadarajah et al., 2001). Most of the identified mechanisms underlying the different steps of radial migration ultimately converge on the dynamic remodeling of both microtubule (MT) and actin cytoskeletons (Liaci et al., 2021; Lian and Sheen, 2015; Moon and Wynshaw-Boris, 2013; Wu et al., 2014). Further reflecting the importance of these cytoskeletons in the regulation of radial migration, variants in genes encoding for tubulin subunits, actin components, microtubule associated proteins, actin binding proteins or motor proteins have been largely associated to neuronal migration disorders (Francis and Cappello, 2020; Stouffer et al., 2016).

Kif21b is a kinesin particularly enriched in the brain from early development onwards (Asselin et al., 2020; Labonte et al., 2014; Marszalek et al., 1999), that promotes intracellular transport along microtubules (Ghiretti et al., 2016; Gromova et al., 2018; Muhia et al., 2016; van Riel et al., 2017) and controls MTs dynamics (Ghiretti et al., 2016; Hooikaas et al., 2020; Muhia et al., 2016; Taguchi et al., 2022; van Riel et al., 2017). In particular, Kif21b accumulates at the MT plus ends, where it stabilizes assembled MT by limiting MT polymerization and suppressing catastrophes (Hooikaas et al., 2020; Masucci et al., 2022; Taguchi et al., 2022; van Riel et al., 2017). During cortical development, Kif21b is specifically expressed in postmitotic neurons where it localizes in dendrites, axons and growth cones (Asselin et al., 2020; Huang and Banker, 2012; Marszalek et al., 1999). Depletion of Kif21b *in vivo* in mice leads to severe brain malformations including microcephaly, hydrocephaly and dysgenesis of the corpus callosum (Kannan et al., 2017), as well as deficits in learning, memory and social behavior (Gromova et al., 2018; Morikawa et al., 2018; Muhia et al., 2016) and impaired neuronal maturation and synaptic function (Morikawa et al., 2018; Muhia et al., 2016; Swarnkar et al., 2018). Although these results clearly point to critical roles of Kif21b in brain development and function, the underlying cellular and molecular mechanisms have not been elicited yet.

Pathological variants in *KIF21B* have been identified in patients presenting with brain malformation and intellectual disability (Asselin et al., 2020; Narayanan et al., 2022). Interestingly, those variants impair neuronal migration and interhemispheric connectivity by enhancing KIF21B canonical motor activity through a gain-of-function mechanism (Asselin et al., 2020; Narayanan et al., 2022). In addition, haploinsufficient *KIF21B* variant also leads to migratory defects, suggesting that dosage of KIF21B is critical for neuronal migration (Asselin et al., 2020), the exact underlying molecular mechanisms of which remains elusive.

Here we uncover the physiological roles of Kif21b during radial migration of cortical projection neurons. By combining *in vivo* genetic perturbation in mouse cortices, complementation assays and time-lapse recording on organotypic brain slices, we show that the kinesin Kif21b is required to maintain bipolar morphology and to promote nucleokinesis and dynamic branching of cortical projection neurons during glia-guided locomotion. Surprisingly, the canonical motor activity of Kif21b is dispensable for its function in migrating neurons. We demonstrate that Kif21b controls radial migration

partly by regulating actin cytoskeleton dynamics through its direct binding to actin filaments. Altogether our data identify an unexpected non-canonical function of Kif21b on actin cytoskeleton participating to the regulation of cortical neurons migration.

Results

Kif21b is cell-autonomously required for radial migration of projection neurons

To explore the function of Kif21b on neuronal migration, we assessed the consequences of acute depletion of *Kif21b* specifically in postmitotic neurons using *in utero* electroporation (IUE) of CRE-dependent inducible shRNA vectors (Matsuda and Cepko, 2007) together with two plasmids allowing expression of CRE or GFP under the control of the NeuroD promoter (NeuroD:CRE and NeuroD:GFP respectively) in mouse embryonic cortices at E14.5. Efficacy of the two shRNAs was confirmed by Western blot in HEK-296T cell line (-93.4% for sh-*Kif21b* #1, -61.4% for sh-*Kif21b* #2 when compared to Kif21b expression in Scramble transfected cells) (**Figures S1A and S1B**). As described previously (Asselin et al., 2020), four days after IUE, the distribution of GFP-positive (GFP+) neurons depleted for *Kif21b* was significantly impaired with a notable reduction of GFP+ neurons reaching the upper cortical plate (Up CP) upon acute depletion of *Kif21b* compared to control (Scramble shRNA) (-19.4% for sh-*Kif21b* #1, -30% for sh-*Kif21b* #2) (**Figures 1A and 1B, Figures S1C and S1D**). *Kif21b*-depleted projection neurons arrested in the intermediate zone expressed the upper-layer marker *Cux1*, supporting a faulty neuronal migration rather than specification defects (**Figure 1C**). As Kif21a, the other member of kinesin-4 family, shares a high sequence similarity with Kif21b (Marszalek et al., 1999), we tested whether the two paralogues have redundant function in neuronal migration. We assessed the ability of mouse wild-type (WT) Kif21b or Kif21a proteins to restore migration defects induced by *Kif21b* knock-down. We performed co-electroporation of plasmids expressing Kif21b or Kif21a under the regulation of the neuronal NeuroD promotor together with NeuroD-driven sh-*Kif21b* #2 that targets the 3'UTR of endogenous *Kif21b* transcripts (**Figure S1B**). Whereas Kif21b fully restored the defective migration induced by sh-*Kif21b* #2 (**Figures 1A and 1B, Figures S3B and S3C**), co-electroporation of Kif21a failed to rescue the impaired distribution of *Kif21b*-depleted neurons, suggesting that loss of Kif21b function in migrating neurons cannot be compensated by Kif21a. Notably, Kif21b likely regulated neuronal migration in a cell-autonomous manner as *Kif21b* silencing did not affect cell survival (**Figure S1E**) and and glia scaffold integrity (data not shown). Finally, we investigated the migration phenotype in *Kif21b*^{flox/flox} conditional knock-out (cKO) embryos by IUE of NeuroD:Cre and NeuroD:GFP plasmids at E14.5. We confirmed the impaired positioning of

Kif21b knock-out neurons four days after IUE, with a reduction of 13.9% of neurons distributed in the upper cortical plate in *Kif21b^{flox/flox}* compared to *Kif21b^{WT/WT}* embryos (**Figures 1D and 1E**).

Given the expression of *Kif21b* in the mouse developing ganglionic eminences where the cortical inhibitory GABAergic neurons are born (**Figures S2A and S2B**), we next asked whether *Kif21b* also regulates tangential migration of interneurons. We performed *in vitro* culture of medial ganglionic explants (MGE) from E13.5 Dlx:Cre-GFP embryos electroporated *ex-vivo* with Cre dependent cherry expressing vector (pCAG-loxPSTOPloxP-Cherry) together with CRE-inducible sh-scramble or sh-*Kif21b* #2 on a layer of WT cortical feeders. This strategy allows concomitant knockdown of *Kif21b* and expression of a cherry fluorescent reporter specifically in migrating cortical interneurons. Time lapse recordings of electroporated explants revealed that, although *Kif21b*-silenced interneurons were able to migrate out of the explant, their kinetics of migration were different from the sh-scramble electroporated interneurons (**Figures S2C and S2D**), with a decreased migration velocity of 24.3%. Altogether, our results revealed the kinesin *Kif21b* as a key regulator of neuronal migration of the two main classes of cortical neurons.

Kif21b depletion impedes glia-guided locomotion of projection neurons

To determine how *Kif21b* controls migration of cortical projection neurons, we further investigated the dynamic cell shape remodeling occurring at the successive steps of migration along radial glia fibers (**Figure 2A**) by time lapse recording. *In utero* electroporation of inducible *Kif21b* shRNA or sh-scramble together with NeuroD:Cre and NeuroD:GFP plasmids were performed in WT E14.5 embryos. Two days later brain organotypic slices were cultured *in vitro* and GFP+ neurons were recorded the next day for 10 hours (**Figures 2B and 2C**). Although *Kif21b* depletion did not affect the initial multipolar to bipolar transition required to start glia-guided locomotion (**Figure 2A**, step 1; **Figure 2D**), the percentage of bipolar neurons that actively initiated the locomotory phase was decreased by 13.8% in sh-*Kif21b* #2 condition compared to sh-scramble control (76% and 88.1% respectively) (**Figure 2A**, step 2; **Figure 2E**). Moreover, compared to control neurons, the *Kif21b*-silenced bipolar neurons that started glia-guided locomotion (step 3 in **Figure 2A**) migrated significantly slower (**Figures 2B-C and 2F**) and spent more time pausing (**Figures 2C and 2G**). Exacerbated pausing was due to increases in both frequency (**Figure 2H**) and duration of the pauses (**Figure 2I**), likely due to a loss of bipolar polarity as shown by *Kif21b*-depleted neurons converting more often to multipolar

shape while pausing (step 4 in **Figure 2A**, **Figure 2J**). Interestingly, the motility index, defined as the velocity during active locomotion excluding the pauses, was decreased in *Kif21b*-silenced neurons (step 5 in **Figure 2A**, **Figure 2K**), demonstrating that Kif21b regulates both pausing and effective processivity of migrating projection neurons.

To properly migrate, projection neurons rely on repetitive cycles of forward progression of the cell body that starts with the translocation of a cytoplasmic dilatation (also known as a swelling) in the proximal region of the extending leading process (Step 5' in **Figure 2L**) and that is followed by the nuclear translocation (hereafter called nucleokinesis) toward the cytoplasmic swelling (Nishimura et al., 2017) (Step 5'' in **Figure 2L**). We showed that *Kif21b*-silenced neurons form less swellings and undergo less frequent and less efficient nucleokinesis with a net nuclear movement of 32.9 μm and 47.8 μm in *kif21b*-depleted and control neurons respectively (**Figures 2M-2P**). Defective nucleokinesis was further confirmed by shorter maximal distances between the nucleus and the centrosome, that is encompassed in the swelling, in neurons electroporated with sh-*Kif21b* #2 (**Figures 2Q and 2R**). We then investigated the dynamic branching of migrating neurons during active locomotion excluding the phases of pausing. While most control neurons persist bipolar during the locomotory phase with a single leading process that branched very transiently, *Kif21b*-depleted neurons, although still polarized, were characterized by multiple and heavily branched leading processes (**Figures 2S**). Overall, sh-*Kif21b* #2 expressing neurons showed an increased total branch length that arose from an increased number of shorter branches sprouting from either the soma or the leading process (**Figures 2S-2V**). As a result, neurons depleted for *Kif21b* spent statistically more time with multiple branches (**Figure 2W**), likely contributing, together with impaired nucleokinesis, to the decrease in migration velocity index observed in mutant projection neurons (**Figure 2K**). Collectively our data indicate that the kinesin Kif21b is critical to regulate neuronal polarization, nucleokinesis and dynamic branching of projection neurons during glia-guided locomotion.

Kif21b motility on microtubules is dispensable for its function in migrating projection neurons.

Given the critical role of Kif21b in regulating intracellular transport in neurons (Ghiretti et al., 2016; Gromova et al., 2018; Muhia et al., 2016; van Riel et al., 2017), we assessed whether Kif21b processive activity on microtubules mediate Kif21b function in migrating neurons. First, we tested for restoration of the sh-*Kif21b* #2-induced phenotype by truncated Kif21b protein that lacks the motor

domain (Kif21b Δ MD, **Figure 3A**) by introducing full-length or Kif21b Δ MD (NeuroD:Kif21b) together with inducible sh-Kif21b #2 and NeuroD:CRE in projection neurons using *in utero* electroporation at E14.5. Interestingly, Kif21b protein that lacks motor domain only partially rescued the distribution of *Kif21b*-depleted neurons with a significant number of neurons still trapped in the intermediate zone at E18.5 (**Figures 3B and 3C**), suggesting that this domain is partially required for Kif21b function in migrating neurons. To further test for the need of Kif21b motility on microtubules for neuronal migration, we performed complementation assays by expressing Kif21b protein that either cannot bind (NeuroD:Kif21b Δ ATP; **Figure 3A**) or hydrolyze ATP (NeuroD:Kif21b-T96N; **Figure 3A**) (Muhia et al., 2016) in *Kif21b*-silenced neurons. Surprisingly, both constructs fully restored the migration phenotype at E18.5, demonstrating that motility of Kif21b is dispensable for its function during radial migration (**Figures 3B and 3C**). Accordingly, the carboxy-terminal WD40 domain of Kif21b (**Figure 3A**), that is thought to promote interaction with cargoes (Marszalek et al., 1999), is not essential for Kif21b migration regulatory activities, as radial migration phenotype is fully rescued by overexpression of Kif21b Δ WD40 construct (**Figures 3B and 3C**). Of note, Kif21b truncated or mutant proteins showed similar expression level in N2A neuroblastoma cell line, except for NeuroD:Kif21b Δ ATP that tends to be lowly expressed (**Figure S3A**) and do not induce migration phenotypes while overexpressed under control conditions (Sh-Scramble) (**Figures S3B and S3C**). We next sought to investigate the migration steps that are regulated by the motor domain of Kif21b. We performed time lapse recording of brain organotypic slices after *in utero* electroporation of Kif21b Δ MD construct together with inducible *Kif21b*-shRNA. In accordance with a partial rescue of *Kif21b*-silenced neurons distribution in the cortical plate, expression of Kif21b lacking the motor domain induced a rescue of 52.6% of the migration velocity of *Kif21b* depleted neurons (**Figures 3D and 3E**). This partial rescue is likely due to inability of Kif21b Δ MD to restore pausing defects. Indeed, while Kif21b Δ MD fully recovered the motility index phenotype (distance with respect to time minus pauses duration) (**Figure 3F**), it failed to restore the increased number of pauses (**Figure 3G**) and even induced more drastic defects on pauses duration (**Figures 3H and 3I**). In line, Kif21b Δ MD expression did not rescue the loss of bipolar morphology of locomoting *Kif21b*-depleted neurons (**Figure 3J**). Collectively those data indicate that the N-terminal motor domain of Kif21b independently of its motility on microtubules is critical to prevent pausing of cortical projection neurons during migration.

Kif21b regulates actin cytoskeletal dynamics through direct binding

We next sought to understand the function of Kif21b that mediates its roles during radial migration of projection neurons. First, to probe for candidate proteins that may interact with Kif21b, we performed Kif21b co-immunoprecipitation on E18.5 mouse cortices followed by mass spectrometry analysis. Among the 41 proteins identified (**Table S1**), 12 were proteins associated either to the microtubule cytoskeleton or, more unexpectedly, to the actin cytoskeleton (**Figures 4A and S4A**). Among those cytoskeleton candidates, we found several actin paralogues, actin-based motor proteins including components of the non-muscle myosin II (NM2) motor protein, that powers actin contractile movement (Brito and Sousa, 2020), the unconventional myosin Va that transports cargoes along actin filaments (Hammer and Burkhardt, 2013) and the actin binding protein Drebrin (Dbrn1). Given the predominant role of the actomyosin remodeling in neuronal cells (Schaar and McConnell, 2005; Solecki et al., 2009; Tsai et al., 2007) and the increasing evidences showing that disruption of actin cytoskeleton associates with neuronal migration defects in human (Francis and Cappello, 2020; Stouffer et al., 2016), the actin cytoskeleton emerged as a strong unlooked-for candidate to mediate Kif21b function in migrating neurons. To validate these interactions, we first performed anti-Kif21b immunoprecipitation assays on extracts from E18.5 wild-type cortices and confirmed the specific binding of Kif21b to both actin and myosin light chain 2 (MLC 2), a subunit of NM2 (**Figures 4B and 4C**). Reciprocal immunoprecipitation analysis using anti-actin antibody confirmed the specific interaction between Kif21b and actin (**Figure 4B**). Next, we purified actin from E18.5 cortices and detected Kif21b in the pellet containing polymerized filamentous actin (F-actin) (**Figure 4D**), further suggesting ability of Kif21b to interact with filaments of actin. Corroborating these findings, Kif21b is enriched in the actin-rich growth cone fraction isolated from postnatal mouse cortices (**Figure 4E**). Immunolabelling of Kif21b, actin and microtubules in primary cortical neurons at day *in vitro* 2 (DIV2) revealed localization of Kif21b both in axons and the central domain of the growth cone that are devoid of microtubules and essentially composed of actin networks (**Figure 4F**). These data suggest that neuronal Kif21b likely interacts with actin cytoskeleton independently of its binding to microtubules. To ascertain the localization of Kif21b on the actin cytoskeleton, we analyzed relative localization of endogenous Kif21b and the actin cytoskeleton labelled with phalloidin using multicolor Single Molecule Localization Microscopy (SMLM) in primary cortical neurons at DIV2. STORM

imaging revealed that Kif21b molecules organized as clusters localized along actin filaments following a spiral pattern in the growth cone as well as in the neurites (**Figure 4G**). We performed quantitative analysis, based on the identification of objects from a Voronoi diagram (Levet et al., 2015), of the shortest distance between the centroid of each Kif21b cluster and the actin lattice border. Computation of the distances indicated that most Kif21b clusters localized within 1.34 nm and 1.86 nm (median) from the actin filament (**Figure 4H**) in growth cone and neurites respectively, demonstrating very close spatial approximation of Kif21b with actin filaments in cortical neurons. We next explored whether Kif21b directly binds to actin by performing *in vitro* co-sedimentation assays of pre-polymerized actin with purified recombinant Kif21b (**Figure S4B**, **Table S2**). Notably, although it contained negligible protein contaminants (**Table S2**), Kif21b purified fractions comprised full-length (FL) His-tagged Kif21b as well as shorter Kif21b fragments (**Table S2**). We detected FL Kif21b as well as most of the short products in the actin-enriched pellet (**Figure 4I**), suggesting a direct binding of Kif21b to polymerized actin. Accordingly, the same experiments in absence of actin revealed that most Kif21b fragments were found in the supernatant. As a control, we also performed a microtubule co-sedimentation assay with Kif21b purified fraction, showing expected enrichment of Kif21b in the MT pellet (data not shown). Finally, we investigated the roles of Kif21b on actin dynamics by recording, using spinning disc microscopy, dynamics of purified actin labelled with phalloidin and incubated with 1 nM of recombinant Kif21b. Actin polymerization was enhanced in presence of 1 nM of Kif21b (**Figure 4J**), indicating that direct binding of Kif21b may favor the initial step of actin dynamics, meaning nucleation (**Figure 4N**). Notably, increasing the concentration of Kif21b to 10 nM had reverse effect on actin nucleation (**Figure S4C**). Conversely, low concentration of Kif21b (1 nM) does not affect assembly of actin when actin is used at higher concentration (5 μ M) (data not shown), suggesting that effect of Kif21b on actin nucleation depends on the relative stoichiometry of actin and Kif21b molecules. To validate this actin-related function in cortices, we performed spinning disc analysis of dynamics of mouse embryonic brain actin labelled with phalloidin using protein extracts from E18.5 WT and KO (*Kif21b*^{tm1a/tm1a}) cortices. Corroborating assays with recombinant proteins, loss of Kif21b in embryonic cortices significantly limits *de novo* assembly of actin filaments as expected for a reduction of actin nucleation capacity (**Figure S4D**). Further analyzes of the G/F actin ratio by ultracentrifugation sedimentation assay in E18.5 WT and *Kif21b* KO (*Kif21b*^{tm1a/tm1a}) cortices revealed a decreased proportion of the filamentous form of actin (F-actin) upon deletion of *Kif21b* compared to the control condition (**Figure**

4K), although measured total actin levels by Western Blot were increased in KO condition (**Figure 4L**). This confirms the positive role of Kif21b in regulating the nucleation of actin filaments in embryonic cortices (**Figure 4N**). Finally, tracking of individual actin filament revealed that Kif21b did not affect filament elongation as similar rates of actin filament growth were measured in presence of Kif21b and in actin alone condition (**Figure 4M**). Altogether these data converged towards a direct role of Kif21b in regulation of actin dynamics (**Figure 4N**).

Kif21b depletion leads to aberrant actin dynamics in migrating neurons

Although well studied in the context of tangential migration of interneurons (Bellion et al., 2005; Godin et al., 2012) or glia-guided migration of cerebellar granular neurons (Solecki et al., 2009), the actin cytoskeletal dynamics in migrating cortical projection neurons has been poorly addressed. We first examined the spatial distribution of actin during glia-guided locomotion of cortical projection neurons using Lifeact as a probe for F-actin (Riedl et al., 2008) in brain organotypic slices after *in utero* electroporation of LifeAct-Ruby in E14.5 cortices. Time lapse imaging in control neurons (sh-Scramble) revealed that LifeAct-labelled F-actin accumulated in the proximal part of leading process before the translocation of the nucleus and dropped severely once the nuclear movement is completed (**Figures 5A and 5B**). Of note, in this experimental setup, the sensitivity of the LifeAct was not compatible with analysis of actin dynamics during branching. Interestingly, although actin dynamics were similar in control and *Kif21b*-depleted neurons before nucleokinesis, F-actin accumulation in the leading process persisted after the forward movement of the nucleus in neurons electroporated with sh-*Kif21b* #2 (**Figures 5A and 5C**). These data demonstrated the critical role of Kif21b in regulating actin dynamics *in vivo* in migrating neurons. Given the predominant role of actomyosin contraction in promoting nuclear translocation of migrating neurons (Schaar and McConnell, 2005; Solecki et al., 2009; Tsai et al., 2007) and the binding of Kif21b to non-muscle myosin II (**Figures 4B and 4C**), we tested the ability of Blebbistatin, which inhibits actomyosin contraction through inhibition of Myosin II motor activity, to rescue the dynamics of migrating neurons. Organotypic slices of brain electroporated with inducible sh-*Kif21b* #2, NeuroD:CRE and NeuroD:GFP were recorded for 4 hours, then treated with Blebbistatin at 3 μ M and imaged for additional 3.5 hours (**Figure 5D**). Nucleokinesis number and amplitude were similar before and after Blebbistatin treatment (**Figures 5E and 5F**), suggesting that faulty nucleokinesis induced by *Kif21b* depletion does not rely

on elevated myosin activity and actomyosin contraction. As we demonstrated that Kif21b regulates migration pausing independently of its motility on microtubules (**Figures 3G-I**), we tested whether pausing could be related to actin-dependent Kif21b function. We showed that inhibition of actomyosin contraction by Blebbistatin failed to rescue number (**Figure 5G**) and duration of pauses (**Figures 5H- and 5I**) indicating that Kif21b likely regulates neuronal polarization independently of actomyosin contractility (**Figure 5J**). Finally, we showed that inhibition of Myosin II motor activity with Blebbistatin rescued the multiple branching observed in *Kif21b*-depleted neurons (**Figures 5K and 5L**), suggesting that Kif21b, at least partly, regulates dynamic branching of the leading process through actomyosin dependent mechanisms. However, the partial rescue of the time spent with multiple branches (26min/3.5h in control condition (**Figure 2W**), 94min/3.5h sh-*Kif21b* #2 pre-Blebbistatin, 41min/3.5h sh-*Kif21b* #2 post- Blebbistatin) is likely not sufficient to rescue the motility index (**Figure 5M**). Collectively, these results showed that Kif21b is required to fine tune actin dynamics during specific steps of glia-guided locomotion including nucleokinesis and branching of the leading process.

Discussion

Our findings uncover physiological roles for Kif21b during radial migration of projection neurons. Although it is dispensable for the new-born pyramidal neurons to reach the intermediate zone and convert to a bipolar shape, Kif21b paces the glia-guided locomotion by controlling nucleokinesis, dynamic branching and pausing of migrating neurons. To date, several members of the kinesin superfamily have been shown to play critical functions during radial migration (Akkaya et al., 2021; Broix et al., 2016; Carabalona et al., 2016; Falnikar et al., 2011; Falnikar et al., 2013; Gilet et al., 2020; Li et al., 2022; Muralidharan et al., 2022; Qian et al., 2022; Sapir et al., 2013; Yu et al., 2020). Yet, unlike Kif21b, many of them regulate the initial multipolar-to-bipolar transition (Broix et al., 2016; Falnikar et al., 2013; Gilet et al., 2020; Qian et al., 2022; Sapir et al., 2013; Yu et al., 2020). Noteworthy, dynamic analysis of each stage of migration (multipolar-to-bipolar transition or bipolar locomotion) has not been performed systematically, preventing the exact delineation of the functions of those kinesins during radial migration.

Our study unravels the molecular mechanisms underlying Kif21b functions in migrating neurons. Several lines of evidence suggest that Kif21b regulates different phases of migration through distinct functional domains. First, our complementation experiments revealed that: i) although the N-terminal motor domain is partially required for Kif21b to promote neuronal migration, its ability to hydrolyze or bind ATP is nonessential; and ii) the C-terminal WD40 repeat (WDR) domain that likely binds cargoes (Marszalek et al., 1999) is not necessary to promote migration. This demonstrates that the N-terminal domain, independently of its motility, and the coiled-coil central region are both necessary but, individually, not sufficient for Kif21b functions in pyramidal neurons during migration. Second, rescue analysis with the truncated Kif21b Δ MD protein showed that the N-terminal domain is dispensable for the processivity of locomoting neurons but necessary to maintain the bipolar morphology and to limit pausing during locomotion. It suggests that the N-terminal domain and the coiled-coil domain ensure the functions of Kif21b in neuronal polarization and active locomotion, respectively. As the N-terminal domain is essential for the inhibition of MT growth (Masucci et al., 2022; Taguchi et al., 2022), it is tempting to postulate that Kif21b maintains bipolar morphology through the regulation of MT polymerization. Indeed, neuronal polarization largely relies on remodeling of the MTs cytoskeleton

(Lasser et al., 2018; Sakakibara et al., 2013) and stabilization of MTs instructs neuronal polarization (Schelski and Bradke, 2022; Witte et al., 2008). Overgrowth of MTs induced by loss of Kif21b (Hooikaas et al., 2020; Masucci et al., 2022; Muhia et al., 2016) could therefore compromise the bipolarity of locomoting neurons. Such hypothesis should be further tested by examining the ability of MT-depolymerizing drugs, like vinblastine, to rescue bipolar morphology of *Kif21b*-depleted migrating neurons (Hooikaas et al., 2020). In line with a MT-dependent effect, we showed that Blebbistatin treatment does not rescue the faulty bipolar-to-multipolar conversion observed upon *Kif21b* knockdown, suggesting that the role of Kif21b in maintaining bipolar morphology is independent of actomyosin contraction. However, as the N-terminal region of Kif21b binds to the unconventional Myosin Va in a neuronal activity dependent manner (Gromova et al, companion manuscript), one cannot exclude that Kif21b cooperates with Myosin Va to regulate actin dynamics in bipolar neurons, although, to date, neuronal activity has been shown to facilitate the initial step of projection neurons migration - the multipolar-to-bipolar conversion - unlikely regulated by Kif21b (**Figure 2**) (Ohtaka-Maruyama et al., 2018). The central coiled coil domain contains secondary MT-binding domain that promotes MT assembly and limits catastrophe frequency, although it is unclear whether it could act alone or exclusively in combination with the other secondary MT-binding domain within the WD40 tail (Ghiretti et al., 2016; Masucci et al., 2022; van Riel et al., 2017). Further work is required to delineate the function of each MT-binding domains in migrating neurons. Third, our *in vitro* co-sedimentation assays of pre-polymerized actin with purified recombinant Kif21b revealed short fragments of Kif21b that might specifically bind to actin (data not shown). Interestingly, those Kif21b fragments encompass all the functional domains of Kif21b, suggesting that Kif21b binds actin through multiple domains, including its central region. Accordingly, our attempts to precisely map Kif21b actin-binding domain(s) using immunoprecipitation of various Kif21b truncated proteins that either lack or only encompass the motor domain, regulatory coiled-coil domain (rCC), coil-coiled domain 1 or 2 or WD40 region were inconsistent and suggest that Kif21b binding to actin filaments requires specific structural conformation involving distinct and potentially distant protein domains. To date, our knowledge about the precise domains of binding to MT, actin or Myosins is limited, with only large domains identified (Ghiretti et al., 2016; Masucci et al., 2022; van Riel et al., 2017) (Gromova et al, companion manuscript). In addition, the high overlap between those domains raises the possibility of a competitive binding of Kif21b to actin and microtubule networks. Refinement of the domains through structural analysis of Kif21b either

bound to actin or microtubule would help, in the future, to understand the cooperative or competitive function(s) of Kif21b on both actin and microtubule cytoskeletons.

Our data provide the first evidence for a direct role of a kinesin on actin cytoskeleton in mammals. Indeed, to date, only a plant- and a *Dictyostelium*-specific kinesin (Iwai et al., 2004; Preuss et al., 2004) were shown to bind actin. Here, we first ascertained a direct binding of Kif21b to actin filaments by super-resolution imaging of cortical neurons in culture and by co-sedimentation assay with purified recombinant proteins (**Figure 4**). This validates previous proteomic data suggesting binding of actin and actin binding partners to exogenous Kif21b purified from HEK293T cells (van Riel et al., 2017). Then, investigations of the role of Kif21b on actin dynamics revealed that Kif21b favors the initial step of actin polymerization, the nucleation, but not the subsequent elongation of actin filaments, suggesting that Kif21b facilitates the formation of actin seeds but does not regulate, at least through direct interaction, the elongation of actin filament once formed. Very interestingly, effect of Kif21b on actin assembly highly depends on the stoichiometric ratio between actin and Kif21b molecules (**Figures 4 and S4**). This is reminiscent of the effect of Kif21b on the dynamics of the MT cytoskeleton in cells, with high and low kinesin concentrations leading to opposite effects on MT growth and stability (Ghiretti et al., 2016; Masucci et al., 2022; van Riel et al., 2017). The complex actin network is further built via Arp2/3-mediated nucleation of new actin branches on the side of pre-existing filaments, hence generating dense fast growing entangled actin networks (Firat-Karalar and Welch, 2011). *In vitro* analysis of filament branching using recombinant Arp2/3 complex and its activator pWA does not reveal changes in branch formation in absence or presence of Kif21b (data not shown). This suggests that Kif21b has likely no direct effect on Arp2/3 dependent nucleation in an assay where no competition with actin binding is present. However, Kif21b might modulate actin branching indirectly through its interaction with Arp2/3 (van Riel et al., 2017) or coronin (Figure S4A), that is known to directly regulate Arp2/3 complexes (Gandhi and Goode, 2008). Notably, in a complementary study, Gromova et al showed that Kif21b promotes polymerization and co-localizes with Arp2/3 complexes at actin foci in Cos-7 cells. Altogether, these findings indicate that Kif21b might regulate all steps of actin network dynamics through either direct (nucleation) or indirect (elongation and branching) mechanisms.

At the cellular level, except for the Kinesin 6 that has been shown to perturb actin localization during the initial multipolar-to-bipolar transition through unknown mechanisms (Falnikar et al., 2013), very few is known about kinesin and actin interplay in migrating cortical projection neurons. Here we showed, in control neurons, that filamentous actin accumulates ahead of the nucleus before nucleokinesis, in line with previous observation in both cortical projection neurons (Martinez-Garay et al., 2016) and in the cerebellar granule neurons that also undergo glia-guided locomotion (Solecki et al., 2009).

Reminiscent of what has been shown in cerebellar neuron, in which a retrograde actin flow away from the proximal region of the leading process drives nucleokinesis (Solecki et al., 2009), actin concentration at the front of the nucleus drastically drops in cortical projection neurons after nuclear movement. Interestingly, this dynamic actin turnover does not occur in migrating cortical neurons lacking Kif21b, suggesting that Kif21b controls nucleokinesis by controlling actin remodeling. Because non-muscle myosin II (NM2) activity ahead of the nucleus is critical for nucleokinesis (Solecki et al., 2009; Tsai et al., 2007), we hypothesized that Kif21b, through its binding to both actin and NM2, might regulate actomyosin contraction during nuclear forward movement. However, our rescue experiments using Blebbistatin indicate that the faulty nucleokinesis induced by the depletion of *Kif21b* is independent of the perturbation of NM2 activity (**Figure 5**). This further suggests that the high concentration of F-actin observed, after nucleokinesis, in the proximal leading process upon *Kif21b* depletion is rather caused by an excessive stabilization of F-actin than a defect in the retrograde actin flow, that is thought to be NM2 dependent (Solecki et al., 2009). This would imply that Kif21b has dual function on actin assembly and disassembly, possibly mediated through distinct binding domains, reminiscent of the double activities of Kif21b on MT nucleation and stability (Ghiretti et al., 2016; Masucci et al., 2022; van Riel et al., 2017). Rescue experiment with Latrunculin A, that depolymerizes actin filaments (Fujiwara et al., 2018), would help better delineating actin-dependent function(s) of Kif21b during nucleokinesis. Finally, in contrast to nucleokinesis and pausing, we showed that Kif21b likely regulates the dynamic branching of the leading process through regulation of actomyosin contraction. Collectively, these results indicate that Kif21b promote glia-guided locomotion of projection neurons by regulating both nucleokinesis and dynamic branching through distinct non-canonical functions on actin cytoskeleton.

In conclusion, our results indicate that Kif21b plays pleiotropic functions during all steps of the glia-guided locomotion of cortical projection neurons. These cellular functions, driven by distinct protein domains, are independent of the canonical processivity of Kif21b and likely rely on regulation of both microtubules and actin cytoskeletons dynamics. As it has been suggested for the plant-specific kinesin GhKCH1 (Preuss et al., 2004) and the *Dictyostelium*-specific kinesin DdKin5 (Iwai et al., 2004), our work opens the question of the roles of Kif21b in the interplay between microtubules and actin during neuronal migration, adding potential novel atypical function of kinesins in the coordination of actin and MT networks during mammalian brain development.

Methods

Cloning and plasmid constructs

shRNAs to deplete the expression of *Kif21b* were directed against the coding sequence 3390-3410 (NM_001252100.1) (sh-*Kif21b* #1) or the 3'-UTR (sh-*Kif21b* #2) and cloned in the pCALSL-mir30(Matsuda and Cepko, 2007) backbone vector as described in (Asselin et al., 2020). Various truncated *Kif21b* constructs were generated by Sequence and Ligation Independent Cloning (SLIC) as follows: *Kif21b*ΔMD (Δ9-371, motor domain), *Kif21b*ΔATP (Δ87-94, ATP binding site), *Kif21b*ΔWD40 (Δ1308-1639, WD40 domain). The c.288 C>T substitution that abolishes *Kif21b* mobility was created from WT CDS by site-directed mutagenesis to generate the *Kif21b*-T96N construct. Wild-type mouse *Kif21a* CDS (NM_001109040.2) was isolated from E18.5 cDNA mouse cortices by PCR and subcloned by restriction-ligation into the NeuroD:IRES-GFP plasmid (Hand and Polleux, 2011). The plasmid pCAGGs-PACT-mKO1 bearing the pericentrin-AKAp450 centrosomal targeting (PACT) domain fused to Kusabira Orange was kindly (Konno et al., 2008) was used to label centrosome and pCAGGS-LifeAct-Ruby (Riedl et al., 2008) was used for F-actin labeling. A Cre/loxP conditional cherry expressing plasmid pCAG-loxPSTOPloxP-Cherry was used for time-lapse imaging of migrating interneurons. Plasmid DNAs used in this study were prepared using the EndoFree plasmid purification kit (Macherey Nagel).

Mice

All animal studies were conducted in accordance with French regulations (EU Directive 86/609 – French Act Rural Code R 214-87 to 126) and all procedures were approved by the local ethics committee and the Research Ministry (APAFIS#15691-201806271458609). Mice were bred at the IGBMC animal facility under controlled light/dark cycles, stable temperature (19°C) and humidity (50%) condition and were provided with food and water *ad libitum*.

Timed-pregnant wild-type (WT) CD1 (Charles River Laboratories) females were used for *In Utero* electroporation (*IUE*) at embryonic day 14.5 (E14.5). NMRI (WT) mice (Janvier Labs) were used for growth cone extraction and actin preparation assays. *Kif21b*^{tm1a(KOMP)Wtsi} were obtained from UC Davis/KOMP repository. *Kif21b*^{Flox/Flox} conditional KO mice were generated using the International Mouse Phenotyping Consortium targeting mutation strategy (Skarnes et al., 2011) by crossing

Kif21b^{tm1a(KOMP)Wtsi} with a Flipase recombinase mouse line (FlpO-2A-eYFP) (Birling et al., 2012).

Genotyping was done as previously described in (Asselin et al., 2020).

In Utero Electroporation. Timed-pregnant mice were anesthetized with isoflurane (2 L per minute (min) of oxygen, 4% isoflurane in the induction phase and 2% isoflurane during surgery: Tem Segal). The uterine horns were exposed, and a lateral ventricle of each embryo was injected using pulled glass capillaries (Harvard apparatus, 1.0OD*0.58ID*100mmL) with Fast Green (1 µg/µl; Sigma) combined with different amounts of DNA constructs using a micro injector (Eppendorf Femto Jet). Embryos were injected with 1 µg/µl of NeuroD:Cre-IRES-GFP vector and 0.5 µg/µl NeuroD:IRES-GFP vector (empty, WT or mutated for *Kif21b* or WT-*Kif21a* construct) together with 3 µg/µl of either Cre inducible pCALSL-miR30-shRNA-*Kif21b* or pCALSL-miR30-sh-scramble plasmids. For rescue experiments and time-lapse imaging of actin dynamics, 1 µg/µl of truncated *Kif21b* constructs (or empty plasmid as control) or 3 µg/µl of pCAGGS-LifeAct-Ruby plasmid (Riedl et al., 2008) were co-injected with the mentioned plasmids. Plasmids were further electroporated into the neuronal progenitors adjacent to the ventricle by discharging five electric pulses (40V) for 50 ms at 950 ms intervals using electrodes (diameter 3 mm; Sonidel CUY650P3) and ECM-830 BTX square wave electroporator (VWR international). After electroporation, embryos were placed back in the abdominal cavity and the abdomen was sutured using surgical needle and thread. Pregnant mice were sacrificed by cervical dislocation, and embryos were collected at E16.5 or E18.5.

In vivo migration analysis

Mouse brain collection, immunolabeling. E16.5 and E18.5 embryos were sacrificed by head sectioning and brains were fixed in 4% paraformaldehyde (PFA, Electron Microscopy Sciences) in Phosphate buffered saline (PBS, HyClone) overnight at 4°C. Dissected brains were embedded in 4% low melt agarose (Bio-Rad), and sectioned with vibratome (Leica VT1000S, Leica Microsystems) in 60 µm slices. Free floating sections were maintained in cryoprotective solution (30 % Ethyleneglycol, 20% Glycerol, 30%DH₂O, 20% PO₄ Buffer) at -20°C until the time of use. Alternatively, for *Cux1* immunostaining, after fixation, brains were rinsed and equilibrated in 20% sucrose in PBS overnight at 4°C, embedded in Tissue-Tek O.C.T. (Sakura), frozen on dry ice and coronal sections were cut at the cryostat (18 µm thickness, Leica CM3050S) and maintained at -80°C until the day of immunolabelling.

Free floating sections were permeabilized and blocked with blocking solution containing 5% Normal Donkey Serum (NDS, Dominic Dutsher), 0.1% Triton-X-100 in PBS. Brain slices were incubated with primary antibodies diluted in blocking solution overnight at 4°C and then rinsed and incubated with secondary antibody diluted in PBS-0.1% Triton for one hour at room temperature (RT). Cell nuclei were stained using DAPI (1mg/ml Sigma). Slices were mounted in Aquapolymount mounting medium (Polysciences Inc). For cryosections immunolabeling, antigen retrieval was performed by incubating the sections in boiling citrate buffer (0.01 M, pH 6) for 10 minutes, followed by standard immunostaining procedure. All primary and secondary antibodies used for immunolabeling are listed in **Table S3**.

Images acquisition and analysis. Cell counting were done in at least three different brain slices from of at least three different embryos for each condition. After histological examination, only brains with comparative electroporated regions and efficiencies were conserved for quantification.

Images were acquired in 1024x1024 mode using confocal microscope (TCS SP5; Leica) at 20x magnification (z stack of 1,55 µm) and analyzed using ImageJ software. Cortical wall areas (UpCP: upper cortical plate, LoCP: lower cortical plate, IZ/SVZ: intermediate zone, subventricular zone/ventricular zone) were identified according to cell density (nuclei staining with DAPI). The total number of GFP-positive cells in the embryonic brain sections was quantified by counting positive cells within a box of fixed size and the percentage of positive cells in each cortical area was calculated.

Organotypic slices culture and real-time imaging

Organotypic slices culture. *IUE* was performed in CD1 mice as indicated above, E16.5 mouse embryos were killed by head sectioning, and brains were embedded in 4% low-melt agarose (BioRad) diluted in HBSS (Hank's Balanced Salt Solution, ThermoFisher Scientific) and sliced (300 µm) with a vibratome (Leica VT1000S, Leica Microsystems). Brain slices were cultured 16 to 24 hours in semi-dry conditions (Millicell inserts, Merck Millipore), in a humidified incubator at 37 °C in a 5% CO₂ atmosphere in wells containing Neurobasal medium supplemented with 2% B27 (Thermofisher #17504044), 1% N2 (Thermofisher #17502048), and 1% penicillin/streptomycin (Gibco, Life Technologies). Slice cultures were placed in a humidified and thermo-regulated chamber maintained at 37 °C on the stage of an inverted confocal microscope.

Time lapse recordings. Time-lapse confocal microscopy was performed with a Leica SP8 scanning confocal microscope equipped with a 25X water immersion objective / N.A. 0.95 and a humidified incubation chamber (37°C, 5% CO₂). 25 successive 'z' optical plans spanning 50 µm were acquired every 30 minutes for 10 hours. Time-lapse acquisitions of actin dynamics in migrating neurons were performed in a confocal Spinning Disk CSU-W1 microscope using a 25X / N.A. 0.95 water immersion objective equipped with a humidified incubation chamber, with acquisitions at 10 minutes intervals for 5 hours. Rescue analysis of neuronal migration with Blebbistatin were done using the same experimental setup except that slices were recorded for 4 hours with 10 minutes intervals, then treated with 3 µM Blebbistatin (abcam, #ab120425) by addition of the drug to the culture media and then recorded for another 3.5 hours.

Analysis of time lapse sequences. All sequences were analyzed using ImageJ by adjusting time-interval in the plugin "Manual tracking", as well adjusting the pixel width with the x/y calibration corresponding to the analyzed sequence. Migrating neurons were manually tracked individually during the time-lapse and the data collected were analyzed for migration velocity calculating the mean velocity during the entire time-lapse acquisition; number of pauses was calculated by counting the number of times that the neuron stopped moving (velocity = 0); mean and total duration of pauses were calculated by the mean and total number of minutes in which the neuron spent without moving (velocity=0), respectively; and motility index was calculated as the mean velocity during the entire time-lapse acquisition subtracting the pausing time (velocity=0). Analysis of the proportions of multipolar-bipolar, persisting multipolar, bipolar-multipolar and persisting bipolar neurons were done by the identification of migrating neurons with either multipolar or bipolar morphology and the follow-up of morphological changes (or absence of them) during the entire duration of the time-lapse. Swelling and nucleokinesis were counted for each neuron during the time-lapse, as well as the time each neuron took to complete a nucleokinesis. Additionally, nucleokinesis amplitude was measured by tracking the maximum length of the movement of the soma of each bipolar neuron. Branching in the leading process was quantified by counting the number of branches of each neuron in every time point of the time-lapse, followed by the calculation of the mean number of branches and the sum of the minutes that the neuron spent with 2 or more branches. Length of the branches was calculated considering the time-point in which the neuron extended at its maximum length the leading process, or main leading

process for branching neurons, in which case, the length of all the branches was counted for that time-point.

LifeAct fluorescence was determined by delimitating the area of the proximal part of the leading process where the LifeAct signal showed increasing levels and measuring the mean grey values of the delimited region during for each time-point of the time-lapse. For each measure, normalization was done with the mean grey fluorescence with a ROI in the soma, where values of fluorescence were constant. Time-lapse analyses were done in at least three different brain slices from different embryos in at least three independent experiments for each condition.

***Ex-vivo* electroporation of medial ganglionic eminence (MGE) explants and time lapse imaging of migrating interneurons.**

Ex-vivo electroporation of MGE and time-lapse imaging has been done as previously described (Tielens et al., 2016). The heads of E13.5 *Dlx5,6* Cre-GFP (Stenman et al., 2003) embryos were harvested and the cortex removed in order to expose the ganglionic eminences. Plasmids to overexpress Cre inducible pCALSL-miR30-shRNA-*Kif21b* or pCALSL-miR30-sh-scramble were used at a concentration of 3 µg/µl and were directly injected in the MGEs. These plasmids were co-electroporated with a Cre/loxP conditional cherry expressing plasmid used at a concentration of 1 µg/µl. Electroporation conditions: 50V, 5 pulses of 50ms duration spaced by 1s interval. Electroporated MGEs were then cultured on cortical cell feeder seeded on glass-bottom petri-dish (MatTek, Ashland, USA). Co-cultures were placed in a humidified and thermo-regulated chamber maintained at 37°C on the stage of an inverted confocal microscope. Time-lapse confocal microscopy was performed with a Leica SP8 scanning confocal microscope with a 25X objective. Images of living cherry-expressing migrating interneurons were acquired every 5 minutes for 4 hours. Migration velocity was analyzed adjusting time interval in the plugin "Manual tracking", as well as the x/y calibration with the pixel width of the analyzed sequence. Migrating neurons were manually tracked individually during the time-lapse and the data collected was analyzed for migration velocity. Analyses were done in at least three different embryos in two independent experiments for each condition.

Neuronal culture, fixation and immunostaining

CD1 mice cortices from E15.5 mice were dissected and collected in cold PBS supplemented with BSA (3 mg/mL), MgSO₄ (1 mM, Sigma), and D-glucose (30 mM, Sigma). Cortices were dissociated in Neurobasal media containing papain (20U/mL, Worthington) and DNase I (100 µg/mL, Sigma) for 20 minutes at 37°C, washed 5 minutes with Neurobasal media containing Ovomucoid (15 mg/mL, Worthington), and manually triturated in OptiMeM supplemented with D-Glucose (20mM). 220 000 cells were plated in Neurobasal Supplemented media supplemented with B27 (Thermofisher #17504044), L-glutamine (2 mM) (Thermofisher #25030-123), and penicillin (5 units/mL) – streptomycin (50 mg/ml) (Thermofisher #15140-130) on round coverslips of N1.H5, 18 mm diameter, pre-coated with Poly-L-Lysine (1 mg/ml). Neurons were incubated in an incubator with controlled CO₂ (5%) and temperature (37°C).

At *Day In Vitro* 2 (DIV2) neurons were incubated with pre-warmed extraction buffer containing 0.25% triton, 0.1% glutaraldehyde, in PEM buffer (80 mM PIPES, 5 mM EGTA, 2 mM MgCl₂, pH 6.8) for 30 seconds and fixed in a pre-warmed fixing solution containing 0.25% Triton, 0.5% Glutaraldehyde, in PEM buffer. Glutaraldehyde was quenched with 0.1 % NaBH₄ prepared with phosphate buffer (PB) for 7 minutes and cells were washed twice with PB. Blocking was performed by incubation with 0.22% gelatine for 2 hours at RT with gentle shaking, primary antibody diluted in blocking buffer was incubated at 4°C overnight. Secondary antibody diluted in blocking buffer was incubated one hour and washed three times with PB. To label F-actin, phalloidin coupled to Alexa Fluor Plus 647 (Invitrogen, A30107) was incubated overnight for aquapolymount mounting for confocal imaging or incubated until the day of acquisition for super resolution microscopy.

Neurons in Figure 4F were imaged using the LiveSR mode of Confocal Spinning Disk CSU-X1 “Nikon” equipped with a Photometrics Prime 75B camera and an APO TIRF 100x/ N.A. 1.49 oil objective controlled by Metamorph 7.10. software.

SMLM imaging protocol

Setup. SMLM was performed with a home-build setup based on an inverted microscope (Eclipse TiE Nikon) equipped with 100x/1.49 NA oil-immersion objective (Apochromat TIRF, Nikon), Perfect Focus and driven with µmanager software (Edelstein et al., 2014). The microscope was equipped with a laser line 532 and 642 nm lasers (Oxxius). Excitation was done in Total Internal Reflection Fluorescence (TIRF) mode to excite only the sample near the surface (< 200 nm). A multiband dichroic mirror was

used to filter emission from the sample (FF560/659-Di01, Semrock) and notch filters were used to remove scattered laser light (532 nm and 642 nm StopLine single-notch filters: NF01-532U and NF03-642, Semrock). Spectral discrimination of the two different fluorescent probes was achieved by splitting the fluorescence emission on the camera chip by an optical separator (Gemini, Hamamatsu associated to a dichroic mirror (FF 640-Di01 Semrock and respectively a LP 532 (Semrock) and a LP 647 (Semrock) for the top and bottom chip areas)). All images were recorded using an EMCCD camera ((C9100-23B ImagEM, Hamamatsu) with 16 x 16 μm pixels), using 240 x 240 top region on the camera for AlexaFluor 555 labelling and 240 x 240 bottom region for AlexaFluor 647 labelling. Chromatic aberration was corrected by imaging TetraSpek fluospheres excited with a low laser power (532nm and 647 nm). A raster scan of a single bead was performed to record a reference image and determined, for each frame, its localization with the help of DOM ImageJ plugin. This plug-in was also used to determine and corrected the optical and chromatic aberration between the two channels.

Acquisition imaging procedure for SMLM. After neurons were cultured, fixed and immunostained as explained above, the coverslips were placed in an observation chamber (Ludin chamber, LIS) and recovered by fresh 700 μL of imaging solution (prepared just before the use by mixing 7 μL of GLOX buffer (56 mg/mL Glucose oxidase, 3.4 mg/mL catalase, 8 mM Tris 10, 40 mM NaCl 50), 70 μL MEA buffer (1 M MEA in 0.25 N HCl) and 620 μL of buffer containing 50 mM Tris (pH 8.0), 10 mM NaCl and 10% Glucose) to control the redox environment. Acquisition was performed by adjusting the laser power to 50 mW at the objective for both lasers that results in 2 kW/cm² excitation intensity and acquisition time to get single fluorophores bursts with the optimal signal-noise ratio. For the dual-color image acquisition, a sequential approach was used with a first dSTORM recording with Alexa Fluor 647 labelling followed by a second dSTORM recording with the Alexa Fluor 555 labelling into two individual image stacks (more than 30 000 frames per stack).

SMLM Data analysis. The two sets of images were read by an imageJ macro, which extracts the appropriate ROI and corrects the chromatic aberrations. Single-molecule localizations in both extract datasets were calculated using the thunderSTORM algorithm (Ovesny et al., 2014). The following parameters were used to find and fit the signal of each particle: image filtering – Difference-of-Gaussians filter (sigma 1 = 1.0 and sigma 2 = 1.6); approximated localization of molecules – Local maximum (peak intensity threshold: std (Wave.F1), connectivity: 8-neighbourhood); sub-pixel localization of molecules – Integrated Gaussian (fitting radius: 4 px, fitting method: Least squares,

initial sigma:1.3 px). The reconstructed images of both channels were combined to generate a two colour-image. To calculate the distances between actin and Kif21b clusters, the localization data of the two channels (obtained with ThunderStorm) were analyzed with the PoCA software (<https://github.com/fleivet/PoCA>, plug-in developed by Floriant Levet). Single molecule localization coordinates were used to compute a Voronoï tessellation, in order to partition the image space in polygons of various sizes centered on each localized molecule (Levet et al., 2015). Using this space-partitioning framework, first-rank densities δ_i^{-1} of the molecules were computed. Segmentations were performed thresholding these density features with a threshold of 5 times (resp. 2 times) the average density δ of the whole dataset for the Kif21b clusters (resp. actin filaments). Finally, we defined the shortest distance between the Kif21b clusters and the actin filaments as the distance between the clusters' centroid and the closest point of the actin filament borders.

Cell culture and transfections

All cells used in this study are provided by the cell culture platform of the IGBMC (Illkirch), are guaranteed mycoplasma free (PCR test Venorgem) and have not been authenticated. Mouse neuroblastoma N2A cells were cultured in DMEM (1g/L glucose) (Dulbecco's Modified Eagle Medium, GIBCO) supplemented with 5% Fetal Calf Serum (FCS) and Gentamycin 40µg/mL and Human embryonic kidney (HEK) 293T cells were cultured in DMEM (1g/L glucose) (GIBCO) supplemented with 10% Fetal Calf Serum (FCS), penicillin 100 UI/mL, streptomycin 100 µg/mL in a cell culture incubator (5% CO₂ at 37°C). Both cell lines were transfected using Lipofectamine 2000 (Invitrogen) according to the manufacturer's protocol. N2A cells were transfected using the different NeuroD:Kif21b-IRES-GFP constructs. HEK293K cells were transfected using sh-scrambled or ShRNA-*Kif21b* #2 together with pEGFP-C1-3'UTR KIF21B or sh-scrambled or ShRNA-*Kif21b* #1 together with pEGFP-C1-WT-Kif21b. Expression of transfected genes was analyzed 48 hours after transfection by RT-qPCR or immunoblotting.

Protein extraction and western blot

Proteins from mouse cortex (E18.5) or transfected cells (N2A or HEK 293T) were extracted as follows: cells were lysed in RIPA buffer (50 mM Tris pH 8.0, 150 mM NaCl, 5 mM EDTA pH 8.0, 1% Triton X-100, 0.5% sodium deoxycholate, 0.1% SDS) supplemented with EDTA-free protease inhibitors

(cOmplete™, Roche) for 30 minutes, then cells debris were removed by high speed centrifugation at 4°C for 25 minutes. Protein concentration was measured by spectrophotometry using Bio-Rad Bradford protein assay reagent. Samples were denatured at 95°C for 10 minutes in Laemmli buffer (Bio-Rad, #1610747) with 2% β-mercaptoethanol (Sigma, #M3148) and then resolved by SDS–PAGE and transferred onto PVDF membranes (Merck, #IPVH00010). Membranes were blocked in 3% milk in PBS buffer with 0.1% Tween (PBS-T) and incubated overnight at 4°C with the antibodies indicated in **Table S3** diluted in blocking solution. Membranes were washed 3 times in PBS-T and incubated at room temperature for 1 hour with the HRP- coupled secondary antibodies indicated in **Table S3**, followed by 3 times PBS-T washes. Visualization was performed by quantitative chemiluminescence using SuperSignal West Pico PLUS Chemiluminescent Substrate (ThermoFisher, #34580). Signal intensity was quantified using ImageJ.

RNA extraction, cDNA synthesis and RT–qPCR.

Total RNA was extracted from the ganglionic eminences of WT NMRI mouse embryos at different time points of development, with TRIzol reagent (Thermo Fisher Scientific). Kif21b ex2-3 (Fwd sequence: AAGGCTGCTTTGAGGGCTAT, Rev sequence: AAAGCCGGTGCCCATAGTA) were used to target mouse *Kif21b* cDNA and actin (Fwd: TATAAAACCCGGCGGCGCA ; Rev: TCATCCATGGCGAACTGGTG) as housekeeping gene normalizer. RT–qPCR was performed in a LightCycler PCR instrument (Roche) using SYBR Green Master Mix (Roche).

Immunoprecipitation

For immunoprecipitation (IP) experiments, E18.5 brain cortices were lysed using 200 µl of IP buffer (Thermofisher IP Kit (#8788) (1% NP40, 5% Glycerol, 1 mM EDTA, 150 mM NaCl, 25 mM Tris-HCl pH 7.4)) supplemented with EDTA-free protease inhibitors (cOmplete, Roche) and proteins were extracted as explained above. 200 µg of protein were incubated with Kif21b antibody (0.20 µg), actin antibody (2 µg) or corresponding control IgG at 4°C overnight with 5 µL of pre-washed Pierce Protein A/G Magnetic Beads (Thermo-Scientific, # 88802) (see **Table S3** for antibodies references). Magnetic beads were collected with a magnetic stand (Invitrogen, 12321D), washed twice with IP buffer and proteins were eluted with 20 µL of Low pH elution buffer (Thermofisher, #1862619) at room temperature for 10 minutes. Neutralization buffer (Tris pH 8, 1.0 M) and 20 µL of 2x Laemmli Elution

Buffer containing 2% β -mercaptoethanol was added to the proteins. Samples were subjected to SDS-PAGE for Western Blot analysis.

Mass spectrometry

Liquid digestion. For mass spectrometry analysis, IP was performed as described above, except that for the protein incubation step, 2 mg of protein, 100 μ L of pre-washed beads and 3 μ g of Kif21b or control IgG antibody were used. After Kif21b elution with 45 μ L of low pH elution buffer (ThermoFisher, #1862619), the same volume of 2x Laemmli Elution Buffer containing 2% β -mercaptoethanol was added to the sample and the proteins were conserved at -20°C until the analysis. Protein mixtures were precipitated with trichloroacetic acid (TCA) overnight at 4°C, pellets were washed twice with 1 mL cold acetone, dried and dissolved in 8 M urea in 0.1 mM Tris-HCl pH 8.5 for reduction (5 mM TCEP, 30 minutes), and alkylation (10 mM iodoacetamide, 30 minutes). Double digestion (LysC - Trypsin) was performed by incubating the proteins first with endoproteinase Lys-C (Wako, #125-05061,) in 8 M urea for 4h at 37°C followed by an overnight trypsin digestion (Promega #V511A,) in 2 M urea at 37°C. Peptide mixtures were then desalted on C18 spin-column and dried on Speed-Vacuum before LC-MS/MS analysis.

LC-MS/MS Analysis. Samples were analyzed using an Ultimate 3000 nano-RSLC (Thermo Scientific, San Jose California) coupled in line with a LTQ-Orbitrap ELITE mass spectrometer via a nano-electrospray ionization source (Thermo Scientific, San Jose California). One microgram of tryptic peptides (in triplicate) were loaded on a C18 Acclaim PepMap100 trap-column (75 μ m ID x 2 cm, 3 μ m, 100Å, Thermo Fisher Scientific) for 3.5 minutes at 5 μ L/minute with 2% ACN, 0.1% FA in H₂O and then separated on a C18 Accucore nano-column (75 μ m ID x 50 cm, 2.6 μ m, 150Å, Thermo Fisher Scientific) with a 90 minutes linear gradient from 5% to 35% buffer B (A: 0.1% FA in H₂O / B: 99% ACN, 0.1% FA in H₂O) followed by a regeneration step (90% B) and a equilibration (5%B). The total chromatography was 120 minutes at 200 nL/minute and at 38°C. The mass spectrometer was operated in positive ionization mode, in Data-Dependent Acquisition (DDA) with survey scans from m/z 350-1500 acquired in the Orbitrap at a resolution of 120,000 at m/z 400. The 20 most intense peaks (TOP20) from survey scans were selected for fragmentation in the Linear Ion Trap with an isolation window of 2.0 Da and were fragmented by CID (Collision-Induced Dissociation) with normalized collision energy of 35%. Unassigned and single charged states were rejected. The Ion

Target Value for the survey scans (in the Orbitrap) and the MS2 mode (in the Linear Ion Trap) were set to 1E6 and 5E3 respectively and the maximum injection time was set to 100 ms for both scan modes. Dynamic exclusion was used. Exclusion duration was set to 20 s, repeat count was set to 1 and exclusion mass width was ± 10 ppm.

MS Data Analysis. Proteins were identified with Proteome Discoverer 2.4 software (PD2.4, Thermo Fisher Scientific) and *Mus Musculus* proteome database (Swissprot, reviewed, release 2020_11_20). Precursor and fragment mass tolerances were set at 7 ppm and 0.6 Da respectively, and up to 2 missed cleavages were allowed. Oxidation (M) was set as variable modification, and Carbamidomethylation (C) as fixed modification. Peptides were filtered with a false discovery rate (FDR) at 1%, rank 1. Proteins were quantified with a minimum of 2 unique peptides based on the XIC (sum of the Extracted Ion Chromatogram). The quantification values were exported in Perseus for statistical analysis involving a log[2] transform, imputation, normalization before Volcano plots (Tyanova et al., 2016).

F-actin sedimentation assay from embryonic cortices

Microdissected E18.5 cortices (3 to 4 cortices per 500 μ l) were lysed in a buffer containing 50 mM PIPES pH 6.9, 50 mM NaCl, 5 mM MgCl₂, 5 mM EGTA, 5% glycerol, 0.1% NP40, 0.1% Triton X-100, 0.1% Tween 20, 0.1% β -mercaptoethanol, supplemented with EDTA-free protease inhibitors (cOmplete™, Roche) for 10 minutes at 37°C. The lysate was first centrifuged at 2,000 g for 5 minutes to remove nuclei then subjected to a high-speed centrifugation (100,000 g, 1 hour, 37°C) to obtain a clear supernatant (G-actin) and a pellet (F-actin). Pellet was dissolved overnight at 4°C in water containing 10 μ M cytochalasin D (Sigma-Aldrich #C8273) at the same volume as the collected supernatant and equal amounts of each fraction were subjected to western blot analysis.

Growth cone extraction from mouse brain.

Isolation of growth cone was performed on WT NMRI mouse cortices at post-natal day (P) 2 as previously described (Li et al., 2013). Five P2 mouse brains were homogenized in 5 mL of homogenization buffer (5 mM Tris-HCl, 0.32 M sucrose, 1 mM MgCl₂) supplemented with EDTA-free protease inhibitors (cOmplete™, Roche), then centrifuged at 1,660 x g for 15 min at 4 °C. Supernatant were loaded on top of a discontinuous 0.75/1.0/2.33 M sucrose density gradient and centrifuge at

242,000 x g for 60 min at 4°C (Beckman SWTi41 swing rotor). The growth cone depleted fraction was collected between 0.75 M and 1.0 M sucrose. The growth cone enriched fraction was collected at the interface between the load and 0.75 M sucrose, re-suspend in the homogenization buffer and centrifuged at 100,000 x g for 40 min at 4°C (Beckman SWTi41 swing rotor). The pellet containing the growth cone were re-suspended in 50 µl of the homogenization buffer. The same volume of each fraction was analyzed by western blot. Non-growth cone membranes, which also contain Golgi membranes, were revealed by the enrichment of Golgi matrix protein (GM130 primary antibody), while the growth cone fraction was revealed by the enrichment of Jip1 protein.

Purification of human KIF21B overexpressed in BHK21 cells

MVA expression vector. A vaccinia virus (strain Modified Vaccinia Ankara - MVA - Bio safe level 1) allowing an inducible expression of human KIF21B in mammalian cells (BHK21) were used. Briefly, KIF21B tagged with 6 His-tag at the C-terminal was integrated by homologous recombination at the HA locus of the MVA viral genome.

BHK21 overexpression. For protein production, a 1.8 L preculture of BHK21 C13-2P cells (10^6 cells/ml) grown in Glasgow's modified Eagle's medium (GMEM; Thermo Fisher, MA, USA) supplemented with Bacto Tryptose Phosphate (1.5 g/L), 10% foetal calf serum and 50 µM Gentamycin was infected with approximately 0.1 PFU/cell of recombinant virus and incubated at 37°C. After 48 hours, the infected cells were mixed with 6 L of uninfected cells at 10^6 cells/mL at a 1:10 ratio (v/v). Overexpression was induced by the addition of 1 mM IPTG to cell mixture and cells were incubated at 37°C in 5% CO₂ at 75% hygrometry for 24 hours. Cells were pelleted at 2000 g for 20 minutes, washed in PBS and pelleted again at 2000 g for 10 minutes. Cell pellet was stored at -20°C until use.

KIF21B-6His purification. Pellets from 5L cells were unfrozen and resuspended in lysis buffer (50 mM HEPES pH7.5, 500 mM NaCl, 1 mM MgCl₂, 10 mM Imidazole, 0.5% IGEPAL® CA-630, 2 mM β-Mercapto-ethanol supplemented with Roche cOmplete inhibitor cocktail tablets) at a ratio of 15 ml of buffer/g of biomass. Lysis was performed by pulse sonication on ice (5 minutes with pulses 2s ON, 2s OFF). Lysate was then clarified by ultracentrifugation for 1 hour at 100.000g at 4°C. After filtration on cellulose filter 5µm, the supernatant was loaded on HisTrap Excel 5mL column (Cytivia). Column was washed with 10 mM imidazole and proteins were eluted with a gradient from 10 to 500 mM of imidazole. Peak fractions at 280 nm were analyzed on SDS-PAGE and fractions containing the

complex were pulled together. The sample was then concentrated using an Amicon Ultra 15 ml with a 100-kDa molecular weight cutoff (MWCO) and further purified using a HiLoad Superdex 200 pg 16/60 column (Cytivia) equilibrated with GF buffer (10 mM HEPES pH7.5, 250 mM NaCl, 1 mM MgCl₂, 2 mM DTT). 2 fractions containing the purest complex (checked by SDS-PAGE) were pooled together to obtain two pooled recombinant sample, concentrated using an Amicon Ultra 15 ml with a 100-kDa molecular weight cutoff (MWCO) to 0.7 mg/ml, flashed frozen in liquid nitrogen and stored at -80°C. The contaminants found in the two pooled samples can be found in **Table S2**.

***In Vitro* F-Actin and microtubules co-sedimentation assay**

Actin was polymerized according to the manufacturer instructions with some modifications to prepare F-actin at 21 µM. Briefly, actin (Cytoskeleton, #AKL99-A) was resuspended in general actin buffer (5 mM Tris-HCl pH 8.0 and 0.2 mM CaCl₂), and incubated 30 minutes at 4°C. Actin polymerization buffer (500 mM KCl, 20 mM MgCl₂, 10 mM ATP) was added and incubated 1 hour at 24°C.

The binding experiments were performed for the following conditions: Kif21b alone and Kif21b+Actin; using 5 µl of recombinant Kif21b (from fraction 1), 29 µl of polymerized actin and adding actin buffer to complete a volume of 50 µl. The reactions were incubated 30 minutes at 24°C and ultracentrifuged 60 minutes at 60 000 rpm in an Optima MAX-E Ultracentrifuge, using the rotor TLA 100.4. Supernatant was collected and resuspended in 10 µl of 4x Laemmli buffer containing 2% β-mercaptoethanol, while the pellet was resuspended adding 30 µl of milliQ water followed by 30 µl of 2% β-mercaptoethanol. Pellet and supernatant fractions were then analysed by Coomassie staining. After running the samples in a SDS-PAGE gel, the gel was warmed for 40 seconds in a microwave in a solution containing 50% ethanol, 10% acetic acid, and incubated on agitation at RT for 10 minutes. It was then incubated overnight in a solution containing 5% ethanol and 7.5% acetic acid with Coomassie blue. The gels were washed in milliQ water to remove background.

Actin polymerization assays *In Vitro*

Coverslips preparation. Glass coverslips were oxidized with oxygen plasma (30s ,35%, Diener Electronic, cat. ZeptoB) and incubated with 5% BSA in HEPES 10 mM at pH 7.4 for 10 minutes RT and washed with HEPES 10 mM.

Actin polymerization of cortices extract. Actin assembly was induced by mixing 7,36 μL of cortex extract with the reaction mixture containing 18 μL fluorescent buffer (15 mM imidazole, pH 7.0, 74 mM KCl, 1.5 mM MgCl_2 , 165 mM DTT, 2 mM ATP, 50 mM CaCl_2 , 5 mM glucose, 30 mg/ml catalase, 155 mg/ml glucose oxidase, and 0.75% methylcellulose.), 2.64 μL of G buffer (2mM Tris-HCl, 0.2 mM Na_2ATP , 0.2 mM CaCl_2 , 5 mM DTT), 0,1% BSA and 1 μL of phalloidin 488 nm (A12379,1/200, diluted in Hepes 10 mM). 5 μL of the reaction mixture were immediately put between coated-coverslip and slide and sealed with VALAP (1:1:1 vaseline, lanolin and paraffin).

Actin polymerization with purified protein. Actin assembly was induced by mixing TicTac buffer (Farina et al., 2016) (10 mM HEPES,16 mM PIPES, 50 mM KCl, 5 mM MgCl_2 ,1 mM EGTA supplemented with - 2.7 mM ATP, 10 mM DTT, 20 $\mu\text{g}/\text{mL}$ Catalase, 3 mg.mL Glucose, 100 $\mu\text{g}/\text{mL}$ Glucose Oxydase, 0.25% Methylcellulose) with 0,1% BSA and 1/60 000 phalloidin (Fisher Scientific A12379). Kif21b (from fraction 2) was added at a final concentration of 1 nM or 10 snM. The reaction mixture was immediately put in a flow chamber (constitute of clean glass slide, a BSA-coated coverslip, and precut adhesive double tape 50 μm thick) and sealed with VALAP (1:1:1 vaseline, lanolin and paraffin).

Image acquisition. Images were taken using an inverted Nikon EclipseTi microscope equipped with a $\times 100$ oil objective (HCX plan APO) and a Photometrics Prime 95B (Teledyne Photometrics). The microscope and devices were driven by MetaMorph (Molecular Devices, Downington, PA). Images of actin polymerization of cortices extract were acquired every 1s with the following parameters: 30% of laser power and 200ms of exposure time. Image of actin polymerization with purified proteins were acquired every 5s with the following parameters: 50% of laser power and 100ms of exposure time.

Image Analysis. Filaments were segmented using TSOAX (V0.2.0, default parameters except for Gaussian-std: 2 and by adjusting the ridge threshold) (Xu et al., 2019). The resulting file was treated using a home-made script on R studio (Version 1.4.1106). The results were plot using a Prism 9. The total amount of polymerized actin was calculated as the sum of all filaments detected at each time. Then, the mean amount of polymerized actin was plotted, the linear regression was calculated, and statistical differences were calculated with GraphPad Prism 9. Mean length of all the detected filaments was measured at each time point. The results were analyzed by fitting the exponential curve and statistical differences was calculated with Prism 9. To quantify actin elongation rate, single filaments were manually tracked: filament length was measured during 90s. The results were plotted,

and the linear regression was calculated, and statistical differences was calculated with GraphPad Prism 9.

Statistical analysis

All statistics were calculated using GraphPad Prism 6 or 9 (GraphPad) and are represented as mean \pm s.e.m. The number of experiment repetitions and statistical tests are indicated in the figure legends and also reported in Supplementary data 1. Adjustments made for multiple comparisons, confidence intervals and exact P-values for Figs. 1B, 1E; 2E-K, M-P, R-W; 3C, E-J; 4H, J-M; 5B-C, E-M; Supplementary 1A, B, D; Supplementary 2A, B, D; Supplementary 3C; Supplementary 4C, D are reported in Supplementary Data 1. Graphs were generated using GraphPad and images were assembled with Adobe Illustrator CS6 (Adobe Systems).

Acknowledgments

This work was funded by grants from INSERM (ATIP-Avenir program, J.D.G.), the Fyssen foundation (J.D.G.), the French state funds through the Agence Nationale de la Recherche under the project JCJC CREDO ANR-14-CE13-0008-01 (J.D.G.), and the programme Investissements d'Avenir labelled (ANR-10-IDEX-0002-02, ANR-10-LABX-0030-INRT, to J.D.G., A-C.R. and M.R.), INSERM/CNRS and University of Strasbourg. This work of the Interdisciplinary Thematic Institute IMCBio, as part of the ITI 2021-2028 program of the University of Strasbourg, CNRS and INSERM, was supported by IdEx Unistra (ANR-10-IDEX-0002), and by SFRI-STRAT'US project (ANR 20-SFRI-0012) and EUR IMCBio (ANR-17-EURE-0023) under the framework of the French Investments for the Future Program. L.A. and J.R.A. were funded through the IGBMC PhD program (ANR-10-IDEX-0002-02, ANR-10-LABX-0030-INRT) and Fondation pour la recherche médicale. R.B. is funded by an ANR JCJC granted to A.C.R. (ANR-19-CE13-0005-01). P.T. and J.B. are, respectively, research assistant and assistant professor at the University of Strasbourg. C.B. is funded by CERBM-GIE. L.R. and B.M. are research engineers at CNRS. F.L. is a research engineer at INSERM. J.D.G. is an INSERM investigator. Y.M. is professor at the University of Strasbourg and Institut Universitaire de France. A-C.R. is a CNRS investigator. We thank the Imaging Center of IGBMC (ici.igbmc.fr), in particular, Elvire Guiot and Erwan Grandgirard for their assistance in the imaging experiments. We are grateful to the staff of the mouse facilities of the Institut Clinique de la souris (ICS) and Institut de Génétique et de Biologie Moléculaire et Cellulaire (IGBMC), the staff of the proteomics platform and of the molecular biology service (in particular Thierry Lerouge and Paola Rossolillo) for their involvement in the project. The SMLM imaging was supported by the Imaging Center PIQ-QuEst (<https://piq.unistra.fr/>). We warmly thank Dr Binnaz Yalcin, Dr Laurent Blanchoin and Christophe Guérin for helpful comments, advice, and reagents. We are also grateful to members of J.D.G. laboratory for discussion and technical assistance.

Author contribution:

J.R.A. and L.A. conceived and designed the experiments, performed the experiments, performed statistical analysis, and analyzed the data related to cellular, and functional studies in mice. P.T. performed *in utero* electroporation. P.T and N.S provided technical assistance. R.B. and A-C.R. conceived, designed, and performed *in vitro* actin experiments. C.B., J.B. and M.R. contributed to the

production of recombinant Kif21b proteins. B.M. performed mass spectrometry analysis and analyzed data. L.R. performed SMLM acquisition and performed quantitative analysis using a plugin developed by F.L. Y.M. contributed to SMLM data analysis and interpretation. J.D.G. conceived, coordinated, and supervised the study, designed experiments, analyzed data and wrote the manuscript.

Competing Interests:

The other authors declare no competing interest.

Figure Legends

Figure 1. Kif21b is cell-autonomously required for radial migration of projection neurons.

(A) Coronal sections of E18.5 mouse cortices electroporated at E14.5 with NeuroD:Cre and NeuroD:IRES-GFP together with either Cre inducible shRNA-*Kif21b* #2 in combination with NeuroD-Empty vector, NeuroD-mKif21b (WT(Wild-type)-mKif21b) or NeuroD-mKif21a (WT(Wild-type)-mKif21a) or sh-scramble in combination with NeuroD-Empty vector. (D) Coronal sections of E18.5 WT or double floxed *Kif21b* conditional knock-out (*Kif21b*^{flox/flox}) mouse cortices electroporated at E14.5 with NeuroD:Cre and NeuroD:IRES-GFP. (A, D) GFP-positive electroporated cells are depicted in green. Nuclei are stained with DAPI. (B, E) Histograms (means \pm s.e.m.) showing the distribution of GFP-positive neurons in different regions (Up CP, Upper cortical plate; Lo CP, Lower cortical plate; SVZ/ IZ, subventricular zone / intermediate zone) showing specific roles of Kif21b and not its paralogue Kif21a in projection neurons migration. Significance was calculated by two-way ANOVA, Bonferroni's multiple comparisons test. ns, non-significant; *P < 0.05; **P < 0.005; ***P < 0.001, ****P < 0.0001. Number of embryos analyzed: (B) sh-scramble + Empty vector, n=6; sh-RNA-*Kif21b* #2 + Empty vector, n=11; sh-RNA-*Kif21b* #2 + WT-Kif21b, n=7; and sh-RNA-*Kif21b* #2 + WT-Kif21a, n=5. (D) Wild type, n=4; and *Kif21b*^{flox/flox}, n=5. (C) Cux1 immunostaining (red) of E18 mouse cortices electroporated at E14.5 with NeuroD:Cre and NeuroD:IRES-GFP together with either Cre inducible sh-scramble or shRNA *Kif21b* #2 showing correct specification of GFP-positive *Kif21b*-depleted arrested neurons (arrowheads in insets). Scale bars (A, C, D) 50 μ m. See also Figures S1 and S2.

Figure 2. *Kif21b* depletion impedes glia-guided locomotion of projection neurons.

(A) Drawing of radial migration of projection neurons depicting the different steps of the process, step 1: multipolar-bipolar transition, step 2: initiation of bipolar migration, step 3: glia-guided locomotion that is paced by pauses (step 4) when bipolarity is transiently lost and active locomotion (step 5). (B-W) Time lapse imaging of neurons electroporated at E14.5 with NeuroD:Cre and NeuroD:IRES-GFP and either Cre inducible shRNA *Kif21b* #2 or sh-scramble in E16.5 brain slices cultured for one day. (B) Locomotor paths (colored lines) of sh-scramble or sh-*Kif21b* #2 expressing neurons recorded every 30 minutes for 10 hours (h). Scale bar: 20 μ m. (C) Time-lapse sequences of representative pyramidal neurons electroporated with the indicated constructs at E14.5. White and red arrowheads indicate respectively forward movement and pausing of the nucleus. Scale bar: 20 μ m. (D) Percentage of GFP+ neurons converting to a bipolar morphology or remaining as multipolar for 10 hours recording. (E-K) Quantification (means \pm s.e.m.) of the percentage of GFP+ bipolar neurons (BP) initiating locomotion (E), the mean velocity of locomotion (μ m/h) (F), the total pause duration (min) (G), the average number of pauses per 10 hours recording (H), the mean pause duration (min) (I), the percentage of neurons maintaining bipolar shape or converting to multipolar morphology (J), and the motility index (velocity without pauses (μ m/h)) (K). (L) Schematic representation of the forward progression of pyramidal neurons during glia guided locomotion, involving cycles of swelling formation (black arrow in 5') and nucleokinesis (5''). (M-P) Analysis (means \pm s.e.m.) of the average number of swelling (M) or nucleokinesis (N) during 10 hours recording and mean amplitude (μ m) (O) and duration (min) (P) of each nucleokinesis. (Q) Representative confocal images of migrating neurons after GFP immunolabelling (green) of E16.5 mouse cortices electroporated at E14.5 with NeuroD:Cre, NeuroD:GFP and pCAGGS-PACT-mKO1 to label centrosome (CTR, red, arrowheads), and either Cre inducible shRNA *Kif21b* #2 or sh-scramble. Nuclei were stained with DAPI (blue). Distances between nuclei and centrosome are indicated by a yellow line. Scale bar: 5 μ m. (R) Quantification (means \pm s.e.m.) of the distance nucleus-centrosome (μ m) in neurons extending a swelling in control and *Kif21b*-depleted cells. (S-W) Analysis (means \pm s.e.m.) of dynamic branching of the leading process showing branching types (S), number (T), mean length (μ m) (U), total length (μ m) (V) of branches, as well as time spent with multiple branches (min) (W). Significance was calculated by unpaired t-test, except in figure S, where significance was calculated by two-way ANOVA. ns, non-significant;

*P < 0.05; ***P < 0.001, ****P < 0.0001. Number of embryos analyzed: **(D)** sh-scramble, n=9; sh-*Kif21b* #2, n=6; **(E)** sh-scramble, n=7; sh-*Kif21b* #2, n=7; **(J)** sh-scramble, n=11; sh-*Kif21b* #2, n=7. Number of cells analyzed from at least 3 embryos: **(F-I,K)** sh-scramble, n=153; sh- *Kif21b* #2, n=248; **(M, N)** sh-scramble, n=77; sh- *Kif21b* #2, n=83; **(O,P)** sh-scramble, n=72; sh- *Kif21b* #2, n=62; **(R)** sh-scramble, n=51; sh- *Kif21b* #2, n=35, **(S-W)** sh-scramble, n=73; sh- *Kif21b* #2, n=71.

Figure 3. Kif21b motility on microtubules is not essential for its function in migrating projection neurons.

(A) Schematic representation of the mouse Kif21b protein indicating its different domains, and the recombinants constructs used for the rescue experiments. **(B)** **(A)** Coronal sections of E18.5 mouse cortices electroporated at E14.5 with NeuroD:Cre and NeuroD:IRES-GFP together with either Cre inducible shRNA-*Kif21b* #2 in combination with NeuroD-Empty vector or Kif21b-expressing constructs as indicated, or sh-scramble in combination with NeuroD-Empty vector. GFP-positive electroporated cells are depicted in green. Nuclei are stained with DAPI. Scale bar, 50 μ m. **(C)** Histograms (means \pm s.e.m.) showing the distribution of GFP-positive neurons in different regions (Up CP, Upper cortical plate; Lo CP, Lower cortical plate; or SVZ /IZ, subventricular zone / intermediate zone) in all conditions as indicated. Number of embryos analyzed per condition: sh-scramble + Empty vector, n=3; sh-RNA-*Kif21b* + Empty vector, n=11; sh-*Kif21b* + indicated Kif21b constructs, n \geq 5. Significance was calculated by two-way ANOVA, Bonferroni's multiple comparisons test. ns, non-significant; *P < 0.05; **P < 0.005; ***P < 0.001, ****P < 0.0001. **(D-J)** Time lapse imaging of neurons electroporated at E14.5 with NeuroD:Cre and NeuroD:IRES-GFP together with either Cre inducible shRNA-*Kif21b* #2 in combination with NeuroD-Empty vector or NeuroD:Kif21b Δ MD, or sh-scramble in combination with NeuroD-Empty vector in E16.5 brain slices cultured for one day. **(D)** Locomotor paths (colored lines) of neurons expressing sh-scramble or sh-*Kif21b* #2 alone or in combination with NeuroD:Kif21b Δ MD and recorded every 30 min for 10 hours (h). Scale bar: 20 μ m. **(E-I)** Analysis (means \pm s.e.m.) of migration dynamics over 10 hours showing that expression of NeuroD:Kif21b Δ MD in Kif21b-depleted neurons partially and totally rescue the mean velocity (μ m/h) **(E)** and the velocity index (μ m/h) **(F)**, respectively, but does not rescue the average number of pauses per 10 hours **(G)**, the mean pause duration (min) **(H)**, the total pause duration (min) **(I)** or the percentage of neurons converting to multipolar morphology **(J)**. Significance was calculated by two-way ANOVA, Bonferroni's multiple comparisons

test. ns, non-significant; * $P < 0.05$; ** $P < 0.005$; *** $P < 0.001$, **** $P < 0.0001$. Number of cells analyzed from at least 3 embryos: **(E-I)** sh-scramble + NeuroD-Empty, $n=77$; sh- *Kif21b* #2 + NeuroD-Empty, $n=66$, sh- *Kif21b* #2 + NeuroD:Kif21b Δ MD, $n=76$. Number of embryos analyzed: **(J)** sh-scramble + NeuroD-Empty, $n=4$; sh- *Kif21b* #2+ NeuroD-Empty, $n=3$; sh- *Kif21b* #2+ NeuroD:Kif21b Δ MD, $n=4$. See also Figure S3.

Figure 4. Kif21b regulates actin cytoskeletal dynamics through direct binding.

(A) Volcano plot analysis of the affinity purification-mass spectrometry (AP-MS) results showing, in red, proteins that are specifically interacting with Kif21b in E18.5 mouse cortices. **(B-C)** Western blot analysis of Kif21b or actin immunoprecipitation (IP) experiments in 3 independent E18.5 mouse cortices (Cx 1 to 3) showing reciprocal interaction between Kif21b and actin **(B)** and binding of Myosin light chain-2 (MLC2) to Kif21b **(C)**. Whole cortices extracts are shown as input. **(D)** Western blot F-actin sedimentation assay from E18.5 wild type mouse cortices showing that Kif21b binds to F-actin. **(E)** Growth cone fractionation assay showing growth cone (GC, enriched for vesicle marker Jip1) and a non-growth cone fraction (NGC, enriched for Golgi marker GM130) isolated from P2 wild type mouse cortices and indicating that Kif21b is enriched in the GC fraction. **(F)** Triple staining of Kif21b (red), α -tubulin (green) and F-actin (phalloidin, in blue) in a growth cone of a DIV2 neuron imaged by confocal microscopy. Scale bar: 5 μ m. **(G)** Single Molecule Localization Microscopy (SMLM) showing Kif21b (green) and F-actin (phalloidin, red) double staining in a growth cone and a neurite of a DIV2 neuron. Scale bar: 5 μ m. Insets are shown by one (*) or two asterisks (**). Scale bar in insets: 1 μ m. **(H)** Analysis of the distribution probability of the distance (nm) between Kif21b clusters and actin filaments in both growth cones and neurites. Growth cones, $n= 259$ particles analyzed from 3 neurons, neurites, $n= 331$ particles analyzed from 4 neurons, experiment done in two independent replicates. **(I)** In vitro co-sedimentation assay of recombinant Kif21b in presence or absence of actin, showing that full-length Kif21b (asterisk) and shorter fragments co-sediment with polymerized actin found in the pellet (P). SN= supernatant. **(J)** Representative spinning-disk images of *in vitro* analysis of actin polymerization dynamics (stained with phalloidin) at the beginning (0') and at the end (10') of the experiment in presence or absence of recombinant Kif21b (1 nM). Scale bar 10 μ m. The graph shows the number of actin filaments assembled during a 600 s time-lapse. Significance was calculated by linear regression to determine differences in curves for each dataset. Number of replicates: Actin 1

μM , $n=7$, Actin $1\ \mu\text{M}$ + Kif21b $1\ \text{nM}$, $n=6$ in three different experiments. **(K)** Quantitative analysis (mean \pm s.e.m.) of Western blot of actin sedimentation assay performed in E18.5 wild type (WT) and *Kif21b*^{Tm1a/Tm1a} (KO) mouse cortices showing increase of G/F ratio upon deletion of *Kif21b*. **(L)** Western blot analysis of total actin levels in three independent E18.5 wild type (WT) and *Kif21b*^{Tm1a/Tm1a} (KO) mouse cortices (Cx 1 to 3) showing (means \pm s.e.m.) increased actin level normalized by GAPDH in KO samples. **(K,L)** Significance was calculated by unpaired t-test, * $P < 0.05$. Number of embryos analyzed: **(K)** WT, $n=7$; KO, $n=10$; **(L)** WT and KO, $n=3$. **(M)** *In vitro* actin polymerization in absence or presence of recombinant Kif21b ($1\ \text{nM}$) analyzed as the length of individual filaments of actin during a 80 s time-lapse. Significance was calculated by linear regression to determine differences in curves for each dataset. Number of filaments analyzed: Actin $1\ \mu\text{M}$, $n=12$, Actin $1\ \mu\text{M}$ + Kif21b $1\ \text{nM}$, $n=14$ in three different experiments. **(N)** Scheme representing monomer actin pool nucleation and polymerization. Lower panel showed the positive effect of Kif21b on actin nucleation without affecting polymerization. See also Figure S4.

Figure 5. *Kif21b* depletion leads to aberrant actin dynamics in migrating neurons.

(A) Representative sequence of migrating pyramidal neurons recorded during 5 hours in E16.5 organotypic slices electroporated at E14.5 with NeuroD:Cre, NeuroD:IRES-GFP and pCAGGS-LifeAct-Ruby together with Cre inducible sh RNA *Kif21b* #2 or sh-scramble and cultured for one day. Intensity of the LifeAct-Ruby is shown by ImageJ fire look up table. Scale bar: $10\ \mu\text{m}$. Arrows points towards the proximal part of the leading process where actin accumulation severely dropped after nucleokinesis in control condition. **(B, C)** Quantification of the relative LifeAct-Ruby fluorescence (A.U.) at the proximal part of the leading process in the LifeAct-Ruby+ control **(B)** or *Kif21b* depleted neurons **(C)** before and after nucleokinesis (pointed by an arrow). Data were analysis by fitting a mixed-model, Tukey's multiple comparisons test. ns, non-significant; * $P < 0.05$. Number of cells analysed: sh-scramble, $n=22$ and sh- *Kif21b* #2, $n=24$. **(D)** Schematic representation of the rescue experimental approach with Blebbistatin. E16.5 organotypic slices electroporated at E14.5 by NeuroD:Cre, NeuroD:IRES-GFP and the Cre inducible shRNA *Kif21b* #2 were imaged by time-lapse microscopy for 4 hours (h), followed by Blebbistatin incubation, and subsequent imaging for an additional 3.5 hours time-lapse. **(E-J)** Analysis (means \pm s.e.m.) of the frequency **(E)** and the amplitude (μm) **(F)** of nucleokinesis as well as the average number of pauses per 3.5h **(G)**, the mean

pause duration (min) (**H**), the total pausing time (min) (**I**) and the percentage of GFP+ neurons converting to multipolar stage (**J**) pre and post-Blebbistatin treatment indicating that Kif21b-induced effect on nucleokinesis and pausing are independent of non-muscle myosin 2 activity. (**K-L**) Quantification (means \pm s.e.m.) of branching parameters before and after Blebbistatin treatment, show rescue of number of branches (**K**) and time spent with multiple branches (min) (**L**) upon non-muscle myosin 2 inhibition. (**M**) Quantification (mean \pm s.e.m.) of motility index ($\mu\text{m/h}$). Significance was calculated by unpaired t-test. ns, non-significant; * $P < 0.05$. Number of cells analyzed from at least 3 embryos: (**E,F**): pre-blebbistatin, n=17 and post-blebbistatin, n=15. (**G-I**) pre-blebbistatin, n=45 and post-blebbistatin, n=33; (**K-L**) pre-blebbistatin, n=20 and post-blebbistatin, n=19; (**M**) pre-blebbistatin, n=25 and post-blebbistatin, n=26. Numbers of embryos analyzed: (**J**) pre-blebbistatin and post-blebbistatin, n=3 embryos.

References

- Akkaya, C., Atak, D., Kamacioglu, A., Akarlar, B.A., Guner, G., Bayam, E., Taskin, A.C., Ozlu, N., and Ince-Dunn, G. (2021). Roles of developmentally regulated KIF2A alternative isoforms in cortical neuron migration and differentiation. *Development* 148.
- Asselin, L., Rivera Alvarez, J., Heide, S., Bonnet, C.S., Tilly, P., Vitet, H., Weber, C., Bacino, C.A., Baranano, K., Chassevent, A., *et al.* (2020). Mutations in the KIF21B kinesin gene cause neurodevelopmental disorders through imbalanced canonical motor activity. *Nat Commun* 11, 2441.
- Barkovich, A.J., Guerrini, R., Kuzniecky, R.I., Jackson, G.D., and Dobyns, W.B. (2012). A developmental and genetic classification for malformations of cortical development: update 2012. *Brain* 135, 1348-1369.
- Bellion, A., Baudoin, J.P., Alvarez, C., Bornens, M., and Metin, C. (2005). Nucleokinesis in tangentially migrating neurons comprises two alternating phases: forward migration of the Golgi/centrosome associated with centrosome splitting and myosin contraction at the rear. *J Neurosci* 25, 5691-5699.
- Birling, M.C., Dierich, A., Jacquot, S., Herault, Y., and Pavlovic, G. (2012). Highly-efficient, fluorescent, locus directed cre and FlpO deleter mice on a pure C57BL/6N genetic background. *Genesis* 50, 482-489.
- Brito, C., and Sousa, S. (2020). Non-Muscle Myosin 2A (NM2A): Structure, Regulation and Function. *Cells* 9.
- Broix, L., Jagline, H., E, L.I., Schmucker, S., Drouot, N., Clayton-Smith, J., Pagnamenta, A.T., Metcalfe, K.A., Isidor, B., Louvier, U.W., *et al.* (2016). Mutations in the HECT domain of NEDD4L lead to AKT-mTOR pathway deregulation and cause periventricular nodular heterotopia. *Nat Genet* 48, 1349-1358.
- Carabalona, A., Hu, D.J., and Vallee, R.B. (2016). KIF1A inhibition immortalizes brain stem cells but blocks BDNF-mediated neuronal migration. *Nat Neurosci* 19, 253-262.
- Edelstein, A.D., Tsuchida, M.A., Amodaj, N., Pinkard, H., Vale, R.D., and Stuurman, N. (2014). Advanced methods of microscope control using muManager software. *J Biol Methods* 1.
- Falnikar, A., Tole, S., and Baas, P.W. (2011). Kinesin-5, a mitotic microtubule-associated motor protein, modulates neuronal migration. *Mol Biol Cell* 22, 1561-1574.

Falnikar, A., Tole, S., Liu, M., Liu, J.S., and Baas, P.W. (2013). Polarity in migrating neurons is related to a mechanism analogous to cytokinesis. *Curr Biol* 23, 1215-1220.

Farina, F., Gaillard, J., Guerin, C., Coute, Y., Sillibourne, J., Blanchoin, L., and Thery, M. (2016). The centrosome is an actin-organizing centre. *Nat Cell Biol* 18, 65-75.

Fernandez, V., Llinares-Benadero, C., and Borrell, V. (2016). Cerebral cortex expansion and folding: what have we learned? *EMBO J* 35, 1021-1044.

Firat-Karalar, E.N., and Welch, M.D. (2011). New mechanisms and functions of actin nucleation. *Curr Opin Cell Biol* 23, 4-13.

Francis, F., and Cappello, S. (2020). Neuronal migration and disorders - an update. *Curr Opin Neurobiol* 66, 57-68.

Fujiwara, I., Zweifel, M.E., Courtemanche, N., and Pollard, T.D. (2018). Latrunculin A Accelerates Actin Filament Depolymerization in Addition to Sequestering Actin Monomers. *Curr Biol* 28, 3183-3192 e3182.

Gandhi, M., and Goode, B.L. (2008). Coronin: the double-edged sword of actin dynamics. *Subcell Biochem* 48, 72-87.

Ghiretti, A.E., Thies, E., Tokito, M.K., Lin, T., Ostap, E.M., Kneussel, M., and Holzbaur, E.L. (2016). Activity-Dependent Regulation of Distinct Transport and Cytoskeletal Remodeling Functions of the Dendritic Kinesin KIF21B. *Neuron* 92, 857-872.

Gilet, J.G., Ivanova, E.L., Trofimova, D., Rudolf, G., Meziane, H., Broix, L., Drouot, N., Courraud, J., Skory, V., Voulleminot, P., *et al.* (2020). Conditional switching of KIF2A mutation provides new insights into cortical malformation pathogeny. *Hum Mol Genet* 29, 766-784.

Godin, J.D., Thomas, N., Laguesse, S., Malinouskaya, L., Close, P., Malaise, O., Purnelle, A., Raineteau, O., Campbell, K., Fero, M., *et al.* (2012). p27(Kip1) Is a Microtubule-Associated Protein that Promotes Microtubule Polymerization during Neuron Migration. *Dev Cell* 23, 729-744.

Greig, L.C., Woodworth, M.B., Galazo, M.J., Padmanabhan, H., and Macklis, J.D. (2013). Molecular logic of neocortical projection neuron specification, development and diversity. *Nat Rev Neurosci* 14, 755-769.

Gromova, K.V., Muhia, M., Rothhammer, N., Gee, C.E., Thies, E., Schaefer, I., Kress, S., Kilmann, M.W., Shevchuk, O., Oertner, T.G., *et al.* (2018). Neurobeachin and the Kinesin KIF21B Are Critical for Endocytic Recycling of NMDA Receptors and Regulate Social Behavior. *Cell Rep* 23, 2705-2717.

Guerrini, R., and Dobyns, W.B. (2014). Malformations of cortical development: clinical features and genetic causes. *Lancet Neurol* 13, 710-726.

Hammer, J.A., 3rd, and Burkhardt, J.K. (2013). Controversy and consensus regarding myosin II function at the immunological synapse. *Curr Opin Immunol* 25, 300-306.

Hand, R., and Polleux, F. (2011). Neurogenin2 regulates the initial axon guidance of cortical pyramidal neurons projecting medially to the corpus callosum. *Neural Dev* 6, 30.

Hooikaas, P.J., Damstra, H.G., Gros, O.J., van Riel, W.E., Martin, M., Smits, Y.T., van Loosdregt, J., Kapitein, L.C., Berger, F., and Akhmanova, A. (2020). Kinesin-4 KIF21B limits microtubule growth to allow rapid centrosome polarization in T cells. *Elife* 9.

Huang, C.F., and Banker, G. (2012). The translocation selectivity of the kinesins that mediate neuronal organelle transport. *Traffic* 13, 549-564.

Hurni, N., Kolodziejczak, M., Tomasello, U., Badia, J., Jacobshagen, M., Prados, J., and Dayer, A. (2017). Transient Cell-intrinsic Activity Regulates the Migration and Laminar Positioning of Cortical Projection Neurons. *Cereb Cortex* 27, 3052-3063.

Iwai, S., Ishiji, A., Mabuchi, I., and Sutoh, K. (2004). A novel actin-bundling kinesin-related protein from *Dictyostelium discoideum*. *J Biol Chem* 279, 4696-4704.

Jabaudon, D. (2017). Fate and freedom in developing neocortical circuits. *Nat Commun* 8, 16042.

Kannan, M., Bayam, E., Wagner, C., Rinaldi, B., Kretz, P.F., Tilly, P., Roos, M., McGillem, L., Bar, S., Minocha, S., *et al.* (2017). WD40-repeat 47, a microtubule-associated protein, is essential for brain development and autophagy. *Proc Natl Acad Sci U S A* 114, E9308-E9317.

Konno, D., Shioi, G., Shitamukai, A., Mori, A., Kiyonari, H., Miyata, T., and Matsuzaki, F. (2008). Neuroepithelial progenitors undergo LGN-dependent planar divisions to maintain self-renewability during mammalian neurogenesis. *Nat Cell Biol* 10, 93-101.

Labonte, D., Thies, E., and Kneussel, M. (2014). The kinesin KIF21B participates in the cell surface delivery of gamma2 subunit-containing GABAA receptors. *Eur J Cell Biol* 93, 338-346.

Lasser, M., Tiber, J., and Lowery, L.A. (2018). The Role of the Microtubule Cytoskeleton in Neurodevelopmental Disorders. *Front Cell Neurosci* 12, 165.

Levet, F., Hosy, E., Kechkar, A., Butler, C., Beghin, A., Choquet, D., and Sibarita, J.B. (2015). SR-Tesseler: a method to segment and quantify localization-based super-resolution microscopy data. *Nat Methods* 12, 1065-1071.

Li, S., Leshchyns'ka, I., Chernyshova, Y., Schachner, M., and Sytnyk, V. (2013). The neural cell adhesion molecule (NCAM) associates with and signals through p21-activated kinase 1 (Pak1). *J Neurosci* 33, 790-803.

Li, W., Cheng, T., Dong, X., Chen, H., Yang, L., Qiu, Z., and Zhou, W. (2022). KIF5C deficiency causes abnormal cortical neuronal migration, dendritic branching, and spine morphology in mice. *Pediatr Res* 92, 995-1002.

Liaci, C., Camera, M., Caslini, G., Rando, S., Contino, S., Romano, V., and Merlo, G.R. (2021). Neuronal Cytoskeleton in Intellectual Disability: From Systems Biology and Modeling to Therapeutic Opportunities. *Int J Mol Sci* 22.

Lian, G., and Sheen, V.L. (2015). Cytoskeletal proteins in cortical development and disease: actin associated proteins in periventricular heterotopia. *Front Cell Neurosci* 9, 99.

LoTurco, J.J., and Bai, J. (2006). The multipolar stage and disruptions in neuronal migration. *Trends Neurosci* 29, 407-413.

Marszalek, J.R., Weiner, J.A., Farlow, S.J., Chun, J., and Goldstein, L.S. (1999). Novel dendritic kinesin sorting identified by different process targeting of two related kinesins: KIF21A and KIF21B. *J Cell Biol* 145, 469-479.

Martinez-Garay, I., Gil-Sanz, C., Franco, S.J., Espinosa, A., Molnar, Z., and Mueller, U. (2016). Cadherin 2/4 signaling via PTP1B and catenins is crucial for nucleokinesis during radial neuronal migration in the neocortex. *Development* 143, 2121-2134.

Masucci, E.M., Relich, P.K., Lakadamyali, M., Ostap, E.M., and Holzbaur, E.L.F. (2022). Microtubule dynamics influence the retrograde biased motility of kinesin-4 motor teams in neuronal dendrites. *Mol Biol Cell* 33, ar52.

Matsuda, T., and Cepko, C.L. (2007). Controlled expression of transgenes introduced by in vivo electroporation. *Proc Natl Acad Sci U S A* 104, 1027-1032.

Molyneaux, B.J., Arlotta, P., Menezes, J.R., and Macklis, J.D. (2007). Neuronal subtype specification in the cerebral cortex. *Nature reviews Neuroscience* 8, 427-437.

Moon, H.M., and Wynshaw-Boris, A. (2013). Cytoskeleton in action: lissencephaly, a neuronal migration disorder. *Wiley Interdiscip Rev Dev Biol* 2, 229-245.

Morikawa, M., Tanaka, Y., Cho, H.S., Yoshihara, M., and Hirokawa, N. (2018). The Molecular Motor KIF21B Mediates Synaptic Plasticity and Fear Extinction by Terminating Rac1 Activation. *Cell Rep* 23, 3864-3877.

Muhia, M., Thies, E., Labonte, D., Ghiretti, A.E., Gromova, K.V., Xompero, F., Lappe-Siefke, C., Hermans-Borgmeyer, I., Kuhl, D., Schweizer, M., *et al.* (2016). The Kinesin KIF21B Regulates Microtubule Dynamics and Is Essential for Neuronal Morphology, Synapse Function, and Learning and Memory. *Cell Rep* 15, 968-977.

Muralidharan, H., Guha, S., Madugula, K., Patil, A., Bennison, S.A., Sun, X., Toyo-Oka, K., and Baas, P.W. (2022). KIFC1 Regulates the Trajectory of Neuronal Migration. *J Neurosci* 42, 2149-2165.

Nadarajah, B., Brunstrom, J.E., Grutzendler, J., Wong, R.O., and Pearlman, A.L. (2001). Two modes of radial migration in early development of the cerebral cortex. *Nature neuroscience* 4, 143-150.

Narayanan, D.L., Rivera Alvarez, J., Tilly, P., do Rosario, M.C., Bhat, V., Godin, J.D., and Shukla, A. (2022). Further delineation of KIF21B-related neurodevelopmental disorders. *J Hum Genet*.

Nishimura, Y.V., Nabeshima, Y.I., and Kawauchi, T. (2017). Morphological and Molecular Basis of Cytoplasmic Dilation and Swelling in Cortical Migrating Neurons. *Brain Sci* 7.

Noctor, S.C., Martinez-Cerdeno, V., Ivic, L., and Kriegstein, A.R. (2004). Cortical neurons arise in symmetric and asymmetric division zones and migrate through specific phases. *Nat Neurosci* 7, 136-144.

Ohtaka-Maruyama, C., Okamoto, M., Endo, K., Oshima, M., Kaneko, N., Yura, K., Okado, H., Miyata, T., and Maeda, N. (2018). Synaptic transmission from subplate neurons controls radial migration of neocortical neurons. *Science* 360, 313-317.

Ovesny, M., Krizek, P., Borkovec, J., Svindrych, Z., and Hagen, G.M. (2014). ThunderSTORM: a comprehensive ImageJ plug-in for PALM and STORM data analysis and super-resolution imaging. *Bioinformatics* 30, 2389-2390.

Preuss, M.L., Kovar, D.R., Lee, Y.R., Staiger, C.J., Delmer, D.P., and Liu, B. (2004). A plant-specific kinesin binds to actin microfilaments and interacts with cortical microtubules in cotton fibers. *Plant Physiol* 136, 3945-3955.

Qian, X., DeGennaro, E.M., Talukdar, M., Akula, S.K., Lai, A., Shao, D.D., Gonzalez, D., Marciano, J.H., Smith, R.S., Hylton, N.K., *et al.* (2022). Loss of non-motor kinesin KIF26A causes congenital

brain malformations via dysregulated neuronal migration and axonal growth as well as apoptosis. *Dev Cell* 57, 2381-2396 e2313.

Rash, B.G., and Grove, E.A. (2006). Area and layer patterning in the developing cerebral cortex. *Curr Opin Neurobiol* 16, 25-34.

Riedl, J., Crevenna, A.H., Kessenbrock, K., Yu, J.H., Neukirchen, D., Bista, M., Bradke, F., Jenne, D., Holak, T.A., Werb, Z., *et al.* (2008). Lifeact: a versatile marker to visualize F-actin. *Nat Methods* 5, 605-607.

Sakakibara, A., Ando, R., Sapir, T., and Tanaka, T. (2013). Microtubule dynamics in neuronal morphogenesis. *Open Biol* 3, 130061.

Sapir, T., Levy, T., Sakakibara, A., Rabinkov, A., Miyata, T., and Reiner, O. (2013). Shootin1 acts in concert with KIF20B to promote polarization of migrating neurons. *J Neurosci* 33, 11932-11948.

Schaar, B.T., and McConnell, S.K. (2005). Cytoskeletal coordination during neuronal migration. *Proc Natl Acad Sci U S A* 102, 13652-13657.

Schelski, M., and Bradke, F. (2022). Microtubule retrograde flow retains neuronal polarization in a fluctuating state. *Sci Adv* 8, eabo2336.

Skarnes, W.C., Rosen, B., West, A.P., Koutsourakis, M., Bushell, W., Iyer, V., Mujica, A.O., Thomas, M., Harrow, J., Cox, T., *et al.* (2011). A conditional knockout resource for the genome-wide study of mouse gene function. *Nature* 474, 337-342.

Solecki, D.J., Trivedi, N., Govek, E.E., Kerekes, R.A., Gleason, S.S., and Hatten, M.E. (2009). Myosin II motors and F-actin dynamics drive the coordinated movement of the centrosome and soma during CNS glial-guided neuronal migration. *Neuron* 63, 63-80.

Stenman, J., Toresson, H., and Campbell, K. (2003). Identification of two distinct progenitor populations in the lateral ganglionic eminence: implications for striatal and olfactory bulb neurogenesis. *J Neurosci* 23, 167-174.

Stouffer, M.A., Golden, J.A., and Francis, F. (2016). Neuronal migration disorders: Focus on the cytoskeleton and epilepsy. *Neurobiol Dis* 92, 18-45.

Swarnkar, S., Avchalumov, Y., Raveendra, B.L., Grinman, E., and Puthanveetil, S.V. (2018). Kinesin Family of Proteins Kif11 and Kif21B Act as Inhibitory Constraints of Excitatory Synaptic Transmission Through Distinct Mechanisms. *Sci Rep* 8, 17419.

Tabata, H., and Nakajima, K. (2003). Multipolar migration: the third mode of radial neuronal migration in the developing cerebral cortex. *J Neurosci* 23, 9996-10001.

Taguchi, S., Nakano, J., Imasaki, T., Kita, T., Saijo-Hamano, Y., Sakai, N., Shigematsu, H., Okuma, H., Shimizu, T., Nitta, E., *et al.* (2022). Structural model of microtubule dynamics inhibition by kinesin-4 from the crystal structure of KLP-12 -tubulin complex. *Elife* 11.

Tanaka, T., Serneo, F.F., Higgins, C., Gambello, M.J., Wynshaw-Boris, A., and Gleeson, J.G. (2004a). Lis1 and doublecortin function with dynein to mediate coupling of the nucleus to the centrosome in neuronal migration. *J Cell Biol* 165, 709-721.

Tanaka, T., Serneo, F.F., Tseng, H.C., Kulkarni, A.B., Tsai, L.H., and Gleeson, J.G. (2004b). Cdk5 phosphorylation of doublecortin ser297 regulates its effect on neuronal migration. *Neuron* 41, 215-227.

Tielens, S., Godin, J.D., and Nguyen, L. (2016). Real-time Recordings of Migrating Cortical Neurons from GFP and Cre Recombinase Expressing Mice. *Curr Protoc Neurosci* 74, 3 29 21-23 29 23.

Tsai, J.W., Bremner, K.H., and Vallee, R.B. (2007). Dual subcellular roles for LIS1 and dynein in radial neuronal migration in live brain tissue. *Nat Neurosci* 10, 970-979.

Tyanova, S., Temu, T., Sinitcyn, P., Carlson, A., Hein, M.Y., Geiger, T., Mann, M., and Cox, J. (2016). The Perseus computational platform for comprehensive analysis of (prote)omics data. *Nat Methods* 13, 731-740.

van Riel, W.E., Rai, A., Bianchi, S., Katrukha, E.A., Liu, Q., Heck, A.J., Hoogenraad, C.C., Steinmetz, M.O., Kapitein, L.C., and Akhmanova, A. (2017). Kinesin-4 KIF21B is a potent microtubule pausing factor. *Elife* 6.

Witte, H., Neukirchen, D., and Bradke, F. (2008). Microtubule stabilization specifies initial neuronal polarization. *J Cell Biol* 180, 619-632.

Wonders, C.P., and Anderson, S.A. (2006). The origin and specification of cortical interneurons. *Nature reviews Neuroscience* 7, 687-696.

Wu, Q., Liu, J., Fang, A., Li, R., Bai, Y., Kriegstein, A.R., and Wang, X. (2014). The dynamics of neuronal migration. *Adv Exp Med Biol* 800, 25-36.

Xu, T., Langouras, C., Koudehi, M.A., Vos, B.E., Wang, N., Koenderink, G.H., Huang, X., and Vavylonis, D. (2019). Automated Tracking of Biopolymer Growth and Network Deformation with TSOAX. *Sci Rep* 9, 1717.

Yu, H.L., Peng, Y., Zhao, Y., Lan, Y.S., Wang, B., Zhao, L., Sun, D., Pan, J.X., Dong, Z.Q., Mei, L., *et al.* (2020). Myosin X Interaction with KIF13B, a Crucial Pathway for Netrin-1-Induced Axonal Development. *J Neurosci* 40, 9169-9185.

Figure 1

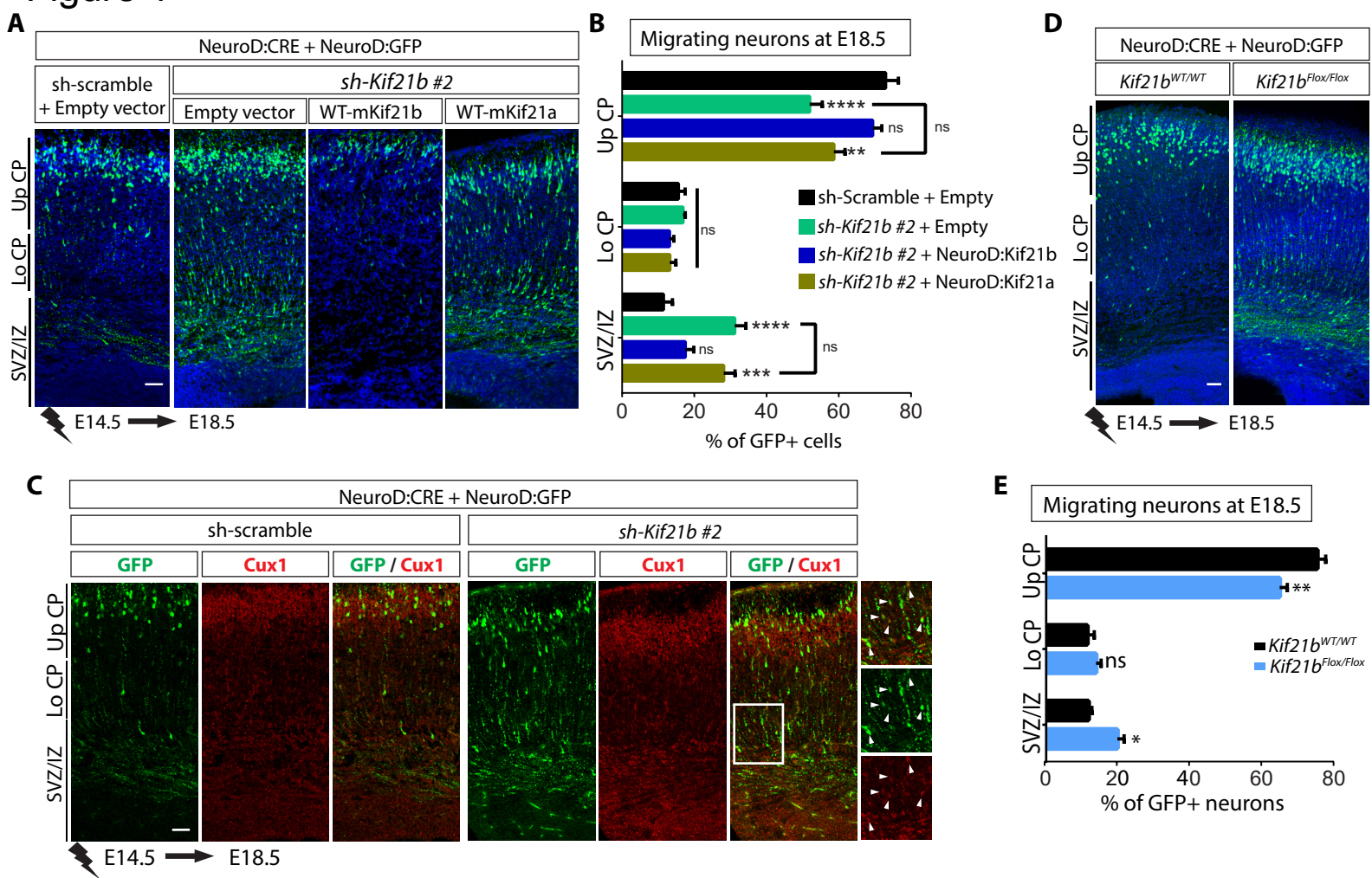


Figure 2

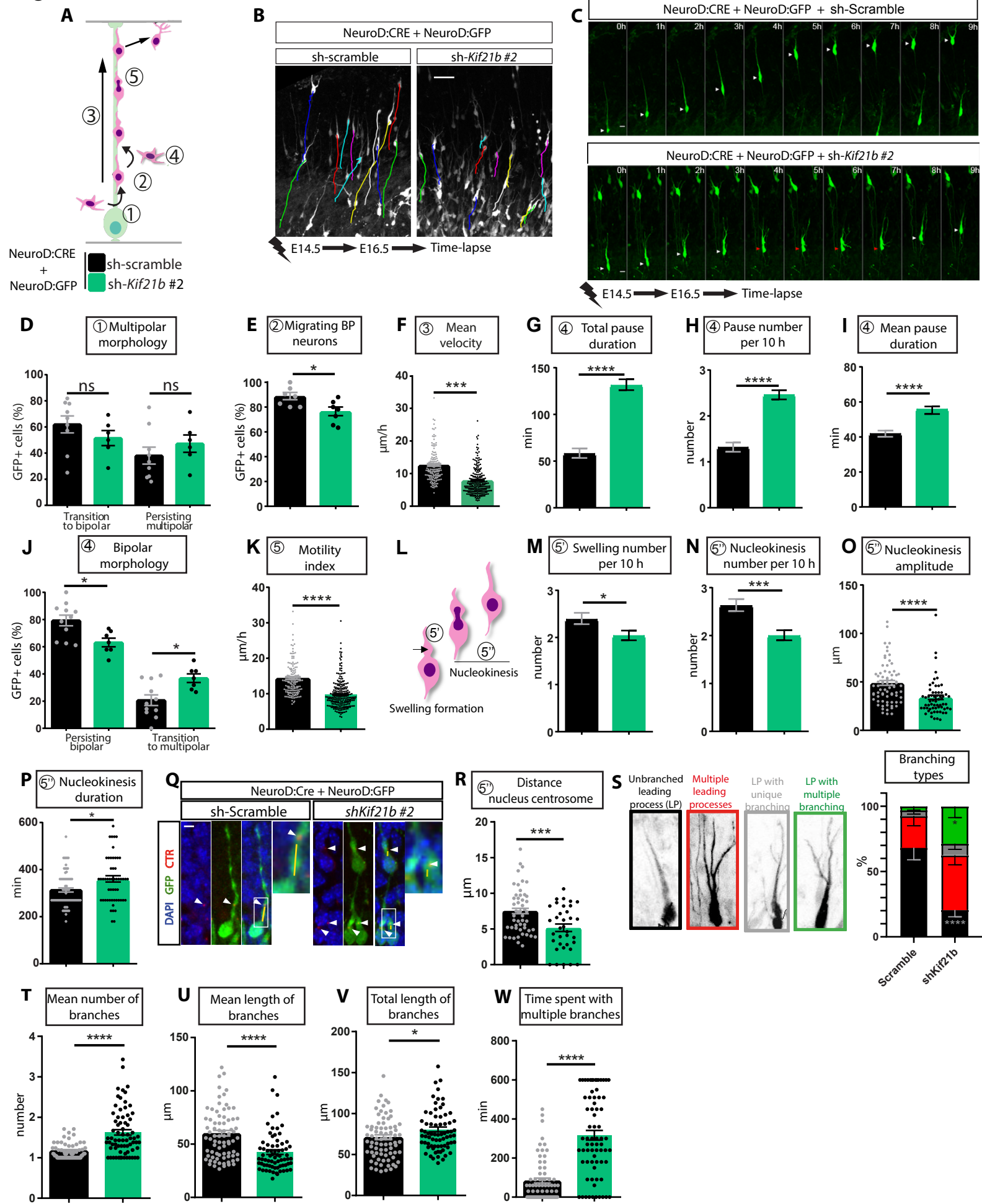


Figure 3

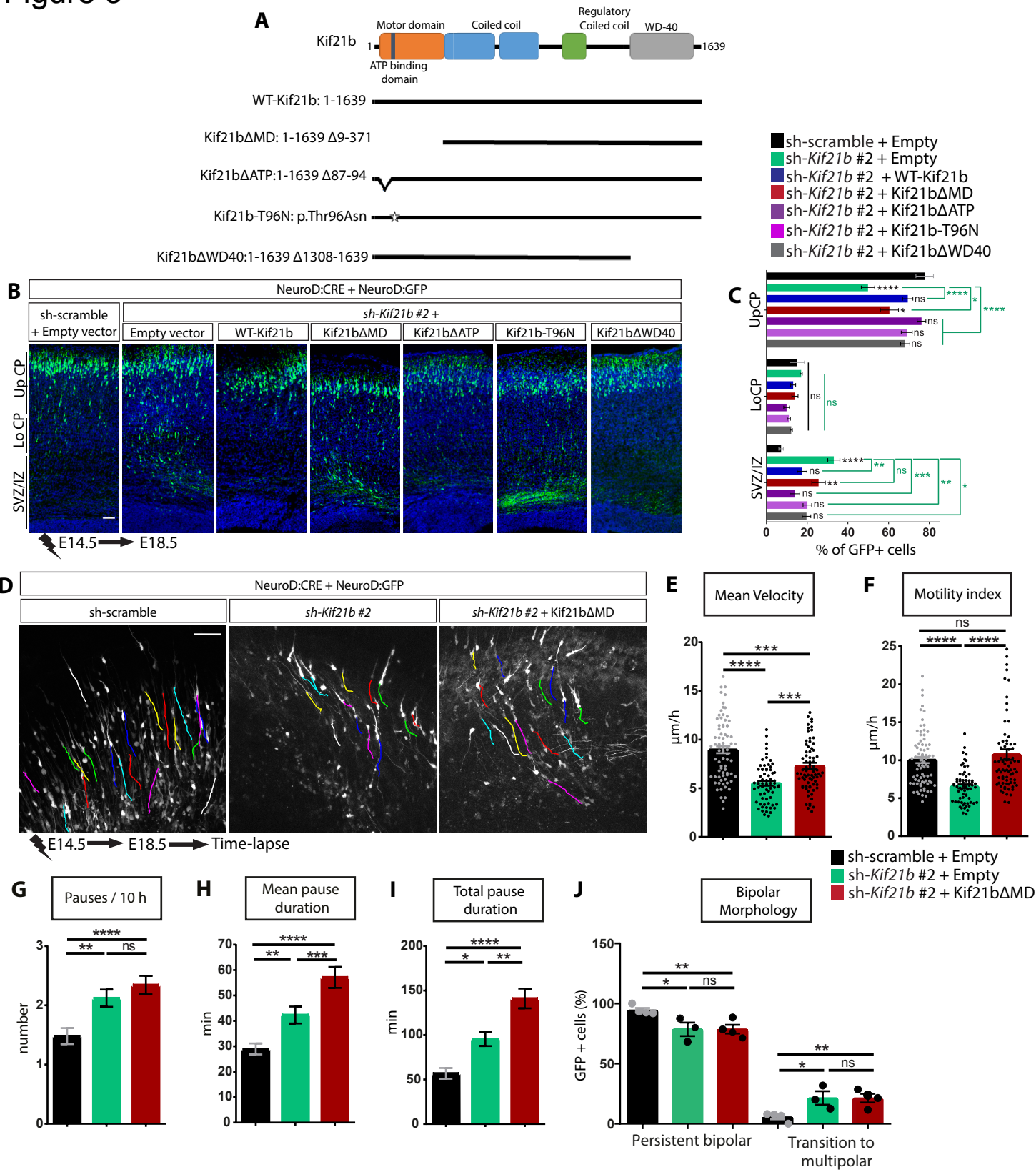


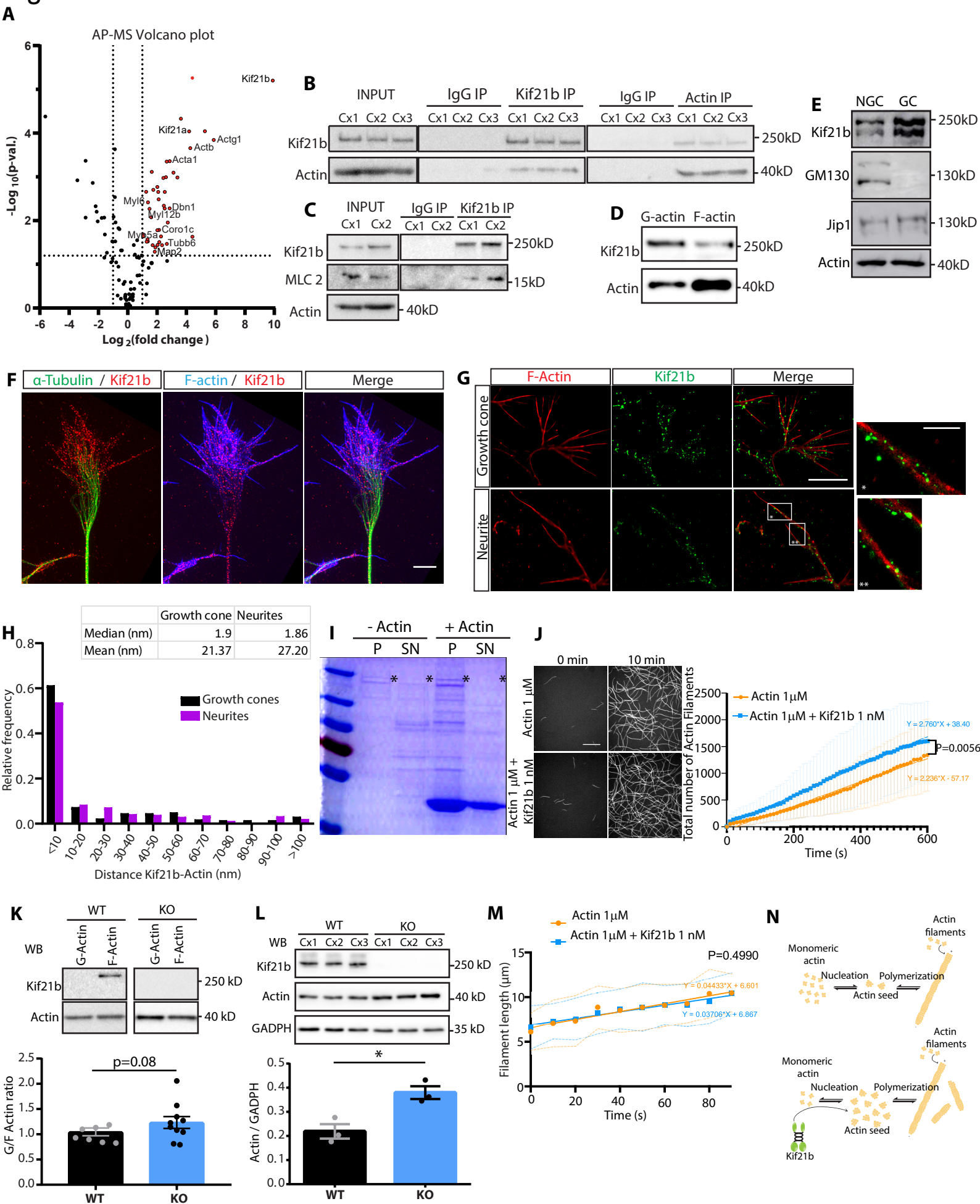
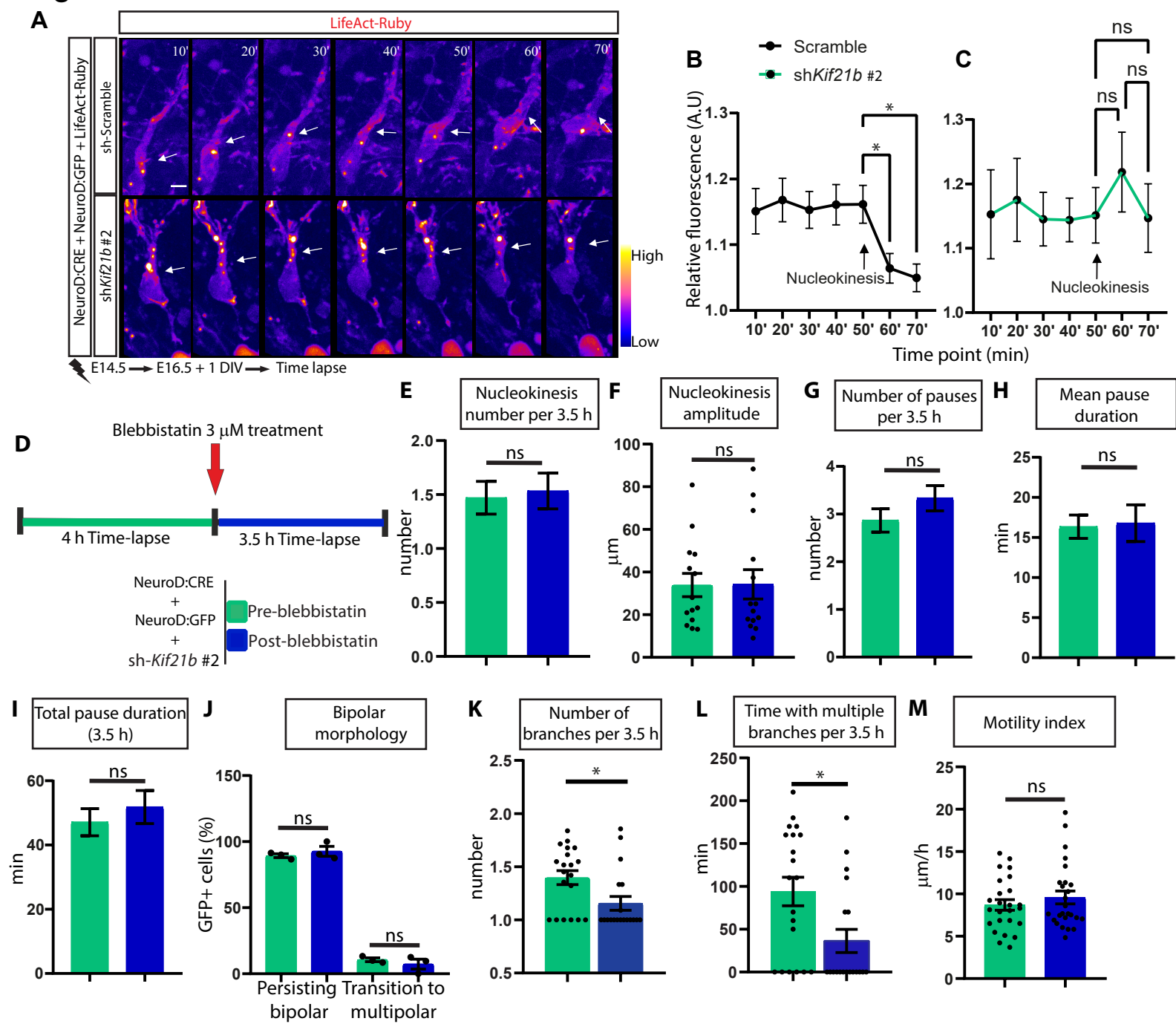
Figure 4

Figure 5



Supplementary Information

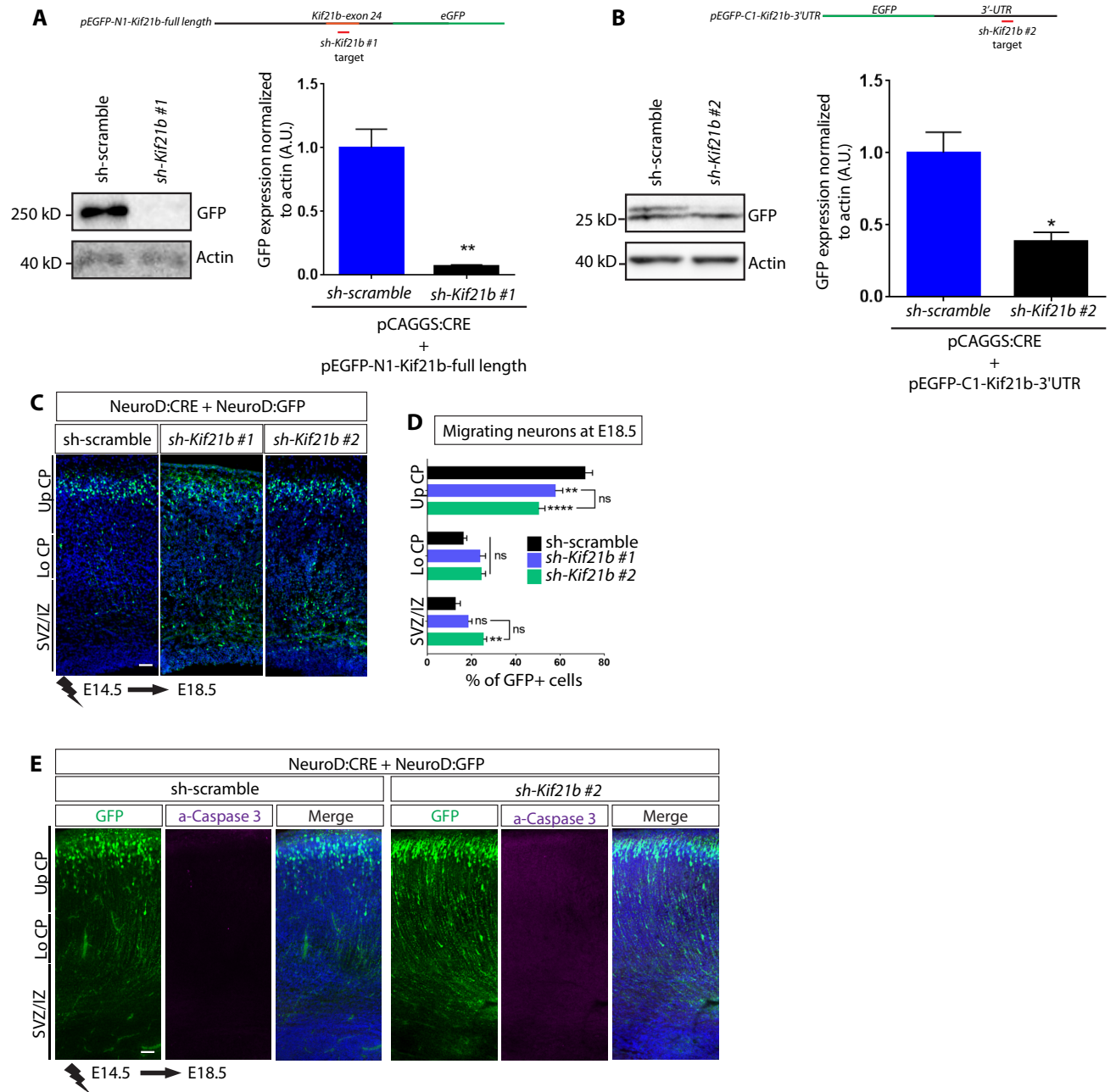
The kinesin Kif21b regulates radial migration of cortical projection neurons through a non-canonical function on actin cytoskeleton.

Rivera Alvarez *et al*

Content:

- **Figure S1:** Depletion of *Kif21b* in projection neurons impairs migration, related to Figure 1.
- **Figure S2:** *Kif21b* depletion induces defects in tangential migration of interneurons, related to Figure 1.
- **Figure S3:** Overexpression of Kif21b-truncated constructs does not alter radial migration, related to Figure 3.
- **Figure S4:** Kif21b interacts with actin and actin binding proteins and regulate actin dynamics, related to Figure 4.

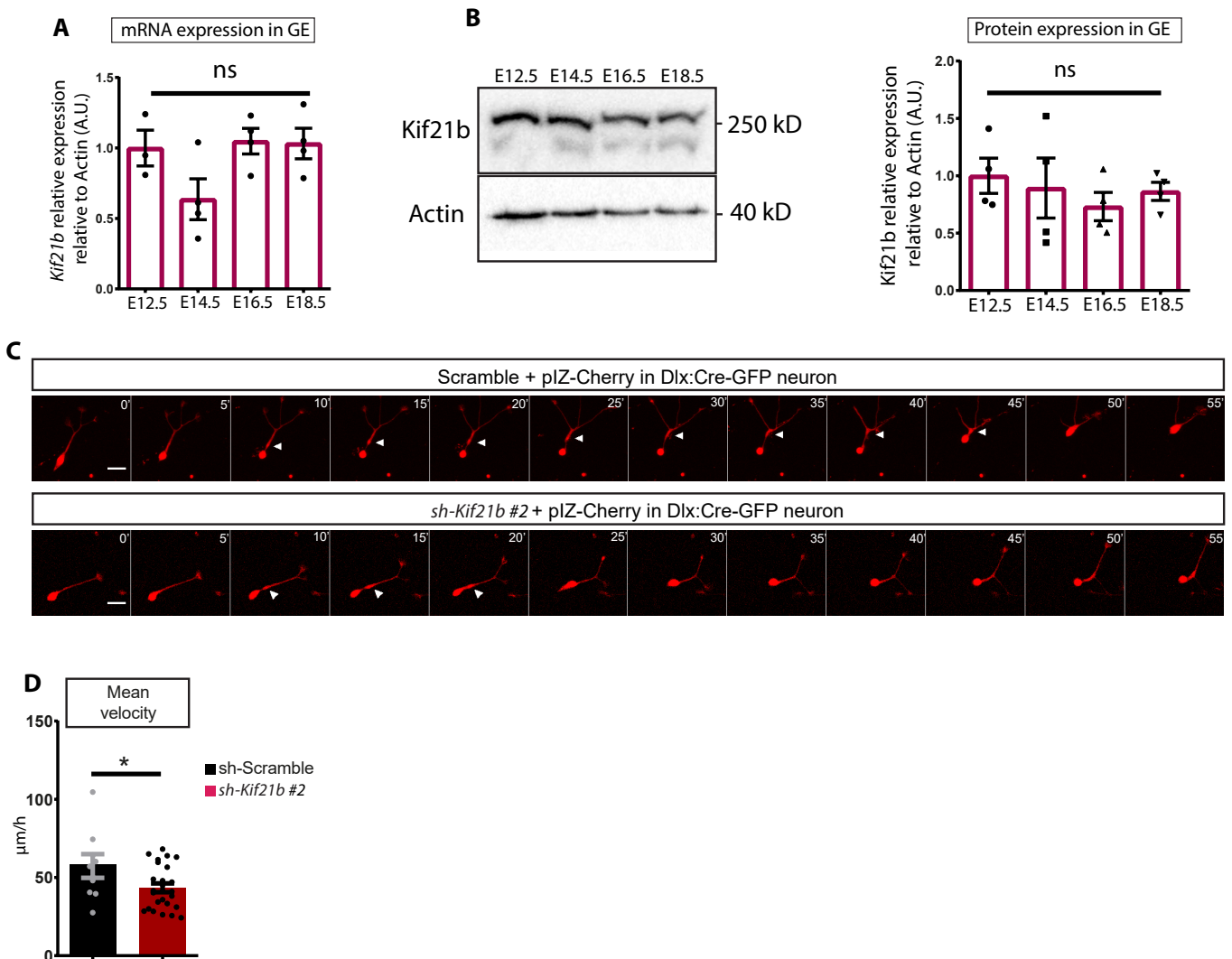
Figure S1: Depletion of *Kif21b* in projection neurons impairs migration, related to Figure 1.



(A,B) Western blots of extracts HEK293T cells transfected with the indicated constructs showing the efficiency of the shRNA-Kif21b #1 directed against the coding exon 24 (A) and shRNA-Kif21b #2 targeting the 3'UTR (B). Data (means \pm s.e.m) from 3 independent experiments were analyzed by unpaired two-tailed Student t-test, $**P < 0.005$. (C) Coronal sections of E18.5 cortices electroporated with NeuroD:Cre and NeuroD:IRES-GFP together with Cre inducible shRNA *Kif21b* #1, *Kif21b* #2 or sh-scramble showing similar migration defects using two different shRNA sequences. D Quantification (means \pm s.e.m.) of the distribution of GFP-positive neurons in different regions (Up CP, Upper cortical plate; Lo CP, Lower cortical plate; SVZ/ IZ, subventricular zone / intermediate zone) in all the indicated conditions. Significance was calculated by two-way ANOVA, Bonferroni's multiple comparisons test. ns,

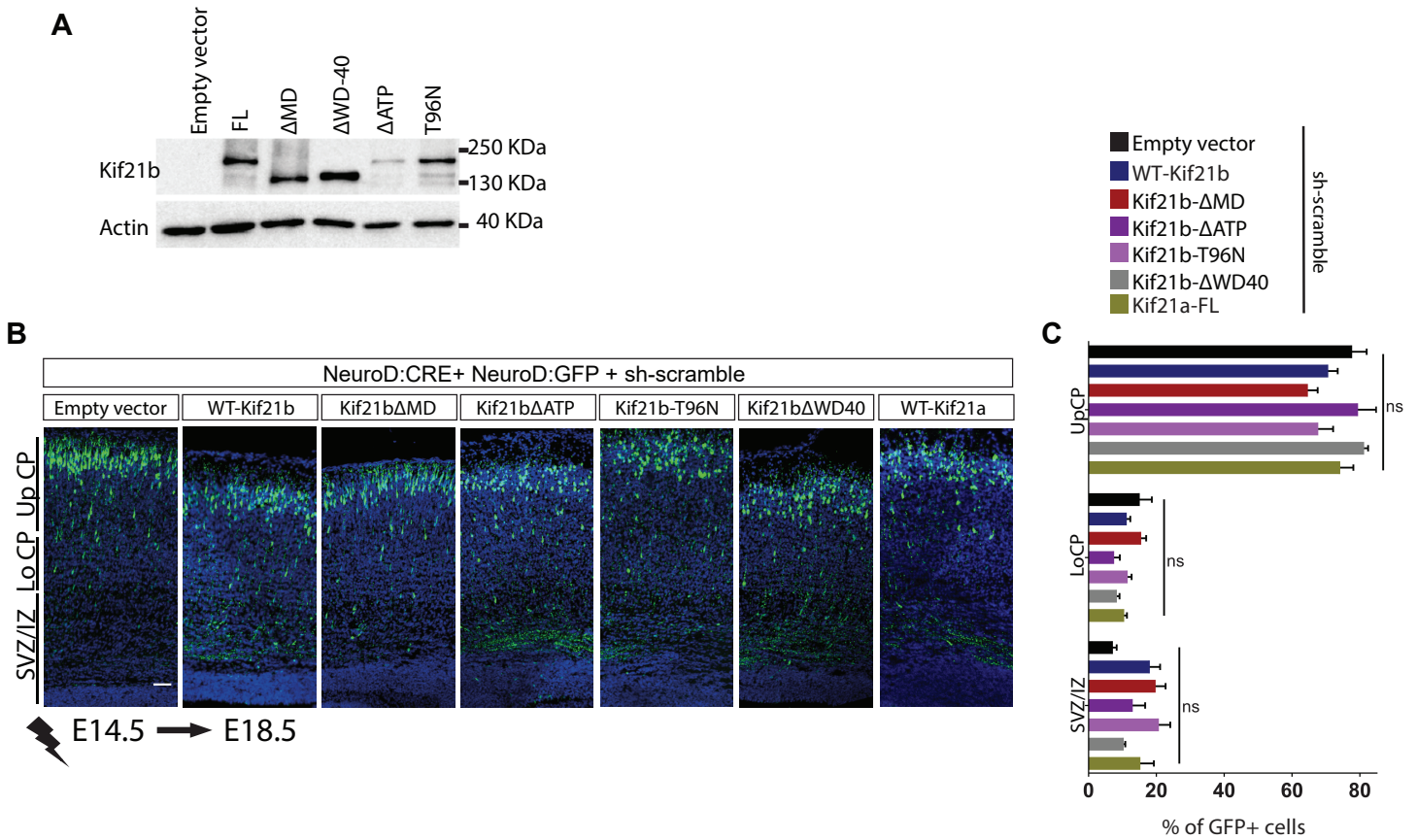
non-significant; ** $P < 0.005$; **** $P < 0.0001$. Number of embryos analyzed: sh-scramble, $n=7$; sh-*Kif21b* #1, $n=8$; sh-*Kif21b* #2, $n=9$. **(E)** Immunolabelling of activated caspase 3 (a-caspase 3, in purple) in E18.5 mouse cortices electroporated at E14.5 with NeuroD:Cre, NeuroD:IRES-GFP and either Cre inducible sh*Kif21b* #2 or sh-scramble. GFP-positive electroporated cells are depicted in green. Nuclei are stained with DAPI. Scale bars: **(C,E)** 50 μm .

Figure S2. *Kif21b* depletion induces defects in tangential migration of interneurons, related to Figure 1.



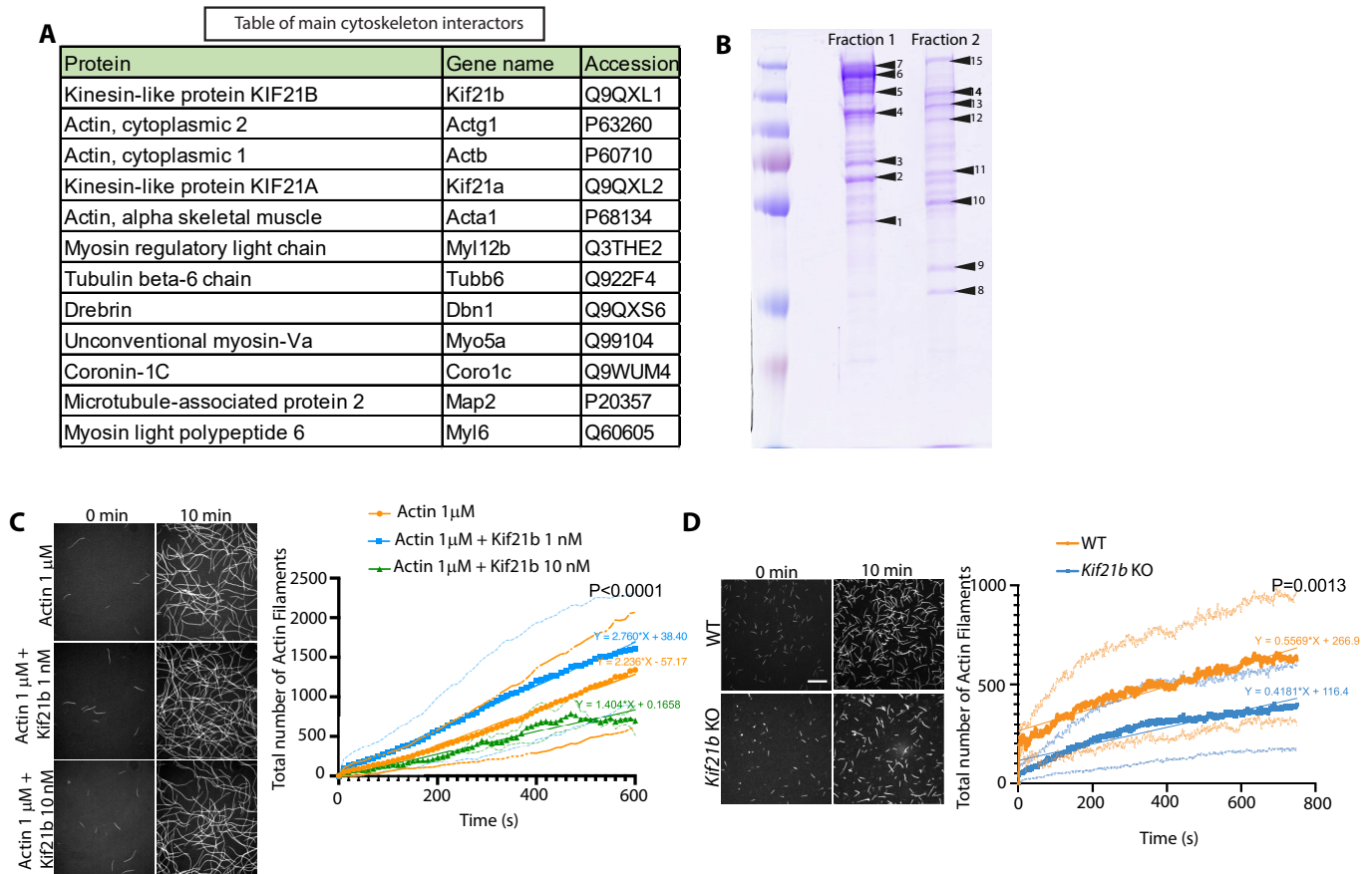
(A,B) RT-qPCR (n=4 brains per stage) (A) and Western blot (n=3 brains per stage) (B) analyses indicating expression of *Kif21b* transcripts and Kif21b proteins in mouse ganglionic eminences (GE) at different embryonic stages (from E12.5 to E18.5) (n=4 brains per stage). Data are represented as means \pm s.e.m. Significance was calculated by one-way ANOVA, Bonferroni's multiple comparisons test, ns, non-significant. (C) Time-lapse sequence (min) showing the migration of interneurons out of MGE explants cultured from Dlx5,6 Cre-GFP E13.5 embryos, electroporated with a Cre-inducible cherry expressing plasmid together with Cre-inducible shRNA-*Kif21b* #2 or sh-scramble. Scale bar: 20 μ m. (D) Quantification (means \pm s.e.m.) of the mean velocity (μ m/h) showing defects in tangential migration of *Kif21b*-depleted interneurons. Number of cells analyzed: scramble=9, sh-*Kif21b* #2= 25, from at least three embryos per condition in two independent experiments. Significance was calculated by unpaired two-tailed Student t-test, ns, non-significant; *P < 0.05.

Figure S3. Overexpression of Kif21b-truncated constructs does not alter radial migration, related to Figure 3.



(A) Western blot of N2A cells transfected with the indicated full length (FL) or truncated Kif21b constructs expressed under the NeuroD promoter. Actin was used as a loading control. (B) Coronal sections of E18.5 mouse cortices electroporated at E14.5 with NeuroD:Cre and NeuroD:GFP together with sh-scramble and the different NeuroD:Kif21b constructs. GFP-positive electroporated cells are depicted in green. Nuclei are stained with DAPI. Scale bars, 50 μ m. (C) Analysis (means \pm s.e.m.) of the distribution of GFP-positive neurons in different regions (Up CP, Upper cortical plate; Lo CP, Lower cortical plate; SVZ / IZ, subventricular zone / intermediate zone) in all conditions as indicated. Number of embryos analyzed per condition: $n \geq 3$ for all conditions. Significance was calculated by two-way ANOVA, Bonferroni's multiple comparisons test. ns, non-significant; * $P < 0.05$.

Figure S4. Kif21b interacts with actin and actin binding proteins and regulate actin dynamics, related to Figure 4.



(A) List of cytoskeleton related partners found in the mass spectrometry analysis among the proteins that significantly interact with Kif21b in E18.5 cortices (see Table S1). **(B)** Isolated fractions of the recombinant Kif21b produced in BHK cells. The bands analyzed for contaminants are shown in arrowheads (see Table S2). **(C)** Representative spinning-disk images of *in vitro* analysis of actin nucleation (stained with phalloidin) at the beginning (0 min) and at the end (10 min) of the experiment in presence or absence of recombinant Kif21b (1 nM or 10 nM). Scale bar 10 μ m. The graph shows the number of actin filaments assembled during a 600 s time-lapse. Number of replicates: Actin 1 μ M, n=7; Actin 1 μ M + Kif21b 1 nM, n=6; Actin 1 μ M + Kif 10 nM, n=2. **(D)** *In vitro* analysis of nucleation of phalloidin-labeled actin from protein extracts of WT or *Kif21b*^{flox/flox} (KO) mouse cortices by spinning-disk microscopy. Scale bar: 10 μ m. The graph shows the number of actin filaments assembled during a 600 s time-lapse. Three independent experiments were performed for both (WT and KO) conditions.

Kif21B immunoprecipitation from E18 mosue cortices followed by MS analysis
Table S1 shows all proteins that significantly bind to Kif21b

Significant	-LOG(P-Value)	Difference log2	Ratio Kif21b/IgG IP	Accession	Description	Gene Name
+	5.201081732	9.896453698	953.0801268	Q9QXL1	Kinesin-like protein KIF21B OS=Mus musculus OX=10090	Kif21b
+	3.842576609	5.873169263	58.61383235	P63260	Actin, cytoplasmic 2 OS=Mus musculus OX=10090	Actg1
+	4.040823499	5.264113824	38.42874145	Q8BMF4	Dihydrolipoyllysine-residue acetyltransferase component of pyruvate dehydrogenase complex, mitochondrial OS=Mus musculus OX=10090	Dlat
+	5.258677389	4.411539078	21.28166436	P35486	Pyruvate dehydrogenase E1 component subunit alpha, somatic form, mitochondrial OS=Mus musculus OX=10090	Pdha1
+	1.631148563	4.41139404	21.27952496	Q9D051	Pyruvate dehydrogenase E1 component subunit beta, mitochondrial OS=Mus musculus OX=10090	Pdhb
+	3.654787735	4.273177465	19.33546379	P60710	Actin, cytoplasmic 1 OS=Mus musculus OX=10090	Actb
+	4.038869384	4.189676523	18.24812745	Q9QXL2	Kinesin-like protein KIF21A OS=Mus musculus OX=10090	Kif21a
+	4.328392954	3.633562406	12.41112859	P68254	14-3-3 protein theta OS=Mus musculus OX=10090	Ywhaq
+	2.986370781	3.393778721	10.51064079	Q8BKZ9	Pyruvate dehydrogenase protein X component, mitochondrial OS=Mus musculus OX=10090	Pdhx
+	3.096201855	3.124877135	8.723318921	P43274	Histone H1.4 OS=Mus musculus OX=10090	H1-4
+	3.35621997	2.864079793	7.280713267	P68134	Actin, alpha skeletal muscle OS=Mus musculus OX=10090	Acta1
+	2.280188105	2.861485084	7.267630559	Q3THE2	Myosin regulatory light chain 12B OS=Mus musculus OX=10090	Myf12b
+	1.954781231	2.733517011	6.65074986	Q3THG9	Alanyl-tRNA editing protein Aarsd1 OS=Mus musculus OX=10090	Aarsd1
+	1.465829263	2.667647441	6.353922271	Q922F4	Tubulin beta-6 chain OS=Mus musculus OX=10090	Tubb6
+	3.34985602	2.659040769	6.316129578	P62259	14-3-3 protein epsilon OS=Mus musculus OX=10090	Ywhae
+	2.990141488	2.609062513	6.10107097	P62264	40S ribosomal protein S14 OS=Mus musculus OX=10090	Rps14
+	2.654186205	2.525267363	5.756801081	Q8CFE4	SCY1-like protein 2 OS=Mus musculus OX=10090	Scyl2
+	2.275610939	2.522186915	5.744522253	Q9QXS6	Drebrin OS=Mus musculus OX=10090	Dbrn1
+	2.339658875	2.46794645	5.532557154	Q9QZ05	eIF-2-alpha kinase GCN2 OS=Mus musculus OX=10090	Eif2ak4
+	2.97214246	2.428147872	5.382020448	Q60972	Histone-binding protein RBBP4 OS=Mus musculus OX=10090	Rbbp4
+	1.438174465	2.344104687	5.07745197	P62754	40S ribosomal protein S6 OS=Mus musculus OX=10090	Rps6
+	1.637086445	2.2667497	4.812377109	Q99104	Unconventional myosin-Va OS=Mus musculus OX=10090	Myo5a
+	1.508706383	2.152390877	4.445639233	P62900	60S ribosomal protein L31 OS=Mus musculus OX=10090	Rpl31
+	1.785975275	2.141403437	4.411910231	Q9WUM4	Coronin-1C OS=Mus musculus OX=10090	Coro1c
+	2.485762976	2.113821348	4.328362553	Q9CQV8	14-3-3 protein beta/alpha OS=Mus musculus OX=10090	Ywhab
+	2.653818558	2.0802176	4.228709925	Q6PDM2	Serine/arginine-rich splicing factor 1 OS=Mus musculus OX=10090	Srsf1
+	1.442247223	2.044054111	4.124027951	Q6NVF9	Cleavage and polyadenylation specificity factor subunit 6 OS=Mus musculus OX=10090	Cpsf6
+	2.766694236	2.025529861	4.07141381	P61982	14-3-3 protein gamma OS=Mus musculus OX=10090	Ywhag
+	1.780567816	2.02542909	4.071129434	Q9CXW4	60S ribosomal protein L11 OS=Mus musculus OX=10090	Rpl11
+	1.385440791	1.885291735	3.694276207	P20357	Microtubule-associated protein 2 OS=Mus musculus OX=10090	Map2
+	2.701464285	1.748967489	3.361179263	P63101	14-3-3 protein zeta/delta OS=Mus musculus OX=10090	Ywhaz
+	1.437686569	1.700069269	3.249165585	P29341	Polyadenylate-binding protein 1 OS=Mus musculus OX=10090	Pabpc1
+	3.112898904	1.641625404	3.120171663	P0DP27	Calmodulin-2 OS=Mus musculus OX=10090	Calm2
+	2.074411582	1.600621541	3.032739415	P63276	40S ribosomal protein S17 OS=Mus musculus OX=10090	Rps17
+	2.26630776	1.489894867	2.808685068	P42932	T-complex protein 1 subunit theta OS=Mus musculus OX=10090	Cct8
+	2.415489381	1.378574371	2.600113086	Q60605	Myosin light polypeptide 6 OS=Mus musculus OX=10090	Myf6
+	1.521837694	1.375297546	2.594214094	P14869	60S acidic ribosomal protein P0 OS=Mus musculus OX=10090	Rplp0
+	1.568535198	1.344968478	2.540246461	P43277	Histone H1.3 OS=Mus musculus OX=10090	H1-3
+	1.518035557	1.288894653	2.443407777	P01027	Complement C3 OS=Mus musculus OX=10090	C3
+	2.658792602	1.253885587	2.384828608	P63017	Heat shock cognate 71 kDa protein OS=Mus musculus OX=10090	Hspa8
+	1.684900849	1.047639529	2.067144912	P61979	Heterogeneous nuclear ribonucleoprotein K OS=Mus musculus OX=10090	Hnnpk
+	1.642668012	1.040415128	2.056819407	P19001	Keratin, type I cytoskeletal 19 OS=Mus musculus OX=10090	Krt19

Masss spectrometry analysis of the fraction 1 presented in Supplementary Figure S4B - sample number below correspond to the number of the analysed band in the fraction (see arrowheads in Figure S4B)

Sample 1

Accession	Description	Coverage	# Peptides	# PSMs	# Unique f	# AAs	MW [kDa]	calc. pl	Score	SeqL	# Peptides Found in S	# Protein Groups
AOA061I0W0	Non-POU domain-containing octamer-binding protein OS=Cricetulus griseus OX=10029 GN=H671_xg20122 PE=4 SV=1	14	11	37	11	686	77.8	5.24	107.58		11 High	1
G3HG95	Lamin-A/C OS=Cricetulus griseus OX=10029 GN=I79_009616 PE=3 SV=1	26	16	26	16	563	64	8.02	81.7		16 High	1
G3I088	Homer protein-like 1 OS=Cricetulus griseus OX=10029 GN=I79_016765 PE=3 SV=1	39	14	18	13	366	41.3	5.53	52.05		14 High	1
AOA3L7HIJW1	KIF21B OS=Cricetulus griseus OX=10029 GN=CgPICR_000914 PE=3 SV=1	7	10	11	10	1722	191.6	7.78	35.72		10 High	1
G3I7M2	Elongation factor Tu OS=Cricetulus griseus OX=10029 GN=H671_3g10221 PE=3 SV=1	14	7	10	7	452	49.5	7.78	26.07		7 High	1
AOA3L7I839	SFPQ OS=Cricetulus griseus OX=10029 GN=CgPICR_007108 PE=4 SV=1	10	4	7	2	474	53.8	7.94	20.94		4 High	1
G3HDG6	Paraspeckle component 1 OS=Cricetulus griseus OX=10029 GN=I79_008512 PE=3 SV=1	11	6	6	6	522	58.6	6.67	15.95		6 High	1
Q60455	Tubulin beta chain OS=Cricetulus griseus OX=10029 PE=2 SV=1	10	4	6	1	444	49.7	4.89	18.14		4 High	1
G3HQP8	Tubulin beta chain OS=Cricetulus griseus OX=10029 GN=CgPICR_019487 PE=3 SV=1	10	4	6	1	444	49.6	4.89	18.61		4 High	1
G3H9U3	Splicing factor, proline-and glutamine-rich OS=Cricetulus griseus OX=10029 GN=I79_007174 PE=4 SV=1	13	3	6	1	351	40.2	6.74	19.57		3 High	1
AOA061I6G9	Septin-7 (Fragment) OS=Cricetulus griseus OX=10029 GN=H671_4g12516 PE=3 SV=1	12	5	5	5	515	59.3	8.57	14.66		5 High	1
AOA061I127	Splicing factor 45 OS=Cricetulus griseus OX=10029 GN=H671_3g8664 PE=4 SV=1	17	5	5	5	356	39.4	6.48	15.46		5 High	1
AOA3L7HDW9	DNA topoisomerase 2 OS=Cricetulus griseus OX=10029 GN=CgPICR_018688 PE=3 SV=1	4	5	5	4	1479	167.7	8.38	13.1		5 High	1
AOA3L7HXD2	HOMER2 OS=Cricetulus griseus OX=10029 GN=CgPICR_008567 PE=3 SV=1	7	3	4	2	390	44.4	7.43	11.12		3 High	1
AOA3L7II90	26S proteasome AAA-ATPase subunit RPT1 OS=Cricetulus griseus OX=10029 GN=CgPICR_013869 PE=3 SV=1	6	3	4	3	617	68.2	9.38	11.93		3 High	1
G3H2U6	Splicing factor 3B subunit 4 OS=Cricetulus griseus OX=10029 GN=H671_1g3059 PE=3 SV=1	6	2	3	2	424	44.3	8.56	11.66		2 High	1
AOA3L7HXQ3	SF3B2 OS=Cricetulus griseus OX=10029 GN=CgPICR_009519 PE=4 SV=1	4	3	3	3	853	95.4	5.76	8.48		3 High	1
AOA061I8C5	Ataxin-2-like protein OS=Cricetulus griseus OX=10029 GN=H671_3g10220 PE=3 SV=1	3	3	3	3	1039	110	8.63	8.69		3 High	1
G3IJ29	PITSLRE serine/threonine-protein kinase CDC2L1 OS=Cricetulus griseus OX=10029 GN=I79_024191 PE=4 SV=1	6	3	3	3	529	62.2	5.63	8.6		3 High	1
G3IJF2	Nuclear fragile X mental retardation-interacting protein 2 OS=Cricetulus griseus OX=10029 GN=I79_023986 PE=4 SV=1	7	3	3	3	530	56.6	7.44	8.95		3 High	1
AOA061IM20	Putative homer protein OS=Cricetulus griseus OX=10029 GN=H671_1g1156 PE=3 SV=1	5	2	3	1	359	40	5.29	9.03		2 High	1
AOA3L7ILS4	SEPT11 OS=Cricetulus griseus OX=10029 GN=CgPICR_018977 PE=3 SV=1	6	3	3	3	473	54.4	7.37	7.7		3 High	1

Sample 2

Accession	Description	Coverage	# Peptides	# PSMs	# Unique f	# AAs	MW [kDa]	calc. pl	Score	SeqL	# Peptides Found in S	# Protein Groups
AOA061I0W0	Non-POU domain-containing octamer-binding protein OS=Cricetulus griseus OX=10029 GN=H671_xg20122 PE=4 SV=1	13	10	40	9	686	77.8	5.24	120.74		10 High	1
AOA061IPK2	RNA-splicing ligase RtcB homolog OS=Cricetulus griseus OX=10029 GN=RTCB PE=3 SV=1	23	11	27	11	505	55.2	7.23	85.07		11 High	1
G3HG95	Lamin-A/C OS=Cricetulus griseus OX=10029 GN=I79_009616 PE=3 SV=1	23	13	14	13	563	64	8.02	44.54		13 High	1
AOA061IR66	Serine hydroxymethyltransferase OS=Cricetulus griseus OX=10029 GN=H671_1g1569 PE=3 SV=1	13	6	11	6	476	52.9	8.66	34.06		6 High	1
AOA3L7HIJW1	KIF21B OS=Cricetulus griseus OX=10029 GN=CgPICR_000914 PE=3 SV=1	5	7	9	7	1722	191.6	7.78	30		7 High	1
AOA3L7H2X3	RBBP7 OS=Cricetulus griseus OX=10029 GN=CgPICR_008031 PE=4 SV=1	10	4	6	4	405	45.6	5.34	15.28		4 High	1
AOA3L7GVU3	Glutamate dehydrogenase (NAD(P)(+)) OS=Cricetulus griseus OX=10029 GN=CgPICR_006231 PE=3 SV=1	9	5	6	5	525	57.3	7.81	15.1		5 High	1
AOA3L7I839	SFPQ OS=Cricetulus griseus OX=10029 GN=CgPICR_007108 PE=4 SV=1	10	4	6	2	474	53.8	7.94	16.47		4 High	1
AOA3L7IAV7	Tubulin alpha chain (Fragment) OS=Cricetulus griseus OX=10029 GN=CgPICR_000155 PE=3 SV=1	14	6	6	6	460	51.2	5.06	15.79		6 High	1
G3HIC5	RuvB-like helicase OS=Cricetulus griseus OX=10029 GN=I79_010385 PE=3 SV=1	12	5	5	5	456	50.2	6.42	14.26		5 High	1
AOA3L7HDW9	DNA topoisomerase 2 OS=Cricetulus griseus OX=10029 GN=CgPICR_018688 PE=3 SV=1	4	4	5	3	1479	167.7	8.38	15.67		4 High	1
AOA3L7HXQ3	SF3B2 OS=Cricetulus griseus OX=10029 GN=CgPICR_009519 PE=4 SV=1	6	5	5	5	853	95.4	5.76	14.6		5 High	1
AOA061I997	Dual-specificity kinase OS=Cricetulus griseus OX=10029 GN=H671_4g12631 PE=3 SV=1	5	4	4	4	830	93	8.97	11.81		4 High	1
G3H9U3	Splicing factor, proline-and glutamine-rich OS=Cricetulus griseus OX=10029 GN=I79_007174 PE=4 SV=1	12	3	4	1	351	40.2	6.74	11.42		3 High	1
G3IJF2	Nuclear fragile X mental retardation-interacting protein 2 OS=Cricetulus griseus OX=10029 GN=I79_023986 PE=4 SV=1	6	3	4	3	530	56.6	7.44	11.86		3 High	1
G3IJG2	Fatty acyl-CoA reductase OS=Cricetulus griseus OX=10029 GN=I79_023997 PE=3 SV=1	7	3	3	3	515	59.4	9.17	8.67		3 High	1
AOA3L7GURS	DNA topoisomerase 2 OS=Cricetulus griseus OX=10029 GN=CgPICR_006188 PE=3 SV=1	1	2	3	1	1533	172.9	8.75	8.39		2 High	1

Sample 3

Accession	Description	Coverage	# Peptides	# PSMs	# Unique f	# AAs	MW [kDa]	calc. pl	Score	SeqL	# Peptides Found in S	# Protein Groups
AOA061I0W0	Non-POU domain-containing octamer-binding protein OS=Cricetulus griseus OX=10029 GN=H671_xg20122 PE=4 SV=1	18	13	147	13	686	77.8	5.24	465.59		13 High	1
AOA3L7HIJW1	KIF21B OS=Cricetulus griseus OX=10029 GN=CgPICR_000914 PE=3 SV=1	9	13	16	13	1722	191.6	7.78	53.14		13 High	1
AOA3L7HSU5	CCT-theta OS=Cricetulus griseus OX=10029 GN=CgPICR_001873 PE=3 SV=1	16	7	7	4	489	53	5.5	22.46		7 High	1
G3IER2	Cleavage and polyadenylation specificity factor subunit 7 OS=Cricetulus griseus OX=10029 GN=I79_022214 PE=3 SV=1	13	4	7	1	361	40.6	7.37	21.03		4 High	1
AOA3L7HAZ7	CPSF7 OS=Cricetulus griseus OX=10029 GN=CgPICR_006755 PE=3 SV=1	10	4	6	1	428	46	6.47	17.26		4 High	1
G3GT05	T-complex protein 1 subunit theta OS=Cricetulus griseus OX=10029 GN=I79_000778 PE=3 SV=1	26	5	5	2	205	22.2	4.91	15.63		5 High	1
AOA3L7HDW9	DNA topoisomerase 2 OS=Cricetulus griseus OX=10029 GN=CgPICR_018688 PE=3 SV=1	4	4	4	4	1479	167.7	8.38	13.65		4 High	1
G3HG95	Lamin-A/C OS=Cricetulus griseus OX=10029 GN=I79_009616 PE=3 SV=1	8	4	4	4	563	64	8.02	11.82		4 High	1
AOA3L7HU56	PDCD7 OS=Cricetulus griseus OX=10029 GN=CgPICR_005263 PE=4 SV=1	7	3	3	3	484	54.5	10.29	10.29		3 High	1
AOA3L7INC4	RNA helicase OS=Cricetulus griseus OX=10029 GN=CgPICR_004361 PE=4 SV=1	3	2	3	2	795	90.9	7.46	10.58		2 High	1
AOA3L7HXQ3	SF3B2 OS=Cricetulus griseus OX=10029 GN=CgPICR_009519 PE=4 SV=1	4	3	3	3	853	95.4	5.76	8.53		3 High	1
G3IJF2	Nuclear fragile X mental retardation-interacting protein 2 OS=Cricetulus griseus OX=10029 GN=I79_023986 PE=4 SV=1	7	3	3	3	530	56.6	7.44	10.41		3 High	1
G3IIM7	GTF3C5 OS=Cricetulus griseus OX=10029 GN=CgPICR_012467 PE=4 SV=1	6	3	3	3	518	60.1	6.99	8.25		3 High	1

Sample 4

Accession	Description	Coverage	# Peptides	# PSMs	# Unique f	# AAs	MW [kDa]	calc. pl	Score	SeqL	# Peptides Found in S	# Protein Groups
G3HG95	Lamin-A/C OS=Cricetulus griseus OX=10029 GN=I79_009616 PE=3 SV=1	50	34	152	34	563	64	8.02	476.23		34 High	1
AOA3L7HIJW1	KIF21B OS=Cricetulus griseus OX=10029 GN=CgPICR_000914 PE=3 SV=1	7	11	16	11	1722	191.6	7.78	51.17		11 High	1
G3HDG6	Paraspeckle component 1 OS=Cricetulus griseus OX=10029 GN=I79_008512 PE=3 SV=1	15	8	12	8	522	58.6	6.67	33.22		8 High	1
AOA061I5D1	Heat shock cognate protein OS=Cricetulus griseus OX=10029 GN=H671_4g13251 PE=3 SV=1	14	8	10	8	673	73.8	5.74	31.17		8 High	1
G3I220	Cytoskeleton-associated protein 4 OS=Cricetulus griseus OX=10029 GN=I79_017443 PE=4 SV=1	16	6	9	6	324	36.3	4.81	25.69		6 High	1
AOA061I0W0	Non-POU domain-containing octamer-binding protein OS=Cricetulus griseus OX=10029 GN=H671_xg20122 PE=4 SV=1	7	5	9	4	686	77.8	5.24	24.37		5 High	1
AOA3L7HXQ3	SF3B2 OS=Cricetulus griseus OX=10029 GN=CgPICR_009519 PE=4 SV=1	6	5	5	5	853	95.4	5.76	14.27		5 High	1
AOA3L7HDW9	DNA topoisomerase 2 OS=Cricetulus griseus OX=10029 GN=CgPICR_018688 PE=3 SV=1	3	4	5	3	1479	167.7	8.38	16.69		4 High	1
G3HEZ0	75 kDa glucose-regulated protein OS=Cricetulus griseus OX=10029 GN=I79_009139 PE=3 SV=1	7	4	4	4	605	65.8	6.1	11.33		4 High	1
AOA3L7IBAO	ATAD3 OS=Cricetulus griseus OX=10029 GN=CgPICR_019152 PE=4 SV=1	7	4	4	4	576	65	9.13	11.21		4 High	1
AOA098KXG8	DNA topoisomerase 2 OS=Cricetulus griseus OX=10029 GN=H671_1g2063 PE=3 SV=1	2	3	4	2	1612	182	8.15	11.53		3 High	1
AOA3L7HCE5	Glyoxylate reductase 1 homolog OS=Cricetulus griseus OX=10029 GN=CgPICR_017508 PE=3 SV=1	4	2	4	2	546	59.9	9.23	12.96		2 High	1
AOA061IH34	Cleavage and polyadenylation specificity factor subunit 6 OS=Cricetulus griseus OX=10029 GN=H671_1g3754 PE=3 SV=1	6	3	3	3	552	59.3	7.37	9.99		3 High	1
AOA3L7HAZ7	CPSF7 OS=Cricetulus griseus OX=10029 GN=CgPICR_006755 PE=3 SV=1	8	3	3	3	428	46	6.47	8.27		3 High	1
G3HG83	T-complex protein 1 subunit gamma OS=Cricetulus griseus OX=10029 GN=I79_009604 PE=3 SV=1	6	3	3	3	545	60.6	6.64	8.64		3 High	1
AOA3L7GU20	Guanine nucleotide-binding protein-like 3 OS=Cricetulus griseus OX=10029 GN=CgPICR_006286 PE=4 SV=1	6	3	3	3	535	60.5	9.23	8.61		3 High	1
G3IJZ9	PITSLRE serine/threonine-protein kinase CDC2L1 OS=Cricetulus griseus OX=10029 GN=I79_024191 PE=4 SV=1	5	3	3	3	529	62.2	5.63	8.85		3 High	1

Sample 5

Accession	Description	Coverage	# Peptides	# PSMs	# Unique	F # AAs	MW [kDa]	calc. pI	Score	SeqL	# Peptides Found in S	# Protein Groups
AOA3L7I839	SFPQ OS=Cricetulus griseus OX=10029 GN=CgPICR_007108 PE=4 SV=1	38	18	141	6	474	53.8	7.94	447.72		18 High	1
G3H9U3	Splicing factor, proline-and glutamine-rich OS=Cricetulus griseus OX=10029 GN=I79_007174 PE=4 SV=1	40	14	133	2	351	40.2	6.74	437.04		14 High	1
AOA3L7HIJW1	KIF21B OS=Cricetulus griseus OX=10029 GN=CgPICR_000914 PE=3 SV=1	18	25	79	25	1722	191.6	7.78	267.74		25 High	1
AOA3L7HDW9	DNA topoisomerase 2 OS=Cricetulus griseus OX=10029 GN=CgPICR_018688 PE=3 SV=1	12	14	20	9	1479	167.7	8.38	66.56		14 High	1
AOA098KXG8	DNA topoisomerase 2 OS=Cricetulus griseus OX=10029 GN=H671_1g2063 PE=3 SV=1	5	7	13	2	1612	182	8.15	45		7 High	1
AOA3L7H7P2	ACTN4 OS=Cricetulus griseus OX=10029 GN=CgPICR_018652 PE=3 SV=1	15	11	12	7	1220	139.5	5.47	44.46		11 High	1
AOA061I8C5	Ataxin-2-like protein OS=Cricetulus griseus OX=10029 GN=H671_3g10220 PE=3 SV=1	10	7	9	7	1039	110	8.63	30.28		7 High	1
G3HCI9	Scaffold attachment factor B1 OS=Cricetulus griseus OX=10029 GN=I79_008200 PE=4 SV=1	8	6	8	5	929	102.8	5.21	30.74		6 High	1
AOA3L7I9I9	CDK11B OS=Cricetulus griseus OX=10029 GN=CgPICR_019145 PE=4 SV=1	10	7	8	7	789	92	5.34	25.74		7 High	1
AOA3L7IQI9	STIM2 OS=Cricetulus griseus OX=10029 GN=CgPICR_004347 PE=4 SV=1	13	7	8	7	637	72.4	7.75	25.58		7 High	1
AOA3L7H4V4	TRIM28 OS=Cricetulus griseus OX=10029 GN=CgPICR_021444 PE=4 SV=1	9	6	7	6	803	86.6	6.14	20.66		6 High	1
AOA3L7HIW9	ACTN1 OS=Cricetulus griseus OX=10029 GN=CgPICR_008314 PE=3 SV=1	10	7	7	3	865	100	5.47	24.1		7 High	1
AOA3L7HXQ3	SF3B2 OS=Cricetulus griseus OX=10029 GN=CgPICR_009519 PE=4 SV=1	4	3	4	3	853	95.4	5.76	11.46		3 High	1
G3GX75	Hepatocyte growth factor-regulated tyrosine kinase substrate OS=Cricetulus griseus OX=10029 GN=I79_002390 PE=4 SV=1	6	4	4	4	776	86.1	6.16	12.75		4 High	1
G3HSC4	Leucine-rich repeat-containing protein 8C OS=Cricetulus griseus OX=10029 GN=I79_013754 PE=3 SV=1	4	3	4	3	803	92.5	7.49	12		3 High	1
AOA3L7IP17	TOX high mobility group box family member 4 (Fragment) OS=Cricetulus griseus OX=10029 GN=CgPICR_017413 PE=4 SV=1	8	4	4	4	603	64.1	5.12	13.25		4 High	1
G3IGZ4	LRRC8A OS=Cricetulus griseus OX=10029 GN=CgPICR_012498 PE=3 SV=1	5	3	3	3	810	94.2	7.84	8.46		3 High	1
AOA3L7I8G0	KIF20A OS=Cricetulus griseus OX=10029 GN=CgPICR_011076 PE=3 SV=1	5	3	3	3	820	93	7.14	8.96		3 High	1
G3HVG9	Matrin-3 OS=Cricetulus griseus OX=10029 GN=I79_014957 PE=4 SV=1	6	3	3	3	847	94.6	6.25	7.48		3 High	1
G3HG95	Lamin-A/C OS=Cricetulus griseus OX=10029 GN=I79_009616 PE=3 SV=1	6	3	3	3	563	64	8.02	8.32		3 High	1
AOA3L7HIM4	HNRNP U OS=Cricetulus griseus OX=10029 GN=CgPICR_010161 PE=4 SV=1	6	3	3	3	744	81.5	6.47	9.03		3 High	1

A0A3L7GQL2	CCAR2 (Fragment) OS=Cricetulus griseus OX=10029 GN=CgPICR_007461 PE=4 SV=1	7	4	4	4	873	97.8	5.63	12.01	4	High	1
G3HL16	Splicing factor 3B subunit 1 OS=Cricetulus griseus OX=10029 GN=H671_2g6483 PE=3 SV=1	4	4	4	4	1304	145.7	7.09	13.34	4	High	1
A0A3L7I9I9	CDK11B OS=Cricetulus griseus OX=10029 GN=CgPICR_019145 PE=4 SV=1	4	3	3	3	789	92	5.34	9.27	3	High	1
G3GUH8	Serine/threonine-protein kinase WNK2 OS=Cricetulus griseus OX=10029 GN=I79_001340 PE=4 SV=1	1	2	3	2	1877	201.1	7.03	8.92	2	High	1
G3HWP7	FACT complex subunit OS=Cricetulus griseus OX=10029 GN=I79_015425 PE=3 SV=1	4	3	3	3	927	106.1	5.62	8.08	3	High	1
A0A061I2E8	Ubiquitin carboxyl-terminal hydrolase 7 OS=Cricetulus griseus OX=10029 GN=H671_7g18767 PE=3 SV=1	3	3	3	3	1110	128.9	5.62	8.61	3	High	1

Sample 7

Accession	Description	Coverage	# Peptides	# PSMs	# Unique	F # AAs	MW [kDa]	calc. pI	Score	SeqL	# Peptides Found in S	# Protein Groups
G3I5N5	DNA topoisomerase 2 OS=Cricetulus griseus OX=10029 GN=I79_018788 PE=3 SV=1	21	26	138	22	1526	173.1	8.75	484.35	26	High	1
A0A3L7HJW1	KIF21B OS=Cricetulus griseus OX=10029 GN=CgPICR_000914 PE=3 SV=1	24	34	101	6	1722	191.6	7.78	369.65	34	High	1
p00001	Protein sequence of hKIF21B-6His,HistaginCterminal	20	30	89	2	1646	183.6	7.15	322.89	30	High	1
A0A098KXG8	DNA topoisomerase 2 OS=Cricetulus griseus OX=10029 GN=H671_1g2063 PE=3 SV=1	7	11	70	7	1612	182	8.15	242.72	11	High	1
A0A3L7HKZ1	SAFB OS=Cricetulus griseus OX=10029 GN=CgPICR_020010 PE=4 SV=1	7	5	7	3	885	99.7	5.22	27.5	5	High	1

Masss spectrometry analysis of the fraction 2 presented in Supplementary Figure S4B - sample number below correspond to the number of the analysed bands in the fraction (see arrowheads in Figure S4B)

Sample 8

Accession	Description	Coverage	# Peptides	# PSMs	# Unique F # AAs	MW [kDa]	# Peptides	(by Search Engine): A2 Sequest HT
A0A3L7HDW9	DNA topoisomerase 2 OS=Cricetulus griseus OX=10029 GN=CgPICR_018688 PE=3 SV=1	7	9	17	7	1479	167.7	9
A0A3L7HJW1	KIF21B OS=Cricetulus griseus OX=10029 GN=CgPICR_000914 PE=3 SV=1	9	11	15	2	1722	191.6	11
A0A098XG8	DNA topoisomerase 2 OS=Cricetulus griseus OX=10029 GN=H671_1g2063 PE=3 SV=1	3	4	13	2	1612	182	4
A0A3L7HAC5	RPL5 OS=Cricetulus griseus OX=10029 GN=CgPICR_015136 PE=3 SV=1	12	4	5	4	297	34.4	4
A0A3L7GVU3	Glutamate dehydrogenase (NAD(P)(+)) OS=Cricetulus griseus OX=10029 GN=CgPICR_006231 PE=3 SV=1	6	3	4	3	525	57.3	3

Sample 9

Accession	Description	Coverage	# Peptides	# PSMs	# Unique F # AAs	MW [kDa]	# Peptides	(by Search Engine): A2 Sequest HT
A0A3L7HQJ8	Protein FAM76B OS=Cricetulus griseus OX=10029 GN=CgPICR_014314 PE=3 SV=1	25	9	19	9	339	38.6	9
A0A3L7HJW1	KIF21B OS=Cricetulus griseus OX=10029 GN=CgPICR_000914 PE=3 SV=1	6	9	11	9	1722	191.6	9
G3HV08	Cell division protein kinase 9 OS=Cricetulus griseus OX=10029 GN=I79_014781 PE=3 SV=1	11	4	7	4	372	42.7	4
A0A3L7HDW9	DNA topoisomerase 2 OS=Cricetulus griseus OX=10029 GN=CgPICR_018688 PE=3 SV=1	4	5	7	3	1479	167.7	5
A0A098XG8	DNA topoisomerase 2 OS=Cricetulus griseus OX=10029 GN=H671_1g2063 PE=3 SV=1	3	4	6	2	1612	182	4
A0A3L7IGI7	LMNA (Fragment) OS=Cricetulus griseus OX=10029 GN=CgPICR_013515 PE=3 SV=1	8	4	6	4	553	61.5	4
A0A3L7I839	SFPQ OS=Cricetulus griseus OX=10029 GN=CgPICR_007108 PE=4 SV=1	6	3	4	2	474	53.8	3
A0A3L7I345	FAM98A OS=Cricetulus griseus OX=10029 GN=CgPICR_005301 PE=3 SV=1	8	2	3	2	251	27.7	2
A0A3L7HB29	DCAF7 OS=Cricetulus griseus OX=10029 GN=CgPICR_016826 PE=4 SV=1	10	3	3	3	290	33.2	3
A0A061IOW0	Non-POU domain-containing octamer-binding protein OS=Cricetulus griseus OX=10029 GN=H671_xg20122 PE=4 SV=1	4	3	3	2	686	77.8	3
A0A061IR66	Serine hydroxymethyltransferase OS=Cricetulus griseus OX=10029 GN=H671_1g1569 PE=3 SV=1	7	3	3	3	476	52.9	3

Sample 10

Accession	Description	Coverage	# Peptides	# PSMs	# Unique F # AAs	MW [kDa]	# Peptides	(by Search Engine): A2 Sequest HT
A0A3L7GVU3	Glutamate dehydrogenase (NAD(P)(+)) OS=Cricetulus griseus OX=10029 GN=CgPICR_006231 PE=3 SV=1	38	15	75	15	525	57.3	15
Q60455	Tubulin beta chain OS=Cricetulus griseus OX=10029 PE=2 SV=1	20	8	16	2	444	49.7	8
G3HQP8	Tubulin beta chain OS=Cricetulus griseus OX=10029 GN=CgPICR_019487 PE=3 SV=1	20	8	15	2	444	49.6	8
A0A3L7IHW1	ATP synthase subunit beta OS=Cricetulus griseus OX=10029 GN=CgPICR_002492 PE=3 SV=1	15	6	12	6	496	53.3	6
A0A3L7HJW1	KIF21B OS=Cricetulus griseus OX=10029 GN=CgPICR_000914 PE=3 SV=1	5	7	8	7	1722	191.6	7
Q540F6	Elongation factor 1-alpha OS=Cricetulus griseus OX=10029 PE=3 SV=1	11	5	7	5	462	50.1	5
A0A3L7HDW9	DNA topoisomerase 2 OS=Cricetulus griseus OX=10029 GN=CgPICR_018688 PE=3 SV=1	5	6	6	4	1479	167.7	6
G3HZY1	RuvB-like helicase OS=Cricetulus griseus OX=10029 GN=I79_016646 PE=3 SV=1	13	6	6	6	518	57.2	6
G3HTU4	SAP30-binding protein OS=Cricetulus griseus OX=10029 GN=I79_014324 PE=4 SV=1	16	5	5	5	308	33.7	5
A0A061IOW0	Non-POU domain-containing octamer-binding protein OS=Cricetulus griseus OX=10029 GN=H671_xg20122 PE=4 SV=1	5	3	4	3	686	77.8	3
A0A3L7GPV9	AP-2 transcription factor OS=Cricetulus griseus OX=10029 GN=CgPICR_015510 PE=3 SV=1	9	4	4	4	439	48.2	4
A0A061IR66	Serine hydroxymethyltransferase OS=Cricetulus griseus OX=10029 GN=H671_1g1569 PE=3 SV=1	7	3	3	3	476	52.9	3
G3HL13	60 kDa chaperonin OS=Cricetulus griseus OX=10029 GN=I79_011398 PE=3 SV=1	6	3	3	3	526	56.5	3
A0A098XG8	DNA topoisomerase 2 OS=Cricetulus griseus OX=10029 GN=H671_1g2063 PE=3 SV=1	2	3	3	1	1612	182	3
G3H7M8	Heterogeneous nuclear ribonucleoprotein U OS=Cricetulus griseus OX=10029 GN=I79_006363 PE=4 SV=1	4	2	3	2	512	57.6	2
A0A3L7HC71	ATP-dependent RNA helicase DDX1 OS=Cricetulus griseus OX=10029 GN=CgPICR_006450 PE=3 SV=1	4	3	3	3	724	80.9	3
A0A061IA65	Acyl-CoA dehydrogenase family member 10 OS=Cricetulus griseus OX=10029 GN=H671_4g11405 PE=3 SV=1	1	3	3	3	2661	295.6	3
A0A3L7I839	SFPQ OS=Cricetulus griseus OX=10029 GN=CgPICR_007108 PE=4 SV=1	5	2	3	2	474	53.8	2
G3HCS4	26S proteasome non-ATPase regulatory subunit 12 OS=Cricetulus griseus OX=10029 GN=I79_008289 PE=3 SV=1	8	3	3	3	456	52.9	3
G3HSI3	Nuclear factor 1 C-type OS=Cricetulus griseus OX=10029 GN=I79_013826 PE=4 SV=1	13	2	3	2	142	15.4	2
A0A061ICE4	ATP synthase subunit alpha OS=Cricetulus griseus OX=10029 GN=CgPICR_017589 PE=3 SV=1	6	3	3	3	553	59.7	3

Sample 11

Accession	Description	Coverage	# Peptides	# PSMs	# Unique F # AAs	MW [kDa]	# Peptides	(by Search Engine): A2 Sequest HT
A0A061IOW0	Non-POU domain-containing octamer-binding protein OS=Cricetulus griseus OX=10029 GN=H671_xg20122 PE=4 SV=1	14	11	52	10	686	77.8	11
A0A3L7HSU5	CCT-theta OS=Cricetulus griseus OX=10029 GN=CgPICR_001873 PE=3 SV=1	17	7	12	4	489	53	7
G3HYB7	T-complex protein 1 subunit eta OS=Cricetulus griseus OX=10029 GN=H671_8g19533 PE=3 SV=1	11	5	12	5	499	54.9	5
G3HTK5	CCT5 OS=Cricetulus griseus OX=10029 GN=CgPICR_008840 PE=3 SV=1	15	10	10	10	541	59.5	10
A0A3L7INC4	RNA helicase OS=Cricetulus griseus OX=10029 GN=CgPICR_004361 PE=4 SV=1	7	5	7	5	795	90.9	5
A0A3L7GVU3	Glutamate dehydrogenase (NAD(P)(+)) OS=Cricetulus griseus OX=10029 GN=CgPICR_006231 PE=3 SV=1	13	6	7	6	525	57.3	6
A0A3L7IPI6	NudC domain-containing protein 1 OS=Cricetulus griseus OX=10029 GN=CgPICR_010700 PE=4 SV=1	6	3	7	3	625	71.6	3
G3T05	T-complex protein 1 subunit theta OS=Cricetulus griseus OX=10029 GN=I79_000778 PE=3 SV=1	26	5	7	2	205	22.2	5
A0A3L7HJW1	KIF21B OS=Cricetulus griseus OX=10029 GN=CgPICR_000914 PE=3 SV=1	4	5	6	5	1722	191.6	5
G3H6B5	Interleukin enhancer-binding factor 3 OS=Cricetulus griseus OX=10029 GN=I79_005870 PE=4 SV=1	6	5	6	5	909	97.5	5
A0A061IFT2	Acetyl-CoA carboxylase kinase OS=Cricetulus griseus OX=10029 GN=H671_2g5838 PE=3 SV=1	13	5	5	5	451	51.8	5
G3HL13	60 kDa chaperonin OS=Cricetulus griseus OX=10029 GN=I79_011398 PE=3 SV=1	9	5	5	5	526	56.5	5
A0A3L7HPC7	CCT6A OS=Cricetulus griseus OX=10029 GN=CgPICR_012143 PE=3 SV=1	6	3	4	3	459	50	3
G3H7M8	Heterogeneous nuclear ribonucleoprotein U OS=Cricetulus griseus OX=10029 GN=I79_006363 PE=4 SV=1	6	3	4	3	512	57.6	3
A0A3L7HDW9	DNA topoisomerase 2 OS=Cricetulus griseus OX=10029 GN=CgPICR_018688 PE=3 SV=1	3	4	4	2	1479	167.7	4
G3HMB1	RNA helicase OS=Cricetulus griseus OX=10029 GN=CgPICR_005025 PE=4 SV=1	6	3	3	3	545	61.2	3
G3HDG6	Paraspeckle component 1 OS=Cricetulus griseus OX=10029 GN=I79_008512 PE=3 SV=1	7	3	3	3	522	58.6	3
G3HQ69	Src substrate cortactin OS=Cricetulus griseus OX=10029 GN=I79_012963 PE=4 SV=1	6	3	3	3	550	61.4	3
A0A098XG8	DNA topoisomerase 2 OS=Cricetulus griseus OX=10029 GN=H671_1g2063 PE=3 SV=1	2	3	3	1	1612	182	3
A0A061HY04	F-box-like/WD repeat-containing protein TBL1X OS=Cricetulus griseus OX=10029 GN=H671_xg20387 PE=4 SV=1	4	2	3	2	628	68	2

Sample 12

Accession	Description	Coverage	# Peptides	# PSMs	# Unique F # AAs	MW [kDa]	# Peptides	(by Search Engine): A2 Sequest HT
A0A3L7INC4	RNA helicase OS=Cricetulus griseus OX=10029 GN=CgPICR_004361 PE=4 SV=1	27	23	78	23	795	90.9	23
A0A3L7HC71	ATP-dependent RNA helicase DDX1 OS=Cricetulus griseus OX=10029 GN=CgPICR_006450 PE=3 SV=1	20	14	33	14	724	80.9	14
G3H6B5	Interleukin enhancer-binding factor 3 OS=Cricetulus griseus OX=10029 GN=I79_005870 PE=4 SV=1	16	13	24	13	909	97.5	13
G3HCV0	RNA helicase OS=Cricetulus griseus OX=10029 GN=I79_008317 PE=4 SV=1	9	9	10	9	928	101.6	9
A0A3L7HIM4	HNRNPU OS=Cricetulus griseus OX=10029 GN=CgPICR_010161 PE=4 SV=1	10	7	10	7	744	81.5	7
A0A3L7HJW1	KIF21B OS=Cricetulus griseus OX=10029 GN=CgPICR_000914 PE=3 SV=1	5	7	10	7	1722	191.6	7
G3HKN8	NCK-interacting protein with SH3 domain OS=Cricetulus griseus OX=10029 GN=CgPICR_013314 PE=4 SV=1	10	7	9	7	714	78.2	7
A0A3L7HXF3	PRKRIR OS=Cricetulus griseus OX=10029 GN=CgPICR_008679 PE=4 SV=1	9	8	9	8	770	88.2	8
A0A3L7HL04	HSP90AA1 OS=Cricetulus griseus OX=10029 GN=CgPICR_019896 PE=3 SV=1	11	8	8	3	733	84.7	8
G3GXG0	CUL1 OS=Cricetulus griseus OX=10029 GN=CgPICR_006838 PE=3 SV=1	9	7	7	7	776	89.7	7
G3IOX3	Cell cycle regulator Mat89Bb-like OS=Cricetulus griseus OX=10029 GN=I79_017015 PE=3 SV=1	6	4	6	4	706	80.1	4
A0A3L7INC2	HSP90AB1 OS=Cricetulus griseus OX=10029 GN=CgPICR_018150 PE=3 SV=1	18	6	6	2	313	36	6
G3HWY6	Dynamin-like 120 kDa protein, form S1 OS=Cricetulus griseus OX=10029 GN=I79_015501 PE=4 SV=1	6	6	6	6	1015	117.4	6
G3I133	Heterogeneous nuclear ribonucleoprotein U-like protein 2 OS=Cricetulus griseus OX=10029 GN=I79_023494 PE=4 SV=1	8	5	5	5	627	72.4	5
A0A061I997	Dual-specificity kinase OS=Cricetulus griseus OX=10029 GN=H671_4g12631 PE=3 SV=1	7	5	5	5	830	93	5
A0A061IAE3	Cullin-5-like isoform 2 (Fragment) OS=Cricetulus griseus OX=10029 GN=H671_4g12082 PE=3 SV=1	7	5	5	5	789	91.9	5
G3HWN6	DNA topoisomerase I (Fragment) OS=Cricetulus griseus OX=10029 GN=I79_015397 PE=3 SV=1	5	4	5	4	715	84.4	4
G3HRJ1	FACT complex subunit SSRP1 OS=Cricetulus griseus OX=10029 GN=I79_013463 PE=3 SV=1	8	5	5	5	709	81	5
G3HC84	Heat shock protein HSP 90-beta OS=Cricetulus griseus OX=10029 GN=I79_008088 PE=3 SV=1	13	5	5	4	412	47.8	5
G3H9L2	Ubiquitin carboxyl-terminal hydrolase OS=Cricetulus griseus OX=10029 GN=I79_007088 PE=3 SV=1	6	5	5	5	870	100	5
A0A061IQE2	WD repeat-containing protein mio OS=Cricetulus griseus OX=10029 GN=H671_1g2310 PE=3 SV=1	6	4	4	4	849	95.2	4
A0A3L7HDW9	DNA topoisomerase 2 OS=Cricetulus griseus OX=10029 GN=CgPICR_018688 PE=3 SV=1	4	4	4	2	1479	167.7	4
A0A061HZF8	DnaI homolog subfamily C member 10 OS=Cricetulus griseus OX=10029 GN=H671_6g15452 PE=4 SV=1	5	4	4	4	838	95.9	4
G3HJQ2	Histone acetyltransferase OS=Cricetulus griseus OX=10029 GN=I79_010901 PE=3 SV=1	4	2	3	2	584	67	2
A0A098XG8	DNA topoisomerase 2 OS=Cricetulus griseus OX=10029 GN=H671_1g2063 PE=3 SV=1	2	3	3	1	1612	182	3
A0A3L7HNU1	DNA replication licensing factor MCM7 OS=Cricetulus griseus OX=10029 GN=MCM7 PE=3 SV=1	4	3	3	3	770	86.3	3
G3I2F8	U4/U6.U5 tri-snRNP-associated protein 1 OS=Cricetulus griseus OX=10029 GN=I79_017600 PE=3 SV=1	3	3	3	3	1215	136.9	3
A0A3L7I839	SFPQ OS=Cricetulus griseus OX=10029 GN=CgPICR_007108 PE=4 SV=1	6	3	3	2	474	53.8	3

Sample 13

Accession	Description	Coverage	# Peptides	# PSMs	# Unique F # AAs	MW [kDa]	# Peptides	(by Search Engine): A2 Sequest HT
G3HWN6	DNA topoisomerase I (Fragment) OS=Cricetulus griseus OX=10029 GN=I79_015397 PE=3 SV=1	28	20	53	20	715	84.4	20
A0A3L7HJW1	KIF21B OS=Cricetulus griseus OX=10029 GN=CgPICR_000914 PE=3 SV=1	12	19	45	19	1722	191.6	19
A0A3L7I839	SFPQ OS=Cricetulus griseus OX=10029 GN=CgPICR_007108 PE=4 SV=1	18	7	27	2	474	53.8	7
G3H9U3	Splicing factor, proline- and glutamine-rich OS=Cricetulus griseus OX=10029 GN=I79_007174 PE=4 SV=1	23	6	25	1	351	40.2	6
G3H6B5	Interleukin enhancer-binding factor 3 OS=Cricetulus griseus OX=10029 GN=I79_005870 PE=4 SV=1	16	13	19	13	909	97.5	13
G3HCV0	RNA helicase OS=Cricetulus griseus OX=10029 GN=I79_008317 PE=4 SV=1	10	10	14	10	928	101.6	10
G3HKE3	Cap methyltransferase 1 OS=Cricetulus griseus OX=10029 GN=I79_011163 PE=4 SV=1	12	10	13	10	833	95.2	10
A0A3L7HIM4	HNRNPU OS=Cricetulus griseus OX=10029 GN=CgPICR_010161 PE=4 SV=1	9	6	9	6	744	81.5	6
G3HWM5	Ribosome biogenesis protein BOP1 OS=Cricetulus griseus OX=10029 GN=BOP1 PE=3 SV=1	6	6	8	6	732	82.6	6
A0A3L7HLW4	DNA helicase OS=Cricetulus griseus OX=10029 GN=CgPICR_001008 PE=3 SV=1	7	6	6	1	801	90.6	6
G3GZQ9	DNA helicase OS=Cricetulus griseus OX=10029 GN=I79_003354 PE=3 SV=1	2	6	6	1	2669	301.1	6
G3I1H7	Cleavage and polyadenylation specificity factor 100 kDa subunit OS=Cricetulus griseus OX=10029 GN=I79_017234 PE=3 SV=1	4	5	5	5	1206	134.8	5
A0A3L7INC4	RNA helicase OS=Cricetulus griseus OX=10029 GN=CgPICR_004361 PE=4 SV=1	6	4	4	4	795	90.9	4

G3IJZ9	PITSLRE serine/threonine-protein kinase CDC2L1 OS=Cricetulus griseus OX=10029 GN=I79_024191 PE=4 SV=1	8	4	4	4	529	62.2	4
G3IIZ3	Heterogeneous nuclear ribonucleoprotein U-like protein 2 OS=Cricetulus griseus OX=10029 GN=I79_023494 PE=4 SV=1	6	4	4	4	627	72.4	4
A0A3L7H4V4	TRIM28 OS=Cricetulus griseus OX=10029 GN=CgPICR_021444 PE=4 SV=1	4	3	3	3	803	86.6	3
G3GVY6	Oxysterol-binding protein OS=Cricetulus griseus OX=10029 GN=I79_001892 PE=3 SV=1	4	3	3	3	736	83.2	3
A0A3L7HBS3	KPNB1 OS=Cricetulus griseus OX=10029 GN=CgPICR_018745 PE=3 SV=1	3	3	3	3	784	87.3	3
G3GU41	Putative RNA-binding protein 19 OS=Cricetulus griseus OX=10029 GN=I79_001190 PE=4 SV=1	3	2	3	2	954	106.1	2
G3HQM6	Endoplasmrin OS=Cricetulus griseus OX=10029 GN=I79_013131 PE=3 SV=1	4	3	3	3	803	92.6	3
A0A3L7HC71	ATP-dependent RNA helicase DDX1 OS=Cricetulus griseus OX=10029 GN=CgPICR_006450 PE=3 SV=1	4	3	3	3	724	80.9	3
A0A3L7IQI9	STIM2 OS=Cricetulus griseus OX=10029 GN=CgPICR_004347 PE=4 SV=1	5	3	3	3	637	72.4	3

Sample 14

Accession	Description	Coverage	# Peptides	# PSMs	# Unique F	# AAs	MW [kDa]	# Peptides	(by Search Engine): A2 Sequest HT
A0A3L7HIM4	HNRNPU OS=Cricetulus griseus OX=10029 GN=CgPICR_010161 PE=4 SV=1	18	17	61	17	744	81.5	17	
A0A061IRA2	Ubiquitin carboxyl-terminal hydrolase OS=Cricetulus griseus OX=10029 GN=H671_1g1368 PE=3 SV=1	23	21	32	19	981	112.2	21	
G3H6B5	Interleukin enhancer-binding factor 3 OS=Cricetulus griseus OX=10029 GN=I79_005870 PE=4 SV=1	19	16	30	16	909	97.5	16	
G3IIZ3	Heterogeneous nuclear ribonucleoprotein U-like protein 2 OS=Cricetulus griseus OX=10029 GN=I79_023494 PE=4 SV=1	25	17	26	17	627	72.4	17	
G3HCV0	RNA helicase OS=Cricetulus griseus OX=10029 GN=I79_008317 PE=4 SV=1	19	18	25	18	928	101.6	18	
A0A3L7HJW1	KIF21B OS=Cricetulus griseus OX=10029 GN=CgPICR_000914 PE=3 SV=1	10	14	20	14	1722	191.6	14	
G3HWN6	DNA topoisomerase I (Fragment) OS=Cricetulus griseus OX=10029 GN=I79_015397 PE=3 SV=1	18	12	19	12	715	84.4	12	
G3HVG9	Matrin-3 OS=Cricetulus griseus OX=10029 GN=I79_014957 PE=4 SV=1	14	9	18	9	847	94.6	9	
A0A061ICN7	Superkiller viralicidic activity 2-like 2 OS=Cricetulus griseus OX=10029 GN=H671_2g6766 PE=4 SV=1	11	11	16	11	1041	117.7	11	
A0A3L7GLU9	TAOK1 OS=Cricetulus griseus OX=10029 GN=CgPICR_003496 PE=4 SV=1	12	10	12	10	925	107.6	10	
G3GU41	Putative RNA-binding protein 19 OS=Cricetulus griseus OX=10029 GN=I79_001190 PE=4 SV=1	12	10	12	10	954	106.1	10	
G3I2F8	U4/U6.U5 tri-snRNP-associated protein 1 OS=Cricetulus griseus OX=10029 GN=I79_017600 PE=3 SV=1	11	11	11	11	1215	136.9	11	
G3H7V9	DNA replication licensing factor MCM2 OS=Cricetulus griseus OX=10029 GN=I79_006453 PE=3 SV=1	11	8	9	8	905	102.1	8	
A0A3L7I9I9	CDK11B OS=Cricetulus griseus OX=10029 GN=CgPICR_019145 PE=4 SV=1	9	7	9	7	789	92	7	
G3H8G1	Ubiquitin carboxyl-terminal hydrolase OS=Cricetulus griseus OX=10029 GN=I79_006661 PE=3 SV=1	7	6	9	4	940	105.8	6	
A0A3L7HDW9	DNA topoisomerase 2 OS=Cricetulus griseus OX=10029 GN=CgPICR_018688 PE=3 SV=1	6	8	8	6	1479	167.7	8	
A0A3L7INC4	RNA helicase OS=Cricetulus griseus OX=10029 GN=CgPICR_004361 PE=4 SV=1	9	6	7	6	795	90.9	6	
G3IGS8	Arsenite-resistance protein 2 OS=Cricetulus griseus OX=10029 GN=I79_023004 PE=3 SV=1	6	5	6	5	841	96.3	5	
A0A3L7H4V4	TRIM28 OS=Cricetulus griseus OX=10029 GN=CgPICR_021444 PE=4 SV=1	9	6	6	6	803	86.6	6	
A0A3L7IPU4	Transcription initiation factor TFIID 150 kDa subunit OS=Cricetulus griseus OX=10029 GN=CgPICR_011623 PE=3 SV=1	4	5	6	5	1152	131.5	5	
G3IKP7	Putative RNA-binding protein 15 OS=Cricetulus griseus OX=10029 GN=CgPICR_003975 PE=3 SV=1	8	6	6	6	912	99.8	6	
G3IB76	WD repeat-containing protein 6 OS=Cricetulus griseus OX=10029 GN=CgPICR_013308 PE=4 SV=1	4	4	5	4	1072	116.6	4	
G3GZ85	Staphylococcal nuclease domain-containing protein OS=Cricetulus griseus OX=10029 GN=I79_003116 PE=4 SV=1	7	5	5	5	886	99.7	5	
A0A3L7IPN3	POP1 OS=Cricetulus griseus OX=10029 GN=CgPICR_010747 PE=4 SV=1	5	4	5	4	953	105.9	4	
A0A061HWP9	LRRC8D OS=Cricetulus griseus OX=10029 GN=CgPICR_015116 PE=3 SV=1	5	4	4	4	855	97.7	4	
A0A3L7IJM3	PRSS2 OS=Cricetulus griseus OX=10029 GN=CgPICR_006786 PE=4 SV=1	4	1	4	1	239	25.6	1	
A0A3L7IC37	PSMD1 (Fragment) OS=Cricetulus griseus OX=10029 GN=CgPICR_000541 PE=4 SV=1	8	3	4	1	469	52.1	3	
G3HVC2	Pre-rRNA-processing protein TSR1-like OS=Cricetulus griseus OX=10029 GN=I79_014904 PE=4 SV=1	6	2	4	2	380	44.4	2	
G3IDS0	Pre-mRNA-processing factor 40-like A OS=Cricetulus griseus OX=10029 GN=I79_021853 PE=4 SV=1	5	3	3	3	714	81.4	3	
G3GU10	Formyltetrahydrofolate synthetase OS=Cricetulus griseus OX=10029 GN=I79_001156 PE=3 SV=1	3	3	3	3	975	105.3	3	
A0A098KXG8	DNA topoisomerase 2 OS=Cricetulus griseus OX=10029 GN=H671_1g2063 PE=3 SV=1	2	3	3	1	1612	182	3	
G3IM40	26S proteasome non-ATPase regulatory subunit 1 OS=Cricetulus griseus OX=10029 GN=I79_024971 PE=4 SV=1	7	3	3	1	539	59.6	3	
A0A3L7HFJ9	Diacylglycerol kinase OS=Cricetulus griseus OX=10029 GN=CgPICR_001729 PE=3 SV=1	5	3	3	3	911	102	3	
A0A061I540	DNA-directed RNA polymerase OS=Cricetulus griseus OX=10029 GN=H671_5g15076 PE=3 SV=1	3	2	3	2	850	96.9	2	
G3HL16	Splicing factor 3B subunit 1 OS=Cricetulus griseus OX=10029 GN=H671_2g6483 PE=3 SV=1	2	3	3	3	1304	145.7	3	

Sample 15

Accession	Description	Coverage	# Peptides	# PSMs	# Unique F	# AAs	MW [kDa]	# Peptides	(by Search Engine): A2 Sequest HT
A0A3L7HJW1	KIF21B OS=Cricetulus griseus OX=10029 GN=CgPICR_000914 PE=3 SV=1	13	21	52	21	1722	191.6	21	
G3ISN5	DNA topoisomerase 2 OS=Cricetulus griseus OX=10029 GN=I79_018788 PE=3 SV=1	10	12	34	9	1526	173.1	12	
A0A098KXG8	DNA topoisomerase 2 OS=Cricetulus griseus OX=10029 GN=H671_1g2063 PE=3 SV=1	4	6	19	3	1612	182	6	
G3HAF4	Splicing factor 3B subunit 3 OS=Cricetulus griseus OX=10029 GN=I79_007403 PE=4 SV=1	8	8	11	8	1217	135.5	8	
A0A3L7HIM4	HNRNPU OS=Cricetulus griseus OX=10029 GN=CgPICR_010161 PE=4 SV=1	10	6	8	6	744	81.5	6	
G3HWL7	Cleavage and polyadenylation specificity factor subunit 1 OS=Cricetulus griseus OX=10029 GN=I79_015349 PE=4 SV=1	5	7	7	7	1419	158.2	7	
A0A061I3J0	Keratin, type I cytoskeletal 10-like protein OS=Cricetulus griseus OX=10029 GN=H671_7g18232 PE=4 SV=1	5	5	7	1	1117	124.3	5	
A0A061IEW4	PRP4 pre-mRNA-processing factor 4 homolog OS=Cricetulus griseus OX=10029 GN=H671_3g8962 PE=4 SV=1	3	3	5	3	999	115.9	3	
A0A3L7IPU4	Transcription initiation factor TFIID 150 kDa subunit OS=Cricetulus griseus OX=10029 GN=CgPICR_011623 PE=3 SV=1	3	3	4	3	1152	131.5	3	
A0A3L7IJM3	PRSS2 OS=Cricetulus griseus OX=10029 GN=CgPICR_006786 PE=4 SV=1	4	1	3	1	239	25.6	1	
G3HKS8	Ribosome biogenesis protein BMS1-like OS=Cricetulus griseus OX=10029 GN=I79_011308 PE=4 SV=1	3	3	3	3	1276	145	3	

Supplementary table 3.- List of antibodies used in this study

Antibody	Host	Dilution	Used for	Manufacturer	Reference
KIF21B	Rabbit	1/1 000	WB	Sigma-Aldrich	HPA027274
		0.20 µg Ab / 200 µg proteins	IP		
α-Tubulin	Mouse	1/200	IF	Sigma	024M4767V
Cux2	Rabbit	1/200	IF	Sigma	HPA003317
Caspase-3	Mouse	1/200	IF	R&D systems	AF835
GFP	Goat	1/600	IF	Abcam	Ab6673
GM130	Rabbit	1/2 000	WB	Protein Tech	113081AP
Jip-1	Mouse	1/ 2 000	WB	Santa Cruz	Sc-25267
Myosin light chain-II	Rabbit	1/ 1 000	WB	Cell Signalling	3672S
Actin coupled-HRP	Mouse	1/ 50 000	WB	Sigma-Aldrich	A3854
		2.0 µg Ab / 200 µg proteins	IP		
Goat-rabbit-HRP	Rabbit	1/ 10 000	WB	Thermo Fischer Sc	G-21234
Goat-mouse-HRP	Mouse	1/ 10 000	WB	Thermo Fischer Sc	G-21040
Donkey-mouse-488	Mouse	1/ 1 000	IF	Thermo Fischer Sc	A-21202
Donkey-goat-488	Goat	1/ 1 000	IF	Thermo Fischer Sc	A-11055
Donkey-rabbit-555	Rabbit	1/ 1 000	IF	Thermo Fischer Sc	A-31572
IgG control mouse	Rabbit	2.0 µg IgG / 200 µg proteins	IP	Sigma Aldrich	NI03
IgG control Rabbit	mouse	0.20 µg Ab / 200 µg proteins	IP	Protein Tech	30000-0- AP

IF= Immunofluorescence, **WB**=Western blot, **IP**= Immunoprecipitation

DISCUSSION

In light of the essential role that kinesins play during corticogenesis, and the cortical malformations associated with their dysfunction (Tables 3 and 4), we investigated the role of the neuronal kinesin Kif21b during cortex development. My contribution to this work was focused on the mechanisms driving migration, as the first process that neurons undergo after committing to this cellular fate. In this work, I elucidated the processes in which Kif21b participates during pyramidal neuronal migration in both pathological and physiological conditions (Asselin et al., 2020; Narayanan, et al. 2022; Rivera Alvarez, et al. in preparation).

Before the start of this project, information about Kif21b was focused mainly on adult hippocampus (Gromova et al., 2018; Labonté et al., 2014; Muhia et al., 2016), and despite some existing studies suggesting Kif21b participation in diseases like Alzheimer (Kreft, et al. 2014) and multiple sclerosis (Goris, et al. 2010), there were no reports about the role that Kif21b plays during development. Therefore, this work is a pioneer study of Kif21b in the events contributing to brain development. In this section, I will discuss the significance of the discoveries I made during my PhD studies, and I will describe how they can be related and integrated into diverse fields of knowledge concerning pyramidal neuronal migration, cytoskeleton regulation and kinesins biology.

1. Kif21b relevance for human neurodevelopmental disease

In collaboration with clinicians, we discovered that KIF21B is mutated in 4 patients with intellectual disability and cortical malformations, finding 3 missense mutations (p.Gln313Lys, p.Ile678Leu and p.Ala1001Thr) and one duplication that led to a premature stop codon (p.Asn988Serfs*4). The complete study showing how these mutations affect corticogenesis can be found in Asselin et al., 2020 (see results, article 1), containing information about how these mutations are responsible for the presence of microcephaly, agenesis of corpus callosum and migratory defects using zebrafish and mice as working models. In this study, I contributed to the elucidation of the mechanisms by which KIF21B mutations drive to defective migration.

Adding more information about the importance of KIF21B during human development, an additional missense mutation (p.Ser505Arg) was recently found in another patient with developmental delay and intellectual disability. In this study I performed the experiments demonstrating pathogenicity of the variant in neuronal migration, the report can be found in Narayanan et al., 2022 (see results, article 2). As presented in paper 1 (Asselin, et al. 2020), the heterozygous mutation p.Asn988Serfs*4 induced a frameshift that produced a stop codon in exon 20, leading to mRNA decay. This induces a loss of function, with a concomitant haploinsufficiency that is probably not pathogenic in humans, since different *KIF21B* loss of function variants have been reported in populations with no pathologic

development. Therefore, we focused in the missense mutations, where the change of a nucleotide led to the substitution of an amino acid: p.Gln313Lys, p.Ile678Leu and p.Ala1001Thr and the recently found p.Ser505Arg.

We studied in mice the effects of these pathological variants in neuronal migration by *in utero* electroporation of plasmids expressing the mentioned KIF21B missense mutations under the neuronal specific promoter NeuroD. In all the four variants we observed migratory delay induced by the expression of the variants, with different degrees of severity. The more severe phenotype was found with the expression of the mutation p.Ile678Leu, exhibiting neurons arrested permanently at the SVZ/IZ. These experiments highlight the importance of KIF21B in neuronal migration, and establish a link to intellectual disability, a common feature among all the patients with *KIF21B* mutations. This is supported by all the studies where it is shown that mutations linked to cortical malformations and intellectual disability induce defects in neuronal migration, including mutations in proteins like TUBG1 (Poirier, et al. 2013), TUBA1A (Belvindrah et al., 2017), NEDD4L (Broix et al., 2016), to mention some (for reviews see Francis & Cappello, 2021; Romero, et al. 2018). Defects in migration also happen when exposing mouse embryos to experimental paradigms that emulate adverse environmental conditions associated with the development of intellectual disabilities and autism spectrum disorder. These paradigms include the exposition of the embryos to ethanol (Delatour et al., 2019), glucocorticoids (Fukumoto et al., 2009), or hypoxia (Zechel et al., 2005), to mention some.

To further study the cognitive impact of these missense mutations, it can be proposed the establishment of Knock-In mouse lines, expressing the human variants in a heterozygous manner in order to have a model that replicates the conditions happening in the studied patients. A similar approach was used in the study of KIF2A (Gilet, et al. 2019), where they generated a conditional KI mouse that expressed the pathogenic variant p.His321Asp, and observed defects in memory related tasks. In our study, it would be interesting to implement behavioural experiments that can be linked to cognitive skills, like novel object recognition tasks or Y maze, to mention some.

Is interesting to note that there is a variation of phenotypes between the mutations presented in patients showing different degrees of intellectual disability and presenting diverse cortical malformations, like microcephaly or agenesis of corpus callosum. There are cases where it is possible to observe that different mutations of the kinesin produce difference in the severity of the phenotypes, this is the case for example for mutations in KIF11 that lead to different degrees of microcephaly (Ostergaard, et al. 2012), or different missense KIF2A mutations that lead to different phenotypes, such as microcephaly or pachygyria (Poirier, et al. 2013; Cavallini, et al. 2017). These differences are explained by different factors, including diverse defects in structural conformations that can be produced by the mutations and alter the function of the protein, like happens with missense mutations

in KIF21A, where missense mutations induce relief of autoinhibition (Bianchi et al., 2016); in second place, and also related, is how these defects in protein structure affect association to binding partners, like it happens with KIF5A mutations, that increase mitochondria transportation (Baron et al., 2022). In order to have an insight about the pathological mechanisms of *KIF21B* mutations, we investigated if pathogenicity produced by the variants was the result of a dominant negative function or by a gain of function.

1.1 Test of a possible dominant negative function

The dominant negative mechanism means that the expression of the protein abolishes the activity of the WT protein (Herskowitz, 1987), and in the case of the mutations in this study, as they are heterozygous, it made sense to study if they would be inhibiting the function of the WT protein. In this context, we tested the rescue of the possible dominant negative mechanism by co-expression of the WT protein. However, co-electroporation of the mutant versions with the WT KIF21B did not produce rescue of the phenotype, indicating that the effect could not be compensated by the presence of the normal protein.

1.2 *KIF21B* mutations induced a gain of function of the protein

Since we proved that the migratory phenotype was not the result of a dominant negative function, we focused on the alternative, the gain of function, in which the protein potentiates its function or acquires a completely new activity (Wilkie, 1994). One hint that pointed towards a gain of function of the mutant KIF21B versions, was the fact that increased concentration of electroporated WT-KIF21B caused increased migratory delay. Increasing amounts of the protein can produce overactivity of the protein associated to defects in migration.

In the literature, we observed that patients with congenital fibrosis of the extraocular muscles (CFEOM) presented mutations in the regulatory coiled coil (rCC) domain of KIF21A (van der Vaart, et al. 2013), the closest KIF21B relative. rCC was demonstrated to be a hinge that assists conformational changes in the protein, inducing intramolecular interactions between motor and tail domains of KIF21A to produce autoinhibition. Mutations found in rCC of KIF21A responsible for CFEOM abolished kinesin autoinhibition by suppressing interaction between motor and tail domain as demonstrated by structural and biochemical studies (Bianchi et al., 2016; van der Vaart et al., 2013). Interestingly, the rCC domain affected upon KIF21A mutation, also participates in KIF21B autoinhibition, as demonstrated by Van Riel, et al. (2017). Moreover, one of the missense mutations found in the studied patients in this work, is located in the residue 1001 (Ala1001Thr) in the rCC domain, indicative that

autoinhibition could be affected, and as a consequence, the protein would be overactive upon KIF21B mutations.

With the information that rCC domain is required for autoinhibition, I expressed a truncated version of Kif21b missing the rCC domain (Δ rCC) in migrating neurons with the purpose of introducing an overactive Kif21b, unable to induce autoinhibition. As expected, given the relief in autoinhibition hypothesis, defects in migration were induced by the expression of the Kif21b- Δ rCC protein. To further prove that the mutations induce migratory delay by this overactivation, we used an approach where we abolished this suggested overactivation in the mutants. To do this, we produced KIF21B constructs that presented the human mutations, but with the motor domain truncated in order to abolish motility and abrogate the migratory delay. Strikingly, and according to the hypothesis, the expression of these mutant constructs in migrating neurons was unable to induce migratory defects, suggesting like this, that overactivation of KIF21B by relief in autoinhibition is the mechanism inducing defects in migration. Furthermore, as shown in COS-7 cells, mutant versions of KIF21B bound to GFP presented higher speed of movement than the WT, adding evidence to the hypothesis of defective autoinhibition upon pathological mutations.

Although we proved that relief in autoinhibition is most likely the pathological mechanism taking place with the presence of the pathological variants, more experiments can be proposed to strengthen the hypothesis. The more direct evidence can come from structural biology, where we could produce the recombinant KIF21B mutated proteins and research in detail the structure that they adopt using approaches like X-ray crystallography or cryo-EM. Also, by immunoprecipitation experiments we can look at the interaction between domains involved in autoinhibition and search for possible disruptions upon missense mutations. It would be helpful to know more in detail the cargoes binding to KIF21B during neuronal migration, so we can study in different cellular models the transportation of such cargoes upon the mutation of KIF21B.

As it was mentioned in the introduction (Chapter II, section 3.2.1), autoinhibition can be relieved physiologically by post-translational modifications (Espeut, et al. 2008), cargo binding (Soppina, et al. 2014) or a protein partner binding (Bassius, et al. 2007). In that sense, it remains to be discovered the nature of the KIF21B autoinhibition relief at the physiological level. This can be solved by studying the effect of the different KIF21B posttranslational modifications and cargo binding on the structure and motile properties of the kinesin.

As it is known that KIF21B regulates microtubules dynamics (Ghiretti, et al. 2016; Van Riel, et al. 2017), it would be interesting to go deeper into the way that the pathological variants affect MTs growth, pausing or severing using *in vitro* experiments, where we could measure those parameters in isolated MTs and find a role for cytoskeleton stability.

1.3 Relief in auto-inhibition induces pathological outcomes in other kinesins

Besides the mentioned KIF21A, there is compelling evidence that defective kinesins autoinhibition is a mechanism responsible for pathogenesis in many diseases, here I mention some of these kinesins as examples:

KIF7, from the kinesin-4 family (including KIF21A and KIF21B) is an immotile kinesin that binds to microtubules in ciliary tips, and it is associated to the Sonic hedgehog (Shh) signalling pathway (Bangs & Anderson, 2017). Patients presenting with KIF7 mutations show ciliopathies, including Bardet-Biedl, Joubert and hydrolethrus syndromes (Putoux et al., 2011; Ali et al., 2012; Barakeh et al., 2015). It was shown that the mutation p.Gln1127Pro of KIF7, relieves autoinhibition, and in this case, the kinesin binds more abundantly to cytosolic and axonemal microtubules, despite mostly binding to ciliary tips in WT conditions. Differently from its relatives KIF21A and KIF21B, mutations in rCC are not enough to relieve autoinhibition in KIF7 (Lynne Blasius et al., 2021).

Increasing evidence is observed in Kinesin-1 (KIF5A), for which deleterious mutation of the “IAK” motif in the C-terminal domain is presented in patients with Amyotrophic lateral sclerosis (ALS), a neurodegenerative disease that produces motoneuron damage. The authors showed that mutated KIF5A presented a higher number of kinesins binding to the microtubules and increased anterograde mitochondria velocity *in vitro*, accumulating at the distal part of the axon (Baron et al., 2022).

In the motor domain of the *KIF1A* gene, 10 missense mutations were found in patients presenting with Hereditary spastic paraplegia (SPG), a disease related to motor neurons defects. These mutations were tested in *C. elegans*, using the ortholog Unc-104. Expression of all the mentioned mutant versions was observed to induce hyper motility of synaptic vesicle precursors, with excessive accumulation of them in the distal part of the axons (Chiba et al., 2019). This was supported by previous studies where KIF1A truncated versions, relieved of autoinhibition presented with hypermotility and excessive microtubules binding in COS-7 cells (Hammond et al., 2009).

Moreover, a KIF22 mutation in the coiled coil domain (p.Val475Gly) observed in a patient with defects in skeletal development, was associated to defective autoinhibition. Since KIF22 is a kinesin that participates in the alignment of chromosomes during mitosis and it has to be inactivated during anaphase, it was seen that both mutant KIF22 and constitutively active KIF22 presented disrupted chromosome segregation during anaphase, as seen in different cell lines (Thompson et al., 2021).

Altogether, there is compelling evidence that autoinhibition is a general mechanism necessary for the correct functioning of many kinesins, and when this is defective, diverse pathological outcomes are produced.

1.4 Study in other neuronal types

Adding to the impact of pyramidal neuronal migration, the study of interneuron migration to the contribution of pathological phenotypes is something that would be very interesting to see in the future. The importance of dysfunctional interneuron migration in the development of cortical malformations and intellectual disability has been studied in multiple investigations (see review Yang et al., 2022). This topic can be addressed by the IUE of the variants in ganglionic eminences or also with a KI model where we can study interneuron migration by the presence of fluorescent markers. Interestingly, in our data, we show that physiologically *Kif21b* regulates migration in interneurons, as shown in our results in article 3, where we depleted the expression of *Kif21b* (Rivera Alvarez, et al. in preparation). The effects in migration in other neuronal types should not be neglected and expression of the mutants in other systems like cerebellar neurons or adult migratory neurons can be informative about a general or a more restricted pathological role of KIF21B variants in different migrating neurons.

1.5 Contribution of this work to the knowledge of kinesins in cortex development

Our study reported for the first time that *KIF21B* is a locus of susceptibility for cortical malformations and intellectual disability in humans. In contrast to other studies that reported the effect of KIF21B abnormalities in human health (Goris, et al. 2010; Kreft, et al. 2014), we showed experimental *in vivo* evidence that supports our discoveries. An advantage of the mouse model we used, is that the basic elements of corticogenesis are recapitulated in mammals, and the events taking place in mouse provide information about what could be happening in human. Regarding the mechanism, KIF21B can be added as one of the many kinesins for which autoinhibition disruption induces pathological outcomes.

2. *Kif21b* in physiological condition – a detailed glance at migration

For this second part of the work, we depleted the expression of *Kif21b* specifically in neurons. In order to do that, we introduced a shRNA that was inducible under the expression of a CRE recombinase with the neuronal promoter *NeuroD*. We observed that the silencing of *Kif21b* induces delay in migration of pyramidal neurons in the SVZ/IZ. To exclude side effects inducing cell death or specification defects, we analysed the expression of markers like caspase 3 and *Cux1*, and we didn't observed differences in those aspects.

Compensatory effects by the paralogue *Kif21a* can be discarded, because despite finding the presence of *Kif21a* in our mass spectrometry analysis of *Kif21b* protein partners, co-electroporation experiments of the *Kif21b* KD with *Kif21a* do not show any rescue to migratory phenotype. In addition to this,

different studies are not able to find Kif21a as a heterodimer with Kif21b (Marszalek et al., 1999; van Riel et al., 2017).

2.1 Kif21b participates in locomotion, but not in the multipolar-bipolar transition

The aim of this part of the study was to know in detail how Kif21b participates in neuronal migration, and to describe at what step it is required for pyramidal neuronal migration. First, we studied the role of Kif21b in multipolar to bipolar transition. Soon after neurons start to migrate, they acquire a multipolar shape at the upper SVZ and lower IZ, and then they need to transition to a bipolar shape (Noctor et al., 2004). We investigated the possibility that Kif21b had an influence in this process. However, after analysing the neurons that pass from multipolar to bipolar, or the number of multipolar cells, we were not able to account for differences. Thus, we looked at the locomotion phase.

Locomotion is a complex phase in which many sequential changes take place to drive the neurons to the cortical plate. Considering this, we analysed by time-lapse microscopy parameters related to the neuronal movement and morphology that could account for defects related to migration. Remarkably, most of these parameters are affected under depletion of Kif21b, with neurons showing slower velocity, increased and longer pauses and showing defects on the leading process that produces multiple and shorter branches.

This differentiates Kif21b from other kinesins, for example KIF2A (Gilet, et al. 2020), KIF1A (Carabalona, et al. 2016), KIF20B (Sapir, et al. 2013) and kinesin 6 (Falkinar, et al. 2013), that are involved in the multipolar bipolar transition. However, similarly to our study, *KifC1* depletion induced decrease in locomotor velocity, which was related to defects in microtubules dynamics. Authors observed by fluorescent EB3 that microtubules in control conditions grow mostly in direction to the trailing process, but upon *KifC1* depletion, growth of microtubules changed in direction of the leading process, also altering nucleus rotation, as it was seen by the expression of the nuclear histone HP1 β tagged with RFP (Muralidharan, et al. 2022). Nucleus dynamics and microtubules growth is then an interesting topic to address in future experiments.

In contrast to what we saw with Kif21b, depletion of *Kif11* (Kinesin 5) by siRNA expression induced an increase in migration velocity due to shorter pauses duration, with an increased length of the leading process. Accordingly, overexpression of Kif11 produced slower migration and shorter leading process (Falkinar, et al. 2011). In the case of *Kif13b* depletion, it is possible to see defects in polarization, with shorter neurites during migration, however, further migratory mechanisms were not investigated (Yu, et al. 2020). Altogether, these studies can provide a link between velocity and leading process morphology, due to mechanisms that possibly involve microtubules, but that require further research to explain the different phenotypes.

Kif21b participation in velocity regulation could converge with other mechanisms that also regulate this property. Cdk5 is an important node for pyramidal neuron migration regulation, exerting a role in velocity modulation through the phosphorylation of targets like Dcx, Lis1 and p27, regulating also swelling formation (Nishimura, et al. 2014). Additionally, p27 regulates microtubules polymerization and actin contraction in migratory interneurons (Godin, et al. 2012), and Kif21b being also a regulator of actin contraction (see article 3, Rivera Alvarez, in preparation; and section 2.5 of discussion), it could exert a complementary role with p27.

Regarding cell adhesions, it was observed in different studies that different adhesion molecules are important regulators of velocity and pauses during pyramidal radial migration, including Connexin 43 (Elias, et al. 2007), cadherins 2 and 4 (Martinez-Garay, et al. 2016), N-cadherin (Barnat, et al. 2017) and protocadherins DCHS1-FAT4 (Klaus, et al. 2019). It is known that cell adhesions proper localization is mediated by kinesins (Mary et al., 2002; Teng et al., 2005), and it will be interesting to study the role of Kif21b regarding this. This topic will be further expanded in section 2.3 of this discussion.

The importance of Kif21b during interneuron migration is something that we started to address and so far, we have proved that depletion of *Kif21b* induces slower velocity, but that's a topic that should be investigate with more details and mechanisms in future studies, in order to establish common and differential mechanisms of function between pyramidal neurons and interneurons. In this regard, work with Kif2a was studied also for interneuron migration (Broix, et al. 2018). It was seen that electroporation of ganglionic eminences with a pathological variant of Kif2a induced slower velocity of and misdirection in the migratory route. Additionally, interneurons expressing the mutant kinesin showed decreased number and amplitude of nucleokinesis. In line with this, migration velocity was boosted after overexpression of the WT Kif2a (Broix, et al. 2018).

With the presented data, we can conclude then, that Kif21b regulates locomotion in its different steps and morphological parameters.

2.2 Kif21b motility does not participate in radial migration

Kif21b is a protein with different functions dependent and independent of transport, and with different domains that regulate its activity (Marszalek, et al. 1999; Labonté et al., 2014; van Riel et al., 2017). To start the elucidation of the intricate puzzle about how Kif21b regulates migration, we expressed truncated Kif21b versions in order to perform complementation experiments and see what functions of the protein were participating in migration

First, we completely rescued the phenotype with two imotile versions of Kif21b, one with the truncated ATPase domain ($\Delta 84-97$), and one with a mutation in the residue p.Thr96Asn that induces immobility on the kinesin. With this result we can think that the functions that depend on cargo

transportation are not determinant for Kif21b participation in neuronal migration. Hence, we discard the involvement of the transportation of cargoes like the BDNF receptor TrkB and the glutamate receptor GluN2B, both of them regulating neuronal locomotion (Nakamuta, et al. 2011; Jiang, et al. 2015), and both of them transported by Kif21b (Ghiretti, et al. 2016; Gromova, et al. 2018).

The same as the motility function, the truncated WD40 (Δ 1308-1639) domain fully rescues the migration phenotype, meaning that this domain does not participate in migration. About the function of this domain, it has been hypothesized its interaction with cargoes (Marszalek et al., 1999), although this has not been found experimental evidence. In support of the cargo interaction function of this domain, it has been reported that WD40 participates as one of the top protein-protein interacting domains in the eucaryotic genome (Stirnimann et al., 2010; Xu & Min, 2011), and this could account for many different interactions happening during transportation. Adding importance to this domain, as studied by Masucci, et al (2021), the C- terminal part of Kif21b participates by switching the direction of motility in antiparallel microtubules filaments (Masucci, et al. 2021), and assists to the binding of Kif21b to the plus ends of the microtubules (Van Riel, et al. 2017). However, as seen in our rescue experiment, these potential interactions and functions are not necessary for the neuron to successfully migrate.

Altogether, this research demonstrated that Kif21b motility is not essential for neuronal migration. This could be also true for other kinesins, since motility and transport, are not experimentally shown as mechanisms that regulate migration in those cases (Sapir, et al. 2013; Falinkar, et al. 2011; Falnikar, et al. 2013; Caraballona, et al. 2016). Since regulation of multipolar to bipolar shape depends on the re-organization of the cytoskeleton (Kawaguchi, et al. 2006; Ip, et al. 2012), it is possible that at least some of the kinesins that participate in this process, do it by remodelling the microtubules or actin networks. Additionally, one recent example of a kinesin that participates in radial migration by the regulation of microtubules dynamics is the previously mentioned KIFC1, which is important for locomotion velocity and direction (Muralidharan, et al. 2022).

Therefore, motility is a topic that will be important to address for future studies with kinesins and it will be also interesting to revisit previously studied kinesins in order to provide more clarity about how these proteins exert different functions from the canonical molecular motor action.

2.3 Implication of the motor domain in migration

In contrast to the complete rescue with the immotile (p.Thr96Asn and Kif21b- Δ ATP) versions and the Kif21b- Δ WD40, the truncated Kif21b- Δ Motor domain produced a partial rescue of the migration phenotype. Interestingly, this means that a property of the motor domain that does not require kinesin

motility, is required for neurons to undergo locomotion. This also means that even at some degree, there is a property of migration that can be rescued by the tail of the kinesin, more likely by the coiled coil domain, since the WD40 domain was seen dispensable for migration.

Microtubules binding domains are contained in the residues 1-660 for the motor domain and from the residues 669 to 1163 for the CC domain (Van Riel, et al; 2017). Then, it is interesting to notice that despite the fact that both motor and CC domains possess microtubules binding properties (Ghiretti, et al. 2016; Van Riel, et al. 2017), they probably exert different, yet complementary functions during radial migration.

To dissect in detail the characteristics controlled by each part of the protein, we performed time-lapse microscopy of organotypic cultures depleted of *Kif21b* by expression of an inducible shRNA and rescue by the co-expression of the Kif21b- Δ Motor domain (Δ MD). After analysing different parameters, we realized that there is a partial rescue of the velocity of the migrating neurons that at least can be explained by the recovery of the velocity index (velocity without pauses), but not in the number and time of pauses, which are dependent on the Kif21b motor domain. In the present section I will present hypothesis that can explain this phenomenon.

First, the co-expression of Δ MD fails to rescue pauses, and moreover, neurons show an increase in the number and duration of pauses, meaning that the motor domain possesses a faculty that prevents pausing, but the rest of the protein by itself might increase time of neuronal stops and promote the pausing, explaining the lack of complete rescue.

Second, to explain the failure in the number of pauses is the possibility that the motor domain is necessary to stabilize the bipolar morphology, and when it is not present, the neuron fails to maintain a bipolar shape, as we observe when depleting *Kif21b*. It was shown previously when knocking out the protein LKB1 and its downstream targets SAD1/2, that migration was arrested in IZ by perturbing neuronal bipolar morphology (Barnes, et al. 2007); by knock down of the microtubules plus -end binding protein CLASP2, with similar effects on neuronal polarity (Dillon, et al. 2017); and more directly associated to kinesins, KD of *Kif20b* produces defects in polarization by mis regulation of the protein Shootin1 (Sapir, et al. 2013). At this moment we cannot conclude about this morphology issue, but experiments are being performed to test this hypothesis by quantifying the aberrant transitions from bipolar to multipolar during locomotion upon MT overexpression.

Third, looking at nucleokinesis, we should remember that radially migrating neurons travel in a saltatory fashion, where the nucleus jumps forward at the final step of each cycle of movement. *Kif21b* depleted neurons produce shorter jumps that take longer to be produced (see article 3, Rivera Alvarez, et al. in preparation). Preliminary time lapse analysis in rescue experiment with the Δ MD show recovery of the duration of nucleokinesis, but not the distance of movement in each cycle. One of the mechanisms regulating nucleokinesis and pauses are cell adhesions, which cadherins 2 and 4 cKO, for

example, were shown to induce shorter nucleokinesis (Martinez-Garay, et al. 2016), and in the case of *Htt* KD, it was seen an increased number of pauses during migration due to defects in N-cadherin distribution (Barnat, et al. 2017). Decrease in the levels of the cell adhesion protein Cx43 also induces shorter nucleokinesis (Elias, et al. 2017). Besides all these data showing the importance of cell adhesions in nucleokinesis, there is data showing that in other systems, kinesins regulate cell junctions positioning. This is the case for Kinesin 1, that regulates positioning of N-cadherin in the plasma membrane, in an association to microtubules close to the cell cortex in fibroblasts (Mary et al., 2002). Also, the heterotrimeric KIF3 participates in localization of N-cadherin in the plasma membrane in neuroepithelial cells (Teng et al., 2005). Following this logic, we could suggest the idea that cell adhesions could be stabilized by Kif21b during nucleokinesis, and the motor domain participates in this stabilization. Then, rescuing the *Kif21b* depletion by the expression of N-cadherin (for example) can be proposed to rescue nucleokinesis and pauses during migration.

Fourth, another hypothesis is related to how nucleokinesis is regulated by motor proteins. Knowing that motor proteins (dynein, kinesin-1, myosin-II) are recruited to the nucleus to perform nucleokinesis (Tsai, et al. 2007; Goncalves, et al; 2020), it is possible to speculate that the tail domain is needed to stabilize interactions of the molecular motors with the nucleus during a defined length of time, but the motor domain is required to assist the execution of this movement in an efficient manner. By this means, the rescue with the Δ MD explains the recovery of the time spent in nucleokinesis (correct attachment to the motile machinery) and the fail to rescue distances travelled by the nucleus (incorrect execution of the movement).

Integrating the data of pausing, we could think that the motor domain, absent in the rescue experiment, is necessary to recruit / uncouple the molecular motors machinery, and then, when trying to rescue with the Δ MD, those events are failed and take longer to be produced, pausing the neuron at these points. With the results that will be discussed in further sections, we can hypothesize that the actomyosin network, involving myosins, could be involved in these mechanisms and not necessarily the microtubules motor machinery, which would involve proteins like dynein and kinesin-1 (Tsai, et al. 2007; Goncalves, et al. 2020).

We could have an indirect insight into this nuclear-molecular motors machinery function by studying the effect of the rescue with the Δ MD during nuclear dynamics in time-lapse microscopy by following the expression of a nuclear marker, like the histone HP1 β , fluorescently tagged molecular motors (dynein, kinesin-1 and myosin), and endogenously tagged Kif21b, in order to follow the dynamic of the three of them during nucleokinesis.

To further test microtubules dependent and independent functions, we can perform migration rescue experiments with drugs that allow us to interfere with microtubules dynamics. Another way would be to test the full-length protein missing the microtubules binding regions contained in the motor domain,

CC2 and linker domains and study the parameters that are able to be rescued. An informative experiment about microtubules dynamics would be to study the microtubules growth by expression of a fluorescent version of the plus-end MAP EB3, in order to follow up the growth of microtubules in migrating neurons either in *Kif21b* depleted and rescue conditions.

Hence, in this study we elucidated the differential role that the motor domain of the kinesin Kif21b exerts during migration, and the specific mechanisms are remaining to be known.

2.4 Kif21b is an actin binding protein

After knowing how the different domains participate in migration, we further investigated Kif21b partners in embryonic cortex to get a clue about the cellular mechanisms in which it participates. One of the most interesting discoveries we made in this work was that main interacting partners of Kif21b are different actin isoforms. This fact encouraged us to test by different means the nature of this interaction with actin and elucidate if direct binding was taking place.

Binding of kinesins with actin was seen previously just in the case of the plant specific kinesin GhKCH1, which interacts with actin through its N-terminal region containing Calponin Homology (CH) domains (Preuss et al., 2004); and in the case of DdKin5, a *Dictyostelium discoideum* specific kinesin that was shown to bind actin through its C-terminal domain (Iwai et al., 2004). However, to our knowledge, this is the first time that a kinesin was seen to interact with the actin cytoskeleton in neurons and in general in mammals.

With that information in mind, we decided to investigate deep into the interaction of Kif21b with actin and the actin related mechanisms in which Kif21b could be implicated. We were able to prove actin interaction through different experimental approaches. First, through verification by western blot of immunoprecipitated Kif21b with actin, which was shown to be specific. Second, we looked by confocal microscopy the presence of Kif21b particles in the peripheral region of the growth cone, a structure enriched in actin filaments, and at a more detailed level, by Single Molecule Localization Microscopy (SMLM) we found that Kif21b particles were interacting with the actin filaments in some cases and in some other cases were detached, suggesting a possible dynamic interaction that is regulated by different conformations or by other proteins. This is an area of study that we could further investigate by using fluorescently tagged Kif21b and looking at different patterns of binding/unbinding to the actin filaments.

To definitively prove that Kif21b is an actin binding protein, we produced the recombinant Kif21b in BHK mammalian cells, and isolated it in order to study its interaction with F-actin. We proved that Kif21b co-sediments with actin filaments, indicating direct interaction. Unfortunately, we could not

prove the domain by which Kif21b binds actin, as we tried to test by co-immunoprecipitation of actin with different Kif21b truncated constructs expressed in HEK-239 cells. We observed a high variability in the amount of actin bound to different domains (data not shown), and therefore we were unable to raise a conclusion about this point. However, we hypothesize that these levels in variability in actin interaction might come from structural requirements from the protein that cannot be reproduced with the fragments of the protein. To test this point, experiments of Cryo-EM would be helpful to determine the structure of the protein and determine the conformations that interacts with actin.

A phenotype that we observed in *Kif21b* depleted neurons, and we could relate to actin dysfunction is the abnormal overbranching of the leading process. This overbranching phenotype is frequent when depleting or overexpressing actin related proteins in migrating pyramidal neurons. The overexpression of Nyap2, that participates in signalling inducing actin nucleation, produced overbranched locomoting neurons (Wang, et al. 2019); when knocking down the Rho activator PlexinB2, shorter processes are seen in migrating neurons (Azarelli, et al. 2014); overexpression of non-phosphorylatable or pseudo-phosphorylated cofilin in serine 3 also produces this overbranched phenotype during locomotion (Chan, et al. 2019); additionally, MACF1 depletion produces defects in locomotion associated to the protrusion of multiple leading processes (Ka, et al. 2014); furthermore, the depletion of the protein Connexin 43 (Cx43) induces overbranching with an associated decrease in actin levels (Elias, et al. 2007).

This study is the first in demonstrate that in mammals, a kinesin is able to interact with the actin cytoskeleton, which opens the field to many interesting questions about the nature of these interaction.

2.5 Kif21b regulates actin dynamics in migrating neurons

Interestingly, in the rescue with the Δ MD we did not see any recovery on the branching phenotype, indicating that the motor domain is required to stabilize the morphology of the leading process. One line of evidence that supports that this branching phenotype could be related to actin dysfunction, is the fact that the incubation of *Kif21b* depleted neurons with the myosin-II inhibitor blebbistatin produced recovery in the morphology of the leading process. Similarly, in a previous study made in interneurons, it was seen that overactivation of contractile activity induced defective branching during migration and blebbistatin incubation rescued this phenotype (Godin, et al. 2012).

Myosin activity is also important for leading process morphology, as it was shown by Ju, et al (2014), where they demonstrated that knock down of Myosin X induced morphological defects on the leading process. Later on, another study showed that KIF13B interacts with myosin X, in an interaction that mediates migration downstream of the Netrin-1 signalling pathway (Yu et al., 2020). The precise mechanism by which this myosin dysfunction affects migration is not clear.

Knowing that Kif21b interacts with actin, we decided to study the effect of *Kif21b* depletion on actin dynamics in radially migrating neurons. The study of actin cytoskeleton in pyramidal neurons has been delimited to the depletion or overexpression of actin related proteins (see table 1), but direct evidence of actin dynamics *in vivo* has not been addressed. Actin dynamics *in vivo* was previously studied just in interneurons by the expression of the F-actin binding peptide LifeAct coupled to GFP (Bellion, et al. 2005) and in cerebellar granular neurons by the expression of the F-actin binding protein Utrophin coupled to GFP (Solecki, et al. 2009). Therefore, how actin is dynamically regulated *in vivo* during the migratory cycle of pyramidal neurons is something that was addressed for the first time in this study. In order to study actin dynamics, we expressed the actin probe LifeAct coupled to the fluorescent protein Ruby (LifeAct-Ruby) in radially migrating neurons, and in contrast to interneurons, where cyclic changes happen at the rear of the migrating nucleus, we saw cyclic changes that corresponded to an increase in fluorescence upon engorgement of the swelling in the leading process, with a corresponding drop in fluorescence after nucleokinesis took place. This would be more similar to actin cycles observed in migrating cerebellar neurons (Solecki, et al. 2009). By endogenously tagging actin with GFP by a CRISPR/Cas9 knock-in approach, we were able to label actin dynamics in migrating neurons and observe an additional cyclic rise and drop in fluorescence in the trailing process of the migrating neuron, indicating that pyramidal neurons also require this actin reorganization in the trailing process to impulse nucleokinesis, as in interneurons.

Using the LifeAct-Ruby experimental approach, we co-expressed inducible shRNA for *Kif21b* in addition to LifeAct-Ruby and observed that the cyclic changes in actin dynamics were disrupted, with a failure in the drop of F-actin signal after nucleokinesis, in contrast to what happens with control neurons. As the cyclic changes in actin fluorescence levels are co-related to myosin II phosphorylation (Martini & Valdeolmillos, 2010), we can conclude that *Kif21b* depletion impairs myosin activity. In interneurons, it has been shown that these abnormal increases in LifeAct levels are associated with over-activity of myosin and it can they be counteracted by the incubation with myosin inhibitors (Godin et al., 2012; Silva et al., 2018).

Suggesting a role of Kif21b regulating migration through actomyosin contraction, is the fact that different myosins were found among the other Kif21b interacting partners in the mass spectrometry analysis, a discovery that was also seen by Gromova, et al (2022), where they find Kif21b interaction with Myosin V. Myosins interaction was brought to our interest since it contributes to neuronal nucleokinesis (Bellion, et al. 2005; Tsai, et al. 2007, Martini & Valdeolmillos, 2010) and branching during migration (Godin, et al. 2012).

Regarding visualization of actin contraction in the leading process, in our study, the actin probe LifeAct was not sensitive enough to detect consistent levels of fluorescence in the leading process, but we can

speculate that myosin disruption can account as one of the mechanisms leading to overbranching in *Kif21b* depleted neurons, as explained before with the effect that blebbistatin had in the branching phenotype. We can further study this branching phenotype with endogenously tagged actin, that would account for more stable levels of actin fluorescence.

Another function of Kif21b related to myosins was shown in the study by Gromova, et al (2022), where they discovered that in hippocampal neurons, Kif21b binding to myosin V is relevant for actin dynamics and found that *Kif21b* KO neurons are unable to mobilize actin in dendritic spines at the same level than the WT neurons, as seen in FRAP experiments where actin fluorescence in dendrites of KO neurons failed to reach normal levels at the same time than the control. They describe the motor domain as the region of Kif21b participating in interaction with Myosin V (Gromova, et al. 2022). Importantly, this same region is a microtubule binding domain (Ghiretti, et al. 2016; Van Riel, et al. 2017). It can be possible that this interaction presents an overlap with the microtubule cytoskeleton or alternatively, it can represent binding in an exclusive manner, exerting specific functions to actomyosin cytoskeleton. One experiment that could clarify this issue would be the fluorescent labelling in neurons of myosin V, actin and Kif2b full length or Kif21b-Motor domain in order to see if Kif21b is present in co-localization with both elements or if it is present in different pools.

Also related to the leading process, Myosin X exerts a role in regulation orientation of the leading process, and when depleted, the leading process presents shorter size and crooked morphology in an effect related to the N-cadherin localization (Lai, et al. 2015). Tsai et al (2007) discovered that inhibition of neuronal myosin IIB by RNAi, produces increase in the number of branches in the leading process. In contrast, in our experimental conditions, we saw that incubation with the myosin inhibitor blebbistatin at a concentration of 3 μ M induced decrease in branching in the *Kif21b* depleted condition. The difference can be explained by the fact that they acutely depleted myosin, while in our conditions, we are incubating with an inhibitor, that probably does not completely block the activity of the protein.

We can conclude with our observations that Kif21b exerts a role on actin dynamics during pyramidal neuronal migration, at least regulating actomyosin contraction to keep stable the morphology of the leading process. However, the complete mechanisms are still remaning to be discovered.

2.6 Other roles of Kif21b regulating actin cytoskeleton dynamics

We were interested in the study of other mechanisms by which Kif21b could be altering actin dynamics. It is known that in migrating pyramidal neurons, depletion of proteins related to actin

nucleation (necessary for polymerization start) induce migratory defects, as it happens with the knock down of WAVE (Xie, et al. 2013) or Ena/VASP (Yoshinaga, et al. 2012), both of them inducing aberrant multipolar morphology; or cKO of the Arpc2 subunit of the Arp 2/3 complex, that produces a decrease in locomotor velocity (Wang, et al. 2014), similarly to what we see with *Kif21b* depletion. Therefore, it is interesting to investigate actin polymerization dynamics regulation by Kif21b.

Adding to this, we know that cycles of actin polymerization/ depolymerization are important for actomyosin contraction, a phenotype we see affected upon *Kif21b* deficiency. It was shown by *in vitro* studies in other systems that increase in polymerization precedes contractile activity by myosin light chain (Goeckeler & Wysolmerski, 1995), and that contraction of myosin IIA requires assembly of networks by actin polymerization through formins participation and crosslinking by Filamin A (Luo et al., 2013).

In order to have an insight into how the actin polymerization rates can be regulated by Kif21b, first we observed by western blot that the total actin concentration is increased in KO brains in comparison to WT brains, and the ratio G/F actin tends towards an increase in the amount in G actin. This suggested the Kif21b deficiency affects production of actin filaments, and somehow, actin accumulates in its monomeric form. This result goes in line with our discovery about Kif21b regulation on actin nucleation *in vitro*, where incubation of monomeric actin with recombinant Kif21b increases the number of nucleated filaments in comparison with the control without recombinant Kif21b. This result is interesting, because besides having a direct interaction with actin, we show that Kif21b also possesses a direct effect on actin dynamics.

Additionally, the data of the paper of Gromova, et al (2022), show that over-expression of Kif21b in COS-7 cells induces faster growing of actin filaments, labelled by LifeAct, in this case, supporting the role of Kif21b as a positive regulator of actin polymerization.

More experiments are being performed in order to study how Kif21b regulates actin filament polymerization. Among them, we are studying *in vitro* by TIRF microscopy the rates of actin polymerization in presence or absence of the recombinant Kif21b. In light of the obtained results, we expect that Kif21b exerts a positive role on actin polymerization. It will be interesting to see additional effects on actin filaments, such as bundling, branching or crosslinking. On the other hand, there might be indirect effects of Kif21b in the actin dynamics, which can be studied by looking at actin polymerization using cell extracts with or without Kif21b (KO) and determining filament growth, branching or crosslinking by looking at actin dynamics *in vitro*.

Recently, another kinesin, KIFC1, was related to actin polymerization in mouse oocytes. It was seen to be involved in the spindle positioning and chromosome alignment during meiosis through regulation of actin nucleating proteins. The authors observed that upon KIFC1 depletion, actin nucleators formin 2 and Arp 2/3 are no longer in the spindle, where they normally are regulating spindle migration (Shan

et al., 2022). Interestingly, KIFC1 also regulates radial migration, and the study by Muralidharan, et al (2022) related to microtubule defects the decrease in velocity and faulty direction of the leading process during locomotion, but they did not report at actin dynamics, which probably are also affected.

The evidence provided in this study indicate that Kif21b has a direct effect on actin dynamics, at least promoting nucleation.

2.7. Hypothesized microtubules actin crosslink

Kif21b possesses activities that regulate microtubule dynamics, even if in this study we focused on a phenotype that is dependent on a novel discovered actin interaction, we cannot discard that some of the characteristics of the migratory delay depend on defects in microtubules dynamics. A recent study described that the ortholog of Kif21b in *C. elegans*, KLP-12, binds to both lattice and plus ends through an interaction with the motor domain (Taguchi et al., 2022), and it was previously studied that Kif21b binds to the plus-end of the microtubules, inducing a pausing activity on the growth of the filament (Van, Riel, et al. 2017).

Considering that Kif21b is associated to the plus ends of microtubules, and that plus end binding proteins are frequently associated as actin-microtubules crosslinkers (Alkemade et al., 2022), this could be an interesting field of study regarding Kif21b function. To determine the possible function of Kif21b as an actin-microtubules crosslinker, we could label in neurons the three elements (Kif21b, actin and microtubules) to perform super resolution microscopy and elucidate if there is co-localization. Additionally, by time-lapse microscopy, it would be possible to follow the localization of fluorescently tagged Kif21b to study how these interactions with actin and microtubules are regulated in time, and study pools of Kif21b binding specifically to actin, microtubules or both.

One of the most important regions of actin-microtubules crosslinking is the cell cortex, which in GnRH neurons was shown to be important for locomotion. I was seen that the forward translocation of the microtubules in the leading process induce protrusion of this part of the cell and regulates neuronal velocity (Hutchins & Wray, 2014). This regulation in velocity is one of the possible mechanisms that could also explain the decrease in velocity in depleted *Kif21b* neurons. We could study this aspect by the introduction of a microtubule fluorescent probe, such as SiR tubulin or by expression of tdEos tubulin, which when expressed in the cell can be photoconverted to visualize the microtubules dynamics, as it was used by Muralidharan, et al (2022).

It would be interesting to elucidate a cytoskeleton crosslinking in an autonomous way or mediated by a partner. For crosslinking mediated by other proteins, we can propose drebrin, one of the partners of Kif21b that we found in our mass spect analysis and previously implicated as a microtubules-actin

crosslinker (Geraldo et al., 2008). In different migrating neuronal types, drebrin was shown to play an important regulatory role. In migrating neuroblasts from the rostral migratory stream, drebrin KD induces decrease in velocity and overbranching (Sonego et al., 2015); drebrin KD in cerebellar granular neurons affects migration by affecting directionality and distance travelled (Trivedi et al., 2014), and finally, in pyramidal migrating neurons, Drebrin-like protein, a member of the drebrin family, is involved in migration by regulating polarity of migrating pyramidal neurons (Inoue, et al. 2019). All of these phenotypes are encouraging to look for a possible interaction of Kif21b with drebrin and study if this is relevant for neuronal migration.

Then, the study of the role of Kif21b in MTs during pyramidal neuronal migration is promising and should be addressed.

2.8. Summary

To summarize, this work provided different novelties that establish how future studies about kinesins roles during migration can be performed, among our most important discoveries, we elucidated the next:

- 1) Detailed definition of the stages of locomotion in which Kif21b participates.
- 2) Investigation of the different functional domains required for Kif21b mediated locomotion, discovering that kinesin motility is dispensable for migration.
- 3) By discovering Kif21b binding to actin, we elucidated a previously unseen interaction of the actin cytoskeleton to kinesins, which are normally associated to microtubules.
- 4) Described for the first time actin dynamics during pyramidal neuron migration.
- 5) Observed a regulatory function of Kif21b on actomyosin contraction.

3. General conclusion

With this work we were able to elucidate the mechanisms by which Kif21b regulates neuronal migration in disease and health. On one hand, we realized that excessive activity by pathological Kif21b variants induces defects that delay migration, but on the other hand, depleting the levels of *Kif21b* produce the same effect, with a defective migration. Therefore, a balance in the activity of Kif21b is necessary for correct neuronal migration.

BIBLIOGRAPHY

- Abe, P., Molnár, Z., Tzeng, Y. S., Lai, D. M., Arnold, S. J., & Stumm, R. (2015). Intermediate progenitors facilitate intracortical progression of thalamocortical axons and interneurons through CXCL12 chemokine signaling. *Journal of Neuroscience*, 35(38), 13053–13063. <https://doi.org/10.1523/JNEUROSCI.1488-15.2015>
- Adams, G., López, M. P., Cartagena-Rivera, A. X., & Waterman, C. M. (2021). Survey of cancer cell anatomy in nonadhesive confinement reveals a role for filamin-A and fascin-1 in leader bleb-based migration. *Molecular Biology of the Cell*, 32(18), 1772–1791. <https://doi.org/10.1091/mbc.e21-04-0174>
- Akhmanova, A., & Hammer, J. A. (2010). Linking molecular motors to membrane cargo. In *Current Opinion in Cell Biology* (Vol. 22, Issue 4, pp. 479–487). <https://doi.org/10.1016/j.ceb.2010.04.008>
- Akhmanova, A., Hoogenraad, C. C., Drabek, K., Stepanova, T., Dortland, B., Verkerk, T., Vermeulen, W., Burgering, B. M., de Zeeuw, C. I., Grosveld, F., & Galjart, N. (2001). CLASPs Are CLIP-115 and-170 Associating Proteins Involved in the Regional Regulation of Microtubule Dynamics in Motile Fibroblasts. In *Cell* (Vol. 104).
- Akhmanova, A., & Steinmetz, M. O. (2015). Control of microtubule organization and dynamics: Two ends in the limelight. In *Nature Reviews Molecular Cell Biology* (Vol. 16, Issue 12, pp. 711–726). Nature Publishing Group. <https://doi.org/10.1038/nrm4084>
- Akhshi, T. K., Wernike, D., & Piekny, A. (2014). Microtubules and actin crosstalk in cell migration and division. In *Cytoskeleton* (Vol. 71, Issue 1, pp. 1–23). <https://doi.org/10.1002/cm.21150>
- Akkaya, C., Atak, D., Kamacioglu, A., Akarlar, B. A., Guner, G., Bayam, E., Taskin, A. C., Ozlu, N., & Ince-Dunn, G. (2021). Roles of developmentally regulated KIF2A alternative isoforms in cortical neuron migration and differentiation. *Development (Cambridge)*, 148(4). <https://doi.org/10.1242/dev.192674>
- Ali, B. R., Silhavy, J. L., Akawi, N. A., Gleeson, J. G., & Al-Gazali, L. (2012). A mutation in KIF7 is responsible for the autosomal recessive syndrome of macrocephaly, multiple epiphyseal dysplasia and distinctive facial appearance. *Orphanet Journal of Rare Diseases*, 7(1). <https://doi.org/10.1186/1750-1172-7-27>
- Alkemade, C., Wierenga, H., Volkov, V. A., Preciado López, M., Akhmanova, A., Rein Ten Wolde, P., Dogterom, M., Koenderink, G. H., & Goldman, Y. E. (2022). Cross-linkers at growing microtubule ends generate forces that drive actin transport. *PNAS*. <https://doi.org/10.1073/pnas>
- Alkuraya, F. S., Cai, X., Emery, C., Mochida, G. H., Al-Dosari, M. S., Felie, J. M., Hill, R. S., Barry, B. J., Partlow, J. N., Gascon, G. G., Kentab, A., Jan, M., Shaheen, R., Feng, Y., & Walsh, C. A. (2011). Human mutations in NDE1 cause extreme microcephaly with lissencephaly. *American Journal of Human Genetics*, 88(5), 536–547. <https://doi.org/10.1016/j.ajhg.2011.04.003>
- Allendoerfer, K. L., & Shatz, C. J. (1994). The subplate, a transient neocortical structure: its role in the development of connections between thalamus and cortex. *Annual Review of Neuroscience*, 17, 185–218. <https://doi.org/10.1146/annurev.ne.17.030194.001153>
- Alsabban, A. H., Morikawa, M., Tanaka, Y., Takei, Y., & Hirokawa, N. (2020a). Kinesin Kif3b mutation reduces NMDAR subunit NR 2A trafficking and causes schizophrenia-like phenotypes in mice . *The EMBO Journal*, 39(1). <https://doi.org/10.15252/emboj.2018101090>

- Alsabban, A. H., Morikawa, M., Tanaka, Y., Takei, Y., & Hirokawa, N. (2020b). Kinesin Kif3b mutation reduces NMDAR subunit NR 2A trafficking and causes schizophrenia-like phenotypes in mice. *The EMBO Journal*, 39(1). <https://doi.org/10.15252/emboj.2018101090>
- Alves, M. M., Burzynski, G., Delalande, J. M., Osinga, J., van der Goot, A., Dolga, A. M., de Graaff, E., Brooks, A. S., Metzger, M., Eisel, U. L. M., Shepherd, I., Eggen, B. J. L., & Hofstra, R. M. W. (2010). KBP interacts with SCG10, linking Goldberg-Shprintzen syndrome to microtubule dynamics and neuronal differentiation. *Human Molecular Genetics*, 19(18), 3642–3651. <https://doi.org/10.1093/hmg/ddq280>
- Anderson, S. A., Eisenstat, D. D., Shi, L., & Rubenstein, J. L. R. (1997). Interneuron Migration from Basal Forebrain to Neocortex: Dependence on Dlx Genes. In *New Series* (Vol. 278, Issue 5337).
- Anderson, S. A., Marín, O., Horn, C., Jennings, K., & Rubenstein, J. L. (2001). Distinct cortical migrations from the medial and lateral ganglionic eminences. *Development (Cambridge, England)*, 128(3), 353–363. <https://doi.org/10.1242/dev.128.3.353>
- Angevine, J., & Sidman, R. (1961). Autoradiographic Study of Cell Migration during Histogenesis of Cerebral Cortex in the Mouse. *Nature*.
- Antón, Z., Weijman, J. F., Williams, C., R Moody, E. R., Mantell, J., Yip, Y. Y., Cross, J. A., Williams, T. A., Steiner, R. A., Crump, M. P., Woolfson, D. N., & Dodding, M. P. (2021). Molecular mechanism for kinesin-1 direct membrane recognition. In *Sci. Adv* (Vol. 7). <https://www.science.org>
- Arimura, N., Kimura, T., Nakamuta, S., Taya, S., Funahashi, Y., Hattori, A., Shimada, A., Ménager, C., Kawabata, S., Fujii, K., Iwamatsu, A., Segal, R. A., Fukuda, M., & Kaibuchi, K. (2009). Anterograde Transport of TrkB in Axons Is Mediated by Direct Interaction with Slp1 and Rab27. *Developmental Cell*, 16(5), 675–686. <https://doi.org/10.1016/j.devcel.2009.03.005>
- Asselin, L., Rivera Alvarez, J., Heide, S., Bonnet, C. S., Tilly, P., Vitet, H., Weber, C., Bacino, C. A., Baranaño, K., Chassevent, A., Dameron, A., Faivre, L., Hanchard, N. A., Mahida, S., McWalter, K., Mignot, C., Nava, C., Rastetter, A., Streff, H., ... Godin, J. D. (2020). Mutations in the KIF21B kinesin gene cause neurodevelopmental disorders through imbalanced canonical motor activity. *Nature Communications*, 11(1). <https://doi.org/10.1038/s41467-020-16294-6>
- Atherton, J., Hummel, J. J. A., Olieric, N., Locke, J., Peña, A., Rosenfeld, S. S., Steinmetz, M. O., Hoogenraad, C. C., & Moores, C. A. (2020). The mechanism of kinesin inhibition by kinesin binding protein. *ELife*, 9, 1–78. <https://doi.org/10.7554/eLife.61481>
- Azzarelli, R., Pacary, E., Garg, R., Garcez, P., van den Berg, D., Riou, P., Ridley, A. J., Friedel, R. H., Parsons, M., & Guillemot, F. (2014). An antagonistic interaction between PlexinB2 and Rnd3 controls RhoA activity and cortical neuron migration. *Nature Communications*, 5, 3405. <https://doi.org/10.1038/ncomms4405>
- Bai, J., Ramos, R. L., Ackman, J. B., Thomas, A. M., Lee, R. v., & LoTurco, J. J. (2003). RNAi reveals doublecortin is required for radial migration in rat neocortex. *Nature Neuroscience*, 6(12), 1277–1283. <https://doi.org/10.1038/nn1153>
- Bando, Y., Hirano, T., & Tagawa, Y. (2014). Dysfunction of KCNK potassium channels impairs neuronal migration in the developing mouse cerebral cortex. *Cerebral Cortex*, 24(4), 1017–1029. <https://doi.org/10.1093/cercor/bhs387>
- Bangs, F., & Anderson, K. v. (2017). Primary cilia and Mammalian Hedgehog signaling. *Cold Spring Harbor Perspectives in Biology*, 9(5). <https://doi.org/10.1101/cshperspect.a028175>
- Barakeh, D., Faqieh, E., Anazi, S., S Al-Dosari, M., Softah, A., Albadr, F., Hassan, H., Alazami, A. M., & Alkuraya, F. S. (2015). The many faces of KIF7. *Human Genome Variation*, 2(1). <https://doi.org/10.1038/hgv.2015.6>
- Barnabé-Heider, F., Wasylnka, J. A., Fernandes, K. J. L., Porsche, C., Sendtner, M., Kaplan, D. R., & Miller, F. D. (2005). Evidence that embryonic neurons regulate the onset of cortical

- gliogenesis via cardiotrophin-1. *Neuron*, 48(2), 253–265.
<https://doi.org/10.1016/j.neuron.2005.08.037>
- Barnat, M., le Fric, J., Benstaali, C., & Humbert, S. (2017). Huntingtin-Mediated Multipolar-Bipolar Transition of Newborn Cortical Neurons Is Critical for Their Postnatal Neuronal Morphology. *Neuron*, 93(1), 99–114. <https://doi.org/10.1016/j.neuron.2016.11.035>
- Barnes, A. P., Lilley, B. N., Pan, Y. A., Plummer, L. J., Powell, A. W., Raines, A. N., Sanes, J. R., & Polleux, F. (2007). LKB1 and SAD Kinases Define a Pathway Required for the Polarization of Cortical Neurons. *Cell*, 129(3), 549–563.
<https://doi.org/10.1016/j.cell.2007.03.025>
- Baron, D. M., Fenton, A. R., Saez-Atienzar, S., Giampetruzzi, A., Sreeram, A., Shankaracharya, Keagle, P. J., Doocy, V. R., Smith, N. J., Danielson, E. W., Andresano, M., McCormack, M. C., Garcia, J., Bercier, V., van den Bosch, L., Brent, J. R., Fallini, C., Traynor, B. J., Holzbaur, E. L. F., & Landers, J. E. (2022a). ALS-associated KIF5A mutations abolish autoinhibition resulting in a toxic gain of function. *Cell Reports*, 39(1), 110598.
<https://doi.org/10.1016/j.celrep.2022.110598>
- Baron, D. M., Fenton, A. R., Saez-Atienzar, S., Giampetruzzi, A., Sreeram, A., Shankaracharya, Keagle, P. J., Doocy, V. R., Smith, N. J., Danielson, E. W., Andresano, M., McCormack, M. C., Garcia, J., Bercier, V., van den Bosch, L., Brent, J. R., Fallini, C., Traynor, B. J., Holzbaur, E. L. F., & Landers, J. E. (2022b). ALS-associated KIF5A mutations abolish autoinhibition resulting in a toxic gain of function. *Cell Reports*, 39(1).
<https://doi.org/10.1016/j.celrep.2022.110598>
- Bedogni, F., & Hevner, R. F. (2021). Cell-Type-Specific Gene Expression in Developing Mouse Neocortex: Intermediate Progenitors Implicated in Axon Development. *Frontiers in Molecular Neuroscience*, 14. <https://doi.org/10.3389/fnmol.2021.686034>
- Beffert, U., Dillon, G. M., Sullivan, J. M., Stuart, C. E., Gilbert, J. P., Kambouris, J. A., & Ho, A. (2012). Microtubule plus-end tracking protein CLASP2 regulates neuronal polarity and synaptic function. *Journal of Neuroscience*, 32(40), 13906–13916.
<https://doi.org/10.1523/JNEUROSCI.2108-12.2012>
- Bellion, A., Baudoin, J.-P., Alvarez, C., Bornens, M., & Métin, C. (2005). Nucleokinesis in Tangentially Migrating Neurons Comprises Two Alternating Phases: Forward Migration of the Golgi/Centrosome Associated with Centrosome Splitting and Myosin Contraction at the Rear. *Journal of Neuroscience*, 25(24), 5691–5699.
<https://doi.org/10.1523/JNEUROSCI.1030-05.2005>
- Belvindrah, R., Graus-Porta, D., Goebbels, S., Nave, K. A., & Müller, U. (2007). $\beta 1$ integrins in radial glia but not in migrating neurons are essential for the formation of cell layers in the cerebral cortex. *Journal of Neuroscience*, 27(50), 13854–13865.
<https://doi.org/10.1523/JNEUROSCI.4494-07.2007>
- Belvindrah, R., Natarajan, K., Shabajee, P., Bruel-Jungerman, E., Bernard, J., Goutierre, M., Moutkine, I., Jaglin, X. H., Savariradjane, M., Irinopoulou, T., Poncer, J. C., Janke, C., & Francis, F. (2017). Mutation of the α -tubulin Tuba1a leads to straighter microtubules and perturbs neuronal migration. *Journal of Cell Biology*, 216(8), 2443–2461.
<https://doi.org/10.1083/jcb.201607074>
- Bhabha, G., Johnson, G. T., Schroeder, C. M., & Vale, R. D. (2016). How Dynein Moves Along Microtubules. In *Trends in Biochemical Sciences* (Vol. 41, Issue 1, pp. 94–105). Elsevier Ltd.
<https://doi.org/10.1016/j.tibs.2015.11.004>
- Bianchi, S., van Riel, W. E., Kraatz, S. H. W., Olieric, N., Frey, D., Katrukha, E. A., Jaussi, R., Missimer, J., Grigoriev, I., Olieric, V., Benoit, R. M., Steinmetz, M. O., Akhmanova, A., & Kammerer, R. A. (2016). Structural basis for misregulation of kinesin KIF21A autoinhibition by CFEOM1 disease mutations. *Scientific Reports*, 6. <https://doi.org/10.1038/srep30668>

- Blanchoin, L., Boujemaa-Paterski, R., Sykes, C., & Plastino, J. (2014). Actin dynamics, architecture, and mechanics in cell motility. *Physiological Reviews*, 94(1), 235–263. <https://doi.org/10.1152/physrev.00018.2013>
- Blasius, T. L., Cai, D., Jih, G. T., Toret, C. P., & Verhey, K. J. (2007). Two binding partners cooperate to activate the molecular motor Kinesin-1. *Journal of Cell Biology*, 176(1), 11–17. <https://doi.org/10.1083/jcb.200605099>
- Bodakuntla, S., Jijumon, A. S., Villablanca, C., Gonzalez-Billault, C., & Janke, C. (2019). Microtubule-Associated Proteins: Structuring the Cytoskeleton. In *Trends in Cell Biology* (Vol. 29, Issue 10, pp. 804–819). Elsevier Ltd. <https://doi.org/10.1016/j.tcb.2019.07.004>
- Broix, L., Jagline, H., Ivanova, E. L., Schmucker, S., Drouot, N., Clayton-Smith, J., Pagnamenta, A. T., Metcalfe, K. A., Isidor, B., Louvier, U. W., Poduri, A., Taylor, J. C., Tilly, P., Poirier, K., Saillour, Y., Lebrun, N., Stemmelen, T., Rudolf, G., Muraca, G., ... Chelly, J. (2016). Mutations in the HECT domain of NEDD4L lead to AKT-mTOR pathway deregulation and cause periventricular nodular heterotopia. *Nature Genetics*, 48(11), 1349–1358. <https://doi.org/10.1038/ng.3676>
- Brouhard, G. J., Stear, J. H., Noetzel, T. L., Al-Bassam, J., Kinoshita, K., Harrison, S. C., Howard, J., & Hyman, A. A. (2008). XMAP215 Is a Processive Microtubule Polymerase. *Cell*, 132(1), 79–88. <https://doi.org/10.1016/j.cell.2007.11.043>
- Buchsbaum, I. Y., Kielkowski, P., Giorgio, G., O'Neill, A. C., di Giaimo, R., Kyrousi, C., Khattak, S., Sieber, S. A., Robertson, S. P., & Cappello, S. (2020). ECE 2 regulates neurogenesis and neuronal migration during human cortical development. *EMBO Reports*, 21(5). <https://doi.org/10.15252/embr.201948204>
- Butkevich, E., Bodensiek, K., Fakhri, N., von Roden, K., Schaap, I. A. T., Majoul, I., Schmidt, C. F., & Klopfenstein, D. R. (2015). Drebrin-like protein DBN-1 is a sarcomere component that stabilizes actin filaments during muscle contraction. *Nature Communications*, 6. <https://doi.org/10.1038/ncomms8523>
- Camargo Ortega, G., Falk, S., Johansson, P. A., Peyre, E., Broix, L., Sahu, S. K., Hirst, W., Schlichthaerle, T., de Juan Romero, C., Draganova, K., Vinopal, S., Chinnappa, K., Gavranovic, A., Karakaya, T., Steininger, T., Merl-Pham, J., Feederle, R., Shao, W., Shi, S. H., ... Götz, M. (2019). The centrosome protein AKNA regulates neurogenesis via microtubule organization. *Nature*, 567(7746), 113–117. <https://doi.org/10.1038/s41586-019-0962-4>
- Cammarata, G. M., Bearce, E. A., & Lowery, L. A. (2016). Cytoskeletal social networking in the growth cone: How +TIPs mediate microtubule-actin cross-linking to drive axon outgrowth and guidance. In *Cytoskeleton* (Vol. 73, Issue 9, pp. 461–476). John Wiley and Sons Inc. <https://doi.org/10.1002/cm.21272>
- Canty, J. T., Tan, R., Kusakci, E., Fernandes, J., & Yildiz, A. (2021). Structure and Mechanics of Dynein Motors. In *Annual Review of Biophysics* (Vol. 50, pp. 549–574). Annual Reviews Inc. <https://doi.org/10.1146/annurev-biophys-111020-101511>
- Capello, S., Bohringer, C., Bergami, M., Conzelmann, K., Ghanem, A., Tomassy, G., Arlotta, P., Mainardi, M., Allegra, M., Caleo, M., van Hengel, J., Brakebusch, C., & Gotz, M. (2012). A Radial Glia-Specific Role of RhoA in Double Cortex Formation. *Neuron*.
- Cappello, S., Monzo, P., & Vallee, R. B. (2011). NudC is required for interkinetic nuclear migration and neuronal migration during neocortical development. *Developmental Biology*, 357(2), 326–335. <https://doi.org/10.1016/j.ydbio.2011.07.001>
- Carabalona, A., Hu, D. J. K., & Vallee, R. B. (2016). KIF1A inhibition immortalizes brain stem cells but blocks BDNF-mediated neuronal migration. *Nature Neuroscience*, 19(2), 253–262. <https://doi.org/10.1038/nn.4213>

- Carter, A. P., Diamant, A. G., & Urnavicius, L. (2016). How dynein and dynactin transport cargos: A structural perspective. In *Current Opinion in Structural Biology* (Vol. 37, pp. 62–70). Elsevier Ltd. <https://doi.org/10.1016/j.sbi.2015.12.003>
- Casarosa, S., Fode, C., & Guillemot, F. (1999). Mash1 regulates neurogenesis in the ventral telencephalon. *Development*.
- Causeret, F., Terao, M., Jacobs, T., Nishimura, Y. v., Yanagawa, Y., Obata, K., Hoshino, M., & Nikolić, M. (2009). The p21-activated kinase is required for neuronal migration in the cerebral cortex. *Cerebral Cortex*, 19(4), 861–875. <https://doi.org/10.1093/cercor/bhn133>
- Cavallin, M., Bijlsma, E. K., el Morjani, A., Moutton, S., Peeters, E. A. J., Maillard, C., Pedespan, J. M., Guerrot, A. M., Drouin-Garard, V., Coubes, C., Genevieve, D., Bole-Feysot, C., Fourrage, C., Steffann, J., & Bahi-Buisson, N. (2017). Recurrent KIF2A mutations are responsible for classic lissencephaly. *Neurogenetics*, 18(2), 73–79. <https://doi.org/10.1007/s10048-016-0499-8>
- Chai, X., Zhao, S., Fan, L., Zhang, W., Lu, X., Shao, H., Wang, S., Song, L., Failla, A. V., Zobiak, B., Mannherz, H. G., & Frotscher, M. (2016). Reelin and cofilin cooperate during the migration of cortical neurons: A quantitative morphological analysis. *Development (Cambridge)*, 143(6), 1029–1040. <https://doi.org/10.1242/dev.134163>
- Chang, H. Y., Cheng, H. Y., Tsao, A. N., Liu, C., & Tsai, J. W. (2019). Multiple Functions of KBP in Neural Development Underlie Brain Anomalies in Goldberg-Shprintzen Syndrome. *Frontiers in Molecular Neuroscience*, 12. <https://doi.org/10.3389/fnmol.2019.00265>
- Chauvin, S., & Sobel, A. (2015). Neuronal stathmins: A family of phosphoproteins cooperating for neuronal development, plasticity and regeneration. In *Progress in Neurobiology* (Vol. 126, pp. 1–18). Elsevier Ltd. <https://doi.org/10.1016/j.pneurobio.2014.09.002>
- Chen, K., Saw, W.-G., Lama, D., Verma, C., Grüber, G., & Koh, C.-G. (2018). Phosphorylation regulates auto-inhibition of kinesin KIF3A. *BioRxiv*. <https://doi.org/10.1101/503680>
- Chen, Z. L., Haegeli, V., Yu, H., & Strickland, S. (2009). Cortical deficiency of laminin $\gamma 1$ impairs the AKT/GSK-3 β signaling pathway and leads to defects in neurite outgrowth and neuronal migration. *Developmental Biology*, 327(1), 158–168. <https://doi.org/10.1016/j.ydbio.2008.12.006>
- Chenn, A., Zhang, Y. A., Chang, B. T., & McConnell, S. K. (1998). Intrinsic Polarity of Mammalian Neuroepithelial Cells. *Molecular and Cellular Neuroscience*, 11(183–193).
- Cheon, C. K., Lim, S. H., Kim, Y. M., Kim, D., Lee, N. Y., Yoon, T. S., Kim, N. S., Kim, E., & Lee, J. R. (2017). Autosomal dominant transmission of complicated hereditary spastic paraplegia due to a dominant negative mutation of KIF1A, SPG30 gene. *Scientific Reports*, 7(1). <https://doi.org/10.1038/s41598-017-12999-9>
- Chesarone, M. A., & Goode, B. L. (2009). Actin nucleation and elongation factors: mechanisms and interplay. In *Current Opinion in Cell Biology* (Vol. 21, Issue 1, pp. 28–37). <https://doi.org/10.1016/j.ceb.2008.12.001>
- Chiba, K., Takahashi, H., Chen, M., Obinata, H., Arai, S., Hashimoto, K., Oda, T., McKenney, R. J., & Niwa, S. (2019). Disease-associated mutations hyperactivate KIF1A motility and anterograde axonal transport of synaptic vesicle precursors. *Proceedings of the National Academy of Sciences of the United States of America*, 116(37), 18429–18434. <https://doi.org/10.1073/pnas.1905690116>
- Clovis, Y. M., Enard, W., Marinaro, F., Huttner, W. B., & de Pietri Tonelli, D. (2012). Convergent repression of Foxp2 3' UTR by miR-9 and miR-132 in embryonic mouse neocortex: Implications for radial migration of neurons. *Development (Cambridge)*, 139(18), 3332–3342. <https://doi.org/10.1242/dev.078063>
- Coffinier, C., Jung, H. J., Nobumori, C., Chang, S., Tu, Y., Barnes, R. H., Yoshinaga, Y., de Jong, P. J., Vergnes, L., Reue, K., Fong, L. G., & Young, S. G. (2011). Deficiencies in lamin B1 and lamin B2 cause neurodevelopmental defects and distinct nuclear shape abnormalities in

- neurons. *Molecular Biology of the Cell*, 22(23), 4683–4693. <https://doi.org/10.1091/mbc.E11-06-0504>
- Coles, C. H., & Bradke, F. (2015). Coordinating Neuronal Actin-Microtubule Dynamics. In *Current Biology* (Vol. 25, Issue 15, pp. R677–R691). Cell Press. <https://doi.org/10.1016/j.cub.2015.06.020>
- Conti, V., Carabalona, A., Pallesi-Pocachard, E., Parrini, E., Leventer, R. J., Buhler, E., McGillivray, G., Michel, F. J., Striano, P., Mei, D., Watrin, F., Lise, S., Pagnamenta, A. T., Taylor, J. C., Kini, U., Clayton-Smith, J., Novara, F., Zuffardi, O., Dobyns, W. B., ... Guerrini, R. (2013). Periventricular heterotopia in 6q terminal deletion syndrome: Role of the C6orf70 gene. *Brain*, 136(11), 3378–3394. <https://doi.org/10.1093/brain/awt249>
- Coquand, L., Victoria, G. S., Tata, A., Carpentieri, J. A., Brault, J. B., Guimiot, F., Fraissier, V., & Baffet, A. D. (2021). CAMSAPs organize an acentrosomal microtubule network from basal varicosities in radial glial cells. *Journal of Cell Biology*, 220(8). <https://doi.org/10.1083/jcb.202003151>
- Corbo, J. C., Deuel, T. A., Long, J. M., Laporte, P., Tsai, E., Wynshaw-Boris, A., & Walsh, C. A. (2002). *Doublecortin Is Required in Mice for Lamination of the Hippocampus But Not the Neocortex*.
- Creppe, C., Malinouskaya, L., Volvert, M. L., Gillard, M., Close, P., Malaise, O., Laguesse, S., Cornez, I., Rahmouni, S., Ormenese, S., Belachew, S., Malgrange, B., Chapelle, J. P., Siebenlist, U., Moonen, G., Chariot, A., & Nguyen, L. (2009). Elongator Controls the Migration and Differentiation of Cortical Neurons through Acetylation of α -Tubulin. *Cell*, 136(3), 551–564. <https://doi.org/10.1016/j.cell.2008.11.043>
- da Silva, F., Zhang, K., Pinson, A., Fatti, E., Wilsch-Bräuninger, M., Herbst, J., Vidal, V., Schedl, A., Huttner, W. B., & Niehrs, C. (2021). Mitotic WNT signalling orchestrates neurogenesis in the developing neocortex. *The EMBO Journal*, 40(19). <https://doi.org/10.15252/embj.2021108041>
- Davidson, D. (1989). The House Mouse: Atlas of Embryonic Development. *Genetical Research*, 54(3), 240–241. <https://doi.org/10.1017/S001667230002872X>
- de Anda, F. C., Meletis, K., Ge, X., Rei, D., & Tsai, L. H. (2010). Centrosome motility is essential for initial axon formation in the neocortex. *Journal of Neuroscience*, 30(31), 10391–10406. <https://doi.org/10.1523/JNEUROSCI.0381-10.2010>
- de Felipe, J. (1993). Neocortical Neuronal Diversity: Chemical Heterogeneity Revealed by Colocalization Studies of Classic Neurotransmitters, Neuropeptides, Calcium-binding Proteins, and Cell Surface Molecules. *Cerebral Cortex*. <http://cercor.oxfordjournals.org/>
- Dehmelt, L., & Halpain, S. (2004). *The MAP2/Tau family of microtubule-associated proteins Gene organization and evolutionary history*. <http://genomebiology.com/2004/6/1/204>
- del Toro, D., Ruff, T., Cederfjäll, E., Villalba, A., Seyit-Bremer, G., Borrell, V., & Klein, R. (2017). Regulation of Cerebral Cortex Folding by Controlling Neuronal Migration via FLRT Adhesion Molecules. *Cell*, 169(4), 621–635.e16. <https://doi.org/10.1016/j.cell.2017.04.012>
- Delatour, L. C., Yeh, P. W., & Yeh, H. H. (2019). Ethanol exposure in utero disrupts radial migration and pyramidal cell development in the somatosensory cortex. *Cerebral Cortex*, 29(5), 2125–2139. <https://doi.org/10.1093/cercor/bhy094>
- Deng, C. Y., Lei, W. L., Xu, X. H., Ju, X. C., Liu, Y., & Luo, Z. G. (2014). JIP1 mediates anterograde transport of Rab10 cargos during neuronal polarization. *Journal of Neuroscience*, 34(5), 1710–1723. <https://doi.org/10.1523/JNEUROSCI.4496-13.2014>
- des Portes, V., Pinard, J. M., Billuart, P., Vinet, M. C., Gelot, A., Anoinette, Dupuis, E., Motte, J., Berwald-Netter, Y., Catala, M., Kahn, A., Beldjord, C., & Chelly, J. (1998). A Novel CNS Gene Required for Neuronal Migration and Involved in X-Linked Subcortical Laminar Heterotopia and Lissencephaly Syndrome. *Cell*.

- Deuel, T. A. S., Liu, J. S., Corbo, J. C., Yoo, S. Y., Rorke-Adams, L. B., & Walsh, C. A. (2006). Genetic interactions between doublecortin and doublecortin-like kinase in neuronal migration and axon outgrowth. *Neuron*, 49(1), 41–53. <https://doi.org/10.1016/j.neuron.2005.10.038>
- Dillon, G. M., Tyler, W. A., Omuro, K. C., Kambouris, J., Tyminski, C., Henry, S., Haydar, T. F., Beffert, U., & Ho, A. (2017). CLASP2 Links Reelin to the Cytoskeleton during Neocortical Development. *Neuron*, 93(6), 1344–1358.e5. <https://doi.org/10.1016/j.neuron.2017.02.039>
- Dimitrova-Paternoga, L., Jagtap, P. K. A., Cyrklaff, A., Vaishali, V., Lapouge, K., Sehr, P., Perez, K., Heber, S., Löw, C., Hennig, J., & Ephrussi, A. (2021). Molecular basis of mRNA transport by a kinesin-1-atypical tropomyosin complex. *Genes and Development*, 35(13), 1–16. <https://doi.org/10.1101/GAD.348443.121>
- Downhill, J. E., Buchsbaum, M. S., Wei, T., Spiegel-Cohen, J., Hazlett, E. A., Mehmet Haznedar, M., Silverman, J., & Siever, L. J. (2000). Shape and size of the corpus callosum in schizophrenia and schizotypal personality disorder. In *Schizophrenia Research* (Vol. 42). www.elsevier.com/locate/schres
- Drerup, C. M., Lusk, S., & Nechiporuk, A. (2016). Kif1B interacts with KBP to promote axon elongation by localizing a microtubule regulator to growth cones. *Journal of Neuroscience*, 36(26), 7014–7026. <https://doi.org/10.1523/JNEUROSCI.0054-16.2016>
- Drummond, D. R. (2011). Regulation of microtubule dynamics by kinesins. In *Seminars in Cell and Developmental Biology* (Vol. 22, Issue 9, pp. 927–934). Elsevier Ltd. <https://doi.org/10.1016/j.semcdb.2011.09.021>
- D’Souza-Schorey, C., & Chavrier, P. (2006). ARF proteins: Roles in membrane traffic and beyond. In *Nature Reviews Molecular Cell Biology* (Vol. 7, Issue 5, pp. 347–358). <https://doi.org/10.1038/nrm1910>
- Dugina, V. B., Shagieva, G. S., & Kopnin, P. B. (2019). Biological Role of Actin Isoforms in Mammalian Cells. In *Biochemistry (Moscow)* (Vol. 84, Issue 6, pp. 583–592). Pleiades journals. <https://doi.org/10.1134/S0006297919060014>
- Dulabon, L., Olson, E. C., Taglienti, M. G., Eisenhuth, S., Mcgrath, B., Walsh, C. A., Kreidberg, J. A., & Anton, E. S. (2000). Reelin Binds 31 Integrin and Inhibits Neuronal Migration. In *Neuron* (Vol. 27).
- Eckler, M. J., Nguyen, T. D., McKenna, W. L., Fastow, B. L., Guo, C., Rubenstein, J. L. R., & Chen, B. (2015). Cux2-Positive Radial Glial Cells Generate Diverse Subtypes of Neocortical Projection Neurons and Macroglia. *Neuron*, 86(4), 1100–1108. <https://doi.org/10.1016/j.neuron.2015.04.020>
- Elias, L. A. B., Wang, D. D., & Kriegstein, A. R. (2007). Gap junction adhesion is necessary for radial migration in the neocortex. *Nature*, 448(7156), 901–907. <https://doi.org/10.1038/nature06063>
- Elie, A., Prezel, E., Guérin, C., Denarier, E., Ramirez-Rios, S., Serre, L., Andrieux, A., Fourest-Lieuvain, A., Blanchoin, L., & Arnal, I. (2015). Tau co-organizes dynamic microtubule and actin networks. *Scientific Reports*, 5. <https://doi.org/10.1038/srep09964>
- Englund, C., Fink, A., Lau, C., Pham, D., Daza, R. A. M., Bulfone, A., Kowalczyk, T., & Hevner, R. F. (2005). Pax6, Tbr2, and Tbr1 are expressed sequentially by radial glia, intermediate progenitor cells, and postmitotic neurons in developing neocortex. *Journal of Neuroscience*, 25(1), 247–251. <https://doi.org/10.1523/JNEUROSCI.2899-04.2005>
- Eom, T. Y., Stanco, A., Guo, J., Wilkins, G., Deslauriers, D., Yan, J., Monckton, C., Blair, J., Oon, E., Perez, A., Salas, E., Oh, A., Ghukasyan, V., Snider, W. D., Rubenstein, J. L. R., & Anton, E. S. (2014). Differential regulation of microtubule severing by APC underlies distinct patterns of projection neuron and interneuron migration. *Developmental Cell*, 31(6), 677–689. <https://doi.org/10.1016/j.devcel.2014.11.022>
- Epifanova, E., Salina, V., Lajkó, D., Textoris-Taube, K., Naumann, T., Bormuth, O., Bormuth, I., Horan, S., Schaub, T., Borisova, E., Ambrozkiwicz, M. C., Tarabykin, V., & Rosário, M.

- (2021). Adhesion dynamics in the neocortex determine the start of migration and the post-migratory orientation of neurons. In *Sci. Adv* (Vol. 7). <https://www.science.org>
- Espeut, J., Gaussen, A., Bieling, P., Morin, V., Prieto, S., Fesquet, D., Surrey, T., & Abrieu, A. (2008). Phosphorylation Relieves Autoinhibition of the Kinetochore Motor Cenp-E. *Molecular Cell*, 29(5), 637–643. <https://doi.org/10.1016/j.molcel.2008.01.004>
- Espinós, A., Fernández-Ortuño, E., Negri, E., & Borrell, V. (2022). Evolution of genetic mechanisms regulating cortical neurogenesis. In *Developmental Neurobiology*. John Wiley and Sons Inc. <https://doi.org/10.1002/dneu.22891>
- Falace, A., Buhler, E., Fadda, M., Watrin, F., Lippiello, P., Pallesi-Pocachard, E., Baldelli, P., Benfenati, F., Zara, F., Represa, A., Fassio, A., & Cardoso, C. (2014). TBC1D24 regulates neuronal migration and maturation through modulation of the ARF6-dependent pathway. *Proceedings of the National Academy of Sciences of the United States of America*, 111(6), 2337–2342. <https://doi.org/10.1073/pnas.1316294111>
- Falk, S., Wurdak, H., Ittner, L. M., Ille, F., Sumara, G., Schmid, M. T., Draganova, K., Lang, K. S., Paratore, C., Leveen, P., Suter, U., Karlsson, S., Born, W., Ricci, R., Götz, M., & Sommer, L. (2008). Brain Area-Specific Effect of TGF- β Signaling on Wnt-Dependent Neural Stem Cell Expansion. *Cell Stem Cell*, 2(5), 472–483. <https://doi.org/10.1016/j.stem.2008.03.006>
- Falnikar, A., Tole, S., & Baas, P. W. (2011). Kinesin-5, a mitotic microtubule-associated motor protein, modulates neuronal migration. *Molecular Biology of the Cell*, 22(9), 1561–1574. <https://doi.org/10.1091/mbc.E10-11-0905>
- Falnikar, A., Tole, S., Liu, M., Liu, J. S., & Baas, P. W. (2013). Polarity in migrating neurons is related to a mechanism analogous to cytokinesis. *Current Biology*, 23(13), 1215–1220. <https://doi.org/10.1016/j.cub.2013.05.027>
- Farkas, L. M., & Huttner, W. B. (2008). The cell biology of neural stem and progenitor cells and its significance for their proliferation versus differentiation during mammalian brain development. In *Current Opinion in Cell Biology* (Vol. 20, Issue 6, pp. 707–715). <https://doi.org/10.1016/j.ceb.2008.09.008>
- Farmer, V., Arpağ, G., Hall, S. L., & Zanic, M. (2021). Xmap215 promotes microtubule catastrophe by disrupting the growing microtubule end. *Journal of Cell Biology*, 220(10). <https://doi.org/10.1083/jcb.202012144>
- Feng, L., Hatten, M. E., & Heintz, N. (1994). Brain lipid-binding protein (BLBP): a novel signaling system in the developing mammalian CNS. *Neuron*, 12(4), 895–908. [https://doi.org/10.1016/0896-6273\(94\)90341-7](https://doi.org/10.1016/0896-6273(94)90341-7)
- Fenlon, L. R. (2022). Timing as a Mechanism of Development and Evolution in the Cerebral Cortex. In *Brain, Behavior and Evolution* (Vol. 97, Issue 2, pp. 8–32). S. Karger AG. <https://doi.org/10.1159/000521678>
- Ferenz, N. P., Gable, A., & Wadsworth, P. (2010). Mitotic functions of kinesin-5. In *Seminars in Cell and Developmental Biology* (Vol. 21, Issue 3, pp. 255–259). Elsevier Ltd. <https://doi.org/10.1016/j.semcdb.2010.01.019>
- Fernández, V., Llinares-Benadero, C., & Borrell, V. (2016). Cerebral cortex expansion and folding: what have we learned? *The EMBO Journal*, 35(10), 1021–1044. <https://doi.org/10.15252/embj.201593701>
- Fietz, S. A., Lachmann, R., Brandl, H., Kircher, M., Samusik, N., Schröder, R., Lakshmanaperumal, N., Henry, I., Vogt, J., Riehn, A., Distler, W., Nitsch, R., Enard, W., Paäbo, S., & Huttner, W. B. (2012). Transcriptomes of germinal zones of human and mouse fetal neocortex suggest a role of extracellular matrix in progenitor self-renewal. *Proceedings of the National Academy of Sciences of the United States of America*, 109(29), 11836–11841. <https://doi.org/10.1073/pnas.1209647109>

- Fili, N., Hari-Gupta, Y., dos Santos, Á., Cook, A., Poland, S., Ameer-Beg, S. M., Parsons, M., & Toseland, C. P. (2017). NDP52 activates nuclear myosin VI to enhance RNA polymerase II transcription. *Nature Communications*, 8(1). <https://doi.org/10.1038/s41467-017-02050-w>
- Fogarty, M., Grist, M., Gelman, D., Marín, O., Pachnis, V., & Kessar, N. (2007). Spatial genetic patterning of the embryonic neuroepithelium generates GABAergic interneuron diversity in the adult cortex. *Journal of Neuroscience*, 27(41), 10935–10946. <https://doi.org/10.1523/JNEUROSCI.1629-07.2007>
- Fox, J., Lamperti, E., Eksioğlu, Y., Hong, S., Feng, Y., Graham, D., Scheffer, I., Dobins, W., Hirsch, B., Radtke, R., Berkovic, S., Huttenlocher, P., & Walsh, C. (1998). Mutations in Filamin 1 Prevent Migration of Cerebral Cortical Neurons in Human Periventricular Heterotopia. *Neuron*.
- Frantz, G. D., & McConnell, S. K. (1996). Restriction of Late Cerebral Cortical Progenitors to an Upper-Layer Fate. In *Neuron* (Vol. 17).
- Frotscher, M., Zhao, S., Wang, S., & Chai, X. (2017). Reelin signaling inactivates cofilin to stabilize the cytoskeleton of migrating cortical neurons. In *Frontiers in Cellular Neuroscience* (Vol. 11). Frontiers Media S.A. <https://doi.org/10.3389/fncel.2017.00148>
- Fu, C., Xu, J., Cheng, W., Rojas, T., Chin, A. C., Snowman, A. M., Harraz, M. M., & Snyder, S. H. (2017). Neuronal migration is mediated by inositol hexakisphosphate kinase 1 via α -actinin and focal adhesion kinase. *Proceedings of the National Academy of Sciences of the United States of America*, 114(8), 2036–2041. <https://doi.org/10.1073/pnas.1700165114>
- Fujita, S. (1962). Kinetics of cellular proliferation. *Experimental Cell Research*, 28, 52–60.
- Fujita, S. (1963). The Matrix Cell and Cytogenesis in the Developing Central Nervous System. *Journal of Comparative Neurobiology*.
- Fukuda, Y., Pazyra-Murphy, M. F., Silagi, E. S., Tasdemir-Yilmaz, O. E., Li, Y., Rose, L., Yeoh, Z. C., Vangos, N. E., Geffken, E. A., Seo, H. S., Adelmant, G., Bird, G. H., Walensky, L. D., Marto, J. A., Dhe-Paganon, S., & Segal, R. A. (2021). Binding and transport of sfpq-rna granules by kif5a/klc1 motors promotes axon survival. *Journal of Cell Biology*, 220(1). <https://doi.org/10.1083/jcb.202005051>
- Fukumoto, K., Morita, T., Mayanagi, T., Tanokashira, D., Yoshida, T., Sakai, A., & Sobue, K. (2009). Detrimental effects of glucocorticoids on neuronal migration during brain development. *Molecular Psychiatry*, 14(12), 1119–1131. <https://doi.org/10.1038/mp.2009.60>
- Furukawa, T., Yamada, J., Akita, T., Matsushima, Y., Yanagawa, Y., & Fukuda, A. (2014). Roles of taurine-mediated tonic GABA receptor activation in the radial migration of neurons in the fetal mouse cerebral cortex. *Frontiers in Cellular Neuroscience*, 8(MAR). <https://doi.org/10.3389/fncel.2014.00088>
- Gao, P., Postiglione, M. P., Krieger, T. G., Hernandez, L., Wang, C., Han, Z., Streicher, C., Papusheva, E., Insolera, R., Chugh, K., Kodish, O., Huang, K., Simons, B. D., Luo, L., Hippenmeyer, S., & Shi, S. H. (2014). Deterministic progenitor behavior and unitary production of neurons in the neocortex. *Cell*, 159(4), 775–788. <https://doi.org/10.1016/j.cell.2014.10.027>
- Geraldo, S., Khanzada, U. K., Parsons, M., Chilton, J. K., & Gordon-Weeks, P. R. (2008). Targeting of the F-actin-binding protein drebrin by the microtubule plus-tip protein EB3 is required for neuriteogenesis. *Nature Cell Biology*, 10(10), 1181–1189. <https://doi.org/10.1038/ncb1778>
- Ghiretti, A. E., Thies, E., Tokito, M. K., Lin, T., Ostap, E. M., Kneussel, M., Holzbaur, E. L. F., Ghiretti, A. E., Thies, E., Tokito, M. K., Lin, T., Ostap, E. M., & Kneussel, M. (2016). Activity-Dependent Regulation of Distinct Transport and Cytoskeletal Remodeling Functions of the Article Activity-Dependent Regulation of Distinct Transport and Cytoskeletal Remodeling Functions of the Dendritic Kinesin KIF21B. *Neuron*, 92(4), 857–872. <https://doi.org/10.1016/j.neuron.2016.10.003>

- Ghosh, D. K., Dasgupta, D., & Guha, A. (2012). Models, Regulations, and Functions of Microtubule Severing by Katanin. *ISRN Molecular Biology*, 2012, 1–14. <https://doi.org/10.5402/2012/596289>
- Gialluisi, A., Reccia, M. G., Modugno, N., Natile, T., Lombardi, A., di Giovannantonio, L. G., Pietracupa, S., Ruggiero, D., Scala, S., Gambardella, S., Iacoviello, L., Gianfrancesco, F., Acampora, D., D'Esposito, M., Simeone, A., Ciullo, M., & Esposito, T. (2021). Identification of sixteen novel candidate genes for late onset Parkinson's disease. *Molecular Neurodegeneration*, 16(1), 35. <https://doi.org/10.1186/s13024-021-00455-2>
- Gilet, J. G., Ivanova, E. L., Trofimova, D., Rudolf, G., Meziane, H., Broix, L., Drouot, N., Courraud, J., Skory, V., Voulleminot, P., Osipenko, M., Bahi-Buisson, N., Yalcin, B., Birling, M. C., Hinckelmann, M. V., Kwok, B. H., Allingham, J. S., & Chelly, J. (2020). Conditional switching of KIF2A mutation provides new insights into cortical malformation pathogeny. *Human Molecular Genetics*, 29(5), 766–784. <https://doi.org/10.1093/hmg/ddz316>
- Gö Tz, M., Stoykova, A., & Gruss, P. (1998). Pax6 Controls Radial Glia Differentiation in the Cerebral Cortex. In *Neuron* (Vol. 21).
- Godin, J. D., Thomas, N., Laguesse, S., Malinowskaya, L., Close, P., Malaise, O., Purnelle, A., Raineteau, O., Campbell, K., Fero, M., Moonen, G., Malgrange, B., Chariot, A., Metin, C., Besson, A., & Nguyen, L. (2012). P27Kip1 Is a Microtubule-Associated Protein that Promotes Microtubule Polymerization during Neuron Migration. *Developmental Cell*, 23(4), 729–744. <https://doi.org/10.1016/j.devcel.2012.08.006>
- Goeckeler, Z. M., & Wysolmerski, R. B. (1995). Myosin Light Chain Kinase-regulated Endothelial Cell Contraction: The Relationship between Isometric Tension, Actin Polymerization, and Myosin Phosphorylation. *The Journal of Cell Biology*.
- Goedert, M. (2018). Tau filaments in neurodegenerative diseases. In *FEBS Letters* (Vol. 592, Issue 14, pp. 2383–2391). Wiley Blackwell. <https://doi.org/10.1002/1873-3468.13108>
- Gonçalves, J. C., Quintremil, S., Yi, J., & Vallee, R. B. (2020). Nesprin-2 Recruitment of BicD2 to the Nuclear Envelope Controls Dynein/Kinesin-Mediated Neuronal Migration In Vivo. *Current Biology*, 30(16), 3116–3129.e4. <https://doi.org/10.1016/j.cub.2020.05.091>
- Gongidi, V., Ring, C., Moody, M., Brekken, R., Sage, E. H., Rakic, P., & Anton, E. S. (2004). SPARC-like 1 Regulates the Terminal Phase of Radial Glia-Guided Migration in the Cerebral Cortex. In *Neuron* (Vol. 41).
- Goodson, H. v., & Jonasson, E. M. (2018). Microtubules and microtubule-associated proteins. *Cold Spring Harbor Perspectives in Biology*, 10(6). <https://doi.org/10.1101/cshperspect.a022608>
- Goris, A., Boonen, S., M-b, D., & Dubois, B. (2010). *Replication of KIF21B as a susceptibility locus for multiple sclerosis*. 664, 2009–2011. <https://doi.org/10.1136/jmg.2009.075911>
- Götz, M., & Huttner, W. B. (2005). The cell biology of neurogenesis. In *Nature Reviews Molecular Cell Biology* (Vol. 6, Issue 10, pp. 777–788). <https://doi.org/10.1038/nrm1739>
- Greenstein, B., & Greenstein, A. (2000). *Color Atlas of Neuroscience: Neuroanatomy and Neurophysiology*.
- Gromova, K. v, Muhia, M., Rothammer, N., Shevchuk, O., Oertner, T. G., Kneussel, M., Gromova, K. v, Muhia, M., Rothammer, N., Gee, C. E., Thies, E., Schaefer, I., & Kress, S. (2018). Neurobeachin and the Kinesin KIF21B Are Critical for Endocytic Recycling of NMDA Receptors and Regulate Social Behavior. *CellReports*, 23(9), 2705–2717. <https://doi.org/10.1016/j.celrep.2018.04.112>
- Guedes-Dias, P., Nirschl, J. J., Abreu, N., Tokito, M. K., Janke, C., Magiera, M. M., & Holzbaur, E. L. F. (2019). Kinesin-3 Responds to Local Microtubule Dynamics to Target Synaptic Cargo Delivery to the Presynapse. *Current Biology*, 29(2), 268–282.e8. <https://doi.org/10.1016/j.cub.2018.11.065>

- Guillaud, L., Wong, R., & Hirokawa, N. (2008). Disruption of KIF17-Mint1 interaction by CaMKII-dependent phosphorylation: A molecular model of kinesin-cargo release. *Nature Cell Biology*, 10(1), 19–29. <https://doi.org/10.1038/ncb1665>
- Gupta, A., Sanada, K., Miyamoto, D. T., Rovelstad, S., Nadarajah, B., Pearlman, A. L., Brunstrom, J., & Tsai, L. H. (2003). Layering defect in p35 deficiency is linked to improper neuronal-glial interaction in radial migration. *Nature Neuroscience*, 6(12), 1284–1291. <https://doi.org/10.1038/nn1151>
- Hamada, N., Negishi, Y., Mizuno, M., Miya, F., Hattori, A., Okamoto, N., Kato, M., Tsunoda, T., Yamasaki, M., Kanemura, Y., Kosaki, K., Tabata, H., Saitoh, S., & Nagata, K. I. (2017). Role of a heterotrimeric G-protein, Gi2, in the corticogenesis: possible involvement in periventricular nodular heterotopia and intellectual disability. *Journal of Neurochemistry*, 140(1), 82–95. <https://doi.org/10.1111/jnc.13878>
- Hammond, J. W., Cai, D., Blasius, T. L., Li, Z., Jiang, Y., Jih, G. T., Meyhofer, E., & Verhey, K. J. (2009). Mammalian Kinesin-3 motors are dimeric in vivo and move by processive motility upon release of autoinhibition. *PLoS Biology*, 7(3), 0650–0663. <https://doi.org/10.1371/journal.pbio.1000072>
- Hannabuss, J., Lera-Ramirez, M., Cade, N. I., Fourniol, F. J., Nédélec, F., & Surrey, T. (2019). Self-Organization of Minimal Anaphase Spindle Midzone Bundles. *Current Biology*, 29(13), 2120–2130.e7. <https://doi.org/10.1016/j.cub.2019.05.049>
- Hansen, A. H., & Hippenmeyer, S. (2020). Non-Cell-Autonomous Mechanisms in Radial Projection Neuron Migration in the Developing Cerebral Cortex. In *Frontiers in Cell and Developmental Biology* (Vol. 8). Frontiers Media S.A. <https://doi.org/10.3389/fcell.2020.574382>
- Hansen, D. v., Lui, J. H., Parker, P. R. L., & Kriegstein, A. R. (2010). Neurogenic radial glia in the outer subventricular zone of human neocortex. *Nature*, 464(7288), 554–561. <https://doi.org/10.1038/nature08845>
- Hanson, E., Armbruster, M., Lau, L. A., Sommer, M. E., Klaft, Z. J., Swanger, S. A., Traynelis, S. F., Moss, S. J., Noubary, F., Chadchankar, J., & Dulla, C. G. (2019). Tonic activation of GluN2C/GluN2D-containing NMDA receptors by ambient glutamate facilitates cortical interneuron maturation. *Journal of Neuroscience*, 39(19), 3611–3626. <https://doi.org/10.1523/JNEUROSCI.1392-18.2019>
- Hatakeyama, J., Wakamatsu, Y., Nagafuchi, A., Kageyama, R., Shigemoto, R., & Shimamura, K. (2014). Cadherin-based adhesions in the apical endfoot are required for active Notch signaling to control neurogenesis in vertebrates. *Development (Cambridge)*, 141(8), 1671–1682. <https://doi.org/10.1242/dev.102988>
- Hatanaka, Y., Hisanaga, S. I., Heizmann, C. W., & Murakami, F. (2004). Distinct migratory behavior of early- and late-born neurons derived from the cortical ventricular zone. *Journal of Comparative Neurology*, 479(1), 1–14. <https://doi.org/10.1002/cne.20256>
- Haubensak, W., Attardo, A., Denk, W., Huttner, W. B., & Simons, K. (2004). Neurons arise in the basal neuroepithelium of the early mammalian telencephalon: A major site of neurogenesis. In *PNAS March* (Vol. 2, Issue 9). www.pnas.org/cgi/doi/10.1073/pnas.0308600100
- Hausrat, T. J., Radwitz, J., Lombino, F. L., Breiden, P., & Kneussel, M. (2021). Alpha- and beta-tubulin isoforms are differentially expressed during brain development. *Developmental Neurobiology*, 81(3), 333–350. <https://doi.org/10.1002/dneu.22745>
- Hébert, J. M., & Fishell, G. (2008). The genetics of early telencephalon patterning: Some assembly required. In *Nature Reviews Neuroscience* (Vol. 9, Issue 9, pp. 678–685). <https://doi.org/10.1038/nrn2463>
- Heimer, G., van Woerden, G. M., Barel, O., Marek-Yagel, D., Kol, N., Munting, J. B., Borghei, M., Atawneh, O. M., Nissenkorn, A., Rechavi, G., Anikster, Y., Elgersma, Y., Kushner, S. A.,

- & ben Zeev, B. (2020). Netrin-G2 dysfunction causes a Rett-like phenotype with areflexia. *Human Mutation*, 41(2), 476–486. <https://doi.org/10.1002/humu.23945>
- Heissler, S. M., & Sellers, J. R. (2014). Myosin light chains: Teaching old dogs new tricks. In *Bioarchitecture* (Vol. 4, Issue 6, pp. 169–188). <https://doi.org/10.1080/19490992.2015.1054092>
- Hendershott, M. C., & Vale, R. D. (2014). Regulation of microtubule minus-end dynamics by CAMSAPs and Patronin. *Proceedings of the National Academy of Sciences of the United States of America*, 111(16), 5860–5865. <https://doi.org/10.1073/pnas.1404133111>
- Herskowitz, I. (1987). Functional inactivation of genes by dominant negative mutations. *Nature*, 329(6136), 219–222. <https://doi.org/10.1038/329219a0>
- Hippenmeyer, S., Youn, Y. H., Moon, H. M., Miyamichi, K., Zong, H., Wynshaw-Boris, A., & Luo, L. (2010). Genetic mosaic dissection of Lis1 and Ndel1 in neuronal migration. *Neuron*, 68(4), 695–709. <https://doi.org/10.1016/j.neuron.2010.09.027>
- Hirokawa, N., Niwa, S., & Tanaka, Y. (2010). Molecular motors in neurons: Transport mechanisms and roles in brain function, development, and disease. In *Neuron* (Vol. 68, Issue 4, pp. 610–638). <https://doi.org/10.1016/j.neuron.2010.09.039>
- Hodge, R. G., & Ridley, A. J. (2016). Regulating Rho GTPases and their regulators. In *Nature Reviews Molecular Cell Biology* (Vol. 17, Issue 8, pp. 496–510). Nature Publishing Group. <https://doi.org/10.1038/nrm.2016.67>
- Hoff, K. J., Aiken, J. E., Gutierrez, M. A., Franco, S. J., & Moore, J. K. (2022). Tubulinopathy mutations in TUBA1A that disrupt neuronal morphogenesis and migration override XMAP215/Stu2 regulation of microtubule dynamics. *ELife*, 11. <https://doi.org/10.7554/eLife.76189>
- Hooikaas, P. J., Damstra, H. G. J., Gros, O. J., van Riel, W. E., Martin, M., Smits, Y. T. H., Loosdregt, J. van, Kapitein, L. C., Berger, F., & Akhmanova, A. (2020). Kinesin-4 kif21b limits microtubule growth to allow rapid centrosome polarization in t cells. *ELife*, 9, 1–75. <https://doi.org/10.7554/ELIFE.62876>
- Hor, C. H. H., & Goh, E. L. K. (2018). Rab23 regulates radial migration of projection neurons via N-cadherin. *Cerebral Cortex*, 28(4), 1516–1531. <https://doi.org/10.1093/cercor/bhy018>
- Horiuchi, D., Collins, C. A., Bhat, P., Barkus, R. v, Diantonio, A., & Saxton, W. M. (2008). Control of a kinesin-cargo linkage mechanism by JNK pathway kinases. *Current Biology*.
- Hurni, N., Kolodziejczak, M., Tomasello, U., Badia, J., Jacobshagen, M., Prados, J., & Dayer, A. (2017). Transient Cell-intrinsic Activity Regulates the Migration and Laminar Positioning of Cortical Projection Neurons. *Cerebral Cortex*, 27(5), 3052–3063. <https://doi.org/10.1093/cercor/bhx059>
- Hutchins, B. I., & Wray, S. (2014). Capture of microtubule plus-ends at the actin cortex promotes axophilic neuronal migration by enhancing microtubule tension in the leading process. *Frontiers in Cellular Neuroscience*, 8(NOV). <https://doi.org/10.3389/fncel.2014.00400>
- Inoue, M., Kuroda, T., Honda, A., Komabayashi-Suzuki, M., Komai, T., Shinkai, Y., & Mizutani, K. I. (2014). Prdm8 regulates the morphological transition at multipolar phase during neocortical development. *PLoS ONE*, 9(1). <https://doi.org/10.1371/journal.pone.0086356>
- Inoue, S., Hayashi, K., Fujita, K., Tagawa, K., Okazawa, H., Kubo, K. I., & Nakajima, K. (2019). Drebrin-like (Dbnl) controls neuronal migration via regulating N-cadherin expression in the developing cerebral cortex. *Journal of Neuroscience*, 39(4), 678–691. <https://doi.org/10.1523/JNEUROSCI.1634-18.2018>
- Ip, J. P. K., Shi, L., Chen, Y., Itoh, Y., Fu, W. Y., Betz, A., Yung, W. H., Gotoh, Y., Fu, A. K. Y., & Ip, N. Y. (2012). α 2-chimaerin controls neuronal migration and functioning of the cerebral cortex through CRMP-2. *Nature Neuroscience*, 15(1), 39–47. <https://doi.org/10.1038/nn.2972>

- Ishii, M., & Maeda, N. (2008). Oversulfated chondroitin sulfate plays critical roles in the neuronal migration in the cerebral cortex. *Journal of Biological Chemistry*, 283(47), 32610–32620. <https://doi.org/10.1074/jbc.M806331200>
- Itoh, K., & Fushiki, S. (2015). The role of L1cam in murine corticogenesis, and the pathogenesis of hydrocephalus. In *Pathology International* (Vol. 65, Issue 2, pp. 58–66). <https://doi.org/10.1111/pin.12245>
- Ivanova, E. L., Gilet, J. G., Sulimenko, V., Duchon, A., Rudolf, G., Runge, K., Collins, S. C., Asselin, L., Broix, L., Drouot, N., Tilly, P., Nusbaum, P., Vincent, A., Magnant, W., Skory, V., Birling, M. C., Pavlovic, G., Godin, J. D., Yalcin, B., ... Hinckelmann, M. V. (2019). TUBG1 missense variants underlying cortical malformations disrupt neuronal locomotion and microtubule dynamics but not neurogenesis. *Nature Communications*, 10(1). <https://doi.org/10.1038/s41467-019-10081-8>
- Iwai, S., Ishiji, A., Mabuchi, I., & Sutoh, K. (2004). A Novel Actin-bundling Kinesin-related Protein from Dictyostelium discoideum. *Journal of Biological Chemistry*, 279(6), 4696–4704. <https://doi.org/10.1074/jbc.M308022200>
- Jacobshagen, M., Niquille, M., Chaumont-Dubel, S., Marin, P., & Dayer, A. (2014). The serotonin 6 receptor controls neuronal migration during corticogenesis via a ligand-independent Cdk5-dependent mechanism. *Development (Cambridge)*, 141(17), 3370–3377. <https://doi.org/10.1242/dev.108043>
- Jaglin, X. H., Poirier, K., Saillour, Y., Buhler, E., Tian, G., Bahi-Buisson, N., Fallet-Bianco, C., Phan-Dinh-Tuy, F., Kong, X. P., Bomont, P., Castelnau-Ptakhine, L., Odent, S., Loget, P., Kossorotoff, M., Snoeck, I., Plessis, G., Parent, P., Beldjord, C., Cardoso, C., ... Chelly, J. (2009). Mutations in the B-tubulin gene TUBB2B result in asymmetrical polymicrogyria. *Nature Genetics*, 41(6), 746–752. <https://doi.org/10.1038/ng.380>
- Janisch, K. M., Vock, V. M., Fleming, M. S., Shrestha, A., Grimsley-Myers, C. M., Rasoul, B. A., Neale, S. A., Cupp, T. D., Kinchen, J. M., Liem, K. F., & Dwyer, N. D. (2013). The vertebrate-specific Kinesin-6, Kif20b, is required for normal cytokinesis of polarized cortical stem cells and cerebral cortex size. *Development (Cambridge)*, 140(23), 4672–4682. <https://doi.org/10.1242/dev.093286>
- Janke, C., & Magiera, M. M. (2020). The tubulin code and its role in controlling microtubule properties and functions. *Nature Reviews Molecular Cell Biology*. <https://doi.org/10.1038/s41580-020-0214-3>
- Jaulin, F., & Kreitzer, G. (2010). KIF17 stabilizes microtubules and contributes to epithelial morphogenesis by acting at MT plus ends with EB1 and APC. *Journal of Cell Biology*, 190(3), 443–460. <https://doi.org/10.1083/jcb.201006044>
- Javaherian, A., & Kriegstein, A. (2009). A stem cell niche for intermediate progenitor cells of the embryonic cortex. *Cerebral Cortex*, 19(SUPPL. 1). <https://doi.org/10.1093/cercor/bhp029>
- Jiang, H., Jiang, W., Zou, J., Wang, B., Yu, M., Pan, Y., Lin, Y., Mao, Y., & Wang, Y. (2015). The GluN2B subunit of N-methyl-D-aspartate receptor regulates the radial migration of cortical neurons in vivo. *Brain Research*, 1610, 20–32. <https://doi.org/10.1016/j.brainres.2015.03.031>
- Jossin, Y., & Cooper, J. A. (2011). Reelin, Rap1 and N-cadherin orient the migration of multipolar neurons in the developing neocortex. *Nature Neuroscience*, 14(6), 697–703. <https://doi.org/10.1038/nn.2816>
- Ju, X. da, Guo, Y., Wang, N. N., Huang, Y., Lai, M. M., Zhai, Y. H., Guo, Y. G., Zhang, J. H., Cao, R. J., Yu, H. L., Cui, L., Li, Y. T., Wang, X. Z., Ding, Y. Q., & Zhu, X. J. (2014). Both myosin-10 isoforms are required for radial neuronal migration in the developing cerebral cortex. *Cerebral Cortex*, 24(5), 1259–1268. <https://doi.org/10.1093/cercor/bhs407>
- Juanes, M. A., Isnardon, D., Badache, A., Brasselet, S., Mavrikakis, M., & Goode, B. L. (2019). The role of APC-mediated actin assembly in microtubule capture and focal adhesion turnover. *Journal of Cell Biology*, 218(10), 3415–3435. <https://doi.org/10.1083/JCB.201904165>

- Ka, M., Jung, E. M., Mueller, U., & Kim, W. Y. (2014). MACF1 regulates the migration of pyramidal neurons via microtubule dynamics and GSK-3 signaling. *Developmental Biology*, 395(1), 4–18. <https://doi.org/10.1016/j.ydbio.2014.09.009>
- Kalantari, S., & Filges, I. (2020a). “Kinesinopathies”: Emerging role of the kinesin family member genes in birth defects. In *Journal of Medical Genetics*. BMJ Publishing Group. <https://doi.org/10.1136/jmedgenet-2019-106769>
- Kalantari, S., & Filges, I. (2020b). “Kinesinopathies”: Emerging role of the kinesin family member genes in birth defects. In *Journal of Medical Genetics* (Vol. 57, Issue 12, pp. 797–807). BMJ Publishing Group. <https://doi.org/10.1136/jmedgenet-2019-106769>
- Kannan, M., Bayam, E., Wagner, C., Rinaldi, B., Kretz, P. F., Tilly, P., Roos, M., McGillemie, L., Bär, S., Minocha, S., Chevalier, C., Po, C., Chelly, J., Mandel, J.-L., Borgatti, R., Piton, A., Kinnear, C., Loos, B., Adams, D. J., ... Yalcin, B. (2017). WD40-repeat 47, a microtubule-associated protein, is essential for brain development and autophagy. *Proceedings of the National Academy of Sciences*, 114(44), E9308–E9317. <https://doi.org/10.1073/pnas.1713625114>
- Kapitein, L. C., & Hoogenraad, C. C. (2015). Building the Neuronal Microtubule Cytoskeleton. *Neuron*, 87(3), 492–506. <https://doi.org/10.1016/j.neuron.2015.05.046>
- Kashina, A. S., Baskin, R. J., Cole, D. G., Wedaman, K. P., Saxton, W. M., & Scholey, J. M. (1996). A bipolar kinesin. *Nature*, 379(6562), 270–272. <https://doi.org/10.1038/379270a0>
- Kawaguchi, A. (2021). Neuronal Delamination and Outer Radial Glia Generation in Neocortical Development. In *Frontiers in Cell and Developmental Biology* (Vol. 8). Frontiers Media S.A. <https://doi.org/10.3389/fcell.2020.623573>
- Kawauchi, T., Chihama, K., Nabeshima, Y. I., & Hoshino, M. (2006). Cdk5 phosphorylates and stabilizes p27kip1 contributing to actin organization and cortical neuronal migration. *Nature Cell Biology*, 8(1), 17–26. <https://doi.org/10.1038/ncb1338>
- Kawauchi, T., Chihama, K., Nabeshima, Y.-C., & Hoshino, M. (2003). The in vivo roles of STEF/Tiam1, Rac1 and JNK in cortical neuronal migration. *The EMBO Journal*.
- Kawauchi, T., Sekine, K., Shikanai, M., Chihama, K., Tomita, K., Kubo, K. ichiro, Nakajima, K., Nabeshima, Y. ichi, & Hoshino, M. (2010). Rab GTPases-dependent endocytic pathways regulate neuronal migration and maturation through N-cadherin trafficking. *Neuron*, 67(4), 588–602. <https://doi.org/10.1016/j.neuron.2010.07.007>
- Keays, D. A., Tian, G., Poirier, K., Huang, G. J., Siebold, C., Cleak, J., Oliver, P. L., Fray, M., Harvey, R. J., Molnár, Z., Piñon, M. C., Dear, N., Valdar, W., Brown, S. D. M., Davies, K. E., Rawlins, J. N. P., Cowan, N. J., Nolan, P., Chelly, J., & Flint, J. (2007). Mutations in α -Tubulin Cause Abnormal Neuronal Migration in Mice and Lissencephaly in Humans. *Cell*, 128(1), 45–57. <https://doi.org/10.1016/j.cell.2006.12.017>
- Kelkar, M., Bohec, P., & Charras, G. (2020). Mechanics of the cellular actin cortex: From signalling to shape change. *Current Opinion in Cell Biology*, 66, 69–78. <https://doi.org/10.1016/j.ceb.2020.05.008>
- Kelliher, M. T., Yue, Y., Ng, A., Kamiyama, D., Huang, B., Verhey, K. J., & Wildonger, J. (2018). Autoinhibition of kinesin-1 is essential to the dendrite-specific localization of Golgi outposts. *Journal of Cell Biology*, 217(7), 2531–2547. <https://doi.org/10.1083/jcb.201708096>
- Kevenaar, J. T., Bianchi, S., van Spronsen, M., Olieric, N., Lipka, J., Frias, C. P., Mikhaylova, M., Harterink, M., Keijzer, N., Wulf, P. S., Hilbert, M., Kapitein, L. C., de Graaff, E., Ahkmanova, A., Steinmetz, M. O., & Hoogenraad, C. C. (2016). Kinesin-Binding Protein Controls Microtubule Dynamics and Cargo Trafficking by Regulating Kinesin Motor Activity. *Current Biology*, 26(7), 849–861. <https://doi.org/10.1016/j.cub.2016.01.048>
- Klaus, J., Kanton, S., Kyrousi, C., Ayo-Martin, A. C., di Giaino, R., Riesenberger, S., O'Neill, A. C., Camp, J. G., Tocco, C., Santel, M., Rusha, E., Drukker, M., Schroeder, M., Götz, M., Robertson, S. P., Treutlein, B., & Cappello, S. (2019). Altered neuronal migratory trajectories

- in human cerebral organoids derived from individuals with neuronal heterotopia. *Nature Medicine*, 25(4), 561–568. <https://doi.org/10.1038/s41591-019-0371-0>
- Klingler, E., Francis, F., Jabaudon, D., & Cappello, S. (2021). Mapping the molecular and cellular complexity of cortical malformations. *Science*, 371(6527), eaba4517. <https://doi.org/10.1126/science.aba4517>
- Kodani, A., Kenny, C., Lai, A., Gonzalez, D. M., Stronge, E., Sejourne, G. M., Isacco, L., Partlow, J. N., O'Donnell, A., McWalter, K., Byrne, A. B., Barkovich, A. J., Yang, E., Hill, R. S., Gawlinski, P., Wiszniewski, W., Cohen, J. S., Fatemi, S. A., Baranano, K. W., ... Walsh, C. A. (2020). Posterior Neocortex-Specific Regulation of Neuronal Migration by CEP85L Identifies Maternal Centriole-Dependent Activation of CDK5. *Neuron*, 106(2), 246–255.e6. <https://doi.org/10.1016/j.neuron.2020.01.030>
- Kollman, J. M., Merdes, A., Mourey, L., & Agard, D. A. (2011). Microtubule nucleation by γ -tubulin complexes. In *Nature Reviews Molecular Cell Biology* (Vol. 12, Issue 11, pp. 709–721). <https://doi.org/10.1038/nrm3209>
- Kon, E., Calvo-Jimé Nez, E., Cossard, A., Na, Y., Cooper, J. A., & Jossin, Y. (2019). *N-cadherin-regulated FGFR ubiquitination and degradation control mammalian neocortical projection neuron migration*. <https://doi.org/10.7554/eLife.47673.001>
- Konjikusic, M. J., Gray, R. S., & Wallingford, J. B. (2021). The developmental biology of kinesins. In *Developmental Biology* (Vol. 469, pp. 26–36). Elsevier Inc. <https://doi.org/10.1016/j.ydbio.2020.09.009>
- Konno, D., Yoshimura, S., Hori, K., Maruoka, H., & Sobue, K. (2005). Involvement of the phosphatidylinositol 3-kinase/Rac1 and Cdc42 pathways in radial migration of cortical neurons. *Journal of Biological Chemistry*, 280(6), 5082–5088. <https://doi.org/10.1074/jbc.M408251200>
- Kreft, K. L., van Meurs, M., Wierenga-Wolf, A. F., Melief, M. J., van Strien, M. E., Hol, E. M., Oostra, B. A., Laman, J. D., & Hintzen, R. Q. (2014). Abundant kif21b is associated with accelerated progression in neurodegenerative diseases. *Acta Neuropathologica Communications*, 2(1). <https://doi.org/10.1186/s40478-014-0144-4>
- Kriegstein, A. R., & Noctor, S. C. (2004). Patterns of neuronal migration in the embryonic cortex. In *Trends in Neurosciences* (Vol. 27, Issue 7, pp. 392–399). <https://doi.org/10.1016/j.tins.2004.05.001>
- Kühn, S., Erdmann, C., Kage, F., Block, J., Schwenkmezger, L., Steffen, A., Rottner, K., & Geyer, M. (2015). The structure of FMNL2-Cdc42 yields insights into the mechanism of lamellipodia and filopodia formation. *Nature Communications*, 6. <https://doi.org/10.1038/ncomms8088>
- Kuznetsov, S. A., Vaisberg, E. A., Shanina, N. A., Magretova, N. N., Chernyak, V. Y., & Gelfand, V. I. (1988). The quaternary structure of bovine brain kinesin. *The EMBO Journal*, 7(2), 353–356. <https://doi.org/10.1002/j.1460-2075.1988.tb02820.x>
- Labonté, D., Thies, E., & Kneussel, M. (2014). The kinesin KIF21B participates in the cell surface delivery of α 2 subunit-containing GABA A receptors. *European Journal of Cell Biology*, 93(8–9), 338–346. <https://doi.org/10.1016/j.ejcb.2014.07.007>
- Lai, M., Guo, Y., Ma, J., Yu, H., Zhao, D., Fan, W., Ju, X., Sheikh, M. A., Malik, Y. S., Xiong, W., Guo, W., & Zhu, X. (2015). Myosin X regulates neuronal radial migration through interacting with N-cadherin. *Frontiers in Cellular Neuroscience*, 9(AUGUST). <https://doi.org/10.3389/fncel.2015.00326>
- Lawrence, C. J., Dawe, R. K., Christie, K. R., Cleveland, D. W., Dawson, S. C., Endow, S. A., Goldstein, L. S. B., Goodson, H. v., Hirokawa, N., Howard, J., Malmberg, R. L., McIntosh, J. R., Miki, H., Mitchison, T. J., Okada, Y., Reddy, A. S. N., Saxton, W. M., Schliwa, M., Scholey, J. M., ... Wordeman, L. (2004). A standardized kinesin nomenclature. In *Journal of Cell Biology* (Vol. 167, Issue 1, pp. 19–22). <https://doi.org/10.1083/jcb.200408113>

- Lehtinen, M. K., Zappaterra, M. W., Chen, X., Yang, Y. J., Hill, A. D., Lun, M., Maynard, T., Gonzalez, D., Kim, S., Ye, P., D'Ercole, A. J., Wong, E. T., LaMantia, A. S., & Walsh, C. A. (2011). The Cerebrospinal Fluid Provides a Proliferative Niche for Neural Progenitor Cells. *Neuron*, 69(5), 893–905. <https://doi.org/10.1016/j.neuron.2011.01.023>
- Liang, C., Carrel, D., Omelchenko, A., Kim, H., Patel, A., Fanget, I., & Firestein, B. L. (2019). Cortical Neuron Migration and Dendrite Morphology are Regulated by Carboxypeptidase e. *Cerebral Cortex*, 29(7), 2890–2903. <https://doi.org/10.1093/cercor/bhy155>
- Liang, C., Carrel, D., Singh, N. K., Hiester, L. L., Fanget, I., Kim, H., & Firestein, B. L. (2022). Carboxypeptidase E Independently Changes Microtubule Glutamylation, Dendritic Branching, and Neuronal Migration. *ASN Neuro*, 14. <https://doi.org/10.1177/17590914211062765>
- Lin Goh, K., Cai, L., Cepko, C. L., Gertler, F. B., Menzies, A., & Fassler, R. (2002). Ena/VASP Proteins Regulate Cortical Neuronal Positioning. In *Current Biology* (Vol. 12).
- Liu, X., Sun, L., Torii, M., & Rakic, P. (2012). Connexin 43 controls the multipolar phase of neuronal migration to the cerebral cortex. *Proceedings of the National Academy of Sciences of the United States of America*, 109(21), 8280–8285. <https://doi.org/10.1073/pnas.1205880109>
- Lombino, F. L., Muhia, M., Lopez-Rojas, J., Brill, M. S., Thies, E., Ruschkies, L., Lutz, D., Richter, M., Hausrat, T. J., Lopes, A. T., McNally, F. J., Hermans-Borgmeyer, I., Dunleavy, J. E. M., Hoffmeister-Ullerich, S., Frotscher, M., Misgeld, T., Kreutz, M. R., de Anda, F. C., & Kneussel, M. (2019). The Microtubule Severing Protein Katanin Regulates Proliferation of Neuronal Progenitors in Embryonic and Adult Neurogenesis. *Scientific Reports*, 9(1). <https://doi.org/10.1038/s41598-019-52367-3>
- Luhmann, H. J., & Fukuda, A. (2020). Can we understand human brain development from experimental studies in rodents? *Pediatrics International : Official Journal of the Japan Pediatric Society*, 62(10), 1139–1144. <https://doi.org/10.1111/ped.14339>
- Luo, W., Yu, C. han, Lieu, Z. Z., Allard, J., Mogilner, A., Sheetz, M. P., & Bershadsky, A. D. (2013). Analysis of the local organization and dynamics of cellular actin networks. *Journal of Cell Biology*, 202(7), 1057–1073. <https://doi.org/10.1083/jcb.201210123>
- Lynne Blasius, T., Yue, Y., Prasad, R. R., Liu, X., Gennerich, A., & Verhey, K. J. (2021). Sequences in the stalk domain regulate auto-inhibition and ciliary tip localization of the immotile kinesin-4 KIF7. *Journal of Cell Science*, 134(13). <https://doi.org/10.1242/jcs.258464>
- Lyons, D. A., Naylor, S. G., Mercurio, S., Dominguez, C., & Talbot, W. S. (2008). KBP is essential for axonal structure, outgrowth and maintenance in zebrafish, providing insight into the cellular basis of Goldberg-Shprintzen syndrome. *Development*, 135(3), 599–608. <https://doi.org/10.1242/dev.012377>
- Malatesta, P., Hack, M. A., Hartfuss, E., Kettenmann, H., Klinkert, W., & Kirchhoff, F. (2003). Neuronal or Glial Progeny: Regional Differences in Radial Glia Fate. *Neuron*, 37, 751–764. <http://www.neuron>.
- Marin, O., & Rubenstein, J. (2001). A long, Remarkable Journey: Tangential migration in the telencephalon. *Nature Reviews*.
- Marszalek, J. R., Weiner, J. A., Farlow, S. J., Chun, J., & Goldstein, L. S. B. (1999). Novel Dendritic Kinesin Sorting Identified by Different Process Targeting of Two Related Kinesins : KIF21A and KIF21B. 145(3), 469–479.
- Martín, C., Bueno, D., Alonso, M. I., Moro, J. A., Callejo, S., Parada, C., Martín, P., Carnicero, E., & Gato, A. (2006). FGF2 plays a key role in embryonic cerebrospinal fluid trophic properties over chick embryo neuroepithelial stem cells. *Developmental Biology*, 297(2), 402–416. <https://doi.org/10.1016/j.ydbio.2006.05.010>
- Martínez-Martínez, M., Ciceri, G., Espinós, A., Fernández, V., Marín, O., & Borrell, V. (2019). Extensive branching of radially-migrating neurons in the mammalian cerebral cortex. *Journal of Comparative Neurology*, 527(10), 1558–1576. <https://doi.org/10.1002/cne.24597>

- Martini, F. J., & Valdeolmillos, M. (2010). Actomyosin Contraction at the Cell Rear Drives Nuclear Translocation in Migrating Cortical Interneurons. *Journal of Neuroscience*, 30(25), 8660–8670. <https://doi.org/10.1523/JNEUROSCI.1962-10.2010>
- Martini, F. J., Valiente, M., López Bendito, G., Szabó, G., Moya, F., Valdeolmillos, M., & Marín, O. (2009). Biased selection of leading process branches mediates chemotaxis during tangential neuronal migration. *Development*, 136(1), 41–50. <https://doi.org/10.1242/dev.025502>
- Mary, S., Charrasse, S., Meriane, M., Comunale, F., Travo, P., Blangy, A., & Gauthier-Rouvière, C. (2002). Biogenesis of N-cadherin-dependent cell-cell contacts in living fibroblasts is a microtubule-dependent kinesin-driven mechanism. *Molecular Biology of the Cell*, 13(1), 285–301. <https://doi.org/10.1091/mbc.01-07-0337>
- Masters, T. A., Kendrick-Jones, J., & Buss, F. (2017). Myosins: Domain organisation, motor properties, physiological roles and cellular functions. *Handbook of Experimental Pharmacology*, 235, 77–122. https://doi.org/10.1007/164_2016_29
- Masucci, E. M., Relich, P. K., Lakadamyali, M., Ostap, E. M., & Holzbaur, E. L. F. (2021). *Microtubule dynamics influence the retrograde biased motility of kinesin-4 motor teams in neuronal dendrites.*
- Mayer, C., Hafemeister, C., Bandler, R. C., Machold, R., Batista Brito, R., Jaglin, X., Allaway, K., Butler, A., Fishell, G., & Satija, R. (2018). Developmental diversification of cortical inhibitory interneurons. *Nature*, 555(7697), 457–462. <https://doi.org/10.1038/nature25999>
- McNeely, K. C., Cupp, T. D., Little, J. N., Janisch, K. M., Shrestha, A., & Dwyer, N. D. (2017). Mutation of Kinesin-6 Kif20b causes defects in cortical neuron polarization and morphogenesis. *Neural Development*, 12(1). <https://doi.org/10.1186/s13064-017-0082-5>
- Medvedeva, V. P., & Pierani, A. (2020). How Do Electric Fields Coordinate Neuronal Migration and Maturation in the Developing Cortex? In *Frontiers in Cell and Developmental Biology* (Vol. 8). Frontiers Media S.A. <https://doi.org/10.3389/fcell.2020.580657>
- Mennella, V., Rogers, G. C., Rogers, S. L., Buster, D. W., Vale, R. D., & Sharp, D. J. (2005). Functionally distinct kinesin-13 family members cooperate to regulate microtubule dynamics during interphase. *Nature Cell Biology*, 7(3), 235–245. <https://doi.org/10.1038/ncb1222>
- Meyerink, B. L., Kc, P., Tiwari, N. K., Kittock, C. M., Klein, A., Evans, C., & Pilaz, L.-J. (2022). Breasi-CRISPR: an efficient genome editing method to interrogate protein localization and protein-protein interactions in the embryonic mouse cortex Protein-tagging in corticogenesis. *Development*. <https://doi.org/10.1101/2022.02.02.478837>
- Meyerink, B. L., Tiwari, N. K., & Pilaz, L. J. (2020). Ariadne's Thread in the Developing Cerebral Cortex: Mechanisms Enabling the Guiding Role of the Radial Glia Basal Process during Neuron Migration. In *Cells* (Vol. 10, Issue 1). NLM (Medline). <https://doi.org/10.3390/cells10010003>
- Mi, D., Li, Z., Lim, L., Li, M., Moissidis, M., Yang, Y., Gao, T., Hu, T. X., Pratt, T., Price, D. J., Sestan, N., & Marín, † Oscar. (2018). Early emergence of cortical interneuron diversity in the mouse embryo. *Science*. <https://www.science.org>
- Mirzaa, G. M., Vitre, B., Carpenter, G., Abramowicz, I., Gleeson, J. G., Paciorkowski, A. R., Cleveland, D. W., Dobyns, W. B., & O'Driscoll, M. (2014). Mutations in CENPE define a novel kinetochore-centromeric mechanism for microcephalic primordial dwarfism. *Human Genetics*, 133(8), 1023–1039. <https://doi.org/10.1007/s00439-014-1443-3>
- Miyata, T., Kawaguchi, A., Saito, K., Kawano, M., Muto, T., & Ogawa, M. (2004). Asymmetric production of surface-dividing and non-surface-dividing cortical progenitor cells. *Development*, 131(13), 3133–3145. <https://doi.org/10.1242/dev.01173>
- Miyata, T., Okamoto, M., Shinoda, T., & Kawaguchi, A. (2015). Interkinetic nuclear migration generates and opposes ventricular-zone crowding: Insight into tissue mechanics. In *Frontiers*

- in Cellular Neuroscience* (Vol. 8, Issue JAN). Frontiers Research Foundation.
<https://doi.org/10.3389/fncel.2014.00473>
- Miyoshi, G., & Fishell, G. (2012). Dynamic FoxG1 Expression Coordinates the Integration of Multipolar Pyramidal Neuron Precursors into the Cortical Plate. *Neuron*, 74(6), 1045–1058.
<https://doi.org/10.1016/j.neuron.2012.04.025>
- Molyneaux, B., Arlotta, P., Menezes, J., & Macklis, J. (2007). Neuronal subtype specification in the cerebral cortex. *Nature Reviews Neuroscience*, 8(June), 427–437.
<https://doi.org/10.1038/nrn2151>
- Monroy, B. Y., Tan, T. C., Oclaman, J. M., Han, J. S., Simó, S., Niwa, S., Nowakowski, D. W., McKenney, R. J., & Ori-McKenney, K. M. (2020). A Combinatorial MAP Code Dictates Polarized Microtubule Transport. *Developmental Cell*, 53(1), 60–72.e4.
<https://doi.org/10.1016/j.devcel.2020.01.029>
- Morikawa, M., Tanaka, Y., Cho, H., Yoshihara, M., & Hirokawa, N. (2018). The Molecular Motor KIF21B Mediates Synaptic Plasticity and Fear Extinction by Terminating Rac1 Activation. *CellReports*, 23(13), 3864–3877. <https://doi.org/10.1016/j.celrep.2018.05.089>
- Moslehi, M., Ng, D. C. H., & Bogoyevitch, M. A. (2017). Dynamic microtubule association of Doublecortin X (DCX) is regulated by its C-terminus. *Scientific Reports*, 7(1).
<https://doi.org/10.1038/s41598-017-05340-x>
- Mostowy, S., & Cossart, P. (2012). Septins: The fourth component of the cytoskeleton. In *Nature Reviews Molecular Cell Biology* (Vol. 13, Issue 3, pp. 183–194).
<https://doi.org/10.1038/nrm3284>
- Muhia, M., Thies, E., Labonté, D., Ghiretti, A., Gromova, K., Xompero, F., Lappe-Siefke, C., Hermans-Borgomeyer, I., Kuhl, D., Schweizer, M., Ohana, O., Schwartz, J., Holzbaur, E., & Kneussel, M. (2016). *The Kinesin KIF21B Regulates Microtubule Dynamics and Is Essential for Neuronal Morphology, Synapse Function, and Learning and Memory*. 968–977.
<https://doi.org/10.1016/j.celrep.2016.03.086>
- Murali, A., & Rajalingam, K. (2014). Small Rho GTPases in the control of cell shape and mobility. In *Cellular and Molecular Life Sciences* (Vol. 71, Issue 9, pp. 1703–1721). Birkhauser Verlag AG. <https://doi.org/10.1007/s00018-013-1519-6>
- Muralidharan, H., Guha, S., Madugula, K., Patil, A., Bennison, S. A., Sun, X., Toyo-Oka, K., & Baas, P. W. (2022). KIFC1 Regulates the Trajectory of Neuronal Migration. *The Journal of Neuroscience: The Official Journal of the Society for Neuroscience*, 42(11), 2149–2165.
<https://doi.org/10.1523/JNEUROSCI.1708-21.2022>
- Murrell, M., Oakes, P. W., Lenz, M., & Gardel, M. L. (2015). Forcing cells into shape: The mechanics of actomyosin contractility. In *Nature Reviews Molecular Cell Biology* (Vol. 16, Issue 8, pp. 486–498). Nature Publishing Group. <https://doi.org/10.1038/nrm4012>
- Mustyatsa, V. v., Boyakhchyan, A. v., Ataullakhanov, F. I., & Gudimchuk, N. B. (2017). EB-family proteins: Functions and microtubule interaction mechanisms. In *Biochemistry (Moscow)* (Vol. 82, Issue 7, pp. 791–802). Maik Nauka Publishing / Springer SBM.
<https://doi.org/10.1134/S0006297917070045>
- Myshrall, T. D., Moore, S. A., Ostendorf, A. P., Satz, J. S., Kowalczyk, T., Nguyen, H., Daza, R. A. M., Lau, C., Campbell, K. P., & Hevner, R. F. (2012). Dystroglycan on radial glia end feet is required for pial basement membrane integrity and columnar organization of the developing cerebral cortex. *Journal of Neuropathology and Experimental Neurology*, 71(12), 1047–1063.
<https://doi.org/10.1097/NEN.0b013e318274a128>
- Nadarajah, B., Brunstrom, J. E., Grutzendler, J., Wong, R. O. L., & Pearlman, A. L. (2001). *Two modes of radial migration in early development of the cerebral cortex*.
<http://neurosci.nature.com>

- Nadarajah, B., & Parnavelas, J. G. (2002). Modes of neuronal migration in the developing cerebral cortex. In *Nature Reviews Neuroscience* (Vol. 3, Issue 6, pp. 423–432). European Association for Cardio-Thoracic Surgery. <https://doi.org/10.1038/nrn845>
- Nag, S., Larsson, M., Robinson, R. C., & Burtneck, L. D. (2013). Gelsolin: The tail of a molecular gymnast. In *Cytoskeleton* (Vol. 70, Issue 7, pp. 360–384). <https://doi.org/10.1002/cm.21117>
- Nagano, T., Yoneda, T., Hatanaka, Y., Kubota, C., Murakami, F., & Sato, M. (2002). Filamin A-interacting protein (FILIP) regulates cortical cell migration out of the ventricular zone. *Nature Cell Biology*, 4(7), 495–501. <https://doi.org/10.1038/ncb808>
- Nakamuta, S., Funahashi, Y., Namba, T., Arimura, N., Picciotto, M. R., Tokumitsu, H., Soderling, T. R., Sakakibara, A., Miyata, T., Kamiguchi, H., & Kaibuchi, K. (2011). *Local Application of Neurotrophins Specifies Axons Through Inositol 1,4,5-Trisphosphate, Calcium, and Ca²⁺/Calmodulin-Dependent Protein Kinases*. www.SCIENCESIGNALING.org
- Nakazawa, N., & Kengaku, M. (2020a). Mechanical Regulation of Nuclear Translocation in Migratory Neurons. *Frontiers in Cell and Developmental Biology*, 8. <https://doi.org/10.3389/fcell.2020.00150>
- Nakazawa, N., & Kengaku, M. (2020b). Mechanical Regulation of Nuclear Translocation in Migratory Neurons. In *Frontiers in Cell and Developmental Biology* (Vol. 8). Frontiers Media S.A. <https://doi.org/10.3389/fcell.2020.00150>
- Narayanan, D. L., Rivera Alvarez, J., Tilly, P., do Rosario, M. C., Bhat, V., Godin, J. D., & Shukla, A. (2022). Further delineation of KIF21B-related neurodevelopmental disorders. *Journal of Human Genetics*. <https://doi.org/10.1038/s10038-022-01087-0>
- Narita, A. (2020). ADF/cofilin regulation from a structural viewpoint. *Journal of Muscle Research and Cell Motility*, 41(1), 141–151. <https://doi.org/10.1007/s10974-019-09546-6>
- Nelson, B. R., Hodge, R. D., Bedogni, F., & Hevner, R. F. (2013). Dynamic interactions between intermediate neurogenic progenitors and radial glia in embryonic mouse neocortex: Potential role in Dll1-notch signaling. *Journal of Neuroscience*, 33(21), 9122–9139. <https://doi.org/10.1523/JNEUROSCI.0791-13.2013>
- Nieto, M., Monuki, E. S., Tang, H., Imitola, J., Haubst, N., Khoury, S. J., Cunningham, J., Gotz, M., & Walsh, C. A. (2004). Expression of Cux-1 and Cux-2 in the subventricular zone and upper layers II–IV of the cerebral cortex. *Journal of Comparative Neurology*, 479(2), 168–180. <https://doi.org/10.1002/cne.20322>
- Nishimura, Y. v., Sekine, K., Chihama, K., Nakajima, K., Hoshino, M., Nabeshima, Y. I., & Kawauchi, T. (2010). Dissecting the factors involved in the locomotion mode of neuronal migration in the developing cerebral cortex. *Journal of Biological Chemistry*, 285(8), 5878–5887. <https://doi.org/10.1074/jbc.M109.033761>
- Nishimura, Y. v., Shikanai, M., Hoshino, M., Ohshima, T., Nabeshima, Y. I., Mizutani, K. I., Nagata, K. I., Nakajima, K., & Kawauchi, T. (2014). Cdk5 and its substrates, Dcx and p27kip1, regulate cytoplasmic dilation formation and nuclear elongation in migrating neurons. *Development (Cambridge)*, 141(18), 3540–3550. <https://doi.org/10.1242/dev.111294>
- Noctor, S. C., Martínez-Cerdeño, V., Ivic, L., & Kriegstein, A. R. (2004). Cortical neurons arise in symmetric and asymmetric division zones and migrate through specific phases. *Nature Neuroscience*, 7(2), 136–144. <https://doi.org/10.1038/nn1172>
- Noctor, S. C., Martínez-Cerdeño, V., & Kriegstein, A. R. (2008). Distinct behaviors of neural stem and progenitor cells underlie cortical neurogenesis. *Journal of Comparative Neurology*, 508(1), 28–44. <https://doi.org/10.1002/cne.21669>
- Ohi, R., Wordeman, L., & Vikash, V. (2021). Cytoskeleton | Kinesins as Microtubule Disassembly Enzymes. In *Encyclopedia of Biological Chemistry III (Third Edition)* (Vol. 5, pp. 220–227).
- Ohshima, T., Hirasawa, M., Tabata, H., Mutoh, T., Adachi, T., Suzuki, H., Saruta, K., Iwasato, T., Itohara, S., Hashimoto, M., Nakajima, K., Ogawa, M., Kulkarni, A. B., & Mikoshiba, K. (2007). Cdk5 is required for multipolar-to-bipolar transition during neuronal migration and

- proper dendrite development of pyramidal neurons in the cerebral cortex. *Development*, 134(12), 2273–2282. <https://doi.org/10.1242/dev.02854>
- Ohtaka-Maruyama, C., & Okado, H. (2015). Molecular pathways underlying projection neuron production and migration during cerebral cortical development. In *Frontiers in Neuroscience* (Vol. 9, Issue DEC). Frontiers Media S.A. <https://doi.org/10.3389/fnins.2015.00447>
- Ohtaka-Maruyama, C., Okamoto, M., Endo, K., Oshima, M., Kaneko, N., Yura, K., Okado, H., Miyata, T., & Maeda, N. (2018). Synaptic transmission from subplate neurons controls radial migration of neocortical neurons. *Neurodevelopment*, 1–4. <http://science.sciencemag.org/>
- Ostergaard, P., Simpson, M. A., Mendola, A., Vasudevan, P., Connell, F. C., van Impel, A., Moore, A. T., Loeys, B. L., Ghalamkarpour, A., Onoufriadis, A., Martinez-Corral, I., Devery, S., Leroy, J. G., van Laer, L., Singer, A., Bialer, M. G., McEntagart, M., Quarrell, O., Brice, G., ... Jeffery, S. (2012). Mutations in KIF11 cause autosomal-dominant microcephaly variably associated with congenital lymphedema and chorioretinopathy. *American Journal of Human Genetics*, 90(2), 356–362. <https://doi.org/10.1016/j.ajhg.2011.12.018>
- Parrini, E., Ramazzotti, A., Dobyns, W. B., Mei, D., Moro, F., Veggiotti, P., Marini, C., Brilstra, E. H., Bernardina, B. D., Goodwin, L., Bodell, A., Jones, M. C., Nangeroni, M., Palmeri, S., Said, E., Sander, J. W., Striano, P., Takahashi, Y., van Maldergem, L., ... Guerrini, R. (2006). Periventricular heterotopia: Phenotypic heterogeneity and correlation with Filamin a mutations. *Brain*, 129(7), 1892–1906. <https://doi.org/10.1093/brain/awl125>
- Peregrina, C., & del Toro, D. (2020). FLRTing Neurons in Cortical Migration During Cerebral Cortex Development. In *Frontiers in Cell and Developmental Biology* (Vol. 8). Frontiers Media S.A. <https://doi.org/10.3389/fcell.2020.578506>
- Petryniak, M. A., Potter, G. B., Rowitch, D. H., & Rubenstein, J. L. R. (2007). Dlx1 and Dlx2 Control Neuronal versus Oligodendroglial Cell Fate Acquisition in the Developing Forebrain. *Neuron*, 55(3), 417–433. <https://doi.org/10.1016/j.neuron.2007.06.036>
- Pilz, D. T., Matsumoto, N., Minnerath, S., Mills, P., Gleeson, J. G., Allen, K. M., Walsh, C. A., Barkovich, A. J., Dobyns, W. B., Ledbetter, D. H., & Ross, M. E. (1998). LIS1 and XLIS (DCX) mutations cause most classical lissencephaly, but different patterns of malformation. In *Human Molecular Genetics* (Vol. 7, Issue 13).
- Poirier, K., Lebrun, N., Broix, L., Tian, G., Saillour, Y., Boscheron, C., Parrini, E., Valence, S., Pierre, B. saint, Oger, M., Lacombe, D., Geneviève, D., Fontana, E., Darra, F., Cances, C., Barth, M., Bonneau, D., Bernadina, B. D., N’Guyen, S., ... Chelly, J. (2013). Mutations in TUBG1, DYNC1H1, KIF5C and KIF2A cause malformations of cortical development and microcephaly. *Nature Genetics*, 45(6), 639–647. <https://doi.org/10.1038/ng.2613>
- Pollard, T. D. (2016). Actin and actin-binding proteins. *Cold Spring Harbor Perspectives in Biology*, 8(8). <https://doi.org/10.1101/cshperspect.a018226>
- Preuss, M. L., Kovar, D. R., Lee, Y. R. J., Staiger, C. J., Delmer, D. P., & Liu, B. (2004). A plant-specific kinesin binds to actin microfilaments and interacts with cortical microtubules in cotton fibers. *Plant Physiology*, 136(4), 3945–3955. <https://doi.org/10.1104/pp.104.052340>
- Price, D. J., Aslam, S., Tasker, L., & Gillies, K. (1997). Fates of the Earliest Generated Cells in the Developing Murine Neocortex. In *J. Comp. Neurol* (Vol. 377). Wiley-Liss, Inc.
- Putoux, A., Thomas, S., Coene, K. L. M., Davis, E. E., Alanay, Y., Ogur, G., Uz, E., Buzas, D., Gomes, C., Patrier, S., Bennett, C. L., Elkhartoufi, N., Frison, M. H. saint, Rigonnot, L., Joyé, N., Pruvost, S., Utine, G. E., Boduroglu, K., Nitschke, P., ... Attié-Bitach, T. (2011). KIF7 mutations cause fetal hydroletharus and acrocallosal syndromes. *Nature Genetics*, 43(6), 601–606. <https://doi.org/10.1038/ng.826>
- Rafiq, N. B. M., Nishimura, Y., Plotnikov, S. v., Thiagarajan, V., Zhang, Z., Shi, S., Natarajan, M., Viasnoff, V., Kanchanawong, P., Jones, G. E., & Bershadsky, A. D. (2019). A mechano-signalling network linking microtubules, myosin IIA filaments and integrin-based adhesions. *Nature Materials*, 18(6), 638–649. <https://doi.org/10.1038/s41563-019-0371-y>

- Rago, L., Beattie, R., Taylor, V., & Winter, J. (2014). MiR379-410 cluster miRNAs regulate neurogenesis and neuronal migration by fine-tuning N-cadherin. *EMBO Journal*, 33(8), 906–920. <https://doi.org/10.1002/emboj.201386591>
- Rakic, P. (1972). Mode of Cell Migration to the Superficial Layers of Fetal Monkey Neocortex '. *Journal of Comparative Biology*.
- Rakic, P. (1974). Neurons in Rhesus Monkey Visual Cortex: Systematic Relation between Time of Origin and Eventual Dispositi. *Science*, 183.
- Rakic, P. (2009). Evolution of the neocortex: A perspective from developmental biology. In *Nature Reviews Neuroscience* (Vol. 10, Issue 10, pp. 724–735). <https://doi.org/10.1038/nrn2719>
- Rallu, M., Machold, R., Gaiano, N., Corbin, J., McMahon, A., & Fishel, G. (2002). Dorsoventral patterning is established in the telencephalon of mutants lacking both Gli3 and Hedgehog signaling. *Development*, 129, 4963–4974.
- Ravenscroft, G., di Donato, N., Hahn, G., Davis, M. R., Craven, P. D., Poke, G., Neas, K. R., Neuhaus, T. M., Dobyns, W. B., & Laing, N. G. (2016). Recurrent de novo BICD2 mutation associated with arthrogryposis multiplex congenita and bilateral perisylvian polymicrogyria. *Neuromuscular Disorders*, 26(11), 744–748. <https://doi.org/10.1016/j.nmd.2016.09.009>
- Riccio, O., Jacobshagen, M., Golding, B., Vutsits, L., Jabaudon, D., Hornung, J. P., & Dayer, A. G. (2011). Excess of serotonin affects neocortical pyramidal neuron migration. *Translational Psychiatry*, 1. <https://doi.org/10.1038/tp.2011.49>
- Romero, D. M., Poirier, K., Belvindrah, R., Moutkine, I., Houllier, A., LeMoing, A. G., Petit, F., Boland, A., Collins, S. C., Soiza-Reilly, M., Yalcin, B., Chelly, J., Deleuze, J. F., Bahi-Buisson, N., & Francis, F. (2022). Novel role of the synaptic scaffold protein Dlgap4 in ventricular surface integrity and neuronal migration during cortical development. *Nature Communications*, 13(1). <https://doi.org/10.1038/s41467-022-30443-z>
- Rubenstein, J. L. R., Shimamura, K., Martinez, S., & Puelles, L. (1998). REGIONALIZATION OF THE PROSENCEPHALIC NEURAL PLATE. In *Annu. Rev. Neurosci* (Vol. 21). www.annualreviews.org
- Saillour, Y., Broix, L., Bruel-Jungerman, E., Lebrun, N., Muraca, G., Rucci, J., Poirier, K., Belvindrah, R., Francis, F., & Chelly, J. (2014). Beta tubulin isoforms are not interchangeable for rescuing impaired radial migration due to Tubb3 knockdown. *Human Molecular Genetics*, 23(6), 1516–1526. <https://doi.org/10.1093/hmg/ddt538>
- Salmi, M., Bruneau, N., Cillario, J., Lozovaya, N., Massacrier, A., Buhler, E., Cloarec, R., Tsintsadze, T., Watrin, F., Tsintsadze, V., Zimmer, C., Villard, C., Lafitte, D., Cardoso, C., Bao, L., Lesca, G., Rudolf, G., Muscatelli, F., Pauly, V., ... Szepietowski, P. (2013). Tubacin prevents neuronal migration defects and epileptic activity caused by rat SrpX2 silencing in utero. *Brain*, 136(8), 2457–2473. <https://doi.org/10.1093/brain/awt161>
- Sapir, T., Frotscher, M., Levy, T., Mandelkow, E. M., & Reiner, O. (2012). Tau's role in the developing brain: Implications for intellectual disability. *Human Molecular Genetics*, 21(8), 1681–1692. <https://doi.org/10.1093/hmg/ddr603>
- Sapir, T., Levy, T., Sakakibara, A., Rabinkov, A., Miyata, T., & Reiner, O. (2013). Shootin1 acts in concert with KIF20B to promote polarization of migrating neurons. *Journal of Neuroscience*, 33(29), 11932–11948. <https://doi.org/10.1523/JNEUROSCI.5425-12.2013>
- Saud, K., Cánovas, J., Lopez, C. I., Berndt, F. A., López, E., Maass, J. C., Barriga, A., & Kukuljan, M. (2017). SFPQ associates to LSD1 and regulates the migration of newborn pyramidal neurons in the developing cerebral cortex. *International Journal of Developmental Neuroscience*, 57, 1–11. <https://doi.org/10.1016/j.ijdevneu.2016.12.006>
- Sauer. (1935). *Mitosis in the neural tube*.
- Sayas, C., & Avila, J. (2014). Regulation of EB1/3 proteins by classical MAPs in neurons. In *Bioarchitecture* (Vol. 4, Issue 1, pp. 1–5). <https://doi.org/10.1038/nrn2631>

- Schaar, B. T., & McConnell, S. K. (2005). *Cytoskeletal coordination during neuronal migration* (Vol. 102, Issue 38). Genentech, Inc. www.pnas.org/cgi/doi/10.1073/pnas.0506008102
- Schaffer, A. E., Breuss, M. W., Caglayan, A. O., Al-Sanaa, N., Al-Abdulwahed, H. Y., Kaymakçalan, H., Yilmaz, C., Zaki, M. S., Rosti, R. O., Copeland, B., Baek, S. T., Musaev, D., Scott, E. C., Ben-Omran, T., Kariminejad, A., Kayserili, H., Mojahedi, F., Kara, M., Cai, N., ... Gleeson, J. G. (2018). Biallelic loss of human CTNNA2, encoding α N-catenin, leads to ARP2/3 complex overactivity and disordered cortical neuronal migration. In *Nature Genetics* (Vol. 50, Issue 8, pp. 1093–1101). Nature Publishing Group. <https://doi.org/10.1038/s41588-018-0166-0>
- Sessa, A., Mao, C. A., Colasante, G., Nini, A., Klein, W. H., & Broccoli, V. (2010). Tbr2-positive intermediate (basal) neuronal progenitors safeguard cerebral cortex expansion by controlling amplification of pallial glutamatergic neurons and attraction of subpallial GABAergic interneurons. *Genes and Development*, 24(16), 1816–1826. <https://doi.org/10.1101/gad.575410>
- Shan, M. M., Zou, Y. J., Pan, Z. N., Zhang, H. L., Xu, Y., Ju, J. Q., & Sun, S. C. (2022). Kinesin motor KIFC1 is required for tubulin acetylation and actin-dependent spindle migration in mouse oocyte meiosis. *Development (Cambridge, England)*, 149(5). <https://doi.org/10.1242/dev.200231>
- Shibata, T., Yamada, K., Watanabe, M., Ikenaka, K., Wada, K., Tanaka, K., & Inoue, Y. (1997). Glutamate transporter GLAST is expressed in the radial glia-astrocyte lineage of developing mouse spinal cord. *The Journal of Neuroscience : The Official Journal of the Society for Neuroscience*, 17(23), 9212–9219.
- Shikanai, M., Nakajima, K., & Kawauchi, T. (2011). N-cadherin regulates radial glial fiber-dependent migration of cortical locomoting neurons. *Communicative & Integrative Biology*, 4, 588–602. <https://doi.org/10.1016/j.neuron.201>
- Shinoda, T., Ito, H., Sudo, K., Iwamoto, I., Morishita, R., & Nagata, K.-I. (2010). Septin 14 Is Involved in Cortical Neuronal Migration via Interaction with Septin 4. *Molecular Biology of the Cell*, 21, 1324–1334. <https://doi.org/10.1091/mbc.E09>
- Shintani, T., Takeuchi, Y., Fujikawa, A., & Noda, M. (2012). Directional neuronal migration is impaired in mice lacking adenomatous polyposis coli 2. *Journal of Neuroscience*, 32(19), 6468–6484. <https://doi.org/10.1523/JNEUROSCI.0590-12.2012>
- Shipp, S. (2007). Structure and function of the cerebral cortex. In *Current Biology* (Vol. 17, Issue 12). Cell Press. <https://doi.org/10.1016/j.cub.2007.03.044>
- Shu, T., Ayala, R., Nguyen, M.-D., Xie, Z., Gleeson, J. G., & Tsai, L.-H. (2004a). Ndel1 Operates in a Common Pathway with LIS1 and Cytoplasmic Dynein to Regulate Cortical Neuronal Positioning Ndel1 forms a common pathway with LIS1 and dynein. In *Neuron* (Vol. 44). <http://www.neuron.org/cgi/content/full/>
- Shu, T., Ayala, R., Nguyen, M.-D., Xie, Z., Gleeson, J. G., & Tsai, L.-H. (2004b). Ndel1 Operates in a Common Pathway with LIS1 and Cytoplasmic Dynein to Regulate Cortical Neuronal Positioning Ndel1 forms a common pathway with LIS1 and dynein. In *Neuron* (Vol. 44). <http://www.neuron.org/cgi/content/full/>
- Siegenthaler, J. A., Ashique, A. M., Zarbalis, K., Patterson, K. P., Hecht, J. H., Kane, M. A., Folias, A. E., Choe, Y., May, S. R., Kume, T., Napoli, J. L., Peterson, A. S., & Pleasure, S. J. (2009). Retinoic Acid from the Meninges Regulates Cortical Neuron Generation. *Cell*, 139(3), 597–609. <https://doi.org/10.1016/j.cell.2009.10.004>
- Silva, C. G., Peyre, E., Adhikari, M. H., Tielens, S., Tanco, S., van Damme, P., Magno, L., Krusy, N., Agirman, G., Magiera, M. M., Kessar, N., Malgrange, B., Andrieux, A., Janke, C., & Nguyen, L. (2018). Cell-Intrinsic Control of Interneuron Migration Drives Cortical Morphogenesis. *Cell*, 172(5), 1063–1078.e19. <https://doi.org/10.1016/j.cell.2018.01.031>

- Silva, C. G., Peyre, E., & Nguyen, L. (2019). Cell migration promotes dynamic cellular interactions to control cerebral cortex morphogenesis. In *Nature Reviews Neuroscience* (Vol. 20, Issue 6, pp. 318–329). Nature Publishing Group. <https://doi.org/10.1038/s41583-019-0148-y>
- Sirajuddin, M., Rice, L. M., & Vale, R. D. (2014). Regulation of microtubule motors by tubulin isoforms and post-translational modifications. *Nature Cell Biology*, 16(4), 335–344. <https://doi.org/10.1038/ncb2920>
- Sokpor, G., Brand-Saberi, B., Nguyen, H. P., & Tuoc, T. (2022). Regulation of Cell Delamination During Cortical Neurodevelopment and Implication for Brain Disorders. In *Frontiers in Neuroscience* (Vol. 16). Frontiers Media S.A. <https://doi.org/10.3389/fnins.2022.824802>
- Solecki, D. J., Model, L., Gaetz, J., Kapoor, T. M., & Hatten, M. E. (2004). Par6 α signaling controls glial-guided neuronal migration. *Nature Neuroscience*, 7(11), 1195–1203. <https://doi.org/10.1038/nn1332>
- Solecki, D. J., Trivedi, N., Govek, E. E., Kerekes, R. A., Gleason, S. S., & Hatten, M. E. (2009). Myosin II motors and F-actin dynamics drive the coordinated movement of the centrosome and soma during CNS glial-guided neuronal migration. *Neuron*, 63(1), 63–80. <https://doi.org/10.1016/j.neuron.2009.05.028>
- Sonego, M., Oberoi, M., Stoddart, J., Gajendra, S., Hendricusdottir, R., Oozeer, F., Worth, D. C., Hobbs, C., Eickholt, B. J., Gordon-Weeks, P. R., Doherty, P., & Lalli, G. (2015). Drebrin regulates neuroblast migration in the postnatal mammalian brain. *PLoS ONE*, 10(5). <https://doi.org/10.1371/journal.pone.0126478>
- Soppina, V., Norris, S. R., Dizaji, A. S., Kortus, M., Veatch, S., Peckham, M., & Verhey, K. J. (2014). Dimerization of mammalian kinesin-3 motors results in superprocessive motion. *Proceedings of the National Academy of Sciences of the United States of America*, 111(15), 5562–5567. <https://doi.org/10.1073/pnas.1400759111>
- Spiering, D., & Hodgson, L. (2011). Dynamics of the rho-family small GTPases in actin regulation and motility. In *Cell Adhesion and Migration* (Vol. 5, Issue 2, pp. 170–180). Taylor and Francis Inc. <https://doi.org/10.4161/cam.5.2.14403>
- Stirnimann, C. U., Petsalaki, E., Russell, R. B., & Müller, C. W. (2010). WD40 proteins propel cellular networks. *Trends in Biochemical Sciences*, 35(10), 565–574. <https://doi.org/10.1016/j.tibs.2010.04.003>
- Stouffer, M. A., Golden, J. A., & Francis, F. (2016). Neuronal migration disorders: Focus on the cytoskeleton and epilepsy. *Neurobiology of Disease*, 92(Part A), 18–45. <https://doi.org/10.1016/j.nbd.2015.08.003>
- Sturgill, E. G., & Ohi, R. (2013). Microtubule-regulating kinesins. In *Current Biology* (Vol. 23, Issue 21). Cell Press. <https://doi.org/10.1016/j.cub.2013.08.012>
- Su, Y. S., Wang, J., Asada, N., Neumayer, G., Hong, C. T., Ishiguro, K. I., Sanada, K., Nakatani, Y., & Minh, D. N. (2008). Protein 600 is a microtubule/endoplasmic reticulum-associated protein in CNS neurons. *Journal of Neuroscience*, 28(14), 3604–3614. <https://doi.org/10.1523/JNEUROSCI.5278-07.2008>
- Subramaniam, Y., Murthy, D., Ayyappa Raja, D., Ramkumar, A., Sivasubbu, S., Mcewan, D. G., Gokhale, R. S., & Natarajan, V. T. (2021). kinesin recruitment by adapter SKIP on melanosomes is dynamically controlled by LC3B phosphorylation Classification: Cell Biology Running Title: Dynamic control of melanosome transport. *BioRxiv*. <https://doi.org/10.1101/2021.03.11.434917>
- Sultan, K. T., Brown, K. N., & Shi, S. H. (2013). Production and organization of neocortical interneurons. In *Frontiers in Cellular Neuroscience* (Vol. 7, Issue NOV). <https://doi.org/10.3389/fncel.2013.00221>

- Sutherland, A., & Lesko, A. (2020). Pulsed actomyosin contractions in morphogenesis. In *F1000Research* (Vol. 9). F1000 Research Ltd. <https://doi.org/10.12688/f1000research.20874.1>
- Svitkina, T. (2018). The actin cytoskeleton and actin-based motility. *Cold Spring Harbor Perspectives in Biology*, 10(1). <https://doi.org/10.1101/cshperspect.a018267>
- Szczurkowska, J., Pischedda, F., Pinto, B., Manag, F., Haas, C., Summa Maria, Bertorelli, R., Papaleo, F., Schafer, M., Piccoli, G., & Cancedda, L. (2018). NEGR1 and FGFR2 cooperatively regulate cortical development and core behaviours related to autism disorders in mice. *Brain*, 141(9), 2542–2544. <https://doi.org/10.1093/brain/awy218>
- Taguchi, S., Nakano, J., Imasaki, T., Kita, T., Saijo-Hamano, Y., Sakai, N., Shigematsu, H., Okuma, H., Shimizu, T., Nitta, E., Kikkawa, S., Mizobuchi, S., Niwa, S., & Nitta, R. (2022). Structural model of microtubule dynamics inhibition by kinesin-4 from the crystal structure of KLP-12 -tubulin complex. *ELife*, 11. <https://doi.org/10.7554/eLife.77877>
- Takahashi, T., Nowakowski, R. S., & Caviness, V. S. ' (1993). Cell Cycle Parameters and Patterns of Nuclear Movement in the Neocortical Proliferative Zone of the Fetal Mouse. In *The Journal of Neuroscience* (Vol. 73, Issue 2).
- Takeuchi, M., Hata, Y., Hirao, K., Toyoda, A., Irie, M., & Takai, Y. (1997). SAPAPs a family of PSD-95/SAP90-associated proteins localized at postsynaptic density. <http://www-jbc.stanford.edu/jbc/>
- Tanaka, T., Serneo, F. F., Higgins, C., Gambello, M. J., Wynshaw-Boris, A., & Gleeson, J. G. (2004). Lis1 and doublecortin function with dynein to mediate coupling of the nucleus to the centrosome in neuronal migration. *Journal of Cell Biology*, 165(5), 709–721. <https://doi.org/10.1083/jcb.200309025>
- Taverna, E., Götz, M., & Huttner, W. B. (2014). The cell biology of neurogenesis: toward an understanding of the development and evolution of the neocortex. In *Annual review of cell and developmental biology* (Vol. 30, pp. 465–502). <https://doi.org/10.1146/annurev-cellbio-101011-155801>
- Taverna, E., & Huttner, W. B. (2010). Neural progenitor nuclei IN motion. In *Neuron* (Vol. 67, Issue 6, pp. 906–914). <https://doi.org/10.1016/j.neuron.2010.08.027>
- Telley, L., Agirman, G., Prados, J., Amberg, N., Fièvre, S., Oberst, P., Bartolini, G., Vitali, I., Cadilhac, C., Hippenmeyer, S., Nguyen, L., Dayer, A., & Jabaudon, D. (2019). Temporal patterning of apical progenitors and their daughter neurons in the developing neocortex. *Science*, 364(6440). <https://doi.org/10.1126/science.aav2522>
- Teng, J., Rai, T., Tanaka, Y., Takei, Y., Nakata, T., Hirasawa, M., Kulkarni, A. B., & Hirokawa, N. (2005). The KIF3 motor transports N-cadherin and organizes the developing neuroepithelium. *Nature Cell Biology*, 7(5), 474–482. <https://doi.org/10.1038/ncb1249>
- Teng, J., Takei, Y., Harada, A., Nakata, T., Chen, J., & Hirokawa, N. (2001). Synergistic effects of MAP2 and MAP1B knockout in neuronal migration, dendritic outgrowth, and microtubule organization. *Journal of Cell Biology*, 155(1), 65–76. <https://doi.org/10.1083/jcb.200106025>
- Theil, T., Alvarez-Bolado, G., Walter, A., & Ruther, U. (1999). Gli3 is required for Emx gene expression during dorsal telencephalon development. *Development*, 126, 3561–3571.
- Thompson, A. F., Blackburn, P. R., Babovic-Vuksanovic, D., Lian, J. B., Klee, W., & Stumpff, J. K. (2021). Pathogenic mutations in the chromokinesin KIF22 disrupt anaphase chromosome 1 segregation. *BioRxiv*. <https://doi.org/10.1101/2021.09.29.462402>
- Tole, S., Ragsdale, C. W., & Grove, E. A. (2000). Dorsoventral patterning of the telencephalon is disrupted in the mouse mutant extra-toes. *Developmental Biology*, 217(2), 254–265. <https://doi.org/10.1006/dbio.1999.9509>
- Toriyama, M., Shimada, T., Kim, K. B., Mitsuba, M., Nomura, E., Katsuta, K., Sakumura, Y., Roepstorff, P., & Inagaki, N. (2006). Shootin 1: A protein involved in the organization of an

- asymmetric signal for neuronal polarization. *Journal of Cell Biology*, 175(1), 147–157. <https://doi.org/10.1083/jcb.200604160>
- Tortosa, E., Adolfs, Y., Fukata, M., Pasterkamp, R. J., Kapitein, L. C., & Hoogenraad, C. C. (2017). Dynamic Palmitoylation Targets MAP6 to the Axon to Promote Microtubule Stabilization during Neuronal Polarization. *Neuron*, 94(4), 809–825.e7. <https://doi.org/10.1016/j.neuron.2017.04.042>
- Toyo-oka, K., Shionoya, A., Gambello, M. J., Cardoso, C., Leventer, R., Ward, , Heather L, Ayala, R., Tsai, K.-H., Dobyns, W., Ledbetter, D., Hirotsune, S., & Wynshaw-Boris, A. (2003). 14-3-3 ϵ is important for neuronal migration by binding to NUDEL: a molecular explanation for Miller–Dieker syndrome. *Nature Genetics*. <https://doi.org/10.1038/ng1169>
- Tripodi, M., Filosa, A., Armentano, M., & Studer, M. (2004). The COUP-TF nuclear receptors regulate cell migration in the mammalian basal forebrain. *Development*, 131(24), 6119–6129. <https://doi.org/10.1242/dev.01530>
- Trivedi, N., Ramahi, J. S., Karakaya, M., Howell, D., Kerekes, R. A., & Solecki, D. J. (2014). Leading-process actomyosin coordinates organelle positioning and adhesion receptor dynamics in radially migrating cerebellar granule neurons. *Neural Development*, 9(1). <https://doi.org/10.1186/1749-8104-9-26>
- Tsai, J. W., Bremner, K. H., & Vallee, R. B. (2007a). Dual subcellular roles for LIS1 and dynein in radial neuronal migration in live brain tissue. *Nature Neuroscience*, 10(8), 970–979. <https://doi.org/10.1038/nn1934>
- Tsai, J. W., Bremner, K. H., & Vallee, R. B. (2007b). Dual subcellular roles for LIS1 and dynein in radial neuronal migration in live brain tissue. *Nature Neuroscience*, 10(8), 970–979. <https://doi.org/10.1038/nn1934>
- Tsai, J. W., Chen, Y., Kriegstein, A. R., & Vallee, R. B. (2005). LIS1 RNA interference blocks neural stem cell division, morphogenesis, and motility at multiple stages. *Journal of Cell Biology*, 170(6), 935–945. <https://doi.org/10.1083/jcb.200505166>
- Tsai, M. H., Cheng, H. Y., Nian, F. S., Liu, C., Chao, N. H., Chiang, K. L., Chen, S. F., & Tsai, J. W. (2020). Impairment in dynein-mediated nuclear translocation by BICD2 C-terminal truncation leads to neuronal migration defect and human brain malformation. *Acta Neuropathologica Communications*, 8(1). <https://doi.org/10.1186/s40478-020-00971-0>
- Umeshima, H., Hirano, T., & Kengaku, M. (2007). *Microtubule-based nuclear movement occurs independently of centrosome positioning in migrating neurons* (Vol. 104).
- Uzquiano, A., Gladwyn-Ng, I., Nguyen, L., Reiner, O., Götz, M., Matsuzaki, F., & Francis, F. (2018). Cortical progenitor biology: key features mediating proliferation versus differentiation. In *Journal of Neurochemistry* (Vol. 146, Issue 5, pp. 500–525). Blackwell Publishing Ltd. <https://doi.org/10.1111/jnc.14338>
- van den Wildenberg, S. M. J. L., Tao, L., Kapitein, L. C., Schmidt, C. F., Scholey, J. M., & Peterman, E. J. G. (2008). The Homotetrameric Kinesin-5 KLP61F Preferentially Crosslinks Microtubules into Antiparallel Orientations. *Current Biology*, 18(23), 1860–1864. <https://doi.org/10.1016/j.cub.2008.10.026>
- van der Vaart, B., van Riel, W. E., Doodhi, H., Kevenaar, J. T., Katrukha, E. A., Gummy, L., Bouchet, B. P., Grigoriev, I., Spangler, S. A., Yu, K. lou, Wulf, P. S., Wu, J., Lansbergen, G., van Battum, E. Y., Pasterkamp, R. J., Mimori-Kiyosue, Y., Demmers, J., Olieric, N., Maly, I. v., ... Akhmanova, A. (2013). CFEOM1-associated kinesin KIF21A is a cortical microtubule growth inhibitor. *Developmental Cell*. <https://doi.org/10.1016/j.devcel.2013.09.010>
- van Erp, S., van den Heuvel, D. M. A., Fujita, Y., Robinson, R. A., Hellemons, A. J. C. G. M., Adolfs, Y., van Battum, E. Y., Blokhuis, A. M., Kuijpers, M., Demmers, J. A. A., Hedman, H., Hoogenraad, C. C., Siebold, C., Yamashita, T., & Pasterkamp, R. J. (2015). Lrig2 Negatively Regulates Ectodomain Shedding of Axon Guidance Receptors by ADAM Proteases. *Developmental Cell*, 35(5), 537–552. <https://doi.org/10.1016/j.devcel.2015.11.008>

- van Riel, W. E., Rai, A., Bianchi, S., Katrukha, E. A., Liu, Q., Heck, A. J., Hoogenraad, C. C., Steinmetz, M. O., Kapitein, L. C., & Akhmanova, A. (2017). Kinesin-4 KIF21B is a potent microtubule pausing factor. *ELife*, 6, 1–30. <https://doi.org/10.7554/eLife.24746>
- Varga, B. v., Faiz, M., Pivonkova, H., Khelifi, G., Yang, H., Gao, S., Linderöth, E., Zhen, M., Karadottir, R. T., Hussein, S. M., & Nagy, A. (2022). Signal requirement for cortical potential of transplantable human neuroepithelial stem cells. *Nature Communications*, 13(1). <https://doi.org/10.1038/s41467-022-29839-8>
- Verhey, K. J., & Hammond, J. W. (2009). Traffic control: Regulation of kinesin motors. In *Nature Reviews Molecular Cell Biology* (Vol. 10, Issue 11, pp. 765–777). <https://doi.org/10.1038/nrm2782>
- Vuolo, L., Stevenson, N. L., Mukhopadhyay, A. G., Roberts, A. J., & Stephens, D. J. (2020). Cytoplasmic dynein-2 at a glance. In *Journal of cell science* (Vol. 133, Issue 6). NLM (Medline). <https://doi.org/10.1242/jcs.240614>
- Wang, D., Nitta, R., Morikawa, M., Yajima, H., Inoue, S., Shigematsu, H., Kikkawa, M., & Hirokawa, N. (2016). Motility and microtubule depolymerization mechanisms of the kinesin-8 motor, KIF19A. *ELife*, 5(September2016). <https://doi.org/10.7554/eLife.18101.001>
- Wang, P. S., Chou, F. S., Ramachandran, S., Xia, S., Chen, H. Y., Guo, F., Suraneni, P., Maher, B. J., & Li, R. (2016). Crucial roles of the Arp2/3 complex during mammalian corticogenesis. *Development (Cambridge)*, 143(15), 2741–2752. <https://doi.org/10.1242/dev.130542>
- Wang, S., Li, X., Zhang, Q., Chai, X., Wang, Y., Förster, E., Zhu, X., & Zhao, S. (2019). Nyp1 Regulates Multipolar–Bipolar Transition and Morphology of Migrating Neurons by Fyn Phosphorylation during Corticogenesis. *Cerebral Cortex*. <https://doi.org/10.1093/cercor/bhz137>
- Wegmann, S., Biernat, J., & Mandelkow, E. (2021). A current view on Tau protein phosphorylation in Alzheimer’s disease. In *Current Opinion in Neurobiology* (Vol. 69, pp. 131–138). Elsevier Ltd. <https://doi.org/10.1016/j.conb.2021.03.003>
- Westerlund, N., Zdrojewska, J., Padzik, A., Komulainen, E., Björkblom, B., Rannikko, E., Tararuk, T., Garcia-Frigola, C., Sandholm, J., Nguyen, L., Kallunki, T., Courtney, M. J., & Coffey, E. T. (2011). Phosphorylation of SCG10/stathmin-2 determines multipolar stage exit and neuronal migration rate. *Nature Neuroscience*, 14(3), 305–313. <https://doi.org/10.1038/nn.2755>
- Wilde, J. J., Petersen, J. R., & Niswander, L. (2014). Genetic, epigenetic, and environmental contributions to neural tube closure. *Annual Review of Genetics*, 48, 583–611. <https://doi.org/10.1146/annurev-genet-120213-092208>
- Wilkie, A. O. (1994). The molecular basis of genetic dominance. *Journal of Medical Genetics*, 31(2), 89–98. <https://doi.org/10.1136/jmg.31.2.89>
- Willemsen, M. H., Ba, W., Wissink-Lindhout, W. M., de Brouwer, A. P. M., Haas, S. A., Bienek, M., Hu, H., Vissers, L. E. L. M., van Bokhoven, H., Kalscheuer, V., Kasri, N. N., & Kleefstra, T. (2014). Involvement of the kinesin family members KIF4A and KIF5C in intellectual disability and synaptic function. *Journal of Medical Genetics*, 51(7), 487–494. <https://doi.org/10.1136/jmedgenet-2013-102182>
- Willemsen, M. H., Vissers, L. E. L., Willemsen, M. A. A. P., van Bon, B. W. M., Kroes, T., de Ligt, J., de Vries, B. B., Schoots, J., Lugtenberg, D., Hamel, B. C. J., van Bokhoven, H., Brunner, H. G., Veltman, J. A., & Kleefstra, T. (2012). Mutations in DYNC1H1 cause severe intellectual disability with neuronal migration defects. *Journal of Medical Genetics*, 49(3), 179–183. <https://doi.org/10.1136/jmedgenet-2011-100542>
- Winkelman, J. D., Bilancia, C. G., Peifer, M., & Kovar, D. R. (2014). Ena/VASP Enabled is a highly processive actin polymerase tailored to self-assemble parallel-bundled F-actin networks with Fascin. *Proceedings of the National Academy of Sciences of the United States of America*, 111(11), 4121–4126. <https://doi.org/10.1073/pnas.1322093111>

- Winterhoff, M., & Faix, J. (2015). Actin-filament disassembly: It takes two to shrink them fast. In *Current Biology* (Vol. 25, Issue 11, pp. R450–R452). Cell Press.
<https://doi.org/10.1016/j.cub.2015.04.050>
- Wloga, D., & Gaertig, J. (2011). Post-translational modifications of microtubules (Journal of Cell Science 123, (3447-3455)). In *Journal of Cell Science* (Vol. 124, Issue 1, p. 154).
<https://doi.org/10.1242/jcs.083576>
- Woolner, S., & Bement, W. M. (2009). Unconventional myosins acting unconventionally. *Trends in Cell Biology*, 19(6), 245–252. <https://doi.org/10.1016/j.tcb.2009.03.003>
- Wordeman, L. (2010). How kinesin motor proteins drive mitotic spindle function: Lessons from molecular assays. In *Seminars in Cell and Developmental Biology* (Vol. 21, Issue 3, pp. 260–268). Elsevier Ltd. <https://doi.org/10.1016/j.semcdb.2010.01.018>
- Wozniak, M. J., Melzer, M., Dorner, C., Haring, H. U., & Lammers, R. (2005). The novel protein KBP regulates mitochondria localization by interaction with a kinesin-like protein. *BMC Cell Biology*, 6. <https://doi.org/10.1186/1471-2121-6-35>
- Wu, Q. F., Yang, L., Li, S., Wang, Q., Yuan, X. bin, Gao, X., Bao, L., & Zhang, X. (2012). Fibroblast growth factor 13 is a microtubule-stabilizing protein regulating neuronal polarization and migration. *Cell*, 149(7), 1549–1564.
<https://doi.org/10.1016/j.cell.2012.04.046>
- Xie, M. J., Yagi, H., Kuroda, K., Wang, C. C., Komada, M., Zhao, H., Sakakibara, A., Miyata, T., Nagata, K. I., Oka, Y., Iguchi, T., & Sato, M. (2013). WAVE2-Abi2 complex controls growth cone activity and regulates the multipolar-bipolar transition as well as the initiation of glia-guided migration. *Cerebral Cortex*, 23(6), 1410–1423. <https://doi.org/10.1093/cercor/bhs123>
- Xie, X., Wang, S., Li, M., Diao, L., Pan, X., Chen, J., Zou, W., Zhang, X., Feng, W., & Bao, L. (2021). α -TubK40me3 is required for neuronal polarization and migration by promoting microtubule formation. *Nature Communications*, 12(1). <https://doi.org/10.1038/s41467-021-24376-2>
- Xu, C., Funahashi, Y., Namba, T., Takano, T., Nakamuta, S., Namba, T., & Kaibuchi, K. (2015). Radial glial cell–neuron interaction directs axon formation at the opposite side of the neuron from the contact site. *Journal of Neuroscience*, 35(43), 14517–14532.
<https://doi.org/10.1523/JNEUROSCI.1266-15.2015>
- Xu, C., & Min, J. (2011). Structure and function of WD40 domain proteins. In *Protein and Cell* (Vol. 2, Issue 3, pp. 202–214). Higher Education Press Limited Company.
<https://doi.org/10.1007/s13238-011-1018-1>
- Yamada, K. H., Hanada, T., & Chishti, A. H. (2007). The effector domain of human Dlg tumor suppressor acts as a switch that relieves autoinhibition of kinesin-3 motor GAKIN/KIF13B. *Biochemistry*, 46(35), 10039–10045. <https://doi.org/10.1021/bi701169w>
- Yamazaki, H., Nakata, T., Okada, Y., & Hirokawa, N. (1996). Cloning and characterization of KAP3: A novel kinesin superfamily-associated protein of KIF3A/3B (microtubule/axonal transport/motor protein). In *Cell Biology (KIFs)* (Vol. 93, Issue 10). <https://www.pnas.org>
- Yang, J., Yang, X., & Tang, K. (2022). Interneuron development and dysfunction. In *FEBS Journal* (Vol. 289, Issue 8, pp. 2318–2336). John Wiley and Sons Inc.
<https://doi.org/10.1111/febs.15872>
- Yang, T., Sun, Y., Zhang, F., Zhu, Y., Shi, L., Li, H., & Xu, Z. (2012). POSH Localizes Activated Rac1 to Control the Formation of Cytoplasmic Dilation of the Leading Process and Neuronal Migration. *Cell Reports*, 2(3), 640–651. <https://doi.org/10.1016/j.celrep.2012.08.007>
- Yoshinaga, S., Ohkubo, T., Sasaki, S., Nuriya, M., Ogawa, Y., Yasui, M., Tabata, H., & Nakajima, K. (2012). A phosphatidylinositol lipids system, lamellipodin, and Ena/VASP regulate dynamic morphology of multipolar migrating cells in the developing cerebral cortex. *Journal of Neuroscience*, 32(34), 11643–11656. <https://doi.org/10.1523/JNEUROSCI.0738-12.2012>

- Youn, Y. H., Pramparo, T., Hirotsume, S., & Wynshaw-Boris, A. (2009). Distinct dose-dependent cortical neuronal migration and neurite extension defects in *Lis1* and *Ndel1* mutant mice. *Journal of Neuroscience*, 29(49), 15520–15530. <https://doi.org/10.1523/JNEUROSCI.4630-09.2009>
- Yu, H. L., Peng, Y., Zhao, Y., Lan, Y. S., Wang, B., Zhao, L., Sun, D., Pan, J. X., Dong, Z. Q., Mei, L., Ding, Y. Q., Zhu, X. J., & Xiong, W. C. (2020). Myosin X interaction with KIF13B, a crucial pathway for Netrin-1-Induced axonal development. *Journal of Neuroscience*, 40(48), 9169–9185. <https://doi.org/10.1523/JNEUROSCI.0929-20.2020>
- Yuen, M., & Ottenheijm, C. A. C. (2020). Nebulin: big protein with big responsibilities. *Journal of Muscle Research and Cell Motility*, 41(1), 103–124. <https://doi.org/10.1007/s10974-019-09565-3>
- Yuki Hirota, & Kazunori Nakajima. (2017). Control of Neuronal Migration and Aggregation by Reelin Signaling in the Developing Cerebral Cortex. In *Frontiers in Cell and Developmental Biology* (Vol. 5, Issue APR). Frontiers Media S.A. <https://doi.org/10.3389/fcell.2017.00040>
- Zechel, J. L., Gamboa, J. L., Peterson, A. G., Puchowicz, M. A., Selman, W. R., & Lust, W. D. (2005). Neuronal migration is transiently delayed by prenatal exposure to intermittent hypoxia. *Birth Defects Research Part B - Developmental and Reproductive Toxicology*, 74(4), 287–299. <https://doi.org/10.1002/bdrb.20051>
- Zhang, C., Mejia, L. A., Huang, J., Valnegri, P., Bennett, E. J., Anckar, J., Jahani-Asl, A., Gallardo, G., Ikeuchi, Y., Yamada, T., Rudnicki, M., Harper, J. W., & Bonni, A. (2013). The X-Linked Intellectual Disability Protein PHF6 Associates with the PAF1 Complex and Regulates Neuronal Migration in the Mammalian Brain. *Neuron*, 78(6), 986–993. <https://doi.org/10.1016/j.neuron.2013.04.021>
- Zhang, F., Yu, J., Yang, T., Xu, D., Chi, Z., Xia, Y., & Xu, Z. (2016). A novel c-Jun N-terminal kinase (JNK) signaling complex involved in neuronal migration during brain development. *Journal of Biological Chemistry*, 291(22), 11466–11475. <https://doi.org/10.1074/jbc.M116.716811>
- Zhang, J. H., Zhao, Y. F., He, X. X., Zhao, Y., He, Z. X., Zhang, L., Huang, Y., Wang, Y. B., Hu, L., Liu, L., Yu, H. L., Xu, J. H., Lai, M. M., Zhao, D. D., Cui, L., Guo, W. X., Xiong, W. C., Ding, Y. Q., & Zhu, X. J. (2018). DCC-Mediated Dab1 Phosphorylation Participates in the Multipolar-to-Bipolar Transition of Migrating Neurons. *Cell Reports*, 22(13), 3598–3611. <https://doi.org/10.1016/j.celrep.2018.03.005>
- Zhang, J., Neal, J., Lian, G., Hu, J., Lu, J., & Sheen, V. (2013). Filamin A regulates neuronal migration through brefeldin A-inhibited guanine exchange factor 2-dependent Arf1 activation. *Journal of Neuroscience*, 33(40), 15735–15746. <https://doi.org/10.1523/JNEUROSCI.1939-13.2013>
- Zhang, X., Lei, K., Yuan, X., Wu, X., Zhuang, Y., Xu, T., Xu, R., & Han, M. (2009). SUN1/2 and Syne/Nesprin-1/2 Complexes Connect Centrosome to the Nucleus during Neurogenesis and Neuronal Migration in Mice. *Neuron*, 64(2), 173–187. <https://doi.org/10.1016/j.neuron.2009.08.018>
- Zhao, C.-T., Li, K., Li, J.-T., Zheng, W., Liang, X.-J., Geng, A.-Q., Li, N., & Yuan, X.-B. (2009). PKC regulates cortical radial migration by stabilizing the Cdk5 activator p35. *PNAS*. www.pnas.org/cgi/content/full/
- Zheng, Y., Wong, M. L., Alberts, B., & Mitchison, T. (1995). Nucleation of microtubule assembly by a γ -tubulin-containing ring complex. *Nature*, 301, 341–357.
- Zhu, X., & Kaverina, I. (2013). Golgi as an MTOC: Making microtubules for its own good. In *Histochemistry and Cell Biology* (Vol. 140, Issue 3, pp. 361–367). <https://doi.org/10.1007/s00418-013-1119-4>

Résumé du projet

Introduction

Le développement du cortex cérébral suit une série d'étapes qui génère une structure composée par six couches de neurones. Le processus commence dans la zone sous-ventriculaire avec la glie radiaire (progéniteur apical), le principal progéniteur neuronal, qui génère de neurones soit dans une manière directe ou d'une manière indirecte, via la production de progéniteurs intermédiaires pour amplifier le nombre total de neurones produits (Paridaen & Huttner, 2014). Une fois générés, les neurones migrent dans la plaque cortical pour atteindre leur location finale où ils vont se différencier. La migration est caractérisée par plusieurs phases distinctes. Les neurones transitent tout d'abord par une phase multipolaire, caractérisée par la protrusion et la rétraction des multiples projections, qui sert à l'exploration de l'environnement. Plus tard, ces neurones vont adopter à nouveau une morphologie bipolaire et initier la phase de locomotion. Au cours de la locomotion, les neurones étendent une projection connue comme « leading process » (LP) qui s'attache au processus basal de la glie radiaire. Après cette extension, une dilatation dans la partie proximale du LP se forme, suivi par le mouvement vers l'avant du noyau. Ce cycle de mouvement est répété jusqu'à la fin de la migration. Les neurones de projection sont organisés dans le cortex d'une façon dite inside-out, où les premiers neurones générés sont ceux qui occupent les couches profondes et les derniers neurones générés occupent les couches superficielles (Francis & Capello, 2021 ; Ohtaka-Maruyama & Okado, H. 2015).

Parmi les facteurs qui interviennent dans la neurogenèse, le cytosquelette de microtubules (MT) est l'un des plus importants. En effet, des mutations dans des gènes codant pour la tubuline ou les protéines associées aux MTs (MAPs) sont associées à malformations corticales, comme l'hétérotopie, l'agénésie de corpus calleux ou la microcéphalie (Fernandez, *et al.* 2016). Les kinésines sont des MAPs avec une fonction motrice médiant le transport antérograde de divers cargos, en utilisant l'énergie produite par l'hydrolyse de l'ATP. Quelques exemples de kinésines importants pour le correct développement du cortex cérébral sont KIF4A (Najmabadi, H. *et al.* 2011), KIF7 (Putoux, A. *et al.* 2011), KIF2A (Poirier, K. *et al.* 2013), KIF5C (Michels, S. *et al.* 2017), KIF1A (Ohba, C. *et al.* 2015) et KIF14 (Makrythanasis, P. *et al.* 2018), dont leurs mutations ont été mise en évidence chez des patients avec déficience intellectuelle, hydrocéphalie ou microcéphalie.

KIF21B est une kinésine neuronale qui appartient à la famille 4 des kinésines et possède trois domaines principaux : le domaine moteur (avec activité ATPase) dans la partie N-terminale de la protéine, un domaine coiled-coil (CC) et un domaine WD40 dans la partie C-terminale de la protéine. Le domaine CC contient un domaine CC régulateur (rCC) nécessaire à l'auto-inhibition de l'activité motrice de KIF21B via des interactions intramoléculaires avec le domaine moteur (Van Riel, *et al.* 2017).

Dans les neurones, KIF21B est connu pour réguler le transport de récepteurs de neurotransmetteurs (Gromova, *et al.* 2018 ; Morikawa, *et al.* 2018) et la stabilité de MT (Van Riel, *et al.* 2017). *In vitro*, KIF21B régule l'arborisation dendritique de neurones hippocampaux (Muhia, *et al.* 2016). En outre, *Kif21b* knock-out (KO) chez la souris produit microcéphalie et un corps calleux fin (Kannan, *et al.* 2017) suggérant la possibilité que KIF21B joue un rôle important dans le développement cortical.

Au cours de ma thèse, j'ai élucidé le rôle physiologique et pathologique de *Kif21b* dans le développement cortical:

- **Caractérisation des mécanismes moléculaires induits par des mutations faux-sens de KIF21B**
- **Régulation de la migration radiaire des neurones de projection par *Kif21b* en conditions physiologiques.**

Résultats

Caractérisation des mécanismes moléculaires induits par des mutations faux-sens de KIF21B

On a identifié en collaboration avec des cliniciens que KIF21B était muté chez 4 patients qui présentent des troubles du neurodéveloppement impliquant des malformations corticales et de la déficience intellectuelle. Parmi ces 4 mutations, trois sont des mutations faux-sens et une impliquait l'ajoute d'un codon de stop prématuré. Pour étudier les mécanismes physiopathologiques impliqués, nous avons décidé d'electroporer les mutations humaines avec un promoteur neuronal pour les exprimer spécifiquement dans les neurones dans le cortex murin en développement. Nous avons constaté que l'expression des versions mutantes de KIF21B induit un retard dans la migration neuronale.

Ma contribution à ce projet a consisté à élucider les mécanismes par lesquels les mutations faux-sens induisent un retard dans la migration neuronale. Pour déterminer si la protéine mutée induit des défauts migratoires par un effet dominant négative, j'ai electroporé la version wild-type (WT) de la protéine avec chaque mutation pour sauver le phénotype. Après l'analyse de résultats, nous avons vu que cette co-électroporation ne sauvait pas le phénotype, signifiant que le retard migratoire est généré par un mécanisme de gain de fonction.

Autre preuve en faveur d'un mécanisme gain de fonction, j'ai montré que l'électroporation de concentration croissante de la protéine WT induit un effet similaire à celui des mutations de KIF21B. Suite à cette observation, nous avons proposé comme un mécanisme possible une hyperactivation (activité motrice) des protéines mutantes, plus précisément un relâchement de l'auto-inhibition. En accord, avec le mécanisme proposé, l'électroporation de la protéine tronquée dans le domaine rCC (Δ rCC), important pour l'auto-inhibition, induit un retard dans la migration neuronale. Pour vérifier que l'hypermobilité était responsable du défaut de migration neuronale induit par les différentes mutations, nous avons électroporé les formes mutantes de la protéine dépourvues du domaine de liaison à l'ATP, et par conséquent, incapables de se déplacer. On a montré que les l'immobilité des mutants de KIF21B abroge les déficits de migration radiaire induit par les mutations, ce qui démontre que les mutations de KIF21B induisent un retard de la migration neuronal par la levée de l'auto-inhibition entraînant en conséquence une hypermobilité de la protéine.

Les résultats complets de cette recherche peuvent être trouvés dans la publication Asselin, *et al.* 2020, parue dans nature communications, à laquelle je participe en tant que second auteur.

Régulation de la migration radiaire par Kif21b dans conditions physiologiques

Pour découvrir comment Kif21b contrôle la migration neuronale pendant le développement cortical, nous avons invalidé l'expression de Kif21b dans la population neuronale par l'électroporation d'un shRNA inductible dans les neurones chez la souris. La déplétion de Kif21b induit une réduction de 27.8% des cellules qui ont atteint la plaque corticale supérieure (UpCP). Il est intéressant de noter que le phénotype n'est que partiellement sauvé par la version dépourvue du domaine moteur (Δ MD), indiquant que ce domaine joue un rôle important pour la fonction de Kif21B dans la migration neuronale, mais également que toute fois nous avons observé un sauvetage total du phénotype de migration par une version de Kif21B incapable d'hydrolyser l'ATP (Δ ATP et T96N), suggérant que la fonction de Kif21B dans la régulation de la migration neuronale est indépendante de l'activité motrice sur les microtubules.

Pour avoir un aperçu des mécanismes cellulaires auxquels Kif21b participe, nous avons réalisé des expériences de vidéo-microscopie en temps réel sur des tranches de cerveau électroporé avec un plasmide contrôle ou le shRNA *Kif21b*. la déplétion de kif21b altère aussi bien la locomotion que la morphologie des neurones en migration. Les caractéristiques principales affectées par la déplétion de Kif21b sont la vitesse, le nombre et longueur des pauses et la transition bipolaire-multipolaire. Une observation intéressante est que des paramètres comme la ramification du LP, la nucléokinese et la

formation de dilations dans le LP sont aussi affectées, toutes ces caractéristiques dépendant du cytosquelette d'actine (Wang, *et al.* 2019; Guerrier, *et al.* 2009).

Notamment, l'analyse des partenaires protéiniques de Kif21b par mass spectrométrie a révélé différentes isoformes de l'actine et des protéines de liaison à l'actine, comme la drebrine et la Myosine associées à Kif21b dans le cortex embryonnaire. Pour corroborer ces interactions j'ai fait l'immunoprécipitation de Kif21b et testé par western blot les différentes interactions indiquées par l'analyse de mass spectrométrie. De plus, par microscopie de super-résolution dans le cône de croissance des neurones corticaux, j'ai observé une association de Kif21b avec des filaments d'actine, et aussi des particules de Kif21b détachées des filaments, ce qui suggère une interaction dynamique de Kif21b avec l'actine.

Les expériences réalisées indiquent une interaction de Kif21b avec le cytosquelette d'actine, et pour déterminer si cette interaction est cruciale pour la migration radiaire, j'ai analysé la dynamique d'actine par vidéo-microscopie sur des tranches de cerveaux électroporés avec le shRNA et le plasmide LifeAct-Ruby, qui quand il s'exprime, produit une protéine fluorescente qui se lie au cytosquelette d'actine. Dans les neurones contrôles, on observe une augmentation de la contraction des filaments d'actine pendant la formation de la dilation du LP, puis une forte diminution à la fin du cycle de nucléokinese. Dans les neurones électroporés avec le shRNA, l'augmentation de la fluorescence était maintenue après la nucléokinese, indiquant que la contraction du cytosquelette d'actomyosine est altérée pendant la migration neuronale.

Conclusions

Au cours de ma thèse, j'ai contribué à définir le rôle de Kif21b lors de la migration radiaire dans le développement cortical, à la fois au niveau physiologique et au niveau pathologique. J'ai établi un lien entre l'hyperactivation de la kinésine produit par des mutations pathologiques et les phénotypes observés chez les patients. Un cas similaire de levée de l'auto-inhibition a été observé par Bianchi et al (2016) observé pour KIF21A (homologue le plus proche de KIF21B) dans le contexte de fibrose congénitale des muscles extra-oculaires de type 1.

Concernant les mécanismes physiologiques, nous avons découvert que la mobilité de Kif21b n'est pas impliquée dans la migration neuronale. De plus, les expériences de vidéo-microscopie indiquent que la déplétion de Kif21b affecte le cytosquelette d'actine. Par exemple, la formation de multiples ramifications dans le LP ou le nombre réduit de nucléokineses. Soutenant ce point, j'ai trouvé que la contraction du cytosquelette d'actomyosine est affectée pendant la migration radiaire.

Il est important de noter que c'est la première fois qu'une kinésine est associée aux filaments d'actine, la différenciant de la fonction normale des kinésines soit comme une protéine motrice ou comme un

régulateur de la structure du cytosquelette de MT. Aussi, nous décrivons une fonction non canonique de Kif21b qui peut être aussi importante pour réguler des mécanismes pathologiques.

En plus de la fonction que nous décrivons dans cette recherche, Kif21B peut aussi avoir une fonction dépendante des MT, puisque il est décrit que la connexion des différents cytosquelettes est importante pour l'homéostasie cellulaire (Seethamaran & Etienne- Manneville, 2020; Sanchez-Huertas, *et al.* 2020).

References:

- Asselin L, Rivera Alvarez, J, *et al.* Mutations in the *KIF21B* kinesin gene cause neurodevelopmental disorders through imbalanced canonical motor activity. *Nature Communications* 11: 1-18
- Bianchi, *et al.* 2016. Structural basis for misregulation of kinesin KIF21A autoinhibition by CFEOM1 disease mutations. *Scientific Reports*. 1-16
- Fernandez, V, Llinares, C, Borrel, V. 2016. Cerebral cortex expansion and folding: what have we learned? *The EMBO Journal* 35. 1021-1044.
- Gromova, K. Muhia, M. Rothamer, N. Gee, C. Thies, E. Schaefer, I. Kress, S. Kiliman, M. Shevuk, O. Oerter, T. Kneussel, M. 2018. Neurobeachin and the kinesin KIF21B are critical for endocytic Recycling of NMDA Receptors and Regulate Social Behavior. *Cell Reports* (23). 2705-2717.
- Guerrier, *et al.* 2009. The F-BAR Domain of srGAP2 Induces membrane Protrusions Required for Neuronal Migration and Morphogenesis. *Cell* 138: 990-1004
- Kannan, M. Bayam, E. Wagner, C. Rinaldi, B. Kretz, P. Tilly, P. Roos, M. McGillewie, L. Bar, S. Minocha, S. Chevalier, C. Po, C. Chelly, J. Mandel, J.L. Borgatti, R. Piton, A. Kinnear, C. Loos, B. Adams, D. Herault, Y. Collins, S. Friant, S. Godin, J. Yalcin, B. 2017. WD40-repeat 47, a microtubule-associated protein, is essential for brain development and autophagy. *PNAS*. 114 (44). 9304-9317
- Makrythanasis, P. *et al.* 2018. Biallelic variants in KIF14 cause intellectual disability with microcephaly. *European Journal of Human genetics*. (3):330-339
- Michels, S. *et al.* 2017. Mutations of KIF5C cause a neurodevelopmental disorder of infantile-onset epilepsy, absent language, and distinctive malformations of cortical development. *American journal of medical genetics*. 173(12): 3127–3131.
- Morikawa, M. Tanaka, Y. Cho, H. Yoshihara, M. Hirokawa, N. 2018. The Molecular Motor KIF21B Mediates Synaptic Plasticity and Fear Extinction by Terminating Rac1 Activation.
- Muhia, *et al.* 2016. The Kinesin KIF21B Regulates Microtubule Dynamics and Is Essential for Neuronal Morphology, Synapse Function, and Learning and Memory. *Cell Reports* 15: 968 - 977
- Ohtaka-Maruyama & Okado, H. 2015. Molecular Pathways Underlying Projection Neuron Production and Migration during Cerebral Cortical Development. *Frontiers in Neuroscience* 9: 1-24
- Ohba, C. *et al.* 2015. *De novo* KIF1A mutations cause intellectual deficit, cerebellar atrophy, lower limb spasticity and visual disturbance. *Journal of Human Genetics*. 60: 739–742
- Paridaen & Huttner. 2014. Neurogenesis during development of the vertebrate central nervous system. *EMBO Reports* (15). Vol 4. 351-364
- Sanchez-Huertas, *et al.* 2020. The +TIP Navigator-1 is an actin–microtubulecrosslinker that regulates axonal growth conomotility. *Journal of Cell Biology* (219). Vol 9: 1 -21
- Seethamaran & Etienne- Manneville, 2020. Cytoskeletal cross-talk in cell migration. *Cell reviews* (30). Vol 9: 720-735.
- Van Riel, W. Rai, A. Bianchi, S. Katrukha, E. Liu, Q. Heck, J. Hoogenraad, C. Steinmetz, M. Kapitein. L. Akhmanova, A. 2017. Kinesin-4 KIF21B is a potent microtubule pausing factor. *eLIFE*
- Wang, *et al.* 2019. Nyap1Regulates Multipolar–Bipolar Transition and Morphology of Migrating Neurons by Fyn Phosphorylation during Corticogenesis. *Cerebral cortex*. 00: 1-13

José RIVERA ALVAREZ
**Physiological and pathological
role of the kinesin Kif21b
during neuronal migration**

Résumé

La fonction défectueuse des kinésines, moteurs moléculaires, est liée à des malformations corticales telles que la microcéphalie, la lissencéphalie et la pachygyrie. Dans ce travail, j'ai étudié les rôles pathologiques et physiologiques de la kinésine Kif21b pendant la migration des neurones de projection corticaux. Premièrement, nous avons élucidé un soulagement de l'auto-inhibition comme mécanisme à l'origine de la migration défectueuse des neurones exprimant les mutations faux-sens de KIF21B trouvées chez les patients atteints de déficience intellectuelle et de troubles neurodéveloppementaux. Deuxièmement, afin d'étudier le rôle physiologique de Kif21b pendant la migration des neurones de projection, nous avons montré que l'extinction de Kif21b induit des défauts morphologiques et de locomotion, et que la motilité de la kinésine est dispensable pour la migration des neurones. De manière inattendue, nous avons découvert que Kif21b se lie directement à l'actine et régule sa dynamique. De plus, les neurones dépourvus de Kif21b présentent des défauts dans la dynamique de l'actine. Dans l'ensemble, ce travail a permis d'élucider les rôles clés de Kif21b pendant la migration des neurones pyramidaux corticaux.

Mot-clés : Kif21b, kinesin, microtubules, actin, migration of cortical pyramidal neurons

Résumé en anglaise

The defective function of the molecular motors kinesins is related to the development of cortical malformations such as microcephaly, lissencephaly and pachygyria. In this work I studied the pathological and physiological roles of the kinesin Kif21b during migration of cortical projection neurons. First, we elucidated a relief in autoinhibition as the mechanism behind defective migration of neurons that expressed KIF21B missense mutations found in patients that presented with intellectual disability and neurodevelopmental disorders. Secondly, to study the physiological role of Kif21b during migration of projection neurons, we showed that *Kif21b* silencing induces morphological and locomotion defects, and that the motility of the kinesin is dispensable for neurons to migrate. Unexpectedly, we found that Kif21b directly binds to actin and regulates its dynamics *In Vitro*, moreover, *Kif21b* depleted neurons showed defects in actin dynamics during migration. Overall, this work elucidated key roles of Kif21b during migration of cortical pyramidal neurons.

Keywords: Kif21b, kinesin, microtubules, actin, migration of cortical pyramidal neurons